THE JOURNAL OF

PHYSICAL CHEMISTRY

The High Temperature Vaporization Properties of Boron Carbide

and the Heat of Sublimation of Boron[1]

by Harry E. Robson and Paul W. Gilles

Department of Chemistry, University of Kansas, Lawrence, Kansas   (*Received December 19, 1963*)

The vaporization behavior of boron carbide solid solutions is shown to be the preferential loss of gaseous boron regardless of the sample composition. An invariant system consisting of a graphite crucible and a carbon-saturated boron carbide sample was used to measure the vapor pressure over the temperature range 2184–2522°K. The Knudsen technique employing condensation targets was used, and boron was specifically assayed by a coulometric titration of the mannitol complex. The derived third-law heats of sublimation in kcal./mole of boron are $\Delta H^{\circ}_0 = 136.8 \pm 0.1$ and $\Delta H^{\circ}_{298} = 138.0 \pm 0.1$ for boron carbide and $\Delta H^{\circ}_0 = 133.8 \pm 0.7$ and $\Delta H^{\circ}_{298} = 135.0 \pm 0.7$ for boron.

Introduction

The high melting and boiling points, the great hardness, and the chemical inertness of the refractory borides cause them to be a unique group of substances. These very properties, however, make their thermodynamic properties difficult to obtain except by vaporization studies, which themselves must employ a reliable value for the heat of sublimation of boron. Elemental boron is so reactive at high temperatures that values of its vapor pressure and heat of sublimation obtained from experimental studies with the element are subject to great errors arising from reactions between the sample and the other parts of the system. One of the purposes of the present work is to obtain the heat of sublimation of boron from a vaporization study of boron carbide.

Searcy and Myers,[2] Chupka,[3] Schissel and Williams,[4] Akishin, Nikitin, and Gorokhov,[5] Priselkov, Sapozhnikov, and Tseplyaeva,[6] Alcock and Grieveson,[7] Verhaegen, Stafford, Ackerman, and Drowart,[8] Verhaegen and

Drowart,[9] Paule and Margrave,[10] and Hildenbrand and Hall[11] all have sought to obtain the sublimation energy of boron, but the results are in disagreement.

(1) Abstracted in part from the Ph.D. Thesis of H. E. Robson, University of Kansas, 1958.

(2) A. W. Searcy and C. E. Myers, *J. Phys. Chem.*, **61**, 957 (1957).

(3) W. A. Chupka, Argonne National Laboratory Report ANL-5667, 1957, p. 75.

(4) P. Schissel and W. Williams, *Bull. Am. Phys. Soc.*, **4**, 139 (1959).

(5) P. A. Akishin, O. T. Nikitin, and L. N. Gorokhov, *Dokl. Akad. Nauk SSSR*, **129**, 1075 (1959).

(6) Yu. A. Priselkov, Yu. A. Sapozhnikov, and A. V. Tseplyaeva, *Izv. Akad. Nauk SSSR, Otd. Tekhn. Nauk Met. i Toplivo*, 134 (1960).

(7) C. Alcock and P. Grieveson, "Thermodynamics of Nuclear Materials," International Atomic Energy Agency, Vienna, Austria, 1962, pp. 571, 572.

(8) G. Verhaegen, F. E. Stafford, M. Ackerman, and J. Drowart, *Nature*, **193**, 1280 (1962).

(9) G. Verhaegen and J. Drowart, *J. Chem. Phys.*, **37**, 1367 (1962).

(10) R. C. Paule and J. L. Margrave, *J. Phys. Chem.*, **67**, 1368 (1963).

(11) D. L. Hildenbrand and W. F. Hall, *ibid.*, **68**, 989 (1964).

In the present work, boron carbide, saturated with carbon and contained in graphite Knudsen cells, was vaporized under high vacuum; the sublimate was collected and analyzed chemically; the dissociation pressure and the heat of sublimation of boron from boron carbide were measured; and the heat of sublimation of elemental boron was calculated.

Graphite crucibles were used to provide a fixed composition for the samples so that meaningful pressures could be obtained. Although the measurements were made several years ago, uncertainty has existed until the present concerning the nature of the gaseous species. Verhaegen, Stafford, Ackerman, and Drowart[8] have recently shown mass spectrometrically that monatomic boron is the predominant species arising from the vaporization of boron from graphite Knudsen cells although BC_2 and B_2C constitute about 5 and 1% of the vapor, respectively.

The boron–carbon system contains only one firmly established intermediate phase which is usually described as B_4C, but it shows extensive solid solution on the boron-rich side of this composition. The crystals exhibit the space group D^5_{3d}-$R\bar{3}m$ and our measurements give hexagonal parameters, $a_0 = 5.601 \pm 0.001$ and $c_0 = 12.072 \pm 0.002$ Å.[12-18]

Experimental

Materials. Some samples of carbon-saturated boron carbide were obtained through the courtesy of Dr. Gordon Finlay of the Norton Co. in the form of 12.5-mm. rods. Other samples of various compositions were synthesized from mixtures of previously outgassed amorphous boron and graphite. The boron was purchased from Fairmount Chemical Co., which supplied the analysis 99.10% boron, 0.40% Fe, and 0.30% C; the spectrographic graphite powder with negligible impurities was purchased from the National Carbon Co. These samples were prepared by sintering the mixed powders *in vacuo* for 0.1 to 2 hr. at temperatures between 1600 and 2300° in graphite crucibles about 20 mm. in diameter and 25 mm. tall which had been machined from spectroscopic grade graphite rod. The pressure during preparation was always less than 10^{-3} mm. and usually below 10^{-4} mm. These rather high pressures are attributable to gases present in the graphite.

Apparatus. The apparatus for effusion studies is shown in Fig. 1. For the preparations, the coolant reservoir and target receiver sections of the apparatus were replaced by a simple cylindrical tube. The crucible assembly is shown in Fig. 2. The spectrographic graphite inner crucible, of about 16 mm. inside diameter and 16 mm. inside height, was contained in a close-
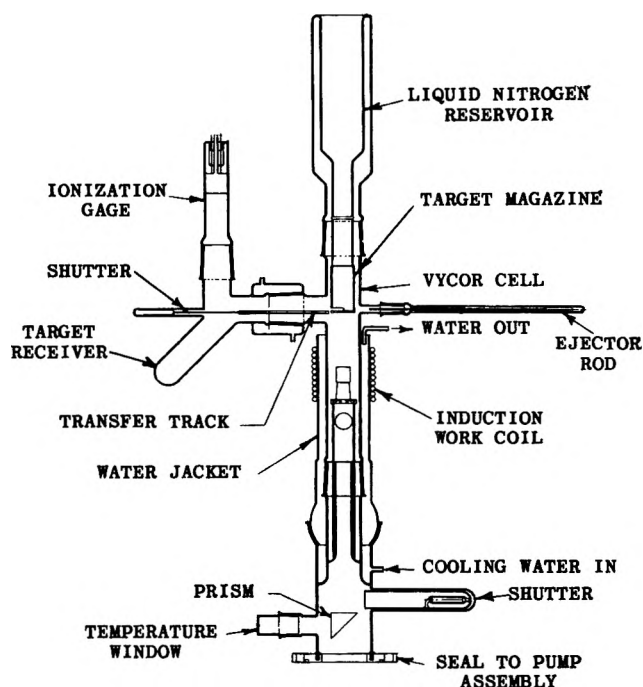
Figure 1. High vacuum effusion apparatus for vapor pressure measurements.

fitting tantalum outer crucible. The two crucibles sat on a tripod formed from tantalum wire. Tungsten shields on top of the crucible served to keep the lid at least as warm as the walls of the crucible. The thin-edged orifice was defined by the tantalum lid, and its size was measured carefully with a comparator both before and after a series of experiments. The ratio of inside surface area to orifice area was 200 or larger.

Platinum targets were contained in individual cassettes stacked in the target magazine which was cooled by liquid nitrogen. Vapor escaping through the orifice in the lid of the crucible was condensed either on the walls of the apparatus or on the platinum targets. After one platinum target had been exposed to the molecular beam it could be ejected from its position and stored in the receiver on the left. As an exposed target was removed, the next target fell into receiving position:

(12) F. Laves, *Nachr. Ges. Wiss. Goettingen, Math-physik. Kl.,* Fachgruppe IV, 57, 1 (1934).

(13) G. S. Zhdanov and N. G. Sevast'yanov, *Russ. J. Phys. Chem.,* 17, 326 (1943).

(14) H. K. Clark and J. L. Hoard, *J. Am. Chem. Soc.,* 65, 2115 (1943).

(15) F. L. Glaser, D. Moskowitz, and B. Post, *J. Appl. Phys.,* 24, 731 (1953).

(16) R. D. Allen, *J. Am. Chem. Soc.,* 75, 3582 (1953).

(17) G. S. Zhdanov, N. N. Zhuravlev, and L. S. Zevin, *Dokl. Akad. Nauk SSSR,* 92, 767 (1953).

(18) G. S. Zhdanov, G. A. Meerson, N. N. Zhuravlev, and G. V. Samsonov, *Zh. Fiz. Khim.,* 28, 1076 (1954).
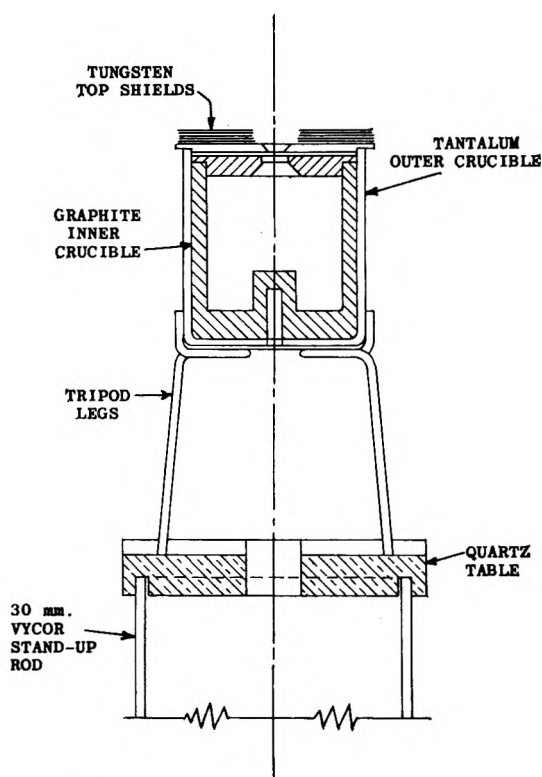
Figure 2. Crucible assembly.

A magnetically operated shutter was opened and closed to define the time during which the target was exposed to the molecular beam. The platinum targets were 31.8 mm. in diameter and 0.13 mm. in thickness and were held in the stainless steel cassettes by stainless steel springs. The distance between the orifice and target was measured with a cathetometer. Definition of the beam was established by a collimator which also supported the cassettes. Its diameter was measured with a micrometer. An auxiliary experiment demonstrated that there was no reflection from the targets. Before being introduced into the system, the targets were cleaned in hot chromic acid, washed in distilled water, dried in a 100° oven, and heated in air for about 10 min. at 1000° in a separate induction heater.

Heating was accomplished by high-frequency induction from a 25-kw. 450-kc. General Electric induction heater. The shutter at the bottom protected the light-deflecting prism from becoming coated with vapor. The pumping system consisted of an oil diffusion pump, a mechanical pump, a thermocouple gage, and a Philips gage. The pumps and gages are below the apparatus shown in Fig. 1.

Temperature Measurement. Because temperature errors would lead to errors in the final results, considerable care was taken in the measurement of the temperature

in the effusion experiments. A Leeds and Northrup disappearing filament optical pyrometer was sighted through a calibrated window and prism into a blackbody hole in the bottom of the crucible. This pyrometer was compared with a similar one which had been standardized at the U. S. National Bureau of Standards. Both pyrometers had been standardized at Argonne National Laboratory. Auxiliary experiments consisting of alternate measurements of the temperature in the blackbody hole and through the orifice established that no correction need be applied to the blackbody observation to obtain the corresponding orifice temperature. The calibration of the window and prism was made both before and after a series of experiments, but no significant change was found.

Procedure. After the crucible assembly and target chamber had been properly placed, the system was pumped for 16 hr. or more without refrigerant in either the pump baffles or the top dewar. During this time the pressure fell to about 10^{-6} mm. Liquid nitrogen was added to the dewar and a CO_2–acetone slush to the pump baffles. A warm-up period of several hours was allowed to keep the pressure below 10^{-4} mm. When the pressure had fallen to 5×10^{-6}, exposures were begun by opening the shutter. Temperatures were measured every 10 min. during exposure. After appropriate exposure time had elapsed, the shutter was closed, the target was ejected, and the procedure was repeated. At the completion of a series of measurements, the targets were removed and assayed for boron.

Analyses. Combustion analyses of boron carbide samples were kindly performed by Prof. Paul Arthur and Dr. Raymond Annino at Oklahoma State University. Details are given in Dr. Annino's dissertation.[19] The assay of boron collected on the platinum targets during the vaporization experiment was performed coulometrically. The targets were inductively heated for 1 min. as they rested in a clean 30-ml. silica beaker with the boron-containing surface down. Then 2 ml. of 1.1 N NaOH was added to the beaker to dissolve the resulting B_2O_3. That this procedure removed all the boron was substantiated by spark spectrographic analysis. After the target had been rinsed with distilled water, the solution was acidified with HCl and was analyzed coulometrically between a platinum cathode and silver anode in the following manner. When a pH of 6.0 was attained, 5 ml. of saturated mannitol solution was added and the titration continued to a pH of 6.3. This value was determined by preliminary studies to be equivalent to a titration to the break in the pH curve between 7.0 and 7.5 followed by a blank correction.

(19) R. Annino, Ph.D. Thesis, Oklahoma State University, 1956.

Eight successive experiments at the same temperature, but for different lengths of time, show that the boron assay was proportional to the exposure time over a four-fold range and that the target weight gains, though less reliable, were approximately proportional to the boron assay.

Results

Characterization of Vaporization Processes. Four qualitative experiments demonstrated that boron is preferentially vaporized even from carbon-saturated boron carbide, and that the vaporization reaction is

$$0.25B_4C(s) = 0.25C(s) + B(g) \qquad (1)$$
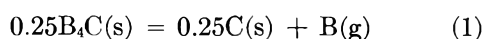
In the first experiment, a Norton Company boron carbide cylinder, 12.5 mm. in diameter and 12.5 mm. long, was heated to about 2200° for about 30 min. by radiation from an inductively heated tantalum susceptor. A tantalum lid on the tantalum susceptor gained weight and an X-ray pattern on the surface revealed substantial amounts of TaB_2 and smaller amounts of TaC. The sample exhibited a black coating which was too thin for X-ray identification. The second experiment consisted of a succession of heatings of a similar boron carbide cylinder followed by X-ray examination of the boron carbide surface which had been polished. The strong graphite X-ray diffraction line was observed to appear and to increase in intensity with progressive vaporization. Since there was no other source of carbon in the system, graphite appeared as the result of reaction 1. The third observation was made on a specimen of synthetic boron carbide from which 6% of the sample had been vaporized during a Knudsen experiment. An X-ray examination of the top surface showed a significant increase in the graphite content. The fourth experiment consisted of a preferential vaporization of a carbon-deficient sample contained in a tantalum crucible that had been previously thoroughly borided by heating it with boron. During the course of the vaporization, the lattice parameters showed changes characteristic of an increase in carbon content.

Some doubt concerning the nature of the vaporization process was indicated early in the investigation by the presence of boron carbide in an orifice following some vaporization experiments. The diffusion of carbon from the close inner graphite crucible probably is the source of the carbon needed to form the boron carbide, yet some carbon may have come directly from the sample by vapor transport as the molecules B_2C and BC_2.

Vapor Pressure Measurements. Ten sets of effusion measurements were performed with synthetic boron carbide containing small amounts of excess graphite.

No other phase was detected in the sample by X-ray diffraction, and spectrographic analysis did not indicate any impurities above the trace level.

The results of 39 measurements are given in Table I in which the first column gives the series and exposure numbers, the second column gives the time interval of collection of the effusing vapor, the third gives the mass of boron in micrograms collected on the target as obtained by the analysis, and the fourth gives the corrected temperature of the sample. The fifth column gives the pressure and the sixth, its logarithm, calculated from the Knudsen equation

$$p \text{ (atm.)} = m(T/M)^{1/2}/44.33Gat \qquad (2)$$

in which m is the mass of boron, T is the temperature, M is the molecular weight of boron, a is the area of the orifice, t is the time duration of the exposure, and G is the geometry factor calculated in the usual manner from the dimensions of the apparatus. The pressure is calculated on the basis that only B(g) is important. The last two columns contain the change in the free-energy function and $\Delta H°_0$ for reaction 1 from the equation

$$\Delta H°_0 = T[(-R \ln p) - (\Delta F° - \Delta H°_0)/T] \qquad (3)$$

The necessary free-energy functions for B(g) and C(s) were obtained from N.B.S. Circular 500[20] and values for boron carbide from a linear extrapolation of the results of Evans, Wagman, and Prosen[21] according to the expression

$$C_p = 26.8 \pm 0.2 + (2.0 \pm 0.2) \times 10^{-3}T \qquad (4)$$

Except for the experiments of run 8 which are low in pressure by about a factor of about 1.8, the results from the different sets are in good agreement with one another. The pressure does not appear to vary appreciably with orifice area. Run 8 was performed with a previously unused graphite liner whereas all the others employed preconditioned graphite liners which had been exposed to boron vapor for long periods of time. The discrepancy between the results of run 8 and the others is attributed to under-saturation, and the results are not included in the final analysis.

The results from run 2, which are about 20% low, are subject to uncertainty because the targets were

(20) F. D. Rossini, D. D. Wagman, W. H. Evans, S. Levine, and I. Jaffe, "Selected Values of Thermodynamic Properties," U. S. National Bureau of Standards, Circular 500, Series III, U. S. Govt. Printing Office, Washington, D. C., 1952.

(21) W. H. Evans, D. D. Wagman, and E. J. Prosen, U. S. National Bureau of Standards, Report No. 4943, U. S. Govt. Printing Office, Washington, D. C., 1956.

Table I : Vapor Pressure Measurements on Boron Carbide[a]

$$0.25B_4C(s) = 0.25C(gr) + B(g)$$

Series-exposure	t, sec.	m, μg.	T, °K.	p, 10^{-6} atm.	log p	$-(\Delta F° - \Delta H°_0)/T$, e.u.	$\Delta H°_0$, kcal.
2-13	606	11.3	2303	6.31	−5.200	35.103	135.6
2-14	1202	16.5	2302	4.64	−5.334	35.102	137.0
2-15	2401	33.0	2308	4.65	−5.332	35.103	137.3
2-16	4806	62.0	2306	4.37	−5.359	35.102	137.5
2-17	2399	30.4	2300	4.28	−5.368	35.103	137.2
3-1	1203	9.4	2299	5.88	−5.230	35.103	135.7
3-2	2400	18.7	2296	5.86	−5.232	35.101	135.6
3-7	1204	8.4	2294	5.25	−5.280	35.102	136.0
3-8	2404	18.4	2297	5.76	−5.240	35.102	135.7
3-10	9601	80.5	2300	6.31	−5.200	35.102	135.5
3-11	4800	41.9	2299	6.57	−5.182	35.102	135.2
3-12	2405	20.3	2298	6.35	−5.197	35.102	135.3
4-13	1204	23.8	2392	15.52	−4.809	35.102	136.5
4-14	2401	48.4	2389	15.82	−4.801	35.102	136.3
5-15	1231	28.1	2390	18.20	−4.740	35.103	135.7
5-16	1200	23.5	2395	15.63	−4.806	35.102	136.7
5-17	1200	21.7	2392	14.42	−4.841	35.102	136.9
5-18	2400	48.5	2391	16.11	−4.793	35.104	136.3
5-19	3601	68.9	2392	15.26	−4.816	35.102	136.6
5-20	4817	87.3	2392	14.45	−4.840	35.102	136.9
5-21	3601	65.6	2396	14.10	−4.837	35.102	137.1
5-22	2401	46.0	2396	15.29	−4.815	35.102	136.8
5-23	1200	21.9	2395	14.56	−4.837	35.102	137.0
7-1	3600	22.1	2308	4.79	−5.319	35.102	137.2
7-2	7200	3.2	2199	0.34	−6.469	35.103	142.3
7-3	3610	57.8	2376	12.67	−4.897	35.102	136.6
7-4	1800	49.6	2421	22.02	−4.657	35.101	136.5
7-5	1800	87.5	2464	39.18	−4.407	35.099	136.1
7-6	1800	177.8	2522	80.55	−4.094	35.093	135.7
8-1	6000	14.7	2270	1.75	−5.757	35.102	139.4
8-2	3600	20.2	2343	4.07	−5.390	35.102	140.0
8-3	2400	39.3	2405	12.05	−4.919	35.102	138.5
8-4	2400	68.4	2483	21.30	−4.672	35.099	140.2
10-7	2400	19.5	2283	2.90	−5.538	35.103	137.9
10-8	3600	18.4	2236	1.80	−5.745	35.102	137.2
10-9	6004	15.5	2184	0.900	−6.046	35.101	137.0
10-10	3604	25.5	2261	2.51	−5.600	35.101	137.2

[a] The orifice areas in cm.², orifice to collimator distance in cm., collimator radius in cm., and geometry factors were, respectively: run 2: 0.04722, 9.28, 1.346, 0.02061; run 3: 0.02307, 9.69, 1.346, 0.01893; run 4: 0.02307, 9.85, 1.353, 0.01852; run 5: 0.02312, 9.94, 1.353, 0.01819; run 7: 0.02285, 9.86, 1.353, 0.01848; run 8: 0.02141, 9.16, 1.353, 0.02135; run 10: 0.04490, 9.36, 1.353, 0.02047.

sparked in the emission apparatus before the chemical analysis was performed. The quantities of boron in runs 3, 4, and exposures 5-15 and 5-16, though in good agreement with others, represent the sum of two or more titrations. The final treatment uses the sixteen data from runs 5-17 to 5-23, 7 (except for 7-2), and 10.

The linear second-law values for the enthalpy and entropy of reaction 1 at 2300°K. are $\Delta H = 146.8 \pm 1.7$ kcal./mole of boron and $\Delta S = 39.2 \pm 0.7$ e.u./mole of boron. From the same set of sixteen data,

the average third-law value for reaction 1 is $\Delta H°_0 = 136.8 \pm 0.1$ kcal./mole of boron and $\Delta H°_{298} = 138.0 \pm 0.1$ kcal./mole of boron.

We take the third-law result to be the more reliable. To obtain the heat of sublimation of boron, one needs the heat of formation of B_4C. A value of -12.2 ± 2.2 was obtained by Smith, Dworkin, and Van Artsdalen.[22] The heat of sublimation of boron calcu-

(22) D. Smith, A. S. Dworkin, and E. R. Van Artsdalen, *J. Am. Chem. Soc.*, **77**, 2654 (1955).

lated from the third-law result and this value of 3.0 per mole of boron is 133.8 ± 0.7 kcal./mole at 0°K. and 135.0 ± 0.7 at 298°K.

Discussion

The present work firmly establishes the vaporization behavior of boron carbide to be the preferential loss of boron to the vapor phase regardless of the composition of the sample and gives its vapor pressure from 2184 to 2522°K. This work is the only vapor pressure endeavor in which boron is collected and specifically assayed.

The interpretation of the vapor pressure measurements on the basis of reaction 1 is justified by the proven nature of the vaporization reaction and by the absence of gaseous molecules of great importance. The few per cent of BC_2 and B_2C^8 and of $B_2{}^9$ in the vapor are of negligible importance in the third-law calculation of the heat of sublimation of boron.

A discrepancy exists between the second-law and the third-law values for the heat of sublimation, the former being higher by about 10 kcal. A slight trend with temperature of the third-law heats amounting to about 1.2 kcal. also exists and is consistent with the difference between the second- and the third-law values. That is, the second-law plot is too steep; the second-law entropy is too high; and the high temperature points give third-law heats slightly lower than the low temperature points. Several possible errors or conditions might have contributed to the discrepancy.

The temperature error required to take the trend out of the third-law values and to make the second- and third-law values agree is about 30° more at one end of the range than at the other, but such a progressive error of this magnitude is not likely in view of the care taken in the experiments and the calibrations. Errors in the estimated free energy functions which could amount to 1 e.u. would cause an error in the third-law enthalpy of sublimation of about 2.3 kcal., but could not remove the trend and would not, of course, alter the second-law result. Errors in the boron analysis would cause errors in the derived pressures and are most likely to occur in the low temperature region. Some difficulty with the target analyses was encountered, but errors in the blank corrections or the titers large enough to force agreement between the second- and the third-law results are not likely.

The onset of another vaporization reaction at the highest temperatures could cause the discrepancies. The proportions of $B_2(g)$, $B_2C(g)$, and $BC_2(g)$, however, seem too small to be of importance.

The crucibles used for these experiments had surface to orifice area ratios of about 200 and 400. No appreciable effect attributable to orifice size was found, and hence the pressures are close to the equilibrium values. The points of run 10 were taken with the large orifice and appear to be slightly low, but only by 7-10% instead of the factor of two required for an extremely low vaporization coefficient. Though in the correct direction, undersaturation, if present, cannot remove much of the discrepancy.

Finally, an enhanced, abnormal transport of boron at the highest temperatures, possibly caused by reaction with the residual gases in the system, could account for the discrepancies. Such an increased transport would amount to about 35% at the highest temperature and progressively less at lower temperatures.

None of the foregoing can be selected with certainty as the source of the discrepancies, but the last seems the most probable. Most of them would have a greater effect on the second-law values than on the third-law values, and hence we have chosen the average of the latter results for the sixteen best points.

The heat of sublimation of boron at 298°K. of 135.0 obtained in the present work clearly depends on the heat of formation of B_4C, a quantity which has been measured but once. Our result for the heat of sublimation is in excellent agreement with the value of 135.7 obtained from torsion effusion vapor pressure measurements on boron carbide at about the same temperatures as ours by Hildenbrand and Hall[11] and the value of 136.9 obtained by Paule and Margrave[10] from Langmuir vaporization measurements on boron at lower temperatures. It is in good agreement with the value of 139 obtained by Searcy and Myers[2] from Knudsen measurements on boron. The agreement among these different types of experiments indicates the lack of serious errors. Except for the results of Akishin, et al.,[5] whose range includes practically all the values, the results obtained by mass spectrometric studies are lower by several kcal. and are in serious disagreement with the direct vapor pressure measurements. The most likely source of error in the mass spectrometric studies is the temperature measurement. The temperature in a crucible heated by electron bombardment in a mass spectrometer may not be well defined and is surely considerably harder to measure than in a typical effusion vaporization study. Buchler and Berkowitz-Mattuck[23] have demonstrated the extreme care which must be taken

(23) A. Buchler and J. B. Berkowitz-Mattuck, J. Chem. Phys., 39, 286 (1963).

to ensure that good temperature coefficients are obtained from mass spectrometric measurements. Another likely source of error in the mass spectrometric measurements is in the absolute pressure measurement.

One possible interpretation, and the most reasonable one in the authors' view, is that the mass spectrometric measurements are in error because of temperature errors or pressure errors, that the vaporization coefficient of boron is nearly unity, that the vaporization coefficient of boron from boron carbide is greater than the value of about 0.005 which is the reciprocal of the surface to orifice ratio in the present work, and that it is perhaps about the 0.07 value that Hildenbrand and Hall[11] suggest. On the other hand, the

apparent agreement among the mass spectrometric values on one value and the agreement among the direct vapor pressure values for another value suggests that some unusual factor, as yet unrecognized, may actually exist.

The Decomposition Pressure of Boron Carbide and the

Heat of Sublimation of Boron[1]

by D. L. Hildenbrand and W. F. Hall

Research Laboratories, Philco Corporation, Newport Beach, California   (*Received December 19, 1963*)

The boron decomposition pressure over boron carbide, B_4C, has been measured by the torsion–effusion method in the range 2350 to 2615°K. A small "hole-size effect" indicates a condensation coefficient of roughly 0.07 for $B(g)$ on $B_4C(s)$. The heat of dissociation of B_4C to $B(g)$ and C(graphite) at 298°K. has been derived as 138.7 ± 1.2 kcal./mole of boron from a third-law analysis of the vaporization data. From this result, the heat of sublimation of boron at 298°K. has been evaluated as 135.7 ± 1.3 kcal./mole. An approximate value of 171 kcal./mole has been obtained for the heat of formation of $BC_2(g)$ at 298°K.

In spite of a number of recent determinations, there remains a relatively large uncertainty in the heat of sublimation of elemental boron. This uncertainty affects all bond-energy calculations involving boron compounds and all equilibrium calculations involving gaseous boron. All of the determinations to date[2-10] are based on vapor pressure measure-

(1) This work was supported by the Advanced Research Projects Agency and Bureau of Naval Weapons under Contract NOw 61-0905-C.

(2) A. W. Searcy and C. E. Myers, *J. Phys. Chem.*, **61**, 957 (1957).

(3) H. E. Robson and P. W. Gilles, *ibid.*, **68**, 983 (1964).

(4) R. G. Paule and J. L. Margrave, *ibid.*, **67**, 1368 (1963).

(5) Yu. A. Priselkov, Y. A. Sapozhnikov, and A. V. Tseplyaeva, *Izv. Akad. Nauk SSSR, Otd. Tekhn. Nauk, Met. i Toplivo*, 134 (1960).

ments made by effusion or free-evaporation methods in the range 2000 to 2500°K., as summarized in Table I. Although vacuum vaporization techniques are

Table I: Comparison of Boron Heat of Sublimation Values

Investigator	Ref.	ΔH_{298}, kcal./mole
Searcy and Myers[a]	2	138 ± 4[d,e]
Robson and Gilles[a]	3	135.0 ± 0.7
Paule and Margrave[c]	4	136.5[d]
Priselkov, et al.[a]	5	101 ± 2
Alcock and Grieveson[a]	6	140
Chupka[b]	7	129.9
Schissel and Williams[b]	8	129 ± 5
Akishin, et al.[b]	9	132.8 ± 5
Verhaegen and Drowart[b]	10	129.2 ± 2.5
This research		135.7 ± 1.3

[a] Knudsen effusion method. [b] Mass spectrometer–effusion method. [c] Free evaporation method. [d] Recalculated from original data with more reliable free-energy functions. [e] Data obtained with ZrB_2 cell.

probably the most feasible under the circumstances, the thermodynamic data obtained are often subject to large uncertainties resulting from errors in temperature measurement. Another complicating factor in this case arises from the reactivity of boron at high temperatures, which makes it difficult to find a suitable container material and, consequently, to specify the condensed phase involved in the vaporization process. These two sources of error are probable responsible for much of the variation among the heats of sublimation in Table I. Robson and Gilles[3] avoided the reactivity problem by measuring the decomposition pressure of boron carbide in a graphite effusion cell, after having established the composition of the carbide phase in equilibrium with graphite at the temperatures involved; the heat of sublimation was evaluated from the measured boron decomposition pressure and the known heat of formation of the carbide. It is interesting that the four mass spectrometric determinations of the heat of sublimation are all lower than the values obtained by direct vaporization experiments, with the exception of the result of Priselkov, et al.,[5] which must surely be in error; it is included only for completeness.

This paper presents additional information on the heat of sublimation of boron, obtained from boron carbide decomposition pressures measured by the torsion–effusion method.[11-13] Effusion of vapor from eccentrically placed orifices imparts a twisting force to an effusion cell which is suspended from a small-

diameter filament. When molecular flow conditions prevail, the pressure within the effusion vessel can be evaluated from the relation

$$P_T = \frac{2k\theta}{\Sigma a f q} \tag{1}$$

where k is the torsion constant of the filament, θ is the angle through which the cell is deflected, and a, f, and q are the area, force factor,[14] and moment arm of each of the orifices. Vapor composition does not enter the pressure calculation.

Experimental

Boron carbide powder was obtained from A. D. Mackay, Inc., New York, N. Y. The X-ray diffraction pattern of the starting material was identical with that on file for B_4C in the ASTM catalog, although a somewhat higher than normal background indicated the presence of noncrystalline impurities. The amorphous material was probably boric oxide. After heating for several hours at 2000° under vacuum, the background essentially disappeared. There were no peaks in the X-ray pattern not attributable to B_4C.

All of the measurements on B_4C were made using graphite effusion cells (National Carbon Co. Grade ATJ). The effusion cells and the remainder of the torsion–effusion apparatus have been described previously.[13] The cells were heated by radiation from a cylindrical susceptor which was in turn heated by a radiofrequency induction generator. Temperatures were measured with a calibrated optical pyrometer by sighting into a blackbody cavity in the bottom of the cell. Corrections were applied for window and prism transmissivities. Because of the high temperatures involved in this work, it was necessary to water-cool the silica vacuum enclosure in the vicinity of the susceptor. Other aspects of the experimental technique have also been described previously,[13] along with

(6) C. Alcock and P. Grieveson, "Thermodynamics of Nuclear Materials," International Atomic Energy Agency, Vienna, Austria, 1962, p. 571.

(7) W. A. Chupka, quoted in National Bureau of Standards Report No. 7093, U. S. Govt. Printing Office, Washington, D. C., 1961.

(8) P. O. Schissel and W. S. Williams, Bull. Am. Phys. Soc., [2] 4, 139 (1959).

(9) P. A. Akishin, O. T. Nikitin, and L. N. Gorokhov, Dokl. Akad. Nauk SSSR, 129, 1075 (1959).

(10) G. Verhaegen and J. Drowart, J. Chem. Phys., 37, 1367 (1962).

(11) A. W. Searcy and R. D. Freeman, J. Am. Chem. Soc., 76, 5229 (1954).

(12) M. D. Scheer, J. Phys. Chem., 61, 1184 (1957).

(13) D. L. Hildenbrand and W. F. Hall, ibid., 66, 754 (1962); 67, 888 (1963).

(14) R. D. Freeman and A. W. Searcy, J. Chem. Phys., 22, 762 (1954).

some measurements on gold which indicate reliable operation of the apparatus.

Results

Decomposition pressures were measured in the range 2350 to 2615°K. with effusion cells of various orifice size. The results are summarized in Table II, where the data are listed in the order in which measurements were made. A close inspection of the observed pressure (P_T) values indicates a regular trend in the direction of increasing pressure with decreasing orifice size (other cell geometrical factors are maintained constant). Behavior of his type is generally characteristic of substances with condensation coefficients less than unity. Whitman,[15] Motzfeldt,[16a] and Stern and Gregory[16b] have discussed the relation of condensation coefficient and cell geometry to pressures determined by the effusion method. Experience has shown that "hole-size effects" can generally be correlated rather well by a simplified form of Motzfeldt's equation, viz.

$$P_e = P_T(1 + \beta C a) \qquad (2)$$

where P_e and P_T are equilibrium and observed pressures, C is the orifice Clausing factor,[17] a is the orifice area, and β is a constant which is characteristic of a particular cell configuration and sample particle size. In Motzfeldt's terminology, β is the reciprocal of the product of condensation coefficient and effective vaporizing surface area. It is recognized, however, that β might contain certain apparatus-dependent factors which could preclude a direct determination of the condensation coefficient from measurements of pressure as a function of orifice size. Nevertheless, it has been found that, in accordance with eq. 2, reliable equilibrium pressure data can be obtained from an extrapolation of observed pressures to zero Ca values. For boron carbide, a β-value of 40 brings the equilibrium pressure (P_e) values calculated from the data of all four effusion cells into close agreement. The calculated P_e data are given in Table II; over the experimental range, the data can be represented by the least-squares equation

$$\log P_e \text{ (atm.)} = 7.506 - (29,630/T) \qquad (3)$$

If Motzfeldt's simplified equation[16a] is assumed to hold, the effusion data indicate a condensation coefficient of less than 0.066. In this evaluation, the cell cross-sectional area was taken as the lower limit to the vaporizing surface area. A similar treatment has yielded a condensation coefficient of 0.025 or less for the related substance ZrB_2.[18]

Verhaegen, Stafford, Ackerman, and Drowart[19]

have examined the mass spectrum of the beam issuing from a Knudsen cell containing boron carbide and have identified B^+, BC_2^+, and B_2C^+ as parent ions. The species B_2C is apparently a very minor one. From the reported intensity ratios $I(B^+)/I(BC_2^+)$ of 38 and 6.3 at 2014 and 2470°K., respectively, together with the relative atomic ionization cross sections of Otvos and Stevenson,[20] it is estimated that the mole fraction of B(g) over B_4C is 0.95 or larger in the range of the measurements reported here. Elemental carbon species are not of importance at these temperatures. Also, Robson and Gilles[3] have shown that vaporization of a carbon-saturated B_4C sample yields a graphite residue, whereas vaporization of a carbon-deficient sample produces a carbon-enriched residue. On the basis of the above, it is clear that vaporization occurs principally by the process

$$0.25 B_4 C(s) = B(g) + 0.25 C(s) \qquad (4)$$
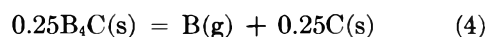
in the temperature range investigated.

Third-law heats for reaction 4 have been derived from the equilibrium pressure data by means of the relation

$$\Delta H_{298} = -T\left[\Delta\left(\frac{F - H_{298}}{T}\right) + R \ln P_e\right] \qquad (5)$$

and are shown in Table II. Values of $-\Delta[(F - H_{298})/T]$ for reaction 4 were calculated as 35.67, 35.63, and 35.58 cal./mole deg. at 2200, 2400, and 2600°K., respectively, using tabulated data from standard sources.[21-23] The average third-law ΔH_{298}, 138.7 ± 0.2 kcal./mole, agrees well with a corresponding second-law value of 136.9 kcal./mole, which is further support for the choice of reaction 4. The third-law value is considered to be more reliable and it is assigned an uncertainty of 1.2 kcal./mole, based

(15) C. I. Whitman, J. Chem. Phys., 20, 161 (1952).

(16) (a) K. Motzfeldt, J. Phys. Chem., 59, 139 (1955); (b) J. H. Stern and N. W. Gregory, ibid., 61, 1226 (1957).

(17) P. Clausing, Ann. Physik, 12, 961 (1932).

(18) J. M. Leitnaker, M. G. Bowman, and P. W. Gilles, J. Chem. Phys., 36, 350 (1962).

(19) G. Verhaegen, F. E. Stafford, M. Ackerman, and J. Drowart, Nature, 193, 1280 (1962); see also WADD Technical Report 60-782, Part III, Contract AF61(052)-225, Nov., 1961.

(20) J. W. Otvos and D. P. Stevenson, J. Am. Chem. Soc., 78, 546 (1956).

(21) D. R. Stull and G. C. Sinke, "Thermodynamic Properties of the Elements," Advances in Chemistry Series, No. 18, American Chemical Society, Washington, D. C., 1956.

(22) JANAF Thermochemical Tables, issued by The Dow Chemical Co., Dec. 31, 1960.

(23) National Bureau of Standards Report No. 7093, U. S. Govt. Printing Office, Washington, D. C., 1961.

Table II: Decomposition Pressure of Boron Carbide
and Heat of the Reaction $0.25B_4C(s) = B(g) + 0.25C(s)$

T, °K.	$\theta \times 10^3$, radian	$P_T \times 10^5$, atm.	$P_e \times 10^5$, atm.	ΔH_{298}, kcal.
Cell 15				
2351	40.2	0.46	0.84	138.4
2374	50.4	0.58	1.05	138.7
2414	68.7	0.79	1.43	139.5
2440	104.6	1.20	2.18	139.0
2429	93.8	1.07	1.95	138.9
2459	130.9	1.50	2.73	139.0
2418	83.8	0.96	1.74	138.8
2406	68.7	0.79	1.43	139.1
2485	171.3	1.96	3.57	139.1
2469	147.2	1.69	3.07	138.9
2428	94.7	1.08	1.97	138.8
Cell 16				
2485	131.9	2.58	3.80	138.7
2474	123.3	2.42	3.56	138.5
2445	82.0	1.61	2.37	138.9
2394	49.5	0.97	1.43	138.4
2341	26.6	0.52	0.76	138.3
2483	128.6	2.52	3.70	138.8
2445	86.4	1.69	2.49	138.7
2508	167.8	3.29	4.84	138.8
2485	129.5	2.54	3.74	138.8
2445	86.9	1.70	2.50	138.6
2410	57.1	1.12	1.65	138.7
Cell 17				
2431	47.7	1.86	2.30	138.2
2480	74.2	2.90	3.58	138.8
2482	82.0	3.20	3.96	138.4
2466	67.3	2.63	3.24	138.5
2447	53.5	2.09	2.58	138.5
2426	38.8	1.52	1.87	138.9
2488	85.8	3.36	4.14	138.5
2502	107.8	4.22	5.20	138.2
2488	93.5	3.66	4.50	138.1
2461	59.5	2.32	2.87	138.8
2463	64.4	2.51	3.10	138.6
Cell 18				
2582	89.5	9.66	10.5	138.9
2610	122.2	13.2	14.3	138.8
2570	81.0	8.75	9.48	138.8
2538	57.7	6.23	6.75	138.8
2502	37.7	4.07	4.41	139.0
2615	128.8	13.9	15.1	138.8
2599	108.1	11.7	12.7	138.8
2580	90.8	9.81	10.6	138.8
2538	58.6	6.33	6.86	138.7
2514	42.9	4.63	5.02	139.0
				138.7 ± 0.2

Cell	$\overline{C_a}$, cm.^{2}	$\Sigma a f_q$, cm.^{3}	k, dyne cm./ radian	P_e/P_T
15	0.0205	0.04940	2.86	1.82
16	0.0118	0.02893	2.86	1.47
17	0.0058	0.01448	2.87	1.23
18	0.0021	0.00520	2.84	1.08

chiefly on estimated error limits of 20° in temperature measurement and 0.2 cal./mole deg. in $\Delta[(F - H_{298})/T]$.

The data in Table III illustrate the effect of changing orifice area on the derived third-law heats and the effectiveness with which eq. 2 correlates these results. Average deviations in the derived ΔH_{298} values for the various cells range from 0.1 to 0.3 kcal./mole. It is evident that a satisfactory correlation is obtained when the β of eq. 2 is assigned a value of 40. The Knudsen effusion data of Robson and Gilles[3] yield for reaction 4 the third-law value $\Delta H_{298} = 138.0$ kcal./mole, in good agreement with the value reported here. Although Robson and Gilles did not consider a non-unit condensation coefficient, they employed cells with considerably larger cross-sectional area than those used in this work, so that their pressures should be close to equilibrium values. Equilibrium boron pressures derived from this work (eq. 3) are within 20% of those reported by Robson and Gilles[3] over the entire region of overlap.

**Table III:** Effect of Orifice Geometry on Third-Law Heats

Cell	C_a, cm.^{2}	ΔH_{298}, kcal./mole $\beta = 1$	$\beta = 40$
15	0.0205	141.7	138.8
16	0.0118	140.5	138.6
17	0.0058	139.5	138.5
18	0.0021	139.2	138.8

Smith, Dworkin, and Van Artsdalen[24] have measured the heat of combustion of crystalline B_4C to glassy B_2O_3 and CO_2, leading to $\Delta Hf°_{298} = -12.2 \pm 2.2$ kcal./mole for $B_4C(s)$. When this value is combined with the heat of reaction 4 derived from the vaporization studies, $\Delta H_{298} = 138.7 \pm 1.2$ kcal./mole, the heat of sublimation of elemental boron at 298°K. is derived as 135.7 ± 1.3 kcal./mole. The heat of sublimation of boron so obtained is in good agreement with the value of Robson and Gilles[3] and agrees with most of the other values in Table I within their stated uncertainties. A substantial error in the heat of formation of boron carbide would be required to bring the present results into close agreement with the mass spectrometric values; such an error seems unlikely. Since the formation of boron carbide from the elements is certainly an exothermic process, the decomposition pressure data fix a definite upper

(24) D. Smith, A. S. Dworkin, and E. R. Van Artsdalen, *J. Am. Chem. Soc.*, **77**, 2654 (1955).

limit of 138.7 kcal./mole for the heat of sublimation of boron at 298°K.

An approximate value for the heat of formation of $BC_2(g)$ can be obtained from the B^+/BC_2^+ intensity ratios given by Verhaegen, *et al.*[19] An extrapolation of their results indicates that at 2500°K. $I(B^+)/I(BC_2^+)$ = 5.6. Combination of this result with the atomic ionization cross sections of Otvos and Stevenson[20] yields $P(B)/P(BC_2) = 15$ at 2500°K. Thus for the reaction

$$0.25B_4C(s) + 1.75C(s) = BC_2(g) \qquad (6)$$
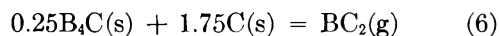
$K = P(BC_2) = 2.9 \times 10^{-6}$ atm. at 2500°K. The estimated molecular constants of Verhaegen, *et al.*,[19] yield $-(F - H_{298})/T = 64.4$ cal./mole deg. for $BC_2(g)$ at 2500°K., which is reasonable when compared to data for the related gaseous molecule C_3. Therefore, for reaction 6, $-\Delta[(F - H_{298})/T]_{2500} = 44.3$ cal./mole deg. and $\Delta H_{298} = 174$ kcal. This leads to a value of 171 kcal./mole for the heat of formation of $BC_2(g)$ at 298°K.

Ion Exchange in Concentrated Electrolyte Solutions.   III.

Zeolite Systems with Salts of Group I and II Metals

by Stanley Bukata[1,2] and Jacob A. Marinsky[3]

The Department of Chemistry, State University of New York at Buffalo, Buffalo, New York
(Received June 18, 1963)

The selectivity coefficients for the ion exchange of cesium with sodium A-zeolite, cesium and sodium with potassium A-zeolite, and sodium and barium with calcium A-zeolite have been determined in dilute and concentrated solutions.   The exchanging ions were at radioactive tracer level concentrations so that the fraction of the exchanged ion of the zeolite was essentially unity in both the resin and external liquid phases.   Quantitative treatment of the observed data was accomplished by assuming that the zeolite phase may be treated as a highly concentrated electrolyte solution having only one diffusible ion and as a cross-linked network which exerts a pressure on the internal solution phase.   The special properties of the zeolite, rigidity and resistance of electrolyte incursion, facilitate the treatment and permit the accurate prediction of selectivity at any external electrolyte concentration of two mobile counter ions at micro- and macroconcentration levels, respectively, on the basis of one selectivity measurement if the thermodynamic properties of the mixed electrolyte in the aqueous phase are known.   Conversely, in the absence of such thermodynamic data, activity coefficients of the trace component can be computed from the experimentally determined selectivity coefficients.

Introduction

The ion-exchange behavior of natural and synthetic zeolites has been rather extensively investigated for many years, the bulk of the work having been done in dilute electrolyte solutions.[4]   Recently, Platek and Marinsky[5] reported work in concentrated solutions with the lithium form of the synthetic A-type zeolite[6] whose structure is well-characterized.[7]   They suggested that this zeolite may be considered to be a highly "cross-linked" exchanger and that a relationship of the type suggested by Gregor[8] and Glueckauf[9] for organic resins may also apply for this exchanger; namely

$$\ln a_j = \ln \bar{a}_j + \frac{\pi}{RT} V_j \tag{1}$$

where a_j and V_j represent the activity and partial molar volume of component j, π is the difference in osmotic pressure between the interior of the zeolite and

the external solution, and the bar placed above the symbol is used to differentiate the resin phase from the aqueous phase.   Equation 2a then governs the exchange process for uni-univalent exchange in 1 : 1 electrolyte solutions with the A-zeolite in the M^+ form and the exchange carried out in solutions of $NX + MX$.[10]

(1)   Union Carbide Doctoral Fellow, 1961–1962.

(2)   This paper is based on a dissertation submitted by S. Bukata in partial fulfillment of the requirements for the degree of Doctor of Philosophy.

(3)   Correspondence to be addressed to this author.

(4)   F. Helfferich, "Ion Exchange," McGraw-Hill Book Co., Inc., New York, N. Y., 1962, Chapter 5, particularly pp. 183–193.

(5)   W. A. Platek and J. A. Marinsky, *J. Phys. Chem.*, **65**, 2118 (1961).

(6)   R. M. Barrer and E. A. D. White, *J. Chem. Soc.*, 1561 (1952).

(7)   D. W. Breck, *et al.*, *J. Am. Chem. Soc.*, **78**, 5963, 5972 (1956).

(8)   H. P. Gregor, *ibid.*, **70**, 1923 (1948); **73**, 642 (1951).

(9)   E. Glueckauf, *Proc. Roy. Soc.* (London), **A214**, 207 (1952).

(10)   G. E. Boyd and B. A. Soldano, *Z. Elektrochem.*, **57**, 162 (1953).

$$\ln\left[\frac{\bar{m}_N m_M}{m_N \bar{m}_M}\right] = \ln K = \frac{\pi}{RT}(\bar{V}_M - \bar{V}_N) +$$

$$\ln\frac{\bar{\gamma}_M}{\bar{\gamma}_N} - 2\ln\frac{\gamma_{\pm MX}}{\gamma_{\pm NX}} \quad (2a)$$

For the univalent–divalent ($NX + MX_2$) and divalent–divalent ($NX_2 + MX_2$) systems, also studied in this research program, the working equations are

$$\ln\frac{(\bar{m}_{N^+})^2(m_{M^{++}})}{(m_{N^+})^2(\bar{m}_{M^{++}})} = \ln K = \ln\frac{(\bar{\gamma}_{M^{++}})}{(\bar{\gamma}_{N^+})^2} -$$

$$\ln\frac{(\gamma_{\pm MX_2})^3}{(\gamma_{\pm NX})^4} + \pi(\bar{V}_{M^{++}} - 2\bar{V}_{N^+})/RT \quad (2b)$$

and

$$\ln\frac{(\bar{m}_{N^{++}})(m_{M^{++}})}{(m_{N^{++}})(\bar{m}_{M^{++}})} = \ln K = \ln\frac{(\bar{\gamma}_{M^{++}})}{(\bar{\gamma}_{N^{++}})} -$$

$$3\ln\frac{\gamma_{\pm MX_2}}{\gamma_{\pm NX_2}} + \pi(\bar{V}_{M^{++}} - \bar{V}_{N^{++}})/RT \quad (2c)$$

where K is the experimentally determined selectivity coefficient, m is the molal concentration of the species, $\bar{\gamma}$ is the activity coefficient of the ion in the zeolite phase, and $\gamma_{\pm}$, is the mean molal activity coefficient of the electrolyte in the external solution phase.

It was the objective of the first phase of this research to demonstrate the applicability of the above model for the analysis of the ion-exchange behavior of the A-zeolite. Its special properties of rigidity and high resistance to electrolyte intrusion, because of the high negative charge due to the ring of oxygen atoms in the faces and corners of the cubic unit cell and the small opening available to the exchanging ions,[7] were expected to facilitate evaluation of the terms on the right-hand side of eq. 2a to provide a quantitative prediction of K with varying ionic strength in uni-univalent electrolyte systems containing one macro- and one microelectrolyte component whose activity behavior in the presence of the bulk electrolyte was calculable.

Once the value of this model was demonstrated it was the objective of the second phase of this research to employ the model further to estimate activity coefficients of trace components, not otherwise obtainable, in bulk electrolyte from a series of selectivity measurements made as a function of the concentration.

In order to obtain the first objective with organic exchangers it has been necessary to limit investigation to dilute solutions where electrolyte invasion is not a complicating factor. Weakly cross-linked exchangers, to represent the unrestrained macromolecule, are then needed to permit estimate of the $\bar{\gamma}_M/\bar{\gamma}_N$ and $\pi/RT(\bar{V}_M - \bar{V}_N)$ terms to be employed in eq. 2 for the cross-linked systems.[8-11] Platek and Marinsky[5] have

pointed out that for zeolites the methods used for organic exchangers are not applicable since the zeolite cannot be made in an "uncross-linked" form. It was believed, however, assuming the applicability of the model to the A-zeolite, that the special properties of framework inflexibility and resistance of electrolyte intrusion, even at high external electrolyte concentration, eliminated the need for this type of approach for the attainment of our objective.

In the first phase of the program the exchanging ion N was kept at radioactive tracer level concentrations in solutions of MX (0.1 m and greater). Thus the ion fraction of M was essentially unity in both the zeolite and external solution phases. According to our model, the zeolite is rigid, its composition in these studies is essentially constant, and $\ln \bar{\gamma}_M/\bar{\gamma}_N$ is constant. If the model is correct this term should be available from a single measurement of K at any external electrolyte concentration and, using this value, K should be calculable at any other concentration with eq. 2a. To demonstrate this result the value of π was obtained as a function of electrolyte concentration from eq. 1 by assigning a value to the water activity (also constant on the basis of our model) in the zeolite phase. It was assumed for these computations, also, that the partial molar volume of solvent and ions were constant. The mean activity coefficient ratio of micro- and macrocomponent in the mixed electrolyte systems were calculated.

In the second phase of this study, the zeolite parameters, $\ln \bar{\gamma}_{M^{++}}/(\bar{\gamma}_{N^+})^2$ and $\ln \bar{\gamma}_{M^{++}}/\bar{\gamma}_{N^{++}}$ were determined from the experimental selectivity coefficients at low concentrations of MX_2. It was assumed that, at these dilutions, the effect of the MX_2 on the mean molal activity coefficients of the microcomponent would not be noticeable within the error limits of the experimental measurement. The published $\gamma_{\pm}$-value for the pure electrolyte at the ionic strength of the experiment was used.

The selectivity coefficient values that were measured at the higher concentrations of MX_2 were then employed in eq. 2b and 2c to calculate the mean activity coefficient of the microcomponent at the higher concentrations. Since NX_2 or NX was present in very low concentrations the activity coefficients for MX_2 are identical with those for the pure electrolyte and the literature values were employed for the computation in every case.

Experimental

Materials. The sodium A-zeolite was kindly sup-

(11) B. A. Soldano, et al., J. Am. Chem. Soc., 77, 1331 1334, 1336 (1955).
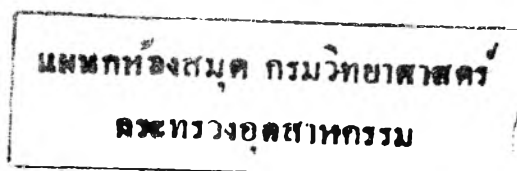
plied by the Linde Company. Its preparation for use in equilibration experiments included a sedimentation technique which was repeated five times to remove amorphous silica and alumina adhering to the commercial product. About 50 g. of zeolite were slurried with 500 ml. of a 0.1 M NaCl solution in a 500-ml. graduated cylinder. The zeolite crystals were allowed to settle for about 30 min. The fine material remaining in suspension was discarded by decantation. The residual zeolite was filtered, washed with deionized water, dried at 80° to remove surface moisture, and stored over a saturated ammonium chloride solution to maintain a constant water content.

Subsequent preparation of the potassium A-zeolite, based on the reactions

$$NaZ + Ag^+ = AgZ + Na^+$$

$$AgZ + K^+ + 2CNS^- = KZ + Ag(CNS)_2^-$$
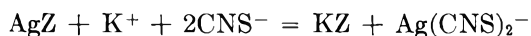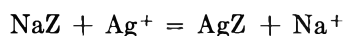
consisted of the following operations. Thirty grams of hydrated sodium A-zeolite were converted to the silver form by equilibration with 500 ml. of a 0.3 M silver nitrate solution for 1 hr. in the dark. The mixture was filtered and the solid product was washed and again equilibrated for 1 hr. with 500 ml. of 0.3 M silver nitrate solution. This procedure was repeated two more times. The zeolite was separated by filtration and washed with deionized water and then was added to 300 ml. of a saturated potassium thiocyanate solution and stirred for 0.5 hr. The solid after filtration was added to 150 ml. of a saturated potassium thiocyanate solution and equilibrated for 1 hr. After another equilibration the product was filtered, washed, dried at 80°, and stored over a saturated ammonium chloride solution.

Conversion to the calcium A-zeolite was accomplished as follows. About 100 g. of hydrated sodium A-zeolite were equilibrated with 500 ml. of a 2 M calcium nitrate solution for 2 hr. The zeolite was filtered and again equilibrated with 500 ml. of 2 M calcium nitrate solution for 2 hr. The procedure was repeated five more times. The final product was washed with deionized water, dried at 80° to remove surface moisture, and stored over a saturated ammonium chloride solution to maintain a constant water content. The final product contained about 0.01% sodium as ascertained by flame photometry.

The γ-emitting, radioactive nuclides, 2.3-year Cs[134] and 12.8-day Ba[140]-40-hr. La[140], were purchased from the Radioisotopes Division of the Oak Ridge National Laboratories. Carrier-free 2.6-year Na[22] was obtained from the Nuclear Science and Engineering Corporation. Analytical grade reagents were from

J. T. Baker Co. and were used without further purification.

Equilibration Procedure. The hydrated zeolite was equilibrated at the ambient temperature, 24 ± 3°, with a solution containing MX or MX$_2$ in macroscopic quantities and NX or NX$_2$ in radioactive tracer quantities. For an experiment, zeolite was accurately weighed into a 2-ounce capacity polyethylene bottle. Plastic equipment was used since glass was found to adsorb appreciable quantities of the radioactive Cs tracer. The weight of the zeolite was varied with the concentration of the external solution to keep the uptake of the tracer at about 25–75% of the initial amount. About 0.1 g. was used with the 0.1 m solutions and 2 to 3 g. was used at 6 m. About 15 ml. of the equilibrating solutions of (MX + NX) was added and its weight determined. The mixture was shaken from 24–48 hr. on a shaking machine at a speed sufficient to keep the zeolite from settling. After equilibration, the mixture was transferred to a 15-ml. conical polypropylene centrifuge tube which was stoppered and centrifuged for 0.5 hr. Two ml. of the supernatant liquid were pipetted (polyethylene pipet) into a 16 × 105 mm. lusteroid test tube. The weight of the liquid transferred was determined. The activity of the samples and standards were measured in a 1.25 × 2 in. well-type sodium iodide, thallium-activated, γ-ray scintillation crystal detector.

In the case of the Ca–Ba exchange the liquid was separated from the equilibrated mixture and was
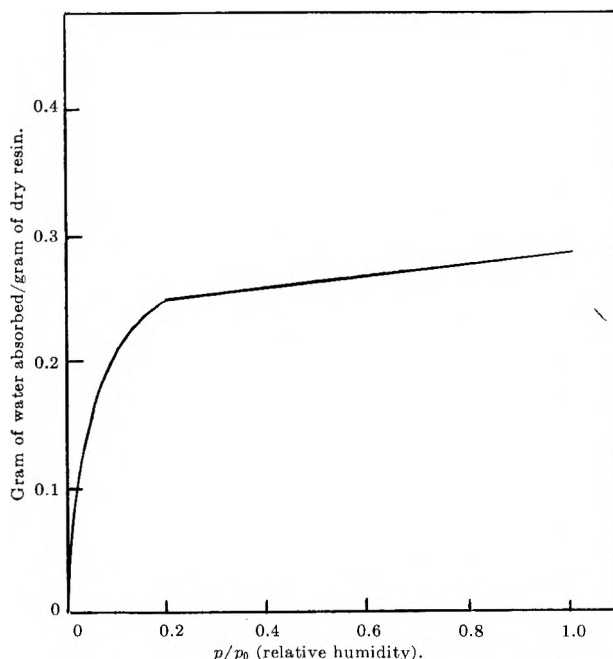

Figure 1. Water sorption isotherm of sodium A-zeolite.

allowed to stand for 14 days to ensure restoration of transient equilibrium between the 12.8-day Ba^{140} parent and its 40-hr. La^{140} daughter prior to measurement of the γ-activity in the sample.

Evaluation of Zeolite Parameters. The osmotic pressure term, π, was evaluated by use of eq. 1 assuming $\bar{a}_w = 0.16$ and is constant. In Fig. 1, the water adsorption isotherm (25°) is given for sodium A-zeolite.[12] There is little change in the amount of water taken up per gram of zeolite as the value of p/p_0 ($\approx a_w$) varies from unity to a value of about 0.16. A sharp decrease in water content of the zeolite occurs below 0.16. Similar behavior is observed for other zeolites. This result is considered to indicate that at $a_w = 0.16$ the activity of water inside and outside of the zeolite is equivalent. When the external water activity is greater than 0.16 the internal water activity remains about constant and to a first approximation is equal to 0.16. At lower a_w values the π-term is believed to disappear ($\bar{a}_w = a_w$).

A value of 18 ml. was used for the partial molar volume of water. Values published for the partial molal volumes of the ions at infinite dilution[13] were used. Another approximation, constancy of partial molar volumes, was employed as a simplification.

The values of $\gamma_\pm$, the activity coefficients in mixed electrolyte solutions, were computed for the uniunivalent systems. Since NX is present in trace quantities the activity coefficients for MX are identical with those for pure MX solutions and are found in the literature.[14] The activity coefficients for trace NX in the presence of MX were calculated by use of the Harned–Cooke[14] equation in the form

$$\log \gamma_{0(NX)} = \log \gamma_{NX(0)} + \alpha m + \beta m^2 \qquad (3)$$

where $\gamma_{0(NX)}$ is the activity coefficient of a trace of NX in the presence of MX at molality m, $\gamma_{NX(0)}$ is the activity coefficient of pure NX at molality m, and α and β are experimentally determined parameters. The $\ln \bar{\gamma}_M/\bar{\gamma}_N$ term is evaluated, as previously mentioned, by using the above parameters in eq. 2a after a single measurement of K at any concentration value.

In the case of the univalent–divalent and divalent–divalent systems K was measured at 0.127 and 0.094 m $Ca(NO_3)_2$, respectively. The effect of the $Ca(NO_3)_2$ on the mean activity coefficient of the trace ion, Na^+ or Ba^{++}, was neglected.

The $\ln \bar{\gamma}_{Ca}/(\bar{\gamma}_{Na})^2$ and $\ln \bar{\gamma}_{Ca}/\bar{\gamma}_{Ba}$ parameters obtained in this manner were used in eq. 2b and 2c to calculate the activity coefficients of the trace electrolyte $NaNO_3$ or $Ba(NO_3)_2$ as a function of the change in K with $Ca(NO_3)_2$ concentration.

Constancy of $\bar{\gamma}_M/\bar{\gamma}_N$ is to be expected in all the systems since electrostatic interactions are essentially unchanged. The zeolite is rigid and electrolyte incursion is essentially absent. It was experimentally determined that the Na A-zeolite is not noticeably invaded by NaCl under the conditions employed in this work. It was assumed that no incursion occurs in any of the other systems studied since the bromides, nitrates, and acetates that were also used are larger than the chloride ion.

Results

In Table I, selectivity coefficients for the system, NaA–NaCl–CsCl, are given. Using the experimental value of K at 2.255 m NaCl (K_e) the $\ln \bar{\gamma}_{Na^+}/\bar{\gamma}_{Cs^+}$ term was calculated to be 3.390. The values of K_e were obtained from eq. 2a using this number. The $\gamma_\pm$-values were obtained from the data of Robinson.[15] Modified selectivity coefficients, K_e', are also given in the table for comparison

$$K_e' = K_e \frac{(\gamma_{\pm MX})^2}{(\gamma_{\pm NX})^2} \qquad (4)$$

Table I: Selectivity Data for the System NaA–NaCl–CsCl

External NaCl molality	$K_e{}^a$	$K_c{}^b$	$K_e'{}^c$
0.053	2.77	2.81	2.86
0.106	2.78	2.83	2.86
0.537	2.56	2.55	2.78
1.085	2.22	2.31	2.58
2.255	1.85	1.85	2.47
3.383	1.61	1.52	2.44
4.510	1.37	1.32	2.31
6.068	1.18	1.09	2.32

^{a} K_e = experimental selectivity. ^{b} K_c = calculated from eq. 2a. ^{c} K_e' = calculated from eq. 4.

In Tables II and III the data for the systems NaA–NaBr–CsBr and NaA–Na acetate–Cs acetate are similarly presented. The values of K_c as a function of molality were calculated again using $\ln \bar{\gamma}_{Na^+}/\bar{\gamma}_{Cs^+} = 3.390$. In the absence of imbibement and significant expansion or contraction of the zeolite matrix, this zeolite parameter for the Na–Cs exchange should be

(12) Permission to use these data was kindly granted by D. W. Breck.

(13) P. Mukerjee, *J. Phys. Chem.*, **65**, 740 (1961).

(14) R. A. Robinson and R. H. Stokes, "Electrolyte Solutions," 2nd Ed., Butterworth Scientific Publications, London, 1959.

(15) R. A. Robinson, *J. Am. Chem. Soc.*, **74**, 6035 (1952).

constant regardless of the anionic form of the salts in the external solution. The $\gamma_{\pm}$-values for NaBr and CsBr were calculated using eq. 3. The unavailability of any interaction coefficients for this system, however, necessitated re-employment of the α- and β-terms that were used for the NaCl–CsCl system[15] as the most reasonable approximation. The activity coefficients up to 3.5 m were taken from Robinson and Stokes.[14] Beyond 3.5 m the values are from Landolt–Bornstein[16] since Robinson and Stokes do not report any values above 3.5 m. There is disagreement between the two sources below 3.5 m and we believe the data of Robinson and Stokes to be more valid on the basis of the good correlation that is obtained between K_c and K_e in the lower concentration range. The values at 5.503 and 7.903 m are used only to demonstrate the prediction of the trend of selectivity by this approach.

Table II: Selectivity Data for System NaA–NaBr–CsBr

External NaBr molality	K_e	K_c	K_e'
0.080	2.86	2.84	2.94
0.401	2.48	2.54	2.71
0.810	2.26	2.25	2.64
1.660	1.84	1.69	2.53
3.490	1.14	1.08	2.06
5.503	0.72	0.60	2.25
7.903	0.47	0.32	1.92

Table III: Selectivity Data for System NaA–NaAc–CsAc

External NaAc molality	K_e	K_c	K_e'
0.186	3.06	3.09	3.02
0.470	3.20	3.15	3.15
0.959	3.35	3.31	3.23
2.001	3.73	3.70	3.52
2.558	3.89	3.89	3.63
3.554	4.31	4.36	3.92

In the NaA–NaAc–CsAc system the trend in activity coefficients of the acetates are opposite to those of the chlorides and bromides and study of the selectivity of this system was expected to be a useful test of the approach that has been employed herein. Unfortunately there are no published α-values for this system as well. The interaction parameters needed to be approximated by using the relation[14]

$$\phi_B - \phi_C = 2.303 m \alpha_B \tag{5}$$

where ϕ_B = osmotic coefficient of CsAc at molality m, ϕ_C = osmotic coefficient of NaAc at molality m, and α_B = interaction coefficient.

In Tables IV and V selectivity data for the system KA–KCl–CsCl and KA–KCl–NaCl are given. The values of ln $\bar{\gamma}_{K^+}/\bar{\gamma}_{N^+}$ = 2.340 and 0.1793 were determined from K_e at 2.090 and 1.831 m KCl, respectively. The $\gamma_{\pm}$-values and interaction parameters were obtained from the data of Robinson.[16,17]

Table IV: Selectivity Data for the Systems KA–KCl–CsCl

External KCl molality	K_e	K_c	K_e'
0.049	2.92	2.80	3.00
0.098	2.77	2.80	2.83
0.499	2.67	2.72	2.76
1.000	2.58	2.66	2.74
2.090	2.48	2.48	2.78
3.220	2.45	2.39	2.82
4.414	2.45	2.36	2.90

Table V: Selectivity Data for the System KA–KCl–NaCl

External KCl molality	K_e	K_c	K_e'
0.1089	3.42	3.41	3.40
0.4394	3.52	3.48	3.45
0.8905	3.49	3.51	3.39
1.8308	3.59	3.59	3.42
2.8291	3.75	3.69	3.49
3.8851	3.80	3.77	3.46

Tables VI and VII contain known aqueous phase activity coefficient data for the heterovalent systems. Tables VIII and IX present the experimental selectivity coefficient values together with the estimated values of (1) the π-term and (2) the activity coefficient of the trace component at the various experimental concentrations of $Ca(NO_3)_2$.

Also included in Table VIII are interaction coefficients (α_{12}), estimated for the Na–Ca systems studied, from the experimentally determined selectivity coefficients. The presumption for evaluation of α_{12} is that the Harned rule[14] is valid for this system.

(16) Landolt–Bornstein, "Physikalisch-Chemischen Tabellen," 5 Auflage, Vol. 2, part 2, Verlag von Julius Springer, 1931, p. 1125.

(17) R. A. Robinson, Trans. Faraday Soc., 49, 1147 (1953).

Table VI: Activity Coefficients in the Aqueous Phase for the System CaZ–Ca(NO₃)₂–NaNO₃(trace)–H₂O

Ca(NO₃)₂ molality	Ca(NO₃)₂ $\gamma_{1(0)}$	NaNO₃ $\gamma_{1(0)}$	a_w
0.127	0.486	0.740	0.994
0.256	0.410	0.680	0.989
0.517	0.363	0.614	0.997
1.055	0.338	0.543	0.959
2.218	0.353	0.468	0.890
5.036	0.513	0.386	0.709

Table VII: Activity Coefficients in the Aqueous Phase for the System CaZ–Ca(NO₃)₂–Ba(NO₃)₂(trace)–H₂O

Ca(NO₃)₂ molality	Ca(NO₃)₂ $\gamma_{1(0)}$	NaNO₃ $\gamma_{1(0)}$	a_w
0.0941	0.490	0.432	0.996
0.1900	0.434	0.348	0.991
0.381	0.381	0.266	0.983
0.773	0.344		0.966
1.599	0.339		0.924
3.469	0.406		0.809

Table VIII: Selectivity Data for the System CaZ–Ca(NO₃)₂–NaNO₃(trace)–H₂O

Ca(NO₃)₂ molality	K_{exp}	$\pi\Delta V/RT$	$\gamma_{1(0)}$	$\gamma_{0(1)}$	α_{12}
0.127	7.59 × 10²	−1.491	0.740	0.740	...
0.256	7.54 × 10²	−1.487	0.680	0.668	+0.03
0.517	6.34 × 10²	−1.477	0.614	0.583	+0.04
1.055	5.26 × 10²	−1.458	0.543	0.524	+0.015
2.218	3.37 × 10²	−1.401	0.468	0.478	−0.004
5.036	1.59 × 10²	−1.215	0.386	0.501	−0.022

Table IX: Selectivity Data for the System CaZ–Ca(NO₃)₂–Ba(NO₃)₂(trace)–H₂O

Ca(NO₃)₂ molality	K_{exp}	$\pi\Delta V/RT$	$\gamma_{1(0)}$	$\gamma_{1(0)}$
0.0941	2.14	−0.548	0.432	0.432
0.1900	2.01	−0.547	0.348	0.374
0.381	2.02	−0.544	0.266	0.329
0.773	0.97	−0.539		0.232
1.599	0.63	−0.526		0.198
3.469	0.35	−0.485		0.191

Discussion

The excellent agreement of K_e and K_c in each of the uni-univalent systems over the total concentration range that was studied indicates attainment of the first objective of this investigation. The model that

has been employed to describe the selectivity behavior of organic exchangers has been shown to be applicable to the A-zeolite. The special properties of the zeolite permit the accurate prediction of selectivity at any external electrolyte concentration of two mobile counter ions at micro- and macroconcentrations levels, respectively, on the basis of one selectivity measurement if the thermodynamic properties of the mixed electrolyte in the aqueous phase is known.

The factors that contribute importantly to the ion-exchange behavior of the A-type zeolite in dilute electrolyte mixtures are apparent from examination of Table X presented below. The value of the $\pi\Delta V/RT$ terms in the dilute solution region and the corresponding ratio of the activity coefficient of the ions in the zeolite phase are given in Table X together with the selectivity coefficients that were evaluated for the several systems studied. The activity coefficient ratio of the salts in the external dilute solutions is close to unity so that the third term of eq. 2 becomes of minor importance in this region.

Table X: Zeolite Parameters

System	$\pi\Delta V/RT$	K_e	$\ln K_e$	$\ln \gamma_M/\gamma_N$
NaZ–NaCl–CsCl	−2.299	2.77	1.0819	3.390
NaZ–NaBr–CsBr	−2.299	2.86	1.0508	3.390
NaZ–NaAc–CsAc	−2.293	3.06	1.1184	3.390
KZ–KCl–NaCl	+1.036	3.42	1.2296	0.1793
KZ–KCl–CsCl	−1.261	2.92	1.0716	2.3405

The $\pi\Delta/VRT$ values are large and thus cannot be neglected in considering selectivity. For all the systems except the KZ–KCl–NaCl system the values are negative. Only in this system does the $\pi\Delta V/RT$ term become the major term. In the other systems the $\pi\Delta V/RT$ and the resin activity coefficient ratio are of the same order of magnitude with the activity coefficient ratio predominating. One cannot generalize as to which term predominates.

The third term in eq. 2 is of minor importance in dilute solution (0.1 m or less) but in concentrated solutions it becomes quite important. Figure 2 shows its effect. The $\pi\Delta V/RT$ term is such to increase the selectivity coefficient slightly with increasing concentration. However, the selectivity coefficients decrease with increasing concentration for the systems NaZ–NaCl–CsCl and NaZ–NaBr–CsBr showing the pronounced effect that the external solution has. The selectivity coefficient increases with concentration for the NaAc–CsAc system due to the $\pi\Delta/RT$ term and
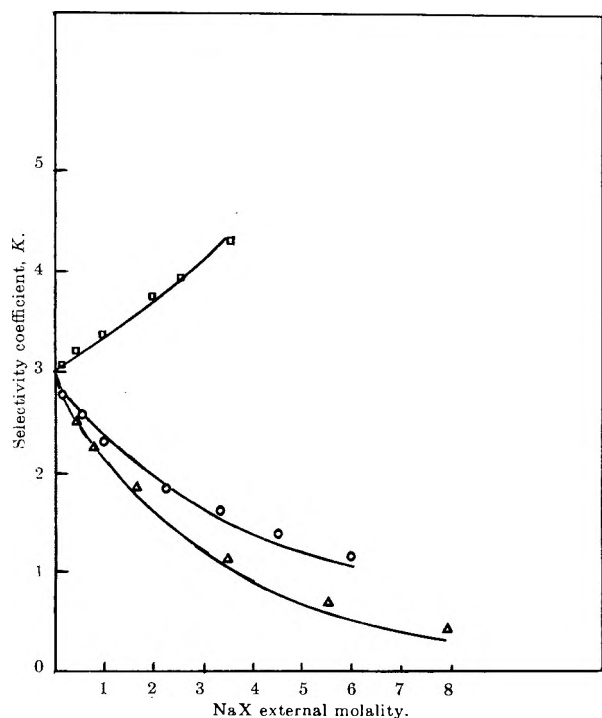
Figure 2. Selectivity data for systems NaZ–NaX–CsX(trace)–
H_2O: □, X = Ac⁻; △, X = Br⁻; O, X = Cl⁻.

the term involving activity coefficients in the external solution.

The selectivity coefficients for the systems in Fig. 2 approach each other 3.0 at infinite dilution as they should since the exchanging ions are the same and the zeolite is at a constant mole fraction, $\bar{X}_{Na^+} = 1$.

The good agreement found by use of this model for the zeolite also suggests that one might use experimentally determined selectivity coefficients to obtain Harned interaction coefficients in mixed electrolyte solutions. Table XI contains interaction coefficients calculated from experimental K values· for the KZ–

KCl–CsCl system assuming no β-term. These are compared to the values obtained by Robinson[18] using the isopiestic method. The agreement is good.

Table XI: Interaction Coefficient Calculations

KCl molality	$-\alpha_{12}$ calcd.	$-\alpha_{12}$[a]
1.00	0.014	0.019
2.09	0.009	0.009
3.22	0.006	0.004
4.41	0.004	0.004

[a] Values from ref. 18.

This result indicates the potential utility of the model for estimating the activity coefficients of trace components in the presence of bulk electrolyte, our second objective. In fact when we examine the results given in Tables VIII and IX we note that the derived observations are indeed reasonable.

The calculated α_{12} values for $NaNO_3$ are of the order of magnitude observed for other systems. They change sign. This behavior is observed in other systems when the $\gamma_{1(0)}$ of one electrolyte is higher than the other electrolyte and with increasing concentration becomes lower as is the case in the $Ca(NO_3)_2$–$NaNO_3$ system. The $\gamma_{1(0)}$ of $Ca(NO_3)_2$ is higher than that of $Ba(NO_3)_2$ and interactions would be such as to make $\gamma_{0(1)}$ of $Ba(NO_3)_2$ higher than $\gamma_{1(0)}$. Such a trend is observed.

(18) R. A. Robinson, *J. Phys. Chem.*, **65**, 662 (1961).

Infrared Studies of Amine Complexes. I. Self-Association of

Aniline in Cyclohexane Solution[1]

by J. H. Lady and Kermit B. Whetsel

Tennessee Eastman Company, Division of Eastman Kodak Company, Kingsport, Tennessee (Received July 19, 1963)

The first overtone N–H symmetric stretching band of aniline in cyclohexane solution has been studied over the concentration range 0.02 to 10 M at temperatures from 10 to 70° as permitted by solubility. The data have been interpreted in terms of self-association through hydrogen bonding. A model based on monomer, dimer, and tetramer is consistent with the experimental data for concentrations up to 4 M and gives $\Delta H°$ values of -1.64 ± 0.25 and -7.7 ± 0.5 kcal. mole^{-1} for the formation of dimer and tetramer, respectively. A model based on dimerization and subsequent stepwise formation of higher multimers is applicable only for concentrations up to 1.5 M.

The question of whether aniline and other primary aromatic amines undergo self-association through hydrogen bonding in nonpolar solvents has been discussed extensively. The discussion has been concerned primarily with the interpretation of the observed effects of concentration upon the ultraviolet, infrared, and nuclear magnetic resonance spectra of the amines. Several workers have interpreted their infrared results in terms of hydrogen bonding interactions,[2-7] but others have attributed the spectral variations to van der Waals interactions or to dipolar and dielectric effects.[8-10] A similar situation exists with respect to the nuclear magnetic resonance data with two groups of workers favoring self-association[11,12] and two opposing it.[13,14] The available ultraviolet data have been interpreted in favor of hydrogen bonding association.[15]

Most of the infrared data on the amines have been qualitative in nature with particular emphasis being placed upon the frequency shifts exhibited by the fundamental N–H stretching bands. Although band intensities are sometimes more sensitive than band positions to hydrogen bonding interactions,[16,17] little attention has been given to the intensities of the N–H bands.[18] In the present investigation, the intensity of the first overtone N–H symmetric stretching band of aniline in cyclohexane solution was studied at a variety of concentrations and temperatures. The results have been interpreted in terms of hydrogen

bonding association, and formation constants and thermodynamic properties of the associated species have been calculated.

Experimental

Instrumentation. A Cary Model 14 spectrophotometer equipped with a log absorbance slide wire

(1) Presented at the 14th Pittsburgh Conference on Analytical Chemistry and Applied Spectroscopy, Pittsburgh, Pa., March, 1963.

(2) W. Gordy, *J. Am. Chem. Soc.*, 59, 464 (1937).

(3) W. Gordy, *J. Chem. Phys.*, 7, 167 (1939).

(4) V. Williams, R. Hofstadter, and R. C. Herman, *ibid.*, 7, 802 (1939).

(5) N. Fuson, M. Josien, R. L. Powell, and E. Utterback, *ibid.*, 20, 145 (1952).

(6) R. A. Friedel, *ibid.*, 62, 1341 (1958).

(7) M. P. Lisitsa and I. N. Khalimonova, *Opt. Spectry.* (USSR), 11, 179 (1961).

(8) M. Freymann, *Ann. Chim.*, 11, 11 (1939).

(9) A. M. Buswell, J. R. Downing, and W. H. Rodebush, *J. Am. Chem. Soc.*, 61, 3252 (1939); 62, 2759 (1940).

(10) L. J. Bellamy and R. L. Williams, *Spectrochim. Acta*, 9, 341 (1957).

(11) I. Yamagucki, *Bull. Chem. Soc. Japan*, 34, 1606 (1961).

(12) B. D. N. Rao and C. N. R. Rao, *Can. J. Chem.*, 40, 963 (1962).

(13) C. Griessner-Prettre, *Compt. rend.*, 252, 3238 (1961).

(14) J. Feeny and L. H. Sutcliffe, *J. Chem. Soc.*, 1123 (1962).

(15) J. C. Dearden and W. F. Forbes, *Can. J. Chem.*, 33, 896 (1960).

(16) G. C. Pimentel and A. L. McClellan, "The Hydrogen Bond," W. H. Freeman and Co., San Francisco, Calif., 1960, Chapter 6.

(17) R. E. Kagarise, *Spectrochim. Acta*, 19, 629 (1963).

(18) K. B. Whetsel, W. E. Roberson, and M. W. Krell, *Anal. Chem.*, 32, 1281 (1960).

was used. The scan speed was 5 Å./sec. and the spectral slit width was about 4 cm.$^{-1}$ at 6696 cm.$^{-1}$. The cells varied in thickness from 0.1 to 5.0 cm. and had quartz or Corex windows. The sample cell was placed in a jacketed cell holder connected to a constant temperature water bath. The solution temperature was determined by inserting an iron–constantan thermocouple into the cell.

With concentrations of aniline below 2 M, the temperature of the cell was varied by increments of 2 or 3° by intermittent circulation of water from the temperature bath. The temperature change was observed on a recorder, and when a steady state was obtained the spectrum was recorded. Solutions were allowed to equilibrate with the light passing through the sample because the intense nondispersed radiation caused the samples to heat about 2° above the temperature of the water jacket. Measurements made by increasing and decreasing the temperature of the cell were in good agreement, indicating no appreciable effects of solvent evaporation or temperature lag. For concentrations above 2 M the water bath was adjusted to the desired temperature and the water was circulated continuously. The estimated temperature accuracy was ±1°. The cell compartments were flushed with dry nitrogen to prevent condensation of moisture on the cell windows when measurements were being made below room temperature.

Reagents. Reagent grade aniline and Eastman Kodak Spectro grade cyclohexane were used without further purification.

Spectral Data. The spectra of cyclohexane solutions of aniline were measured against reference solutions of cyclohexane containing a volume per cent of carbon tetrachloride equal to the volume per cent of aniline in the sample. Background corrections were applied to all measured absorbances by subtracting the absorbance at 6211 cm.$^{-1}$ (1.610 μ) from the absorbance at 6696 cm.$^{-1}$ (1.4935 μ). An additional correction was applied to compensate for the solvent unbalance which resulted when the sample and reference cells were at different temperatures.

Aniline concentrations were corrected for density changes by determining the density of each sample solution as a function of temperature. Apparent absorptivities, ϵ_a, were calculated from the relation $\epsilon_a = A/lC$, where A is corrected absorbance, C is concentration in moles per liter, and l is cell length in centimeters. With concentrations less than 2 M, the apparent molar absorptivities were plotted as a function of temperature for each concentration to obtain curves such as those shown in Fig. 2. Values of ϵ_a were read from the resulting smooth curves at

temperature intervals of 10° from 10 to 70°. With concentrations greater than 2 M, the values of ϵ_a were determined directly at the desired temperatures. The absorptivity data are presented in Table I, and a few typical plots of absorptivity $vs.$ concentration are shown in Fig. 3.

Calculations. *1. Limiting Slope Method.* Dimerization constants, K_D, were calculated from the limiting slopes of apparent absorptivity $vs.$ concentration plots using the relation derived by Liddel and Becker.[19] For the reaction

$$\mathrm{M + M} \rightleftharpoons \mathrm{D} \qquad K_D = \frac{[C_D]}{[C_M]^2} \qquad (1)$$

these authors have shown that

$$\lim_{C \to 0} \frac{d\epsilon_a}{dC} = -\left[2 - \frac{\epsilon_D}{\epsilon_M}\right] K_D \epsilon_M \qquad (2)$$

where C_D and C_m are the equilibrium concentrations of dimer and monomer, C is the total solute concentration expressed as monomer, and ϵ_D and ϵ_M are the molar absorptivities of dimer and monomer, respectively.

In the present work the limiting slopes were determined by a least-squares treatment of the data for concentrations between about 0.03 and 0.2 M. For systems having values of ϵ_M, ϵ_D, and K_D similar to those found for aniline, it can be shown that over this concentration range the plots of ϵ_a $vs.$ C are linear within the limits of normal experimental error; however, the values of K_D obtained from the slopes are 15 to 20% lower than the true values. This inherent weakness of the limiting slope method is partially offset in the aniline–cyclohexane system by the formation of a more highly associated species which is discussed in the following section of the paper. The error in K_D resulting from this effect is believed to be less than 10%.

The value of ϵ_D required for the solution of eq. 2 could not be determined directly, but it was estimated to be approximately 1.0 l. mole^{-1} cm.$^{-1}$. The absorptivity of the aniline–chloroform complex, in which aniline is the proton acceptor, is about 0.6 l. mole^{-1} cm.$^{-1}$, and the absorptivity of the aniline–dimethyl aniline complex, in which aniline is the proton donor, is about 0.4 l. mole^{-1} cm.$^{-1}$.[20] For a dimer in which one molecule serves as the proton donor and the other as the proton acceptor, it is reasonable that the absorptivity should be approximately 1.0 l. mole^{-1} cm.$^{-1}$

(19) U. Liddel and E. D. Becker, *Spectrochim. Acta*, **10**, 70 (1957).
(20) K. B. Whetsel and J. H. Lady, *J. Phys. Chem.*, **68**, 1010 (1964), and unpublished results.

Table I: Apparent Absorptivities of Aniline in Cyclohexane Solution[a]

10° Concn., M	ε_a	20° Concn., M	ε_a	30° Concn., M	ε_a	35° Concn., M	ε_a	40° Concn., M	ε_a	50° Concn., M	ε_a	60° Concn., M	ε_a	70° Concn., M	ε_a
0.0291	1.889	0.0288	1.861	0.0284	1.832	0.0282	1.818	0.0281	1.804	0.0277	1.775	0.0273	1.746	0.0270	1.718
0.0351	1.887	0.0347	1.864	0.0342	1.842	0.0340	1.830	0.0338	1.818	0.0333	1.796	0.0329	1.774	0.0325	1.751
0.0531	1.888	0.0528	1.864	0.0522	1.840	0.0518	1.828	0.0515	1.816	0.0508	1.792	0.0501	1.768	0.0495	1.745
0.0830	1.828	0.0819	1.823	0.0809	1.813	0.0804	1.806	0.0789	1.797	0.0788	1.781	0.0778	1.744	0.0768	1.718
0.1105	1.784	0.1092	1.781	0.1078	1.780	0.1070	1.760	0.1064	1.752	0.1050	1.734	0.1037	1.717	0.1023	1.700
0.1444	1.734	0.1426	1.732	0.1409	1.727	0.1399	1.724	0.1391	1.719	0.1372	1.709	0.1355	1.697	0.1337	1.679
0.1870	1.679	0.1846	1.682	0.1824	1.685	0.1812	1.684	0.1801	1.682	0.1778	1.673	0.1757	1.660	0.1734	1.646
0.2202	1.649	0.2174	1.652	0.2148	1.653	0.2136	1.649	0.2121	1.644	0.2094	1.632	0.2069	1.621	0.2042	1.610
0.2740	1.545	0.2707	1.572	0.2663	1.590	0.2658	1.597	0.2641	1.600	0.2609	1.603	0.2578	1.604	0.2545	1.606
0.3363	1.475	0.3322	1.505	0.3268	1.531	0.3263	1.543	0.3242	1.551	0.3203	1.562	0.3163	1.567	0.3124	1.571
0.4258	1.360	0.4206	1.414	0.4154	1.447	0.4129	1.460	0.4103	1.470	0.4051	1.484	0.3999	1.491	0.3948	1.493
0.5563	1.222	0.5495	1.285	0.5428	1.332	0.5395	1.349	0.5361	1.364	0.5294	1.387	0.5228	1.403	0.5161	1.413
		0.7345	1.138	0.7254	1.203	0.7208	1.228	0.7164	1.252	0.7073	1.290	0.6983	1.322	0.6892	1.348
		0.8708	1.050	0.8604	1.122	0.8553	1.151	0.8501	1.177	0.8401	1.218	0.8298	1.252	0.8196	1.278
		1.0960	0.949	1.0830	1.013	1.0760	1.040	1.0690	1.065	1.0560	1.110	1.0430	1.150	1.0290	1.188
		1.3060	0.863	1.2910	0.934	1.0906	1.020	1.0840	1.044	1.0716	1.114	1.0587	1.124	1.0445	1.149
						1.2840	0.964	1.2760	0.992	1.2610	1.037	1.2460	1.078	1.2310	1.116
						2.1823	0.736	2.1707	0.768	2.1418	0.816	2.1189	0.855	2.0946	0.880
						3.2537	0.621	3.2354	0.649	3.1956	0.676	3.1620	0.715	3.1242	0.755
						4.3623	0.546		...	4.2920	0.592	4.2529	0.618	4.2133	0.646
						5.4145	0.493	5.4047	0.509	5.3426	0.543	5.2927	0.567	5.2303	0.602
						6.5486	0.463	6.5140	0.465	6.4465	0.495	6.3839	0.523	6.3192	0.556
						8.7181	0.395	8.6790	0.408	8.5991	0.426	8.5310	0.444	8.4492	0.468
						9.7892	0.366	9.7464	0.378	9.6608	0.393	9.5832	0.415	9.4957	0.430
						10.7810	0.336	10.7670	0.345	10.6658	0.369	10.5927	0.379	10.5079	0.404

[a] For concentrations up to 1.3 M, the values of ϵ_a are interpolated ones read from curves such as those shown in Fig. 2; for higher concentrations the values of ϵ_a were measured only at the temperatures shown in this table.

Table II: Formation Constants and Thermodynamic Quantities for Self-Association of Aniline ($\epsilon_D/2 = 0.40$; $\epsilon_T/4 = 0.15_8$)[a]

Temp., °C	Limiting slope[b] $K_D \pm \sigma$	Dimer-tetramer model[b] K_D	K_T	Stepwise association model[b] K_D	K
10	$0.44_3 \pm 0.02_0$	. . .	. . .	. . .	. . .
20	$0.39_9 \pm 0.02_0$	0.41	2.28	0.40	1.18
30	$0.35_6 \pm 0.02_5$	0.39	1.39	0.37	0.97
35	. . .	0.37	1.13	0.34	0.89
40	$0.32_8 \pm 0.02_6$	0.36	0.90	0.33	0.83
50	$0.30_6 \pm 0.03_2$	0.38	0.60	0.31	0.72
60	$0.28_0 \pm 0.02_8$	0.30	0.43	0.28	0.59
70	$0.25_9 \pm 0.03_4$	0.27	0.31	0.26	0.54
$\Delta H° \pm 2\sigma$, kcal. mole⁻¹	-1.72 ± 0.06	-1.69 ± 0.22	-7.96 ± 0.26	-1.72 ± 0.14	-3.17 ± 0.18
$\Delta F°_{25}$, kcal. mole⁻¹	$+0.58$	$+0.54$	-0.33	$+0.58$	-0.04
$\Delta S°_{25} \pm 2\sigma$, e.u.	-7.7 ± 0.2	-7.7 ± 0.6	-25.6 ± 0.9	-7.7 ± 0.5	-10.5 ± 0.6

[a] Formation constants are expressed in concentration units; all error limits represent precision only; see Table III for effect of $\epsilon_D/2$ and text for discussion of errors. [b] The values shown were derived from data covering the following ranges of concentration: limiting slope, 0.03 to 0.2 M; dimer-tetramer model, 0.07 to 4.3 M; stepwise association model, 0.07 to 1.5 M.

Table III: Formation Constants and Thermodynamic Quantities for Self-Association of Aniline ($\epsilon_D/2 = 0.60$; $\epsilon_T/4 = 0.14_5$)[a]

Temp., °C	Limiting slope[b] $K_D \pm \sigma$	Dimer-tetramer model[b] K_D	K_T	Stepwise association model[b] K_D	K
10	$0.50_9 \pm 0.02_3$	. . .	. . .	. . .	. . .
20	$0.46_0 \pm 0.02_3$	0.47	2.62	0.44	1.18
30	$0.41_2 \pm 0.02_9$	0.44	1.68	0.41	1.02
35	. . .	0.42	1.36	0.40	0.91
40	$0.38_0 \pm 0.03_0$	0.41	1.08	0.38	0.85
50	$0.35_6 \pm 0.03_7$	0.38	0.77	0.35	0.76
60	$0.32_7 \pm 0.03_2$	0.34	0.55	0.32	0.64
70	$0.30_3 \pm 0.03_9$	0.32	0.40	0.29	0.61
$\Delta H° \pm 2\sigma$, kcal. mole⁻¹	-1.62 ± 0.06	-1.58 ± 0.16	-7.49 ± 0.22	-1.68 ± 0.22	-2.74 ± 0.26
$\Delta F°_{25}$, kcal. mole⁻¹	$+0.49$	$+0.46$	-0.42	$+0.50$	-0.04
$\Delta S°_{25} \pm 2\sigma$, e.u.	-7.1 ± 0.20	-6.8 ± 0.5	-23.7 ± 0.7	-7.3 ± 0.7	-9.1 ± 0.9

[a] Formation constants are expressed in concentration units; all error limits represent precision only; see Table II for effect of $\epsilon_D/2$ and text for discussion of errors. [b] The values shown were derived from data covering the following ranges of concentrations: limiting slope, 0.03 to 0.2 M; dimer-tetramer model, 0.07 to 4.3 M; stepwise association model, 0.07 to 1.5 M.

($\epsilon_D/2 = 0.50$ based on the formal concentration of aniline in the dimeric form). To demonstrate the effect of the value of ϵ_D on K and ΔH, calculations are presented for ϵ_D-values of 0.80 and 1.20 l. mole⁻¹ cm.⁻¹ ($\epsilon_D/2 = 0.40$ and 0.60) in Tables II and III, respectively.

2. Monomer–Dimer–Tetramer Model. At concentrations greater than 0.2 M, the experimental data are not consistent with a simple monomer–dimer equilibrium. The rapid decrease in absorptivity with increasing concentration indicated that one or more higher multimer was being formed. This observation led to an analysis of the data by the curve-fitting methods developed by Rossotti and Rossotti.[21]

The monomer concentrations required by the Rossotti method could not be determined directly from the experimental values of ϵ_a at 6696 cm.⁻¹ because of the absorption of associated species at this frequency. First approximations of the monomer concentration, b, were obtained by assuming that all multimers above monomer have an equal absorptivity, ϵ_n/n, per molecule of aniline. Monomer fractions, α, and the monomer concentrations, b, were then calculated from the relations

(21) F. J. C. Rossotti and J. Rossotti, *J. Phys. Chem.*, **65**, 926, 930 (1961).

$$\epsilon_a = \alpha\epsilon_M + (1 - \alpha)\epsilon_n/n \qquad (3)$$

$$b = \alpha B \qquad (3a)$$

using the extrapolated values of ϵ_M, assumed values of ϵ_n/n, and the total aniline concentration, B. With assumed values of ϵ_n/n between 0.15 and 0.30, the experimental data fit the normalized curve for the system $B + B_2 + B_Q$ where $Q = 4$, i.e., a system composed of monomer, dimer, and tetramer. The range of values chosen for ϵ_n/n is reasonable, since $\epsilon_D/2$ is approximately 0.5 and ϵ_n/n for higher multimers is probably less than 0.2. The latter conclusion is based on the fact that ϵ_a for pure aniline at 5° is only 0.28; since this sample contains some monomer and dimer, the absorptivity of more highly associated species must be quite low.

Once it was established that a system composed of monomer, dimer, and tetramer gave a reasonable fit of the data, the value of the tetramer absorptivity, ϵ_T, was approximated from the 50° data using a method similar to that used by Drago and Rose[22] to calculate formation constants and absorptivities of complexes. The calculations were carried out using the relations

$$\epsilon_a = \alpha\epsilon_M + \beta\frac{\epsilon_D}{2} + \delta\frac{\epsilon_T}{4} \qquad (4)$$

$$\beta = 2K_D\alpha^2 B \qquad (5)$$

$$\delta = 4K_T\alpha^4 B^3 \qquad (6)$$

where α, β, and δ are the fractions of aniline in the form of monomer, dimer, and tetramer, K_D and K_T are formation constants for the dimer and tetramer, respectively, and B is the total aniline concentration. Assuming that no other species are present

$$\alpha + \beta + \delta = 1 \qquad (7)$$

Combining eq. 4 through 7 yields

$$2K_DB\left(\frac{\epsilon_D}{2} - \frac{\epsilon_T}{4}\right)\alpha^2 + \left(\epsilon_M - \frac{\epsilon_T}{4}\right)\alpha - \left(\epsilon_a - \frac{\epsilon_T}{4}\right) = 0 \qquad (8)$$

The values of K_D and $\epsilon_D/2$ from the limiting slope treatment and assumed values of $\epsilon_T/4$ were substituted into eq. 8 to obtain sets of α-values for various values of B. The α-values and eq. 5–7 were used to calculate corresponding sets of values for K_T. Plotting K_T against $\epsilon_T/4$ for several concentrations gave a cross point which corresponded to the best estimate of $\epsilon_T/4$. This value of $\epsilon_T/4$ was assumed to be independent of temperature and was substituted into eq. 8 to obtain a second approximation of α at all temperatures.[23] New values of b were calculated from the second

approximation of α and treated by Rossotti's curve-fitting method. The variables defined by

$$F = \frac{B - b}{b^2}; \qquad \mathbf{F} = (2 + Q\mathbf{b}^{Q-2}) \qquad (9)$$

were used to prepare the experimental function log F vs. log b and the normalized function log $\mathbf{F}$ vs. log $\mathbf{b}$. The experimental function was superimposed on the normalized function for $Q = 4$, and values of K_D and K_T were calculated by substituting corresponding values of these functions into eq. 10 and 11. The

$$\log \mathbf{F} = \log F - \log K_D \qquad (10)$$

$$\log \mathbf{b} = \log b + \frac{1}{Q - 2}\log\frac{K_q}{K_D} \qquad (11)$$

validity of the values of K_D and K_T thus obtained was tested by calculating β and δ from eq. 5 and 6 and then constructing error curves based on eq. 7.

3. Stepwise Association Model. A model based on dimerization followed by successive stepwise association was studied using the method described by Rossotti under hypothesis I in ref. 21. In this method the stepwise association constants for the reaction

$$B_{q-1} + B \rightleftharpoons B_q \qquad (12)$$
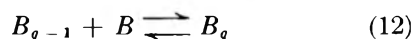
are assumed to be equal and to have a value K when $q \geq 3$; therefore

$$K_q = K_DK^{q-2} \qquad (13)$$

The auxiliary concentration variables used in the graphical treatment are defined by

$$T = \frac{(B - b)}{b} \qquad (14)$$

and the normalized variables by

$$\mathbf{T} = \frac{TK}{K_D} \qquad (15)$$

and

$$\mathbf{b} = bK \qquad (16)$$

The monomer concentrations obtained in the monomer–dimer–tetramer treatment were used for the stepwise model. Using these values is equivalent to assuming that ϵ_n/n is a constant for all multimers higher than the dimer. Error curves for the stepwise model were constructed from the relation

(22) N. J. Rose and R. S. Drago, *J. Am. Chem. Soc.*, **81**, 6138 (1959).

(23) An electronic computer was used to obtain solutions of eq. 8.

$$\text{error, \%} = 100\left(1 - \alpha \sum_{n=1}^{n=i}(n+1)K_\mathrm{D}K^{n-1}\alpha^{n+1}C'^n\right)$$

(17)

Results

The general effects of concentration on the N–H bands of aniline in cyclohexane solution are shown in Fig. 1. The effects of temperature and concentration on the absorptivity at 6696 cm.$^{-1}$ are shown in Fig. 2 and 3. The monomer absorptivity, ϵ_M, obtained by extrapolating ϵ_a to infinite dilution, decreases with
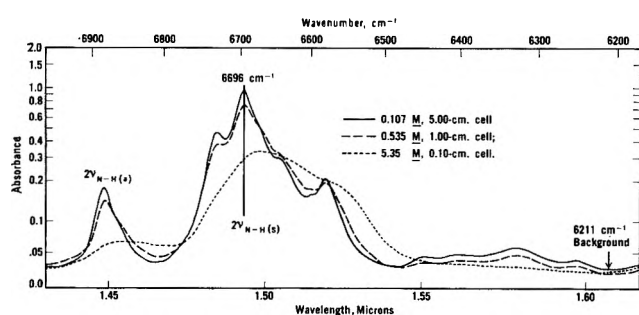

Figure 1. Near-infrared spectra of aniline in cyclohexane solution at 40°.
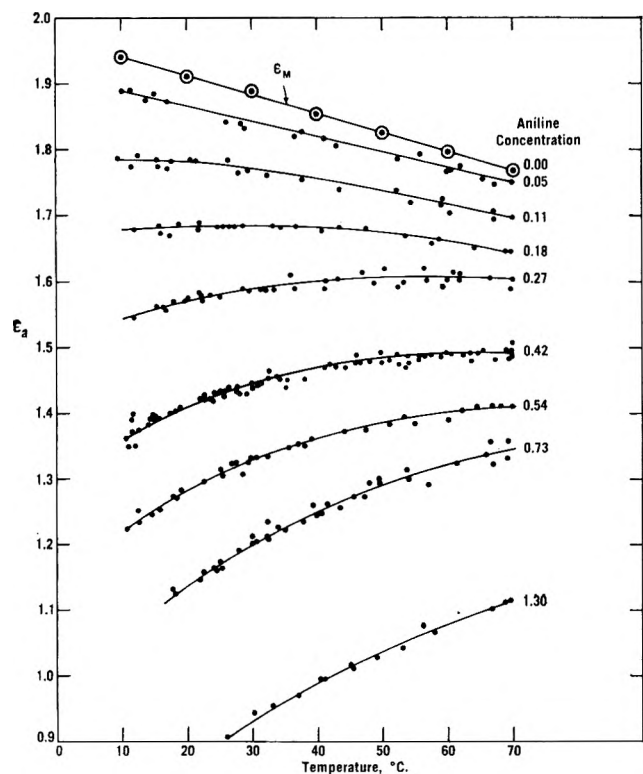
Figure 2. Apparent absorptivity of aniline at 6696 cm.$^{-1}$ as a function of temperature at various concentrations.
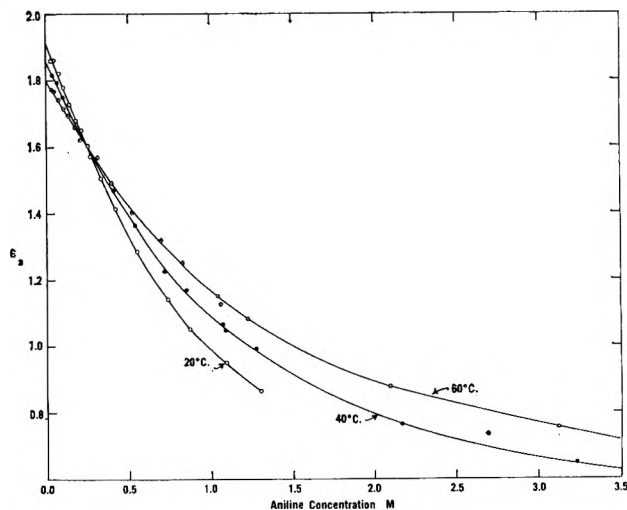
Figure 3. Apparent absorptivity of aniline at 6696 cm.$^{-1}$ as a function of concentration at various temperatures.

increasing temperature. This effect has been observed with alcohols and other compounds,[7,19,24–27] and the necessity of taking it into account in the calculation of formation constants has been pointed out by Drago and co-workers.[28,29] The temperature effect is the predominant one until the concentration exceeds about 0.25 M. At higher concentrations it is over-ridden by the effects of multimer dissociation, and the apparent absorptivity increases with temperature.

Limiting Slope Method. Dimerization constants obtained by the limiting slope method using assumed values of 0.40 and 0.60 for $\epsilon_\mathrm{D}/2$ are shown in Tables II and III, respectively. The error limits shown for K_D correspond to one standard deviation of the limiting slope and represent the precision of the results for a particular assumed value of $\epsilon_\mathrm{D}/2$. The choice of $\epsilon_\mathrm{D}/2$ introduces a further uncertainty of approximately ±0.03 l. mole^{-1} into the estimate of the true value of K_D. In order to take both sources of error into account, the values of K_D shown in Tables II and III for a given temperature should be averaged and error limits of about ±0.06 l. mole^{-1} should be applied. Since the limiting slope method tends to give low results, the true values of K_D probably lie

(24) R. H. Hughes, R. J. Martin, and N. D. Coggeshall, *J. Chem. Phys.*, 24, 489 (1956).

(25) R. M. Hammaker, Ph.D. Dissertation, Northwestern University, 1961.

(26) M. P. Lisitsa and I. N. Khalimonova, *Opt. Spectry.* (USSR), 11, 97 (1961).

(27) M. P. Lisitsa, *et al., ibid.*, 7, 386 (1959).

(28) M. D. Joesten and R. S. Drago, *J. Am. Chem. Soc.*, 84, 2037 (1962).

(29) R. L. Carlson and R. S. Drago, *ibid.*, 84, 2320 (1962).

near the upper ends of the ranges established by these error limits. The error in ϵ_M was neglected in the calculations since it amounts to less than $\pm 1\%$ and has a correspondingly small effect on K_D.

The value chosen for $\epsilon_D/2$ has a much smaller effect on the heat of formation of the dimer than it does on the individual values of K_D. Plots of log K_D vs. $1/T$ gave values of -1.72 ± 0.06 and -1.62 ± 0.06 kcal. mole^{-1} for $\Delta H°$ when $\epsilon_D/2$ was taken as 0.40 and 0.60, respectively. These error limits correspond to two standard deviations of the log K_D vs. $1/T$ plots and represent precision only. In order to take the uncertainty of $\epsilon_D/2$ into acount, the best estimate of $\Delta H°$ from the limiting slope treatment is expressed as -1.67 ± 0.11 kcal. mole^{-1}.

At first thought, the precision expressed for the $\Delta H°$ values appear rather small in view of the precision of the individual values of K_D. Further consideration shows, however, that much of the uncertainty in the individual values of K_D is cancelled out in the determination of $\Delta H°$. The error limits on K_D represent scatter about the ϵ_a vs. C plots at a particular temperature. Since the ϵ_a values were read from smooth curves such as those shown in Fig. 2, the random errors associated with instrument noise and chart readibility were minimized. Much of the scatter, therefore, arises from errors associated with the preparation of the solutions, the positioning of the cells, and the photometric accuracy of the instrument. Since the variation of ϵ_a with temperature was determined for each sample without removing it from the instrument, these errors are essentially independent of temperature. In other words, they vertically displace the ϵ_a vs. temperature curves shown in Fig. 2 without changing their shapes. These displacements are reflected in the error limits of the individual values of K_D, but they have relatively little effect on the change of K_D with temperature. The standard deviations of the individual values of K_D determined from the limiting slope plots are about ± 0.03, but the standard deviation of K_D in the log K_D vs. $1/T$ plot is only 0.005.

Monomer–Dimer–Tetramer Model. The Drago–Rose-type plot from which the absorptivity of the tetramer was obtained is shown in Fig. 4. Values of 0.158 and 0.145 l. mole^{-1} cm.$^{-1}$ were obtained for $\epsilon_T/4$ when $\epsilon_D/2$ was taken as 0.40 and 0.60, respectively. These values are not significantly different, but for the sake of internal consistency the individual values were used in the calculations of α by eq. 8.

Curves of the normalized function log F vs. log b for the system $B + B_2 + B_Q$ where $Q = 3$ and $Q = 4$ are shown in Fig. 5. The experimental function repre-
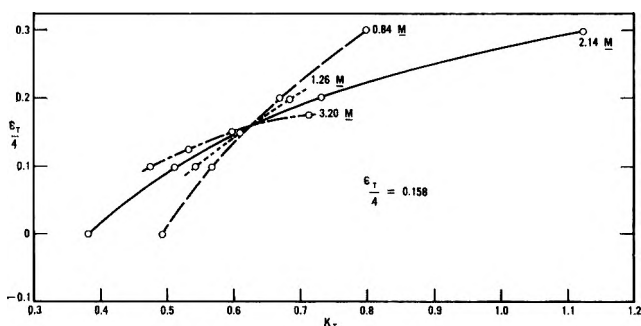

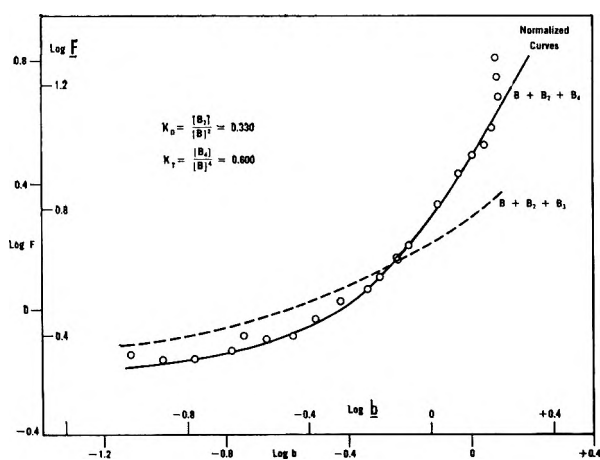Figure 4. Estimation of tetramer absorptivity by a Drago–Rose-type plot (50°, $\epsilon_D/2 = 0.40$).

Figure 5. Rossotti plot of the experimental data for log F vs. log b for the aniline system at 50° superimposed on the normalized curve of log F vs. log b for $Q = 4$ (solid line). The broken line is the corresponding curve for $Q = 3$. (Inside captions for normalized curves.)

senting the 50° data is superimposed on the curve for $Q = 4$. A good fit is obtained over a wide range of concentration. The two points that deviate markedly from the upper end of the curve correspond to 90 and 100% aniline.

The values of K_D and K_T obtained from plots similar to the one shown in Fig. 5 are listed in Tables II and III for the two sets of absorptivities. The values of K_D obtained by the curve-fitting method are 5 to 10% higher than those obtained by the limiting slope method. This result probably reflects the bias of the limiting slope method that was discussed earlier.

The precision of the individual formation constants determined by the curve-fitting method cannot be expressed statistically, but the reproducibility of K_D is estimated to be ± 0.02 l. mole^{-1}; that of K_T probably varies from ± 0.02 to about ± 0.06 l. mole^{-1} as the temperature decreases. These error limits must be increased about threefold and applied to the average

values of the formation constants at any one temperature to show the total uncertainty arising from the choce of $\epsilon_D/2$ and from the experimental error.

Three typical error curves for the monomer–dimer–tetramer treatment are shown in Fig. 6. The vertical bars on the 50° curve show the effect of 1% error in the apparent absorptivity. The values of K_D and K_T obtained by the curve-fitting method are consistent with the experimental data until the total concentration of aniline exceeds 4 M. Inf act, the deviations amount to little more than the experimental error at concentrations less than 8 M.

Plots of log K_D and log K_T vs. $1/T$ gave $\Delta H°$ values of -1.69 ± 0.22 and -7.96 ± 0.26 kcal. mole^{-1} for the dimer and tetramer, respectively, when $\epsilon_D/2$ was taken as 0.40 (Table II); the corresponding values when $\epsilon_D/2$ was taken as 0.60 were -1.58 ± 0.16 and -7.49 ± 0.22 kcal. mole^{-1} (Table III). These limits represent two standard deviations of the slope of the $\Delta H°$ plot for a particular value of $\epsilon_D/2$. When both the experimental error and the uncertainty in $\epsilon_D/2$ are taken into account, the average values of -1.64 ± 0.25 and -7.7 ± 0.5 kcal. mole^{-1} are obtained for the best estimates of the heats of formation from the Rossotti treatment. The value for the dimer is in good agreement with the one obtained by the limiting slope method, but the error limits are almost doubled. At least part of the loss of precision can be attributed to the fact that the apparent absorptivities for concentrations greater than 2 M were measured at only five temperatures.

Stepwise Association Model. Figure 7 shows a typical set of data in which the experimental function
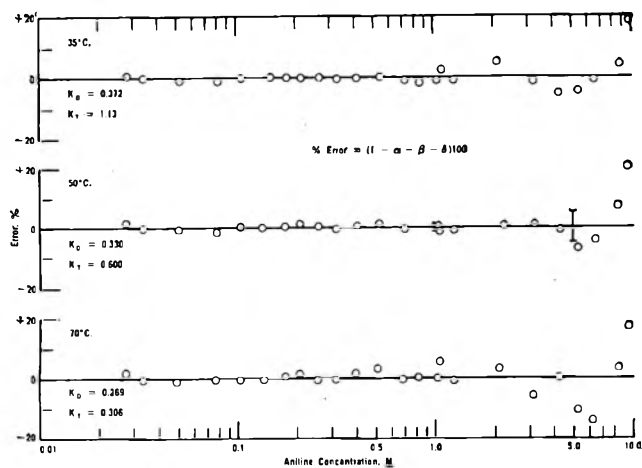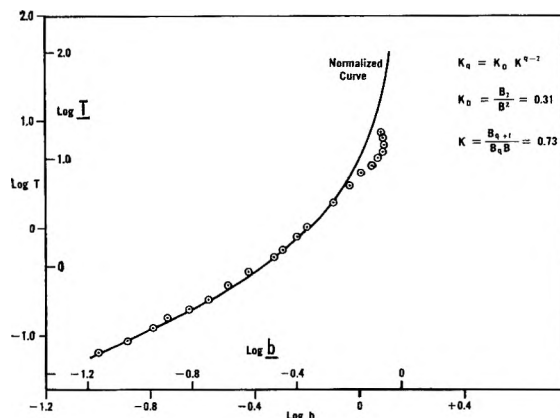
Figure 7. Rossotti plot for the stepwise association of aniline at 50°. The curve for the experimental data of log T vs. log b is superimposed on the normalized curve of log T vs. log b. (Inside captions for normalized curve.)

log T vs. log b is superimposed on the normalized curve of log T vs. log b for the stepwise association model. Although the points corresponding to aniline concentrations greater than 1.5 M deviated seriously from the normalized curve, apparent values of K and K_D were calculated by substituting corresponding values of the experimental and normalized functions into eq. 15 and 16. The results listed in Tables II and III show that the values of K_D and $\Delta H°$ for the formation of dimer are in good agreement with those obtained by the other treatments. The best estimate of $\Delta H°$ for the stepwise formation of higher multimers is -2.96 ± 0.44 kcal. mole^{-1}.

It should be emphasized that the results reported for this model apply only to concentrations of aniline up to about 1.5 M. At a concentration of 3 M, the error calculated by eq. 17 exceeds -35%. Even at the relatively low concentration of 1.5 M, at least 10 terms (corresponding to 10 species) are required in eq. 17 before succeeding terms become insignificant.

Discussion

This study has shown that the effects of concentration on the infrared spectrum of aniline in cyclohexane solution can be interpreted quantitatively in terms of self-association involving dimer and tetramer species. The fact that this model is consistent with the experimental data over wide ranges of concentration and temperature lends strong support to its validity.

A simple model involving only dimerization is inconsistent with the experimental data except at very low concentrations. Even if the absorptivity of the dimer is assumed to be zero, this model fails at concentrations greater than 0.2 M. Attempts to make

Figure 6. Error curves for the formation constants derived from the monomer–dimer–tetramer model at various temperatures.

the data fit a monomer–dimer–trimer model using a variety of absorptivities were unsuccessful at concentrations greater than about 0.5 M. The data will fit a model based on the formation of a dimer, trimer, and tetramer species if the trimer formation constant is quite small relative to the other two. We do not believe that the accuracy of the data justifies the use of an additional constant when an equally good fit of the experimental data can be obtained without it.

Little information on the strength of the N–H---N bond is available for comparison, but our results are consistent with the ones that have been reported. Feeny and Sutcliffe,[14] using nuclear magnetic resonance techniques, found a $\Delta H°$ of -6.7 kcal. mole^{-1} for the formation of the tetramer of monoethylamine from the monomer in carbon tetrachloride solution. From vapor pressure measurements, Wolff and Hoepfner[30] obtained a heat of formation of -1.8 kcal. mole^{-1} for the dimer of monomethylamine in normal hexane solution. Alcohols and phenols generally have heats of formation of -3 to -5 kcal. mole^{-1} per hydrogen bond,[31] and somewhat smaller values are to be expected for the N–H---N bond.

Anderson, Duncan, and Rossotti[32] found dimerization constants for imidazole, pyrazole, and substituted pyrazoles over a hundred times greater than the values we report for aniline. These compounds are apparently able to form relatively stable cyclic complexes because they contain proton donating groups ortho to proton accepting groups. Recently Vinogradov and Kilpatrick[33] have reported a ΔH of -4.6 kcal. mole^{-1} per bond for the self-association of 3,5-dimethylpyrazole.

The relative values of the thermodynamic quantities for dimer and tetramer formation indicate that the tetramer is cyclic. If ones assumes a cyclic tetramer containing three hydrogen bonds in addition to the one associated with dimer formation, the average $\Delta H°$ for the three bonds is about -2 kcal. mole^{-1}. If a linear tetramer is assumed, the average $\Delta H°$ for the two hydrogen bonds formed after the first one is close to -3 kcal. mole^{-1}. While one might expect some increase in the strength of the additional bonds compared to that of the bond in the dimer,[34] the difference between -3 and -1.7 kcal. mole^{-1} seems unreasonably large. According to the statistical treatment of Sarolea-Mathot,[35] the decrease in entropy per bond for multimer formation must be less than that for dimer formation. Although our entropy values are not accurate enough to be considered as conclusive evidence, they meet the Sarolea-Mathot requirement only if one assumes a cyclic tetramer.

The absorptivity–concentration relations of m-toluidine and m-chloroaniline in cyclohexane solution at room temperature are qualitatively similar to the ones shown in Fig. 3 for aniline.[18] The dimer–tetramer model is probably also valid for these amines. With o-chloroaniline a somewhat different relation is observed,[18] indicating that a different model may be required to describe this system.

(30) H. Wolff and A. Hoepfner, Z. Elektrochem., 66, 149 (1962).

(31) See ref. 16, Appendix B.

(32) D. M. W. Anderson, J. L. Duncan, and F. J. C. Rossotti, J. Chem. Soc., 140, 2165, 4201 (1961).

(33) S. N. Vinogradov and M. Kilpatrick, J. Phys. Chem., 68, 181 (1964).

(34) N. J. Coggeshall, J. Chem. Phys., 18, 978 (1950).

(35) L. Sarolea-Mathot, Trans. Faraday Soc., 49, 8 (1953).

Infrared Studies of Amine Complexes. II. Formation Constants and

Thermodynamic Properties of Amine–Chloroform Complexes[1]

by Kermit B. Whetsel and J. H. Lady

Tennessee Eastman Company, Division of Eastman Kodak Company, Kingsport, Tennessee
(Received July 19, 1963)

The association of chloroform with primary and secondary amines in cyclohexane solution was studied by measuring the effects of solvent composition and temperature on the near-infrared N–H bands of the amines. Formation constants, K_C, were determined at 35° for the 1:1 complexes of chloroform with the following amines: aniline, p-phenetidine, p-chloroaniline, m-chloroaniline, o-chloroaniline, p-aminoacetophenone, N-methylaniline, N-ethylaniline, and cyclohexylamine. With the primary aromatic amines, a linear relation exists between log K_C and pK_a (H_2O). Thermodynamic constants for the aniline and cyclohexylamine complexes were calculated from equilibrium data obtained at temperatures between 10 and 50°. The heats of formation of these complexes are -1.7 ± 0.2 and -3.6 ± 0.3 kcal. mole^{-1}, respectively. The results are related to those obtained previously in a general study of the effects of chloroform on the near-infrared N–H bands of primary aromatic amines.

The effects of chloroform on the N–H stretching bands of aromatic amines have been studied in both the fundamental and the first overtone regions of the spectrum.[2-4] Although the observed solvent effects have been interpreted in terms of hydrogen bonding of chloroform with the amino group, no values have been reported for the formation constants and heats of formation of the complexes.

In the present paper, formation constants are reported for the chloroform complexes of aniline, five ring-substituted anilines, N-methylaniline, N-ethylaniline, and cyclohexylamine. The thermodynamic properties of the aniline and cyclohexylamine complexes are also given. The results were obtained by studying the first overtone and combination N–H bands of the amines in the cyclohexane–chloroform solvent system.

Experimental

Equipment. The spectrophotometer and the temperature-regulating device described previously[5] were used with one modification. Corning No. 7–56 filters were used between the source and the cells in order to remove the bulk of the ultraviolet and visible radiation from the light beams. Without these filters, solu-

tions of p-phenetidine containing chloroform developed a haze upon being exposed to the undispersed radiation of the source. The instrument operating conditions described previously were also used, except that the spectral slit width was kept at about 3 cm.$^{-1}$. Five-centimeter cells were used in the overtone region. Because of the relatively strong absorption of cyclohexane, 1-cm. cells were used in the combination region.

Chemicals. The amines were purified by recrystallization and/or distillation through a 1.4-m. spinning band column. Center cuts from the distillations were analyzed by gas chromatography, usually on two columns of different polarity, and judged to be more than 99% pure. Reagent grade chloroform was passed through a chromatographic column packed with partially deactivated alumina to remove the ethanol used

(1) Presented at the 14th Pittsburgh Conference on Analytical Chemistry and Applied Spectroscopy, Pittsburgh, Pa., March, 1963.

(2) A. G. Moritz, *Spectrochim. Acta*, **17**, 365 (1961).

(3) K. B. Whetsel, *ibid.*, 614 (1961).

(4) F. H. Lohman and W. E. Norteman, Jr., *Anal. Chem.*, **35**, 707 (1963).

(5) J. H. Lady and K. B. Whetsel, *J. Phys. Chem.*, **68**, 1010 (1964).

as a stabilizer. The eluent was dried over calcium chloride and distilled. The center cut, b.p. 60.5°, was collected and used within a few days. Chloroform prepared in this manner gave amine solutions that remained clear and showed constant absorption for at least 1 week. The cyclohexane was Eastman Kodak Spectro grade.

Sample Preparation. The aromatic amines were studied at concentrations between 0.07 and 0.15 M, except that more dilute solutions of acetophenone were required because of the limited solubility of the amine. The concentration of cyclohexylamine was in the range 0.25 to 0.35 M. All concentrations were corrected for the variation of solvent density with temperature.

Reference solutions were prepared by mixing the appropriate volumes of chloroform and cyclohexane with a volume of carbon tetrachloride approximately equal to the volume of the amine in the sample solution. At temperatures other than ambient, differential spectra of the reference solutions were measured to obtain correction factors for the solvent unbalance which resulted from the temperature differential between the two cells.

Formation Constants. Preliminary work showed that self-association of the amines could not be neglected without introducing significant errors into the determination of the complex formation constants. A method described by Grunwald and Coburn[6] for treating systems of this type was modified so that most of the calculations could be performed on an electronic computer.

If dimerization of the amine and formation of the chloroform complex are the only significant interactions occurring in the mixtures, the systems can be described by the equations

$$M + M \rightleftharpoons D \qquad K_D = \frac{[C_D]}{[C_M]^2} \qquad (1)$$

$$M + S \rightleftharpoons C \qquad K_C = \frac{[C_C]}{[C_M][C_S]} \qquad (2)$$
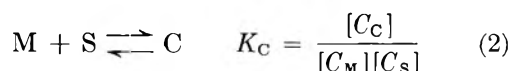
where K_D and K_C are the formation constants of the amine dimer and the amine–chloroform complexes, respectively; C_S, C_M, C_D, and C_C are the equilibrium concentrations in moles per liter of chloroform, amine monomer, amine dimer, and complex, respectively. If C_A^0 and C_S^0 represent the total initial concentrations of amine and chloroform, respectively

$$C_C = C_A^0 - C_M - 2C_D \qquad (3)$$

and

$$C_S = C_S^0 - C_C \qquad (4)$$

Substituting eq. 1, 3, and 4 into eq. 2 and rearranging gives

$$2K_C K_D C_M^3 + (2K_D + K_C)C_M^2 +$$
$$[K_C(C_S^0 - C_A^0) + 1]C_M - C_A^0 = 0 \qquad (5)$$

If Beer's law holds for the individual species

$$A/l = \epsilon_M C_M + \epsilon_D C_D + \epsilon_C C_C \qquad (6)$$

where A is the measured absorbance, l is the path length in centimeters, and ϵ_M, ϵ_D, and ϵ_C are the molar absorptivities of amine monomer, dimer, and complex, respectively. Substituting for C_D and C_C in eq. 6 and rearranging gives

$$\epsilon_C = \frac{A/l - \epsilon_D K_D C_M^2 - \epsilon_M C_M}{K_C[2K_D C_M^3 + C_M^2 + (C_S^0 - C_A^0)C_M]} \qquad (7)$$

The values of ϵ_M, ϵ_D, and K_D required for the solution of eq. 5 and 7 were obtained from separate studies of the amines in cyclohexane solution. The methods described in the preceding paper[5] under the discussion of the limiting slope treatment were used to obtain all of the constants except ϵ_D and K_D for cyclohexylamine. Since ϵ_D of the cyclohexylamine dimer at 2006 mμ appeared to be close to zero, dimerization constants were determined at this wave length and used to calculate values of ϵ_D at 2030 mμ.

Since the values of C_M in this work were always much less than unity, the cubic term of eq. 5 could be neglected without altering the final results. An assumed value of K_C was substituted into the quadratic form of eq. 5 to calculate a set of values of C_M for a series of solutions containing known total concentrations of amine and chloroform. These C_M values and the experimentally determined values of A/l were substituted into eq. 7 to obtain a corresponding set of values of ϵ_C.[7] This procedure was repeated several times using different assumed values of K_C. The standard deviation and the average of each set of ϵ_C values were calculated and plotted against the assumed value of K_C. The best estimate of K_C was obtained from the minimum of the standard deviation plot. The value of ϵ_C corresponding to this value of K_C was obtained from the average ϵ_C plot.

In order to determine the range of K_C values to be substituted into eq. 5, an approximate value of K_C was determined by a graphical method in which self-association of the amine was neglected and the equilibrium concentration of chloroform was assumed to

(6) E. Grunwald and W. C. Coburn, Jr., *J. Am. Chem. Soc.*, 80, 1322 (1958).

(7) An electronic computer was used to obtain solutions of eq. 5 and 7.

be equal to the initial concentration. Equations 5 and 7 then reduce to

$$C_M = \frac{C_A{}^0}{K_C C_S{}^0 + 1} \quad (8)$$

and

$$\epsilon_C = \frac{A/l - \epsilon_M C_M}{K_C C_M C_S{}^0} \quad (9)$$

which, after combining and rearranging, can be written as

$$A/l C_A{}^0 = \frac{1}{K_C} \frac{\epsilon_M - A/l C_A{}^0}{C_S{}^0} + \epsilon_C \quad (10)$$

If $A/l C_A{}^0$ is plotted against $(\epsilon_M - A/l C_A{}^0)/C_S{}^0$, approximate values of K_C and ϵ_C can be obtained from the reciprocal of the slope and the intercept, respectively.

Results

Aromatic Amines. The spectra of 0.107 M solutions of aniline in the cyclohexane–chloroform solvent system at 30.5° are shown in Fig. 1. As the concentration of chloroform increases, the symmetric N–H band at 1493.5 mμ is replaced by a weaker and broader one with a maximum extending from about 1494 to 1501 mμ. At lower temperatures, a distinct maximum occurs at 1501 mμ. Similar changes occur in the region of the asymmetric band near 1450 mμ. The absorbance changes at 1493.5 mμ were used to determine the formation constant of the aniline–chloroform complex. Data and results obtained at several temperatures between 10 and 50° are summarized in Table I. In Fig. 2 the standard deviation of ϵ_C is plotted against K_C for the aniline–chloroform system at three temperatures. Values of K_C determined from the positions

Table I: Aniline–Chloroform Complex in Cyclohexane Solution[a]

CHCl₃, mole/l. at 26°	10°	21.6°	30.5°	41.6°	49.5°
			A/l at 1493.5 mμ[b]		
0.4941[c]	0.1698	0.1688	0.1660	0.1650	0.1622
0.7431[c]	.1634	.1630	.1594	.1588	.1568
1.2336[c]	.1478	.1482	.1458	.1452	.1454
1.7271	.1388	.1386	.1374	.1382	.1390
2.4673	.1260	.1274	.1270	.1276	.1272
3.4542	.1158	.1172	.1172	.1184	.1192
4.9346	.1050	.1068	.1056	.1080	.1080
6.9084	.0970	.0976	.0968	.0988	.0990
8.8823	.0912	.0920	.0914	.0930	.0930
12.2160[c]	.0866	.0874	.0870	.0882	.0886
ϵ_M, l./mole-cm.	1.940	1.905	1.880	1.848	1.826
ϵ_D, l./mole-cm.	0.80	0.80	0.80	0.80	0.80
K_D, l./mole	0.44	0.40	0.36	0.33	0.31
Density correction	1.020	1.006	0.994	0.981	0.971
K_C, l./mole	0.579	0.526	0.500	0.448	0.400
ϵ_C, l./mole-cm.	0.623	0.632	0.630	0.640	0.625
K_C (cor.),[d] l./mole	0.590	0.522	0.500	0.438	0.404

[a] Aniline concentration 0.1074 M at 26°. [b] $A = A_{1493.5\,m\mu} - A_{1610\,m\mu}$; $l = 5.00$ cm. [c] These samples not used in calculation of K_C and ϵ_C. [d] Assuming ϵ_C is 0.630 l./mole-cm. at all temperatures.

of the minima in these plots are summarized in Table I. Since the results obtained with solutions containing low concentrations of chloroform are quite sensitive to experimental error and to small errors in ϵ_M, only the data from solutions containing between about 1.7 and 9 M chloroform were used to determine K_C. Within the limits of experimental error, the values obtained in this manner were consistent with the absorbance data obtained with samples containing as little as 0.4 M or as much as 12.1 M chloroform.

Figure 1. First overtone N–H stretching bands of aniline in cyclohexane–chloroform solutions at 30.5° (5-cm. cells).
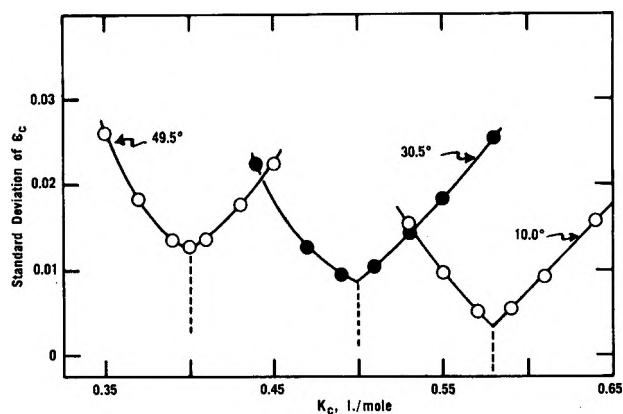

Figure 2. Formation constants of the aniline–chloroform complex.

The values of ϵ_C corresponding to the best estimates of K_C ranged from 0.623 to 0.640 l. mole^{-1} cm.$^{-1}$. Since no systematic variation of ϵ_C with temperature was evident, the average value of 0.630 was used to determine a corrected K_C at each temperature from the ϵ_C vs. assumed K_C plots. The corrected values of K_C differed from the original ones by no more than ±0.011 l. mole^{-1} (Table I).

A plot of log K_C vs. $1/T$ for the aniline–chloroform complex gave a ΔH° value of -1.72 ± 0.12 kcal. mole^{-1}. The comparable value obtained with the uncorrected values of K_C was -1.64 ± 0.16 kcal. mole^{-1}. These error limits represent one standard deviation of the slope of the line. In a following section it will be shown that errors in ϵ_M, ϵ_D, and K_D introduce a further uncertainty of about ±0.10 kcal. mole^{-1} into the determination of ΔH°. When all sources of error are considered, a realistic value for ΔH° is -1.7 ± 0.2 kcal. mole^{-1}.

Formation constants of several other aromatic amine–chloroform complexes at 35° are shown in Table II. The value reported for the p-aminoacetophenone complex is an approximate one determined by the graphical method. The value of ϵ_M for p-aminoacetophenone is subject to considerable error, because the solubility of the amine in cyclohexane is quite low. Since any error in ϵ_M is reflected in K_C, use of the more refined method was not justified.

Table II: Aromatic Amine–Chloroform Complexes in Cyclohexane Solution at 35°

Amine	λ, mμ	ϵ_C, l./mole-cm.	K_C, l./mole	pK_a (H$_2$O)
Aniline	1493.5	0.63	0.47	4.58[a]
p-Phenetidine	1499.5	.76	.65	5.25[a]
p-Chloroaniline	1492.0	.64	.33	4.05[b]
m-Chloroaniline	1490.5	.59	.25	3.52[b]
o-Chloroaniline	1491.5	.43	.16	2.71[b]
p-Aminoaceto-phenone[c]	1485.0	.92	.14	2.19[b]
N-Methylaniline	1485.0	.47	.25	4.85[d]
N-Ethylaniline	1495.0	.38	.23	5.11[d]

[a] N. F. Hall and M. R. Sprinkle, *J. Am. Chem. Soc.*, **54**, 3469 (1932). [b] J. M. Vandenbelt, C. Heinrich, and S. G. Vanden Berg, *Anal. Chem.*, **25**, 726 (1954). [c] Data for this compound treated by graphical method using approximate value of ϵ_M. [d] See ref. 12.

Cyclohexylamine. The first overtone and combination N–H bands of cyclohexylamine in the cyclohexane–chloroform solvent system are shown in Fig. 3.
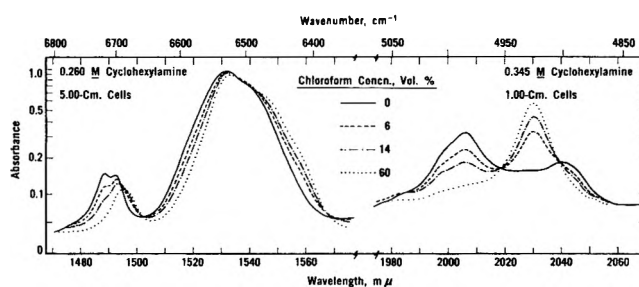
Figure 3. Near-infrared N–H bands of cyclohexylamine in cyclohexane–chloroform solutions at 30°.

In the overtone region the solvent effects are rather small, but in the combination region the addition of chloroform to a cyclohexane solution of the amine results in the progressive disappearance of the band at 2006 mμ and the appearance of a well-resolved new band at 2030 mμ. The combination N–H bands of aromatic amines do not show this pronounced solvent effect,[3] but similar results have been reported by Lohman and Norteman[4] for various aliphatic primary amines.

Formation constants of the cyclohexylamine–chloroform complex calculated from the absorbance changes observed at 2006 and 2030 mμ are summarized in Table III. The constants calculated at 2006 mμ are consistently higher than those obtained at 2030 mμ. The error analysis which follows indicates that this difference represents bias resulting from errors in ϵ_M, ϵ_D, and K_D. The values obtained at 2030 mμ are less sensitive to these errors and are thus the preferred ones.

Table III: Cyclohexylamine–Chloroform Complex in Cyclohexane Solution

Temp., °C.	2006 mμ ϵ_C, l./mole-cm.	2006 mμ K_C, l./mole	2030 mμ ϵ_C, l./mole-cm.	2030 mμ K_C, l./mole
12.0	0.07	1.74	1.71	1.41
17.5	.06	1.50	1.65	1.31
28.0	.06	1.22	1.62	1.04
30.0	.06	1.08	1.59	1.03
38.0	.05	0.94	1.57	0.84
42.5	.06	0.89	1.51	0.84
51.5	.06	0.77	1.49	0.64

Plots of log K_C vs. $1/T$ for the cyclohexylamine complex gave ΔH° values of -3.9 ± 0.2 and -3.6 ± 0.2 kcal. mole^{-1} at 2006 and 2030 mμ, respectively. These values are subject to additional uncertainties of ap-

proximately ±0.3 and ±0.1 kcal. mole^{-1}, respectively, because of possible errors in ϵ_M, ϵ_D, and K_D (see following section). Since the results at 2030 mμ are much less sensitive to these errors, the best value for the heat of formation of the complex is believed to be -3.6 ± 0.3 kcal. mole^{-1}.

Analysis of Errors. The effects of experimental error and of any interactions other than those represented by eq. 1 and 2 are reflected by the precision of the complex constants. Precision limits for ϵ_C were obtained directly from the minimum in the plot of standard deviation of ϵ_C vs. assumed K_C (see Fig. 2). The values varied from ±0.002 to ±0.012 l. mole^{-1} cm.$^{-1}$. These values compare favorably with the estimated experimental error of 0.01 to 0.02 in the measurement of the apparent absorptivities. This condition must be met if the model being used for complex formation is a valid one.[6]

The precision of K_C cannot be determined directly from plots such as those shown in Fig. 2. The values of K_C corresponding to the minima of these plots can be determined exactly, but they still have errors associated with them that are related to the errors in ϵ_C. Precision limits for K_C corresponding to the minimum standard deviation of ϵ_C were obtained from the plot of average ϵ_C vs. assumed K_C. For the aromatic amine complexes the errors in K_C were generally less than ±0.01; for the cyclohexylamine complex the errors ranged from ±0.01 to ±0.05. These errors are consistent with the standard deviation of K_C calculated from the linear $\Delta H°$ plots.

Errors in ϵ_M, ϵ_D, and K_D have relatively little effect upon the precision of ϵ_C, K_C, and $\Delta H°$, but they introduce bias affecting the accuracy of the results. Reasonable errors for ϵ_M, ϵ_D, and K_D were estimated by considering the results of the self-association studies. The calculation of the complex constants were then repeated to obtain the results summarized in Table IV. Since the self-association of aniline has been studied extensively,[5] the estimated errors for ϵ_M, ϵ_D, and K_D were relatively small; their combined effect on the complex constants amounted to only ±0.01 in ϵ_C, ±0.02 in K_C, and ±0.10 in $\Delta H°$. Somewhat larger errors were estimated for the cyclohexylamine system, since the self-association of this amine was not studied exhaustively. At 2006 mμ the uncertainties in ϵ_M, ϵ_D, and K_D correspond to possible errors of ±0.01, ±0.10, and ±0.3 in ϵ_C, K_C, and $\Delta H°$, respectively. At 2030 mμ the corresponding errors are only ±0.01, ±0.05, and ±0.1. Thus, the set of complex constants determined at 2030 mμ is believed to be the more reliable of the two.

The treatment of the data could be refined by cor-

Table IV: Effect of Errors on ϵ_C, K_C, and $\Delta H°$

Factor	Change	$\Delta\epsilon_C$ (30°)	ΔK_C (30°)	$\Delta(\Delta H°)^a$
		Aniline–CHCl₃		
ϵ_D	0.80 to 1.20[b]	+0.005	+0.006	+0.01
K_D	±10%	∓0.004	∓0.005	∓0.04
ϵ_M	±0.5%	±0.003	±0.011	±0.03
		Cyclohexylamine–CHCl₃ at 2006 mμ		
ϵ_D	0.00 to 0.10	+0.001	+0.007	+0.04
K_D	+50%	−0.003	−0.038	−0.10
ϵ_M	±2%	±0.003	±0.062	±0.14
		Cyclohexylamine–CHCl₃ at 2030 mμ		
ϵ_D	±10%	±0.002	∓0.008	∓0.01
K_D	+50%	+0.003	−0.004	−0.06
ϵ_M	±10%	±0.004	∓0.034	∓0.04

^{a} Negative values in this column indicate increases in the heat of formation. ^{b} Correspondingly larger values of K_D were also used. See ref. 5 for discussion of the relation between ϵ_D and K_D.

recting for the effects of chloroform self-association. A dimerization constant of 0.013 l. mole^{-1} has been reported[8] for chloroform in cyclohexane solution at 25°. Using this value to correct our 30.5° data lowered the formation constant only 0.02 l. mole^{-1} and the absorptivity about 0.05 l. mole^{-1} cm.$^{-1}$. Since dimerization constants at other temperatures were not available, the correction was not applied to any of the results shown in Tables I through III.

Discussion

The formation constants at 25° and the associated thermodynamic constants of the chloroform complexes of aniline and cyclohexylamine are summarized in Table V.

Table V: Thermodynamic Data for Chloroform–Amine Complexes

Complex	K_{25}, l./mole	$\Delta F°_{25}$, kcal./mole	$\Delta H°$, kcal./mole	$\Delta S°_{25}$; e.u.
Chloroform–aniline	0.51	+0.41	−1.7 ± 0.2	−7.1 ± 0.7
Chloroform–cyclohexylamine^a	1.10	−0.06	−3.6 ± 0.3	11.9 ± 1.0

^{a} From data obtained at 2030 mμ.

(8) C. F. Jumper, M. T. Emerson, and B. B. Howard, *J. Chem. Phys.*, **35**, 1911 (1961).

The heats of formation of the aniline–chloroform complex and of the aniline dimer[5] are the same within the limits of experimental error. The $\Delta H°$ value for the chloroform complex is also comparable to the value of -1.93 kcal. mole^{-1} reported by Davies[9] for the aniline–water complex in carbon tetrachloride solution.

In a nuclear magnetic resonance study of the chloroform–triethylamine complex in cyclohexane solution, Creswell and Allred[10] found a formation constant of 0.51 l. mole^{-1} at 25° and a $\Delta H°$ of -4.2 kcal. mole^{-1}. A value of -4.2 kcal. mole^{-1} has also been reported for the heat of formation of the diethylamine–chloroform complex in the gas phase.[11] These $\Delta H°$ values are about 10% higher than the value now being reported for the cyclohexylamine complex. The formation constant of the triethylamine complex, however, is about one-half as large as that of the cyclohexylamine complex. This difference probably reflects steric hindrance by the alkyl groups of triethylamine to the approach of a chloroform molecule.

In Fig. 4, log K_C of the aromatic amine–chloroform complexes is plotted against the pK_a of the amines in aqueous solution. The primary amines follow the linear relation

$$\log K_C = 0.247 \text{p}K_a - 1.474 \qquad (11)$$

This relation holds for o-chloroaniline as well as for the meta- and para-substituted derivatives, indicating that steric effects are relatively unimportant in the formation of the o-chloroaniline complex. These results provide direct experimental confirmation for the interpretation of chloroform solvent effects presented previously.[3] For example, much larger effects are observed with p-phenetidine than with p-aminoacetophenone, because the ratio of complexed amine to free amine in chloroform solution is about 8:1 for the first compound and less than 2:1 for the second.

The N-alkylanilines do not follow the linear relation between log K_C and pK_a that characterizes the primary amines. Both N-methylaniline and N-ethylaniline are slightly more basic than aniline,[12] but the formation constants of their chloroform complexes are less than one-half as large as that of the aniline complex. The N-alkyl groups appear to offer substantially greater steric hindrance to formation of the chloroform complexes than to protonation of the amines. The steric effects of the two alkyl groups are quite similar in the formation of the chloroform complexes, but in the dimerization of the amines the effect of the ethyl group must be considerably larger than that of the methyl group. The dimerization
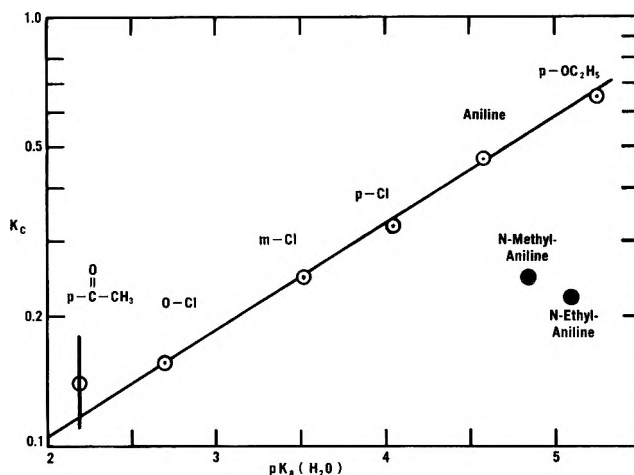
Figure 4. Relation between the formation constant of aromatic amine–chloroform complexes in cyclohexane solution and the pK_a of the amines in aqueous solution.

constants for N-methyl- and N-ethylaniline are approximately 0.30 and 0.15 l. mole^{-1}, respectively.

Kagarise recently reported a formation constant of 0.90 l. mole^{-1} (31°) and a $\Delta H°$ of -3.5 kcal. mole^{-1} for the CDCl$_3$–acetone complex in n-hexane solution.[13] These values are approximately twice as large as the values now being reported for the CHCl$_3$–aniline complex and about equal to those found for the CHCl$_3$–cyclohexylamine complex. Since the basicity of the amines in water is many times greater than that of acetone, it is evident that the linear relation expressed by eq. 11 cannot be used with widely different types of bases.

Using nuclear magnetic resonance spectroscopy, Creswell and Allred[10] found that the chloroform–benzene complex in cyclohexane solution has a formation constant of 0.11 l. mole at 25° and a $\Delta H°$ of -1.97 $\pm$ 0.35 kcal. mole^{-1}. The free N–H bands of the aromatic amines show high frequency shifts of 1 to 2 mμ in cyclohexane solutions containing from 10 to 40 vol. % chloroform. These shifts are believed to arise from the interaction of chloroform with the π-electrons of molecules which are not complexed through the amino group. With higher concentrations of chloroform, the concentration of free amino groups becomes so low that the secondary solvent effect is no

(9) M. Davies, Ann. Rept. Progr. Chem., 43, 5 (1946).

(10) C. J. Creswell and A. L. Allred, J. Phys. Chem., 66, 1469 (1962).

(11) J. D. Lambert, J. S. Clarke, J. F. Duke, C. L. Hicks, S. D. Lawrence, D. M. Morris, and M. G. T. Shane, Proc. Roy. Soc. (London), A249, 414 (1959).

(12) H. C. Brown and A. Cahn, J. Am. Chem. Soc., 72, 2939 (1950).

(13) R. E. Kagarise, Spectrochim. Acta, 19, 629 (1963).

longer observed. The π-electron interaction may persist after the amino group is complexed, but its effect upon the spectrum is not apparent. Since the π-electron interaction results in a very small spectral change, it probably has little effect upon the constants

reported for the amino group interaction. These constants represent the average effects of hydrogen bonding of chloroform to the amino group, irrespective of whether the π-electrons are involved in a secondary interaction.

The Reactions of C_2F_5 and C_3F_7 Radicals with Hydrogen and Deuterium[1]

by G. O. Pritchard and J. K. Foote[2]

Department of Chemistry, University of California, Santa Barbara, Goleta, California
(Received August 26, 1963)

By use of the perfluoroaldehydes as the sources of C_2F_5 and C_3F_7 radicals, the hydrogen abstraction reactions of these radicals with H_2 and D_2 are reinvestigated. The previous anomalously high values for the activation energies of these reactions are confirmed. New data for the reaction $C_2F_5 + D_2 \rightarrow C_2F_5D + D$ are presented.

Introduction

In a previous article[3] the photolysis mechanisms of perfluoroalkylaldehydes were discussed, especially with regard to the H abstraction reactions

$$R_f + R_fCHO \longrightarrow R_fH + R_fCO \qquad (1)$$

relative to the respective radical recombination reactions

$$R_f + R_f \longrightarrow R_{f_2} \qquad (2)$$
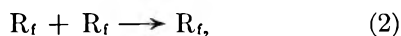
where $R_f = CF_3$, C_2F_5, or C_3F_7. In this work, using C_2F_5CHO and C_3F_7CHO as the radical sources, we have investigated the abstraction reactions of C_2F_5 and C_3F_7 radicals with H_2 and with D_2

$$R_f + H_2 \longrightarrow R_fH + H \qquad (3)$$

and

$$R_f + D_2 \longrightarrow R_fD + D \qquad (4)$$

Reactions 3 and 4 have been quite extensively studied using perfluoroalkyl ketones as the radical sources: CF_3 with H_2 and D_2,[4] C_2F_5 with H_2,[5] C_3F_7 with H_2 and D_2,[6] and C_3F_7 with D_2.[7] The reactions of CF_3 radicals with H_2 and D_2 have also been investi-

gated, using hexafluoroazomethane as the radical source.[8]

Calvert[9] has pointed out that the activation energies obtained for the reactions of C_3F_7 with H_2 and D_2[6,7] (and subsequently $C_2F_5 + H_2$[5]) are anomalously high, when compared to the general pattern of alkyl and perfluoroalkyl H abstraction reactions. It therefore seemed desirable to redetermine values of E_3 and E_1 for $R_f = C_2F_5$ and C_3F_7, using a different photolytic

(1) This work was supported by a grant from the National Science Foundation and is based in part on a thesis submitted by J. K. F. in partial fulfillment of the requirements for the M.A. degree.

(2) Department of Chemistry, University of California, Riverside, California.

(3) G. O. Pritchard, G. H. Miller, and J. K. Foote, *Can. J. Chem.*, **40**, 1830 (1962).

(4) P. B. Ayscough and J. C. Polanyi, *Trans. Faraday Soc.*, **52**, 960 (1956).

(5) S. J. W. Price and K. O. Kutschke, *Can. J. Chem.*, **38**, 2128 (1960).

(6) G. H. Miller and E. W. R. Steacie, *J. Am. Chem. Soc.*, **80**, 6486 (1958).

(7) G. Giacometti and E. W. R. Steacie, *Can. J. Chem.*, **36**, 1493 (1958).

(8) G. O. Pritchard, H. O. Pritchard, H. I. Schiff, and A. F. Trotman-Dickenson, *Trans. Faraday Soc.*, **52**, 849 (1956).

(9) J. G. Calvert, *Ann. Rev. Phys. Chem.*, **11**, 41 (1960).

source of the radicals, and especially in view of the fact that in the C_3F_7 radical work C_6F_{14} was not measured directly, but estimated by radical balance procedures.[6,7]

Experimental

The apparatus, purification of fluorine-containing materials, and the method of analysis have been described previously[3] (volume of fully illuminated reaction cell = 152.6 cc.).

D_2 was purchased from Air Reduction Co. and used without further purification. Analysis on the mass spectrometer indicated 97.3% D_2, 1.8% H_2, and 0.9% HD based on identical sensitivities for the m/e peaks at 2, 3, and 4. H_2 was obtained from Victor Equipment Co. and purified by passing it through a Pd thimble at 300–350°. No detectable impurities were found by analysis on the mass spectrometer.

In the experiments containing added D_2, mixtures of R_fH and R_fD were analyzed by using the relative peak heights at m/e 51 (CF_2H^+) and 52 (CF_2D^+), assuming equal sensitivities on the mass spectrometer. In some cases the C_4F_{10} and C_6F_{14} samples contained small traces ($< 1\%$) of the aldehyde. This was corrected for using the 29 (CHO^+) ion peak.

Results

C_2F_5 with H_2 and D_2. The results of these experiments are presented in Tables I and II.

Table I: Photolysis of C_2F_5CHO with H_2

Time, sec.	Temp., °K.	$[C_2F_5CHO]_0{}^a$	$[H_2]_0{}^a$	$\bar{R}_{C_2F_5H}{}^b$	$\bar{R}_{C_4F_{10}}{}^b$	$k_3/k_2^{1/2c}$
910	419	99.6	581	141	95.0	0.512
240	441	78.2	624	188	79.1	1.41
660	459	88.3	603	213	70.6	1.47
300	465	72.8	583	276	89.0	2.39
210	491	78.1	375	369	103	3.91
120	520	73.7	290	646	141	9.64
120	539	93.4	386	1340	183	15.8
60.0	568	82.1	380	1860	193	24.0
50.5	586	81.6	298	2170	187	37.4

^{a} Mole cc.$^{-1}$ $\times$ 10^8. ^{b} Mole cc.$^{-1}$ sec.$^{-1}$ $\times$ 10^{12}. ^{c} Mole$^{-1/2}$ cc.$^{1/2}$ sec.$^{-1/2}$.

For the reaction of C_2F_5 with H_2 we may write

$$k_3/k_2^{1/2} = \bar{R}_{C_2F_5H}/\bar{R}_{C_4F_{10}}^{1/2}[H_2] -$$
$$k_1[C_2F_5CHO]_{av}/k_2^{1/2}[H_2]$$

where $\bar{R}$ denotes mean rate of formation, and $[C_2F_5CHO]_{av}$ denotes average aldehyde concentration during a run. Aldehyde decomposition varied between 10

and 30% (mean = 20%) based on $(C_2F_5H + 2C_4F_{10})/(C_2F_5CHO)_0$. The ratio $k_1/k_2^{1/2}$ has been determined and this method of treatment has been discussed previously.[3] In the experiments reported in this paper the consumption of H_2 or D_2 was limited to less than 0.5% in any run.

A least-squares treatment of an Arrhenius plot of the above expression yields

$$k_3/k_2^{1/2} = (1.59 \pm 0.16)10^6 \times$$
$$\exp(-12,400 \pm 200/RT) \text{ mole}^{-1/2} \text{ cc.}^{1/2} \text{ sec.}^{-1/2}$$

For the reaction of C_2F_5 with D_2 we have

$$k_4/k_2^{1/2} = \bar{R}_{C_2F_5D}/\bar{R}_{C_4F_{10}}^{1/2}[D_2]$$

Aldehyde decompositions varied between 14 and 44% (mean = 23%). A virtually negligible correction has been applied to allow for the small decrease in D_2 concentration. A least-squares treatment of the Arrhenius plot of the expression gives

$$k_4/k_2^{1/2} = (2.83 \pm 0.31)10^5 \times$$
$$\exp(-12,600 \pm 200/RT) \text{ mole}^{-1/2} \text{ cc.}^{1/2} \text{ sec.}^{-1/2}$$

We may also obtain a rate constant ratio for the reaction of C_2F_5 with C_2F_5CHO. The data give

$$k_1/k_2^{1/2} = \bar{R}_{C_2F_5H}/\bar{R}_{C_4F_{10}}^{1/2}[C_2F_5CHO]_{av}$$
$$= (5.5 \pm 1.5)10^3 \times \exp(-4900 \pm 200/RT)$$
$$\text{mole}^{-1/2} \text{ cc.}^{1/2} \text{ sec.}^{-1/2}$$

which is in good agreement with our previously determined value in experiments on the aldehyde alone,[3] where

$$k_1/k_2^{1/2} = (3.09 \pm 0.12)10^3 \times$$
$$\exp(-4500 \pm 200/RT) \text{ mole}^{-1/2} \text{ cc.}^{1/2} \text{ sec.}^{-1/2}$$

Finally, the rate constant ratio k_1/k_4 is given in Table II, where

$$k_1/k_4 = \bar{R}_{C_2F_5H}[D_2]/\bar{R}_{C_2F_5D}[C_2F_5CHO]_{av}$$

A least-squares treatment of the Arrhenius plot yields

$$k_1/k_4 = (1.55 \pm 0.10)10^{-2} \times \exp(7900 \pm 100/RT)$$

From our previous values[3] we may derive $E_4 - \frac{1}{2}E_2 = 12,400 \pm 300$ cal. mole^{-1} and $A_4/A_2^{1/2} = 2.0 \times 10^5$ mole$^{-1/2}$ cc.$^{1/2}$ sec.$^{1/2}$. There is excellent agreement between the differently derived sets of values.

C_3F_7 with H_2 and D_2. The results of these experiments are presented in Tables III and IV. The corresponding rate constant ratios which can be derived from these data are

Table II: Photolysis of C_2F_5CHO with D_2

Temp., °K.	Time, sec.	$[C_2F_5CHO]_0{}^a$	$[D_2]_0{}^a$	$\bar{R}_{C_2F_6H}{}^b$	$\bar{R}_{C_2F_6D}{}^b$	$\bar{R}_{C_4F_{10}}{}^b$	$k_4/k_2{}^{1/2c}$	$k_1/k_2{}^{1/2c}$	k_1/k_4
408	1500	113	385	135	1.66	100	0.0431	15.3	356
419	1080	92.1	504	131	3.76	76.3	0.0855	17.8	208
442	960	94.7	560	124	7.78	75.6	0.160	17.6	109
458	300	87.5	492	222	16.7	103	0.335	27.1	81.1
481	310	86.2	421	204	23.2	121	0.507	23.6	46.9
510	420	75.8	358	285	41.3	101	1.15	43.8	38.1
566	90	73.8	389	586	177	202	3.21	60.2	18.8
612	70	68.0	288	986	368	179	9.58	119	12.4

^{a} Mole cc.$^{-1}$ $\times$ 10^8. ^{b} Mole cc.$^{-1}$ sec.$^{-1}$ $\times$ 10^{12}. ^{c} Mole$^{-1/2}$ cc.$^{-1/2}$ sec.$^{-1/2}$.

Table III: Photolysis of C_3F_7CHO with H_2

Temp., °K.	Time, sec.	$[C_3F_7CHO]_0{}^a$	$[H_2]_0{}^a$	$\bar{R}_{C_3F_7H}{}^b$	$\bar{R}_{C_6F_{14}}{}^b$	$k_3/k_2{}^{1/2c}$
430	300	99.2	545	225	133	0.662
431	300	94.2	553	217	132	0.654
462	120	84.0	490	283	147	0.855
494	120	83.8	390	448	153	2.82
549	40	72.2	344	1050	270	8.99
559	50	63.3	309	1100	228	13.7
591	30	80.4	251	1850	262	26.8
592	25	65.0	276	1600	186	28.4

^{a} Mole cc.$^{-1}$ $\times$ 10^8. ^{b} Mole cc.$^{-1}$ sec.$^{-1}$ $\times$ 10^{12}. ^{c} Mole$^{-1/2}$ cc.$^{1/2}$ sec.$^{-1/2}$.

$$k_4/k_2{}^{1/2} = \bar{R}_{C_2F_5D}/\bar{R}_{C_6F_{14}}{}^{1/2}[D_2]$$

$$= (9.6 \pm 0.5)10^5 \times \exp(-14,000 \pm 100/RT)$$
$$\text{mole}^{-1/2} \text{ cc.}^{1/2} \text{ sec.}^{-1/2}$$

The aldehyde decomposition varied between 5 and 12% (mean = 8.5%).

$$k_1/k_2{}^{1/2} = \bar{R}_{C_3F_7H}[C_3F_7CHO]_{av}$$

$$= (9.5 \pm 2.0)10^3 \times \exp(-5500 \pm 200/RT)$$
$$\text{mole}^{-1/2} \text{ cc.}^{1/2} \text{ sec.}^{-1/2}$$

This is only in fair agreement with our previous results, obtained by the photolysis of C_3F_7CHO alone.[3]

Table IV: Photolysis of C_3F_7CHO with D_2

Temp., °K.	Time, sec.	$[C_3F_7CHO]_0{}^a$	$[D_2]_0{}^a$	$\bar{R}_{C_3F_7H}{}^b$	$\bar{R}_{C_3F_7D}{}^b$	$\bar{R}_{C_6F_{14}}{}^b$	$k_4/k_2{}^{1/2c}$	$k_1/k_2{}^{1/2c}$	k_1/k_4
438	610	93.4	415	177	4.36	102	0.104	19.9	191
441	600	94.0	459	180	5.37	100	0.117	20.3	174
466	250	103	500	295	15.7	152	0.255	24.0	94.1
473	240	93.0	510	235	17.4	132	0.297	22.7	76.4
506	190	73.9	356	316	34.3	141	0.812	37.6	46.3
528	400	77.2	378	383	66.9	132	1.55	47.9	30.9
532	100	74.4	371	401	74.5	172	1.53	42.2	27.6
567	50	63.6	333	783	209	236	4.09	82.6	20.2
570	70	79.6	310	890	190	197	4.38	82.9	18.9

^{a} Mole cc.$^{-1}$ $\times$ 10^8. ^{b} Mole cc.$^{-1}$ sec.$^{-1}$ $\times$ 10^{12}. ^{c} Mole$^{-1/2}$ cc.$^{1/2}$ sec.$^{-1/2}$.

$$k_3/k_2{}^{1/2} = \bar{R}_{C_3F_7H}/\bar{R}_{C_6F_{14}}{}^{1/2}[H_2] -$$
$$k_1[C_3F_7CHO]_{av}/k_2{}^{1/2}[H_2]$$
$$= (7.2 \pm 1.2)10^5 \times \exp(-12,100 \pm 200/RT)$$
$$\text{mole}^{-1/2} \text{ cc.}^{1/2} \text{ sec.}^{-1/2}$$

Aldehyde decomposition varied between 8 and 15% (mean = 11%). The ratio $k_1/k_2{}^{1/2}$ was obtained from experiments in which C_3F_7CHO was photolyzed alone.[3]

$$k_1/k_2{}^{1/2} = (1.86 \pm 0.14)10^3 \times$$
$$\exp(-4000 \pm 300/RT) \text{ mole}^{-1/2} \text{ cc.}^{1/2} \text{ sec.}^{-1/2}$$

There appears to be a compensating effect between the respective values of the Arrhenius parameters in the two determinations of $k_1/k_2{}^{1/2}$.

The rate constant ratio in Table IV, k_1/k_4 is given by

Table V: Comparison of R_f with H_2, D_2, and CH_4 Data

R_f	$E_a - \frac{1}{2}E_2{}^a$	$A_a/A_2{}^{1/2b}$	Ref.	$E_a - \frac{1}{2}E_2{}^a$	$A_a/A_2{}^{1/2b}$	Ref.	A_4/A_3	$E_a - \frac{1}{2}E_2{}^a$	$A_a/A_2{}^{1/2b}$	Ref.
	H₂			D₂			CH₄			
CF_3	9.5 ± 0.7	14	4	10.2 ± 0.7	5.9	4	0.41	10.3 ± 0.2	10	c
	8.6 ± 0.5	4.2–8.9	8[d]	9.5 ± 0.4	2.9–6.1	8[d]	0.69[e]	10.4	40	f
C_2F_6	11.9	53	5					10.6	4.2	5
	12.4 ± 0.2	158	g	12.6 ± 0.2	28	g	0.18			
C_3F_7	12.3 ± 0.4	44	6	13.8 ± 0.5	60	6	1.37			
						6	1.32[e]			
				12.9 ± 0.8	49	7[h]		9.5 ± 0.5	0.97	7
	12.1 ± 0.2	72	g	14.0 ± 0.1	96	g	1.33			

[a] $E_a - \frac{1}{2}E_2$ in kcal. mole⁻¹. [b] $A_a/A_2{}^{1/2}$ in mole⁻¹/² cc.¹/² sec.⁻¹/² × 10⁻⁴. [c] P. B. Ayscough, J. C. Polanyi, and E. W. R. Steacie, *Can. J. Chem.*, **33**, 743 (1955). [d] E_a values are given for $CF_3 + n$-butane reaction as reference point. $A_a/A_2{}^{1/2}$ values are for either butane or ethane reaction as reference point. See G. O. Pritchard and G. H. Miller, *J. Chem. Phys.*, **35**, 1135 (1961), and P. B. Ayscough and E. W. R. Steacie, *Can. J. Chem.*, **34**, 103 (1956). [e] Direct experimental determination in competitive system $R_f + H_2 + D_2$. [f] R. E. Dodd and J. W. Smith, *J. Chem. Soc.*, 1465 (1957). [g] This work. [h] Competitive experiments, $C_3F_7 + D_2 + CH_4$.

$$k_1/k_4 = \bar{R}_{C_3F_7H}[D_2]/\bar{R}_{C_3F_7D}[C_3F_7CHO]_{av}$$

$$= (8.5 \pm 0.4)10^{-3} \times \exp(8600 \pm 100/RT)$$

Combining with our previous result[3] we obtain $E_4 - \frac{1}{2}E_2 = 12,600 \pm 400$ cal. mole⁻¹ and $A_4/A_2{}^{1/2} = 2.2 \times 10^4$ mole⁻¹/² cc.¹/² sec.⁻¹/². These results are again only in fair agreement with those obtained for these parameters by determining $k_4/k_2{}^{1/2}$ directly.

Discussion

The per cent decompositions of the aldehydes in this work tend to be somewhat high for the rigorous use of the steady state approximation. Due to the low activation energies required for the abstraction of the aldehydic hydrogen (reaction 1), the aldehydes are not particularly good sources of C_2F_5 and C_3F_7 radicals for studies of reactions 3 and 4, which have considerably higher activation energies. Because of this factor, before there is sufficient build-up of product from reaction 3 or 4 for analysis, more aldehyde is decomposed than is desirable. The aldehyde is not only consumed in the initial photolytic step, but by any reaction between an atom or a radical with an aldehyde molecule, e.g., reaction 1; this is a chain propagating step, and the rate of aldehyde decomposition increases greatly with rise in temperature. This is offset somewhat by the relative increase in rate of reactions 3 and 4 over reaction 1, with temperature. However, even at the highest temperatures it did not seem feasible to conduct experiments of less than ∼30 sec. in duration, leading to about 10% aldehyde decomposition. The ratios of the rate constants for reactions 1 and 4 are given in Tables II and IV. There is a factor of over 10² involved at the lowest temperatures.

In Table V we have compared the available data for $E_a - \frac{1}{2}E_2$ (a = abstraction) and $A_a/A_2{}^{1/2}$ for the re-

actions of CF_3, C_2F_5, and C_3F_7 radicals with H_2, D_2, and CH_4. The various values of E_a can be compared directly, as, although E_2 may have a small positive value, it is invariant for the three radical species.[10] It is seen that the "high" values for E_a for the reactions of C_2F_6 and C_3F_7 radicals with H_2 and D_2 are confirmed. For the reactions of the radicals with CH_4, the value of E_a appears to be constant. Similarly, for other substrates R–H, the value of E_a appears to be independent of R_f.[3,10,11] In all cases, ΔE_a for R_f radical attack on D_2 and H_2 is within the limits of the difference in zero-point energy between the two molecules.

The general pattern of the results suggests that there is some compensation between the Arrhenius parameters obtained in our $C_2F_5 + D_2$ system, and that they are low. It appears that $E_a - \frac{1}{2}E_2$ should be about 1 kcal. mole⁻¹ greater, making the ratios $A_a/A_2{}^{1/2}$ and A_4/A_3 correspondingly greater. The errors quoted are the deviations obtained in the least-squares treatment, and are not meant to signify that the values are absolute.

Simple collision theory predicts that the ratio of the frequency factors $A_4/A_3 = 2^{-1/2}$. The values given in Table V are for the cases in which the Arrhenius parameters were derived in the same manner, or for competitive systems. The correlation for the CF_3 radical reactions is good, but the C_3F_7 results are consistently high. (Miller and Steacie[6] erroneously state that their experimental values agree with the ratio of the relative collision numbers, citing $2^{1/2}$, rather than $2^{-1/2}$.)

(10) G. O. Pritchard, G. H. Miller, and J. R. Dacey, *Can. J. Chem.*, **39**, 1968 (1961).

(11) G. O. Pritchard, Y. P. Hsia, and G. H. Miller, *J. Am. Chem. Soc.*, **85**, 1568 (1963); G. O. Pritchard and R. L. Thommarson, *J. Phys. Chem.*, **68**, 568 (1964).
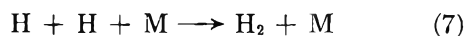
In the perfluoro ketone systems[4-6] the fate of the H and D atoms generated in reactions 3 and 4 was not established. In the CF$_3$ radical system Ayscough and Polanyi[4] contend that rather than
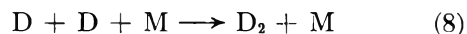
$$R_f + H + (M) \longrightarrow R_fH + (M) \qquad (5)$$

and

$$R_f + D + (M) \longrightarrow R_fD + (M) \qquad (6)$$
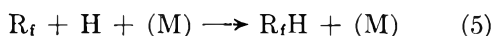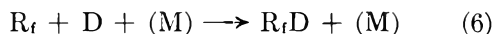
being the fate of the H and D atoms, they are removed from the system by

$$H + H + M \longrightarrow H_2 + M \qquad (7)$$

and

$$D + D + M \longrightarrow D_2 + M \qquad (8)$$

and that all four reactions require a third body. In the C$_2$F$_5$ and C$_3$F$_7$ radical systems[5,6] the opposite point of view is taken, that reactions 5 and 6 do not require a third body, and as a limiting value, the rates of formation of R$_f$H and R$_f$D were divided by a factor of two, in order to obtain the true rates of formation of these products in reactions 3 and 4. It has been assumed that whichever standpoint is taken, the derived values of E_a are unaffected, but the rate constant ratios $k_a/k_2^{1/2}$, and thus the pre-exponential ratios $A_a/A_2^{1/2}$, may vary between a factor of one and two. However, this is an oversimplification of the situation.[12]

In the present work it was anticipated that the H and D atoms would be removed rapidly by

$$H + R_fCHO \longrightarrow H_2 + R_fCO \qquad (9)$$

and

$$D + R_fCHO \longrightarrow HD + R_fCO \qquad (10)$$
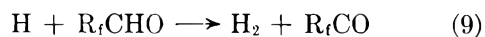
In the C$_3$F$_7$CHO + D$_2$ mixtures we analyzed for HD enrichment in the D$_2$ at the end of the runs.

Values varied from 60 to 100% HD formation based on C$_3$F$_7$D produced. It thus appears that reactions 9 and 10 are the main fates of H and D atoms in the aldehyde systems. It should be pointed out that the decomposition of the formyl radical

$$CHO \longrightarrow CO + \overset{\cdot}{H}$$
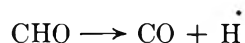
followed by the exchange reaction

$$H + D_2 \longrightarrow HD + D$$
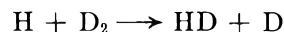
will also lead to HD enrichment.

Finally, we may comment on two further types of errors occurring in our experiments, which render them less reliable than the perfluoro ketone systems. Firstly, in the experiments at higher per cent decompositions, especially so in the C$_2$F$_5$CHO systems, possible loss of products may occur due to subsequent reactions. In the H$_2$ systems, H + C$_2$F$_5$H $\rightarrow$ H$_2$ + C$_2$F$_5$ can occur, and some of the radicals released may eventually dimerize to C$_4$F$_{10}$. In the D$_2$ systems, D and H (from CHO $\rightarrow$ CO + H) atoms may attack the C$_2$F$_5$H and C$_2$F$_5$D which is produced. In view of the rapid occurrence of reactions 9 and 10, these effects are probably minor, but not negligible. They may help to account for the apparently low E_a obtained in the C$_2$F$_5$ + D$_2$ system.[13]

Secondly, if reactions 5 and 6 compete significantly with reactions 9 and 10 as modes of removal of H and D atoms, errors will be introduced due to the differing temperature dependences of the respective pairs of reactions.

A comparison of the various $A_a/A_2^{1/2}$ ratios (excluding C$_2$F$_5$ + D$_2$) in Table V indicates that reactions 7 and 8 may not be insignificant in the perfluoro ketone systems.

(12) K. O. Kutschke, Can. J. Chem., in press.

(13) We are indebted to a referee for discussion on this point.

Polyfunctionality and Equilibruim Selectivity Coefficient of Ion-Exchange System. Reaction of Alkali Metal Cations with Phosphoric Acid Resins[1]

by H. Ti Tien

Department of Chemistry, Northeastern University, Boston 15, Massachusetts (Received September 6, 1963)

The equilibrium selectivity coefficients for the alkali metal cations for polymers containing strongly acidic groups follow the Hofmeister series. The order is inverted, however, for polymers having weakly acidic groups. Using phosphoric acid resins, the order of selectivity has been shown to be a function of pH of the media used in the exchange reactions. The order of equilibrium selectivity coefficients at pH 6.7 and 8.5 is Cs > Rb > K > Na > Li. At pH 10 the order is Cs > Rb > K > Li > Na, whereas at pH 12.6 the order of affinity is quite different, being Li > Na > Rb $\simeq$ Cs > K. The reasons for these inversions are advanced. An equation is presented which enables one to predict the orders of selectivity for such polyfunctional systems. A possible application of this phenomenon is also indicated.

Introduction

Stoichiometric equations for cation-exchange reaction may be represented as

$$C^+ + NaR = CR + Na^+ \qquad (1)$$
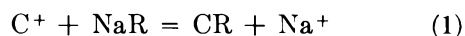
where R denotes ion-exchange polymer containing fixed functional groups and C^+ and Na^+ are the exchanging cations. The thermodynamic equilibrium constant for the reaction is, therefore, defined by the familiar expression

$$K = \frac{[CR][Na^+]f_{CR}\,f_{Na^+}}{[NaR][C^+]f_{NaR}\,f_{C^+}} \qquad (2)$$

It is well-known that the major difficulty lies in our inability to evaluate the activity coefficients of the ions in the polymer phase. Hence, the thermodynamic equilibrium constant K cannot be evaluated rigorously at present.[2] Nevertheless, a useful and measurable quantity has been defined by the workers in the field of ion-exchange resins. This quantity is known as the equilibrium selectivity coefficient and it is defined by

$$K_{Na}^c = \frac{[CR][Na^+]}{[NaR][C^+]} \qquad (3)$$

where the superscript c refers to the exchanging species, and the subscript indicates the reference cation, Na^+ in the present case.

Many experiments have shown that the equilibrium selectivity coefficient of a cation-exchange polymer is influenced by many factors such as (a) the structure of the polymer, (b) the nature of the functional group, and (c) mole fraction of the exchanging cations in the polymer phase.[3-6] The equilibrium selectivity order for the alkali metal cations is usually either that of Hormeister series,[7] or the order which follows the crystal radii.[6,8] Not infrequently, however, neither of these series is observed for the alkali metal cations. Bregman,[5] in studying a certain phosphonic acid resin as a function of pH, found that at low pH values potassium is preferred over sodium, whereas at high pH the reverse is the case. This is particularly true with the biological systems[9,10] and complex natural and synthetic

(1) The experimental work was done at Department of Basic Research, Eastern Pennsylvania Psychiatric Institute, Philadelphia, Pa., while the author was on the staff, 1957–1963.

(2) R. Kunin, "Ion Exchange Resins," John Wiley and Sons, Inc., New York, N. Y., 1958, pp. 20–26.

(3) G. E. Boyd, J. Schubert, and A. W. Adamson. J. Am. Chem. Soc., 69, 2818 (1947).

(4) H. P. Gregor and J. I. Bregman, J. Colloid Sci., 6, 232 (1951).

(5) J. I. Bregman, Ann. N. Y. Acad. Sci., 57, 125 (1953).

(6) C. E. Marshall and G. Garcia, J. Phys. Chem., 63, 1663 (1959).

(7) O. D. Bonner, ibid., 59, 719 (1955).

(8) H. P. Gregor, M. J. Hamilton, R. J. Oza, and F. Bernstein, ibid., 60, 266 (1956).

aluminosilicates.[11-13] It has been suggested that the reversal of the Hofmeister series is connected with the interaction between the cation and the anion. The origin of such reversals has been discussed by Robinson and Harned.[14,15] Little explanation, however, is offered in the literature concerning the "intermediate" orders (i.e., orders other than the ones which follow either the crystal radii or the Hofmeister series.) excepting the hypothesis advanced recently by Eisenman, Rudin, and Casby[16] and Ling.[17] Their hypothesis rests upon, among other things, the changing field strength of the fixed exchange sites, which in turn depend on the interaction between the cation and anion, and cation and solvent water. Hence, according to their hypothesis, the equilibrium selectivity order of a polymer is determined by the charge and the polarizing power of the cation and the polarizability of the fixed anionic sites, and that of the solvent medium. In regard to the detailed discussion of Rudin, Eisenman, Casby, and Ling's hypothesis, their original papers should be consulted. The purpose of this paper is to present a different approach, using phosphoric acid ion-exchange resins as a model, to offer an alternative explanation for the existence of these intermediate orders.

Experimental

Phosphoric acid ion-exchange resins manufactured by the Chemical Process Co., Redwood, Calif., under the trade name Duolite C-65 were used. It is a cation-exchange resin having phosphoric acid groups attached to an inert hydrocarbon matrix. The resin as received was in the hydrogen form. It was conditioned by alternating treatment with 1 N caustic soda and 1 N hydrochloric acid. At the end of the third cycling, the resin was washed with deionized water, converted into sodium form, and air-dried. All solutions used in the experiment were prepared from reagent grade chemicals and deionized water. The establishment of equilibrium was carried out by contacting the resin in the sodium form with the chloride solution of various alkali metals. Four sets of solutions were used with various cations (i.e., Li$^+$, K$^+$, Rb$^+$, Cs$^+$) to Na$^+$ ratios at 1:9, 3:7, 5:5, 7:3, and 9:1. Solutions (0.1 N) of various hydroxides were used for the experiment at pH 12.6. The exchange capacities at various pH values were evaluated by the method suggested by Gregor and Bregman.[18] A number of 1.0-g. portions of resin (H-form) were weighed into polyethylene bottles containing 100 ml. of 5 N NaCl. Different amounts of standard (0.5 N) NaOH solution were added to each bottle, which was then shaken for 48 hr. To confirm the polyfunctional nature of the resin, a sample of Duolite C-65 was titrated rapidly

in 0.1 N KCl in the usual manner. The pH of all solutions was measured employing a Beckman pH meter, Model G. The equilibrium selectivity values were determined with the aid of radioactive sodium-22 as the tracer. After allowing sufficient time for the attainment of equilibrium, as indicated by the constant number of counts, the resin was then separated from the solution phase. The relative quantity of sodium in the resin phase was detected using a Nuclear-Chicago scintillation well detector and scaler. Knowing the exchange capacity of the resin at the given pH, the concentration of the exchanging cation, C$^+$, in the resin phase was obtained by difference. The equilibrium selectivity coefficients were then calculated using eq. 3.

Results

Figure 1 shows the titration curve for the phosphoric acid resin used in the present study. The exchange capacities at various pH values are given in Table I.
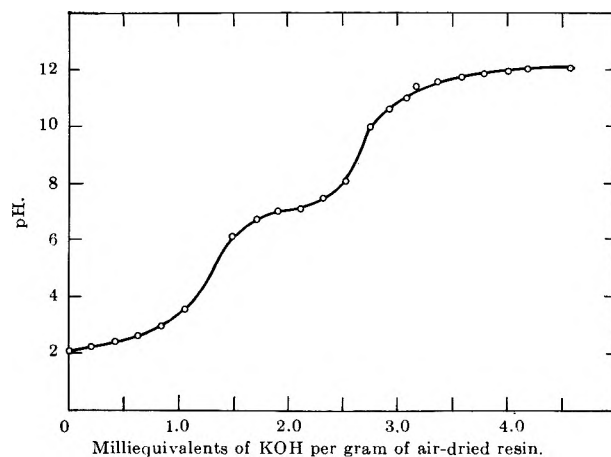

Figure 1. Titration characteristics of phosphoric acid ion exchanger in 0.1 N KCl.

(9) K. Hutschneker and H. Deuel, Helv. Chim. Acta, 39, 1038 (1956).

(10) R. Hober, "Physical Chemistry of Cells and Tissues," Blakiston Co., Philadelphia, Pa., 1950, pp. 289–290 and 313–314.

(11) G. Wiegner and H. Jenny, Kolloid-Z., 42, 270 (1927).

(12) P. Schachtschabel, Kolloid-Beih., 51, 109 (1940).

(13) H. Jenny and R. F. Reitemeier, J. Phys. Chem., 39, 593 (1935).

(14) R. A. Robinson and H. S. Harned, Chem. Rev., 419 (1941).

(15) H. T. Tien, J. Phys. Chem., 67, 532 (1963).

(16) (a) G. Eisenman, D. O. Rudin, and J. Casby, paper presented before the 10th Annual Conference on Electrical Technique in Medicine and Biology of the AIEE, ISA, and IRE, Boston, Mass., November 8, 1957; (b) G. Mattock, "pH Measurement and Titration," Macmillan Co., New York, N. Y., 1961, pp. 130–134.

(17) G. N. Ling, J. Gen. Physiol., 43, 149 (1960).

(18) H. P. Gregor and J. I. Bregman, J. Am. Chem. Soc., 70, 2370 (1948).

Table I

pH	Capacity, mequiv./g. of air-dried resin
6.7	2.1
8.5	2.6
10.0	3.0
12.6	3.9

Equilibrium selectivity values for the five alkali metal cations, at four different pH values, are tabulated in Table II. The reference cation used in all cases was Na^+.

Table II: Equilibrium Selectivity Coefficients, K_{Na}^c, at Various pH Values

Cation	6.7	8.5	10.0	12.6
Li^+	0.95	0.98	1.1	1.2
Na^{+a}	1.00	1.00	1.00	1.00
K^+	2.5	1.6	1.2	0.76
Rb^+	7.0	3.0	2.1	0.90
Cs^+	19.0	5.5	3.2	0.90

a Reference cation.

Discussion

In studies made with synthetic organic resins at moderate cross linking, the selectivity coefficient values have been found to be nearly constant.[2] This is most likely when the exchange is attempted between exchanging cations having similar properties. It can be seen from eq. 3 that the preference of one cation over the other is reflected in the K_{Na}^c value. Whenever the K_{Na}^c value is greater than unity, it simply means that cation "C" is preferred by the resin exchanger. It will be obvious that in an ideal case a log–log plot of $[CR]/[NaR]$ vs. $[Na^+]/[C^+]$ (Na^+ being the reference cation; C^+ represents either Li^+, K^+, Ru^+, or Cs^+) should yield a straight line with the slope equal to unity. Figure 2 shows a typical plot from the data obtained at pH 6.7. Similar linear relationships exist at other pH values. This implies that the selectivity coefficients obtained in the present study were not affected by the ion fraction in the resin phase over the range of resin composition examined. This fact greatly simplified the interpretation which follows.

It is evident from Table II that at pH 6.7 and 8.5 the order of affinity is Cs > Rb > K > Na > Li. At pH 10, the order is Cs > Rb > K > Li > Na, whereas at pH 12.6, the order of affinity is quite different, being Li > Na > Rb = Cs > K. Before
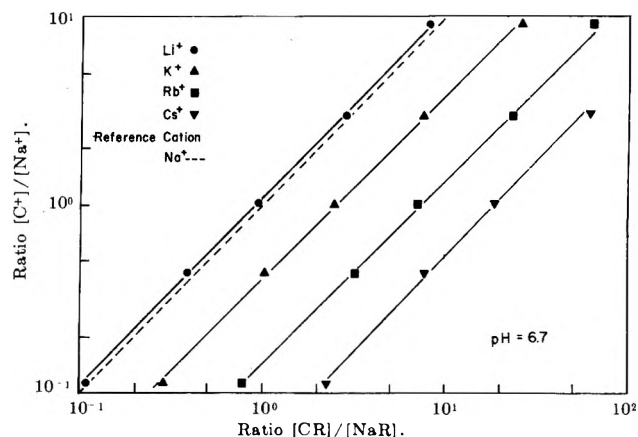

Figure 2. The exchange reaction of sodium ion vs. other alkali metal cations on phosphoric acid ion exchanger.

proceeding to explain the "intermediate" orders observed in this study based upon the heterogeneity of the exchanging groups, it would be more meaningful to review briefly what are the orders generally observed in connection with the synthetic organic exchangers having "theoretically" homofunctional groups. The nature of the functional groups may be roughly divided into "strongly" acidic and "weakly" acidic. At moderate cross linking a resin containing strongly acidic groups such as sulfonic acid resin (e.g., Dowex 50) gives a Hofmeister series, namely, Cs > Rb > K > Na > Li.[7] On the other hand, in a resin having weakly acidic groups such as carboxylic acid resin (e.g., IRC-50), the equilibrium selectivity order follows the crystal radii sequence, Li > Na > K > Rb > Cs.[5,6,8] The exchange resin used in the present study is polyfunctional, having mixed functional groups, as can be seen from the titration curve (Fig. 1). It is reasonable to assume that the first dissociable group, being strongly acidic, should give an equilibrium selectivity order of the Hofmeister series. Analogously, the second dissociable group, being weakly acidic, should give an order following the crystal radii sequence. To explain the observed intermediate orders at pH 10.0 and 12.6, it is, therefore, postulated that there are only two fundamental orders in nature, namely, the Hofmeister series and the inverse. Any other order observed may be explained on the basis of polyfunctionality of the system. If the above postulation is granted, it would be a simple matter to show that such is the case for the orders observed with the phosphoric acid resin at various pH values. To test this hypothesis, eq. 1 is rewritten as

$$C^+ + xNaR_1 + (1 - x)NaR_2 = xCR_1 +$$

$$(1 - x)CR_2 + Na^+ \quad (4)$$
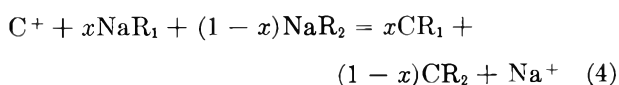
where R_1 and R_2 denote first and second dissociable groups, and x is the fraction of R_1 and $(1 - x)$ is the fraction of R_2. The equilibrium selectivity values K_{Na}° are then expressed by the equation

$$\log K_{Na}^c = x \log k_1 + (1 - x) \log k_2 \qquad (5)$$

where k_1 and k_2 are the equilibrium selectivity values for the first and second dissociable groups, R_1 and R_2, respectively. The experiments were carried out at four different pH values. It is interpreted that by changing the hydrogen ion concentration in the solution phase, the ratios of the first to the second dissociable groups are thus varied, since the second dissociable group prefers the hydrogen ion by a factor of several orders of magnitude. It can be seen from the titration curve (Fig. 1) that K_{Na}^c obtained at pH 6.7 involved only the first dissociable group. Hence, it may be safely assumed that K_{Na}° values represent the selectivity of the first functional group only. Accordingly, eq. 5 may be written as

$$\log K_{Na}^c = \log k_1; \quad K_{Na}^c = k_1 \qquad (6)$$

since x is equal to unity.

In accord with postulation, the observed order follows the Hofmeister series as is shown in Table I, column 2. The test of the hypothesis is then centered on whether the equilibrium selectivity values k_2 of the second dissociable group are the reverse of the Hofmeister series. It is evident from the titration curve that the K_{Na}^c values obtained at pH 12.6 involved both functional groups. The theoretical quantity for each is equal to 2 mequiv./g. of air-dried resin. Hence, eq. 5 at pH 12.6 becomes

$$\log K_{Na}^c = 0.5 \log k_1 + 0.5 \log k_2 \qquad (7)$$

where K_{Na}^c would be the value obtained at pH 12.6. The only quantity which is unknown and sought for is k_2, the selectivity value of the second functional group, which cannot be be determined experimentally in this case. By substituting appropriated values into eq. 7, k_2 values of the second dissociable group are readily calculated. These values thus calculated together with k_1 are given in Table III.

The selectivity values of the second functional group may also be obtained by plotting K_{Na}^c values at various

pH values as functions of per cent involved in the exchange, and the k_2 value is obtained by extrapolation as has been done in Fig. 3. It is evident that the equilibrium selectivity values of the second functional group follow the crystal radii sequence, as mentioned earlier (see second row in Table III). It might be argued, however, that the observed reversals of se-
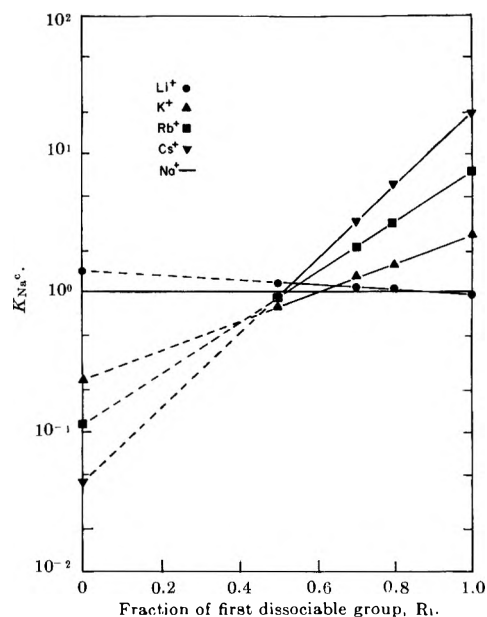

Figure 3. Extrapolation of selectivity coefficients of second dissociable group of phosphoric acid ion exchanger, as shown in dotted lines. Symbols indicate experimental K_{Na}° at various pH values.

lectivity order could be due to the variation of exchange capacities at various pH values. Further, the effect of the swelling of the exchanger at different pH values might also complicate the selectivity pattern. It is not known to what extent these factors affect the equilibrium selectivity coefficients in the present case. However, it might be reasonably assumed that the reversal of affinity order as a function of exchange capacity is not generally observed, apart from the isolated case of pectic acids reported by Hutschneker and Deuel.[9] The question of the effect of swelling on selectivity coefficients is more difficult to answer. In fact, some workers in the field tend to discount its importance except for highly cross-linked resins or large ions.[19] Since the resin used had a low cross linking ($\approx 6\%$ DVB) and the ions involved in the exchange reactions were quite small (the hydrated radius for $Li^+ = 3.4$ Å.), the effect of swelling on K_{Na}^c would be

Table III: Intrinsic Selectivity Coefficients for First and Second Dissociable Groups

	Cs⁺	Rb⁺	K⁺	Na⁺	Li⁺
k_1 (for R_1)	19.0	7.0	2.5	1.0	0.95
k_2 (for R_2)	0.043	0.12	0.23	1.0	1.4

(19) J. A. Kitchener, "Ion-exchange Resin," Methuen & Co., Ltd., London, 1957, pp. 30-33.

negligible. Further, the swelling of resin tends to depress K_{Na}^c, according to Gregor's swelling energy theory.[20] Should this factor be of importance, it should be operative on both k_1 and k_2. Therefore, it is difficult to visualize that the swelling pressure term should cause the reversal of selectivity order.

The nature of polyfunctionality of the exchange resin is of considerable interest, and possibly of technical importance. For instance, in the present case it is desirable to separate lithium and potassium ions from a solution containing sodium. This may be achieved by performing the exchanging reaction at pH 11. It is conceivable that an entirely analogous

situation exists with other groups of elements in the periodic table. Furthermore, the polyfunctionality of exchange resin may be obtained by having different functional groups attached to the same hydrocarbon matrix, as has been done in the present case, or by mixing different types of resin. The equilibrium selectivity values will be governed by eq. 5.

(20) H. P. Gregor, *J. Am. Chem. Soc.*, **73**, 643 (1951).

Thermodynamic Functions and Phase Stability Limits by Electromotive

Force Measurements on Solid Electrolytic Cells

by Giovanni B. Barbi

Euratom C.C.R. Ispra, High Temperature Chemistry Group Materials Department, Ispra, Italy
(Received September 9, 1963)

The possibility of determining the standard free energy of formation of metal oxides through measurements of potential across solid electrolytic chains is illustrated. It is shown how such measurements make it possible to determine the transformation temperatures in a biphasic system. The method was applied for the determination of the standard molar free energy of formation of NiO, Fe_3O_4, WO_2, and MoO_2 and of the eutectoid temperature in the iron–wüstite–magnetite system.

Theoretical

The determination of the thermodynamic functions of metal oxides may be achieved, as previously shown,[1-7] by means of e.m.f. measurements across solid electrolytic chains of the types

$$Pt|Me, MeO_x \begin{vmatrix} \text{intermediate} \\ \text{electrolyte} \end{vmatrix} \frac{Me'O_k, Me'O_{y_-}\ (T > T_0)}{Me'O_k, Me'O_z\ (T < T_0)} \begin{vmatrix} \\ \end{vmatrix} Pt \quad (I)$$

$$Pt|Me, MeO_x \begin{vmatrix} \text{intermediate} \\ \text{electrolyte} \end{vmatrix} \frac{Me'O_{y_+},\ Me'O_z\ (T > T_0)}{Me'O_k, Me'O_z\ (T < T_0)} \begin{vmatrix} \\ \end{vmatrix} Pt \quad (II)$$
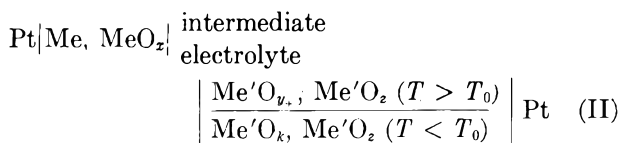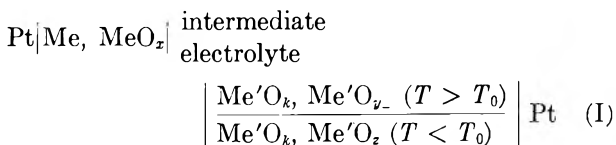
where T_0 is the eutectoid temperature of the $Me'O_y$ phase and y_- and y_+ are the values of the oxygen–

(1) U. Croatto and C. Bruno, *Ric. Sci.*, **17**, 1998 (1947).

(2) M. Katayama, *Z. physik. Chem.*, **61**, 566 (1908).

(3) T. N. Rezukhina, V. I. Lavrent'ev, V. A. Levitskii, and F. A. Kutnezov. *Zh. Fiz. Khim.*, **35**, 1367 (1961).

metal ratio in equilibrium with $Me'O_k$ and $Me'O_z$, respectively. The determination is possible if the intermediate electrolyte is chemically unaffected by metals and oxides that form the ends of the chain and if it shows pure anionic conductivity.

Under these conditions, when $T > T_0$, for cells I and II we have, respectively

$$\frac{\Delta G^\circ{}_{Me'O_{y_-}} - \Delta G^\circ{}_{Me'O_k}}{y_- - k} = \frac{\Delta G^\circ{}_{MeO_z}}{x} + 2\mathfrak{F}E' \quad (1)$$

$$\frac{\Delta G^\circ{}_{MeO_z} - \Delta G^\circ{}_{Me'O_{y_+}}}{z - y_+} = \frac{\Delta G^\circ{}_{MeO_z}}{x} + 2\mathfrak{F}E'' \quad (2)$$

and for both cells at $T < T_0$

$$\frac{\Delta G^\circ{}_{Me'O_z} - \Delta G^\circ{}_{Me'O_k}}{z - k} = \frac{\Delta G^\circ{}_{MeO_z}}{x} + 2\mathfrak{F}E \quad (3)$$

where values of ΔG° represent the standard molar free energies of formation of the oxides and those of E are the measured e.m.f.

Provided that there are no transformation points in the phases MeO_z, $Me'O_k$, and $Me'O_z$ in the close vicinity of T_0, we write

$$(\Delta^\cdot G^\circ{}_{MeO_z, \, Me'O_k, \, Me'O_z}, \, \dot{x}, \, \dot{k}, \, \dot{z})_{T_{0+}} =$$

$$(\Delta^\cdot G^\circ{}_{MeO_z, \, Me'O_k, \, Me \, O_z}, \, \dot{x}, \, \dot{k}, \, \dot{z})_{T_{0-}} \quad (4)$$

where the points represent the derivatives with respect to T.

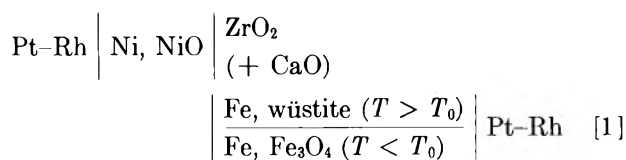By deriving (1), (2), and (3) and combining with (4)

$$2\mathfrak{F}(\dot{E}'_{T_{0+}} - \dot{E}_{T_{0-}}) = \frac{1}{(y_- - k)(z - k)} \times$$

$$[(z - k)\Delta^\cdot G^\circ{}_{Me'O_{y_-}} - (y_- - k)\Delta^\cdot G^\circ{}_{Me'O_z} -$$

$$(z - y_-)\Delta^\cdot G^\circ{}_{Me'O_k} -$$

$$\frac{z - k}{y_- - k}(\Delta G^\circ{}_{Me'O_{y_-}} - \Delta G^\circ{}_{Me'O_k})\dot{y}_-] \quad (5)$$

$$2\mathfrak{F}(\dot{E}''_{T_{0+}} - \dot{E}_{T_{0-}}) = \frac{1}{(z - k)(z - y_+)} \times$$

$$[(y_+ - k)\Delta^\cdot G^\circ{}_{Me'O_z} - (z - k)\Delta^\cdot G^\circ{}_{Me'O_{y_+}} +$$

$$(z - y_+)\Delta^\cdot G^\circ{}_{Me'O_k} +$$

$$\frac{z - k}{z - y_+}(\Delta G^\circ{}_{Me'O_z} - \Delta G^\circ{}_{Me'O_{y_+}})\dot{y}_+] \quad (6)$$

Equations 5 and 6 relate the variation of the slope of the E/T curves with those of the phase diagrams at the eutectoid temperature, thus giving a criterium to evaluate the reliability of the phase diagrams at this temperature.

Experimental

Electromotive force measurements were performed across the cells

$$Pt-Rh \left| Ni, NiO \left| \begin{array}{c} ZrO_2 \\ (+ CaO) \end{array} \right. \right.$$
$$\left| \begin{array}{c} Fe, \text{wüstite } (T > T_0) \\ \hline Fe, Fe_3O_4 \ (T < T_0) \end{array} \right| Pt-Rh \quad [1]$$

$$Pt-Rh \left| Ni, NiO \left| \begin{array}{c} ZrO_2 \\ (+ CaO) \end{array} \right. \right.$$
$$\left| \begin{array}{c} \text{wüstite, } Fe_3O_4 \ (T > T_0) \\ \hline Fe, Fe_3O_4 \ (T < T_0) \end{array} \right| Pt-Rh \quad [2]$$

$$Pt-Rh \left| Fe, \text{wüstite} \left| \begin{array}{c} ZrO_2 \\ (+ CaO) \end{array} \right| W, WO_2 \right| Pt-Rh$$
$$[3]$$

$$Pt-Rh \left| Ni, NiO \left| \begin{array}{c} ZrO_2 \\ (+ CaO) \end{array} \right| W, WO_2 \right| Pt-Rh \quad [4]$$

$$Pt-Rh \left| \begin{array}{c} \text{wüstite, } Fe_3O_4 \ (T > T_0) \\ \hline Fe, Fe_3O_4 \ (T < T_0) \end{array} \right.$$
$$\left| \begin{array}{c} ZrO_2 \\ (+ CaO) \end{array} \right| Mo, MoO_2 \right| Pt-Rh \quad [5]$$
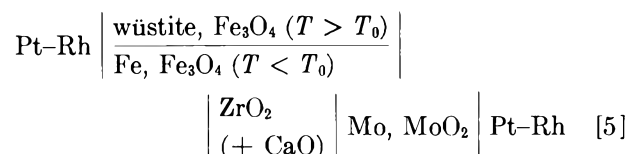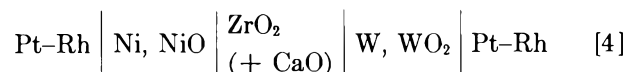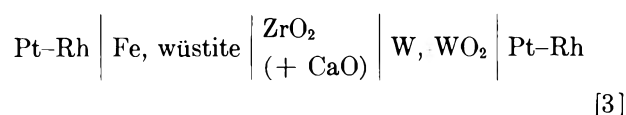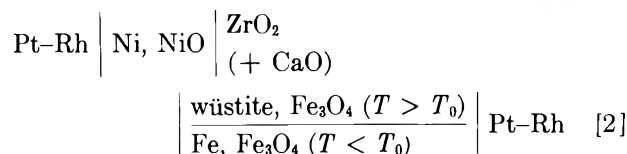
and these made it possible to determine: (1) ΔG° values of NiO, WO_2, and MoO_2 from the knowledge of the ratios of partial pressures of CO_2 and CO in equilibrium with the iron–wüstite and wüstite–magnetite systems at different temperatures; (2) the transformation temperature, T_0, of the iron–wüstite and wüstite–magnetite systems into the iron–magnetite system; and (3) from the values of $\Delta G^\circ{}_{NiO}$ as extrapolated below T_0, the ΔG° value of Fe_3O_4 from iron and oxygen.

Materials. The intermediate electrolyte consisted of a solid solution of calcium oxide and zirconium oxide having a molar ratio 15:85. Electrical conductivity, compactness, and stability of this solution were found to be satisfactory. The electrolyte was prepared from Merck zirconium nitrate and calcium oxide (purity 99.5%) as described elsewhere.[7]

The oxides obtained by heating the nitrates were fired at 1200° for 20 hr., pressed into pellets of 12-mm. diameter and 2–3-mm. thickness, and then sintered at 1650–1700° for 20 hr. The pellets showed a dense and compact appearance.

(4) S. Aronson and J. C. Clayton, *J. Chem. Phys.*, **32**, 749 (1960).

(5) Y. I. Gerasimov, I. A. Vasileva, T. P. Chusova, V. A. Geiderich, and M. A. Timofeeva, *Zh. Fiz. Khim.*, **36**, 358 (1962).

(6) K. Kiukkola and C. Wagner, *J. Electrochem. Soc.*, **104**, 308 (1957).

(7) K. Kiukkola and C. Wagner, *ibid.*, **104**, 379 (1957).

The iron–wüstite and wüstite–magnetite pellets were prepared by pressing iron and magnetite mixtures and then heating at a temperature of about 900° for 10 hr. under oxygen-free argon.

The W–WO₂ and Mo–MoO₂ pellets were prepared from mixtures of 5 molar % WO₃ in W and 5 molar % MoO₃ in Mo. After heating at a temperature of 600° in an argon atmosphere, they were kept at 900° under vacuum $(10^{-4}$ mm.) for about 20 hr.

The Ni–NiO pellets were prepared starting from a mixture containing 90 wt. % Ni. The pellets were annealed at about 600° for 2 hr. in an inert atmosphere.

To facilitate the pressing operation, 1–2 wt. % camphor was added to serve as a lubricant.[8] After pressing, the camphor was removed by heating under vacuum up to 180° for 1 hr.

The surfaces of the pellets must be perfectly flat in order to provide maximum contact surfaces among each other and minimum electric impedance of the cell.

Apparatus. The apparatus for e.m.f. measurements on chains [1], [2], [4], and [5] is similar, with some

modifications, to that described by Kiukkola and Wagner,[7] and is represented in Fig. 1.

The electrodes are small Pt–Rh (30% Rh) plates cemented to the ends of the electrode tube holders (with Melpar CA-100 cement) and connected with platinum leads. A temperature uniformity within ±2° over a region of 5 cm. is assured.

A stream of prepurified argon flows slowly from the bottom to the top of the cell, escaping from the clearances between the electrode tube holder and the stainless steel tubular guide. A weight is applied in order to improve and stabilize the contact among the pellets.

The apparatus with which the measurements on chain [3] were performed consists of a quartz tube which has a cylindrical alumina crucible at the bottom to contain the pellets. The lead from the lower electrode passes through the bored bottom of the crucible and then up the outside wall. The lead of the upper electrode passes inside a quartz tube which facilitates (by its own weight) good and stable contact among the pellets, and also keeps the latter well centered by means of an enlargement of the diameter on its upper section. During the runs a vacuum of better than 10^{-4} mm. was maintained inside. Extreme care was taken to avoid a.c. noise by a careful shielding of the furnace with thick heat-resistant stainless steel sheets and by grounding the cables. An electrometric voltmeter with an input impedance of 10^{-14} ohm (Keithley Model 610 A) was employed and the e.m.f. was recorded.

Results

Chains [1] and [2]. The values of the ratio between the partial pressures of CO_2 and CO in equilibrium with iron–wüstite and wüstite–magnetite systems, as determined by Darken and Gurry[9] as well as those of the standard molar free energy of oxidation of CO to CO_2,[10] enable us to calculate the standard free energy of formation per atom of oxygen of wüstite and the standard free energy of oxidation of wüstite to magnetite per atom of oxygen.

Figure 2 shows e.m.f. values and the eutectoid temperature, T_0, for both chains. By applying eq. 1 and 2, we obtain the values of $\Delta G°_{NiO}$ for chains [1] and [2]

$$-\Delta G°_{NiO} = 58.90 - 0.02335T \quad \text{(kcal./mole)} \quad (7)$$

$$-\Delta G°_{NiO} = 57.10 - 0.02150T \quad \text{(kcal./mole)} \quad (8)$$
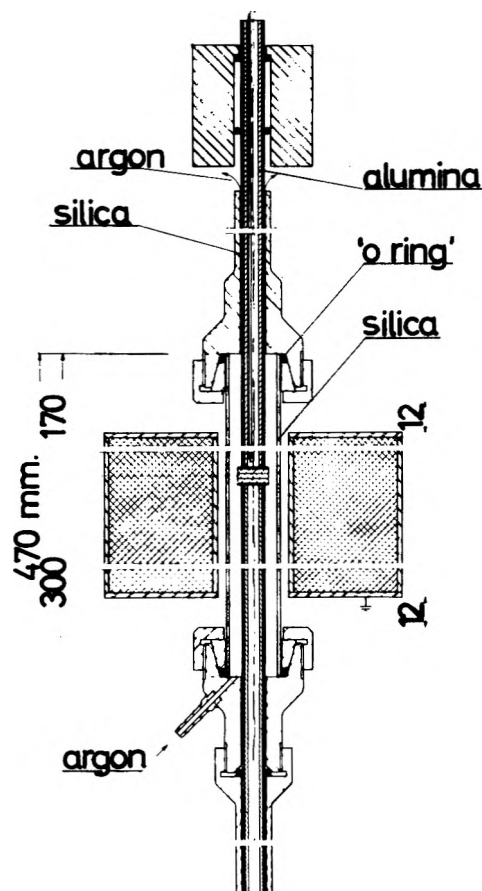

Figure 1. Assembly for e.m.f. measurements on chains [1], [2], [4], and [5].

(8) J. J. Gallay, Thesis, University of Lyon, 1960.

(9) L. S. Darken and R. W. Gurry, *J. Am. Chem. Soc.*, **67**, 1398 (1945).

(10) "International Critical Tables," Vol. VII, McGraw-Hill Book Co., Inc., New York, N. Y., 1930, p. 243.
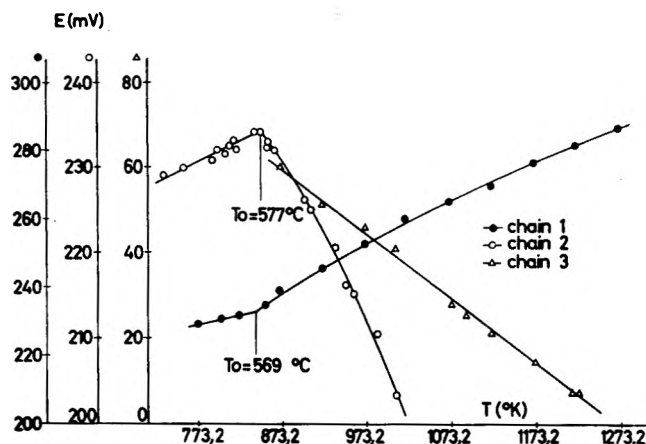
Figure 2. Plot of e.m.f. values vs. temperature
for chains [1], [2], and [3].

Terms of higher order than the first were neglected because of uncertainties due to possible small variation of the electronic transport number[11] with temperature in the intermediate electrolyte

By extrapolating for $T < T_0$ the average of eq. 7 and 8, *i.e.*

$$-\Delta G^{\circ}_{\text{NiO}} = 58.00 - 0.02242T \text{ (kcal./mole)} \quad (9)$$

by eq. 3 we found

$$-\Delta G^{\circ}_{\text{Fe}_3\text{O}_4} = 269.55 - 0.08316T \text{ (kcal./mole)}$$

Taking the Darken and Gurry[9] values: $(y_-)_{842^{\circ}\text{K}}$ = 0.946 and $(y_+)_{850^{\circ}\text{K}}$ = 0.941, we found

$$(\dot{y}_-)_{842^{\circ}\text{K}} = -0.0001054 \ \frac{\text{atoms of oxygen}}{\text{atoms of iron} \times \ ^{\circ}\text{C}}.$$

$$(\dot{y}_+)_{850^{\circ}\text{K}} = 0.000252 \ \frac{\text{atoms of oxygen}}{\text{atoms of iron} \times \ ^{\circ}\text{C}}.$$

Chain [3]. The e.m.f. data are shown in Fig. 2. From the values of the standard molar free energy of formation of wüstite, we found for the standard molar free energy of formation of WO_2 the following expression between 923 and 1223°K.

$$-\Delta G^{\circ}_{\text{WO}_2} = 146.18 - 0.04771T \text{ (kcal./mole)} \quad (10)$$

Chain [4]. In this case, results of e.m.f. measurements were hardly reproducible when the temperature exceeded 750°. This lack of reproducibility can be explained by the existence of WO_3, which is very volatile and whose presence can be accounted for either by disproportion[12,13] or by oxidation of traces of oxygen eventually present in the inert gas. The WO_3 transported toward the Ni–NiO pellet forms NiWO_4, which gives rise to a mixed potential. In fact, the

presence of NiWO_4 on the Ni–NiO pellet surfaces was noticed and, after a long time with working temperatures exceeding 800°, traces of WO_3 were also found on the upper, cooler walls of the cell.

The results of e.m.f. measurements are shown in Fig. 3. From the values of $\Delta G^{\circ}_{\text{NiO}}$ (eq. 9), we obtained

$$-\Delta G^{\circ}_{\text{WO}_2} = 147.08 - 0.0487T \text{ (kcal./mole)}$$

Chain [5]. Electromotive force measurements, reported in Fig. 3, permit us to calculate $\Delta G^{\circ}_{\text{MoO}_2}$

$$-\Delta G^{\circ}_{\text{MoO}_2} = 138.35 - 0.0425T \text{ (kcal./mole)} \quad (11)$$

Above 800° the e.m.f. values diverge somewhat from the extrapolation of the lower temperature straight line. This effect can be explained by local oxidation of MoO_2. The resulting MoO_3, because of its volatility, gets into contact with the other electrolyte and the reactions which occur with iron oxides may give rise to a mixed potential.
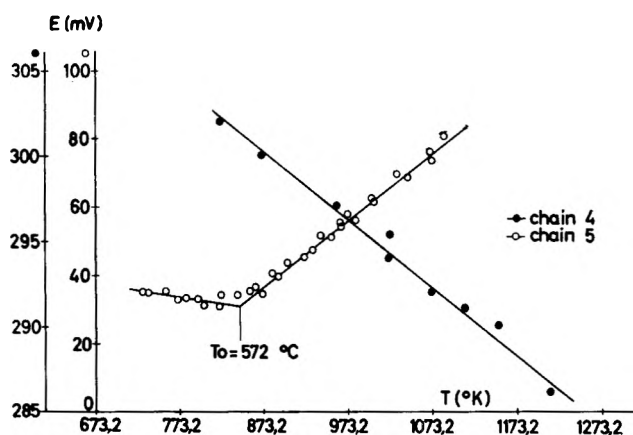

Figure 3. Plot of e.m.f. values vs. temperature
for chains [4] and [5].

Figure 3 shows also the eutectoid temperature of iron–wüstite–magnetite system at 572° (845°K.) in good agreement with the values determined by chains [1] and [2].

Taking the extrapolated values of eq. 11 of $\Delta G^{\circ}_{\text{MoO}_2}$ for $T < 845^{\circ}\text{K}$., we found

$$-\Delta G^{\circ}_{\text{Fe}_3\text{O}_4} = 265.06 - 0.0780T \text{ (kcal./mole)}$$

In Table I a comparison is made of the values of

(11) S. F. Pal'guev and A. D. Neuimin, *Trans. Inst. Electrochem.*, 1, 90 (1960).

(12) P. E. Blackburn, M. Hoch, and H. L. Johnston, *J. Phys. Chem.*, 62, 769 (1958).

(13) L. Brewer, *Chem. Rev.*, 52, 1 (1953).

ΔG° values obtained by e.m.f. measurements with those of the literature.

Table I

Oxide	T, °K.	ΔG°, this work	ΔG°, lit. values
NiO	800	−40.07	−39.61[a]
	1000	−35.58	−34.90[a]
	1200	−31.10	−30.19[a]
Fe_3O_4	700	−211.34	−210.26[b]
	850	−198.87	−197.93[b]
WO_2	800	−108.07	−102.32[a]
	1000	−98.43	−95.00[a]
	1200	−88.79	−87.68[a]
MoO_2	800	−104.35	−106.14[a]
	1000	−95.85	−98.10[a]
	1200	−87.35	−90.14[a]

[a] O. Kubaschewski and E. L. Evans, "Metallurgical Thermochemistry," Pergamon Press, London, 1958, pp. 336–343.
[b] O. Kubaschewski and J. A. Catterall, "Thermochemical Data of Alloys," Pergamon Press, London, 1956, p. 173.

Remarks

In some runs it was noted that the metal and metal oxide may penetrate into the intermediate electrolyte. The total amount of metal and metal oxide which penetrated was greater in the case of W and Mo than in the case of Fe. Nickel did not show any penetration.

This effect was less pronounced if the metallic pellets were previously kept in contact with other pellets of intermediate electrolyte or used in preceding runs.[14] It also decreased as the sintering temperature of the intermediate electrolyte increased and the working temperature decreased.

Because of this effect, the measurements on chains [3], [4], and [5] were performed above 650°, at increasing temperatures and at a relatively fast rate, even if this implies an imperfect stabilization of e.m.f. values to be measured. Thus, the variation of the conduction properties of the intermediate electrolyte during the measurements has been minimized as much as possible.

(14) S. Aronson and J. Belle, J. Chem. Phys., 29, 151 (1958).

The Surface Area of Water Preadsorbed on Powdered Substrates

by William H. Wade

Department of Chemistry, The University of Texas, Austin 12, Texas   (Received September 27, 1963)

The surface areas of powdered solids pre-equilibrated with various amounts of water have been measured by nitrogen adsorption. The data are best interpreted in terms of a dual mode of adsorption, requiring the adsorbate to be held as both a uniform film and as capillary condensate in the contact zone of touching particles.

Introduction

Many models have been employed to explain what is loosely referred to as "multilayer, physical" adsorption and most have fallen into disuse for diverse reasons. The B.E.T. model and its accompanying theoretical formulation would appear to be the sole survivor, not so much because of the correctness of the underlying assumptions, but because of its general utility in providing reasonable values for the surface area of high specific surface area solids. Of probable secondary importance is its ability to fit qualitatively a variety of isotherm shapes. Several apparently valid objections to the B.E.T. model as applied to nonideal surfaces have been raised and even for ideal

surface interactions the B.E.T. model must be an over-simplification. For instance, Karnaukhov and Kiselev[1] have calculated that during surface area measurements by gas adsorption, the adsorption process itself leads to apparent changes in B.E.T. surface areas. They assumed the growth of a uniform film on spherical adsorbent particles. One undeterminable parameter that is not independently evaluable by them is the number of physical contacts made by any one adsorbent particle and its neighbors. The surface area on the outside of an adsorbed gas film depends strongly on this parameter as does the volume in the contacting zones inaccessible to adsorbate molecules of finite size. The work discussed here is addressed to this point and arose from studies on the validity of Harkins–Jura "absolute" area measurements.

Two series of measurements had previously been performed in this laboratory. The first series[2] was an intercomparison of surface area measurements between B.E.T. analyses of krypton, argon, and nitrogen adsorption isotherms and Harkins–Jura calorimetric measurements for a series of alumina powders reported still earlier.[3] The surface areas by gas adsorption were found to be internally consistent, with an average deviation of approximately 4%. However, the Harkins–Jura areas obtained from heats of immersion data on the same samples equilibrated with water vapor at $p/p^0 = 0.95$ uniformly yielded lower surface areas. For particulate samples with no internal pore structure, the discrepancy is 10–15%, but for the one gel sample used, the Harkins–Jura specific surface area is 4 m.^{2}/g. whereas by gas adsorption it was 221 m.^{2}/g. As noted elsewhere,[4] the Harkins–Jura method does measure only the surface area of the adsorbate–gas interface but discrepancies of even 15% should not be overlooked in precise measurements.

A second series of experiments[5] was initiated a year ago to measure differential heats of adsorption by calorimetric immersion techniques but became side-tracked when it was found that heats did not as-sympotically approach the surface enthalpy of the liquid used in the calorimeter (water, in this case). Rather, it was found that immersional heats for particulate alumina samples eventually would fall to 100–110 ergs/cm.^{2} rather than the "theoretical" limit of 118 ergs/cm.^{2}. What is needed is an independent evaluation of the surface area of these powdered solids as a function of the water preadsorbed on the samples. The only apparent experimental approach is equilibration with water vapor, freezing *in situ*, followed finally by a gas adsorption surface area measurement at liquid nitrogen temperatures. Karasz, *et al.*,[6] carrying out such measurements on a TiO_2 sample, apparently

did not consider that the preadsorption of water significantly altered the surface area.

Experimental

Volumetric adsorption isotherms were obtained for nitrogen on four samples—three of Al_2O_3 and one of SiO_2. Additional information on these samples can be obtained elsewhere.[3,7] The previously reported surface areas, Σ, of these samples are: Al_2O_3, 2.72, 65.4, and 104 m.^{2}/g; SiO_2, 188 m.^{2}/g. Areas were estimated on the basis of the following molecular areas: N_2, 16.2 Å.^{2}; Ar, 16.0 Å.^{2}; and Kr, 20.0 Å.^{2}. Samples were outgassed at 200°. Water vapor was added slowly with the water sample bulb initially at −80° and allowed to slowly warm to a final temperature consistent with the required pressure. This was done to preclude any possible irreversible pore condensation caused by "shocking" the sample with a transient pressure higher than the ultimate pressure.[8] This equilibration was considered complete when a pressure drop of <0.02 torr was observed over a 4-hr. period. The sample was cooled to −195° slowly to prevent distillation from the sample to the cold wall.[6] In practice this was accomplished by surrounding the sample tube with a test tube of acetone to increase the heat capacity and provide thermal insulation. This assembly was subsequently positioned in the neck of a deep dewar flask approximately one-third filled with liquid nitrogen. By careful positioning of glass wool insulation, low thermal transfer rates were achieved. The cooling rate was monitored by a pentane thermometer. Equilibration times varied from 4 to 30 hr. depending on the initial pressure of H_2O. During the cooling process the small amount of gaseous water vapor in the dead space was adsorbed but was a negligible perturbation (less than 0.1% of the adsorbate H_2O). Nitrogen isotherms were measured volumetrically over a p/p^0 range of 0.04 to 0.22 and consisted of six or seven experimental points. The temperature of the liquid nitrogen bath was monitored with a nitrogen vapor pressure thermometer and found to be con-

(1) A. P. Karnaukhov and A. V. Kiselev, *Russ. J. Phys. Chem.*, **34**, 1019 (1960).

(2) W. H. Wade, H. D. Cole, F. Stiles, and N. Hackerman, Southwest Regional Meeting of the American Chemical Society, Dallas, Texas, 1962.

(3) W. H. Wade and N. Hackerman, *J. Phys. Chem.*, **64**, 1196 (1960).

(4) A. W. Adamson, "Physical Chemistry of Surfaces," Interscience Publishers, Inc., New York, N. Y., 1960, p. 437.

(5) W. H. Wade and N. Hackerman, unpublished data.

(6) F. E. Karasz, W. M. Champion, and G. D. Halsey, Jr., *J. Phys. Chem.*, **60**, 376 (1956).

(7) A. C. Makrides and N. Hackerman, *ibid.*, **63**, 594 (1959).

(8) J. W. Whalen, *ibid.*, **67**, 2114 (1963).

stant to ±0.02° over the 4-hr. period required for a complete isotherm. The ambient temperature of the volumetric bulbs was thermally damped to ±0.2° by a dead-air space. Pressures were read off a traveling microscope to ±0.02 torr. No corrections were made for gas imperfection. After an adsorption isotherm run, the system was evacuated while being slowly warmed to room temperature, re-equilibrated with water vapor at a higher pressure, and the cycle repeated.

In addition to these measurements, electron micrographs of some the samples were taken to estimate the particle size distribution and to check the validity of the necessary assumption of spheroidicity for a model later assumed valid (see Discussion).

One sample of alumina (104 m.²/g.) was compressed at 10⁴ p.s.i. to give a pellet with a greatly increased but still unknown number of particle contacts.

Results

Plots of surface area vs. volume of water preadsorbed rather than p/p^0 are more easily interpreted and these are shown in Fig. 1 for areas relative to the totally outgassed values. The volumes adsorbed, V_{ads}, are in cc. of liquid H_2O/g. of adsorbate. The last data point of each curve corresponds to a $p/p^0 = 0.95$, and the conversion of relative pressures of water to volumes adsorbed come from previously published results.[9] The volumes adsorbed for the compressed 104 m.²/g. alumina are assumed to be identical with those of the same sample in the uncompressed state.

Electron microscope pictures of the four samples mentioned in Fig. 4 were visually examined. The
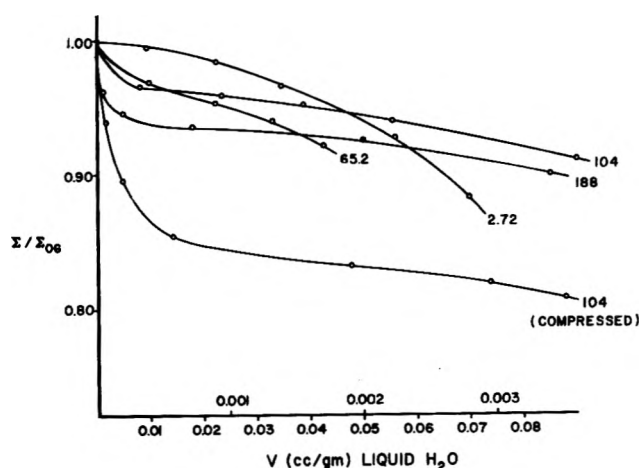
Figure 1. The relative surface area of various powdered samples as a function of the volume of liquid water preadsorbed. $\Sigma = \Sigma_{OG}$ at $V = 0$. The upper abscissa is for the 2.72 sample, the lower abscissa is for the remaining samples.

Alon "C" (65.2 m.²/g.) and Cab-O-Sil (188 m.²/g.) particles were found to be spherical but with a considerable particle size spread, whereas the Alucer "MA" (104 m.²/g.) and Alucer "MC" (2.72 m.²/g.) had a narrow particle size distribution of spherical particles.

Discussion

Before attempting to interpret the experimental data in terms of various models, one risky assumption must be made: *The B.E.T. analysis of N_2 isotherms yields the true surface area of the water adsorbate–gas interface.* This point will be argued later, but meanwhile it should worry the discerning reader.

As mentioned earlier, Karnaukhov and Kiselev[1] derived analytical expressions relating the surface area and volume of the liquid adsorbate to the thickness of a uniform film using the following parameters: R, adsorbent particle radius (assumed spherical); Ω, adsorbate particle radius (assumed spherical); t, thickness of the uniform adsorbate film; n, number of spheres touching any one sphere (assumed constant); and δ, density of the adsorbent particles.

If values of Ω, R, n, and δ are assumed, the surface area, Σ, corresponding to a given volume of adsorbate, V, can be obtained. For values of n less than 3 or 4, the surface area increases with volume adsorbed, but for n-values greater than 3–4, it decreases with V. The only data of Fig. 1 which could possibly fit such a model would be those pertaining to the low area, 2.72-m.²/g. sample. Assuming the individual particles of this sample to be spherical, a surface area of 2.72 m.²/g. corresponds to a particle radius, R, of 2800 Å. For adsorbent particles with this radius, the void volume with $n = 12$ would give a particle radius 0.4% too small (see eq. 4 of ref. 1) which is small compared to the experimental errors. If the radius of a water molecule is assumed to be 1.75 Å., and the maximal contact number, $n = 12$ is chosen, a reasonable fit to the data is obtained other than at the highest relative pressures. For large volumes of water adsorbed on the 2.72-m.²/g. sample, the fit to the data is not altogether satisfactory. The theoretical diminution of surface area with volume of water preadsorbed is only three-fourths that observed in Fig. 1. Moreover, hexagonal close packing would never be realized in practice for loosely packed powders.

The remaining curves of Fig. 1 show a different behavior in that there is an initial rapid drop of surface area followed by a further gradual drop as for the 2.72-m.²/g. sample. This complexity is inexplicable by

(9) W. H. Wade, R. L. Every, and N. Hackerman, *J. Phys. Chem.*, 65, 25, 937 (1961).

the uniform film model. Rather, it is tempting to adopt the much older capillary condensation model, for as will be shown below, it predicts a rapid initial drop in surface area with volume adsorbed.

The adsorbed water is assumed to be held in n contact zones, geometrically bounded by the two spherical adsorbent particles and the assumed[10] circular adsorbate–gas meniscus. The reader can easily show that geometrical considerations for this volume of revolution yields

$$V_{ads} = \frac{3nr_m{}^2}{4R^3\delta} \left\{ R - \sqrt{2Rr_m + r_m{}^2} \times \right.$$
$$\left. \sin^{-1}\frac{R}{R + r_m} \right\} \quad (cc./g.) \quad (1)$$

and for the surface area

$$\Sigma = \frac{3}{2R^2\delta} \left\{ 2R^2 - nRr_m + \right.$$
$$\left. nr_m\sqrt{2Rr_m + r_m{}^2}\ \sin^{-1}\frac{R}{R + r_m} \right\} \quad (cm.^2/g.) \quad (2)$$

where r_m is the radius of meniscus and the other terms have their previous significance.

To proceed further, an analytical expression for an adsorption isotherm must be used and the validity of the Kelvin equation must be assumed. Applied to the problem in hand

$$\ln p/p^0 = \frac{\gamma\bar{V}}{RT} \left\{ \frac{1}{\rho_1} + \frac{1}{\rho_2} \right\} \quad (3)$$

where γ is the surface tension; $\bar{V}$ the molar volume of liquid; R, the gas constant; T, the absolute temperature; and ρ_1, ρ_2, the principle radii of curvature. As applied here for water at 25°, (3) becomes

$$\log p/p^0 = -2.275 \times$$
$$\left\{ \frac{1}{r_m} - \frac{2}{\sqrt{2Rr_m + r_m{}^2} - r_m + R} \right\} \quad (4)$$

Where ρ_2 is taken as the arithmetic mean of its maximum and minimum values.[11] Using (4) in conjunction with (1) yields classical B.E.T. type 3 isotherms inconsistent with experimental water isotherms on the present samples which are type 2. Nevertheless, it is instructive to note as in Fig. 2 that Σ–V plots from eq. 1 and 2 give a rather good fit for the Cab-O-Sil sample. This sample is shown because its water isotherm most closely resembles the type 3 behavior. The fit appears to be best for $n = 1$ to 2, which is an unreasonably low value (for a powder with the individual particles at rest, $n \geq 2$ except at the surface of the powder pack).
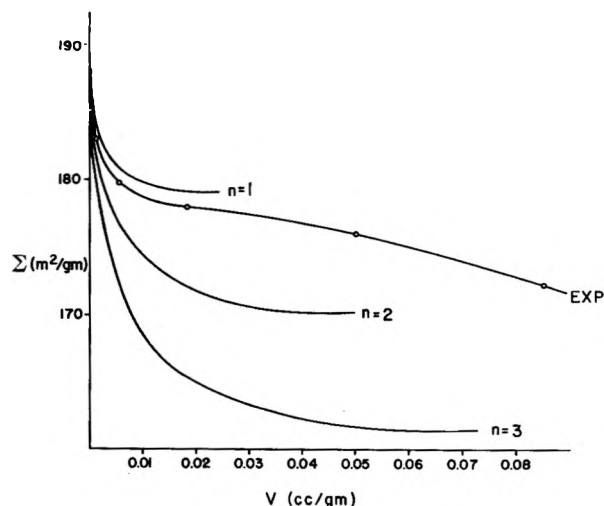
Figure 2. Comparison of experimental and calculated surface areas on the basis of pure capillary condensation.

In the derivations of eq. 1 and 2, it was assumed that adsorbent particle packing geometry need not be considered, i.e., the total volume adsorbed is n times the volume adsorbed per contact zone. This is not true at high relative pressures (large volumes adsorbed) for large values of n because eventually the adjacent menisci will overlap. A quantity called the critical meniscus radius, r_c, can be defined as the radius where adjacent menisci just coincide. Values of r_c/R can easily be determined for various simple geometric packing models as listed in Table I.

Table I: Values of r_c/R for Various Geometric Packing Models

Type of packing	No. of contacts per particle	r_c/R
Linear one-dimensional	2	∞
Plane trigonal	3	1.000
Tetrahedral	4	0.740
Cubic	6	0.414
Hexagonal close-packed	12	0.154

From eq. 4, at $p/p^0 = 1.00$, $r_m/R = 0.854$ as a maximum value. Thus for loosely packed samples ($n = 2$–5) it is unlikely that r_m will exceed r_c during adsorption. However, another difficulty exists. The calculated curves of Fig. 2 terminate where $p/p^0 = 1.00$ via eq. 6. It is therefore not possible to obtain a suf-

(10) Proper minimization of the surface free energy would require a trochoidal rather than a circular meniscus.

(11) B. G. Aristov, A. P. Karnaukhov, and A. V. Kiselev, Russ. J. Phys. Chem., 36, 1159 (1962).

ficient volume of adsorbate below $n = 3$, where the calculated surface areas are already much too low, and would only be further lowered by merging of water menisci. The one promising feature of this model is that it would account for the initial rapid drop of surface area.

The appropriate blend of the two extreme models should give the correct variation (at least qualitatively) of surface area with water adsorbed and should be the most realistic. Following the general approach of Aristov, Karnaukhov, and Kiselev,[11] it is possible to draw a geometric picture such as in Fig. 3. The volume adsorbed is the sum of the uniform film volume and the superimposed capillary condensation volume. It is possible to write once again an expression for V_{ads} in terms of Ω, t, r_m, R, n, and δ, i.e.

$$V_{ads} = \frac{3}{4R^3\delta} \left\{ \frac{4}{3} [(R + t^3) - R^3] + \frac{nRr_m}{R + r_m + t} \times \right.$$

$$[(R + r_m + t)^2 - R^2 + r_m^2] - \frac{Rr_m n}{R + r_m + t} \times$$

$$\sqrt{[(R + r_m + t)^2 - R^2]\left[r_m^2 - \frac{R^2 r_m^2}{R + r_m + t}\right]} -$$

$$\frac{n}{3} \left[\frac{Rr_m}{R + r_m + t} + t\right]^2 \left[3(R + t) - \frac{Rr_m}{R + r_m + t} - t\right]$$

$$- nr_m^2 \sqrt{(R + t + r_m^2) - R^2} \sin^{-1} \frac{R}{R + t + r_m} -$$

$$nR\Omega^2 + n\Omega^2 \sqrt{2R\Omega + \Omega^2} \sin^{-1} \frac{R}{R + \Omega} \right\} \text{ (cc./g.)} \quad (5)$$

The last two terms are now added to correct for the volume excluded to the water molecules.

It is also possible to write an expression for the surface area of the adsorbate–gas interface
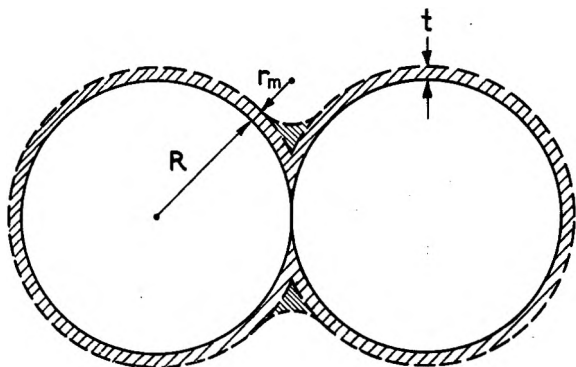
Figure 3. Dual adsorption mechanism consisting of a uniform film of thickness t with capillary condensation superimposed.

$$\Sigma = $$

$$\frac{3}{2R^3\delta} \left\{ 2(R + t)^2 + nr_m \sqrt{(R + t + r_m)^2 - R^2} \times \right.$$

$$\sin^{-1} \frac{R}{R + r_m + t} - \frac{nr_m^2 R}{R + t + r_m} -$$

$$n(R + t) \left(\frac{Rr_m}{R + r_m + t} + t\right) \right\} \text{ (cm.}^2\text{/g.)} \quad (6)$$

Aristov, et al., give no consideration to variation of surface area but proceed to discuss isotherm hysteresis, tacitly assuming that contact zone effects are unimportant for samples with surface areas of 6 m.^{2}/g. or below. From the experimental results on the 2.72-m.^{2}/g. sample, no such assumption seems warranted. The basic difficulty that one encounters is how to apportion the water between the uniform film of thickness, t, and the capillary water in the wedges of revolution with meniscus radius, r_m. The approach used here is: (a) set the relative pressure p/p^0; (b) calculate r_m from the Kelvin equation (6) (assuming $R >>> t$); (c) introduce the value of r_m from (b) along with the appropriate values of R, n, δ, Ω, and V (the latter obtained from the experimental water isotherm at the p/p^0 set in (a)); (d) solve eq. 5 for t; and (e) introduce t, r_m, R, δ, and n into eq. 6 and obtain the surface area, Σ.

To facilitate the preceding calculations, the Control Data Corp. 1604 computer at the University of Texas was programmed for these calculations and simultaneous evaluation of the corresponding surface areas. The calculations were performed for the four samples of Fig. 1 other than the compressed 104-m.^{2}/g. Al$_2$O$_3$. It is apparent that compression of this latter sample increased the number of contacts, causing drastic modification in the surface area when large volumes of water are adsorbed but only minor changes under totally outgassed conditions.

Even on the basis of this latter more refined model, quantitative agreement could not be obtained. However, the qualitative features are as required: for high specific area samples, a rapid drop in surface area primarily due to capillary condensation is observed, followed by a slow decrease due to both modes of water adsorption. Calculations for the uncompressed 104-m.^{2}/g. alumina are given in Fig. 4. The best fit is obtained $n = 5$ at small volumes adsorbed and $n = 3$ for large volumes adsorbed.

In addition to calculating surface areas, the C.D.C. 1604 computer also tabulated the volumes of "film" water and "capillary" water. For $n = 4$ (best average value) the 104-m.^{2}/g. sample has approximately 1% of V_{ads} (total) held as capillary condensate at low p/p^0,
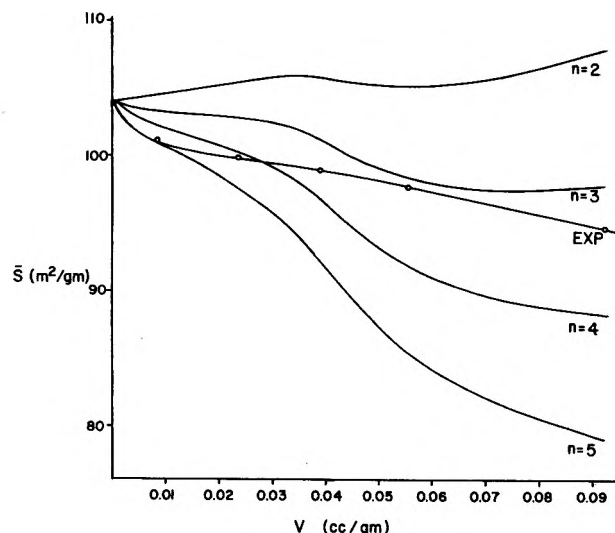
Figure 4. Comparison of experimental and theoretical surface areas with volume of water preadsorbed on the basis of the dual mode model.

increasing to approximately 25% at p/p^0 = 0.95 with an intermediate value of approximately 3% at p/p^0 = 0.30. This indicates that a small percentage of capillary condensate is responsible for the majority of the decrease in surface area at low and intermediate relative pressures (since the simple uniform film model would predict little or no change in surface area for $n = 4$).

The best fit for Alon C (65.2 m.²/g.) is also obtained with $n = 5$ at low p/p^0 and $n = 3$ at high p/p^0, and is very similar to the 104 m.²/g. sample with regard to the percentage of water held by capillarity, ranging from 1 to 30% for $n = 4$.

The Cab-O-Sil sample (188 m.²/g.) has a best fit for $n = 3$, but the calculated percentage of capillary water is much higher—20% at low p/p^0 and up to 30% at high p/p^0, consistent with the almost type 3 shape of the water adsorption isotherm.

The one low area sample (2.72 m.²/g.) shows no initial rapid drop of the surface area. The best fit to the experimental data is for $n = 9$ and the calculations for all values of n show no initial steep drop in the surface area; the calculations for $n = 9$ do apportion only 0.1% to capillary condensate at low relative pressures.

Several possible explanations of the quantitative lack of agreement are possible. (1) For real samples, n and r must be average values and correctly weighed distributions of n and r values would need to be folded

into the calculations. (2) The validity of the Kelvin equation for "meaningless" menisci radii of molecular dimensions is obviously open to question. This point was repeatedly discussed in the literature of 30 to 40 years ago, and no firm conclusions have ever been reached, although its validity is repeatedly assumed in obtaining pore size distributions from hysteresis loops. (3) Packing geometries may need to be considered for large adsorbed volumes as previously discussed. (4) A uniform adsorbate density is assumed without any independent check. (5) With regard to the present study, it is uncertain that the B.E.T. analysis of N_2 adsorption isotherms measures the actual surface area.

The following points can be made supporting the assumption that the B.E.T. analysis still measures the area. (1) Values of n = 3 or 4 predict little or no change in area for a uniform film (B.E.T.) model. (2) For type 2 isotherms (such as all the N_2 isotherms), the N_2 adsorbate held in contact zones by capillarity is only a few per cent of the total. (3) The nitrogen isotherms were measured over a restricted p/p^0 range (0.04 to 0.22) where there is not a large variation in the N_2 adsorbate coverage (less than a 30% total variation). (4) To a first approximation, the void volume problem introduces a constant but usually small constant error and does not affect relative areas for a given sample.

In any event and regardless of the correctness of the model here pictured, the Harkins–Jura areas are usually low by approximately 10%, which is the same approximate percentage lowering of the surface area during equilibration with water at high relative pressures, and it should be noted that these corrections may need to be made for samples in the micron size range.

In conclusion, this study has reaffirmed the existence of commonly overlooked complications encountered in measurements in the multilayer region. Though Harkins and Jura themselves were aware of such possible sources of error, later workers have at times excessively minimized their importance.

The Thermal Decomposition of Mercuric Cyanide Vapor

by J. P. Galvin and H. O. Pritchard

Chemistry Department, University of Manchester, Manchester 13, England (*Received September 27, 1963*)

The thermal decomposition of mercuric cyanide vapor has been studied in the presence of N_2, H_2, and various hydrocarbons, and is shown to take place by two distinct mechanisms. One is a molecular reaction which leads directly to cyanogen and the other involves the production of HgCN radicals, which behave essentially as if they were CN radicals. The vapor pressure and latent heat of vaporization of mercuric cyanide have been measured. The existence of NOCN is reported.

Preliminary Qualitative Experiments. When a stream of nitrogen containing a hydrocarbon RH is passed over solid mercuric cyanide heated to 350°, chromatographic analysis of the effluent gas shows the presence of HCN, C_2N_2, and the corresponding nitrile RCN. Thus methane and ethane give methyl and ethyl cyanide, respectively, propane gives *sec*-propyl cyanide, *n*-butane gives *sec*-butyl cyanide plus some ethyl cyanide, and benzene and toluene give phenyl and benzyl cyanide, respectively; in no case is any isonitrile formed. The simplest explanation of these products is that the radical R is produced by abstraction from RH, and this R then combines with a CN radical. The existence of radicals in the system is further supported by the fact that the products also contain alkyl mercuric compounds, which can easily be recognized by their unmistakable odor. It was also noted that unchanged mercuric cyanide was deposited downstream, and it was decided to study these reactions quantitatively under controlled gas phase conditions.

When unsaturated hydrocarbons were used addition products were found, *i.e.*, ethylene gave ethyl cyanide and succindinitrile, and acetylene and butadiene gave unidentified products, which in the latter case were very high boiling. It was also found that AgCN and $Cu(CN)_2$—actually $Zn(CN)_2$ + $CuCl_2$ mixture—behaved analogously.

Vapor Pressure of Mercuric Cyanide. The vapor pressure of solid mercuric cyanide was measured over the range 237–284° by saturating a carrier gas flowing at a known rate over the heated solid, and weighing the amount of solid transported to the condensation area; no decomposition occurs in this temperature range (except for a minute trace in the presence of H_2).

Variations were made in flow rate and carrier gas composition to ensure that saturation had been achieved. The vapor pressure of mercuric cyanide is about 5.7×10^{-2} mm. at 237° and about 4.7×10^{-1} mm. at 284°, giving a latent heat of vaporization of 26 ± 1 kcal./mole; no previous determination of the vapor pressure has been reported, but an estimate of the latent heat is on record.[1] The vapor pressure is given by

$$\log p \text{ (mm.)} = 9.810 - 26,000/2.3RT$$

In the kinetic experiments reported below, the mercuric cyanide did not always achieve its saturation vapor pressure under the conditions of carrier flow and composition used, and the amount transported in any experiment was always determined by dummy experiments carried out under the same flow conditions.

Thermal Decomposition in Pure Nitrogen. Kinetic experiments were carried out in a flow system in which the carrier gas, at about 1 cm. pressure, first flowed over solid mercuric cyanide maintained at a temperature near 250° and then into a cylindrical Pyrex reaction vessel at a higher temperature; contact times were of the order of 1 sec., and the products were analyzed mass spectrometrically. Little decomposition occurred below 410°, but at higher temperatures, surprisingly, HCN was the main product.

We had previously established that $Hg(CN)_2$ was readily hydrolyzed to HCN by water at high temperature. Consequently, water was rigorously excluded from the carrier gas by refrigeration, and in all experi-

(1) E. Lange and W. Martin, *Z. Physik. Chem.* (Leipzig). **A180**, 233 (1937).

ments the mercuric cyanide was purified by vacuum sublimation and stored until use *in vacuo* at 150°. We had also found from mass spectrometer analyses that C_2N_2 tended to hydrolyze slowly to HCN + HOCN when trapped in recently blown sections of the system, and suitable precautions were always taken; this kind of hydrolysis, analogous to the halogens, has been recorded previously in aqueous solution.[2]

We concluded therefore that the source of the HCN was a reaction involving the traces of hydrogen (0.05–0.1%) in the nitrogen. The reaction of H_2 with C_2N_2 has been studied previously,[3] and blank experiments confirmed that only in the order of 1% of the cyanogen would be converted to HCN in our system. Hence a reaction between hydrogen and mercuric cyanide was indicated, and this was confirmed in experiments with hydrogen as carrier.

Kinetic measurements were made in nitrogen between 420 and 510°. At the lower temperatures, the HCN:C_2N_2 ratio was often as high as 3, but at the highest temperatures, the ratio was nearer 0.3. Over the same temperature range, the over-all order in Hg(CN)$_2$ rose from 1.0 to 1.5 (a similar rise in order from about 1 to about 2 was found when methane was used as carrier). We interpret this to mean that HCN is formed by a first-order reaction of Hg(CN)$_2$ with H_2, and that C_2N_2 is formed from Hg(CN)$_2$ by a second-order mechanism; this interpretation is consistent with the fact that C_2N_2 is only formed in appreciable quantities in the gas phase at 500°, but that the solid decomposes rapidly 200° lower. It will be shown conclusively later that in these reactions, the radical concentration is negligible, and cyanogen could not have been formed by any radical mechanism. Hence it is reasonable to use the rate of formation of cyanogen as a measure of the rate of the second-order reaction

$$Hg(CN)_2(g) \longrightarrow Hg(g) + C_2N_2(g) \qquad (1)$$
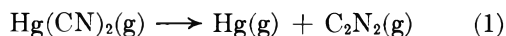
The Arrhenius parameters for this reaction are E_1 = 27 ± 3 kcal., log A_1 = 12.8 (A_1 in cc. mole^{-1} sec.$^{-1}$). Reaction 1 is thermoneutral to within experimental error,[4] *i.e.*, for Hg(CN)$_2$, $(D_1 + D_2) = D(NC-CN)$.

Thermal Decomposition in Hydrogen. When hydrogen was used as a carrier, the rate of decomposition rose so much that satisfactory rates could not be measured above 400°, and even down as low as 250° (the temperature of the solid Hg(CN)$_2$), a small but detectable decomposition occurred. At all temperatures, the product was HCN containing less than 1% C_2N_2. The kinetic results in hydrogen were very variable, and we were unable to establish the order

of the reaction. We believe, however, that a chain sequence is involved in which one step is

$$H + Hg(CN)_2 \longrightarrow HCN + HgCN \qquad (2)$$

It has been previously reported that hydrogen atoms attack solid mercuric cyanide,[5] and we have found that hydrogen atoms, produced by mercury photosensitized decomposition of H_2, considerably enhance the rate of formation of HCN from H_2 and mercuric cyanide vapor at 250°; mercuric cyanide vapor itself is unaffected by irradiation in the presence of mercury. If reaction 2 is to be fast, it must be exothermic which means that $D_2 = D(Hg-CN) > 15$ kcal. if $D(NC-CN)$ = 145 kcal./mole.[6]

Further support for this mechanism comes from experiments using nitrogen–hydrogen mixtures as carrier. The addition of 1% of oxygen caused the over-all rate of decomposition to be reduced, and at the same time there was a similar drop in the (small) amount of cyanogen formed. This suggests that in the low temperature region (300–400°), cyanogen is being formed by a radical mechanism which arises because of reaction 2. The most likely one is

$$HgCN + HgCN \longrightarrow 2Hg + C_2N_2 \qquad (3)$$
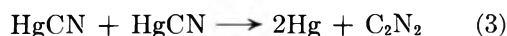
which is exothermic provided that $D_2 < 0.5 D(NC-CN)$; and since D_1 must always be greater[7] than D_2, the thermoneutrality of reaction 1 ensures that this is the case (since $D_1 + D_2 = D(NC-CN)$). However, we can set a more useful limit on D_2 since, if a chain is to be maintained, the hydrogen atoms must be regenerated by

$$HgCN + H_2 \longrightarrow HCN + Hg + H \qquad (4)$$

which is exothermic provided that $D_2 < 26$ kcal. Because of the high concentration of H_2, this reaction could be sufficiently fast even if it had a small activation energy, say $E \leq 4$ kcal. which places an upper limit of about 30 kcal. on D_2. Thus $15 < D_2 < 30$ kcal., which is of comparable magnitude with $D(Hg-Cl)$ and $D(Hg-Br)$. Hence, $130 > D_1 > 115$ kcal., which means that a free-radical decomposition analogous to the mercury alkyl decompositions[8] is impossible. There appears to be no thermochemically favorable

(2) R. Naumann, *Z. Elektrochem.*, 16, 772 (1910).

(3) N. C. Robertson and R. N. Pease, *J. Am. Chem. Soc.*, 64, 1880 (1942).

(4) All thermochemical data from National Bureau of Standards Circular 500 unless stated otherwise.

(5) S. Miyamato, *Chem. Abstr.*, 28, 4319 (1934).

(6) J. Berkowitz, *J. Chem. Phys.*, 36, 2533 (1962).

(7) H. A. Skinner, *Trans. Faraday Soc.*, 45, 20 (1949).

(8) B. G. Gowenlock, *Quart. Rev.* (London), 14, 133 (1960).

reaction through which CN radicals themselves could be produced.

Thermal Decomposition in Methane. Cylinder methane was freed from oxygen and then rigorously purified by repeated trap to trap distillations at temperatures in the range -218 to $-204°$ until it was completely free from ethane; the only remaining impurities were traces of H_2 and N_2. However, in order to maintain suitable flow conditions, the methane had to be diluted with nitrogen, and the final carrier gas composition was N_2 (67%), CH_4 (33%), and H_2 (<0.1%). The over-all rate of decomposition of mercuric cyanide was unaffected by the presence of methane in the nitrogen, and above $410°$ the products were mainly C_2N_2 and HCN, as before, together with small amounts of ethane (1–5%) and methyl cyanide (0.1–0.2%). These new products we assume to be formed by

$$CH_3 + CH_3 \longrightarrow C_2H_6 \qquad (5)$$

and

$$CH_3 + HgCN \longrightarrow CH_3CN + Hg \qquad (6)$$
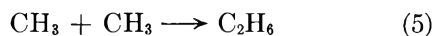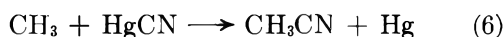
since we have established in separate experiments that methyl radicals do not readily attack mercuric cyanide. The methyl radicals involved in these reactions could be formed in two ways, *i.e.*

$$H + CH_4 \longrightarrow H_2 + CH_3 \qquad (7)$$

or

$$HgCN + CH_4 \longrightarrow Hg + HCN + CH_3 \qquad (8)$$
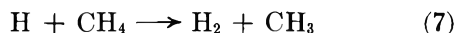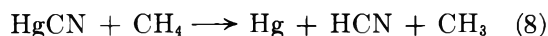
Of these, the latter is the more probable because reaction 8 is more exothermic than reaction 4, whereas reaction 7 is known to have an activation energy of the order of 10 kcal./mole. However, the radical balance shows that not all the HCN is formed by reaction 8 but that most of it comes from reaction 2 since the total HCN always exceeds the sum $[CH_3CN + 2C_2H_6]$ by a factor of from 10 to 50.

Comparison of reactions 3 and 6 shows that the ethane produced is always 10 to 50 times the amount of methyl cyanide. If we assume that reactions 3 and 6 behave as normal recombination reactions like reaction 5, we may write $R_6/R_3^{1/2}R_5^{1/2} \approx 2$, which means that the rate of formation of cyanogen by radical combination is about one-tenth to one-fiftieth that of the methyl cyanide; *i.e.*, at the highest temperatures, reaction 3 accounts for about 10^{-5} of the total cyanogen, which is our justification for assigning Arrhenius parameters to reaction 1.

It is interesting to speculate on the shape of the transition state for reactions 2, 3, 4, 6, and 8. Certainly in reaction 2 one might expect a linear configura-

tion which could lead to the formation of HNC instead of HCN; however, infrared examination of the product hydrogen cyanide under high resolution shows it to be purely HCN. In addition, it has already been noted that when hydrocarbons are present, it is always RCN and not RNC that is produced, indicating that in all these reactions, HgCN behaves as though it were the CN radical. HNC, of course, might readily isomerize to HCN, but this would not be true of the alkyl isonitriles which are thermally quite stable. It is also interesting to note that the products obtained in the preliminary qualitative experiments would not have occurred if the nitrogen diluent used had not contained hydrogen since it is only in the presence of hydrogen that radicals appear to be formed.

Reactions in Packed Vessels. Experiments were performed with the vessel packed with Pyrex beads, increasing the surface area by a factor of 4. With nitrogen as a carrier, the rate of formation of cyanogen from $Hg(CN)_2$ rose, but the extent of the rise was obscured by the formation of paracyanogen particularly at $500°$. This was the only occasion in the whole series of experiments when paracyanogen was produced. It is known that cyanogen is readily polymerized by CN radicals[9,10] and it is possible that HgCN radicals may do likewise when the cyanogen concentration is high enough. Using 20:1 nitrogen–hydrogen mixtures, however, paracyanogen is not formed, even at high temperatures; packing does not cause any change in the rate of formation of HCN at any temperature, but above $400°$ the rate of formation of cyanogen goes up by a factor of 8–10. Thus it seems that reaction 1 is dependent on surface. However, in the chain sequence of reactions 2 and 4, both initiation and termination are equally affected by surface; since termination is probably a wall reaction, this suggests that initiation also takes place on the walls. One might add, as in the case of the C_2N_2–H_2 reaction,[3] there is no homogeneous initiation step which is thermochemically feasible.

The Formation of NOCN. In some experiments, NO was added to the carrier gas but no NOCN was formed. However, in the photolysis of ICN with NO added, the final products did contain NOCN, identified mass spectrometrically; the amount of NOCN was about 0.2 of the C_2N_2, and could be increased by a factor of 2–3 by addition of I_2 to the reaction mixture. At the same time, the radical-catalyzed[11] decomposition of NO to N_2 and NO_2 took

(9) D. E. Paul and F. W. Dalby, *J. Chem. Phys.*, **37**, 592 (1962).

(10) D. E. McElcheran, M. H. J. Wijnen, and E. W. R. Steacie [*Can. J. Chem.*, **36**, 321 (1958)] state that the photolysis of CO(CN)₂ vapor leads to copious formation of paracyanogen.

place, but no NO_2CN was formed. At the moment, our identification of NOCN rests solely on mass spectrometric analysis of the reaction products and an attempt is now being made to isolate a pure sample of NOCN from the mixture of excess NO_2 and C_2N_2. In recent flash photolysis experiments, I + NO have been shown[12] to form the transient NOI, and NO has been reported to react with CN, but the nature of the product was not known.[13]

Silver Cyanide and Cupric Cyanide. Neither of these substances is suitable for kinetic studies similar to those just described. Volatile species do exist over both substances, above about 380 and 190°, respectively. However, thermal decomposition occurs in the condensed phase at all temperatures where volatile species can be detected by flow experiments.[14]

(11) O. P. Strausz and H. E. Gunning, *Can. J. Chem.*, **41**, 1207 (1963).

(12) G. Porter, Z. G. Szabo, and M. G. Townsend, *Proc. Roy. Soc.* (London), **A270**, 493 (1962).

(13) N. Basco, J. E. Nicholas, R. G. W. Norrish, and W. H. J. Vickers, *ibid.*, **A272**, 147 (1963).

(14) D. H. Shaw, unpublished results.

Benzene Production in the Radiation Chemistry of Acetylene

by F. H. Field

Humble Oil and Refining Company, Research and Development, Baytown, Texas
(*Received October 12, 1963*)

Benzene production by the irradiation of acetylene has been investigated as a function of pressure (3–200 torr) at 30 and 80° and at 30° in the presence of added Ar, H_2, and mixtures of Ar and H_2. In the experiments with pure C_2H_2 the fractions of reacted C_2H_2 converted to C_6H_6 and $G(C_6H_6)$ pass through maxima at 20–30 torr, and the amount of C_6H_6 formed increases with temperature. The range of C_6H_6 yield values found is 0.23–0.46, and the range of $G(C_6H_6)$ is 5.1–13.0. Values of $G(-C_2H_2)$ are essentially invariant with pressure, but the average value increases from 68 to 91 when the temperature is increased from 30 to 80°. The fraction of reacted C_2H_2 converted to C_6H_6 is independent of radiation intensity, but $G(C_6H_6)$ and $G(-C_2H_2)$ drop sharply between 6×10^{12} and 42×10^{12} e.v./cm.^{3} sec. but then do not change much as the intensity is increased further. A reaction model and mathematical analysis are given, and a calculated C_6H_6 yield curve of the same form as that observed experimentally is obtained. The addition of both Ar and H_2 by themselves lowers the amount of C_6H_6 formed, but the addition of Ar to a C_2H_2–H_2 mixture has no significant additional effect. The addition of Ar decreases $G(-C_2H_2)$ significantly, but the effect of the addition of H_2 is much less marked. From the effect on $G(-C_2H_2)$ it is concluded that at relatively low pressures both Ar and H_2 are efficient in transferring energy to C_2H_2, but at higher pressures the efficiency decreases. The addition of H_2 depresses the value of $G(C_6H_6)$ more strongly than does Ar. The experiments indicate that C_2H_3 is not greatly involved in C_6H_6 production. In addition, results obtained cause one to question whether an ionic mechanism is involved in polymer production.

In recent years, several investigations of the formation of benzene in the radiolysis of acetylene have been made.[1-4] It has been found that about 20% of the acetylene reacting produces benzene, and almost all of the remaining reaction produces polymer (cuprene). In most experiments only small amounts of other products, usually C_4 and C_8 unsaturates, are found. Dorfman and Wahl[3] found that at acetylene pressures below 20 torr the fraction of acetylene reacting converted to benzene fell monotonically, the amount of the decrease depending somewhat on the size of the radiation vessel. They also found that the presence of rare gases in large excess (electron fraction = 0.86–0.95) almost completely stopped the formation of benzene. It was suggested that the formation of polymer and benzene involve separate primary processes and, in particular, that ionization of acetylene leads to polymerization, whereas benzene formation involves an excited acetylene molecule, probably in a triplet state. Mains, Niki, and Wijnen[4] assert that a free radical mechanism for the formation of benzene is compatible with their results.

In this paper the results of an investigation of benzene formation in the radiolysis of pure acetylene and of mixtures of acetylene with argon and/or hydrogen will be given.

Experimental

The irradiations were made with 2-Mev. electrons produced by a Van de Graaff generator. The radia-

(1) C. Rosenblum, *J. Phys. Chem.*, **52**, 474 (1948).

(2) L. M. Dorfman and F. J. Shipko, *J. Am. Chem. Soc.*, **77**, 4723 (1955).

(3) L. M. Dorfman and A. C. Wahl, *Radiation Res.*, **10**, 680 (1959).

(4) G. J. Mains, H. Niki, and M. H. J. Wijnen, *J. Phys. Chem.*, **67**, 11 (1963).

tion vessel was made of Pyrex glass in the shape of a conventional round-bottom flask, except that the neck of the flask was sealed off at a distance of about 7.5 cm. from the spherical portion of the flask. The seal-off was worked so as to give a gently curving surface, which served as the entrance window for the electrons. This vessel (volume $\cong$ 500 ml.) constituted part of a closed system (total volume, 882 ml.) which allowed one to circulate the gas being irradiated from the vessel to a cold trap to collect low vapor pressure product and back to the vessel. The circulation was accomplished by means of a glass pump, and the flow rate of the gas was between 500 and 1000 ml./min. Thus the average residence time of the gas in the vessel was approximately 1 min. The temperature of the radiation vessel was controlled by immersing it, except for the electron entrance window, in a thermostated liquid bath. The temperature of the bath was controlled to $0.1°$. During the irradiations, the electron entrance window temperature was controlled by directing a blast of air on it.

The product-receiving trap was constructed of glass and was cooled with a Dry Ice–acetone mixture, which served to condense completely the benzene formed in the irradiation. In most experiments the acetylene was irradiated until about 10% of it reacted, which generally required on the order of 1 hr. Thus, given the rate of circulation which existed, about 0.1–0.2% acetylene reacted during the residence time in the reaction vessel. Clearly, secondary reactions of benzene under these circumstances are negligible. However, in the runs at 80°, the technique used was to irradiate without circulation for 5 min., followed by 5 min. of circulation without irradiation to collect the products. This was done so that the temperature of the gas being irradiated was well defined.

The radiation system other than the radiation vessel, product-receiving trap, and circulating pump was made using stainless steel tubing, fittings, valves, and product vessels. No stopcock grease was present in the radiation system, nor were the radiation products allowed to come in contact with stopcock grease at any point in the course of their analysis. The purpose of these precautions was to prevent loss of benzene by solution in stopcock grease and to attempt to reduce contamination of the system. The system was evacuated with an oil diffusion pump, and no difficulty was experienced in evacuating the system to a pressure of 10^{-3} torr or less and maintaining this vacuum when closed off from the pump for periods of the order of hours. Particular care was taken to exclude oxygen from the system during the radiations.

Pressures were measured with a wide bore mercury

manometer read by means of a cathetometer. In the early stages of the work, an investigation was made of the possibility that noncondensables (presumably H_2) might be formed in the irradiations. This was done using a mass spectrometric technique, and it was found that no noncondensables were formed in significant amounts.

To determine the amount of benzene formed as a product, the benzene condensed in the product-receiving trap during the irradiation was distilled into a stainless steel product receiving vessel. The sample vessel was transferred to another gas handling system, and 1.00 ml. (liquid measure) of Phillips research grade n-hexane, as measured by a pipet, was distilled under vacuum into the sample vessel containing the benzene. The vessel was cooled in an ice bath to increase the solubility of benzene in hexane and agitated to accomplish the dissolution. Appropriate sized samples were withdrawn and were immediately charged into a Perkin-Elmer Model 154D gas chromatograph to make the quantitative determination of the amount of benzene present. The chromatograph was periodically calibrated using synthetically prepared solutions of benzene in n-hexane in the concentration range encountered in the radiation samples. A day-to-day check of the sensitivity of the chromatograph was maintained using pure benzene. The stability of the calibration of the instrument was quite good, and the reproducibility of the response to the synthetic samples was satisfactory.

The energy input to the radiation vessel was determined from the amount of current incident on the window of the radiation vessel. The final calibration of the energy input was made using acetylene itself as the dosimeter. The value of 71.9 for $G(-C_2H_2)$ given by Dorfman and Shipko[2,5] was used, and the calibration runs were made at acetylene pressures in the range 100–150 torr. Most of the experiments here reported were made using beam currents of 30.0 μa., which for pure acetylene at 30° corresponds to a nominal energy input of $1.05 \times 10^{12}P$ e.v./cm.^{3} sec., where P is the acetylene pressure in torr. Thus the total energy input in a typical irradiation of 1-hr. duration at 50 torr mean pressure was 1.89×10^{17} e.v./cm.^{3}. The rate energy input used in the experiments here reported is about the same as that used by Mains, Niki, and Wijnen[4] with their X-ray source. Replicate determinations of the apparatus constants for energy input rates showed an average deviation

(5) This value has also been obtained in earlier α-particle studies. See S. C. Lind, C. J. Hochanadel, and J. A. Ghormley, "Radiation Chemistry of Gases," Reinhold Publishing Corp., New York, N. Y., 1961, p. 164.

from average of about 5%. A separate determination of the apparatus constant for the 80° runs was made. Because the value of 71.9 for $G(-C_2H_2)$ refers to acetylene at room temperature, the body of the radiation vessel was maintained at 30°, but the temperature of the electron entrance window was allowed to rise to 80°. A slightly different apparatus constant from that at 30° resulted.

The acetylene used was purified by being passed slowly through a trap immersed in a carbon dioxide–acetone mixture and through a trap filled with activated charcoal. The mass spectrum of the acetylene obtained from this treatment showed no impurities. The argon and hydrogen were the best grades commercially available and no purification operations were attempted. However, mass spectrometric checks of purity were made, and no impurities were found. A particular effort was made to discover whether oxygen was present, for oxygen very strongly inhibits benzene formation. None was found.

Since the chief goal of this work was to determine in detail the quantitative aspects of benzene formation, no serious effort was made to determine the nature and quantities of other products formed in the acetylene radiolysis. Furthermore, the method of benzene analysis involved the addition of a large excess of n-hexane to the condensable product(s) of the radiolysis, and thus the presence of small amounts of products other than benzene might be concealed. However, a few quantitative runs designed to disclose the presence of other products were made and, of course, a large number of radiolyses were made in total, which would have yielded evidence, or at least clues, for the presence of other products. As was mentioned above, no significant amount of noncondensable gas was formed. In some runs quite small amounts of a substance tentatively identified as diacetylene were observed. It may be stated with confidence that no products other than benzene or polymer were formed in significant amounts in these experiments.

In the early stages of the work the polymer deposited in the reaction vessel was removed by oxidation (burning) between experiments. However, as experience accumulated, it became clear that the results obtained were not dependent upon whether polymer was present in the vessel or not. Dorfman and Wahl[3] report the same experience. Thus in the latter part of the work, several experiments at low pressures were made between removal operations. At no time, however, was the polymer in the radiation vessel allowed to build up to more than a light surface dusting. It might also be mentioned that the presence of polymer did not seem to affect in any way the speed and ease

with which the system could be evacuated to low pressure (10^{-3} torr or less). One concludes that the polymer is formed without relatively low molecular weight, high vapor pressure components.

Results

Pure Acetylene. Figure 1 shows the fraction of reacted acetylene converted to benzene as a function of initial acetylene pressure (P_i). The series of results at 30 and 80° are shown. In addition to the experimental points shown in Fig. 1, experiments were made at 80° at initial pressures of 396 and 754 torr. The fractions of reacted acetylene converted to benzene for these two runs were 0.231 and 0.211, respectively.
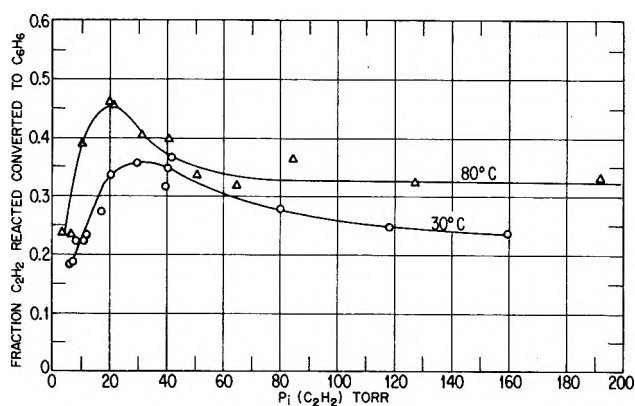

Figure 1.

The shapes of the curves for the runs at the two temperatures are very similar. At the higher temperature somewhat more conversion to benzene occurs and the fall-off at low pressures occurs at somewhat lower pressures. All previous workers agree that at higher pressures, i.e., above 100–200 torr, the fraction of reacted acetylene converted to benzene is on the order of 0.20. From Fig. 1 it may be seen that at 30° the yield curve is approaching this value as the pressure increases, and the values at 80° also approach this value, although at somewhat higher pressures. The maxima in the yield curves at 30 and 20 torr found, respectively, at the lower and higher temperatures have not previously been reported. Dorfman and Wahl[3] found that the fraction of acetylene reacted converted to benzene is constant down to a pressure of 20 torr, and at lower pressures a monotonic decrease occurs. Mains, Niki, and Wijnen[4] made only one run at an acetylene pressure below about 40 torr, but they reported that in the range in which they worked, $G(C_6H_6)$ rises as the initial acetylene pressure de-

creases. From a consideration of their results and those of Dorfman and Wahl[3] they predicted that a maximum in the yield curve should be observed at low acetylene pressures. Aside from the maximum in the benzene yield curve, the results found in this work differ from those reported by Dorfman and Wahl[3] in that the benzene yield is significantly higher over practically the whole pressure range studied, and, in addition, the decrease in benzene production at low pressures is less precipitous.

The production of benzene can be represented in terms of $G(C_6H_6)$, and the values found at 30 and 80° as a function of initial acetylene pressure are given in Fig. 2. In calculating these G-values it has been assumed that with all other variables maintained constant, the energy input to the system is linearly proportional to the pressure. One thus in effect assumes that changes in back scattering, range-energy loss considerations, etc., are negligible. From the essential constancy of the values of $G(-C_2H_2)$ as a function of pressure (discussed later), one concludes that this assumption is reasonably valid. The forms of the $G(C_6H_6)$ vs. P curves are very similar to those of the benzene yield curves shown in Fig. 1. To the extent that comparisons can be made, the G-values found in this work are about 60% of those found by Mains, Niki, and Wijnen[4] with their Co[60] source, and 1.5–3.5 times larger than the values obtained with their X-ray source. At the higher pressures the value of $G(C_6H_6)$ found here approaches the value of 5.1 reported by Dorfman and Shipko[2] for acetylene pressures greater than 100 torr.

Single determinations of $G(C_6H_6)$ were also made at temperatures of 50 and 120°. The values obtained were $G(C_6H_6)$ = 8.5 and 16.5, respectively. The initial acetylene pressure in both cases was 40 torr.
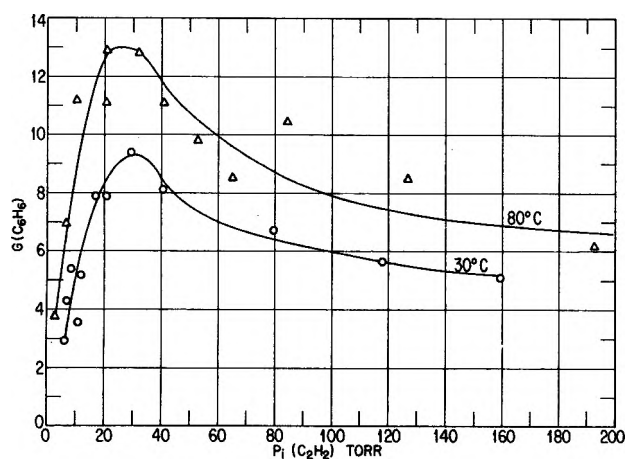
Figure 2.

Thus measurements were made at 40 torr at four different temperatures (30, 50, 80 and 120°), and if one approximates the observed increase of $G(C_6H_6)$ with temperature as being linear, one finds that $\Delta G(C_6H_6)/\Delta t(°C.)$ = 0.10. A similar calculation applied to the given data by Mains, Niki, and Wijnen[4] in the temperature range 12–102° gives $\Delta G(C_6H_6)/\Delta t(°C.)$ = 0.083. The agreement should probably be considered as acceptable. If, as a matter of interest, one makes an Arrhenius type plot for the results obtained in this work, one can calculate that the observed temperature coefficient for $G(C_6H_6)$ corresponds to an activation energy of about 2 kcal./mole.

From the diminution in acetylene pressure, one can calculate values for $G(-C_2H_2)$, and the values obtained in this work at 30 and 80° as a function of initial acetylene pressure are given in Table I. At 30° it is clear that no significant trend in G-values occurs down to a pressure of about 10 torr. Below this value the results are not very reproducible because of the experimental error involved in measuring the small pressure changes encountered, but the data could be interpreted as indicating that a decline in the G-value occurs. However, such an interpretation must be considered as very tentative. At 80°, $G(-C_2H_2)$ is largely constant down to 10 torr, with perhaps a small increase as the pressure decreases. The average value at 80° is about 30% larger than the average value at 30°, and this difference may be considered as experimentally significant.

Table I: G-Values for C_2H_2 Consumption

30°		80°	
$P_i(C_2H_2)$, torr	$G(-C_2H_2)$	$P_i(C_2H_2)$, torr	$G(-C_2H_2)$
7	67 ⎫ 57	9	95
7	47 ⎭	22	97
8	67	40	103
10	48	59	96
12	66	83	83
17	87	97	85
21	71	120	83
30	79	187	84
41	71		
80	72	Av.	90.8
118	68		
160	65		
Av.	68.3		

To investigate the effect of radiation intensity, experiments were made at beam currents of 4 and 100 μa. in addition to the series of measurements at 30 μa.

The values of various quantities of interest at the several beam currents are tabulated in Table II. In making these experiments the total energy input was kept about constant. It is clear from the third column of Table II that the fraction of acetylene converted to benzene is essentially independent of radiation intensity at acetylene pressures of both 40 and 12.5 torr. The value of $G(-C_2H_2)$ falls sharply as the current is increased from 4 to 30 μa., and the change observed is surely experimentally significant. However, as the current increases from 30 to 100 μa., $G(-C_2H_2)$ increases slightly, but it cannot be stated with certainty whether the increase is meaningful. One is inclined to consider $G(-C_2H_2)$ to be essentially constant above 30 μa. As is to be expected from the constancy of the fractional yield of benzene, the variation of $G(C_6H_6)$ is essentially identical with that of $G(-C_2H_2)$.

Table II: Effect of Variation in Radiation Intensity

Beam current, μa.	Energy input rate, e.v./cm.^{3} sec.	Fraction $C_2H_2 \rightarrow$ C_6H_6	$G(-C_2H_2)$	$G(C_6H_6)$
		$P_i(C_2H_2) = 40$ torr		
4.1	5.7×10^{12}	0.356	118	13.8
4.6	6.4×10^{12}	0.384	108	14.2
29.5	41.3×10^{12}	0.315		
30.0	42.0×10^{12}	0.345	70	8.2
32.0	44.8×10^{12}	0.362		
100	140×10^{12}	0.346	78	8.8
109	153×10^{12}	0.338	84	9.4
		$P_i(C_2H_2) = 12.5$ torr		
30	11.7×10^{12}	0.265^a		
104	40.7×10^{12}	0.275		

^{a} Taken from curve, Fig. 1.

Comparing these results with those reported by Mains, Niki, and Wijnen,[4] both agreement and disagreement may be found. Mains, Niki, and Wijnen attribute a difference in the values of $G(C_6H_6)$ found with their Co^{60} source and X-ray source to the fact that irradiation from the X-ray source is about 100 times more intense than that from the γ-ray source, i.e., that $G(C_6H_6)$ exhibits an intensity dependence. The results obtained in the present work show that below an energy input rate of about 40×10^{12} e.v./cm.^{3} sec., an intensity effect does operate in C_6H_6 production, and the intensity variations primarily affect the over-all acetylene consumption rather than changing the relative amounts of C_6H_6 and polymer

formed. However, from the information given by Mains, Niki, and Wijnen, one can estimate that at an acetylene pressure of 40 torr, the energy input rate from their Co^{60} source is about 2×10^{10} e.v./cm.^{3} sec., while that from their X-ray source is about 2×10^{12} e.v./cm.^{3} sec. At a beam current of 4 μa., the energy input in the present work is about three times greater than the larger of these, but even so the value of 14 for $G(C_6H_6)$ given in column five of Table II is very close to the value of 13.6 found by the previous workers at initial acetylene pressure of 43 torr using the Co^{60} source. Mains, Niki, and Wijnen suggest further that intensity considerations play an important additional role in the radiation chemistry of acetylene, namely, that the variation in $G(C_6H_6)$ with pressure observed by them (and corroborated here) is the consequence of changes in the rate of energy input occasioned by the changes in pressure. The intensity results found in this work lead one to question the validity of this suggestion, and, as will be shown later, an alternative explanation for the pressure variation can be advanced.

Mixtures of Acetylene with Argon and/or Hydrogen. All the experiments with mixtures of acetylene and argon and/or hydrogen were made at a temperature of 30°. The effect of the addition of argon, hydrogen, and a mixture of argon and hydrogen on the fraction of reacted acetylene converted to benzene is given in Fig. 3. The initial pressure of acetylene was maintained constant at 40 torr. One sees the rather surprising result that the fraction yielding benzene decreases linearly with pressure of added argon or hydrogen,
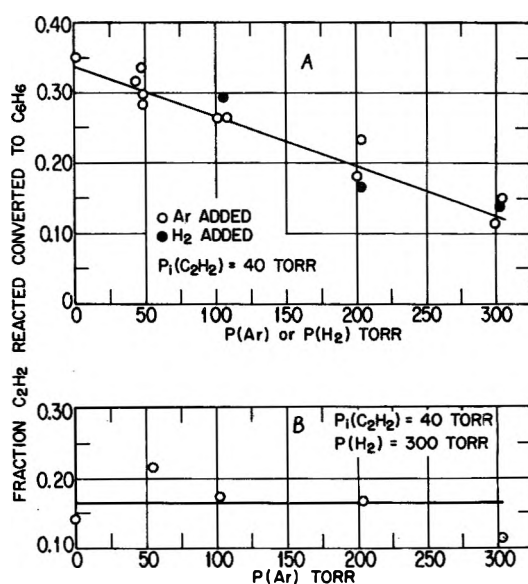

Figure 3.

and the changes with the two added gases are so similar that only one line can be drawn through the points shown in Fig. 3A. From Fig. 3B it may be seen that the addition of various amounts of argon to a mixture of 40 torr of acetylene and 300 torr of hydrogen has no significant effect on the fraction of acetylene reacted to benzene. From the plots of $G(C_6H_6)$ against $P(H_2)$, $P(Ar)$, or $P(Ar + H_2)$ shown in Fig. 4, one can see that both argon and hydrogen depress $G(C_6H_6)$, but argon has the greater effect. The addition of argon to a mixture already containing large excess of hydrogen brings only a small additional depression.

In these experiments with mixtures of substances, the fraction of the total energy absorbed by the various components of the mixture is considered to be proportional to the electron fraction of the components. The G-values are calculated in terms of the total energy input to the system.

By contrast with these results, Dorfman and Wahl[3] found that the addition of rare gases to acetylene brought about essentially complete suppression of benzene formation. Thus in experiments with $P(C_2H_2)$ = 34.24 torr, $P(Ar)$ = 170 torr, $P(C_2H_2)$ = 23.21 torr, and $P(Ar)$ = 127.9 torr, only barely measurable quantities of benzene were formed; that is, a mass equivalent to about 3–10% of the amount of benzene formed in the absence of the rare gas.

Mains, Niki, and Wijnen[4] irradiated acetylene at an initial pressure of about 150 torr in the presence of various (122–422 torr) pressures of krypton, and they find that the rare gas does not suppress the formation of benzene. In the present work one experiment with krypton has been made: $P_i(C_2H_2)$
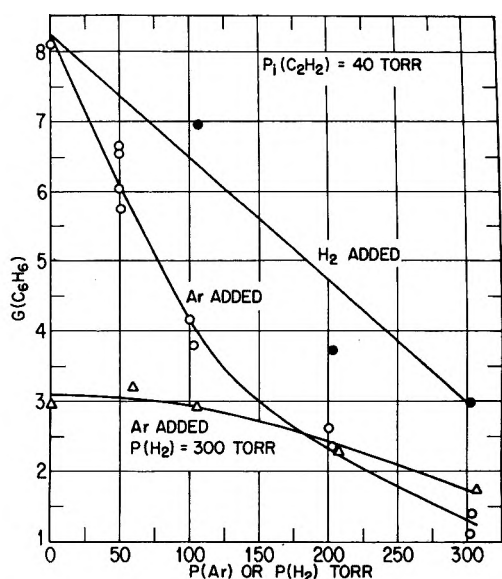
= 40 torr and $P(Kr)$ = 204 torr. The results obtained are: fraction C_2H_2 reacted converted to C_6H_6 = 0.136, $G(C_6H_6)$ = 1.27, and $G(-C_2H_2)$ = 28.1. This corresponds to a somewhat greater suppression of C_6H_6 formation than is found with argon.

Figure 5A shows the effect on $G(-C_2H_2)$ of the addition of argon or hydrogen, and Fig. 5B shows the effect of mixtures of argon and hydrogen. Unlike the effect of these two gases on the fraction of C_2H_2 reacted converted to C_6H_6, the effect of hydrogen on $G(-C_2H_2)$ is much less than the effect of argon. As was the case previously, however, the addition of argon to a mixture already containing a large excess of hydrogen has only a small additional effect.
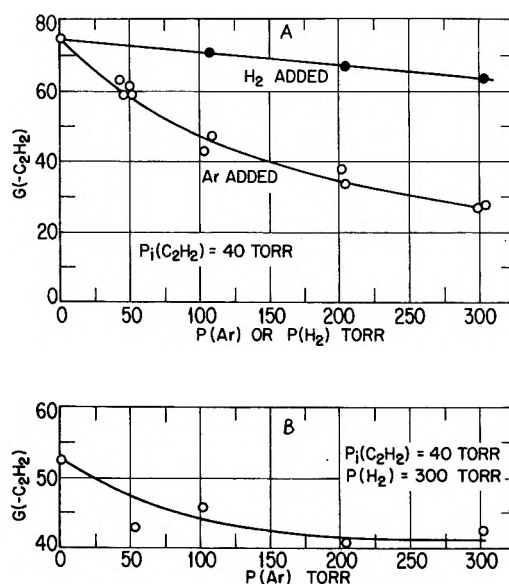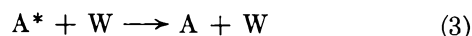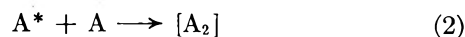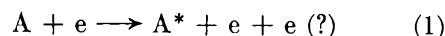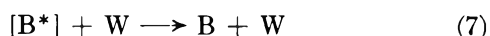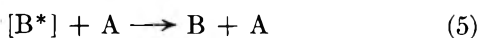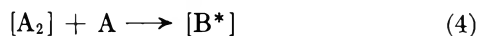

Figure 5.

Discussion

Dorfman and Wahl[3] attributed the decrease in the fraction of acetylene yielding benzene observed by them at low pressures to the quenching by wall reaction of the intermediate(s) involved in the formation of C_6H_6. This hypothesis is quite reasonable, but additional considerations must be invoked to explain the maximum in the benzene production curve observed in the present work.

Thus the processes producing benzene are represented as

$$A + e \longrightarrow A^* + e + e \ (?) \tag{1}$$

$$A^* + A \longrightarrow [A_2] \tag{2}$$

$$A^* + W \longrightarrow A + W \tag{3}$$

Figure 4.

$$[A_2] + A \longrightarrow [B^*] \qquad (4)$$

$$[B^*] + A \longrightarrow B + A \qquad (5)$$

$$[B^*] + A \longrightarrow C \qquad (6)$$

$$[B^*] + W \longrightarrow B + W \qquad (7)$$

In these equations $A = C_2H_2$, $A^* = $ a reactive entity involved in the formation of benzene, $B = C_6H_6$, $B^* = $ an unstabilized entity which is the immediate precursor of benzene; C is some undefined product formed from B^* which is not benzene; and $W = $ wall. Since generally only trace amounts of C_4 products are formed in acetylene radiolysis, it is assumed that the A_2 dimer formed in reaction 2 is a transient intermediate which reacts very rapidly to give B^*. The entity B^* surely requires stabilization to be converted to benzene, for just the exothermicity of the trimerization of C_2H_2 to give C_6H_6 is 142 kcal./mole. The product C conceivably might be a C_8 or high polymer, or it might be a degradation product such as $A^* + 3A$. Because it is assumed that no significant amount of A_2 is formed, it is necessary to postulate that C is not $A_2 + 2A$, i.e., the formation of B^* from A_2 may not be taken as reversible.

Equation 7 represents wall stabilization of B^*, and it assumed that wall collisions are completely efficient in stabilizing B^* molecules. On the other hand, the efficiency of formation of benzene from B^* by homogeneous stabilization is only $k_5/(k_5 + k_6)$. The unit efficiency of (7) is assumed for simplicity; any efficiency factor greater than $k_5/(k_5 + k_6)$ would suffice. Unit quenching efficiency of A^* entities at the wall is assumed, although if one wished, an accommodation coefficient could be introduced.

To treat the system further, it is assumed that the reaction vessel is spherical and that the radiation field fills it uniformly. Then the rate of formation of A^* entities is uniform over the volume of the reactor. The A^* entities are assumed to react homogeneously by (2) and at the wall by (3) and it is further assumed that a steady state has been achieved. The distribution of A^* is given by Fick's law, which in this case takes the form

$$\frac{d^2(A^*)}{dr^2} + \frac{2}{r}\frac{d(A^*)}{dr} + \frac{\alpha I(A)}{D} - \frac{k_2(A^*)(A)}{D} = 0 \qquad (8)$$

where r is the distance from center of reactor; α is a constant of proportionality between I (current) and rate of production of A^*; D is the coefficient of diffusion of A^* in A; and I is the electron beam current. The value of D was calculated from the equation[6]

$$D = \frac{3}{32}\frac{1}{N\sigma^2}\left(\frac{8kT}{\pi\mu}\right)^{1/2} = \frac{169}{P_{torr}} \qquad (9)$$

taking as an approximation that σ is equal to the value applicable to the system CO–N_2.

The solution of (8) obtained assuming as boundary condition that the concentration of A^* at the wall is zero is

$$(A^*)_r = \frac{\alpha I}{k_2}\left(1 - \frac{r_w(e^{br} - e^{-br})}{r(e^{br_w} - e^{-br_w})}\right) \qquad (10)$$

where $(A^*)_r$ is the radial distribution function of $(A)^*$; $b = \sqrt{k_2(A)/D} = \sqrt{1.88 \times 10^{14}k_2 p_{torr}^2}$; and r_w is the radius of reaction vessel = 5 cm.

The average value of (A^*) is obtained by evaluating the equation

$$(A^*)_a = \frac{4\pi\int_0^{r_w}(A^*)_r r^2 dr}{4\pi\int_0^{r_w}r^2 dr} \qquad (11)$$

to obtain

$$(A^*)_a = \frac{\alpha I}{k_2}\left[1 - \frac{3}{br_w^2}\left(\frac{r_w(e^{br_w} + e^{-br_w})}{e^{br_w} - e^{-br_w}} - \frac{1}{b}\right)\right] =$$
$$\frac{\alpha I}{k_2}(1 - f(P)) \qquad (12)$$

The term $\alpha I/k_2$ is the value of (A^*) which would exist in the absence of destruction of A^* at the wall, and the term $f(P)$ represents the fraction of this lost to the wall as a function of pressure.

Values of the quantity $[1 - f(P)]$ for several different values of the rate constant k_2 are plotted against acetylene pressure in Fig. 6. The smaller the rate constant for the homogeneous consumption of A^*, the greater the wall effect, which is the result one expects.

To proceed rigorously, one should solve an equation analogous to (8) for the distribution of B^*. However, in view of the distribution of A^* just calculated, one could not take the production of B^* to be uniform over the volume of the reaction vessel, and the mathematical problem would become very difficult. Since the wall effect for A^* sets in quite sharply below a more or less critical pressure when k_2 is larger than about 10^{-15} cc./molecule sec., one may consider as an approximation that the loss of B^* to the walls is represented by a function of the form of $f(P)$ given in (12). For loss of B^* this function is designated as $f'(P)$. The

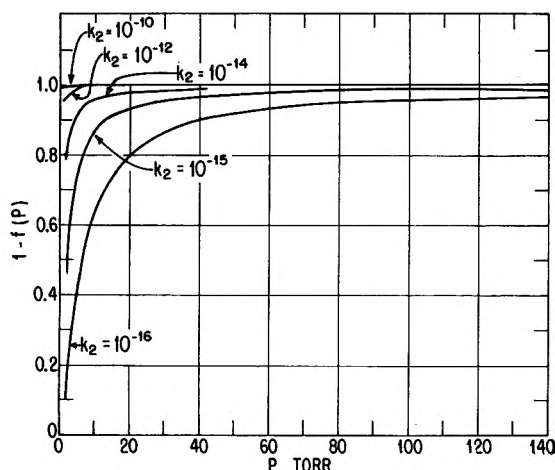(6) S. W. Benson, "The Foundation of Chemical Kinetics," McGraw-Hill Book Co., Inc., New York, N. Y., 1960, p. 184.

Figure 6.

Figure 7.

approximation would be particularly good if the rate of the homogeneous consumption of B* (eq. 5 and 6) were significantly slower than the rate of consumption of A* (eq. 2). At low pressures the loss of A* to the walls will dominate.

By making a steady treatment of (1)–(7) one can show that in the absence of loss of B* to the walls, the concentration of B* will be $k_2(A^*)/(k_5 + k_6)$. When wall effects are considered, the fraction of the B* disappearing at the wall is given by $f'(P)$ and $1 - f'(P)$ is the fraction of B* disappearing, homogeneously. Then one can write for the rate of formation of B the expression

$$R_{C_6H_6} = \left[f'(P) + \frac{k_5}{k_5 + k_6} (1 - f'(P)) \right]\left[\frac{k_2(A^*)}{k_5 + k_6} \right]$$

(13)

The term (A*) is taken from (10), yielding

$$R_{C_6H_6} = \frac{\alpha I}{k_5 + k_6} \left[f'(P) + \frac{k_5}{k_5 + k_6} (1 - f'(P)) \right] \times$$

$$[1 - f(P)] = \frac{\alpha I}{k_5 + k_6} (F(P)) \quad (14)$$

In writing (13) it is assumed that wall deactivation of B* leads to the formation of benzene with unit efficiency. As was the case with A* loss at the wall, an efficiency of less than unity can be accepted as long as it is greater than $k_5/(k_5 + k_6)$.

Values of $F(P)$ as a function of pressure were calculated using a digital computer for several assumed values of k_2, k_5, and k_6. Note that in evaluating $f'(P)$, $k_5 + k_6$ corresponds to the constant k_2 used in evaluating $f(P)$ (see eq. 10). The curve for $F(P)$ shown in Fig. 7 results from the use of the following values for the various rate constants: $k_2 = 10^{-16}$
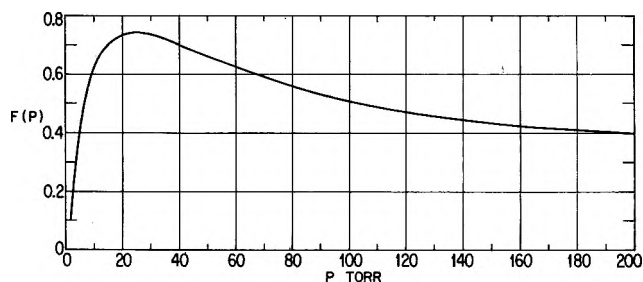
cc./molecule sec., $k_5 + k_6 = 10^{-18}$ cc./molecule sec., and $k_5/(k_5 + k_6) = 0.25$. The form of the curve is very similar to the curve for the fraction of acetylene yielding benzene and $G(C_6H_6)$ shown in Fig. 2.

The agreement of (14) with experiment is taken to indicate that the reaction sequence (1)–(7) is not incompatible with the experimental findings. One is strengthened in this view from the fact that the values of the rate constant needed to give the $F(P)$ curve shown in Fig. 6 are reasonable. The rate constant k_2 refers to the combination of two acetylene-like entities, which may be considered as a combination of two linear molecules. Benson[7] states that for this type of reaction a steric factor of 10^{-3} to 10^{-4} may be expected. A temperature coefficient for benzene formation has been observed, and the corresponding activation energy is 2 kcal./mole. At 30° an activation energy of this magnitude effects a lowering of the reaction rate by a factor of roughly 10^{-2}, and when this is combined with the steric factor one concludes that the value of k_2 should be a factor of 10^{-5} to 10^{-6} times the collision frequency; that is, a value of 10^{-16} cc./molecule sec., for k_2 is not unreasonable assuming A* to be a nonionic entity. The rate constant k_5 involves a stabilization and/or a cyclization, and particularly in the latter case the steric factor will be quite large, possibly such as to give a rate constant 10^{-6} to 10^{-7} times the collision frequency. Thus a value of 10^{-18} for k_5 can be accepted without strain. The analysis requires k_6 to be somewhat larger than k_5, although probably not by more than a factor of ten.

Mains, Niki, and Wijnen[4] assert that a free-radical mechanism involving vinyl radical is compatible with their data. In the present work, acetylene–hydrogen–argon mixtures have been irradiated with varying amounts of argon. From the work of Lampe,[8] one expects the concentration of H atoms to increase, but as can be seen from Fig. 3B the relative amount

(7) See ref. 6, p. 280.

(8) F. W. Lampe, J. Am. Chem. Soc., 82, 1551 (1960).

of benzene formed from the acetylene with an excess of H_2 is essentially independent of argon pressure. To the extent that one can consider that an enhancement of the hydrogen atom concentration in the system will lead to an enhancement of the C_2H_3 radical concentration, these results suggest that vinyl radicals are not much involved in the formation of benzene.

Several points of interest concerning the observed variations in $G(-C_2H_2)$ can be made. It may be seen from Table I that increasing the temperature from 30 to 80° increases the value of $G(-C_2H_2)$ by about 20 units, and this corresponds to an increase in G(polymer) of about 10 units. If polymer is formed by an ionic mechanism · as suggested previously,[3] one would not expect it to have a positive temperature coefficient in view of the known fact that gas phase ionic reactions proceed very rapidly on essentially every collision.

In Table II it is shown that the fraction of acetylene producing benzene is independent of intensity but that between an incident current of 4 and 30 μa. sharp changes in the values of $G(-C_2H_2)$ and $G(C_6H_6)$ occur. Thus these two quantities are varying together, and it is not easy to visualize how this will happen if two different types of reaction (ionic and neutral) are involved in the consumption of acetylene.

In Fig. 8A and 8B, plots of $G(-C_2H_2)/G(-C_2H_2)_0$ and $Y(C_6H_6)/Y(C_6H_6)_0$ are given as a function of $E(C_2H_2)/E_{total}$. In this notation the subscript 0 refers to the value of the quantity in the absence of an added gas and $Y(C_6H_6)$ represents the fraction of reacted acetylene converted to benzene. The added gases were argon and hydrogen, and the G-values are calculated on the basis of the total energy absorbed by the mixture. If no energy were transferred to the acetylene and if the rate of reaction of the energized acetylene molecule were not changed by the presence of the foreign gas, the plot of $G(-C_2H_2)/G(-C_2H_2)_0$ against energy fraction should be linear with unit slope. From Fig. 8A one may see that significant amounts of energy are transferred to the acetylene. At lower values of $E_{C_2H_2}/E_{total}$ (higher values of $P_{Ar}/P_{C_2H_2}$), the G-value ratio falls off rather sharply. This must result either from dissipation of the energy in the added gas before it can be trans-
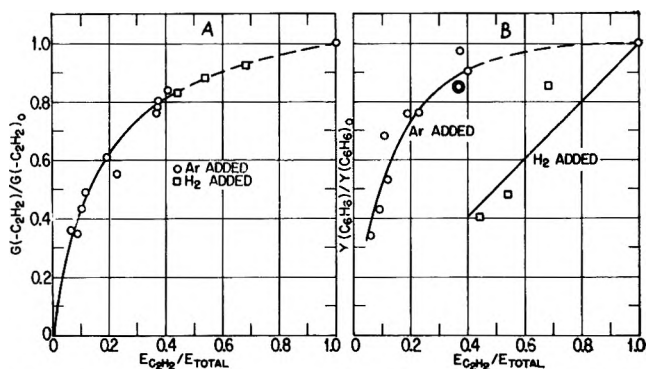

Figure 8.

ferred to the acetylene or to lack of reactivity of the acetylene as a result of the relatively high degree of dilution. Of much interest is the fact that the values of $G(-C_2H_2)/G(-C_2H_2)_0$ obtained when hydrogen is the added gas fall on the curve obtained when argon is the added gas.

Now considering the C_6H_6 yields, one can see from Fig. 8B that significant amounts of energy which will produce C_6H_6 are transferred from the argon at high values of $E_{C_2H_2}/E_{total}$, but at low values the production of C_6H_6 from the energized C_2H_2 molecules is inhibited. While a number of mechanisms for this inhibition can probably be advanced, it might be mentioned that the phenomenon is compatible with the reaction sequence (1)–(7) where the presence of argon may be thought of as enhancing (6) or a reaction analogous to (6).

Conclusions concerning the C_2H_2–H_2 system are limited by the small number of experiments performed, but even so it is apparent that the effect of hydrogen is rather different from that of argon. As is shown in Fig. 8B, hydrogen decreases the yield of benzene much more than argon, which may be taken to indicate that energy transfer to form C_6H_6 does not much occur.

The Decomposition Pressure of Plutonium Nitride[1]

by W. M. Olson and R. N. R. Mulford

University of California, Los Alamos Scientific Laboratory, Los Alamos, New Mexico
(Received October 14, 1963)

Decomposition pressures for the reaction PuN(s) → Pu(l) + 0.5N₂(g) in the temperature range 2290–2770° are reported, and experiments which define some of the properties and methods of preparation of PuN are described. An equation, log p(atm.) = 8.193 − (29.54 × 10³)/T + 11.28 × 10⁻¹⁸T^5 (T in °K.), was found to fit the variation of the decomposition pressure with temperature over the above range.

Introduction

As part of a general program to investigate the fundamental properties of refractory plutonium compounds, measurements of the decomposition pressure–temperature relation for plutonium nitride were made. In addition, a number of supporting experiments intended to give information on the stoichiometry of PuN were done. The decomposition pressure–temperature relation was determined by observing the apparent melting point of PuN as a function of nitrogen pressure.

At nitrogen pressures below that necessary for congruent melting of PuN, the reaction

$$\text{PuN(s)} \longrightarrow \text{Pu(l, satd. with N)} + 0.5\text{N}_2\text{(g)}$$

occurs whenever the temperature is such that the decomposition pressure exceeds the ambient nitrogen pressure, and the solid liquefies.

Thus measurement of the apparent melting point of PuN as a function of nitrogen pressure will give the equilibrium pressure for the decomposition reaction as a function of temperature. A possibility also exists of observing the true congruent melting point of PuN. This possibility will be realized if the nitrogen pressure over the sample is maintained high enough to suppress decomposition at the melting temperature. The highest pressure that could be attained in the present work, 24.5 atm., was too low for us to observe the congruent melting of PuN.

Previous work on plutonium nitride is scanty. The melting point of PuN under 1 atm. of nitrogen has been measured by Carroll[2] who reports 2750 ± 75°. This result differs considerably from ours, which is 2584 ± 30°.

Rand and Street[3] have measured the thermal expansion of PuN at temperatures between 25 and 1000° by X-ray methods. Their PuN samples were made by treating plutonium metal with nitrogen containing a small amount of hydrogen at 600° followed by heating to 1500° *in vacuo* to remove any hydrogen. They report a composition of PuN₀.₉₀₇ with a lattice parameter of a = 4.9069 ± 0.0005 Å. for samples prepared in this way. After subsequent heating to 1000°, the lattice parameter had decreased to 4.9049 ± 0.0005 Å. Our value for the lattice parameter of PuN after heating (4.9055 ± 0.0003 Å.) agrees with the latter value within the limits of error, and also with Carroll's value of 4.905 ± 0.001 Å. Brown, Ockenden, and Welch,[4] and also Zachariasen[5] report a lattice parameter of 4.905 Å.

Experimental

The apparatus and method used in measuring the decomposition pressure of PuN have been described in detail previously.[6]

A tungsten strip 0.25 in. wide and 0.005 in. thick

(1) Work performed under the auspices of the U. S. Atomic Energy Commission.

(2) D. F. Carroll, "Synthesis and Properties of Plutonium Mononitride," Document HW-5A-2755, General Electric Co., Hanford Atomic Products Operation, Richland, Wash., 1962.

(3) M. H. Rand and R. S. Street, "High Temperature X-ray Diffraction Studies. Part 3. Plutonium Nitride and Plutonium Sesquicarbide," Document AERE-M973, United Kingdom Atomic Energy Authority, 1962.

(4) F. Brown, H. M. Ockenden, and G. A. Welch, *J. Chem. Soc.*, 4196 (1955).

(5) W. H. Zachariasen, "The Transuranium Elements," McGraw-Hill Book Co., New York, N. Y., 1949, p. 1448.

(6) W. M. Olson and R. N. R. Mulford, *J. Phys. Chem.*, 67, 952 (1963).

was used to heat the sample. A vee with a 30° included angle was formed in the center of the tungsten strip and the PuN sample was placed in the apex of the vee. The tungsten strip was heated by passing an electric current through it. The behavior of the sample was observed, and the temperature of the strip was determined with an optical pyrometer sighted into the vee through a quartz window in the top of the pressure vessel.

Several methods of preparing PuN were attempted. Heating of the elements for many hours at temperatures up to 1000° did not result in the formation of a significant amount of the compound. Arc melting plutonium under 0.5 atm. of nitrogen converted approximately 80% of the metal to PuN. When pure PuN powder was arc melted under the same conditions, a similar product resulted, and it was concluded that this pressure was insufficient to obtain congruent melting.

It has been reported[3] that PuN may be prepared by direct reaction of the elements at 600° if a small amount of hydrogen is present. This method was successful but only a few samples were prepared in this way.

Most of the plutonium nitride used in the decomposition pressure measurements was prepared from plutonium metal by first forming plutonium hydride, then flowing spectroscopically pure nitrogen over it at 500°. The product was a finely divided powder (estimated from X-ray data to be less than 0.1 μ in particle size), which ignited spontaneously when exposed to the ordinary air in the laboratory. However, when the freshly made powder was first exposed to argon containing a small amount of air, it could then be handled in air without igniting. The stock of PuN thus passivated was stored in vacuo until needed.

For most of the determinations, about 5 mg. of the PuN powder was placed in the vee, the apparatus was evacuated, and then filled with pure nitrogen (either Linde spectroscopically pure or Matheson prepurified) to the desired pressure. The temperature was increased very rapidly until the expected melting point had almost been attained, and then was increased slowly until the sample melted. When the pressure was less than 0.03 atm., melting was not seen. Instead, the sample volatilized suddenly when the decomposition temperature was reached. At pressures above 0.03 atm. the transition of the particles from solid to liquid could be observed, although above 2 atm. it was difficult to see the specimen clearly. It is estimated that the melting point of the PuN could be read to about ±5° with this technique, as the temperature read immediately before melting usually differed

from the temperature read immediately after melting by about 10°.

The possibility that oxygen pickup by the stock of PuN powder when it was handled in air might influence the decomposition pressure was investigated by making several determinations in which the PuN used had never been exposed to air. For these experiments a piece of plutonium wire was placed in the tungsten vee in the apparatus. Then the wire was either hydrided and nitrogen flowed over it at approximately 600° or it was heated to this temperature in a static atmosphere of nitrogen containing a small amount of hydrogen. After the wire was converted to nitride, the gas was pumped out, fresh nitrogen was admitted, and the melting point was determined.

Results

The decomposition pressure–temperature data plotted as $\log p$ vs. $10,000/T$ are shown in Fig. 1. Open circles represent data from the stock PuN handled
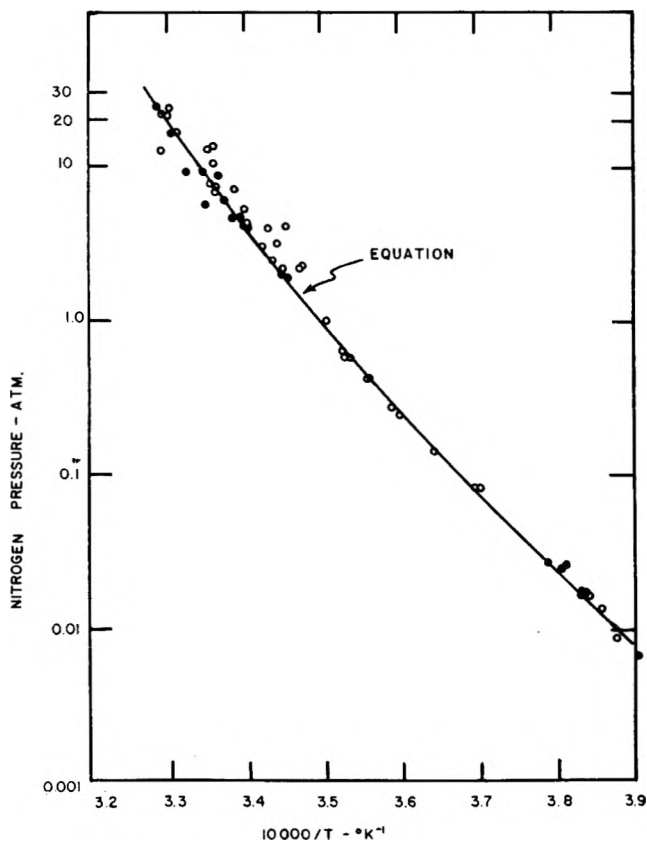

Figure 1. Decomposition pressure of PuN.

in air; solid circles represent data from PuN made in situ and not exposed to air. The agreement between the results for the two kinds of PuN is good, apparently indicating that a slight amount of oxida-

tion does not influence the melting point very much.[7] The data are fitted by a gentle curve over the entire range investigated. Congruent melting of the PuN was not observed, as the apparatus did not permit the use of high enough pressures. There is considerable scatter in both sets of data at pressures above 2 atm. This scatter is probably a result of difficulty in detecting melting. At high pressures the optical path is distorted by strong convection currents and it is difficult to see the sample clearly.

Several experiments were done in an attempt to determine whether or not PuN exists over a composition range. If it does, a variation in nitrogen content should cause a variation in X-ray lattice parameter. A button consisting of PuN dispersed in a plutonium matrix was made by arc melting plutonium in a nitrogen atmosphere. The button was then heat treated at 1500° for about 3 hr. After this treatment the lattice parameter of the PuN phase was found to be 4.9051 ± 0.0002 Å., and analysis showed that the button contained 450 p.p.m. of oxygen. Next, a sample of PuN made in the tungsten vee was held at 1500° for 2 hr. under a nitrogen pressure of 5.1 atm. The lattice parameter of the sample after this treatment was 4.9056 ± 0.0003 Å. Finally, the lattice parameter of a sample also made in situ but heated to 2700° under 17 atm. of nitrogen was 4.9055 ± 0.0002 Å. The tungsten vee cooled very rapidly when the power was shut off and the samples were thus quenched. As no significant difference in lattice parameter was detected between "nitrogen-rich" and "nitrogen-poor" PuN, it appears that at high temperatures if there is any composition range at all it must be small.

Measurement of the nitrogen-to-plutonium ratio was also attempted. Nitrogen was determined by a modified Kjeldahl method in which the sample is initially dissolved in a mixture of hydrochloric and perchloric acids. Samples of PuN were made at 600° via the hydride route from weighed pieces of metal in a glass ampoule which was then sealed off and then later broken under the acid to preclude exposing the sample to air. Four such samples gave nitrogen-to-plutonium ratios of 0.945, 0.946, 0.961, and 0.967. These particular samples were not examined by X-ray, but other samples made in the same way invariably gave diffuse lines in the diffraction pattern and the lattice parameters could not be measured accurately. There is also some doubt as to the absolute accuracy of the nitrogen analyses, since the samples did not dissolve completely in the acid mixture but left a residue. It has been assumed in computing the above ratio that the residue involved only plutonium,

and that all the nitrogen in the sample was determined.

The PuN powder was extremely susceptible to oxidation by air during handling. Even a very brief exposure to air, as, for example, the few seconds required to transfer a weighed sample from its container into the oxygen analysis apparatus, was sufficient to introduce several atomic per cent of oxygen into the sample. Thus, all of the oxygen analyses on powdered PuN, no matter what precautions were taken during its preparation, showed that it contained between 0.47 and 0.90 wt. % oxygen. On the other hand, the massive material, which was made by arc melting plutonium in a nitrogen atmosphere, contained only 450 p.p.m. of oxygen, as mentioned above. Therefore, any oxygen analysis done on powdered PuN would appear to be meaningless unless exposure to air or moisture is rigorously excluded in all handling procedures. Although surface oxidation of the PuN powder does not affect the lattice parameter, the heating of oxidized PuN does cause oxygen to dissolve in the lattice, with consequent enlargement of the lattice parameter. Thus, several samples which had been handled so that they did not contain dissolved oxygen had lattice parameters of 4.9055 Å. despite oxygen analyses of several atomic per cent, while other samples which had been heated after being exposed to air had lattice parameters as high as 4.9099 Å. These latter samples also contained as much as 4 atomic % oxygen according to the analyses.

Discussion

The standard heat and entropy of the decomposition reaction observed cannot be obtained from the present data because the activity of the liquid plutonium formed is not known and thus the equilibrium constant cannot be calculated. However, it is possible to compute a limit for the heat of formation of PuN by using estimates of the standard entropy of formation and the appropriate heat capacities. According to Rand and Kubaschewski,[8] the absolute entropies of

(7) One referee has suggested that the data do indicate an effect of oxygen on the decomposition pressure of PuN, as it appears in Fig. 1 that there is a significant difference between the black points through which the fitted equation passes and the open points. While this interpretation may be correct, it is our opinion that any difference between the two sets of points is not distinct enough for us to draw an unequivocal conclusion. In addition, we would expect an effect from oxygen contamination to appear over the whole temperature range studied, while, if there is any deviation of the oxidized samples from the unoxidized, it appears to exist only at the higher temperatures. The difference between lines through the open points and the black points is about 30° and in view of the scatter we do not feel this to be a significant difference.

It should also be realized that the way we have chosen to fit the line to the data involves only one free parameter, and hence one experimental point. The fact that this line goes through the black points very well, but lies below the open points may be fortuitous.

metallic nitrides having the NaCl-type of structure are not very different from those of the parent metal. Thus, by using $S°_{298}(\text{PuN}) - S°_{298}(\text{Pu}) = 1 \pm 1$, one obtains $\Delta S°_{298} = -22 \pm 1$ cal./mole/deg. for $\text{Pu(s)} + 0.5\text{N}_2(\text{g}) = \text{PuN(s)}$. The average heat capacity change for this process is estimated to be $\Delta C_p° = 1.5$ cal./mole/deg. Using these estimates, the change in the standard free energy function for the reaction at any experimental temperature can be found. The lowest point on the experimental pressure–temperature curve is assumed to be closest to the standard reaction, that is, the liquid plutonium formed at the lowest temperature would be expected to have the least nitrogen in solution and thus to have an activity closest to unity. Hence, a third-law calculation of $\Delta H°_{298}$ can be made by using the estimated free energy function and the lowest experimental point. The value so obtained is $\Delta H°_{298} \leq -64$ kcal./mole. The actual standard heat of formation of PuN will be somewhat more negative than this. From analogy to UN, it is reasonable to guess that the heat of formation of PuN probably will be about -70 kcal./mole. This is in contrast to -95 kcal./mole estimated by Brewer.[9]

In order to present the results in a convenient form, an empirical equation of the form $\log p = A + B/T + CT^5$ was fitted to the experimental points. In previous similar work with UN,[2] the same form of equation was used, in which the A and B coefficients were the standard entropy and enthalpy changes at the temperature, respectively, and the CT^5 term allowed for deviations from the standard states of the liquid uranium and solid uranium nitride. For PuN the standard heat of formation is not known. The stand-ard heat and entropy of formation estimated above for PuN are the same as for UN. Therefore, the A and B coefficients of the UN equation were used for the PuN equation, and the C coefficient was fitted to the PuN data. The resulting equation is

$$\log p(\text{atm.}) = 8.193 - (29.54 \times 10^3)/T + 11.28 \times 10^{-18}T^5$$

with T in °K. This equation fits the observed data well, as can be seen in Fig. 1, and probably can be used for extrapolations to lower temperatures.

It should be pointed out that the pressures we have measured are presumed to be the equilibrium pressures for the univariant equilibrium between nitrogen gas, liquid plutoniums aturated with nitrogen, and plutonium-rich PuN. While some evidence is presented above which indicates that no composition range exists for PuN, it is possible that, perhaps at lower temperatures, there is a stoichiometry range. If so, the pressures given by the equation will represent the decomposition pressure of the PuN of a composition lying on the plutonium-rich boundary of the PuN composition range.

(8) M. H. Rand and O. Kubaschewski, "Thermochemical Properties of Uranium Compounds," Document AERE-R-3487, United Kingdom Atomic Energy Authority, 1960.

(9) L. Brewer, *et al.*, "The Transuranium Elements," McGraw-Hill Book Co., New York, N. Y., 1949, p. 863.

Magnetic Susceptibility Changes during the Adsorption of

Oxygen and Carbon Monoxide on Cuprous Oxide

by John D. Cotton and Peter J. Fensham

Department of Chemistry, University of Melbourne, Parkville, Victoria, Australia   *(Received October 14, 1963)*

Measurements of the magnetic susceptibility of cuprous oxide films on copper powder have been made during the adsorption of oxygen and carbon monoxide. A paramagnetic form of ionized oxygen appears and reaches an equilibrium coverage which is less than a monolayer. No change in susceptibility occurs when carbon monoxide adsorbs on an evacuated surface of the oxide, but on a previously oxygenated surface, carbon monoxide adsorbs and reacts with some of the oxygen and at the same time the paramagnetism is destroyed. The implications of these results for the nature of the adsorbed species are discussed.

The processes occurring during the reaction of oxygen and carbon monoxide on the surface of cuprous oxide have been studied by numerous experimental techniques.[1-5] From these results it is known that oxygen chemisorbs on a thin layer (100–500 Å.) of cuprous oxide to something more than a monolayer coverage and that the reaction involves transfer of electrons from the solid to the oxygen. The positive holes left behind in the surface region of the solid give rise to enhanced conductivity, and the system is a classic case of what has been called cumulative adsorption.[6] It is also known that such a surface can be regenerated for further absorption by treating *in vacuo* at 470°K., and during this anneal the extra oxygen becomes part of the oxide layer by the normal mechanism for oxidation at this temperature. Some earlier attempts to explore this adsorption reaction had shown that there was no change in the magnetic state of the system after the cycle of adsorption and oxidation was complete in accord with reproducible chemical properties of the system.[7,8] However, owing to insufficient sensitivity,[7] the question was left unanswered as to whether a paramagnetic species appears on the surface during the cycle. In the present investigation, a refined technique does lead to evidence of a paramagnetic intermediate.

Experimental

The copper was prepared by reduction of cupric hydroxide with hydrazine. This preparation has also

been used in earlier magnetic studies of the copper–oxygen system[7,8] and measurements at varying field strengths and by e.p.r. techniques have shown that the samples were suitably free of ferromagnetic impurities. After final reduction of the surface with hydrogen at 450°K., it was allowed to oxidize under controlled conditions until oxide films of appropriate thickness (100–300 Å.) were obtained. The surface area of these powdered preparations ranged from 2 to 4 m.^{2} g.$^{-1}$ measured by B.E.T. adsorption of krypton at 77°K.

A thin glass bucket (0.8 cm. diameter × 3.0 cm.), perforated with tiny holes, was loosely packed with 1.5 g. of the powdered copper, and suspended from one arm of a Gulbransen type balance.[9] The balance beam was constructed from quartz rod (0.18 cm. diameter), and it was supported by tungsten wire (0.005 cm. diameter). On the other arm of the balance were hung glass counterweights or a small iron dust core surrounded by a coarse and a fine solenoid. In the

(1) W. E. Garner, T. J. Gray, and F. S. Stone, *Proc. Roy. Soc.* (London), **A197**, 294 (1949).

(2) W. E. Garner, F. S. Stone, and P. F. Tiley, *ibid.*, **A211**, 472 (1952).

(3) T. J. Jennings and F. S. Stone, *Advan. Catalysis*, **9**, 441 (1957).

(4) E. R. S. Winter, *ibid.*, **10**, 196 (1958).

(5) A. W. Czanderna and H. Wieder, *J. Phys. Chem.*, **66**, 816 (1962).

(6) K. Hauffe, *Advan. Catalysis*, **7**, 213 (1955).

(7) P. J. Fensham, Thesis, Bristol University, 1952.

(8) M. O. O'Keefe and F. S. Stone, *Proc. Roy. Soc.* (London), **A267**, 501 (1962).

(9) E. A. Gulbransen, *Rev. Sci. Instr.*, **15**, 201 (1944).

former situation the balance was used as a deflection instrument covering a small range of weight, and the position was observed with a traveling microscope. In the latter situation the balance was used as a null instrument and weight changes (real and magnetic) were observed as current changes applied to the solenoids to restore the beam to its original position. The sensitivity of this balance was 3.0 μg. per 0.01 mm. deflection with a load of 5–6 g., while above a load of 8 g. the balance became unstable. Under deflection conditions the maximum weight change was 4 mg. The whole balance was enclosed in a glass envelope with a flat window for observation and connected to a vacuum and gas handling line.

The Gouy method was employed for measuring susceptibilities and a permanent magnet with shaped pole pieces (2.0 cm. diameter and 1.5 cm. gap) provided the magnetic field. At the center of the gap the field strength was 4850 oersteds and 2.5 cm. from its center it was 1230 oersteds. With the sample tube placed reproducibly with its two ends in these respective fields, the position was maintained during weight changes by coupling the permanent magnet to the travelling microscope. The magnet could be rotated away from the sample on a hinge thereby providing an "on-off" switch for the magnetic field. The minimum volume susceptibility (κ) which could be detected was thus 0.0005×10^{-6} c.g.s. unit.

Oxygen was prepared by heating A.R. grade $KMnO_4$ and purified through KOH pellets and a liquid air trap. Carbon monoxide was prepared by reacting 90% formic acid with A.R. grade sulfuric acid *in vacuo* followed by purification over solid KOH, heated copper, sputtered sodium, and a liquid air trap.

Results

In expressing the results of adsorption experiments in terms of surface coverages, it is assumed[2] that each copper site in the surface can be regarded as a potential adsorption center, and that there are 5.2×10^{18} such sites per m.[2] which is the mean figure for the site density in the three principal planes (100), (110), and (111).

Adsorption of Oxygen. Preliminary experiments on a sample with an oxide layer showed that the uptake of oxygen at room temperature could be readily measured gravimetrically and the weight changes corresponded to the manometric changes in the system. The surface was regenerated by heating *in vacuo* at 450°K. for 12 hr., but evacuation at 520°K. led to sintering and loss of activity. No desorption was detected on reducing the pressure at 295°K., or when the temperature was raised to 450°K. The kinetics and the extent of the uptake agreed with the

earlier observations of Jennings and Stone.[3] A series of adsorptions were made at 295°K. in which the weight of the sample was measured as a function of time with the magnetic field alternatively "on" and "off." Typical results are shown in Fig. 1. The difference in the observed weight, ΔW, between the two curves represents the increase in paramagnetism of the sample during the adsorption time, and this paramagnetic increase rises sharply to a maximum value which is reached before the adsorption is complete, and sometimes before even a coverage of a monolayer (assuming dissociation) is reached (Fig. 2). After this constant value, ΔW_c, had been reached, evacuation for several hours had little effect, but on raising the temperature for a short time, the susceptibility at 295°K. rapidly fell to a value indistinguishable from the magnetic state of the sample prior to adsorption. Variation of the oxygen pressure in the system changed the constant value, ΔW_c, and also the point on the pure uptake curve, W_c, at which the constancy set in. The ratio, $\Delta W_c : W_c$, however remained
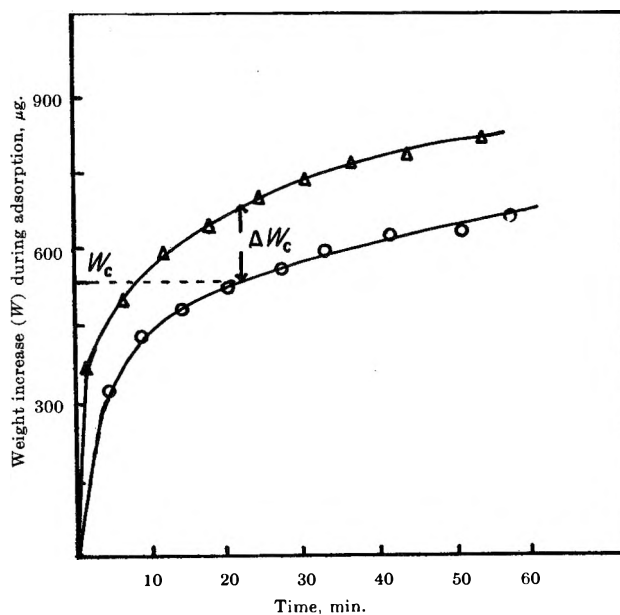

Figure 1. Weight increases during adsorption of oxygen on cuprous oxide at 295°K.: O, weight of oxygen adsorbed with magnet field off; △, apparent weight with magnetic field on.

constant over the pressure range studied as shown in Table I. This ratio is a measure of the apparent weight increase due to paramagnetic species relative to the real weight of the oxygen adsorbed by the time the constancy is established.

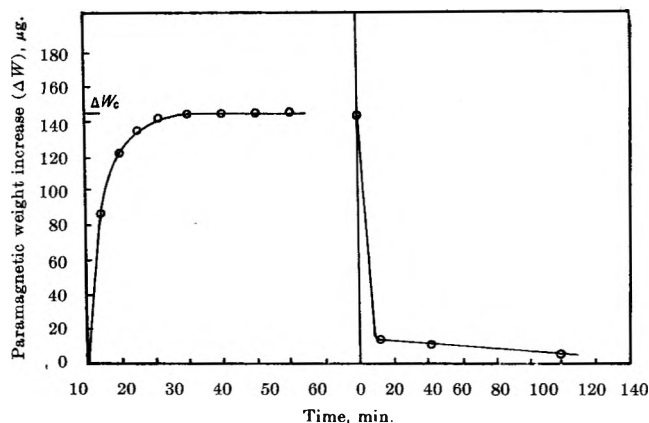*Adsorption of Carbon Monoxide.* When an evacuated oxide surface was exposed to CO at 295°K., adsorption

Figure 2. Increase of paramagnetism during adsorption of oxygen on cuprous oxide at 295°K. (left curve) and its decay during evacuation at 450°K. (right curve).

Table I: Oxygen Uptakes and Paramagnetic Increases during Adsorption on Cuprous Oxide

Expt.	Pressure, mm. Initial	Pressure, mm. Final	ΔW_c, μg.	W_c, μg.	$\dfrac{\Delta W_c}{W_0}$
1	1.46	1.30	156	510	0.31 ± 0.04
2	0.64	0.47	165	510	0.32 ± 0.04
3	0.52	0.17	111	345	0.32 ± 0.06
4	0.12	0.04	84	255	0.33 ± 0.08

was very rapid and reached completion within 5 min. In this case there was no observable change in susceptibility, that is, ΔW was zero. The results of a number of experiments at different pressures are summarized in Table II, in which the extent of desorption by evacuation can also be seen. The surface could be regenerated by heating to 450°K., oxidation at 295°K., and re-evacuation at 450°K.

On exposing a freshly oxygenated surface to CO at 295°K., adsorption occurred rapidly and the weight

Table II: Carbon Monoxide Uptakes and Coverages during Adsorption and Desorption on Cuprous Oxide

Expt.	Pressure, mm.	Total uptake of CO, μg.	Coverage by CO, % Total	Coverage by CO, % Reversible
1	0.11	375	50	38
2	0.22	342	49	37
3	0.03	216	29	25
4	1.00	447	61	47
5	0.46	369	50	?
6	0.19	354	48	38
7	0.22	330	45	35
8	0.25	354	49	38

of the sample increased, passed through a maximum at 3 min., and at 30 min. reached a constant value when the adsorption was complete. This behavior is consistent with the familiar adsorption of CO, and the subsequent desorption of some of it and some of the preadsorbed oxygen. During the time of the adsorption, ΔW, the apparent weight increase due to the paramagnetic species from the oxygen adsorption, decreased steadily to zero. For example, a sample on which 414 μg. of oxygen had been adsorbed, and for which ΔW_0 was 99 μg., adsorbed CO in the above way giving a net increase in weight of 294 μg. by which time ΔW was zero.

Adsorption of Oxygen on Copper. Oxygen was admitted to the reduced surface of the powdered copper at 295°K. and adsorption ensued. However at no stage in the process could any sign of a differential, ΔW, be detected. Since the sensitivity was considerably better than that used by one of us previously when a transient paramagnetism was reported,[7] it must now be concluded that paramagnetic ions do not have an appreciable lifetime on the surface.

Discussion

The adsorption of oxygen on cuprous oxide occurs with electron transfer from the metal ions to the oxygen converting diamagnetic Cu^+ into paramagnetic Cu^{2+}.[1] Several types of adsorbed oxygen may be present, paramagnetic O_2^- and O^-,[4] and diamagnetic $O^{2-}(ads)$[10] and O^{2-}—the last, essentially the same as the surface oxide ions. Adsorption at room temperature proceeds beyond a monolayer, and is explained by the incorporation of $O^{2-}(ads)$ ions into the lattice. Not all the adsorbed oxygen on the surface will react with CO to give CO_2. Garner, Stone, and Tiley[2] showed that not more than 66% of the adsorbed oxygen could be released as CO_2 after 24 hr., and that some CO, even on surfaces saturated with oxygen, was adsorbed by other processes than by forming the CO_3 complex.

There are clearly several possible equilibria inherent in this chemisorption process. First, there is an equilibrium between the process of adsorption and incorporation, and second, between the various forms of adsorbed oxygen. The increase, in Fig. 2, of ΔW to a constant value before adsorption is complete, is indicative of an equilibrium associated with the emergent paramagnetism. It is strong evidence too, that this paramagnetism is essentially associated with the adsorbed oxygen and not with the paramagnetic Cu^{2+} since these ions are steadily produced throughout

(10) F. S. Stone, *Advan. Catalysis,* **13,** 1 (1962).

the whole adsorption process. O'Keefe and Stone[8] have measured the effect of Cu^{2+} ions on the susceptibility of cuprous oxide down to $Cu_2O_{1.05}$, and the lack of a contribution from these ions in our case is surprising although their concentration in the surface may lead to the quenching. This absence of a measurable contribution from the cations is further supported by the removal of all the paramagnetic increase during reaction with CO which is only sufficient to reduce a fraction of the Cu^{2+}.

If then the paramagnetism is due to oxygen, the data suggest an equilibrium on the surface between a singly charged and a doubly charged species of the adsorbed gas. At high pressures, when the adsorption rate is higher, the magnetic equilibrium is not achieved until higher coverages, which indicates that the transfer of the second electron is the rate-determining step. That a concentration of negatively charged ions on the surface would inhibit the transfer of further electrons to complete the ionization of the oxygen is not surprising since these electrons must come from the ionization of Cu^+ ions. However, conversion to O^{2-} on the metal surface could occur because of the availability of electrons in the free-electron band of the metal.

The details of the reactivity with CO suggest that the equilibration inferred from the constancy of $\Delta W_c/W_c$ is related with that between the oxygen which is chemically reactive with CO and that which is not. The association of a singly charged species with reactivity and the doubly charged form with inactivity avoids such a less clear distinction between $O^{2-}(ads)$ and O^{2-} of the oxide surface. It also enables an estimate of the susceptibility of the paramagnetic oxygen to be calculated. In the example given earlier, 99 μg. of paramagnetism was associated with 414 μg. of O_2. Following Garner, Stone, and Tiley,[2] it is reasonable to use 50% as an approximate figure for the amount of adsorbed oxygen which reacts with CO in the experiment. Thus, 207 μg. of oxygen correspond to the ΔW_c value of 99 μg., that is 165×10^{-6} c.g.s. unit of volume susceptibility. Since the sample density was 1.5 g. cm.$^{-3}$ the estimated gram susceptibility χ_g, is $(50 \pm 20) \times 10^{-6}$ c.g.s. unit. We have

assumed that all or most of the paramagnetic oxygen is desorbed, or that the concentration of CO_3 complex on the surface is small as expected in the presence of a large excess of CO.

O_2^- ions in the alkali metal superoxides have a measured χ_g of 33×10^{-6} unit, which agrees well with the figures of 39×10^{-6} unit calculated for a single spin free electron in the molecule ion. The experimental susceptibility, χ_g, of O^- is not available, but a calculated estimate of 165×10^{-6} unit can be obtained for room temperature using the general formula of Van Vleck.[11] The effective susceptibility of the oxide ions on the surface might be expected to be reduced by magnetic interactions; however, Juza[12] did not find any appreciable reduction in the first monolayer of physically adsorbed oxygen from the value for gaseous oxygen molecules. At this stage, it is impossible to differentiate between the two paramagnetic species beyond suggesting that the observed value would seem to be too low if the dominant stable intermediate on the surface is O^-, but that to postulate O_2^- only, raises difficulties with the number of sites involved in the adsorption of the oxygen which is reactive with CO.

The existing model for the adsorption of CO on the evacuated surface of the oxide is supported by the absence of any observed paramagnetism. This rules out any essentially ionic type of bonding involving a charged paramagnetic form of CO. Likewise, the CO_3 complex formed with active oxygen is diamagnetic and must contain an even number of electrons, all of which are paired.

(11) J. H. Van Vleck, "The Theory of Electric and Magnetic Susceptibilities," Oxford University Press, London, England, 1932.

(12) R. Juza and F. Grasenick, *Z. Elektrochem.*, **54**, 145 (1950).

The Effect of Dielectric Constant Difference on

Hyperfiltration of Salt Solutions

by George Scatchard[1]

Oak Ridge National Laboratory, Oak Ridge, Tennessee   (*Received October 17, 1963*)

The equation of Onsager and Samaras for the equilibrium concentrations of an ion near the water–air interface is extended to interfaces between two phases with any dielectric constants, to the concentrations in the phase of lower dielectric constant, and to the minimum concentration in a membrane of the second phase between two exterior phases of the first. Hyperfiltration of sodium chloride through an uncharged membrane is discussed and shown to depend largely upon the equilibrium concentration within the membrane and almost not at all upon the concentrations very near the membrane surfaces.

In the paper in which he first discussed oriented monomolecular films at the water–air interface, Langmuir[2] also suggested that for salt solutions, which increase the surface tension, there is a monomolecular layer of oriented water molecules at the solution–air interface. If the surface concentration is calculated by the Gibbs adsorption isotherm and the thickness of the film is calculated on the assumption that the salt concentration changes abruptly from zero to the bulk concentration, the thickness of the salt-free layer is constant and about 4 Å. for many salts within the scatter of measurements by various observers which were available at that time.

Harkins and McLaughlin[3] and Goard[4] made more measurements and give the thickness of this film for NaCl from 0.1 to 5 M.

The best measurements in dilute solutions are those reported by Heydweiler[5] and those of Schwenker.[6] Heydweiler found that at 18° in dilute solutions the increase of surface tension per equivalent of salt is the same for several uni-univalent salts, some bi-univalent and uni-bivalent salts and the only bi-bivalent salt studied in dilute solutions. The increase per equivalent becomes rapidly smaller with increasing concentration at low concentrations. At moderate concentrations it becomes specific and then passes through a minimum. Schwenker made very precise measurements on LiCl, NaCl, and KCl up to 0.15 M at 0° and confirmed Heydweiler's findings, with very close agreement between the effects of the three salts up to 0.13 M.

Wagner[7] and Onsager and Samaras[8] use the Boltzmann–Debye theory which determines the negative surface concentrations of ions from the mirror-image electrostatic repulsion from a surface at which the dielectric constant changes. They find that some ions penetrate very close to the surface but that the concentration approaches that of the bulk phase rather slowly as the distance increases. They calculate a somewhat smaller increase of the surface tension than Schwenker measured and conclude that there may be other effects very close to the surface, but that the Coulomb expression is valid for distances greater than one molecular diameter, 3 Å.

On the Debye model the ions are charged spheres, all with the same distance of nearest approach A, and the solvent is a continuum, characterized only by its dielectric constant. The radius of the spherical ion within which the dielectric constant is independent

(1) Professor of Physical Chemistry, Emeritus, Massachusetts Institute of Technology. Consultant, Oak Ridge National Laboratory. Work performed for the Office of Saline Water, U. S. Department of the Interior, at the Oak Ridge National Laboratory, Oak Ridge, Tennessee, operated by Union Carbide Corporation for the U. S. Atomic Energy Commission.

(2) I. Langmuir, *J. Am. Chem. Soc.*, **39**, 1848 (1917).

(3) W. D. Harkins and H. M. McLaughlin, *ibid.*, **47**, 2083 (1925).

(4) A. K. Goard, *J. Chem. Soc.*, **127**, 2451 (1925).

(5) A. Heydweiler, *Ann. Physik.*, (4) **33**, 145 (1910).

(6) G. Schwenker, *ibid.*, **11**, 525 (1931).

(7) C. Wagner, *Physik. Z.*, **25**, 474 (1924).

(8) L. Onsager and N. N. T. Samaras, *J. Chem. Phys.*, **2**, 528 (1934).

of the medium is b. The application of this model to the first monomolecular layer is troublesome, but there can be no doubt about the slow approach to the bulk concentration which it pictures.

Recently, Sourirajan[9] has used the Langmuir picture to explain the desalting of sodium chloride solution by hyperfiltration, the removal of small solute molecules by filtering through special membranes. He pictures a successful membrane as one with pores of radii not greater than the thickness of the Langmuir monomolecular water layer so that only pure solvent reaches the membrane.

Sourirajan's explanation should be corrected for the shortcomings of the simple Langmuir picture, and for the fact that the 4-Å. layer corresponds to the water–air interface and not to a water–organic liquid interface at which the change in dielectric constant is much smaller.[10]

Equilibrium

We will use the Boltzmann–Debye picture, and we will talk of the activity coefficient of a single ion, but always with the understanding that the number of equivalents of positive and negative ions is always the same, and only mean activities of components are measurable. According to the theory of Debye[11] the electrostatic contribution, W, to the chemical potential of an ion of charge ϵz and radius b in a solution of dielectric constant D in which all the ions have the distance of closest approach A is

$$W = \frac{\epsilon^2 z^2}{2D}\left[\frac{1}{b} - \frac{\kappa}{1 + \kappa A}\right] \tag{1}$$

in which $1/\kappa$ is the thickness of the ion atmosphere.

When there is a boundary with another phase of dielectric constant $D' = \rho D$, Onsager and Samaras[8] show that there is an additional term depending upon y, the distance from the boundary, so that

$$W_y = \frac{\epsilon^2 z^2}{2D}\left[\frac{1}{b} - \frac{\kappa}{1 + \kappa A} + \frac{(1 - \rho)}{(1 + \rho)}\frac{e^{\kappa A}}{1 + \kappa A}\frac{e^{-2\kappa y}}{2y}\right] \tag{2}$$

$$W'_{y'} = \frac{\epsilon^2 z^2}{2D}\left[\frac{1}{\rho b} - \frac{\kappa'}{\rho(1 + \kappa' A)} - \frac{(1 - \rho)}{\rho(1 + \rho)}\frac{e^{\kappa' A}}{1 + \kappa' A}\frac{e^{-2\kappa' y'}}{2y'}\right] \tag{3}$$

in which the primes refer to the second phase, and the subscripts y and y' refer to the distances y and y' from the interface. These equations depend upon the simplifying assumption that the effective κ is that in the bulk phase.

We define m and m' as the moles of solute in a kilogram of the first solvent in the first and second phases at a very large (infinite) distance from the boundary and m_y and $m'_{y'}$ as the corresponding molalities at a distance y or y'. This rather unusual definition of m' is the one most useful for hyperfiltration. At equilibrium the activity is constant throughout the system and $\gamma = a/m$, $\gamma_y = a/m_y$, $\gamma' = a/m'$, and $\gamma'_{y'} = a/m'_y$. Then the activity coefficients are given by

$$\ln \gamma_y = \frac{W_y}{kT} - \frac{\epsilon^2 z^2}{2DkTb} \tag{4}$$

$$\ln \gamma'_{y'} = \frac{W'_y}{kT} - \frac{\epsilon^2 z^2}{2DkTb} + \ln X_1' \tag{5}$$

in which k is Boltzmann's constant, T is the absolute temperature, and X_1' is the mole fraction of the first solvent in the second. The second term on the right serves to make infinite dilution in the first solvent the reference state in which the activity coefficient is unity, instead of infinite dilution in a solvent of infinite dielectric constant, and the last term in eq. 5 serves to make the ideal activity proportional to the mole fraction of water.

For a salt with ions of valence z_+ and z_-

$$\ln \gamma_{\pm y} = (|z_-| \ln \gamma_{+y} + z_+ \ln \gamma_{-y})/(z_+ + |z_-|) \tag{6}$$

Then

$$\ln \gamma_{\pm y} = \frac{\epsilon^2 z_+ |z_-|}{2DkT}\left[\frac{-\kappa}{1 + \kappa A} + \frac{(1 - \rho)}{(1 + \rho)}\frac{e^{\kappa A}}{1 + \kappa A}\frac{e^{-2\kappa y}}{2y}\right] \tag{7}$$

$$\ln \gamma'_{\pm y'} = \frac{\epsilon^2 z_+ |z_-|}{2DkT}\left[\frac{(1 - \rho)}{\rho b_\pm} - \frac{\kappa'}{\rho(1 + \kappa' A)} - \frac{(1 - \rho)}{\rho(1 + \rho)}\frac{e^{\kappa' A}}{1 + \kappa' A}\frac{e^{-2\kappa' y'}}{2y'}\right] + \ln X_1' \tag{8}$$

if

$$\frac{1}{b_\pm} = \left(\frac{z_+}{b_+} + \frac{|z_-|}{b_-}\right)\bigg/(z_+ + |z_-|) \tag{9}$$

provided that electrical neutrality is maintained at each distance y or y'.

(9) S. Sourirajan, *Ind. Eng. Chem., Fundamentals*, **2**, 51 (1963).

(10) There would be a much more serious difficulty with the model if the measurements of W. C. McC. Lewis, *Phil Mag.*, **17**, 466 (1910), were correct. He found that sodium chloride and other salts decrease the tension at a water-"hydrocarbon oil" interface and have positive interfacial concentrations. The measurements are very difficult, however, and this author has found no other measurements on such systems. Until these are confirmed they may probably be disregarded.

(11) P. Debye and E. Hückel, *Physik. Z.*, **24**, 185 (1923).

At equilibrium $\ln m_{\pm}\gamma_{\pm}$ is the same in both bulk phases and through the boundary layer. The equations involving y or y' cannot hold very close to the interface. At the interface ($y = y' = 0$) eq. 5 makes $\ln m_0$ equal to minus infinity and eq. 6 makes $\ln m'_0$ equal to plus infinity, but the two concentrations in moles per liter must be equal. This error decreases very rapidly, however, as y increases, and $\ln m'_{y'} = \ln m_y - \ln X_1'$ when $y = y' = b/2$. We will therefore assume that the error is negligible when $y = y' \geq b$, that is when the ion is entirely within one of the phases.

The measurements by Åkerlöf[12] of the dielectric constants of mixtures of water with organic liquids show that the dielectric constant is approximately a linear function of the volume fraction, much nearer linear than is the Clausius–Mosotti ratio, $(D - 1)/(D + 2)$. For our purposes we do not need a more sophisticated treatment, since we need only know that a small amount of water causes only a correspondingly small increase in the dielectric constant.

We will illustrate with aqueous solutions of sodium chloride at 25°, where the density of water is 0.997 and its dielectric constant is 78.5, so $\epsilon^2/2DkT = 3.578 \times 10^{-8}$ and $\kappa = 0.3287 \times 10^8\sqrt{I}$ with $I = \Sigma_i m_i z_i^2/2$. For other liquids $\epsilon^2/2D'kT = 3.578 \times 10^{-8}/\rho$ and $\kappa' = 0.3287 \times 10^8\sqrt{I'/\rho}$. For sodium chloride $z_+ = |z_-| = 1$, $A = 4.56 \times 10^{-8}$, and $b = 1.35 \times 10^{-8}$, so $\kappa A = 1.5\sqrt{I}$ and $\epsilon^2/2DkTb = 2.65$.

If ρ is less than one, $\kappa' = \kappa/\sqrt{\rho}$ is greater than κ when $m' = m$; but at equal activity of the salt in the two phases the first term in the bracket of eq. 8 is so large that κ' is less than κ and even $\kappa'/\rho(1 + \kappa'A)$ is less than $\kappa/(1 + \kappa A)$ unless κ is large.

Figure 1 shows the change in the ratio of molality to activity from that at zero molality when the mean activity increases as $\Delta \log (m/m\gamma_{\pm}) = \Delta \log (1/\gamma_{\pm})$ vs. $\sqrt{m}\gamma_{\pm}$ for $\rho = 1$, $1/2$, and $1/4$. As ρ becomes smaller the initial slope and the curvature both become smaller. The difference between the curve for $\rho = 1$ and that for another value of ρ gives $\Delta \log m/m'$ with changing $m\gamma_{\pm}$ at equilibrium. For small values of $m_{\pm}\gamma_{\pm}$, $\log m/m'$ increases with increasing activity. However, the change is never great and it may change sign for larger values of the activity if ρ is near unity.

Figure 2 shows the concentration in the first phase as $(1 + \rho)/(1 - \rho) \log (m_y/m)$ vs. y for $\sqrt{m} = 0$, 0.1, 0.2, 0.5, and 1. Here y is expressed as Ångstroms and the curves are not carried to $y < 1$. If the ordinates are multiplied by $(-1/\rho)$ they represent $[(1 + \rho)/(1 - \rho)] \log (m'_{y'}/m')$ vs. y', and if they are multiplied by $(-2/\rho)$ they represent $\log \gamma'_{min}$, the minimum value of $[(1 + \rho)/(1 - \rho)] \log m'_{y'}/m'$ in a membrane of thickness $2y'$ between two exterior phases with $\rho = 1$.
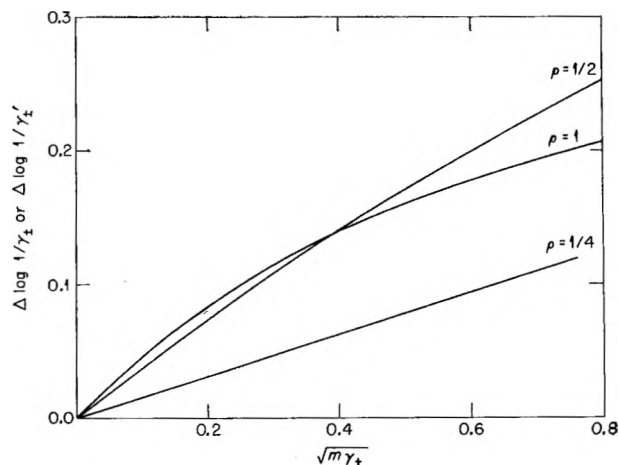

Figure 1. Change of activity coefficient in bulk phase with change in activity $(m\gamma_{\pm})$ (1–1 electrolyte).
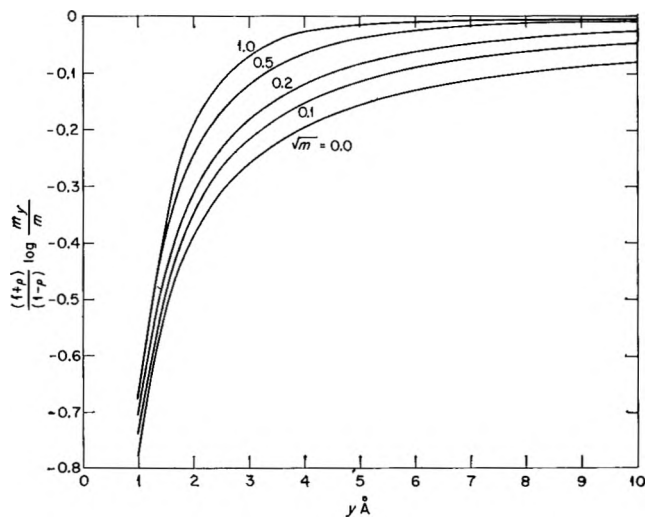

Figure 2. Ion concentration as function of distance from surface, y (1–1 electrolyte).

For the air–water system ρ is $1/78.5$, and $(1 - \rho)/(1 + \rho)$ is 0.975, so $\log m_y/m$ is within 3% of the value shown in Fig. 2. At a distance $y = 1$, where the edges of the ions would be protruding into the air, m_y/m is about 0.17 in the limit of small concentrations. At $y = 2$ the ratio is about 0.4. The ratios at $y = 1$ and $y = 2$ are 0.34 and 0.55 for $\rho = 1/4$, and 0.59 and 0.74 for $\rho = 1/2$. Each of these ratios increases toward unity as m increases.

In the phase of lower dielectric constant, the concentration near the surface is larger than that in the bulk phase, but that is much smaller than the bulk concentration in the phase of higher dielectric constant. We are particularly interested in the concentration in

(12) G. Åkerlöf, J. Am. Chem. Soc., 54, 4125 (1932).

a membrane between two aqueous phases. The molecular weight of the organic material in the membrane is so large that log X_1' may be taken as zero. In the limit of low concentrations for sodium chloride

$$\log m'/m = -1.151(1 - \rho)/\rho \qquad (10)$$

and for a membrane of thickness l

$$\log m'_{y'}/m' = 0.777[(1 - \rho)/\rho(1 + \rho)][l/y'(l - y')] \qquad (11)$$

If y' is the distance from one surface of the membrane, $(l - y')$ is the distance from the other surface. The minimum value of $l/y'(l - y')$ is $4/l$ for $y' = l/2$. For $\rho = 1/2$, $1/4$, and $1/8$, $-\log m'/m$ is 1.151, 3.453, and 8.057, and $l \log m'_{1/2}/m'$ is 2.072, 7.459, and 19.339. For a membrane only 100 Å. thick, $m'_{1/2}/m'$ is 1.05, 1.19, and 1.56, and $m'_{1/2}/m$ is 7.5×10^{-2}, 4.2×10^{-4}, and 1.4×10^{-8}.

Flow Due to Pressure Gradient

We will consider the flow of salt and water through a membrane of low dielectric constant with two parallel plane faces placed between two exterior phases. The exterior phases contain only salt and water, and in the membrane every other component is fixed so that its flow is zero. If ρ is small, the concentration ratio of salt to water within the membrane will be much smaller than in the exterior phases. At equilibrium, the compositions of the two exterior phases will be the same and the temperature and pressure will be constant throughout.

If pressure is applied to one side of the membrane, salt and water flow through it. In the steady state, the flux of each component is the same through any plane parallel to the interfaces. By the thermodynamics of irreversible processes, the flux of water, j_1, and that of salt, j_2, in the direction of increasing x, are

$$j_1 = -L_{11}d(\mu_1/T)/dx - L_{12}d(\mu_2/T)/dx \qquad (12)$$

$$j_2 = -L_{12}d(\mu_1/T)/dx - L_{22}d(\mu_2/T)/dx \qquad (13)$$

since $L_{21} = L_{12}$. The current applications of the thermodynamics of irreversible processes to membranes require the assumption that each boundary of the membrane is a true surface at which there is no change in the potential of any component. Although this is probably the weakest point in the theory, there is at present no alternative.

In general, we do not know any of the five terms on the right-hand side of eq. 12 and 13 within the membrane. We may, however, use Kirkwood's integration[13] to give

$$j_1 = -L_{11}{}^*\Delta(\mu_1/RT) - L_{12}{}^*\Delta(\mu_2/RT) \qquad (14)$$

$$j_2 = -L_{12}{}^*\Delta(\mu_1/RT) - L_{22}{}^*\Delta(\mu_2/RT) \qquad (15)$$

in which Δ is the change from one exterior phase to the other in the direction of increasing x.

For aqueous sodium chloride

$$\Delta(\mu_1/RT) = -0.036\,\Delta(\phi m_2) + 0.00074\Delta P \qquad (16)$$

$$\Delta(\mu_2/RT) = 2\Delta \ln m_2\gamma_\pm + 0.00068\Delta P + 0.00011\Delta(P\sqrt{m_2}) \qquad (17)^{[14]}$$

in which ϕ is the osmotic coefficient, $\gamma_\pm$ is the mean activity coefficient, and P is the pressure in atmospheres. In 0.5 m NaCl, $-0.036\,(\phi m_2)$ is -0.0166 so it cannot be changed much by reducing m_2.

It is instructive to consider the case in which a rigid porous membrane is completely impermeable to component 2 and the pressure is the same on both sides of the membrane but the potential of 1 in the solution with large x is lowered by the presence of 2. There will be a positive flux, and therefore a negative potential gradient, of 1. Since its potential within the membrane depends only on the pressure there must be a pressure drop within the membrane which would require a sudden jump in pressure at the assumed surface between membrane and exterior phase. This brings out clearly the weakness of that assumption. If the membrane is a liquid, however, in which 1 is slightly soluble but 2 absolutely insoluble, there will be no pressure gradient, but the potential gradient will be accompanied by a concentration gradient. Real membranes are probably intermediate between these two extremes.

If the potential difference between the two external solutions is maintained by a hydrostatic pressure difference, the situation is unchanged because the matrix of a rigid membrane or of a rigidly supported membrane is constant throughout. If the membrane is truly porous, the pressure on the liquid component 1 will vary almost linearly from high to low, but if component 1 is dissolved in a liquid membrane, the pressure will be the high pressure throughout and the potential gradient of 1 will be accompanied by a concentration gradient. Real membranes will usually have both pressure and concentration gradients.

Consider the steady-state flux when the high pressure exterior phase contains a solution stirred as effectively as possible. Then the relative flux at every point, j_2/j_1, is m_2 of the low pressure exterior phase or the effluent, m_2(eff), if j_1 is measured in kilograms and j_2

(13) J. G. Kirkwood in "Ion Transport Across Membranes," H. T. Clarke, Ed., Academic Press, New York, N. Y., 1954, p. 119.

(14) From the equation for the apparent molal volume of aqueous NaCl of O. Redlich, J. Phys. Chem., 44, 619 (1940).

in moles. For the strictly semipermeable membrane the effluent is pure 1. Since stirring on the high pressure side cannot be completely effective, the flux of water causes the concentration of 2 at the membrane surface to build up until the back diffusion maintains the steady state.

For aqueous sodium chloride between 0.01 and 2 M, the diffusion coefficient is 1.5×10^{-5} cm.^{2} sec.$^{-1}$. If the linear flow rate is $v \times 10^{-5}$ cm. sec.$^{-1}$, the corresponding gradient is

$$\frac{dm}{dx} = 2v(m - m')/3 \qquad (18)$$

Very efficient stirring is roughly equivalent to a layer 0.01 cm. thick with a constant gradient and a constant concentration beyond that distance. With such stirring the difference between the concentration at the surface and that in the bulk phase is approximately

$$\Delta m \simeq 0.02vm/3 \qquad (19)$$

The linear velocities quoted by Sourirajan[9] are 1–2 gal. (sq. ft.)$^{-1}$ (day)$^{-1}$ or $v = 5$ to 10 and the v's quoted by Loeb and Sourirajan[15] are as high as 50 (cm. $\times$ 10^{-5} sec.$^{-1}$). The latter value corresponds to $\Delta m = m/3$, or to a surface concentration four-thirds that of the bulk concentrations. Poor stirring may lead to a much larger ratio.

Even if the membrane is permeable to both components, there will be hyperfiltration if the mobility of 2 within the membrane is much less than that of 1, or if the ratio of salt to water at equilibrium is smaller within the membrane than outside.

Equations 16 and 17 show that the effect of a pressure difference on the potential of aqueous NaCl is about the same as on that of water, that the concentration change in dilute solutions has a very small effect on the potential of water, approximately 50 atm. per mole of salt, but that each power of ten in ratio of feed to effluent concentration corresponds to a pressure drop of about 6000 atm. for the potential of the salt. If the separation depends on mobility differences, the mobility of salt must be much less than that of water. This means that both $L_{22}*$ and $L_{12}*$ of eq. 14 and 15 must be much smaller than $L_{11}*$.

If m_2' is much smaller than m_2, the ions are repelled from the walls of a porous membrane, and they sort out water from the solution in a liquid membrane.[16] The ions and the water are much more closely associated to each other than to the matrix or the solvent, so that the flux of the salt may be considered as flow with the water plus diffusion relative to the water. For dilute solu-

tions this differs very little from considering the convective flow of the center of mass of the water and salt plus diffusion of these two components relative to their center of mass. The simplest way to consider the flow is to start with the concentrations at the low pressure side of the membrane. Since m_2' at the low pressure surface is smaller than $m_2(\text{eff})$, there must be positive diffusion and a negative concentration gradient. The difference $[m_2(\text{eff}) - m_2']$ decreases exponentially with $j_1(1 - y)/\mathfrak{D}_2'$; $\mathfrak{D}_2'$ is the diffusion coefficient of the salt relative to water in the membrane. The difference does not become negative, however. Therefore, the minimum value of $m_2(\text{eff})$ is m_2' near the high pressure surface if the rejection is due only to the distribution coefficient at the high pressure side. The value of this minimum and the effect of pressure on the approach to the minimum are independent of the thickness of the membrane except for extremely thin membranes.

There are several reasons for the improvement of desalination by increasing pressure[16,17] for any mechanism. There will be improvement because of the increase with pressure of the ratio of the change in potential of the water to that of salt shown in eq. 16 and 17 and because of the sealing by the high pressure of some of the defects (very large pores) and squeezing out solution from the more homogeneous regions, thus decreasing the salt–water ratio in the membrane. This gain will be partially compensated by the greater build-up of salt on the high pressure side because of the more rapid flow.

Just as we know that often the difference in dielectric constant is sufficient to explain the distribution of salt between aqueous and nonaqueous bulk phases but do not know that there is no other difference affecting the distribution, we also know that this distribution is sufficient to explain the rejection of salt in hyperfiltration through an uncharged membrane but do not know that this is the only reason for the rejection. We do know, however, on the basis of the present study, that the distribution of salt in the exterior phase very near the membrane surface does not affect the salt rejection, and that the distribution in the membrane very near the surface has an appreciable effect only for membranes so thin that they can probably not be prepared homogeneous and mechanically stable.

(15) S. Loeb and S. Sourirajan, Advances in Chemistry Series, No. 38, American Chemical Society, Washington, D. C., 1963, p. 117.

(16) G. Scatchard, *J. Chem. Phys.*, 9, 34 (1941).

(17) C. E. Reid and E. J. Breton, *J. Appl. Polymer Sci.*, 1, 133 (1959).

gratitude to Dr. K. A. Kraus. Discussions with him gave the first impulse to study this problem and many of the ideas arose from these discussions in such a way that they cannot be attributed to either one of us. The author is also grateful to Dr. J. S. Johnson and Dr. L. Dresner for very helpful discussions.

Hydrogen Adsorption on Silver, Gold, and Aluminum.

Studies of Parahydrogen Conversion

by S. J. Holden and D. R. Rossington

Department of Physical Science, State University of New York, College of Ceramics at Alfred University,
Alfred, New York   (Received October 22, 1963)

The para–ortho hydrogen conversion has been investigated in order to study aspects of hydrogen adsorption on silver, gold, and aluminum films. The pressure dependence of the first-order rate constant for the conversion obeys a Langmuir isotherm on silver and aluminum. From the temperature dependence of the ratio of the Langmuir adsorption–desorption rate constants, heats of adsorption of hydrogen were calculated. Values of -2.5 kcal./mole in the range 363-413°K. on silver and -7.7 and -8.4 kcal./mole in the range 308-358°K. on aluminum were obtained. No pressure dependence for the conversion on gold was observed in the range 2-20 mm. The normal compensation effect between activation energy and frequency factor for the conversion on the metals was obtained. Calculated values for the activation energies and frequency factors fell on the experimentally obtained line. By comparing the experimentally obtained entropy change upon adsorption with the calculated entropy changes for adsorption into mobile and immobile layers, it is concluded that the adsorbed hydrogen film on silver, in the temperature range studied, is mobile.

Introduction

The para–ortho hydrogen conversion has been shown[1] to be a particularly sensitive test for the chemisorption of hydrogen on those metals such as copper, silver, gold, and aluminum which have been reported as showing negligible adsorption of hydrogen.[2] The process of a chemical parahydrogen conversion (as opposed to a physical or low temperature mechanism) requires the chemisorption of hydrogen regardless of the reaction mechanism[1,3] which may be prevailing.

In such cases where the adsorption of hydrogen is very small, conventional gas-uptake and calorimetric measurements are extremely difficult to interpret,

and a study of the kinetics of the parahydrogen conversion enables the nature of the adsorption process to be studied.

Experimental

The apparatus consisted of a conventional high vacuum system with provision for the preparation and storage of pure normal hydrogen and para-enriched hydrogen. Pure normal hydrogen was prepared by

(1) D. D. Eley and D. R. Rossington, "Chemisorption," W. E. Garner, Ed., Butterworth, London, 1957, p. 137.

(2) B. M. W. Trapnell, Proc. Roy Soc. (London), A218, 566 (1953).

(3) S. J. Holden and D. R. Rossington, Nature, 199, 589 (1963).

allowing tank hydrogen to diffuse through an electrically heated palladium thimble, and para-enriched hydrogen was prepared by adsorbing pure normal hydrogen on charcoal at the triple point of nitrogen (65°K.). This para-enriched hydrogen contained approximately 60% p-H$_2$ and is referred to subsequently as parahydrogen.

The kinetics of the parahydrogen conversion were studied as a function of pressure and temperature in a constant-volume reaction system. The parahydrogen was left in contact with a metal film for known times and the reaction mixture was then analyzed in a micropirani thermal conductivity gage.[4] Reaction temperatures were obtained by immersing the reaction vessel in an oil bath which could be controlled to ±0.2°. Reaction pressures were obtained by reading a mercury manometer to ±0.03 mm. with a cathetometer.

The cylindrical reaction vessels were approximately 15 cm. long with an outside diameter of 2.5 cm. The catalysts were in the form of evaporated metal films with an apparent area of approximately 96 cm.[2]. These were prepared by evaporating a 0.1-mm. diameter wire of the metal under investigation wound around a 10-mil tungsten filament which was sealed down the center of the reaction vessel. The tungsten filament was electrolytically cleaned prior to use. The weights of the films ranged from 14 to 150 mg. and the thicknesses from approximately 3000 to 8600 Å. In order to prevent contamination, the reaction vessel was connected to the main vacuum system via a liquid nitrogen trap. The reaction vessel and cold trap were outgassed at 450 to 500° for 24 hr. prior to the deposition of each film. No deposited film was used for more than 24 hr. and the reaction vessel and cold trap were connected to the rest of the system by mercury float valves.

The metal wires were supplied by Johnson Matthey and Co., Ltd., with a purity of 99.999+% for the gold and silver and 99.99+% for the aluminum. The slopes of all lines shown in the figures were calculated by the method of least squares.

Results

As usual,[1,5] it was found that the kinetics of the conversion were first order at constant pressure at all temperatures studied.

If C_0 denotes the concentration of parahydrogen in excess of its equilibrium value at time zero and C_t at time t, then the experimental rate constant is given by

$$k = \frac{2.303}{t} \log \frac{C_0}{C_t} \qquad (1)$$

C_0 is directly proportional to Ω_0, the difference in resistance of the micropirani gage for normal and parahydrogen and C_t is directly proportional to Ω_t, the gage resistance difference for normal hydrogen and a reacted sample after t minutes.

The effect of temperature on the rate constant k at constant pressure obeys the Arrhenius equation

$$k = B \exp\left(\frac{-E}{RT}\right)$$

where E is the apparent activation energy and B is a frequency factor.

Typical plots are shown in Fig. 1 and 2 for the temperature dependence of the rate constant, over temperature ranges of 363–413, 400–433, and 308–373°K.
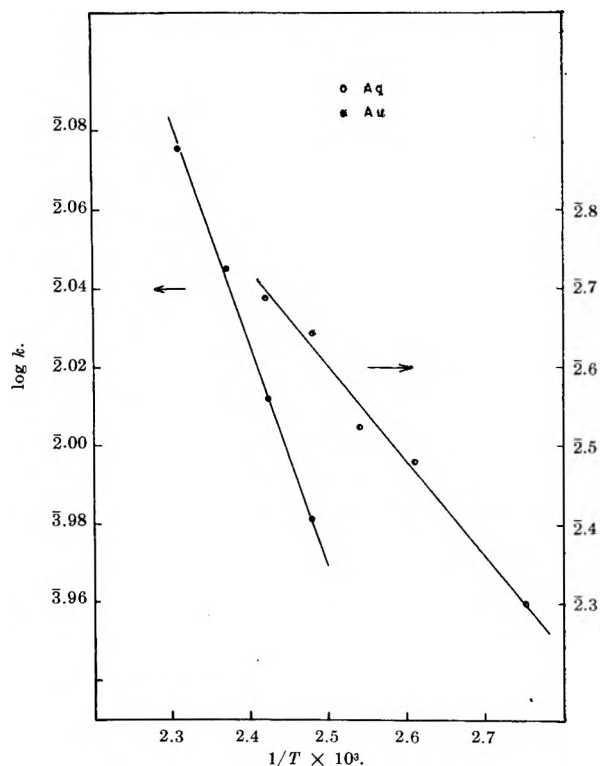

Figure 1. Arrhenius plot for silver and gold films: O, Ag; ●, Au.

for the silver, gold, and aluminum films, respectively. In the case of the aluminum films, there was a sharp decrease in the surface area due to sintering. From the linear parts of Fig. 1 and 2, values for E and B may be obtained. It is more meaningful to correct B to B^0, the frequency factor for unit reaction volume

(4) J. L. Bolland and H. W. Melville, *Trans. Faraday Soc.*, **33**, 1316 (1937).

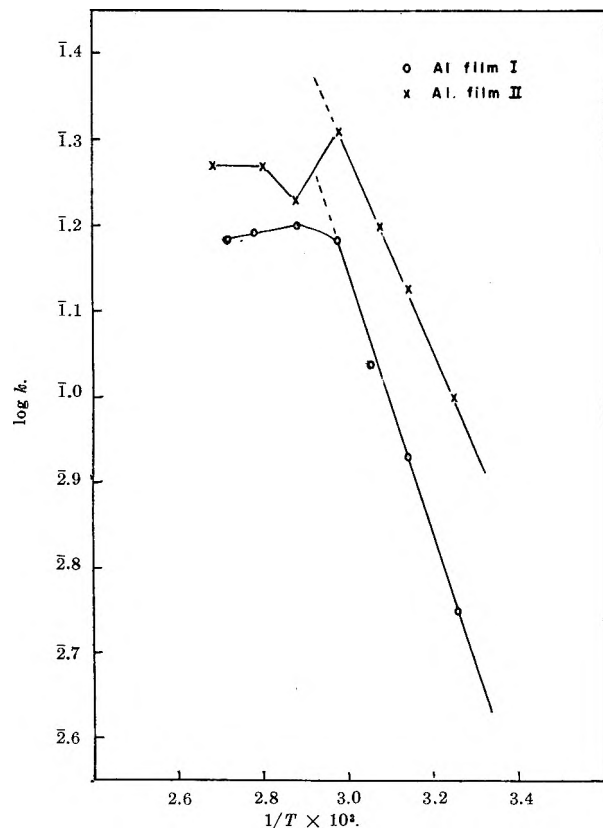(5) D. R. Ashmead, D. D. Eley, and R. Rudham, *ibid.*, **59**, 207 (1963).

Figure 2. Arrhenius plot for aluminum films:
O, Al film I; X, Al film II.

Figure 3. Compensation effect for group IB metal films.
This work: △, Ag; O, Au; ref. 1: ■, Cu; ▲, Ag;
●, Au; ref. 13: □, Cu; calcd. from eq. 8: ▽, Cu; X, Ag.

and unit surface area, i.e., $B^0 = BV/A$, where V is the reaction volume and A is the surface area of the catalyst. The surface area of the catalyst was taken to be equal to its geometric area.[1,6,7]

Values of E and B^0 for all the metal films studied are shown in Fig. 3 and 4.

It has been shown previously,[1] and was confirmed here, that the pressure dependency of the first-order rate constant obeys a Langmuir isotherm. The pressure dependency is therefore expressed by the equation

$$\frac{1}{k} = \frac{a}{b} + ap \qquad (2)$$

where a and b are constants and b represents the ratio of the Langmuir adsorption/desorption rate constants. A plot of the reciprocal of the first-order rate constant vs. pressure at constant temperature should yield a straight line and it is thus possible to obtain values for b at various temperatures. Figures 5 and 6 show such plots for the silver and aluminum films.

Eley and Rossington[1] and Kemball[8] have shown that the heat of adsorption $(-\Delta H_a)$ may be calculated from

the temperature dependency of b in eq. 2, using the equation given by Bond[9]

$$\frac{1}{b} = \frac{k_d}{\alpha} (2\pi mkT)^{1/2} \exp\left(\frac{\Delta H_a}{RT}\right) \qquad (3)$$

where k_d is the rate constant for desorption, α is the condensation coefficient, R is the gas constant, and T is temperature, or

$$-\log b = \frac{\Delta H_a}{2.303RT} + \text{constant} \qquad (4)$$

The "constant" in eq. 4 contains the term $1/2 \log T$. However, over the temperature range used for these experiments (a maximum of 50°), the variation in this term is small, being of the order of 3%.

A plot of the results for the silver film obtained from

(6) J. A. Allen and J. W. Mitchell, Discussions Faraday Soc., 8, 309 (1950).

(7) J. M. Saleh, C. Kemball, and M. W. Roberts, Trans. Faraday Soc., 57, 1771 (1961).

(8) C. Kemball, Advan. Catalysis, 2, 233 (1950).

(9) G. C. Bond, "Catalysis by Metals," Academic Press, London, 1962, p. 70.
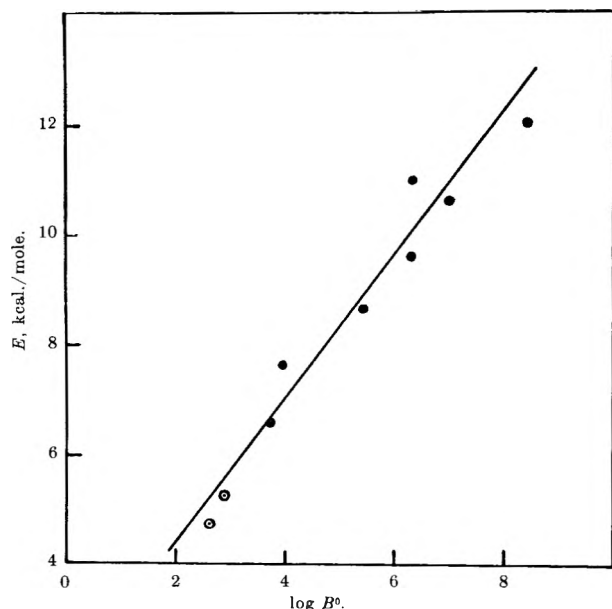
Figure 4. Compensation effect for aluminum films:
O, this work; ●, from work of D. R. Rossington,
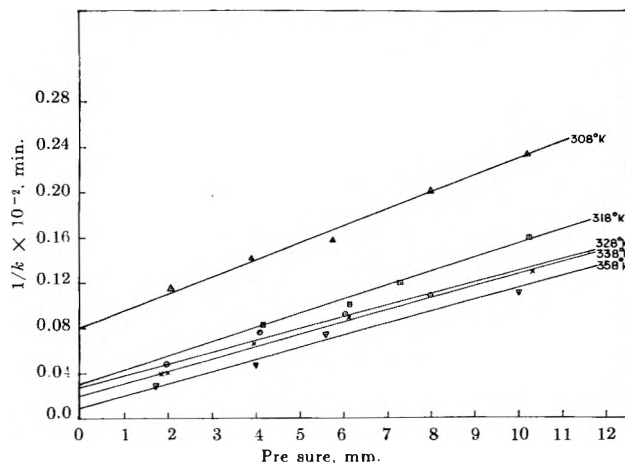Ph.D. Thesis, University of Bristol, 1956.

Figure 6. Pressure dependency of the parahydrogen
conversion on an aluminum film.

Fig. 5, according to eq. 4, gave a straight line of slope 0.56 ± 0.07, yielding a value for the heat of adsorption of hydrogen, at equilibrium coverage, of $(-\Delta H_a)$ silver $= 2.5 \pm 0.3$ kcal./mole.

Figure 7 shows the results obtained on two aluminum films. The pressure dependency results for film I are given in Fig. 6. The results for film II were similar in every respect. The lines in Fig. 7 yield values of the heat of adsorption of hydrogen on aluminum of 7.7 and 8.4 $\pm$ 0.5 kcal./mole.

As has been observed previously,[10] the rate constant for the conversion on gold films was independent of pressure, over the range 2–20 mm. and the temperature range 393–433°K.

Discussion

Activation Energies and Frequency Factors. Figure 3 shows the activation energies and frequency factors obtained in this work (except for aluminum which is shown in Fig. 4), together with previously reported values. It is seen that a normal compensation effect is operative, which has been discussed by other workers.[11] The various results in Fig. 3 and 4 were obtained over a span of 8 years and in different laboratories. These results give support to the view that instead of a characteristic activation energy, there may exist a characteristic E–log B^0 relation for a metal, or series of metals, as was first suggested by Couper and Eley.[12] In such cases, it is not useful to report

Figure 5. Pressure dependency of the parahydrogen
conversion on a silver film.

(10) A. Couper, D. D. Eley, M. J. Hulatt, and D. R. Rossington;
Bull. Soc. Chim. Belges, **67**, 343 (1958).

(11) E. Cremer, *Advan. Catalysis*, **7**, 75 (1955).

(12) A. Couper and D. D. Eley, *Proc. Roy. Soc.* (London), **A211**, 536;
544 (1952).
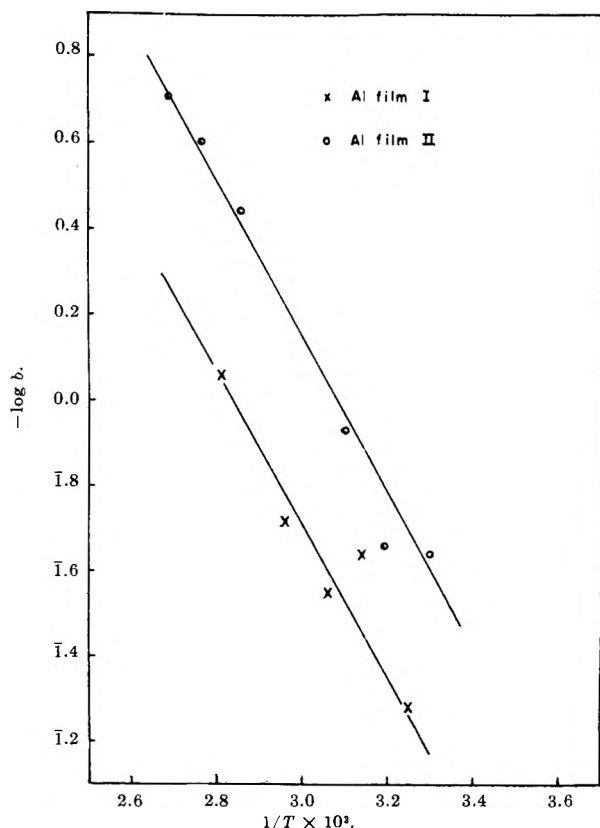
Figure 7. Determination of heat of adsorption on aluminum films, yielding values of ΔH_a = −7.7 and −8.4 kcal./mole: X, Al film I; O, Al film II.

an activation energy without a frequency factor. A similar situation has been found to exist for copper.[13]

Although many workers have reported[6,7] that low melting point metals sinter completely at room temperature, it may be seen that the activity of the films decreased with heat treatment. Not only the activity, but also the activation energy and frequency factor were changed after the temperature was raised above a certain value, as shown in Fig. 4. These changes could be attributed to a change in the physical nature of the film, and while such changes in the surface structure may be quite small, the parahydrogen conversion is an extremely sensitive method for detecting them. Pritchard[14] has recently indicated that structural variations in evaporated films may also affect surface potential measurements.

In discussing the compensation effect, Eley and Rossington[1] have shown that a temperature-dependent activation energy can yield the expression

$$E = 2.303RT \log B^0 + [E(T) - 2.303RT \log B^0(T)] \tag{5}$$

where E and B^0 are temperature-independent values.

If the term in brackets is assumed constant, then a plot of E vs. log B^0 should yield a line of slope $2.303RT$. The calculated value of the slope for an average temperature of 415°K. for the points in Fig. 3 is 1.90 as compared with an experimental slope of 1.50.

Other workers[11,12,15,16] have suggested that the compensation effect could be explained in terms of a relation between energy and entropy. Everett[15] has reported that entropies and heats of adsorption are often related and Kemball[16] showed that this could lead to the compensation effect.

Calculated Activation Energies and Frequency Factors. An equation for the first-order rate constant has been derived by Eley.[17]

$$k = \frac{A\sigma\theta}{n}(k_o + k_p) \tag{6}$$

where A is the surface area of catalyst (cm.^{2}); σ is the number of sites/cm.^{2} of surface; θ is the fraction of surface covered; n is the total number of hydrogen molecules in the system; k_o is the first-order rate constant for the conversion ortho- to parahydrogen; and, k_p is the first-order rate constant for the conversion para- to orthohydrogen. By substituting for the number of hydrogen molecules and replacing θ by a Langmuir isotherm, we obtain

$$k = \frac{A\sigma kT}{V}(k_o + k_p)\frac{b}{(1 + bp)} \tag{7}$$

and $(k_o + k_p)$ represents the net conversion of hydrogen molecules.

As the pressure approaches zero, eq. 7 reduces to

$$(k_o + k_p) = \frac{k_{p\rightarrow0}V}{A\sigma kTb} \tag{8}$$

For silver, the rate constant as the pressure approaches zero and the value of b at a particular temperature may be obtained from Fig. 5. The reaction volume and surface area of the metal films may be measured and the value of σ was taken to be that for the most densely packed plane (111).

If the rate constant $(k_o + k_p)$ calculated from eq. 8 obeys the Arrhenius equation, a plot of its logarithm vs. reciprocal temperature should give a line of slope $-E/2.303R$ and intercept log B^0. The results of these calculations are given in Table I and yield a linear plot of log $(k_o + k_p)$ vs. $1/T$.

(13) S. J. Holden and D. R. Rossington, to be published.

(14) J. Pritchard, *Trans. Faraday Soc.*, 59, 437 (1963).

(15) D. H. Everett, *ibid.*, 46, 957 (1950).

(16) C. Kemball, *Proc. Roy. Soc.* (London), A217, 376 (1953).

(17) D. D. Eley, *Trans. Faraday Soc.*, 44, 216 (1948).

Table I: Calculations of log $(k_o + k_p)$ as a Function of Temperature for a Silver Film

T, °K.	$1/k_{p\to 0}$	$k_{p\to 0}$	b	$(k_o \times k_p)$	log $(k_o \times k_p)$
363	36.01	0.0278	0.0940	9.710×10^{-3}	-3.987
383	22.76	0.0439	0.1104	1.238×10^{-2}	-2.093
393	20.00	0.0500	0.1259	1.205×10^{-2}	-2.081
403	14.81	0.0675	0.1347	1.482×10^{-2}	-2.171
413	12.87	0.0777	0.1457	1.539×10^{-2}	-2.187

The activation energy and frequency factor calculated for pressures approaching zero for eq. 8 ($E = 2.68$ kcal./mole, log $B^0 = -1.61$) were lower than the experimental values, and yet fell on the general compensation effect line, as shown in Fig. 3. It was not possible to calculate an activation energy and frequency factor for aluminum as the calculated points did not lie on a straight line. This may have been due to the fact that the higher activity of the aluminum resulted in the pressure dependency experiments being conducted over a smaller temperature range than for the silver films.

Heat of Adsorption. The rate constant for gold does not appear to be pressure-dependent between 379 and 433°K. It is possible that the small amount of conversion on gold, due to a very low surface coverage, requires a lower range of pressure measurements in order to detect a pressure dependency. Such a low equilibrium surface coverage could be reached even at a reaction pressure of 2 mm. In the present work, the lower pressure limit of reaction of approximately 2 mm. was determined by the fact that there had to be enough reaction mixture to give a pressure of 50 mm. when compressed into the micropirani gage for analysis.

Pritchard[14] has recently shown that hydrogen adsorption on gold at $-183°$ is low ($\theta = 0.15$) and it is quite possible that the coverage would be undetectable in the temperature range of the current experiments.

There was close agreement between the heats of adsorption obtained from the two aluminum films. The chemisorption of hydrogen on aluminum must involve a mechanism other than d–s promotion of electrons, which has been proposed for the mechanism of hydrogen adsorption on copper and silver. A mechanism involving hydrogen atoms being bonded by a hybrid sp orbital at the surface has been suggested.[2] The chemisorption of hydrogen by aluminum is sufficiently small as to be immeasurable by gas-uptake methods.[2]

For silver, the heat of adsorption at equilibrium

coverage was determined as 2.5 kcal./mole, compared to 8.0 kcal./mole for copper.[1]

State of the Adsorbed Surface Film. A knowledge of the heat of adsorption at equilibrium coverage and the ratio of the adsorption–desorption rate constant enables calculations to be made regarding the state of the adsorbed film.

Following Kemball,[8] if the standard surface state is defined as a surface coverage of 0.5 and a pressure of 1 atm., the change in free energy upon adsorption, ΔF_a, is given by

$$\Delta F_a = RT \ln b \qquad (9)$$

The value of b may be obtained from Fig. 6 or 7 using the average temperature of the experiment as T. Therefore, the entropy change upon adsorption, ΔS_a, may be obtained from

$$\Delta S_a = \frac{-\Delta F_a + \Delta H_a}{T} \qquad (10)$$

This experimentally determined entropy change may be compared to a calculated entropy change, which will be dependent upon whether the adsorbed film is mobile or immobile.

The three-dimensional translational entropy of a gas at 1 atm. pressure is given by[8]

$$_3S_{transl} = R \ln [M^{3/2}T^{5/2}] - 2.30 \qquad (11)$$

where M is the molecular weight of the gas.

The two-dimensional translational entropy is given by[8]

$$_2S_{transl} = R \ln [MTA] + 65.80 \qquad (12)$$

where A is the area per adsorbed molecule. Kemball and Rideal[18] have defined a standard state corresponding to a surface layer of thickness 6 Å. which gives the same volume per molecule at 1 atm. pressure as the three-dimensional state. Thus defined, $A = 22.53T$ Å.^{2}. For a mobile layer, upon adsorption, a degree of translational freedom is lost and replaced by a vibration perpendicular to the surface. For chemisorption at ordinary temperatures, the entropy of vibration is small, usually less than 3 e.u.

For an immobile adsorbed layer, the translational entropy which is lost is replaced by a configurational entropy. Kemball[8] has shown that for dissociative adsorption, a surface in which each atom has six nearest neighbors has a configurational entropy of

(18) C. Kemball and E. K. Rideal, *Proc. Roy. Soc.* (London), **A187**, 53 (1946).

$$S_{\text{config}} = R[\sigma(x - \tfrac{1}{6}) \ln (x - \tfrac{1}{6}) + \ln \sigma - 4 \times$$

$$\ln x - 2(x - 1) \ln (x - 1)] \quad (13)$$

where $x = 1/\theta$ and σ is the symmetry number, taken as equal to two if the two ends of a double molecule are indistinguishable. Therefore, if the surface layer of hydrogen on the metal studied is mobile, the entropy change upon adsorption will be approximated by the difference between the translational entropy in three and two dimensions. If the surface film is immobile, the entropy change will be approximated by the difference between the three-dimensional translational entropy and the configurational entropy.

Table II shows the calculated and experimentally determined entropy changes. The calculated values for the three-dimensional translational entropy have been corrected to 1 atm. pressure. The surface standard states were estimated, based on the known surface coverage for copper[3] and the relative activities and areas of copper, silver, and aluminum films.

As may be seen from the table, the film on silver is

Table II :   Experimental and Theoretical Entropy Changes

Metal film	Surface standard state	Average temp., °K.	ΔS_{exptl}, e.u.	$_3S_{\text{transl}} - {}_2S_{\text{transl}}$, e.u.	$_3S_{\text{transl}} - S_{\text{config}}$, e.u.	State of adsorbed layer
Cu I	0.17	413	−21.0	−17.0	−33.2	Mobile[a]
Cu II	0.17	393	−23.5	−24.0	−30.7	Mobile[a]
Ag I	0.10	391	−15.2	−15.4	−29.4	Mobile
Al I	0.25	330	−25.0	−15.3	−30.8	?
Al II	0.25	338	−23.8	−15.4	−30.9	?

[a] See ref. 13.

mobile at the temperature of the experiment, while a definite conclusion cannot be reached in the case of aluminum. A similar analysis to this has shown that the adsorbed hydrogen film on copper is also mobile under similar conditions.[13]

Surface Energy Distributions of a Homogeneous Surface and a

Heterogeneous Surface from Argon Adsorption Isotherms

by P. Y. Hsieh

The National Cash Register Company, Dayton 9, Ohio   (*Received October 25, 1963*)

The adsorption isotherms of argon on carbon black, MT-3100, and a silica–alumina cracking catalyst at 77.8°K. are given. The site-energy distributions of these surfaces were obtained from the isotherms using the method proposed by Adamson and Ling. The results show that the cracking catalyst is heterogeneous while the carbon black is a homogeneous surface. The site-energy distribution on the carbon black is gaussian-like, as assumed by Ross and Olivier, which implies that the method suggested by Adamson and Ling is rather insensible to the local isotherm selected.

Introduction

The equation relating adsorption of a gas onto a solid surface to the experimental quantities P, T can be written in general as

$$\Theta = \left[\int_0^\infty f(Q)\theta(P,T,Q)\, dQ \right]_{P,T} \quad (1)$$

where $\Theta(P,T)$ is the observed adsorption function and is usually obtained as an adsorption isotherm $\Theta(P)$; $f(Q)$ is the site-energy distribution function; $\theta(P,T,Q)$ is the adsorption function representing adsorption for regions obeying local isotherm θ; and Q is the adsorbent–adsorbate interaction energy. The distribution function may be expressed as $f(Q) = dF/dQ$, where $F(Q)$ is the integral site-energy distribution, *i.e.*, F is the fraction of sites with energy $\geq Q$.

The problem of obtaining site-energy distributions of a solid surface from adsorption isotherms is that of finding the solution of eq. 1. The solution to this problem, that is the inversion of this Stieltjes integral to give $f(Q)$, would not be difficult, if $\theta(P,T,Q)$ and $\Theta(P,T)$ were known in simple analytical form.

For the analytical integration of eq. 1, the Langmuir equation has been used for θ and certain simple functions such as the Freudlich and Temkin isotherm equations for Θ by many workers.[1] The approach is convenient mathematically; however, it is practical only for certain types of assumed functions θ and Θ. The Langmuir model postulates no lateral

interaction, homogenity of substrate, and a localized adsorbed film.

Another approach was taken to solve eq. 1 by Ross and Olivier.[2] They took a two-dimensional van der Waals equation of state for θ and assumed a gaussian distribution of adsorptive energies for $f(Q)$. A number of model adsorption isotherms have been computed, using various assumed values of the parameters involved.

The site-energy distribution was finally obtained by comparing the computed isotherms with the experimental isotherms. The use of a two-dimensional van der Waals equation was based on the experimental findings of Ross and his co-workers[3] that an adsorbed gas film is a mobile, two-dimensional nonideal type, and that the more uniform the surface the more closely can the adsorption isotherm be described by the van der Waals equation.

Unfortunately, their method does not provide any possibility for an independent check of the proposed distribution. It is generally believed that experimental adsorption isotherms can be fitted by a number of semi-empirical equations, and agreement with some partic-

(1) R. Sips, *J. Chem. Phys.*, **16**, 490 (1948); J. M. Honig, *ibid.*, **24**, 510 (1956); J. M. Honig and L. H. Reyerson, *ibid.*, **23**, 2179 (1955); J. M. Honig and E. Hill, *ibid.*, **22**, 851 (1954).

(2) S. Ross and J. P. Olivier, *J. Phys. Chem.*, **65**, 608 (1961).

(3) S. Ross and W. Winkler, *J. Am. Chem. Soc.*, **76**, 2637 (1954); *J. Colloid Sci.*, **10**, 319, 330 (1955); S. Ross and W. W. Pultz, *ibid.*, **13**, 397 (1958).

ular one provides no assurance that its basic assumptions are correct.

Recently, Adamson and Ling[4] have demonstrated a convenient way of obtaining the site-energy distributions from the experimental isotherm itself and from any arbitrarily chosen local isotherm function θ.

The adsorption isotherms of butane and oxygen on TiO_2 and of nitrogen on both Graphon and TiO_2 have been used in the illustration of the method.[4] The method was applied to find these distributions functions for silica–alumina cracking catalysts from ammonia adsorption isotherms. The result appeared to agree with the calorimetric heat measurements.[5]

In the present study this method was tested on two extreme substrates: a homogeneous and a heterogeneous surface. The adsorbents chosen were a highly graphitized carbon black, MT-3100, and a silica–alumina cracking catalyst previously used in the ammonia adsorption. Argon was used as the adsorbate. The site-energy distribution obtained from the argon adsorption isotherm on MT-3100 may be used to crosscheck the result reported by Ross and Olivier.[2] Although an independent check cannot be made for the distribution obtained from the adsorption isotherm on the silica–alumina catalyst, it should show the heterogeneous nature of the surface and it should give some comparison with that obtained from the ammonia adsorption isotherm.

Experimental

The adsorbents used in the present study were a carbon black, Sterling MR-3100, and a silica–alumina cracking catalyst. The carbon black was graphitized at $3000 \pm 300°$ in the absence of air and was supplied by the courtesy of Dr. W. R. Smith of Godfrey L. Cabot Corp. The surface area of 6.3 m.^{2}/g., was reported by Beebe, et al.[6] The catalyst was 25% alumina on silica and was kindly supplied by the courtesy of Dr. M. C. Throckmorton of the Texaco Research Center. The surface area of the catalyst from nitrogen B.E.T. measurements was found to be 525 m.^{2}/g. Argon was obtained from Air Reduction Sales Co. as spectroscopically pure and was used directly from the glass container.

Measurements of the adsorptions were carried out with the vacuum apparatus described earlier[5] at liquid nitrogen temperature, $77.8°K$. The outgassing conditions were a minimum of 12 hr. at $150°$ for the carbon black and a minimum of 40 hr. at $260°$ for the cracking catalyst.

Results and Discussion

The experimental data of argon adsorption on MT-3100 at $77.8°K$ obtained previously[7] are shown in Fig.

4 and also shown as Θ $(= v/v_m)$ vs. $1/p$ in Fig. 1. This graphical form of Θ and the Langmuir equation for θ were used for making successive graphical approximations of the integral site-energy distribution $F(Q)$, following the procedure described by Adamson and Ling. Multilayer corrections, which were small in this case, were made by the equation

$$\Theta = (v/v_m)(1 - P/P^0) \qquad (2)$$

and are indicated by the solid circles. The vapor pressure of solid argon which is 212 mm. was used for P^0. The dashed line indicates the final F vs. b distribution for the isotherm, where b is the constant in the Langmuir equation. In order to calculate Θ, the monolayer capacity, V_m, of 2 cc.(STP)/g. was obtained from the isotherm "B" point. The value of 2.3 cc. was reported by Ross and Olivier[2] from their approach. If based on the surface area of 6.3 m.^{2}/g. and 14.6 Å.^{2} for the cross
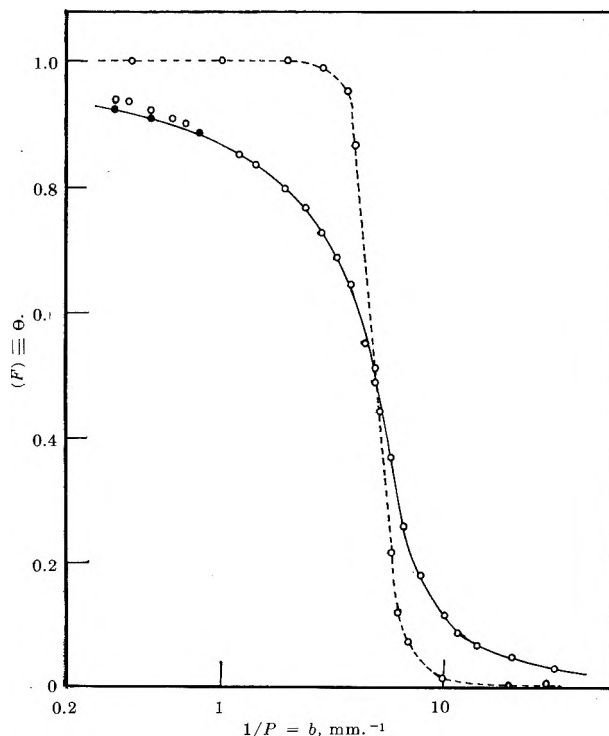

Figure 1. Adsorption isotherm of argon at $77.8°K$. on MT-3100: ———, Θ vs. $1/p$; – – – –, final approximation to F vs. b; O, V/V_m; ●, $(V/V_m)(1 - X)$.

(4) A. W. Adamson and I. Ling, Advances in Chemistry Series, No. 33, American Chemical Society, Washington. D. C., 1961, p. 51.

(5) P. Y. Hsieh, J. Catalysis, 2, 211 (1963).

(6) W. B. Spencer, C. H. Amberg, and R. A. Beebe, J. Phys. Chem., 62, 719 (1958).

(7) P. Y. Hsieh, Ph.D. Thesis, Rensselaer Polytechnic Institute, Troy, N. Y., 1959.

section of argon, the value of V_m would have been about 1.6 cc.

Since it was assumed that the active sites consist of patches, the local isotherms of which obey the Langmuir isotherm, the interaction energy Q was obtained from the relation

$$b = na^0 r^0 (2\pi MRT)^{-1/2} e^{Q/RT} = b_0 e^{Q/RT}$$

The values of 14.6 Å.^{2} and 10^{-13} sec. (see ref. 8) were used here for a^0 and r^0, respectively. The collection of constants b_0 was 9.2 × 10^{-8} at 77.8°K. and pressure was in mm.

The differential site-energy distribution was then obtained by finding the slope of F vs. Q and is shown in Fig. 2.

The site-energy distribution obtained this way appears to be gaussian-like as assumed by Ross and Olivier.[2] The agreement was striking despite the difference in the local adsorption function assumed, that is, the Langmuir isotherm in this work and van der Waals equation of state in Ross and Olivier's paper. Strictly, Langmuir's adsorption isotherm may not be applied to a mobile adsorption film such as argon on carbon black. However, there is no way to confirm that the active site patches really do not obey the Langmuir isotherm. It appears more likely that Adamson and Ling's method is rather insensitive to the isotherm

Figure 3. Differential site-energy distribution for ammonia on silica–alumina catalyst.
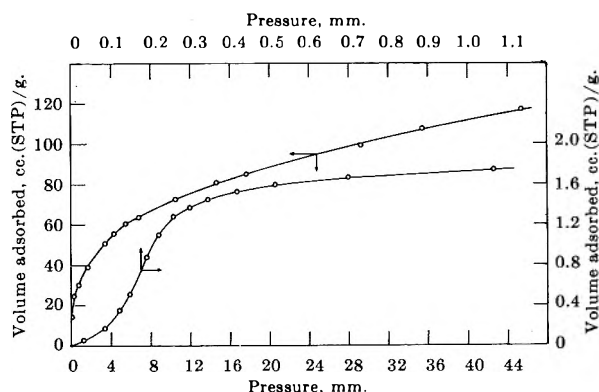
Figure 4. Adsorption isotherm of argon at 77.8°K. on silica–alumina cracking catalyst (upper curve) and MT-3100 (lower curve).

selected, and that any local isotherm function θ may be arbitrarily chosen without giving an entirely different distribution curve.

It is also noted that the site energy found by this method is about 2.75 kcal./mole while 2.12 was calculated by Ross and Olivier's method.[2] The slight difference is possibly due to the value of Frenkel's characteristic adsorption time r^0 used. The value of b_0 which includes an entropy term was treated as constant with surface coverage.

It has been shown[5] from the ammonia adsorption isotherm at 0° that silica–alumina has two predominant energy sites as shown in Fig. 3. The argon adsorption isotherm for the catalyst at 77.8°K. is shown in Fig. 4, and θ vs. $1/p$ for the isotherm is given in Fig. 5. The final result obtained from the successive approximation of F vs. b for the isotherm is also presented as a dashed

Figure 2. Differential site-energy distribution for argon on MT-3100.

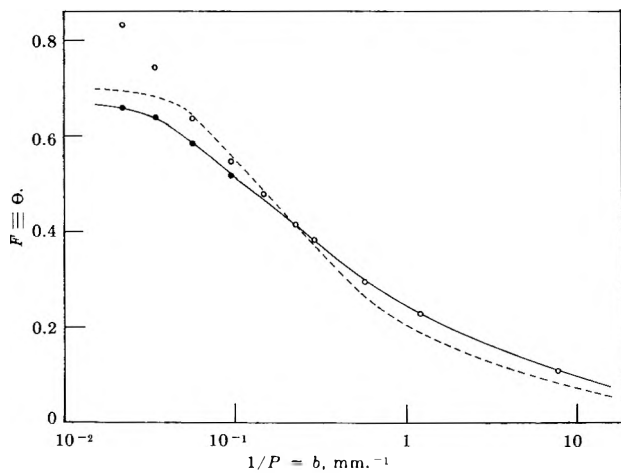(8) J. H. de Boer, "The Dynamical Character of Adsorption," Clarendon Press, Oxford, 1953.

Figure 5.   Adsorption isotherm of argon at 77.8°K.
on silica–alumina cracking catalyst: ————, Θ vs. $1/p$;
– – – –, final approximation to F vs. b;   O, V/V_m;
●, $(V/V_m)(1 - X)$.

Figure 6.   Differential site-energy distribution
on silica–alumina catalyst.

line in Fig. 5. The solid circles are the result of multilayer corrections made according to eq. 2. The monolayer capacity V_m was estimated to be 134 cc.-(STP)/g. based on the specific surface area obtained from nitrogen B.E.T. measurement, taking the cross-sectional area of argon as 14.6 Å.^{2} at 77.8°K.

With argon as the adsorbate, the catalyst surface still maintains its heterogeneous nature as can be seen from the site-energy distribution curve shown in Fig. 6. The majority of the sites have energies of about 2.25 kcal./mole. The site-energy distribution curve from the argon adsorption isotherm has only one peak in-

stead of two as when ammonia was an adsorbate. This is possible, because the integral site-energy distribution $F(Q)$ depends on the nature of both the adsorbent and adsorbate and is not solely a property of a given adsorbent.

The Viscoelastic Properties of Dilute Solutions of Polystyrene in Toluene

by G. Harrison, J. Lamb, and A. J. Matheson

Department of Electrical Engineering, The University, Glasgow W.2., Scotland   (*Received October 31, 1963*)

Quartz crystals resonant in the fundamental torsional mode at frequencies of 38 and 73 kc./sec. have been used to measure the viscoelastic properties of dilute solutions of polystyrene in toluene at temperatures from +50 to −70°. Seven narrow molecular weight fractions ranging in molecular weight from 4.8×10^4 to 1.2×10^6 were employed. Good agreement is found with the theory of Zimm but not with that of Rouse for solutions of polystyrene fractions with a molecular weight 2.39×10^5 and below. Up to this molecular weight, results for the dynamic viscosities of solutions of different molecular weights can be plotted on a single universal curve in agreement with the Zimm theory and similarly those for the rigidity modulus. Deviations from the Zimm theory are found for molecular weights of 3.64×10^5 and above, but in no way do these results approximate to the Rouse theory. It is suggested that these deviations at the higher molecular weights are due to a short time coordination of the motion of two polymer molecules.

Introduction

Molecular theories of the viscoelastic properties of dilute solutions of polymers have been developed by Rouse[1] and by Zimm.[2] The essential difference between these theories lies in the type of interaction between the polymer molecule and the flowing solvent. Rouse assumes that the velocity of the solvent flowing through a molecule is unaffected by the presence of the molecule (free-draining case),[3] while Zimm assumes that the solvent velocity and hence the interaction is less in the region of the center of the molecule than at its perimeter (nonfree-draining case). In both theories, the expressions for the components G' and G'' of the complex shear rigidity modulus, G^* $(= G' + iG'')$, of a polymer solution are[4]

$$G' = nkT\sum\omega^2\tau_p{}^2/(1 + \omega^2\tau_p{}^2) \qquad (1)$$

$$G'' = \omega\eta_s + nkT\sum\omega\tau_p/(1 + \omega^2\tau_p{}^2) \qquad (2)$$

The dynamic viscosity

$$\eta' = G''/\omega = \eta_s + nkT\sum\tau_p/(1 + \omega^2\tau_p{}^2) \qquad (3)$$

where n is the number of polymer molecules per cm.³, k is Boltzmann's constant, T is the absolute temperature, ω $(= 2\pi f)$ is the angular frequency, and η_s is the solvent viscosity. In the Rouse theory the values of the relaxation times τ_p of the different modes of motion of the polymer chain are

$$\tau_p = \frac{6(\eta - \eta_s)}{\pi^2 p^2 nkT} = \frac{6}{\pi^2 p^2}\frac{(\eta - \eta_s)M}{cRT} \qquad (4)$$

where η is the static viscosity of the solution, M is the molecular weight, c the concentration of the solution in g./ml., and $p = 1, 2, 3 \ldots$.

Zimm's values of τ_p on the other hand are

$$\tau_p = \frac{1.71(\eta - \eta_s)}{\lambda_p{}'nkT} = \frac{1.71}{\lambda_p{}'}\frac{(\eta - \eta_s)M}{cRT} \qquad (5)$$

where $\lambda_p{}' = 4.04, 12.79, 24.2 \ldots$.

The shapes of the resulting curves for G', G'', and η are shown with the experimental results in Fig. 1–6.

Some brief results of Rouse and Sittel[5] for polystyrenes of molecular weights 2.53×10^5, 5.2×10^5, and 6.2×10^6 dissolved in toluene agree with the Rouse theory. More recent results of De Mallie, et al.,[6] for a monodisperse polystyrene of molecular weight 2.67×10^5 in a solvent of high viscosity show

(1) P. E. Rouse, *J. Chem. Phys.*, **21**, 1272 (1953).

(2) B. H. Zimm, *ibid.*, **24**, 269 (1956).

(3) P. J. Flory, "Principles of Polymer Chemistry," Cornell University Press, Ithaca, N. Y., 1953.

(4) J. D. Ferry, "Viscoelastic Properties of Polymers," John Wiley & Sons, New York, N. Y., 1961.

(5) P. E. Rouse and K. Sittel, *J. Appl. Phys.*, **24**, 690 (1953).

(6) R. B. De Mallie, M. H. Birnboim, J. E. Frederick, N. W. Tschoegl, and J. D. Ferry, *J. Phys. Chem.*, **66**, 536 (1962).
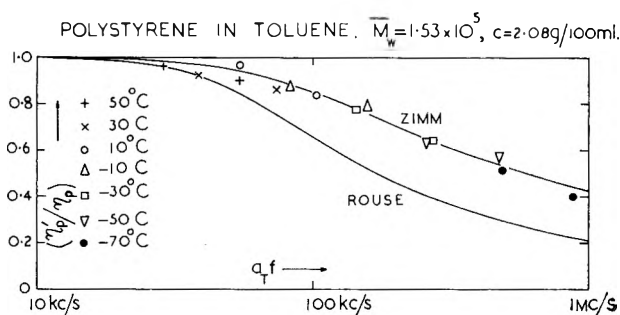
Figure 1.   Linear plot of dynamic viscosity of the solution in toluene of polystyrene C with M_w = 153,000.   The curves are those predicted by the theories of Rouse and Zimm.
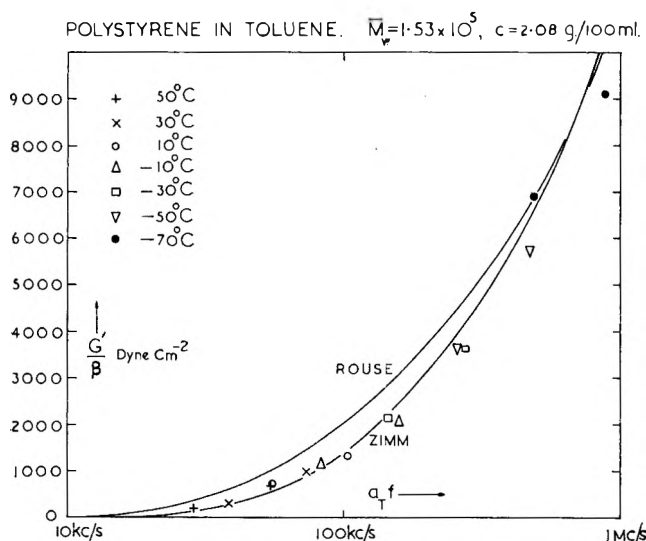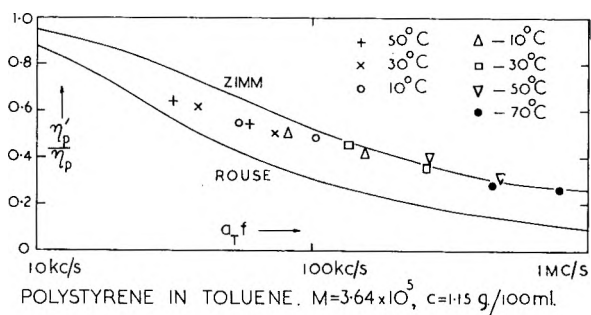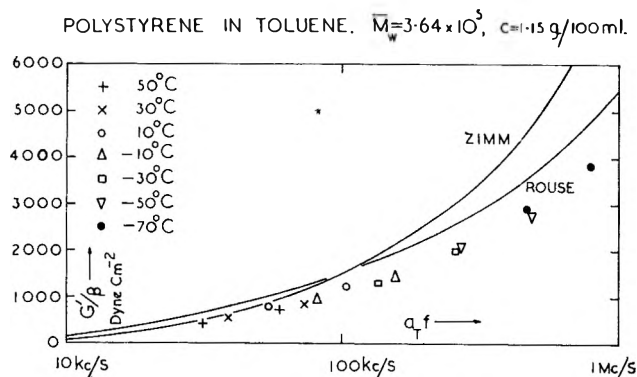

Figure 3.   Linear plot of the dynamic viscosity of the solution in toluene of polystyrene E_1 with M_w = 364,000.   The curves are those predicted by the theories of Rouse and Zimm.

Figure 2.   Linear plot of the shear rigidity modulus of the solution in toluene of polystyrene C with M_w = 153,000.   The curves are those predicted by the theories of Rouse and Zimm.

Figure 4.   Linear plot of the shear rigidity modulus of the solution in toluene of polystyrene E_1 with M_w = 346,000.   The curves are those predicted by the theories of Rouse and Zimm.

good agreement with the Zimm theory, however, as do the results of Tschoegl and Ferry[7] for narrow fractions of polyisobutylene of molecular weights 3.0 × 10^4 and 1.29 × 10^5, again in a solvent of high viscosity. But Tschoegl and Ferry[7,8] also find that in a solvent of high viscosity a polystyrene of molecular weight 1.7 × 10^6 and a polyisobutylene of molecular weight 1.1 × 10^6 agree with the Rouse theory.

We have measured the viscoelastic properties of a range of polystyrenes of molecular weights between 4.8 × 10^4 and 1.2 × 10^6 in a solvent of low viscosity (toluene) and have compared the results with the theories of Rouse and Zimm.   We were only able to cover a substantial part of the relaxation region in a solvent of low viscosity by working at frequencies above the audio range.

Experimental

Method.   The dynamic viscosity and shear rigidity modulus of the solutions were measured using torsional quartz crystals resonant at frequencies of 38 kc./sec. and 73 kc./sec., as described in detail elsewhere.[9] The resonant frequency and the resistance at resonance of the crystals were determined *in vacuo* and then in the solution to be measured.   The resistive and reactive components of the shear mechanical impedance of the liquid are obtained from the change in the resonant frequency Δf, and resistance at resonance ΔR

$$R_L = \frac{\Delta R}{K_1}; \quad X_L = \frac{\Delta f}{K_2} \qquad (6)$$

K_1 and K_2 are constants depending upon the geometrical and electrical characteristics of the quartz crystal and may either be calculated or determined from

(7)   N. W. Tschoegl and J. D. Ferry, *Kolloid-Z.*, in press.

(8)   J. D. Ferry, personal communication.

(9)   A. J. Barlow, G. Harrison, J. Richter, H. Seguin, and J. Lamb, *Lab. Pract.*, **10**, 786 (1961).
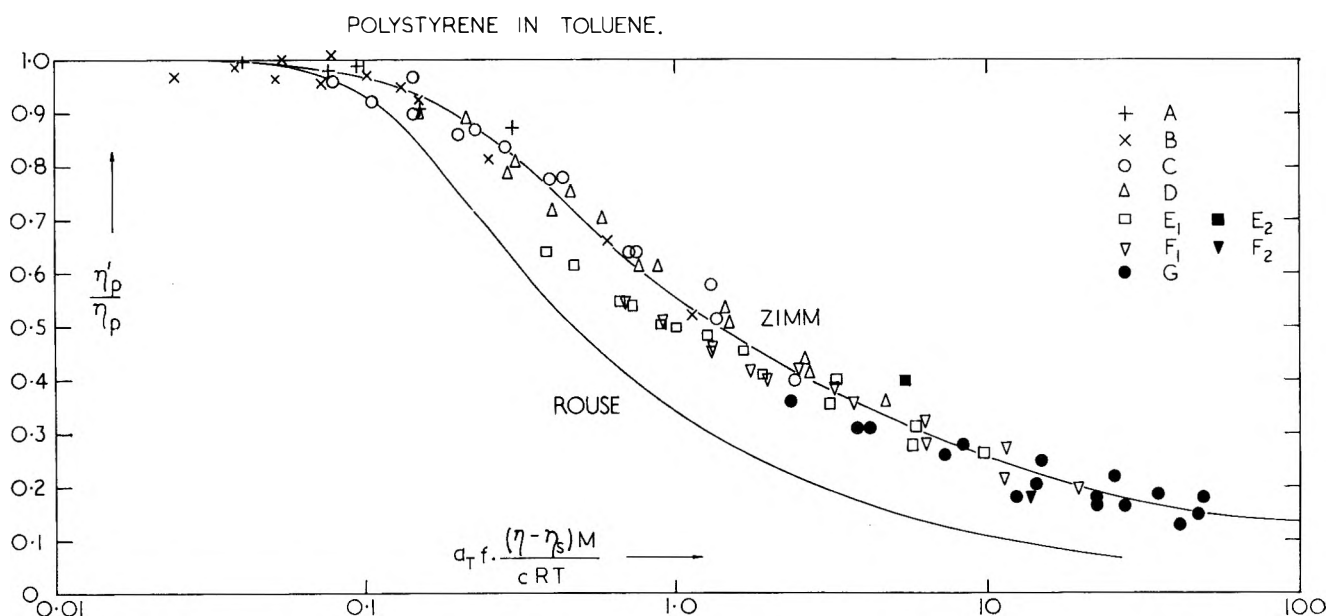
Figure 5. Linear plot of the dynamic viscosities of the polystyrene solutions on a dimensionless frequency scale. The curves are those predicted by the theories of Rouse and Zimm.

measurements using a Newtonian liquid of known shear mechanical impedance. In practice, although the constant K_1 is independent of the viscosity of the liquid under investigation, the constant K_2 varies with the viscosity of the liquid for liquids of low viscosity, owing to the surface roughness of the crystal. The crystal constants were therefore obtained empirically by calibration, using nonconducting liquids of different viscosities but of similar density to those under investigation. Suitable liquids were the homologs of toluene, e.g., n-butylbenzene, or dilute solutions in toluene of a nonrelaxing silicone fluid. The components of the complex shear modulus are[10]

$$G' = \frac{R_L{}^2 - X_L{}^2}{\rho}; \ G'' = \frac{2R_L X_L}{\rho} \qquad (7)$$

ρ is the density of the solution, and the dynamic viscosity of the solution η' is G''/ω.

Measurements were made at intervals of 20° between +50 and −70° and the result reduced to a standard temperature of 30° using the method of reduced variables.[4] The nonrelaxing viscosity of the solvent subtracted from the dynamic viscosity of the solution gives the contribution of the polymer to the dynamic solution viscosity η_p'. This is normalized by dividing by η_p, the contribution of the polymer to the static viscosity of the solution at the temperature of measurement. The values of (η_p'/η_p) are shown plotted against the reduced frequency, $a_T f$, where

$$a_T = \frac{(\eta_p)_T}{(\eta_p)_{30}} \frac{1}{\beta} \qquad (8)$$

and

$$\beta = \frac{(T\rho)_T}{(T\rho)_{30}}$$

Equation 8 is derived from eq. 1 and 2. It is only valid if the temperature dependence of all the relaxation times of a molecule is the same.

The static viscosity of the solutions and the solvent was measured in a suspended-level U-tube viscometer to an accuracy of ±0.5%. Both R_L and X_L are accurate to within ±2% and the probable uncertainties in (η_p'/η_p) and G'/β are ±4% and ±6%, respectively.

Measurements of density were made using a conventional densitometer.

Materials. Seven polystyrene samples were used in this investigation. Sample A was prepared by Dr. J. Pannell of I.C.I. Plastics Division, and the others by Dr. H. W. McCormick of the Dow Chemical Company, using the Szwarc technique, and they were kindly made available to us for this investigation. The molecular weights were estimated by sedimentation velocity analysis. Solutions of these samples of relative viscosity approximately equal to 3.0 were

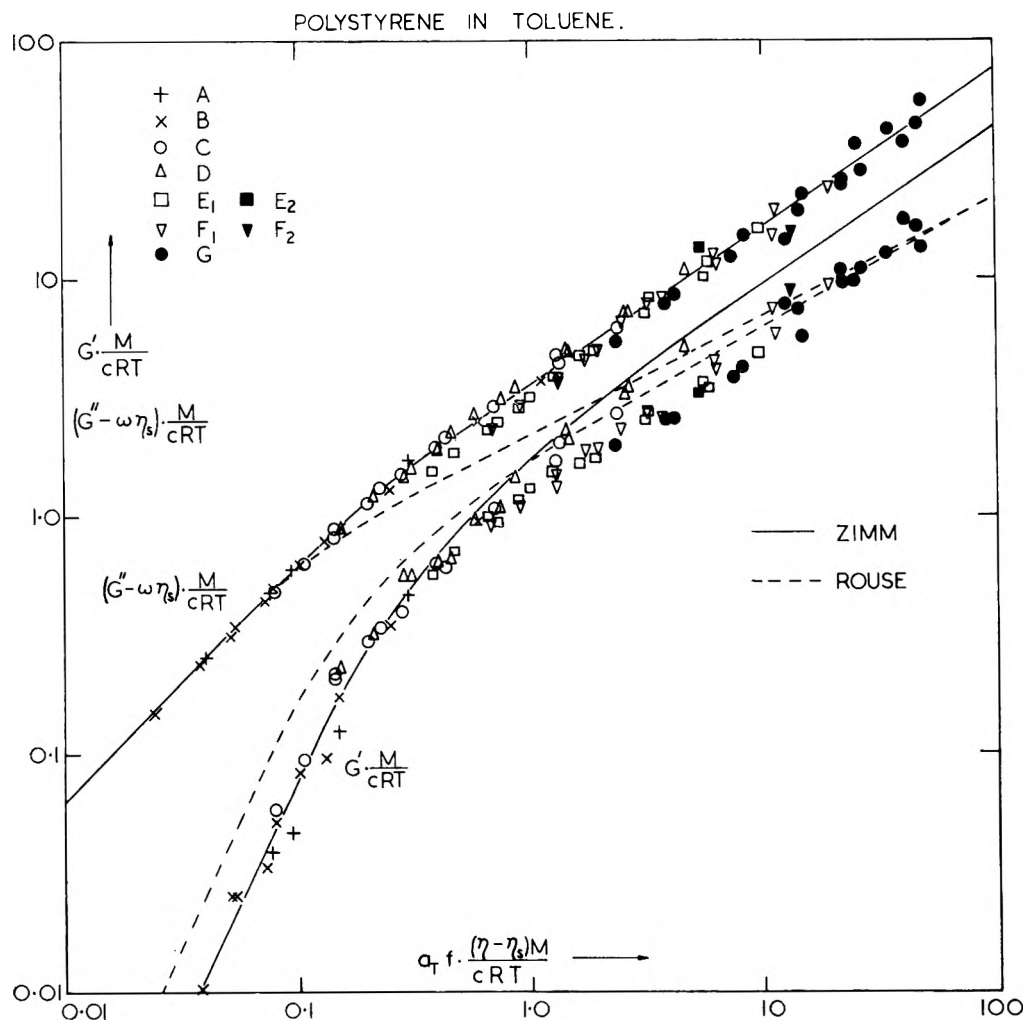(10) A. J. Barlow and J. Lamb, *Proc. Roy. Soc.* (London), **A253**, 52 (1959).

Figure 6. Logarithmic plot of $G'M/cRT$ and $(G'' - \omega\eta_s)M/cRT$ for the polystyrene solutions on a dimensionless frequency scale. The curves are those predicted by the theories of Rouse and Zimm.

made in dry toluene. Details of the solutions are given in Table I.

It transpires that the results for the polymer solutions on which measurements were made fall into two

Table I : Details of Polystyrene Samples and Solutions

Sample	$\overline{M}w$	$\overline{M}w/\overline{M}N$	Concentration, g./dl.	η_{20°, cp.
A	47,700		2.71	1.04
B	82,000	1.05	2.74	1.35
C	153,000	1.04	2.08	1.46
D	239,000	1.08	1.58	1.44
E_1	364,000	1.08	1.15	1.49
E_2	364,000	1.08	0.56	0.90
F_1	570,000	1.09	0.86	1.42
F_2	570,000	1.09	0.57	1.15
G	1,200,000	1.19	0.49	1.66

groups, namely those for polystyrenes with molecular weights below about 2.5 $\times$ 10^5 and those above. Results typical of the low molecular weight polymers are shown in Fig. 1 for the dynamic viscosity and in Fig. 2 for the shear rigidity modulus, along with the curves calculated from the theories of Rouse and Zimm. Likewise, typical results for the high molecular weight polymers are shown in Fig. 3 and 4.

Discussion

Results for both the dynamic viscosity and the shear rigidity modulus for polystyrenes of molecular weight up to 2.39 $\times$ 10^5 show good agreement with the predictions of the Zimm theory but do not agree with curves calculated from the Rouse theory. The application of the Zimm theory has also been confirmed by De Mallie, et al.,[6] for a polystyrene of molecular weight 2.67 $\times$ 10^5 in a high viscosity solvent, and by
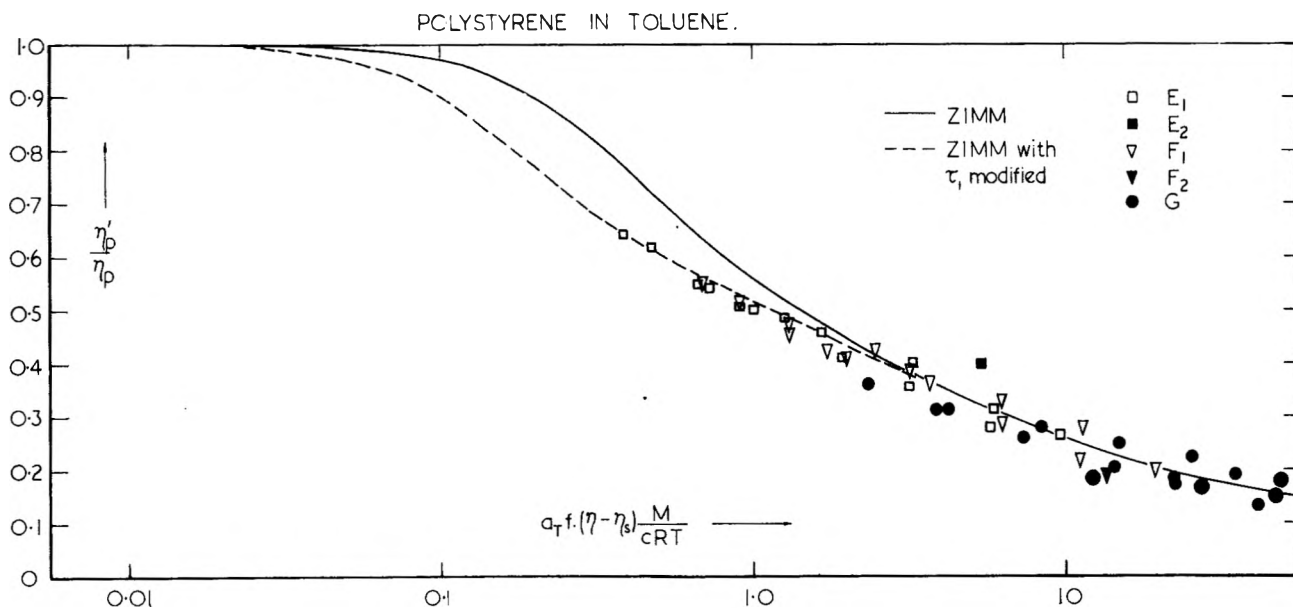
PCLYSTYRENE IN TOLUENE.

Figure 7. Linear plot of the dynamic viscosities of the higher molecular weight polystyrene solutions on a dimensionless frequency scale. The curves are those predicted by the Zimm theory and that obtained with τ_1 doubled as explained in the text.

Tschoegl and Ferry[7] for polyisobutylenes of molecular weight 0.63×10^5 and 2.19×10^5, again in a high viscosity solvent.

Both the Rouse and Zimm theories predict that the relaxation time of the pth mode is proportional to $(\eta - \eta_s)M/cRT$ and G' to cRT/M. Hence it is possible to reduce the results for polymers of different molecular weights to a single curve for the viscosity and to a single curve for the rigidity modulus by using the dimensionless variables $G'M/cRT$, $(G'' - \omega\eta_s)M/cRT$, and $a_Tf(\eta - \eta_s)M/cRT$. This reduction is made for all the polymer solutions in Fig. 5 and 6. For molecular weights up to 2.39×10^5 the experimental points are scattered about the Zimm curve within experimental error.

The experimental results for the polystyrenes of molecular weights 3.64×10^5, 5.7×10^5, and 1.2×10^6 deviate from the curves calculated from the Zimm theory. Measured values of the viscosity fall below the Zimm curve at low frequencies but agree with it at high frequencies (Fig. 3). On the other hand, measured values of the rigidity modulus agree with the curve predicted from the Zimm theory at low frequencies but fall progressively below the calculated curve with increasing frequency and in the direction of the Rouse curve after this has crossed the Zimm curve at the very highest frequencies (Fig. 4). Measurements on more dilute solutions of these polymers (Table I and Fig. 5 and 6) show similar behavior, suggesting that deviations from the Zimm theory

are not due to the solutions being too concentrated, within the limits of measurement.

There appears to be a discontinuity in the viscoelastic behavior occurring at molecular weights in the region of 3×10^5. Moreover, deviations from the curves predicted by the Zimm theory for molecular weights above this critical value appear to be independent of molecular weight when plotted with the same dimensionless variables as are used in Fig. 5 and 6. The results for only the three high molecular weight polystyrenes are shown plotted in this way in Fig. 7 and 8, in which there is no evidence of stepwise changes with differing molecular weights. We are thus led to conclude that a different mechanism becomes operative above a molecular weight of about 3×10^5, in agreement with the findings of Ferry and his co-workers.

It is of interest to note that above the same molecular weight the anomalous sound absorption results of Candau, Zana, and Cerf[11] for polystyrene solutions become independent of molecular weight.

For the higher molecular weights there is no suggestion that the viscosity is tending towards the Rouse theory. In Fig. 8 the slope of the rigidity curve for higher molecular weights is approximately parallel to the Zimm curve with values lying below the latter.

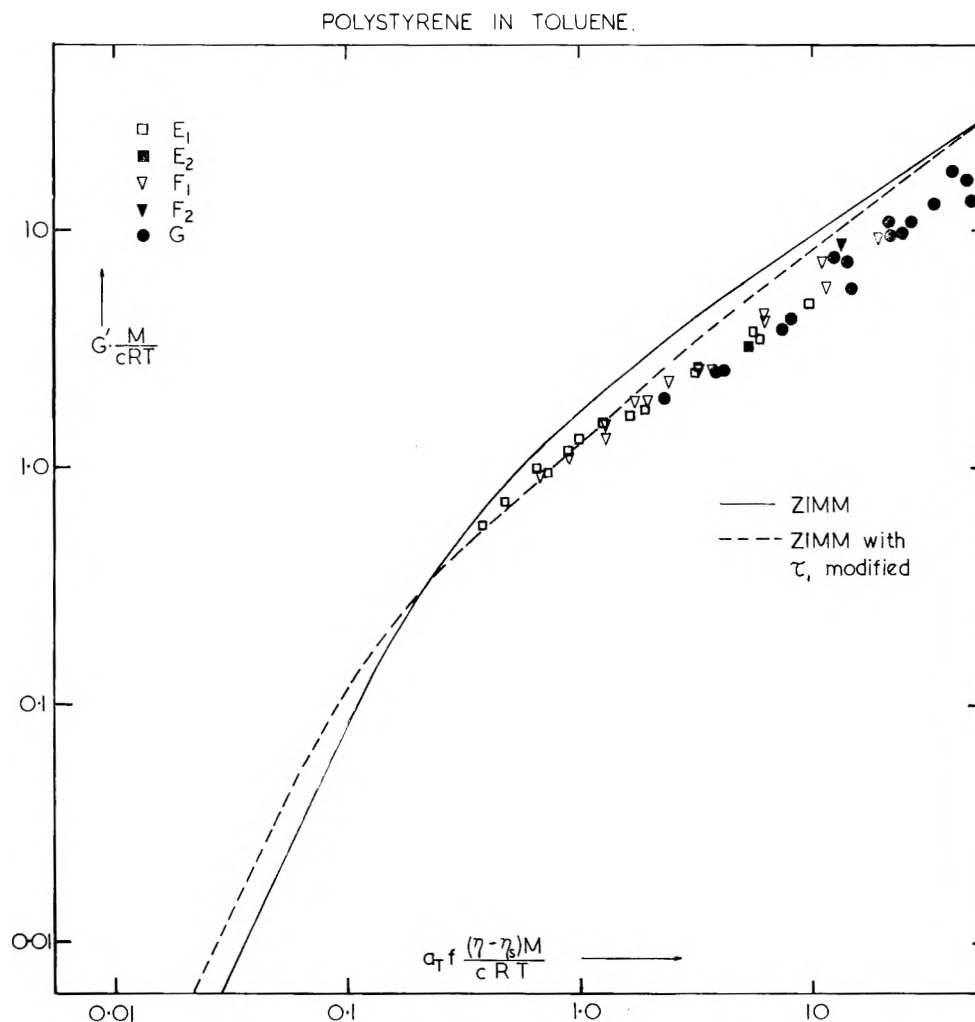(11) S. Candau, R. Zana, and R. Cerf, Compt. rend., 252, 2229 (1961).

Figure 8. Logarithmic plot of $G'M/cRT$ on a dimensionless frequency scale for the higher molecular weight polystyrene solutions. The curves are those predicted by the Zimm theory and that obtained with τ_1 doubled as explained in the text.

At the highest frequencies the experimental values are close to the values predicted from the Rouse theory.

Deviations of the viscosity from the Zimm theory at the lower frequencies with higher molecular weights (Fig. 7) can only be explained by using a value for τ_1 which is greater than that given by eq. 5. This is contrary to what one would expect if the molecule were self-entangled. Rewriting eq. 5

$$\eta - \eta_s = \frac{cRT}{M} \sum \tau_p$$

$$= \frac{cRT}{M} \tau_1 + \frac{cRT}{M} \tau_2 + \dots \quad (9)$$

Thus, for a given polymer contribution to the viscosity $(\eta - \eta_s)$, τ_1 can only be increased if the effective molecular weight associated with τ_1 be increased in the same proportion. The curve of Fig. 7 has been ob-

tained by arbitrarily increasing τ_1 and M in the Zimm theory by a factor of two for the first mode only. This gives a surprisingly good fit to the experimental points for viscosity. It also improves the fit on the rigidity curve of Fig. 8 at the lower frequencies but still leaves a discrepancy at the higher frequencies.

The only explanation which we are able to put forward to account for this behavior is in terms of a short time coordination of the motion of two molecules. We visualize two molecules coming together for a period of time which is greater than the duration of the stress cycle, so that within the time scale of τ_1, the effective molecular weight is increased by a factor of two. During this "time of contact," many intermolecular entanglements are broken and re-formed so that cooperative motion of the two molecules is possible. However, if the rate at which entanglements break and re-form is comparable with τ_2, then co-

operative motion on this shorter time scale may no longer be possible and the higher order modes are then sensibly unaffected by the intermolecular entanglements. The entanglement points are thus "pinned" or "frozen" with respect to the higher modes. Equilibrium properties such as the static viscosity remain unaffected by this process. Its kinetic nature is only evident when the time scale of an experiment is comparable with the contact time of the polymer molecules.

It would be of interest to examine the viscoelastic behavior in a "poorer" solvent, particularly that for the polystyrene of molecular weight 2.39×10^5 which, in solution in toluene, is the highest molecular weight which gives agreement with the theory of Zimm.

Torsion–Effusion Technique for Studying the Kinetics

of Gas-Forming Reactions

by Charles L. Rosen and Alvin J. Melveger

Research and Advanced Development Division, Avco Corporation, Wilmington, Massachusetts
(Received November 7, 1963)

The torsion–effusion technique has been applied to the study of the kinetics of thermal decomposition. An apparatus which includes a thermocouple as an integral part of the suspension system is described. The decomposition of polytetrafluoroethylene (Teflon) was studied and found to obey first-order kinetics with an activation energy of 76.7 ± 7.3 kcal./mole in the temperature range 544 to 590°. The first-order rate constant, k (sec.$^{-1}$), was found to obey the expression $\log k = 17.27 - 16.66 \times 10^3 (1/T)$. The molecular weight of vaporizing species was calculated and found to be 100.0 ± 6.

I. Introduction

The kinetics of reactions that involve the irreversible formation of volatile species have usually been studied by techniques involving weight change or pressure change observations.[1] In most weight change and pressure change experiments that have been reported, the integral amounts of sample weight or system pressure were measured at given times. However, the information most frequently desired is the rate of reaction as a function of time at various temperatures. These isothermal rates can be derived from the integral values.

This paper will show the applicability of the torsion–effusion method to the study of reaction kinetics of irreversible gas-forming reactions. The torsion–effusion method permits pressure rate data to be obtained directly and in addition, if the weight change rate data are available, the molecular weight of the vaporizing species may be determined. The desirability of this method which measures the reaction rate directly rests upon its being an extremely rapid and relatively accurate procedure requiring only small quantities of material and an apparatus that is easy to construct.

The torsion method was first used by Volmer[2] for the measurement of vapor pressures and this has remained its main use. However, in addition to vapor pressure measurements, the torsion–effusion technique has been used to measure the rate of evaporation and the rate of growth of single crystals.[3] In the usual experimental arrangement, a condensed phase is enclosed in a reaction crucible and the vapors which are formed upon heating this condensed phase are allowed to effuse through one or more orifices. It has been shown that in the molecular flow region, the force of the issuing vapor beam depends directly upon the number of molecules leaving the crucible per unit of time.[4] This force, due to the transfer of momentum from the escaping gaseous molecules to the crucible, may be determined by allowing the vapor to flow through crucible orifices that are eccentrically located with respect to a suspension wire calibrated in terms of force per angular displacement and measuring the displacement produced. Thus the angular displacement is actually a measure of the number of molecules leaving the crucible per unit of time and as will be shown, under certain conditions, the rate of reaction.

For vapor pressure measurements, the effusion rates are kept as low as possible by using large evaporating to orifice area ratios in order to ensure that the vapor pressure above the condensed phase approaches, as closely as practical, the equilibrium vapor pressure.

(1) (a) C. D. Doyle, *J. Appl. Polymer Sci.*, **5**, 285 (1961); (b) S. L. Madorsky, V. E. Hart, and S. Straus, *J. Res. Natl. Bur. Std.*, **56**, 343 (1956).

(2) M. Volmer, *Z. physik. Chem.*, 863 (1931).

(3) V. J. Clancey, *Nature*, **166**, 275 (1950).

(4) R. D. Freeman and A. W. Searcy, *J. Chem. Phys.*, **22**, 762 (1954).

II. Theoretical Discussion

The mathematical equations for the application of torsion–effusion are well known.[2,3] The applicability of these equations to the determination of the kinetics of irreversible gas-forming reactions will be demonstrated.

The equations to be discussed are applicable only in the molecular flow region where from kinetic gas theory the rate of weight loss from the reaction crucible can be shown to be[5]

$$\frac{dw}{dt} = 2f\left[\frac{M}{2\pi RT}\right]^{1/2} \tag{1}$$

where dw is the loss of weight from the crucible; dt is the time interval during which the weight change occurs; f is the force of the effusing beam; M is the molecular weight of the vapor species; T is the absolute temperature; and R is the gas constant.

The force exerted by the effusing beam on the crucible can be expressed as

$$f = D\theta \tag{2}$$

where f is the force, D is the torsional constant of the suspension wire, and θ is the angular deflection of the suspension. A combination of eq. 1 and 2 gives

$$\frac{dw}{dt} = 2D\theta\left[\frac{M}{2\pi RT}\right]^{1/2} \tag{3}$$

Equation 3 shows that for a given torsion wire, the angular deflection is dependent only upon the rate of weight loss from the crucible, the temperature, and the molecular weight of the effusing vapors.

If the residence time of a molecule in the crucible is short compared to the apparatus response time, then the rate of weight loss from the crucible equals the rate of formation of gaseous molecules. Thus, the angular deflection at any time becomes proportional to the reaction rate.

The average residence time of a molecule under molecular flow conditions will be estimated. Intermolecular collisions may be neglected in this flow region. The total number of collisions of vapor species with the walls of the crucible during time t can be expressed as[6]

$$Z = \frac{1}{4} CA_T t \frac{n}{V} \tag{4}$$

where Z is the total number of collisions with walls; C is the average velocity of the molecules; A_T is the total area of the crucible walls; t is the time during which collisions occur; n is the number of molecules present; and V is the volume of the crucible.

If it is assumed that any molecule colliding with an effusion hole leads to effective removal from the crucible, then the number of molecules removed from the crucible in time t is

$$Z_1 = \frac{1}{4} CA t \frac{n}{V} \tag{5}$$

where Z_1 is the number of collisions with effusion holes and A is the area of effusion holes. If one considers a molecule having an average velocity, C, then the time necessary for it to make a collision leading to effective removal is

$$t = \frac{4V}{CA} \tag{6}$$

Under the conditions of a typical experiment, the values of V, C, and A are such that a molecule is removed in the order of milliseconds after its formation. Therefore, within this time resolution, the angular deflection at any time is directly proportional to the rate of reaction.

Implicit in the assumption of molecular flow is the occurrence of a cosine law effusion of molecules from the orifices. Corrections for the existence of nondiffuse effusion should be made in certain cases.[3,7] This correction may be important when comparing the results from orifices of different geometry.

It should be emphasized that although eq. 3 reveals the independence of angular deflection and orifice area, this only applies to irreversible reactions and/or cases where the orifice area is not a limiting factor in vapor removal. In reversible zero-order reactions, such as vapor pressure determinations, the amount of material effused per unit of time, and hence the angular deflection, is directly proportional to the orifice area as long as the rate of vapor removal through the orifice is small in comparison to the total rate of evaporation within the crucible. Even though the deflection has been shown to be independent of orifice area, the orifice area does determine the maximum rate of molecular effusion that can be maintained in order to remain in the molecular flow region.

III. Experimental

The usual torsion–effusion assembly has been modified to permit accurate temperature measurement of the decomposing specimen.

The uncertainty associated with temperature measurements has been a factor limiting the accuracy attain-

(5) J. L. Margrave, J. Chem. Phys., 27, 1412 (1957).

(6) I. Langmuir, J. Am. Chem. Soc., 35, 931 (1913).

(7) P. Clausing, Ann. Physik, 12, 961 (1932).

able in torsion–effusion experiments. The nature of the torsion–effusion assembly has, in the past, appeared to preclude the insertion of a thermocouple directly in the sample without introducing an extraneous torque. The usual procedure has been to place a thermocouple close to, but not in contact with, the effusion crucible and to calibrate this thermocouple against readings of a thermocouple placed inside the cell during a "dummy" run without a sample.

Figure 1 is a schematic diagram of the apparatus used in our laboratory. It has the advantage of allowing direct temperature monitoring of the evaporating system, thus helping to eliminate a major source of uncertainty in torsion experiments. A chromel–alumel thermocouple is an integral part of the apparatus; yet it introduces, for our purposes, negligible interference to the angular deflection of 20.2 in. long, 0.003 or 0.005 in. diameter tungsten torsion wire. A two-hole quartz torsion crucible fitted with a standard taper joint connected to twin bore quartz capillary tubing is suspended from the torsion wire. The

capillary tubing is mechanically coupled to an aluminum rod which, in turn, is coupled to the torsion wire. Five-mil chromel–alumel thermocouple wire is fed through the quartz twin bore tubing and terminates in a ceramic-coated junction inside the effusion cell.

The upper end of the capillary tubing contains two holes from which the insulated thermocouple wires may be removed and tightly wrapped and cemented about the aluminum rod. The ends of the thermocouple wires are attached to small clips to which 0.0005-in. diameter tungsten wire is connected and allowed to hang loosely. These very fine tungsten wires are led through the vacuum system by means of metal–ceramic seals and terminate at a recorder that is used for monitoring the sample temperature.

The stability of the torsion constant of a 0.003-in. diameter suspension wire was determined with the thermocouple and fine tungsten wires in place. This was done by measuring the period of oscillation of the system over the range of angular deflection 2–40° of arc under simulated experimental conditions. In 25 determinations over a 1-week interval, the deviation of the period from a mean value of 28.22 sec. was less than 0.5% with a confidence level of 90%. The maximum spread of these determinations was 1.4%. These results indicate that the torsion constant determined with attached tungsten wires remains constant during normal experimental operation. The success of this method appears to depend upon the use of loosely hung wires and the coupling of the wires as close to the center of rotation as possible, thereby reducing extraneous torques.

A possible source of error in temperature measurement with the described apparatus is the presence of tungsten–chromel and tungsten–alumel junctions in the temperature measuring circuit. The temperatures of these junctions were measured during sample heating and found to remain at ambient temperature. As long as such conditions can be maintained, it is felt that this method is more reliable than the use of "dummy" calibrations.

Although the described apparatus can be used only below the softening point of quartz, modification of the torsion crucible and the capillary tubing materials can extend the usable range of the apparatus to higher temperatures.

In order to make the technique practicable, the apparatus must employ a method for critically damping the system so that the angular deflection reaches its steady-state value during the characteristic time of a measurement. The suspension system employs an oil damping arrangement. Two damping vanes shown in Fig. 1 are attached to the rigid part of the suspension
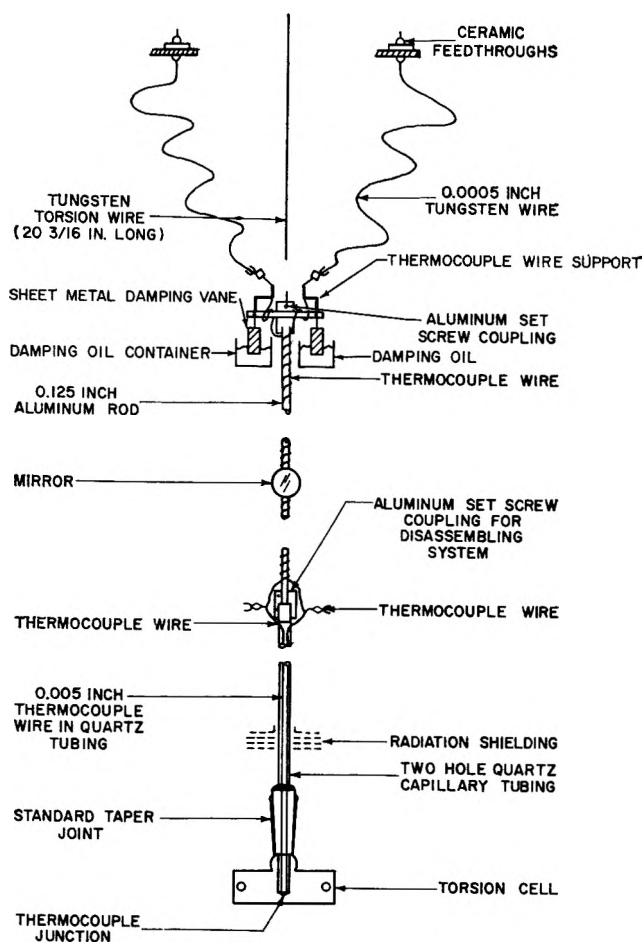

Figure 1. Torsion suspension and damping system.

system and dip into the oil, thus serving to damp out any extraneous oscillations and any overshooting while the torsion system's motion is being monitored. The amount of damping may be varied by increasing or decreasing the depth of immersion of the vanes in the oil. This can be achieved by either adding or removing damping fluid or by raising or lowering the entire suspension system by means of the screw assembly at the top of the torsion system. In any given experiment the damping was adjusted to what was considered the critical amount. This was determined by imparting various torques to the system and monitoring the decay time to reach its equilibrium value. The amount of damping was then adjusted to make this decay time as short as possible. The system's motion was then found to be smooth and regular without any apparent overshooting that one would expect in an underdamped system. In choosing a damping fluid, it was important to consider both its viscosity and vapor pressure since the system was operated under vacuum. Motor oil was found to meet these requirements for our system.

The actual measurements of angular deflection were made by reflecting a light from a mirror mounted on the suspension system onto a scale placed at a distance of 9 ft. from the axis of rotation of the system. The scale was calibrated in degrees of arc.

IV. Results

The decomposition of polytetrafluoroethylene (Teflon), which has been studied previously, was used to test the method and the apparatus. Madorsky and co-workers,[8] by isothermal weight loss and pressure rise methods, reported that the pyrolysis of polytetrafluoroethylene *in vacuo* followed a first-order rate law between 480 and 510° with an activation energy of 75 ± 4 kcal./mole. Anderson[9] determined by thermogravimetry that in the range 450 to 550° the pyrolysis of Teflon *in vacuo* obeyed a first-order rate law with an activation energy of 80.5 kcal./mole.

From eq. 3 it can be seen that the rate of material loss is proportional to the angular deflection at constant temperature and constant molecular weight. Since a simultaneous determination of weight loss and angular deflection was not made, it was assumed that the average molecular weight of the effusing molecules remained constant during the course of an experimental run. Thus if the decomposition of material A (condensed phase) to some vapor phase follows a first-order relation, then one may write

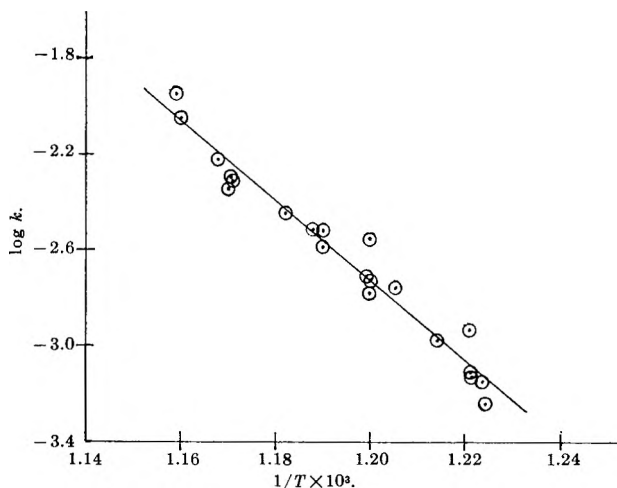$$\frac{-dA}{dt} = kA = k'\theta \tag{7}$$

Figure 2. Arrhenius plot for decomposition of polytetrafluoroethylene.

where $-dA/dt$ is the reaction rate, k is the rate constant, and k' is a proportionality constant between the rate of reaction and angular deflection.

It can be shown that after suitable integration of eq. 7 one may write

$$\log\left(\frac{A_0 k}{k'}\right) - \frac{kt}{2.303} = \log \theta \tag{8}$$

where A_0 is the original concentration of A.

Thus, for a first-order reaction a plot of $\log \theta$ vs. t yields a line with a slope equivalent to $-k/2.303$. Values of $\log k$ at various temperatures can now be determined and plotted against $1/T$ according to the Arrhenius expression

$$\log k = \log k_0 - \frac{E}{2.303RT} \tag{9}$$

where E is the activation energy and k_0 is the Arrhenius constant. The slope of such a plot yields the value $-E/2.303R$ from which the activation energy, E, can be determined.

DuPont Teflon which was cut into small shavings or powdered from a piece of the pressed material was used for the experiments. Sample weights of 50, 100, and 150 mg. were used. It was found that the results were independent of sample weight or form.

The torsion crucible was placed in a vacuum resistance furnace and when ready was brought up to temperature as rapidly as possible and maintained at temperature for the duration of the experimental run. The temperature indicated by the thermocouple

(8) S. L. Madorsky, V. E. Hart, S. Straus, and V. A. Sedlack, J. Res. Natl. Bur. Std., 51, 327 (1953).

(9) H. C. Anderson, Makromol. Chem., 51, 233 (1962).

was displayed on a Sargent strip chart recorder. The temperature range studied was 544 to 590°. There seemed to be some indication of anomalous behavior during the initial pyrolysis before the sample reached its final temperature and usually before 10% of the sample had vaporized. Only those readings of the deflection taken after the attainment of isothermal conditions were used.

A series of 19 experiments was performed in the temperature range indicated. It was assumed that slight temperature changes during any run would be averaged out. Temperature fluctuations were usually kept to within 2°. For each isothermal run, values of log θ vs. time were plotted and a least-squares fit was made of these data to determine k. The logarithms of these values of k were then plotted against $1/T$ to evaluate the activation energy of the decomposition. Such a plot gave a straight line, shown in Fig. 2, which obeyed the equation

$$\log k = 17.27 - 16.66 \times 10^3 \, (1/T) \quad (10)$$

where k is the first-order rate constant in sec.$^{-1}$, and T is the absolute temperature.

The activation energy was then determined to be 76.7 $\pm$ 7.3 kcal./mole with 90% confidence, which agrees with previous workers.

An average molecular weight for the effusing vapors was determined by using the integrated form of eq. 3

$$(M)^{1/2} = \frac{W(2\pi RT)^{1/2}}{2D \int_0^t \theta \mathrm{d}t} \quad (11)$$

The molecular weight was assumed to be constant during an experimental run in making this calculation. The value of $\int_0^t \theta \mathrm{d}t$ was evaluated graphically from plots of θ vs. t. The total weight loss of sample in an experiment was used as the value for W.

The torsion constant, D, was calculated from a knowledge of the modulus of rigidity of the 5-mil tungsten torsion wire and its length. Molecular weights which were determined on the basis of the calculated torsion constant were then corrected by means of an experimentally determined instrument calibration factor. Zinc metal which vaporizes into atomic Zn having a molecular weight of 65.4 and ammonium chloride which decomposes to NH_3 and HCl with an average molecular weight of 26.8 were the calibrating substances used. By use of eq. 11 the molecular weights for the calibrating substances were calculated and found to deviate from their true value by the factor 1.37 $\pm$ 0.05. All molecular weights determined for Teflon were then multiplied by this apparatus constant. In calculating the molecular

weight of the decomposing Teflon, no correction was made for the fact that part of the effusion occurred before the sample reached its nominal temperature.

Values for the molecular weight of Teflon determined in the above manner are listed in Table I. The mean value is 100.0 with an associated mean deviation error of approximately 6%. The estimated error includes the uncertainty associated with the experimental determination of the apparatus calibration factor.

Table I

Sample weight, mg.	Temp., °K.	Mol. wt.
99.6	817	96.9
99.9	846	106.3
101.0	829	115.2
99.9	840	95.1
98.5	833	98.1
99.4	834	97.7
99.4	842	96.3
100.5	824	106.2
100.4	819	100.0
99.7	854	87.3
99.7	854	104.3
100.7	819	104.3
50.3	853	94.3
50.2	856	99.7
51.0	855	95.6
150.3	817	101.1
150.0	819	101.2
150.4	819	99.3
149.4	833	101.1
	Mean	100.0 ± 6

These results indicate that the average molecular weight of Teflon degradation products as determined by this technique is fairly constant and independent of sample size and temperature within the range studied.

In order to investigate the possibility of changes in the molecular weights of the vapors over the duration of the experiment, one would need simultaneous angular deflection and weight loss data.

V. Summary

The torsion–effusion technique has been shown to be applicable to the study of thermal decomposition reactions involving the formation of a gas phase. The method allows for the direct measurement of the rate of formation of a vapor phase using small samples and should be applicable to the study of kinetics in both organic and inorganic systems.

Electrokinetic Flow in Ultrafine Capillary Slits[1]

by D. Burgreen and F. R. Nakache

Development Division, United Nuclear Corporation, White Plains, New York   (*Received November 9, 1963*)

This paper contains an analytical study of electrokinetic flow in very fine capillary channels of rectangular cross section. It is a natural extension of the general theory of electrokinetic flow which heretofore was limited to channels of large electrokinetic radius or to interfaces exhibiting low source potential. The practical implications of the results of the study are explored.

Nomenclature

A	cross section area of capillary channel
B	$M^2\omega^2\mu/K$
c	ion concentration in moles per liter
D	dielectric constant of fluid
E_0	applied axial voltage
E_s	streaming potential
$E(\theta,\kappa)$	elliptic integral of second kind
$F(\theta,\kappa)$	elliptic integral of first kind
$G(\alpha,\omega h)$	parameter plotted in Fig. 6
h	half of distance between plates
I	current in external circuit
I_c	electroosmotic conduction current $= K_0 A Y_0$
I_t	electroosmotic transport current
K	lumped conductivity (fluid path plus external path) $= K_0 + L/2hR_0 = K_0 + L/\pi r_0^2 R_0$
K_0	specific conductivity of fluid
k	Boltzmann constant
L	length of capillary passage
M	mobility $= \psi_0 D/4\pi\mu$ or $\zeta D/4\pi\mu$
$\bar{n}$	average number of positive or negative ions per unit volume
$\bar{n}_i$	average number of ions of ith kind per unit volume
n_i	number of ions of ith kind per unit volume
P	pressure in fluid
Re	Reynolds number
R_0	resistance of external circuit
R_1	internal or fluid resistance
r_0	radius of tube
s	wetted perimeter of capillary channel
T	absolute temperature

u	velocity at a given point in capillary channel
u_0	velocity at center of channel
u_e	electroosmotic velocity
u_p	pressure-induced velocity
u_r	retarding flow component
V	volumetric flow
V_p	volumetric pressure-induced flow
V_r	volumetric retarding flow
W_e	electrokinetic pumping energy
W_p	mechanical pumping energy
x	axial distance along capillary channel
Y	axial electric field $= \mathrm{d}E/\mathrm{d}x$
Y_0	applied axial electric field $= \mathrm{d}E_0/\mathrm{d}x$
Y_s	$\mathrm{d}E_s/\mathrm{d}x =$ streaming axial electric field
Y_{su}	unreduced streaming potential
y	distance measured from capillary wall
z	valence of ions when one kind of salt is present and dissociates into two equal and oppositely charged ions
z_i	valence of ith type of ion

Greek symbols

α	ionic energy parameter $= ez\psi_0/kT$
α_i	ionic energy parameter $= ez_i\psi_0/kT$
η	rectilinear coordinate measured from center of channel in flow between plates
θ	$\sin^{-1}[\cosh(\alpha\psi_c/2\psi_0)/\cosh(\alpha\psi/2\psi_0)]$
θ_0	$\sin^{-1}[\cosh(\alpha\psi_c/2\psi_0)/\cosh(\alpha/2)]$

κ	$[\cosh\,(\alpha\psi_c/2\psi_0)]^{-1}$
λ	Debye length $= [D\psi_0/8\pi\bar{n}ez\alpha]^{1/2}$
μ	viscosity of fluid
ρ	net charge per unit volume
τ	viscous shear stress
ψ	electric potential of ions (relative to solution containing an equal number of positive and negative ions)
ψ_0	potential at surface of capillary
Ω	electrokinetic radius $= 2\omega A/s$, or $2\omega h$, or ωr_0
ω	reciprocal of Debye length $= [8\pi\bar{n}ez\alpha/D\psi_0]^{1/2}$

Introduction

Before proceeding with the analytical development of the theory of electrokinetic flow in ultrafine capillary elements, it is worth reviewing briefly the historical development and present status of the subject.

Electrokinetic phenomena were observed as far back as the beginning of the 19th century. In 1808, Reuss[2] discovered that flow through capillary elements can be induced by the application of an electric field. About half a century later, Wiedemann[3] performed a number of quantitative experiments and promulgated one of the fundamental theories of electrokinetics. This theory, which has been verified many times, states that the volumetric electroosmotic flow is proportional to the applied current. In 1859, Quinke[4] discovered the phenomenon of streaming potential which is the converse of electroosmosis. His experiments showed that when fluid was forced through a diaphragm, the voltage developed across the diaphragm was proportional to the pressure differential causing the flow.

In 1879, Helmholtz[5] developed the double layer theory which related analytically the electrical and flow parameters of electrokinetic transport. Although the theory was based on a somewhat intuitive analysis, it has stood the test of time and still represents an acceptable formulation of the electroosmotic phenomenon in most capillary materials. Smoluchowski,[6] in 1903, expanded on Helmholtz's double layer theory by taking into account the actual distribution of velocity in the capillary channel. In 1909, Freundlich[7] published results of a number of comprehensive experiments dealing with electrokinetic effects, and was the first to use the word electrokinetics to describe the phenomena. He demonstrated that the proportionality constant in electroosmosis, relating volumetric flow to electric current, was identical with the proportionality constant relating streaming potential and applied pressure.

A more realistic concept of the potential and charge distribution in the fluid adjacent to the capillary wall was introduced by Gouy[8] in 1910. He computed the electric charge distribution in a diffuse layer. Debye and Hückel,[9] in 1923, determined the ionic distribu-

tion in solutions of low ionic energy, by means of a linear simplification of the exponential Boltzmann ion energy distribution. Contributions have been made in more recent times to the technology of electrokinetics by Freundlich,[7] Abramson,[10] Bikerman,[11] Davies and Rideal,[12] and others. A comprehensive treatment of the classical theories of electroosmosis and streaming potential is available in a recently published article by the authors.[13]

Analytical solutions exist[13] for electroosmotic flow in slits and capillary tubes when the surface ionic energy $ez\psi_0$ is small in comparison to the thermal energy kT. The solution of these problems indicates that when the electrokinetic radius, defined as $2\omega h$ or ωr_0 (see Nomenclature), becomes moderately large, the electrokinetic effects are confined to the area close to the capillary wall. As a result, it is possible to solve the electroosmotic flow problem for arbitrary cross-section channels applicable to capillaries having any magnitude of ionic energy, provided the electrokinetic radius is sufficiently large. It is difficult to specify an exact range of validity for solutions applicable to large electrokinetic radius since the solution becomes more accurate as the electrokinetic radius increases. For the case of flow in a slit, we find that when $\omega h > 5$ the error is less than 1%. In the case of flow in a tube or in an odd-shaped capillary, the nonrectilinear geometry requires that ωr_0 or the electrokinetic radius be larger than 40 in order to obtain reasonably accurate results. The requirement of large electrokinetic radius would appear, from a practical point of view, not very restrictive, since only in very dilute solutions and in very fine capillaries will the electrokinetic radius be small. However, it is specifically the results of the present treatment, applicable to small electrokinetic radius, that suggest practical application.

(2) F. F. Reuss, Memoires de la Societé Imperiale de Naturalistes de Moscou, Vol. 2, 1809, p. 327.

(3) G. Wiedemann, Pogg. Ann., 87, 321 (1852).

(4) G. Quinke, ibid., 107, 1 (1859).

(5) H. Helmholtz, Ann., 7, 337 (1879).

(6) M. Smoluchowski, Krak. Anz., 182 (1903); also in Graetz, "Handbuch der Elektrizität und des Magnetismus," Vol. 2, Barth, Leipzig, 1921, p. 336.

(7) H. Freundlich, "Kapillarchemie," Akademischer Verlag, 1909.

(8) L. Gouy, J. Phys., 9, 456 (1910).

(9) P. Debye and E. Hückel, Physik. Z., 24, 185, 305 (1923).

(10) H. A. Abramson, "Elecktrokinetic Phenomena and Their Application to Biology and Medicine." Chemical Catalog Co., New York, N. Y., 1934.

(11) J. J. Bikerman, "Surface Chemistry," Academic Press Inc., New York, N. Y., 1958.

(12) J. T. Davies and E. K. Rideal, "Interfacial Phenomena," Academic Press Inc., New York and London, 1961.

(13) D. Burgreen and F. R. Nakache, "Electrokinetic Flow in Capillary Elements," ASD-TDR-63-243, March, 1963.

In solving the streaming potential problem, similar limitations were imposed. Solutions of problems are thus available covering the more common ranges of ionic energy and electrokinetic radius. This paper contains the analysis of the streaming potential generation and flow in a capillary slit for an arbitrary ionic energy and electrokinetic radius. It provides a solution for the case of high ionic energy and small electrokinetic radius, which is not contained in the earlier work. In the treatment which follows, electroosmotic flow and streaming potential generation are included as part of the comprehensive problem.

Charge and Potential Distribution

The theory of electrokinetic flow is based on the fundamental observation that at the interface of a dilute solution and nonconducting surface a potential ψ_0 (relative to the fluid far from the wall where the positive and negative ion concentrations are equal) exists whose magnitude is dependent upon the character of the surface and the solution. The question of how or why such a potential is developed need not be considered here. It exists, and its presence produces a redistribution of ions in the vicinity of the surface. As a result of the surface potential ψ_0, the equilibrium ionic distribution is disturbed, the net electric charge at various points in the solution is not zero, and the number of ions of each type per unit volume in the fluid differs from the average. When the material of the capillary wall is an insulator and the net lateral current is zero, an equilibrium will be obtained between the ionic diffusion and conduction current. This resulting ionic distribution is the Boltzmann distribution which gives the number of ions of a particular kind (n_i) which are at a potential ψ above that of a solution containing uniformly distributed ions. This is expressed as

$$n_i = \bar{n}_i e^{-ez_i\psi/kT} \tag{1}$$

Assuming that we are dealing with a simple electrolyte which ionizes into two equally charged ions of valence z, then the net charge per unit volume, ρ, is given by

$$\rho = \bar{n}ez(e^{-\alpha\psi/\psi_0} - e^{-\alpha\psi/\psi_0}) = -2\bar{n}ez \sinh (\alpha\psi/\psi_0) \tag{2}$$

where $\alpha = ez\psi_0/kT$. The charge density and potential are also related through the one-dimensional Poisson equation

$$\frac{d^2\psi}{dy^2} = -\frac{4\pi}{D}\rho \tag{3}$$

When combined with eq. 2 this yields

$$\frac{d^2(\alpha\psi/\psi_0)}{d(\omega y)^2} = \sinh (\alpha\psi/\psi_0) \tag{4}$$

We have introduced in eq. 4 the inverse of the Debye length, ω, defined as

$$\omega = \left[\frac{8\pi\bar{n}ez\alpha}{D\psi_0}\right]^{1/2} \tag{5}$$

Integration of eq. 4 yields

$$\frac{d(\alpha\psi/\psi_0)}{d(\omega\eta)} = \left(2\cosh\frac{\alpha\psi}{\psi_0} - \text{constant}\right)^{1/2} \tag{6}$$

If ψ_c is the potential at the center of the channel ($\eta = 0$) then by means of the boundary condition

$$\left[\frac{d(\alpha\psi/\psi_0)}{d(\omega\eta)}\right] = 0 \text{ at } \eta = 0 \tag{7}$$

eq. 6 becomes

$$d(\omega\eta) = \frac{d(\alpha\psi/2\psi_0)}{\left(\cosh^2\frac{\alpha\psi}{2\psi_0} - \cosh^2\frac{\alpha\psi_c}{2\psi_0}\right)^{1/2}} \tag{8}$$

or

$$\omega\eta = \omega(h - y) = \int_{\psi}^{\psi = \psi_0} \frac{d(\alpha\psi/2\psi_0)}{\left(\cosh^2\frac{\alpha\psi}{2\psi_0} - \cosh^2\frac{\alpha\psi_c}{2\psi_0}\right)^{1/2}} = \kappa\left[F\left(\frac{\pi}{2}, \kappa\right) - F(\theta,\kappa)\right] \tag{9}$$

where $F(\theta,\kappa)$ is the elliptic integral of the first kind, and

$$\theta = \sin^{-1}\left[\frac{\cosh (\alpha\psi_c/2\psi_0)}{\cosh (\alpha\psi/2\psi_0)}\right];$$

$$\theta_0 = \sin^{-1}\left[\frac{\cosh (\alpha\psi_c/2\psi_0)}{\cosh (\alpha/2)}\right] \tag{10}$$

$$\kappa = [\cosh (\alpha\psi/2\psi_0)]^{-1} \tag{11}$$

The subscript c (center) refers to $\eta = 0$ and the subscript 0 to $\eta = h$. The quantity ψ_c/ψ_0 is defined by the expression

$$\omega h = \kappa\left[F\left(\frac{\pi}{2}, \kappa\right) - F(\theta_0,\kappa)\right] \tag{12}$$

From eq. 12 we can determine, for any given value of $\alpha = ez\psi_0/kT$, the variation of ωh with ψ_c/ψ_0. The relationship between ωh and ψ_c/ψ_0 is shown graphically in Fig. 1. The knowledge of the variation of ψ_c/ψ_0 with ωh permits us to plot, with the use of eq. 9, the distribution of potential. The variation of potential across the slit is shown in Fig. 2, 3, and 4 for several values of α and ωh.

This is the undisturbed transverse distribution of potential, which will be maintained as long as there is no lateral mixing. Since laminar-type flow will
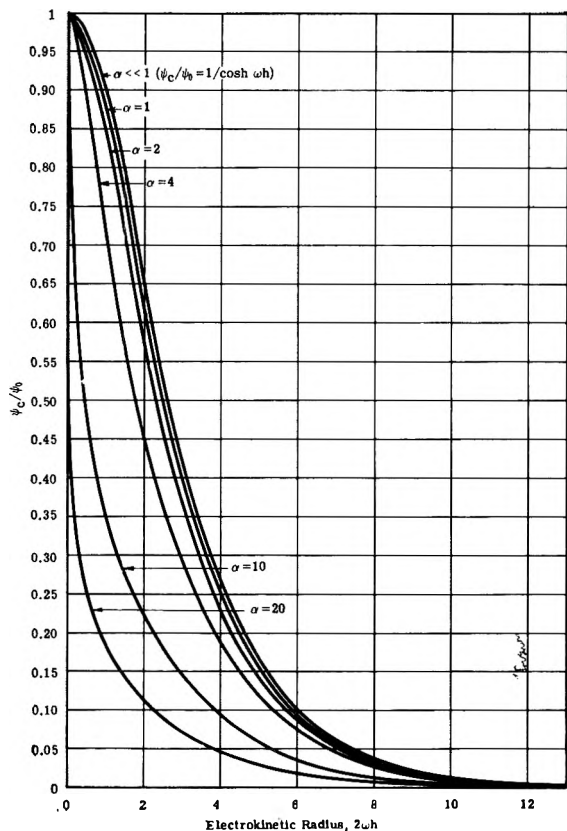
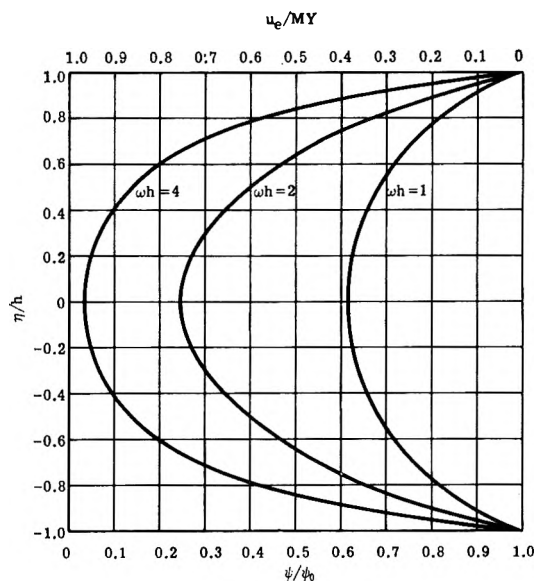Figure 1. Variation of ψ_c/ψ_0 with electrokinetic radius.

Figure 2. Variation of potential and electrokinetic velocity in a slit; $\alpha = 1$.
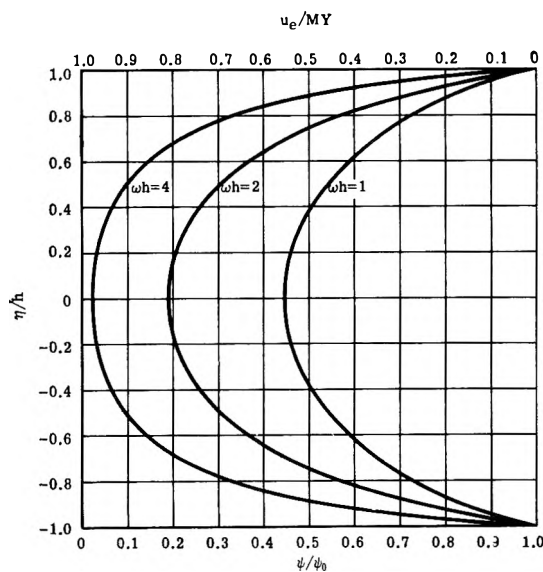
Figure 3. Variation of potential and electrokinetic velocity in a slit; $\alpha = 4$.

normally exist in a fine slit, the foregoing computed variation of potential and charge will remain valid.

General Equation of Electrokinetic Flow

Consider the case of laminar flow between parallel plates. Figure 5 shows an element of fluid of unit width acted upon by pressure forces, viscous forces, and electric body forces generated by an axial electric field, $Y = dE/dy$. Under steady conditions, the sum of these elemental forces is zero, and with the use of the relationship for laminar flow $\tau = \mu du/dy$, the equation

$$-\frac{dP}{dx} + \mu \frac{d^2u}{dy^2} - \rho Y = 0 \qquad (13)$$

is obtained.

In eq. 13, the charge density, ρ, is related to the spatial distribution of potential, ψ, by the Poisson equation (eq. 3) so that eq. 13 may be written as

$$-\frac{dP}{dx} + \mu \frac{d^2u}{dy^2} + \frac{DY}{4\pi} \frac{d^2\psi}{dy^2} = 0 \qquad (14)$$

The velocity, u, is composed of two discrete parts. The first, u_p, is the laminar flow caused by the pressure

gradient, dP/dx, alone. The second is the electroosmotic velocity, u_e.

If only pressure and viscous forces were present, the equation of flow would be

$$-\frac{dP}{dx} + \mu \frac{d^2u_p}{dy^2} = 0 \qquad (15)$$

If only electric body forces and viscous forces were acting, the equation of flow would be eq. 16.
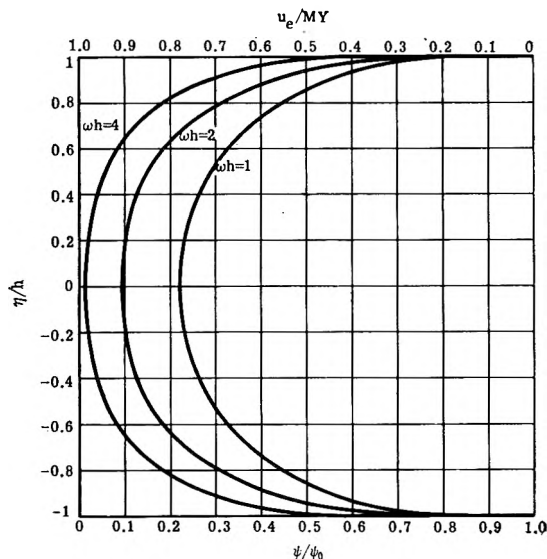
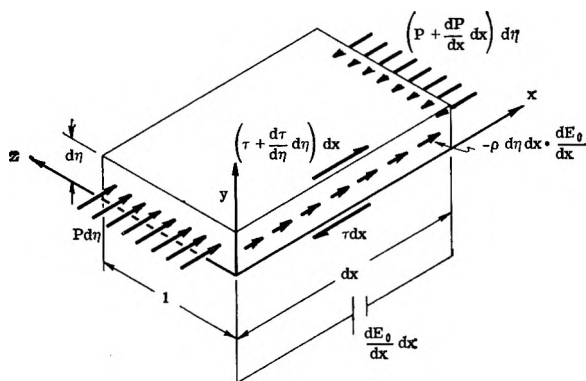Figure 4. Variation of potential and electrokinetic velocity in a slit; $\alpha = 10$.

Figure 5. Forces acting on a capillary fluid element between flat plates.

$$\mu \frac{d^2 u_e}{dy^2} + \frac{DY}{4\pi} \frac{d^2 \psi}{dy^2} = 0 \tag{16}$$

The addition of the foregoing equations yields eq. 14, in which $u = u_e + u_p$. The boundary conditions that apply are $u_p = u_e = 0$, and $\psi = \psi_0$ at the surface of the slit. Also, $du_e/dy = d\psi/dy$ at the center.

The solution for the velocity will always be of the form

$$u = u_p + MY \left(1 - \frac{\psi}{\psi_0}\right) \tag{17}$$

or

$$u = \frac{1}{2\mu} (\eta^2 - h^2) \frac{dP}{dx} + MY \left(1 - \frac{\psi}{\psi_0}\right) \tag{18}$$

where $\eta = h - y$. The mean velocity of flow in a slit is given by the expression

$$\bar{u} = -\frac{h^2}{3\mu} \frac{dP}{dx} + \frac{MY}{h} \int_0^h \left(1 - \frac{\psi}{\psi_0}\right) d\eta \tag{19}$$

We define $G(\alpha, \omega h)$ as

$$G(\alpha, \omega h) = \frac{1}{\omega h} \int_0^h \frac{\psi}{\psi_0} d(\omega \eta) \tag{20}$$

which, by use of eq. 8, becomes

$$G(\alpha, \omega h) =$$
$$\frac{2}{\alpha \omega h} \int_{\psi = \psi_c}^{\psi = \psi_0} \frac{(\alpha \psi / 2\psi_0) \, d(\alpha \psi / 2\psi_0)}{\left(\cosh^2 \frac{\alpha \psi}{2\psi_0} - \cosh^2 \frac{\alpha \psi_c}{2\psi_0}\right)^{1/2}} \tag{21}$$

The mean velocity may, therefore, be written as

$$\bar{u} = -\frac{h^2}{3\mu} \frac{dP}{dx} + MY[1 - G(\alpha, \omega h)] \tag{22}$$

The function G is found by numerical integration. It is plotted in Fig. 6 for various values of the parameters α and ωh.

The Streaming Potential

Up to this point, we have computed the potential and charge distribution and also the local and mean velocities in terms of the axial field Y (eq. 18 and 22). The field Y can be an externally applied field $Y_0 = E_0/L$, as shown in Fig. 7; it can be a self-induced field Y_s, defined as the streaming potential; or it can be a combination of both. If there were only an externally applied voltage (of zero internal resistance) which was maintained at E_0, then the electroosmotic flow could
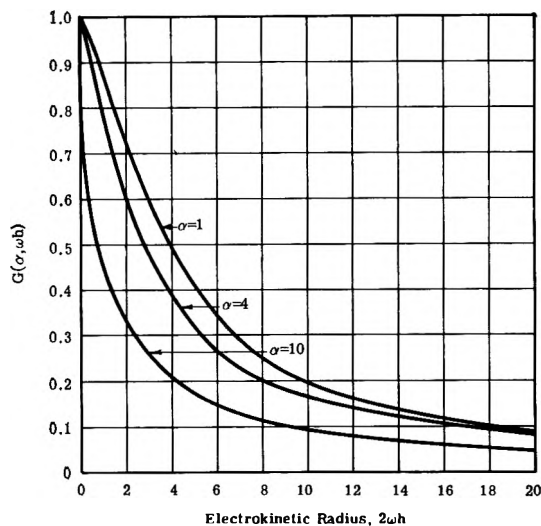

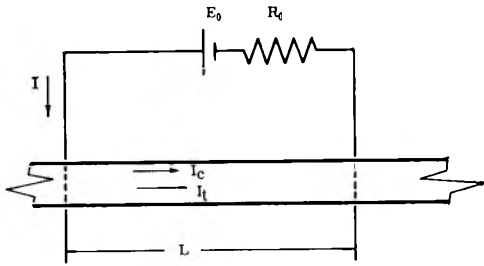Figure 6. Variation of $G(\alpha, \omega h)$ with electrokinetic radius.

Figure 7. Basic electrokinetic circuit.

be computed by means of eq. 22. Practical considerations require, however, that we take into account the external resistance of an applied electric field source in addition to the internal resistance of the fluid in the capillary. The problem is treated below in a general way by including the external voltage and both the internal and external resistances, as shown in Fig. 7.

Assume that across the capillary element there is placed a voltage source E_0 and an internal resistance R_0 in series with the voltage source, as shown in Fig. 7. The net voltage across the capillary element is

$$E = E_0 - IR_0 = \frac{I_c L}{K_0 A} \qquad (23)$$

It is noted that only conduction current is associated with a voltage drop, since Ohm's law is not applicable to the transport current. The current in the external circuit is

$$I = I_c + I_t \qquad (24)$$

where

$$I_t = - \int_A \rho u \, dA \qquad (25)$$

The substitution of eq. 23 and 25 into eq. 24 yields

$$I = \frac{K_0 A E}{L} - \int_A \rho u \, dA \qquad (26)$$

From eq. 26, I is set into eq. 23 and the result is

$$Y = \frac{E_0}{L} + \frac{R_0}{L} \left(\int_A \rho u \, dA - K_0 A Y \right) \qquad (27)$$

The substitution of u from eq. 17 into eq. 27 gives the net electric field explicitly as

$$Y = \frac{\dfrac{E_0}{R_0} + \int_A \rho u_p \, dA}{\dfrac{L}{R_0} + K_0 A - M \int_A \rho \left(1 - \dfrac{\psi}{\psi_0}\right) dA} \qquad (28)$$

We can lump the internal and external resistances by defining the lumped conductivity K as

$$K = K_0 + \frac{L}{AR_0} \qquad (29)$$

Equation 28 becomes

$$Y = \frac{\dfrac{E_0}{KAR_0} + \dfrac{1}{KA} \int_A \rho u_p \, dA}{1 - \dfrac{M}{KA} \int_A \rho \left(1 - \dfrac{\psi}{\psi_0}\right) dA} \qquad (30)$$

The foregoing expression for the net axial field is valid for both electroosmotic flow and streaming potential flow and does not carry any restrictions with regard to ionic energy or electrokinetic radius. Thus, the short circuit condition ($R_0 = 0$) yields the electric field for electroosmotic flow, $Y = E_0/L$, and the open circuit condition ($R_0 \to \infty$) yields the expression for open circuit streaming potential

$$Y = \frac{\dfrac{1}{K_0 A} \int_A \rho u_p \, dA}{1 - \dfrac{M}{K_0 A} \int_A \rho \left(1 - \dfrac{\psi}{\psi_0}\right) dA} \qquad (31)$$

The function $G(\alpha,\omega h)$, evaluated previously (eq. 21) and plotted in Fig. 6, appears in the expression for the electric field Y as given by eq. 30. For flow in a slit, the integral term in the numerator becomes

$$\frac{1}{Kh} \int_0^h \rho u_p \, d\eta = \frac{D}{4\pi Kh} \int_0^h \frac{d^2\psi}{d\eta^2} u_p \, d\eta \qquad (32)$$

By partial integration, eq. 32 becomes

$$\frac{1}{Kh} \int_0^h \rho u_p \, d\eta = \frac{M}{K} \frac{dP}{dx} [1 - G(\alpha,\omega h)] \qquad (33)$$

Thus, the same averaging factor, $1 - G(\alpha,\omega h)$, appears in both the electroosmotic component of the mean flow and in the expression for streaming potential. The integral term in the denominator of eq. 30

$$\frac{M}{K\omega h} \int_0^h \rho \left(1 - \frac{\psi}{\psi_0}\right) d(\omega\eta) \qquad (33a)$$

can be evaluated analytically. The result is

$$\frac{M}{K\omega h} \int_0^h \rho \left(1 - \frac{\psi}{\psi_0}\right) d(\omega\eta) = - \frac{B}{\omega h (\alpha/2)^2 \kappa} \times$$
$$\left[\tanh (\alpha_0/2) \cot \theta_c + E(\theta_0,\kappa) - E\left(\frac{\pi}{2}, \kappa\right) \right] \qquad (34)$$

where $E(\theta,\kappa)$ is an elliptic integral of the second kind, and as before

$$\theta_0 = \sin^{-1} \left[\frac{\cosh (\alpha\psi_c/2\psi_0)}{\cosh (\alpha/2)} \right]$$

$$\kappa = [\cosh (\alpha\psi_c/2\psi_0)]^{-1} \qquad (35)$$

The integral term in eq. 33a has a definite physical significance. In simple short circuit ($R_0 \rightarrow 0$) electroosmotic flow, given by the expression

$$u_e = \frac{ME_0}{L} \left(1 - \frac{\psi}{\psi_0}\right) \qquad (36)$$

from which it follows that the electroosmotic transport current in a slit is

$$I_t = -\frac{2ME_0}{L} \int_0^h \rho\left(1 - \frac{\psi}{\psi_0}\right) d\eta \qquad (37)$$

The electroosmotic conduction current, moving in the same direction as the transport current, is

$$I_c = \frac{2KhE_0}{L} \qquad (38)$$

The ratio of electroosmotic transport current to conduction current, I_t/I_c, is thus

$$\frac{I_t}{I_c} = -\frac{M}{Kh} \int_0^h \rho\left(1 - \frac{\psi}{\psi_0}\right) d\eta$$

or

$$\frac{I_t}{BI_c} = \frac{1}{\omega h(\alpha/2)^2\kappa} \left[\tanh(\alpha/2) \cot \theta_0 + \right.$$

$$\left. E(\theta_0,\kappa) - E\left(\frac{\pi}{2}, \kappa\right) \right] \qquad (39)$$

where $B = M^2\omega^2\mu/K$.

The quantity I_t/BI_c is plotted in Fig. 8 as a function of the surface ionic energy, $ez\psi_0/kT$, and the electrokinetic radius, $2\omega h$. The parameter B, as will be observed, has a strong influence in electrokinetic systems.

The open circuit streaming potential for flow in a slit is thus given by the expression

$$Y_s = \frac{\dfrac{M}{K}\dfrac{dP}{dx}[1 - G(\alpha,\omega h)]}{1 + \dfrac{B}{\omega h(\alpha/2)^2\kappa}\left[\tanh(\alpha/2)\cot\theta_0 + \right.}$$

$$\left. E(\theta_0,\kappa) - E\left(\frac{\pi}{2}, \kappa\right)\right] \qquad (40)$$

or

$$Y_s = \frac{\dfrac{M}{K}\dfrac{dP}{dx}[1 - G(\alpha,\omega h)]}{1 + I_t/I_c} \qquad (41)$$

It is plotted in Fig. 9 as a function of the electrokinetic radius, $2\omega h$, the surface ionic energy, α, and the parameter, B. It can be shown that in the limit, as
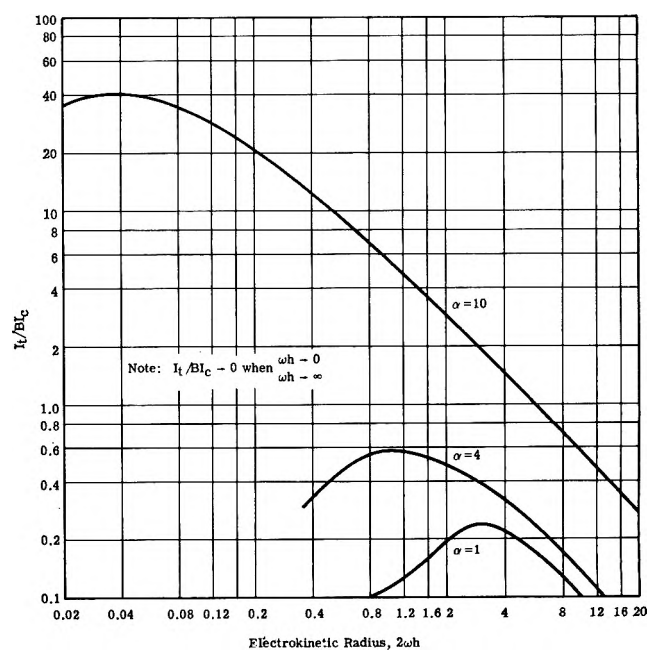
Figure 8. Variation of I_t/BI_c with electrokinetic radius.

$\alpha \rightarrow 0$ and $\omega h \gg d$, eq. 40 approaches the approximate equations obtained in earlier work[13] for low ionic potential and/or large electrokinetic radius.

The usefulness of the curves in Fig. 9 lies primarily in the determination of the streaming potential in the case of small electrokinetic radius and large surface potential. The necessity of using lumped parameters in the presentation of the results obscures somewhat the role of the basic parameters that influence the streaming potential. For example, the surface ionic potential ψ_0 is contained in the ordinate (*i.e.*, in M) as well as in the parameters α and B. It is not clear from the figures what effect will be produced by alter-
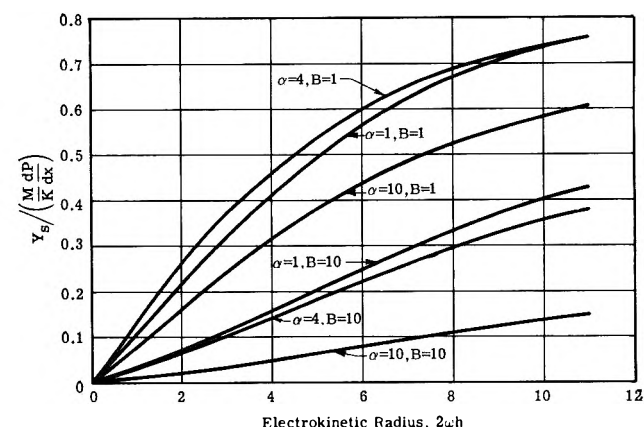

Figure 9. Variation of streaming potential with electrokinetic radius for several values of α and B.

ing the magnitude of ψ_0. A broader generalization of the problem, beyond that shown in Fig. 9, is not feasible because of the large number of basic parameters upon which Y_s depends. These are: ψ_0, D, μ, dP/dx, K, z, T, c, and h.

The solution of the problem of electrokinetic flow in a slit can be used in estimating the electroosmotic velocity and streaming potential in capillary elements having other than slit cross sections. If we assume that the same generalization holds as in the case of low potential flow, then it is possible to substitute $2\omega A/s$ for the electrokinetic radius in capillary elements of arbitrary cross section. The error of this approximation has not been established.

Flow Retardation in Fine Capillary Channels

In mechanical pumping through fine capillary channels, the net velocity, which is the algebraic sum of the pressure-induced velocity and the retarding velocity, is given by eq. 22 and 41 as

$$\bar{u} = -\frac{h^2}{3\mu}\frac{dP}{dx} + \frac{M^2}{K}\frac{dP}{dx}\frac{(1-G)^2}{1+I_t/I_c} \qquad (42)$$

or

$$\bar{u} = \bar{u}_p - \bar{u}_r \qquad (43)$$

The ratio of the electrokinetic counterflow component, $\bar{u}_r$, to the pressure-induced component, $\bar{u}_p$, is

$$\frac{\bar{u}_r}{\bar{u}_p} = \frac{V_r}{V_p} = \frac{3}{(\omega h)^2}\frac{(1-G)^2}{\dfrac{1}{B}+\dfrac{I_t}{BI_c}} \qquad (44)$$

The variation of this ratio with electrokinetic radius is plotted in Fig. 10 for several values of α and B. These curves show that when the electrokinetic radius is greater than 20, the retarding flow will be less than 10% of the pressure-induced flow. However, for the
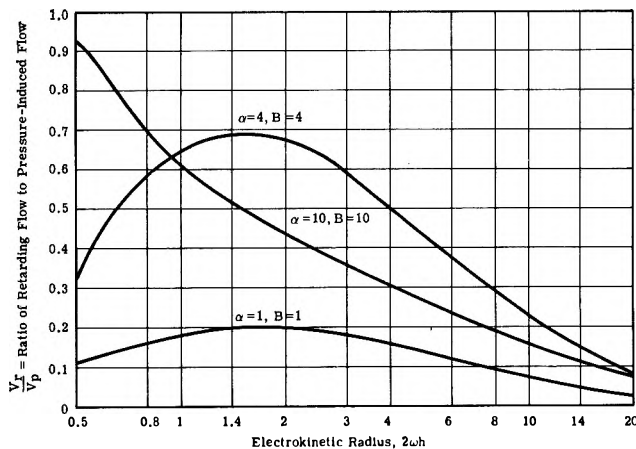

Figure 10. Variation of retarding flow with electrokinetic radius for several values of α and B.

practical case of $\alpha = 4$, $B = 4$, which corresponds roughly to the α and B of distilled water in equilibrium with the CO_2 of the air, one finds that the retarding flow component can be as much as 68% of pressure-induced flow. This occurs when the electrokinetic radius is $2\omega h = 1.6$. Since in equilibrium water $c = 2.1 \times 10^{-6}$ mole/l., the channel width at which the large retardation occurs is

$$h = \frac{0.8}{3.26 \times 10^7 \sqrt{2.1 \times 10^{-6}}} = 1.7 \times 10^{-5}\ \text{cm.}$$

Thus, when the fineness of the capillary element approaches 10^{-5} cm., it is to be expected that a large resistance to the transmission of fluids, via pumping, will be experienced. When the surface ionic potential ψ_0 is sufficiently large, with α and B correspondingly large, Fig. 10 shows that the retardation approaches 100% of the flow. Under these conditions, the porous material would appear completely impermeable.

The Temperature Coefficient of the Polydimethylsiloxane Chain Configuration

from Swelling Equilibrium Measurements

by J. E. Mark

The Department of Chemistry, Stanford University, Stanford, California (*Received November 9, 1963*)

The temperature dependence of the degree of swelling of polydimethylsiloxane (PDMS) networks in equilibrium with an athermal solvent is used to determine the temperature coefficient of the unperturbed dimensions of the polymer chains comprising the network. A moderately large, positive value of d ln $\langle r^2 \rangle_0/dT$ is obtained, in agreement with values determined by other methods.

Introduction

The temperature coefficient of the unperturbed mean square end-to-end distance, d ln $\langle r^2 \rangle_0/dT$, has assumed great importance in the interpretation of the spatial configuration of a polymer chain in terms of basic structural parameters.[1-7] It is the purpose of the present investigation to determine this quantity for PDMS chains from the temperature dependence of the equilibrium extent of swelling of PDMS networks in an athermal solvent. Comparison with values of the same quantity obtained from stress–temperature measurements on unswollen networks[6] and from intrinsic viscosity–temperature data on athermal PDMS solutions[6] can be used to assess the validity of the postulate that the elastic free energies of polymer chains in a network are strictly additive.

The elastic response (*i.e.*, internal pressure) of a polymer network subject to swelling by a solvent depends on the mean square distention of its chains relative to their unperturbed dimensions in the absence of all constraints. Thus the extent to which a polymer network will imbibe solvent with which it is in contact depends on the unperturbed dimensions of the polymer chains comprising the network, at the temperature of measurement, and the change in equilibrium swelling with temperature must therefore depend on the temperature coefficient of $\langle r^2 \rangle_0$. Observation of the temperature dependence of equilibrium swelling should therefore afford a method for determining the temperature coefficient of $\langle r^2 \rangle_0$ if the following quantities are also known: specific volumes and thermal expansion coefficients of polymer and solvent, molecular

weight of the solvent, and the free energy of mixing parameter[8] for the system, χ_1. The determination of χ_1 can be avoided by choosing an athermal solvent (for which χ_1 would be small and independent of temperature).

Dimethylsiloxane oligomers and networks consisting of PDMS chains have close structural similarity; a system of these two components can be expected to exhibit an enthalpy of mixing of virtually zero[9] and a small value of χ_1.

Initial measurements on PDMS networks swollen by dimethylsiloxane oligomers indicated that the approximation $\chi_1 = 0$ could not be made in this analysis; small deviations of the quantity from zero are sufficient to affect the apparent value of d ln $\langle r^2 \rangle_0/dT$. In an attempt to correct for this, the apparent temperature coefficient of $\langle r^2 \rangle_0$ was determined for a series of networks of different degrees of cross-linking swollen by several dimethylsiloxane oligomers differing in molecular weight. From these data it should be pos-

(1) O. B. Ptitsyn and I. A. Sharanov, *Zh. Tekhn. Fiz.*, **27**, 2744, 2762 (1957).

(2) A. Ciferri, C. A. J. Hoeve, and P. J. Flory, *J. Am. Chem. Soc.*, **83**, 1015 (1961).

(3) P. J. Flory, A. Ciferri, and R. Chiang, *ibid.*, **83**, 1023 (1961).

(4) C. A. J. Hoeve, *J. Chem. Phys.*, **35**, 1266 (1961).

(5) K. Nagai and T. Ishikawa, *ibid.*, **37**, 496 (1962).

(6) J. E. Mark and P. J. Flory, *J. Am. Chem. Soc.*, **86**, 138 (1964).

(7) P. J. Flory, V. Crescenzi, and J. E. Mark, *ibid.*, **86**, 146 (1964).

(8) P. J. Flory, "Principles of Polymer Chemistry," Cornell University Press, Ithaca, N. Y., 1953.

(9) G. Delmas, D. Patterson, and D. Böhme, *Trans. Faraday Soc.*, **58**, 2116 (1962).

sible to estimate d ln $\langle r^2 \rangle_0 / dT$ for a PDMS network comprising chains of infinite length between cross links swollen by a dimethylsiloxane oligomer of infinite chain length. Since the effect of end groups of the solvent and junction points of the network are thus eliminated, χ_1 for such a system is assuredly zero at all temperatures and the true value of d ln $\langle r^2 \rangle_0 / dT$ should be obtained.

Experimental

Preparation of PDMS Networks. An unfractionated sample of PDMS[10] having a molecular weight of 1.1×10^6 was used for the preparation of the cross-linked samples. The polymer was pressed between sheets of cellophane to a uniform thickness of approximately 0.10 cm. These sheets were then irradiated with high energy electrons from a General Electric resonant transformer to the desired dose. To ensure network uniformity, samples were irradiated on opposite sides for equal lengths of time. The cellophane was washed off and the cross-linked samples were extracted with carbon tetrachloride at room temperature for at least 12 hr. The soluble portion never exceeded 5% of the sample.

Determination of Degree of Swelling. The solvents were commercially available dimethylsiloxane fluids (General Electric, SF-96 series). The molecular weight of each oligomer was determined from its bulk viscosity at 40° using the empirical relationship of Warrick, *et al.*[11] The specific volumes and cubical thermal expansion coefficients of the solvents (Si-5, 10, 20, 50) and polymer were determined by pycnometry and dilatometry, respectively. These data are summarized in Table I.

Table I: Characteristics of Solvents and Polymer

Material	Specific volume at 30°, cm.^{3}/g.	$\beta \times 10^3$, deg.$^{-1}$ at 67.5°	$M_v \times 10^{-6}$
Si-5[a]	1.0968	0.990	0.716
10	1.0726	0.947	1.19
20	1.0561	0.938	2.06
50	1.0467	0.909	3.71
Cross-linked polymer	1.0360	0.880	

[a] Number designates approximate bulk viscosity in centistokes at 25°.

After extraction and drying, the cross-linked samples were cut into the shape shown in Fig. 1. The absence of horizontal faces on the samples minimized drainage errors. During swelling, the strip was totally immersed in the solvent at constant temperature. At approxi-
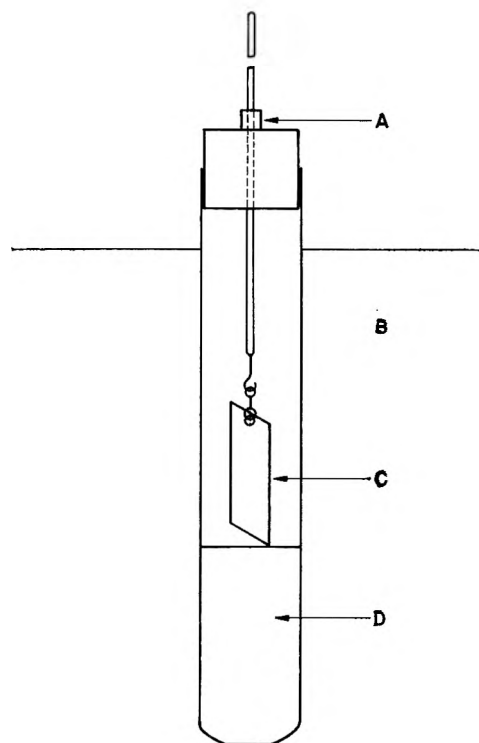

Figure 1. Swelling equilibrium apparatus: A, adjustable collar; B, constant temperature bath; C, swollen network; D, solvent.

mately 8-hr. intervals, the sample was raised within the cell and allowed to drain at constant temperature for a fixed length of time (15 min. for the low viscosity fluids, Si-5 and Si-10; 30 min. for the others). The swollen network was then removed and weighed in an aluminum dish. The sample was immersed in the solvent for another 8-hr. period, drained, and reweighed. When the weight of a sample was constant within a few tenths of a milligram, the system was considered to be at equilibrium. Up to 3 weeks was required for equilibration at the first temperature of measurement, 30°. Once equilibrium was established at this temperature, however, the swollen network attained constant weight at the other temperatures relatively rapidly (within 2 or 3 days). The volume fraction of polymer v_2 was calculated from the weights and specific volumes of polymer and solvent at each temperature (30, 55, 80, 105°). It was necessary to assume additivity of volume in this calculation; in view of the structural similarity of solvent and polymer the error introduced is certainly negligible. Measurements on

(10) This sample was generously provided by the Silicones Department of the General Electric Co., Waterford, N. Y.

(11) E. L. Warrick, W. A. Piccoli, and F. O. Stark, *J. Am. Chem. Soc.*, 77, 5017 (1955).

the descending temperature cycle reproduced those of the ascending cycle well within the limits of experimental error.

In this investigation four networks (A, B, C, D) of varying degrees of cross linking were studied in four solvents varying in molecular weight.

Results

The equilibrium volume fraction of polymer is shown as a function of temperature in Fig. 2. Data for polymer networks A and B in solvents Si-5, 10, 20, and 50 are presented; similar curves were obtained for the other systems but are not shown here.
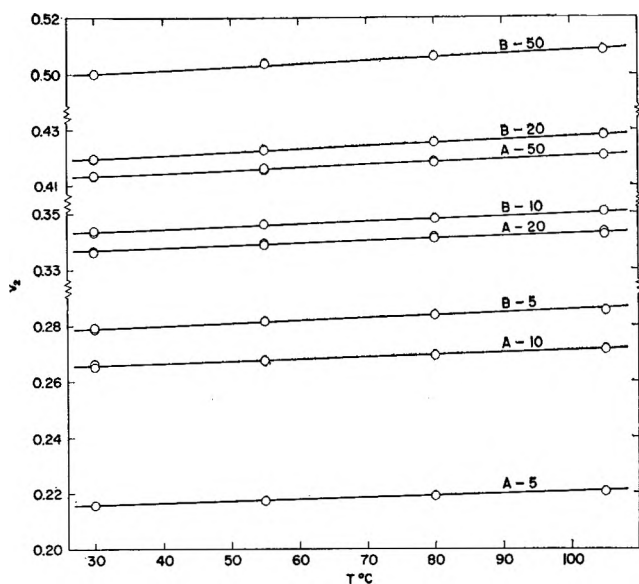

Figure 2. Temperature dependence of volume fraction of polymer at swelling equilibrium; letter and number designate network and solvent, respectively.

According to the theory of swelling of network structures,[3] at equilibrium or maximum swelling

$$(\nu V_1 / V^{*1/3} V_0^{2/3})[v_2^{1/3} - (v_2/2)(V_0/V^*)^{1/3}] =$$

$$- [\ln (1 - v_2) + v_2 + \chi_1 v_2^2] \quad (1)$$

where ν is the number of chains in the network, V_1 the molar volume of the solvent, V^* the specific volume of the unswollen network, V_0 the volume associated with the undistorted chains before the imposition of cross links, v_2 the volume fraction of polymer at swelling equilibrium, and χ_1 the free energy parameter for mixing of solvent with the polymer network. Since all networks considered here were formed in the absence of diluent, the reference volume $V_0 \cong V^*$ at the temperature of cross linking. The second term

on the left-hand side of eq. 1 is small in comparison with the first; this approximation can therefore be introduced in this term without hesitation. As will be shown, this approximation is rendered completely negligible in the consequent treatment of the data. Rearrangement of eq. 1 yields

$$\nu/V_0^{2/3} = - \left[\frac{\ln (1 - v_2) + v_2 + \chi_1 v_2^2}{v_2^{1/3} - v_2/2} \right] \left(\frac{V^{*1/3}}{V_1} \right) \quad (2)$$

Since V_0 is directly proportional to $\langle r^2 \rangle_0^{3/2}$ the fractional change of the right-hand side of eq. 2 with temperature is $-d \ln \langle r^2 \rangle_0/dT$. Values of the temperature coefficient of $\langle r^2 \rangle_0$ calculated on the assumption that $\chi_1 = 0$ at all temperatures (Table II) showed a

Table II: Swelling Equilibrium Results

System	Dose, mrads	v_2 at 30°	$\frac{d \ln v_2}{dT} \times 10^3$	$\frac{d \ln \langle r^2_0 \rangle}{dT} \times 10^3$ (uncor.)
A-5	9.0	0.2158	0.31	0.09
10		0.2659	0.27	0.10
20		0.3367	0.23	0.15
50		0.4138	0.20	0.14
B-5	30.	0.2790	0.33	0.00
10		0.3435	0.27	0.07
20		0.4198	0.26	0.04
50		0.5000	0.24	0.02
C-5	50.	0.5065	0.32	-0.12
10		0.5630	0.27	-0.10
20		0.6510	0.20	0.01
50		0.7490	0.21	-0.15
50		0.7201	0.20	-0.09
D-5	75.	0.5954	0.31	-0.18
10		0.6638	0.26	-0.16
20		0.7469	0.21	-0.10

trend with both the molecular weight of the solvent and the degree of cross linking of the network. This is due to the exceedingly small temperature coefficient of v_2; even small contributions to χ_1 from chain ends of the solvent and junction points in the network are sufficient to affect significantly the apparent value of $d \ln \langle r^2 \rangle_0/dT$. To remove the effect of solvent chain ends, the uncorrected value ($\chi_1 = 0$) of $d \ln \langle r^2 \rangle_0/dT$ for each network was plotted against the reciprocal of the solvent molecular weight M and extrapolated to M equal infinity (Fig. 3). A linear dependence was observed for each network. The vertical lines in each plot indicate the relative reliability of the measurements; the data for the most highly cross-linked networks are less reliable because the changes in weight of the samples with temperature are smaller than those measured for other networks. Values of the tempera-
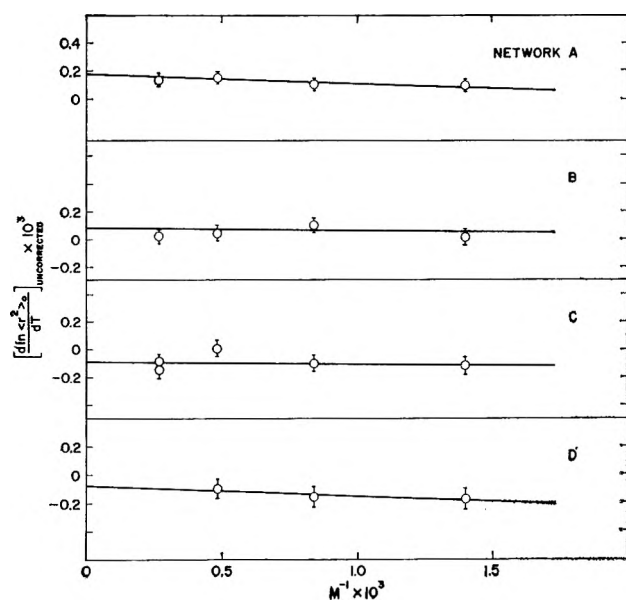
Figure 3. Extrapolation of uncorrected $d \ln \langle r^2 \rangle_0 / dT$ for each network to values for infinite molecular weight of solvent.

ture coefficient of $\langle r^2 \rangle_0$ corrected to infinite molecular weight for the solvent must then be further corrected for the effect of network junctions. Clearly, for an idealized network having infinite chain length between cross links the equilibrium volume fraction of polymer must equal zero, but theory does not indicate how this extrapolation should be performed. Extrapolation to $v_2 = 0$ would also make the approximation in the second term of eq. 1 insignificant (since v_2 approaches zero much more rapidly than does $v_2^{1/3}$). Although this extrapolation cannot be made unambiguously, the data do indicate that as the density of cross links decreases (as indicated, for example, by the relative value of v_2 for a network in equilibrium with Si-5, at 30°), $d \ln \langle r^2 \rangle_0 / dT$ approaches a moderately large, positive value. This result is in agreement with the value obtained by stress–temperature and intrinsic viscosity–temperature measurements,[6] $0.75 \pm 0.15 \times 10^{-3} \deg.^{-1}$.

Unfortunately, this method cannot claim the accuracy and precision obtained in stress–temperature or intrinsic viscosity–temperature studies. This is due to the exceedingly small temperature dependence of v_2 $(d \ln v_2 / dT \cong 10^{-4})$. In stress–temperature measurements the fractional change in force with temperature is of the order of $10^{-3} \deg.^{-1}$ as is also the fractional change in the intrinsic viscosity of an athermal solution with temperature.

Discussion

This method for evaluating the temperature coefficient of the unperturbed dimensions of PDMS chains gives a value in agreement with those obtained by other techniques.[6] The agreement between values for the polymer chains in very different environments consisting of the dilute solution, the swollen network, and the undiluted network is very difficult to reconcile with the claim[12] that intermolecular interactions in the undiluted, amorphous state drastically alter the configuration characteristic of the free chain. Indeed these results corroborate previous work[2,3,6] indicating that the elastic free energies of polymer chains making up a network are additive, and that the configuration of a chain in the amorphous state is not significantly influenced by intermolecular interactions.

These results on networks at swelling equilibrium also give considerable support to the theory[8] developed for such systems.

(12) M. V. Volkenstein, "Configurational Statistics of Polymeric Chains," Interscience Publishers, New York, N. Y., 1963, Chapter 8.

Crystallographic Requirements and Configurational

Entropy in Body-Centered Cubic Hydrides

by Thomas R. P. Gibb, Jr.

Contribution No. 311 from Department of Chemistry, Tufts University, Medford, Massachusetts
(Received November 12, 1963)

The number of ways w in which foreign atoms or ions may be arranged in a b.c.c. host lattice is enumerated as a function of composition for structural units containing two host atoms. The result is shown to be simply related to w for a mole of substance, which leads directly to the configurational entropy. The relatively large contribution of configurational entropy to the free energy of b.c.c. metallic hydrides renders accurate calculation of w particularly important for this class of compounds. It is shown that conventional (combinatorial) calculation of w leads to large errors when site occupation is restricted, e.g., in the case where occupation of a given site renders the nearest sites unavailable. The value of w is obtained by actual enumeration for restricted occupancy of octahedral and of tetrahedral sites by foreign atoms X and the results are presented as graphs of w vs. n where n is the atomic ratio defined by MX_n. A simple method of calculating w for restricted site occupancy is derived heuristically and shown to give excellent results for the cases studied.

Introduction

The number of ways in which interstitial atoms may be arranged in the lattice of a nonstoichiometric crystal may influence or, geometrical factors being equal, even determine the changes in structure and magnetic properties resulting from the insertion of these atoms. The number w of such arrangements controls the configurational or statistical entropy S_c through the well-known relation $S_c = k \ln w$, where k is Boltzmann's constant (3.296 $\times$ 10^{-24} cal./deg.). For highly nonstoichiometric solids where the number of arrangements per mole may be of the order of 10^{24}, and particularly if the heat of formation of the solid is low, the TS term of the general expression for free energy may be nearly comparable to the heat of formation or enthalpy term at room temperature or above. This is the case with some of the metallic hydrides, e.g., of group V metals and palladium.

This article will deal only with the number of ways in which hydrogen atoms, for example, may be arranged in a b.c.c. metal lattice such as that of vanadium. The treatment is designed primarily to bridge the gap between purely geometrical considerations, such as radius ratio, atomic radii, etc.,[1] and the bases for

statistical-mechanical treatment,[2-5] including order-disorder theory.[6-8] One of the difficulties in setting up a statistical-mechanical treatment is always the choice of the array or cluster to be used. In some cases this is straightforward as in Snoek's classical work on martensite (cf. ref. 9), where the carbon atoms are free to occupy *any* of the octahedral sites in the unstressed b.c.c. iron. In other cases, occupancy of one

(1) T. R. P. Gibb, Jr., Advances in Chemistry Series, No. 39, R. F. Gould, Ed., American Chemical Society, Washington, D. C., 1963, p. 99.

(2) S. L. H. Martin and A. L. G. Rees, *Trans. Faraday Soc.*, 50, 343 (1954).

(3) G. G. Libowitz, "Advances in Chemistry Series," No. 39, R. F. Gould, Ed., American Chemical Society, Washington, D. C., 1963.

(4) J. E. Mayer and M. G. Mayer, "Statistical Mechanics," John Wiley and Sons, Inc., New York, N. Y., 1946.

(5) L. Kaufman, ASD-61-445 (1961); *Trans. AIME*, 224, 1006 (1962).

(6) J. M. Honig, *J. Chem. Educ.*, 38, 538 (1961).

(7) F. E. J. K. Aretz, *Physica*, 26, 967, 981 (1960); 28, 736 (1962).

(8) T. Muto and Y. Takagi, "Solid State Physics," Vol. I, F. Seitz and D. Turnbull, Ed., Academic Press, Inc., New York, N. Y., 1955, p. 193.

(9) J. D. Fast, "Entropy," McGraw-Hill Book Co., New York, N. Y., 1962, p. 123.

site by a rather large interstitial atom may prevent occupation of some neighboring sites. The nature of such restrictions is sometimes subtle[1,3] and especially so when progressive anisotropic deformations occur.

Interstitial Configurations in a B.c.c. Lattice

If all of the octahedral sites of a b.c.c. metal are equivalent, as they must be in an undistorted crystal (Fig. 1), then the number of ways w of arranging hydrogens
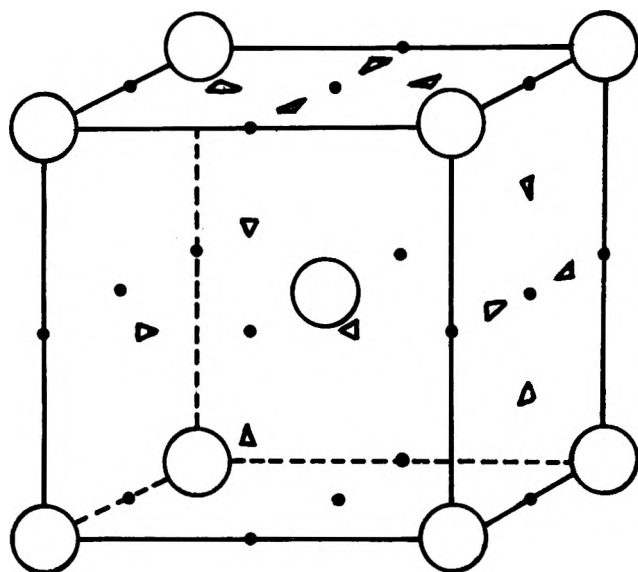

Figure 1. Octahedral sites (black dots) and tetrahedral sites (triangles) in b.c.c. lattice. Tetrahedral sites are shown only on three faces.

in these sites in a gram-atom of metal is given by a simple combinatorial formula

$$w = \frac{(3N)!}{(\theta 3N)![(1 - \theta)3N]!}$$

where N is Avogadro's number, and θ is the occupied fraction of the $3N$ available sites. The number of octahedral sites per unit cell is six, as is evident from Fig. 1, and the unit cell contains two metal atoms, hence $3N$ sites per gram-atom of metal. This formula simplifies via Stirling's approximation to

$$\ln w = -3N[\theta \ln \theta + (1 - \theta) \ln (1 - \theta)]$$

where the number of sites $3N$ is outside the brackets. As long as $3N$ is large enough so that Stirling's approximation is applicable, ln w is directly proportional to the total number of sites at a constant value for the occupancy. If the composition of the interstitial compound were represented by MX_n or MH_n, then $\theta = n/3$. A graph of ln w vs. n is similar in shape to

curve A of Fig. 2, but with the ordinate increased by an appropriate factor of the order of 10^{23} (see below).

If the three octahedral sites per metal atom are not equivalent (but are equally available), then the number of arrangements is given by multiplying together three combinatorial relations of the type shown above with the necessary changes in total sites and fractions occupied. Such methods may be used to evaluate the change in entropy resulting from redistribution of interstitial atoms as in a martensitic transformation, or from stress due to distortion of the crystal structure.[9] A similar formula may be set up for occupancy of tetrahedral sites where the total number of sites per unit cell is twelve.
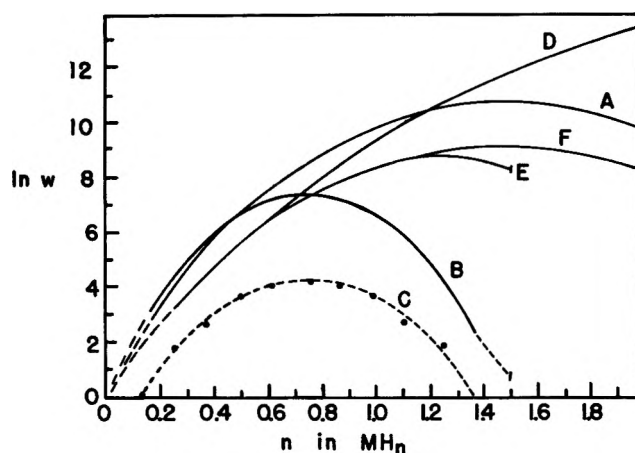

Figure 2. Natural log of the number of ways of arranging interstitial atoms H in one unit cell of an undistorted b.c.c. metal: curve A, equivalent octahedral sites; B, octahedral sites, mutual exclusion of face center and edge center sites; C, nonsuperposable arrangements for B; D, equivalent tetrahedral sites; E, one tetrahedral site per face; F, tetrahedral sites, exclusion of three nearest sites. Curves are guide lines between discrete points.

If the size of the interstitial atom is such that occupancy of a given site prevents or inhibits occupation of certain neighboring sites, the simple combinatorial method used above is no longer applicable, and in most cases the number of arrangements cannot be calculated in this way. To understand the relation between purely crystallographic considerations and the calculation of the number of arrangements, it is necessary to investigate what happens in a simple unit cell or in a minimum assembly of such cells, where the evident relationship between sites helps to visualize what will happen in a very large assembly. In Fig. 2, curve A shows the natural log of the number of arrangements possible in a single unit such as Fig. 1 plotted vs. the stoichiometric proportion of interstitial atoms

represented as n in equivalent octahedral sites. This recapitulates the previous combinatorial calculation but now in a much smaller unit. It is surprising that the number of arrangements is so large (maximum is 48,620) for a single unit cell.

If the interstitial atoms are found not to occupy the edge-center positions (octahedral sites) $0, \frac{1}{2}, 0; \frac{1}{2}, 0, 0; 1, \frac{1}{2}, 0; \frac{1}{2}, 1, 0$ (Fig. 1) when the face center site $\frac{1}{2}, \frac{1}{2}, 0$ is occupied (or vice versa), which is a not uncommon situation in a b.c.c. matrix, then one may not use a simple combinatorial calculation to get the number of possible arrangements for a given fractional occupation. The reason for this is that the availability of sites is no longer a simple function of the fraction filled. The size of the unit shown in Fig. 1 is small enough to permit an actual enumeration of the number of possible arrangements as a function of occupancy.[10] The results of the enumeration are plotted as curve B of Fig. 2. In this curve, the total number of arrangements is counted as a function of the atomic ratio n. In curve C the number of these arrangements not superposable by rotation about any cube axis is shown. This would be of interest if only an isolated "cubic molecule" were under consideration, but if the cube is a portion of a large assembly, then it is rigidly fixed as part of this assembly and arrangements which would be equivalent in a molecule are no longer so.

If the tetrahedral sites of a b.c.c. metal are the only sites available for occupancy, and if they are all equivalent (Fig. 1), then the number of arrangements may also be calculated by a simple combinatorial formula. The result is shown as curve D in Fig. 2. If one makes an arbitrary restriction that only one tetrahedral site per face may be occupied, curve E results. If one makes the more meaningful restriction that occupation of a tetrahedral site prevents occupation of the three nearest tetrahedral sites, curve F is obtained. (This restriction may be stated in the form $r = a_0\sqrt{2}/8$, where r is the radius of the interstitial atom, a_0 is the cube edge, and the radius of the matrix atom or cation is such that contact occurs between interstitial atoms.[3] If in Fig. 1 site $\frac{3}{4}, 0, \frac{1}{2}$ is occupied, for example, sites $\frac{1}{2}, 0, \frac{3}{4}; \frac{1}{2}, 0, \frac{1}{4}$; and $1, \frac{1}{4}, \frac{1}{2}$ are excluded.)

Discussion

The relation of the number of arrangements in a single unit cell to the number of arrangements in a large number of unit cells, say a mole of solid or $(6.02/2) \times 10^{23}$ unit cells, is not obvious, although it is easily demonstrated when a simple combinatorial formula is applicable. Thus for a gram-atom of solid containing three equivalent octahedral sites per atom, the above-mentioned combinatorial formula and its logarithmic

form (Stirling) are applicable. For the single unit cell the number of arrangements for octahedral atoms is $(18)!/(18\theta)!(18 - 18\theta)!$. The ratio of the natural logarithms of these is, accordingly

$$\frac{\ln w_m}{\ln w_c} = \frac{-(3)(6.02 \times 10^{23})[\theta \ln \theta + (1 - \theta) \ln (1 - \theta)]}{\ln [18!/(18\theta)!(18 - 18\theta)!]}$$

$$= 1.16 \times 10^{23}$$

where w_m is the arrangement per gram-atom and w_c is the arrangement per unit cell. The ratio for tetrahedral occupancy is arrived at in a similar fashion and equals 1.69×10^{23}. (The reason these ratios are not equal to $(3)(6.02 \times 10^{23})/18$ and $(6)(6.02 \times 10^{23})/24$, respectively, is, of course, partly due to the failure of Stirling's approximation for small numbers. Since $\theta_m = \theta_c$ the variable terms would cancel save for this failure.)

The above reasoning may be shown empirically to apply with sufficient accuracy to the calculation of $\ln w_m/\ln w_c$ when the number of arrangements is restricted by geometric (etc.) factors and simple combinatorial formulas cannot be used. The proof of this is simply whether $\ln w_c$ may be represented to the desired accuracy by a complex combinatorial formula containing only terms in θ so that $\ln w_m/\ln w_c$ is approximately constant for a given value of n over a range of compositions. It is readily found that curve B, for example, of Fig. 2 may be substantially duplicated in this way. Specifically one finds from Fig. 1 that the maximum interstitial content under the restrictions cited is $n = 1.5$, corresponding to the filling of half of the eighteen octahedral sites. If one calculates the number of arrangements based on nine sites, $9!/(9\theta)!(9 - 9\theta)!$, and multiplies each value of $\ln w$, so found, by $\frac{3}{2}$, one obtains a curve which is practically superposable on curve B of Fig. 2. In the same fashion curve F of Fig. 2 may be approximately reproduced by multiplying the natural log of the combinatorial formula based on the limiting total occupancy, viz., $12!/(12\theta)!(12 - 12\theta)!$ by the empirical factor $\frac{4}{3}$. These empirical factors are obtained by noting that the average number of sites available is greater than that based on maximum occupancy, i.e., on a combinatorial formula based on nine or twelve sites, except as this maximum occupancy is approached. Therefore the number of arrangements will be greater than that given by the combinatorial formula. For the octahedral case, when $n = n_{max}/2 = 0.75$, there may be seven sites available, or there may be as few as

(10) These enumerations for curves B and F, Fig. 2, were performed by Hewes, Holz, and Willard Co., Cambridge, Mass.

four sites. The average number is approximately $^3/_2$ that expected from maximum occupancy. For the tetrahedral case, one would expect only six sites to be available when $n = n_{max}/2 = 1.5$, whereas there may be as many as eight, hence the factor $^4/_3$. Even though such considerations lack mathematical rigor, the resulting equations agree surprisingly well with the enumerated data and they are far less cumbersome than the rigorous alternatives. These simple relationships also appear to be greatly superior in accuracy to those now in use (e.g., ref. 12), partly because usage often ignores the considerable effect of geometrical restrictions on the number of arrangements, or assumes that occupation of a site excludes a *constant* number of other sites.

If we consider more carefully the effect of geometrical restrictions on occupancy of sites, it is clear that on adding the first atom to an octahedral site in a single structural unit (Fig. 1), either two or four other sites in that unit will be prevented from subsequent occupancy (excluded) by the cited restrictions, depending on whether the occupied site is in an edge or a face centered position. The weighted mean number of sites so excluded is $2^2/_3$. It is obviously true that because of these restrictions the number of available sites is reduced rapidly as sites are occupied. Let D_y be the total number of *available* sites and y the number of occupied sites. It may be shown from the enumeration used to obtain curve B of Fig. 2 that D_y varies with y in the sequence shown in Table I as y increases from 0 to 11. This table shows that for $y = 1$ the added atom renders $3^2/_3$ sites unavailable, which is just the weighted mean number found on inspection. The second atom to enter renders 3.40 sites unavailable, etc. The values of D_y are defined by the relation

$$w = D_{y0}D_{y1}D_{y2}D_{y3}/y!$$

or

$$w = \prod_{y=0}^{y=y} D_y/y!$$

which is equivalent to a combinatorial formula where the denominator is $D - 1, D - 2$, etc.) The second and fourth columns of Table I give the values of D_y. The significance of the third and fifth columns requires a further word of explanation. The fractional values are averages over all arrangements for a given y, some of which do not allow an additional atom to enter. The successive values of D_y may be closely approximated by a third-order polynomial based on the easily enumerated number of arrangements for $y = 0, y = 1, y = 11,$ and $y = 12$.[11]

Table I: Number of Available Sites D as a Function of Occupancy y with Occupancy Restricted

y	Octahedral sites D_y	Sites eliminated per added atom	Tetrahedral sites D_y	Sites eliminated per added atom
0	18.00		24	
		3.67		4.00
1	14.33		20	
		3.40		3.46
2	11.16		16.54	
		2.15		2.96
3	8.78		13.58	
		2.01		2.53
4	6.77		11.05	
		1.05		2.14
5	5.72		8.91	
		0.61		1.82
6	5.11		7.09	
		0.64		1.44
7	4.47		5.55	
		0.72		1.33
8	3.75		4.22	
		0.83		1.16
9	2.92		3.06	
		0.92		1.06
10	2.00		2.00	
		1.00		1.00
11	1.00		1.00	
		1.00		1.00
12	0.00		0.00	

The point of the foregoing is that when site occupation is restricted, the number of arrangements is *not* simply combinatorial. The two widely used methods for handling such computations are not particularly accurate. The dashed curve of Fig. 3 indicates what happens if one uses a combinatorial formula of the type suggested, for example, by ref. 12. Here the number of arrangements is based on the formula

$$w = \frac{(18)(18 - k)(18 - 2k)\ldots(18 - (y - 1)k)}{y!}$$

where k, the number of sites excluded per site occupied, is taken here as $3^2/_3$, and the terms in the numerator are supposed to represent the successive number of sites available.

The approximation suggested above and shown by the solid curve of Fig. 3 is closer but still not entirely accurate, *viz.*, a combinatorial formula based on the *maximum* number of sites which can be filled. Note the comparison of curve B of Fig. 2 and curve B' of

(11) R. Willard, private communication.
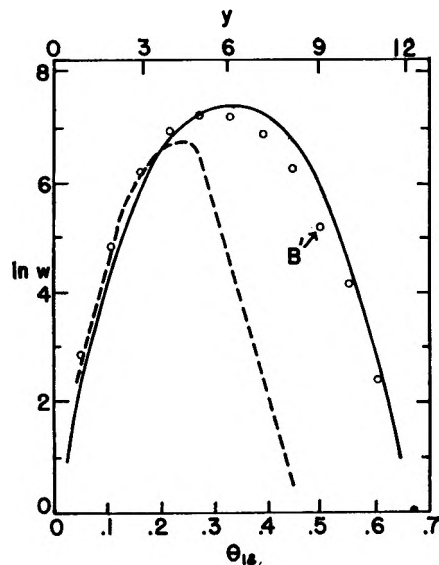(12) R. Speiser and J. W. Spretnak, *Trans. AIME*, **47**, 493 (1955); *cf.* p. 497.

Figure 3. Enumerated number of arrangements (small circles) of atoms in octahedral sites (Fig. 1) as a function of the number y of sites occupied and as a function of the occupied fraction θ of the initially available eighteen sites. Compare with curve B of Fig. 2. The dashed curve is obtained with $k = 3^2/_3 = $ constant number of sites made unavailable by occupation of a single site. The solid curve is $(12/11)[12!/y!(12 - y)!]$.

Fig. 3. Both curves use the same enumeration, but owing to the fact that an occupied face-centered site increases n in MH_n by $^1/_4$ whereas an occupied edge-centered site increases n by $^1/_8$, the curves appear different depending on whether n or y is used as the abscissa. This distinction must be made when a single unit cell is considered, but disappears when a mole is involved.

While it is possible to obtain an accurate expression for computing the number of arrangements, this expression is cumbersome. The purpose of this article is primarily to clarify the relation between a sufficiently small structural unit and the assemblage of these units to make a mole of solid. Two semiempirical formulas have been suggested which provide a means of calculating the configurational entropy due to interstitial atoms in a b.c.c. lattice when site occupancy is limited in two particular ways. Site-preference energies, as estimated from ligand field or similar calculations probably determine whether an entering atom takes up an octahedral or a tetrahedral site; however configurational entropy is by no means unimportant in the choice of energetically equivalent structures. In the case of so-called interstitial hydrides the configurational entropy may also control the stoichiometry.

It is of interest that curves B and F of Fig. 2 show maximum values of configurational entropy to occur at $MH_{0.75}$ and $MH_{1.66}$ for octahedral and tetrahedral sites, respectively, and further that the configurational entropy for hydrogen contents below 0.6 is *higher* for octahedral than for tetrahedral occupation of the interstices of a b.c.c. metal.

A Study of the Desorption of Stearic Acid from Platinum

and Nickel Surfaces Using Ellipsometry

by W. T. Pimbley and H. R. MacQueen

IBM, General Product Division, Development Laboratory, Endicott, New York (*Received November 15, 1963*)

Isothermal desorption experiments were performed for the desorption of many monolayers of stearic acid from both a nickel and a platinum surface. The experiments were performed under ultrahigh vacuum conditions and at a number of different temperatures. An ellipsometer was used to measure the amount of adsorbed stearic acid at any given time. Desorption constants obtained from the isothermal curves were examined for their temperature dependence by plotting them on an Arrhenius plot. The resulting binding energies of the bottom layer to the metal surface were 36.4 kcal./mole to nickel and 30.5 kcal./mole to platinum. The binding energy of the outer layers was 44.1 kcal./mole for desorption from either metal. This energy compares well with the sublimation energy for stearic acid. A theory is presented for isothermal multimolecular desorption. Many features of the experimental results compare well with the predictions of the theory. However, the rate of desorption of the bottom one or two layers is much higher than the theory would indicate. The probable cause and implications of this discrepancy are discussed.

Introduction

Ellipsometry has been used by a number of persons to measure thicknesses of very thin films of transparent materials on reflecting surfaces.[1-5] In the desorption experiments presented in this paper, ellipsometry was used to measure the amount of stearic acid adsorbed on a metal surface under conditions of controlled temperature and ultrahigh vacuum.

Desorption of stearic acid from both nickel and platinum surfaces was studied. About ten monolayers of stearic acid were adsorbed onto the surface, and the temperature was then raised to some desorption temperature. Data were taken for the amount of adsorbed stearic acid vs. time under isothermal conditions. A number of such desorption isotherms were obtained at different temperatures.

The binding energies involved in the adsorption have been determined by observing how the desorption constants vary with temperature. The desorption constant vs. temperature data were compared with the Arrhenius type equation

$$k = k_0 e^{-E/RT} \qquad (1)$$

to determine the binding energies involved. In eq.

1, k is a desorption constant, E is a binding energy, R is the universal gas constant, and T is the absolute temperature corresponding to k.

Theory

The model for the desorption of many layers of an adsorbate presented in this paper has many of the assumptions and many of the limitations of the multimolecular steady-state adsorption theory of Brunauer, Emmett, and Teller.[6] An adsorbed molecule is bound to a molecule in the next lower monolayer, and the binding of molecules within a layer is neglected. The molecules desorb individually, and a molecule is eligible for desorption only if it is uncovered, i.e., if no molecule is adsorbed on top. In any layer, the rate of desorption is directly proportional to the number of molecules eligible for desorption. Further-

(1) P. Drude, *Ann. Physik*, **36**, 865 (1889).

(2) L. Tronstad, *Trans. Faraday Soc.*, **29**, 502 (1933).

(3) A. Rothen and M. Hanson, *Rev. Sci. Instr.*, **20**, 66 (1949).

(4) J. B. Bateman and N. W. Harris, *Ann. N. Y. Acad. Sci.*, **53**, 1064 (1951).

(5) F. Partovi, *J. Opt. Soc. Am.*, **52**, 918 (1962).

(6) S. Brunauer, P. H. Emmett, and E. Teller, *J. Am. Chem. Soc.*, **60**, 309 (1938).

more, all the layers are assumed to have the same desorption constant except the layer next to the adsorbing surface.

Consider that, initially, a number of complete monolayers are adsorbed on a surface. The desorption of the first layer (the top layer) is the same as for Langmuir's monolayer[7]

$$\frac{dN_1}{dt} = -k_1 N_1 \qquad (2)$$

N_1 is the number of molecules adsorbed in the first layer from the top at a time t. Also, k_1 is the desorption constant for the first layer. The expression for the desorption of the nth layer from the top is

$$\frac{dN_n}{dt} = -k_n[N_n - N_{n-1}] \qquad (3)$$

This equation can be modified by multiplying through by $\exp(k_n t)$. Thus

$$\frac{d}{dt}[N_n e^{k_n t}] = k_n N_{n-1} e^{k_n t} \qquad (4)$$

Since the top layers are assumed to have the same desorption constant, the degenerate solutions of eq. 2 and 4 must be used. The solutions are

$$N_n = N_0 e^{-kt} \sum_{j=0}^{n-1} \frac{(kt)^j}{j!} \qquad (5)$$

where N_0 is the number of molecules in a full monolayer. The total number of molecules, if one started with m layers, would be

$$N_T \equiv \sum_{n=1}^{m} N_n = N_0 e^{-kt} \sum_{n=1}^{m} \sum_{j=0}^{n-1} \frac{(kt)^j}{j!} \qquad (6)$$

or

$$N_T = N_0 e^{-kt} \left[(m - kt) \sum_{j=0}^{m-1} \frac{(kt)^j}{j!} + \frac{m(kt)^m}{m!} \right] \qquad (7)$$

The series in eq. 7 approximates the exponential function for small time when m is large. Therefore, for these conditions

$$\left[(m - kt) \sum_{j=0}^{m-1} \frac{(kt)^j}{j!} + \frac{m(kt)^m}{m!} \right] \cong (m - kt)e^{kt} \qquad (8)$$

and so

$$N_T \cong N_0(m - kt) \qquad (9)$$

for small time. Therefore, the desorption of a number of layers of the same desorption constant should start out as a linear decay.

If $m + 1$ layers are initially adsorbed on the surface, the desorption of the first m layers, those with the

same desorption constant, is described by eq. 7. The desorption of the base layer, the layer next to the metal surface, can be found by using eq. 3 and 5. Thus

$$\frac{dN_B}{dt} = -k_B N_B + k_B N_0 e^{-kt} \sum_{j=0}^{m-1} \frac{(kt)^j}{j!} \qquad (10)$$

N_B is the number of molecules in the base layer with m layers initially on top at a time t, k_B is the desorption coefficient of the base layer, while k is the desorption coefficient of the multiple top layers.

The solution to eq. 10 when the $m + 1$ layers are initially filled is

$$N_B = N_0 b^m e^{-k_B t} + N_0 e^{-kt} \times$$
$$\left[\sum_{j=0}^{m-1} \frac{(kt)^j}{j!} - b^m \sum_{j=0}^{m-1} \frac{(at)^j}{j!} \right] \qquad (11)$$

where

$$a \equiv k - k_B \qquad (12)$$

and

$$b \equiv k/a \qquad (13)$$

One can now find an expression for the amount of material adsorbed vs. time by adding eq. 7 and 11. The temperature dependence is introduced, of course, through the constants, k and k_B.

Experiment

The metal specimen off which the desorption was studied was in the form of a ribbon enclosed in an ultrahigh vacuum tube. The ribbon was heated to the desorption temperature by passing a current through it.

An ellipsometer was used to measure the amount of adsorbed material at a given time. The ellipsometer is an instrument that causes monochromatic plane polarized light to fall on the surface from which the desorption is taking place and analyzes the reflected light for elliptical polarization by passing the light first through a quarter-wave plate and then through a polarizing analyzer. An excellent discussion of ellipsometry is given by Partovi.[5] A Rudolph Model 441 ellipsometer was used in these experiments. The green line of mercury, 5461 Å., was used to illuminate the surface.

Figure 1 is a diagram which depicts the working parts of an ellipsometer. The azimuthal position of the quarter-wave plate and the analyzing polarizer, when they are set so as to cause extinction of the light, yield the elliptical polarization properties of the reflected

(7) J. H. deBoer, "The Dynamical Character of Adsorption," Oxford University Press, London, 1953.
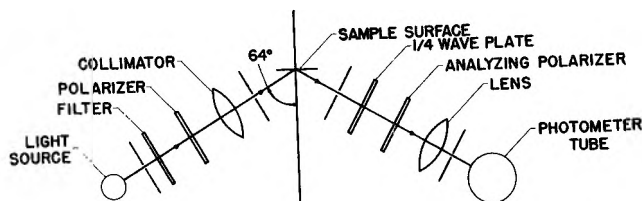
Figure 1. Schematic diagram of an ellipsometer.

light. The minimal setting of the analyzer can be determined with great accuracy if one utilizes the fact that the transmitted light intensity is symmetric about the minimum setting. One determines positions on either side of the minimum that have equal light intensities. The minimum is then halfway between. The reason for the greater accuracy is that the position is much more sensitive to light intensity as one gets away from the minimum.

In the measurements for the amount of adsorbate on the reflecting surface, the quarter-wave plate and the analyzer were set for light extinction when the surface was clean of adsorbed material. Thereafter, only the position of the analyzer was changed to achieve a light minimum when material was adsorbed on the surface. The change in analyzer setting from the clean surface setting is a measure of the amount of adsorbed material.

The calibration of the ellipsometer was made using a barium stearate wedge. Chromium was evaporated on glass slides to a thickness of over 1000 Å. Monolayers of barium stearate were deposited over this surface using the Blodgett technique.[8] The monolayers were deposited in such a manner that there were areas of 0, 1, 3, 5, 7, and up to 15 monolayers coverage on the surface. Each complete monolayer of barium stearate had a thickness of 24.3 Å.[9]

The barium stearate wedge was placed in the ellipsometer, and the change in analyzer setting from the clean surface was measured. The resulting calibration curve is a straight line with a slope of 1.07° per layer. The analyzer angle change is, therefore, directly proportional to the amount of adsorbed material.

The sensitivity of the ellipsometer (the slope of the calibration curve) was found to differ somewhat from surface to surface. The differences in surface condition and polish accounted for the variation. For the work presented in this paper, an exact knowledge of the sensitivity is not required. The amounts of adsorbate are all given in degrees of analyzer angle change, and the amounts in other units would be proportional to this.

A cross section of the desorption tube is shown in Fig. 2. The polished metal ribbon, which is 0.013

cm. thick, 0.317 cm. wide, and about 9 cm. long, is held along the axis of the glass vacuum tube. Potential leads contact the ribbon about 2.5 cm. from its center.

A platinum cylindric shield surrounds the ribbon. It contains two holes through which the incident and reflected beams of light can pass. During an experiment, a mixture of solid and liquid benzene is kept in the dewar section of the tube. The shield is then at a temperature of 5.2°. Since the vapor pressure of stearic acid is less than 10^{-10} mm. at this temperature, the stearic acid will not adsorb back onto the ribbon during the experiment.
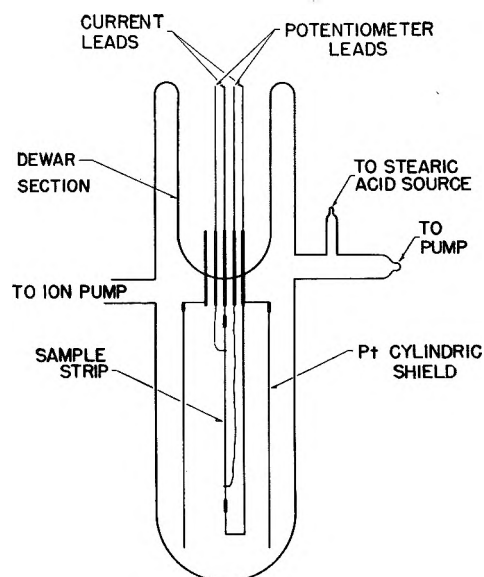

Figure 2. Desorption tube.

The desorption tube was evacuated on an all-glass mercury diffusion vacuum system containing two liquid nitrogen traps in series before the tube. The tube and the second trap were baked out at 430° for 2 days. Moreover, the metal parts were outgassed appropriately. The first trap was kept at liquid nitrogen temperature.

The stearic acid was in a tube projecting from the oven. The acid was distilled over five times with the used glass segment being sealed off and discarded. These distillations were designed to take out absorbed gases. The stearic acid used was Eastman White Label brand.

A 1-l./sec. Varian VacIon pump was attached to the desorption tube to provide pumping after tube seal-off.

(8) K. B. Blodgett, J. Am. Chem. Soc., 57, 1007 (1935).

(9) K. B. Blodgett and I. Langmuir, Phys. Rev., 51, 964 (1937).

Except for the vapor pressure of the stearic acid, the pressure in the tube was about 10^{-10} mm. during the experiments.

During the desorption experiments, the light had to pass into and out of the glass desorption tube. The effect of the glass on the measurements was tested by putting a glass tube around the barium stearate wedge during calibration. The presence of the glass tube had no effect.

The metal ribbons off which the stearic acid was desorbed were prepared, first by polishing them to a mirror-like finish, completing the polishing with γ-alumina which had a particle size of 0.1 μ. The ribbons were then thoroughly washed. During the evacuation of the desorption tube, the ribbons were heated a number of times to red heat for 10 or 15 min. After the stearic acid was introduced into the tube, the ribbons were not heated higher than 100°.

Before each desorption experiment, stearic acid was condensed onto the ribbon. This condensation was accomplished by warming the outside of the desorption tube to about 80°. After cooling the tube, the ribbon was heated to the desorption temperature and the experiment started. After each desorption run, the ribbon was heated to about 100° to assure the desorption of all the stearic acid for the zero thickness measurement.

Thermometry

The temperature of the ribbon was controlled and measured using a four-lead potentiometer–ammeter circuit. The ribbon could be heated to the desired range of temperature, from 20 to 40°, using a current of from 1 to 1.5 amp. The ribbon served as its own resistance thermometer. The resistance measurements were taken with the current passing first in one direction and then in the other. In this way, the thermal e.m.f.'s in the potential measuring circuit could be eliminated.

The temperature calibration was made before the final assembly of the desorption tube. The ribbon assembly was placed in a toluene temperature bath for the calibration. For both the platinum and the nickel ribbons, the calibrations yielded values of temperature coefficient that agreed with the literature.[10]

The leads supporting the ribbon are quite heavy. They have both an electrical and a thermal conductivity at least one order of magnitude greater than that of the ribbon. It can therefore be seen that the ends of the ribbon would remain at about the temperature of the benzene bath in the dewar section while the center of the strip would rise to the desired temperature.

The steady-state heat diffusion problem was worked out for the case of these ribbons. Values for the temperature at the center of the ribbon and for the resistance of the ribbon between the potential leads were calculated as a function of the ribbon current. For both the platinum and nickel ribbons, the resistance vs. current data agreed rather well with experiment. Therefore, the data for the temperature at the center vs. the resistance of the ribbon were used for the final corrected temperature calibration.

It was estimated that the temperature could be measured to within 0.1°. When temperature equilibrium was reached, the temperature of the ribbon would remain constant to within 0.3°.

Results

Figures 3 and 4 present the experimental data for the desorption experiments. For most of these desorption runs, data were taken every minute. For the shortest runs, data were taken every 30 sec., and
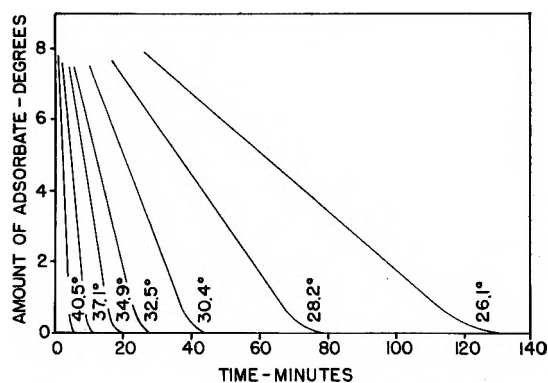
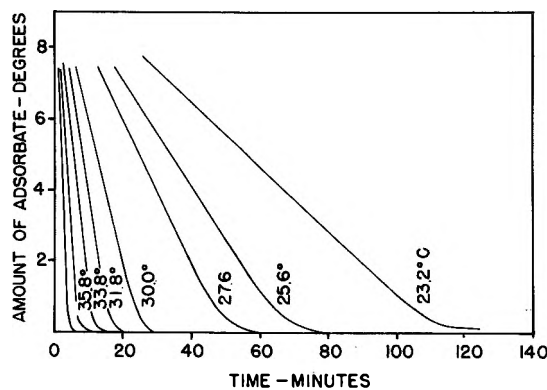Figure 3. Experimental isotherms for the desorption of stearic acid from nickel.

Figure 4. Experimental isotherms for the desorption of stearic acid from platinum.

(10) "Handbook of Chemistry and Physics," 35th Ed., Chemical Rubber Publishing Co., Cleveland, Ohio, 1953.

for the longest, every 2 min. No point deviated from the curves shown in the figures by more than 0.05°.

The first feature to note about the curves is that the decay is linear along a good portion of the desorption. This linearity is in agreement with the theory as can be seen from eq. 9. Equation 9 also indicates that the slopes of the linear portion of the deposition curves are proportional to the desorption coefficients of the multiple layers.

Figures 5 and 6 show Arrhenius plots of the slopes of the desorption curves. For desorption from both the nickel and platinum surfaces, the Arrhenius plots yield the expected straight line. Furthermore, the resulting desorption energies from both plots have the

Figure 6. Arrhenius plots for the desorption of stearic acid from platinum. Line A is a plot of the negative slope of the desorption of the outer layers. The resulting binding energy is 44.1 kcal./mole. Line B is a plot of the time required to desorb from a degree of coverage of 0.5 to 0.1. The resulting binding energy is 30.5 kcal./mole.

Figure 5. Arrhenius plots for the desorption of stearic acid from nickel. Line A is a plot of the negative slope of the desorption of the outer layers. The resulting binding energy is 44.1 kcal./mole. Line B is a plot of the time required to desorb from a degree of coverage of 0.5 to 0.1. The resulting binding energy is 36.4 kcal./mole.

same value, 44.1 kcal./mole. According to the theoretical model, this desorption energy is the binding energy of all of the layers except the layer next to the metal surface. This energy, therefore, is to be compared with either the vaporization or the sublimation energy of stearic acid (see Discussion).

The isothermal desorption curves do not trail off in an exponential decay (see Discussion). For this reason, the binding energy of the bottom layer was determined by plotting, on an Arrhenius plot, the time that it took for the desorption to pass from degrees of coverage of 0.5 to 0.1. Figures 5 and 6 also show these plots. The resulting binding energies are 36.4 kcal./mole for the binding of stearic acid to a nickel surface, and 30.5 kcal./mole for the binding of stearic acid to a platinum surface.

Arrhenius plots were also made for the time it took for the desorption to pass between other degrees of coverage, all starting below 0.8. The slopes of these plots were all the same within the limits of accuracy of the data. Therefore, the desorption below a 0.8-degree of coverage was singly activated, as far as the data from the experiments could detect.

Experiments were also performed for the desorption of stearic acid from a nickel surface under poor vacuum conditions, about 10^{-4} mm. The results of these experiments indicate that there is a layer of material next to the metal surface that desorbs with a relatively high desorption energy, an energy greater than the desorption energy of the outer layers. This tightly bound layer could be a layer of a contaminant. However, the presence of such a layer could also be explained if the bottom layer of stearic acid adheres to a contaminated surface more tenaciously than to a relatively clean one.

Discussion

The binding energy of the outer layers of stearic acid, 44.1 kcal./mole, should be compared to the vaporization and sublimation energies of stearic acid. Lederer[11] calculated the vaporization energy of stearic acid at 25° to be 25.5 kcal./mole. An estimate of the sublimation energy can be obtained by adding the fusion energy to the vaporization energy. The fusion energy of stearic acid has been determined by Singleton, Ward, and Dollear[12] to be 16.4 kcal./mole. Therefore,

(11) E. L. Lederer, Seifensieder-Z., 57, 67 (1930).

one obtains 41.9 kcal./mole as an estimate of the sublimation energy of stearic acid at 25°. It can be seen that the binding energy of the outer layers compares well to the sublimation energy, not the vaporization energy.

The outer layers desorb at a rate of 1 layer/min. at about 34°. The reasonableness of this value can be ascertained by comparing it to what would be expected in the sublimation process. Lederer's calculations[11] give a value of 1.7×10^{-4} mm. as the vapor pressure of stearic acid at its melting point, 69.4°. Using the Arrhenius-type equation with a value of 44.1 kcal./mole for the sublimation energy, one can calculate the vapor pressure at 34° to be 9×10^{-8} mm. This vapor pressure at 34° yields a desorption rate of 1.5 layers/min. for stearic acid. It can be seen, therefore, that the value of the desorption rate of the outer layers agrees well with what would be expected in the sublimation process. This correspondence between multilayer adsorption and sublimation of stearic acid would suggest that the multilayer adsorption process would have a first-order phase change at about the melting point of stearic acid.

Other workers have studied the adsorption of materials at temperatures well below their melting points. The adsorption of carbon dioxide,[13] ethylene,[14] and krypton[15] has been studied at such temperatures. These workers found that in order to obtain agreement between their experiments and the Brunauer–Emmett–Teller adsorption theory, they had to use the extrapolated liquid vapor pressure, not the solid vapor pressure. This need for the use of the liquid vapor pressure indicates that these materials when adsorbed to a thickness of many monolyayers act as a super-cooled liquid and that the binding energy of their molecules in the outer layers is equal to the vaporization energy instead of the sublimation energy. The results of this present paper, therefore, represent a departure from former experiences.

Both desorption energies for the first layer from the metal surface, 36.4 kcal./mole from nickel and 30.5 kcal./mole from platinum, are between the vaporization and sublimation energies for stearic acid. Since the outer layers desorb with an energy equal to the sublimation energy, the adsorption of stearic acid on nickel and platinum corresponds to type III adsorption according to the classifications of Brunauer, et al.[16]

Another feature of type III adsorption evident in the results is that the desorption isotherms do not trail off into an exponential decay. For type II adsorption, the case where the first layer is bound more tightly than the outer layers, the second term of eq. 11 becomes negligible as compared with the first, for large time. The desorption isotherm therefore approaches an exponential decay with k_B as the decay constant. For type III adsorption, however, the second term of eq. 11 never becomes negligible relative to the first and therefore no exponential tail would exist.

Many features of the experimental desorption curves agree with the predictions of the theory presented herein. However, where the desorption progressed down to one or two monolayers, the experimental curves decayed much faster than the theory predicts. The assumptions of the theory, therefore, are not all valid in this region. Lateral interaction of the molecules, for example, would be expected to be important in this region for type III adsorption.

The results for the desorption experiments performed in a poor vacuum show that one can be easily misled by such poor vacuum conditions. The vacuum conditions present in the rest of the experiments were fairly good. However, the metal surfaces could only be said to be relatively clean. They certainly were not atomically clean. The ribbons were cleaned by heating. However, the temperature could not be raised nearly high enough to clean them atomically. It is suggested that in addition to the experiments presented herein, the monolayer adsorption should be studied using another technique such as field emission microscopy. In this way, one could be sure to get the binding energy of the adsorbate molecule to an atomically clean surface.

(12) W. S. Singleton, T. L. Ward, and F. G. Dollear, *J. Am. Oil Chemists' Soc.*, **27**, 143 (1950).

(13) P. H. Emmett and S. Brunauer, *J. Am. Chem. Soc.*, **59**, 1553, 1564 (1937).

(14) L. A. Wooten and C. Brown, *ibid.*, **65**, 113 (1943).

(15) R. A. Beebe, J. B. Beckwith, and J. M. Honig, *ibid.*, **67**, 1554 (1945).

(16) S. Brunauer, L. S. Deming, W. E. Deming, and E. Teller, *ibid.*, **62**, 1723 (1940).

Hydride Ion Transfer and Radiolysis Reactions in Pentane and Isopentane

by J. H. Green and D. M. Pinkerton

Department of Nuclear and Radiation Chemistry, University of New South Wales, Sydney, Australia
(Received November 18, 1963)

The rates of hydride ion transfer reactions leading to the $C_5H_{11}{}^+$ ion in pentane and isopentane have been measured. These rates are briefly discussed with relevance to the radiolysis of pentane.

It has been clearly shown by Stevenson[1] that ion–molecule reactions must be considered in formulating mechanisms in radiation chemistry. Evidence now available convincingly points to the significant role of ion–molecule reactions in gas phase radiolysis.

The early results of the β- and γ-ray radiolysis of liquid pentane in our laboratory have previously been reported[2]; the yield of products, particularly isomerized radicals, was adequately explained by ion formation, rearrangement, and neutralization followed by reactions of radicals. Futrell[3,4] has since studied the radiolysis of gaseous n-pentane and n-hexane and has proposed reaction mechanisms involving hydride ion transfer reactions. In order to provide further information on these mechanisms we resolved to measure the rates of any ion–molecule reactions occurring in n- and isopentane.

Experimental

In general, the method consisted of the measurement of the mass spectrum of the appropriate system, at elevated ionization chamber pressures. The instrument used was a Metropolitan-Vickers mass spectrometer, MS-SG, a general purpose spectrometer, accommodating both gaseous and solid samples.

Appearance potential measurements were made, where possible, using the vanishing current method. The voltage scale was calibrated by the addition of argon as a primary standard.

Secondary ions were characterized by making a plot of the ion abundance ratio of the suspected secondary to the parent ion against the inlet reservoir pressure. A linear pressure dependence of the ratio signifies a secondary reaction and a finite intercept of the ratio at zero pressure indicates the contribution from the primary unimolecular process. It is well-known that

the intensities of secondary ion currents diminish with increasing ionization chamber field strength and so repeller studies were also used to distinguish the secondary ion.

The reaction cross section for the reaction

$$P^+ + R \longrightarrow S^+ + \ldots$$
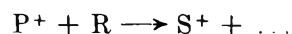
is given by

$$Q = \frac{i_s}{i_p} [l n_r]^{-1}$$

where i_s is the secondary ion current, i_p is the primary ion current, n_r is the concentration of reactant gas, and l is the distance traveled by the primary ions through the reactant gas (1.6 mm.).

To obtain a relation between the gas concentration in the ionization chamber and the measured reservoir pressure, the total ion current produced in argon in the ionization chamber per unit ionizing electron current was measured and used in conjunction with the absolute cross section for ionization by single electron impact. For $Q_{\text{argon}} = 3.52 \times 10^{-16}$ cm.^{2} per molecule and d being 1.8 cm. (electron path length), we find by substituting in the equation

$$\gamma = \frac{I_i}{I_e Q_i d p_r}$$

where I_e is the electron current, p_r is the reservoir pressure, and I_i is the total ion current collected on a

(1) D. P. Stevenson, *J. Phys. Chem.*, **61**, 1453 (1957).

(2) K. H. Napier and J. H. Green, Proceedings of the Australasian Conference on Radiation Biology, Melbourne, Dec., 1958; Australian Atomic Energy Symposium, Sydney, 1958.
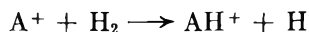
(3) J. H. Futrell, *J. Am. Chem. Soc.*, **81**, 5921 (1959).

(4) J. H. Futrell, *J. Phys. Chem.*, **64**, 1634 (1960).

negatively biased repeller electrode, that $\gamma = 3.02 \times 10^9$ molecules cc.$^{-1}$ μ^{-1}. The concentration of gas molecules in the ionization chamber is then given by

$$n_r = 3.02 \times 10^9 p_r \text{ molecules cc.}^{-1} \mu^{-1}$$

Due to an appreciable divergence of the electron beam in the MS2-SG, which would lead to error in d, the reaction

$$A^+ + H_2 \longrightarrow AH^+ + H$$

was studied. The reaction rate constant determined, 1.4×10^{-9} cm.^{3} molecule^{-1} sec.$^{-1}$, is in reasonable agreement with a previously reported value of 1.89×10^{-9} cm.^{3} molecule^{-1} sec.$^{-1}$.[1] A theoretical treatment by Gioumousis and Stevenson[5] gives the specific rate of reaction as 1.5×10^{-9} cm.^{3} molecule^{-1} sec.$^{-1}$. The experimental reaction rate constant thus supports our value for γ and the over-all error in values of Q and k is about 25%.

The pentanes were distilled and the middle fraction was used for the experiments. Normal high vacuum "degassing" procedures were adopted for the preparation of the reaction samples. All pentane experiments, other than the repeller studies, were conducted with an ionization field strength of 4 v./cm.

Results

A secondary ion occurring at mass $M - 1$, where M is the molecule-ion mass, first appeared in measurable amounts at a reservoir pressure of about 1 mm. No other secondary ions were found. A plot of the ratio of the mass 71 ion intensity to the mass 72 ion intensity (the parent peak) against the reservoir pressure of n-pentane is presented in Fig. 1.

Over the pressure range used the ratio increases and the conditions of the experiment are such that this increase indicates that a secondary reaction is occurring. This result is in accord with the findings of Field and Lampe[6] in their study of hydride ion transfer reactions in the lower hydrocarbons. The relative constancy of a similar plot of the $M + 1$ ion (isotope peak) indicates that the observed increase of the i_{71}/i_{72} ratio is indeed a real effect and not an instrumental artifact. A study of the effect of the ionization chamber field strength on the same abundance ratios endorses the above conclusion (see Fig. 2). Similar results were obtained with isopentane.

Since the reactant primary ion may be one of many, even though the $C_3H_7^+$ fragment is most likely, essentially one must determine which ions are thermodynamically allowed reactant ions. On the basis of present thermodynamic data the ions CH_3^+, $C_2H_3^+$, $C_2H_4^+$, $C_2H_5^+$, $C_3H_3^+$, $C_3H_5^+$, $C_3H_6^+$, and $C_3H_7^+$ can
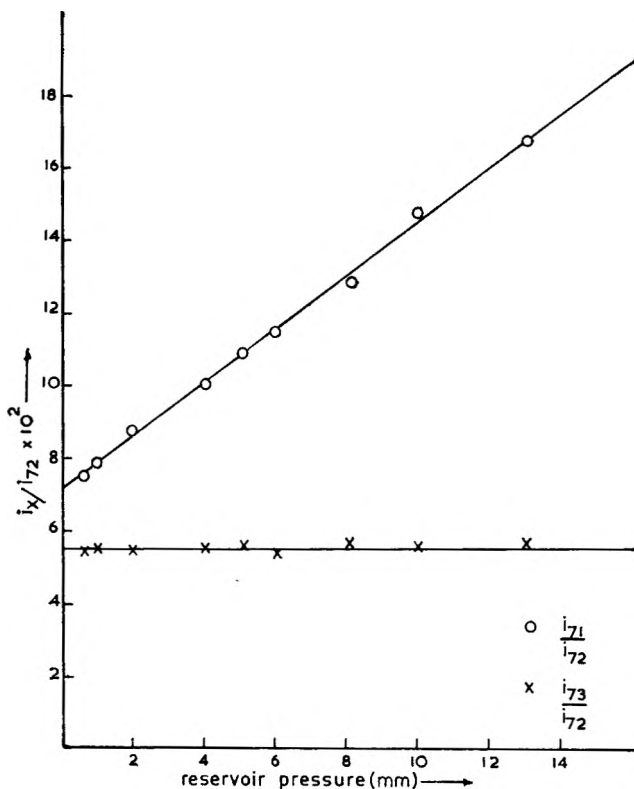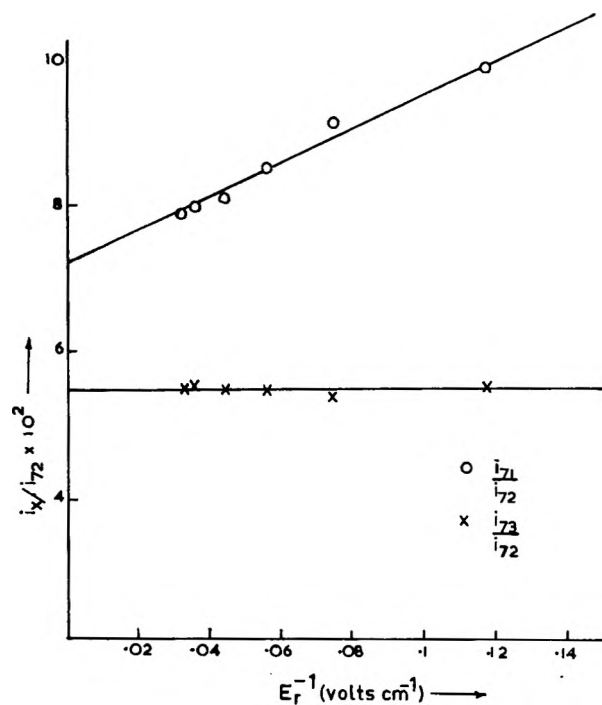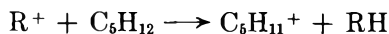

Figure 1. Hydride ion transfer in n-pentane.

Figure 2. Effect of field strength on current ratios.

(5) G. Gioumousis and D. P. Stevenson, *J. Chem. Phys.*, 28, 294 (1958).

(6) F. H. Field and F. W. Lampe, *J. Am. Chem. Soc.*, 80, 5587 (1958).

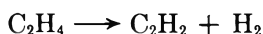react according to the following hydride ion transfer reaction

$$R^+ + C_5H_{12} \longrightarrow C_5H_{11}^+ + RH$$

The heats of reactions were calculated for the allowed reactant ions for various decomposition reactions of the neutral product of the transfer reaction. For example the reaction

$$C_2H_3^+ + C_5H_{12} \longrightarrow C_5H_{11}^+ + C_2H_4$$
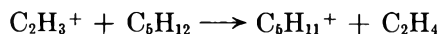
is exothermic as is the decomposition reaction

$$C_2H_4 \longrightarrow C_2H_2 + H_2$$

Although the energy of the hydride ion transfer reaction exceeds that of the decomposition reaction, we must acknowledge, because of our incomplete knowledge of the energy distribution, that exothermic radical decompositions may also occur. It can be shown[6] that

$$\lambda = \frac{\gamma \bar{K} \bar{\tau}}{\beta}$$

where λ is the slope of the line in Fig. 1, γ is the "spectrometer constant," $\bar{K}$ is the average reaction rate constant, $\bar{\tau}$ is the average ion residence time in the ionization chamber, and β is a correction factor defined below.

To simplify calculations, the parent ion intensity at any given pressure can be used as a measure of the summed intensities of the possible reacting primary fragment ions

$$I_R = \beta \sum_i I_{pi}$$

The possible reactant ions in pentane and isopentane are listed above and the values of β were 3.75×10^{-2} and 2.78×10^{-2}, respectively. These values were obtained from the mass spectral intensities of the allowed reactant ions, correcting the measured intensity of the molecule-ion to allow for all primary ions. We have also[7] $\bar{K}\bar{\tau} = QQ'$, where Q is the reaction cross section and Q' is a constant. Then

$$Q = \frac{\lambda \beta}{\gamma Q'}$$

Over the range of pressures studied, the ion current varies linearly with pressure, to a good approximation, and the value of γ may be taken to be the same for related compounds. We determined the value of λ for the reaction

$$CH_4^+ + CH_4 \longrightarrow CH_5^+ + CH_3$$
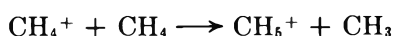
and found 3.48×10^{-3} mm.$^{-1}$. Taking an earlier result[7] for comparison[8] which gave $Q = 71 \times 10^{-16}$

cm.^{2} molecule^{-1} (at a field strength of 4 v. cm.$^{-1}$) we have

$$Q = \frac{\beta \lambda}{4.9 \times 10^{11}} \text{ cm.}^2 \text{ molecule}^{-1}$$

For n-pentane β is deduced to be 3.75×10^{-2} and λ is 7.5×10^{-3} mm.$^{-1}$. The corresponding values in isopentane are 2.78×10^{-2} and 9.75×10^{-3} mm.$^{-1}$. Thus the reaction cross sections for hydride ion transfer in n- and isopentane are 5.8×10^{-16} and 5.6×10^{-16} cm.^{2} molecule^{-1}, respectively. The corresponding specific rate constant can be shown to be 5×10^{-11} cm.^{3} molecule^{-1} sec.$^{-1}$ in both cases.[9] Results of hydride ion transfer reaction studies are given in Table I. The reason the values of Q should be somewhat smaller than one would expect from the results of Field and Lampe[6] is not understood at present and further work is in progress with pentane and heavier hydrocarbons.

Table I: Hydride Ion Transfer Reactions

| Reaction	Reaction cross section, $Q \times 10^{16}$ cm.^{2}/molecule		Reaction rate constant, $k \times 10^{10}$ cm.^{3} molecule^{-1} sec.$^{-1}$
	This work	Field and Lampe	This work
$R^+ + C_2H_6 \rightarrow C_2H_5^+ + RH$		264	
$R^+ + C_3H_8 \rightarrow C_3H_7^+ + RH$		66	
$R^+ + n\text{-}C_4H_{10} \rightarrow C_4H_9^+ + RH$		32	
$R^+ + i\text{-}C_4H_{10} \rightarrow C_4H_9^+ + RH$		34	
$R^+ + n\text{-}C_5H_{12} \rightarrow C_5H_{11}^+ + RH$	5.8		0.51
$R^+ + i\text{-}C_5H_{12} \rightarrow C_5H_{11}^+ + RH$	5.6		0.50
$R^+ + neo\text{-}C_5H_{12} \rightarrow C_5H_{11}^+ + RH$		14	
$R^+ + neo\text{-}C_6H_{14} \rightarrow C_6H_{13}^+ + RH$		7	

(Due to an appreciable abundance of the pentyl ion in the primary mass spectrum it was not possible to use the conventional method of appearance potential measurements to elucidate the reacting ion(s). The thermodynamically allowed reactant ions are listed above. If one ion were incorrectly allowed, there would only be a small error in β, because the ion intensities from pentane are spread over a large number of ions. For example, if the most intense ion, $C_3H_7^+$, were excluded from the list the reaction cross section in pentane would change from 5.8 to 9 Å.^{2}.)

(7) F. W. Field, J. L. Franklin, and F. W. Lampe, *J. Am. Chem. Soc.*, **79**, 2419 (1957).

(8) A similar determination in the MS2-SG, using our value for γ, gave $Q = 72 \times 10^{-16}$ cm.^{2} molecule^{-1} at 4 v. cm.$^{-1}$.

(9) D. M. Pinkerton, Ph.D. Dissertation, University of New South Wales, 1962.

A hydrogen abstraction reaction of the type

$$C_5H_{12}^+ + C_5H_{12} \longrightarrow C_5H_{13}^+ + C_5H_{11}$$
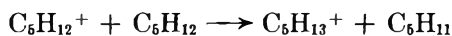
has been supposed to occur in radiolytic systems. Throughout the course of our experimental work on pentane the ratio of the mass 73 ion intensity, which corresponds to $C_5H_{13}^+$, to the molecule-ion intensity was used as a reference against which we measured the observed secondary reaction. Over the range of pressures used (up to about 2×10^{-3} mm. ionization chamber pressure) no significant variation of the ratio was noticed. The possibility of rapid decomposition of the $C_5H_{13}^+$ was considered, but no ion in the spectrum showed the growth in intensity that would be expected if the reaction cross section for the formation of $C_5H_{13}^+$ was of a measurable magnitude. This means that this reaction cross section must be smaller than 10^{-16} cm.^{2}/molecule.

In a further study on the radiolysis of n-hexane vapor Dewhurst[10] suggests that the ion–molecule theory used for an explanation of radiolytic products may require the consideration of chain-lengthening ion–molecule reactions. The same considerations apply to pentane radiolysis. However, a limited study in our mass spectrometer gave no indication of the appearance of such ions even though the energetics are favorable.

Discussion

One reaction sequence in the radiolysis of n-pentane has been assumed[3] to be ionization of the molecule, fragmentation, reaction of the fragment ions with pentane molecules, and neutralization of the product ions, followed by intercombination and disproportionation of free radicals from these processes. After fragmentation, ion–molecule reactions may occur at every collision of the fragment ions (about 10^{-10} sec.) and the hydride ion transfer reaction was believed to dominate this phase of the reaction. On this basis Futrell[3] has expressed 29% of the total products in the gas phase radiolysis of n-pentane as arising from a hydride ion transfer reaction. However, our measured reaction rate constant for this reaction in n- and isopentane is so small that it is difficult to treat it as the dominant reaction.

Futrell himself points out that one obvious limitation to his proposed reaction scheme was that nonionizing excitation events were ignored. The objection that the time interval appropriate to the radiation chemistry of gases is about 10^{-10} sec., while the mass spectrum represents the extent of unimolecular decomposition of the molecule-ion in about 1 μsec., was countered by referring to the work of Stevenson[11], who had used the

statistical theory of mass spectra to show that, for alkanes such as pentane, the rates of dissociation of the molecule-ion are comparable with the rates of bimolecular ion–molecule reactions and so reactions of the fragment ions must be considered. (Recent work in this laboratory[12] shows that some ions from electron impact on alkanes are formed with kinetic energy well above thermal energy. Since most mass spectrometers discriminate against such ions this is a further reason why the mass spectral pattern may not give a reasonable indication of the extent of fragmentation.)

The reaction rate constant for hydride ion transfer in n- and isopentane we find to be 3×10^{10} l. mole^{-1} sec.$^{-1}$ in both cases. Methyl and ethyl radical disproportionation and recombination rate constants are 3.6×10^{10} and 2.0×10^{10} l. mole^{-1} sec.$^{-1}$,[13] respectively, of the same order as for the ionic reaction and so is the rate constant, 4.2×10^{10} l. mole^{-1} sec.$^{-1}$, for the reaction of methyl and ethyl radicals to give propane.[14]

Wagner[15] has found a high yield of pentyl radicals in the radiolysis of pure liquid pentane. Previous scavenger studies in our laboratory had shown a similar result: 16% as n-C_5H_{11} and 59% as sec-C_5H_{11}.[2] The hydrogen abstraction reaction just discussed would, if it occurred in pentane, readily account for these observations. A study of the radiolysis of liquid n-hexane by Hardwick[16] has revealed no evidence that ion–molecule reactions play a significant role, while on the other hand, free radical mechanisms appear to supply a quantitative explanation of the method of formation of products. Hardwick[17] has found that the rate constant for the radical–molecule reaction

$$H + RH \longrightarrow H_2 + R$$
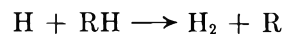
is about 10^9–10^{10} l. mole^{-1} sec.$^{-1}$ (the precise value depending on the structural group). Further, evidence is provided for assuming the rate constant in the liquid phase to be equal to that found in the gas phase.

Now, since the hydride ion transfer rate constant in pentane is of the same order, then the nonobservance of $C_5H_{13}^+$ indicates that, if formed, it must be from a much slower reaction. On a rate basis the high pentyl

(10) H. A. Dewhurst, *J. Am. Chem. Soc.*, **83**, 1050 (1961).

(11) D. P. Stevenson, *Radiation Res.*, **10**, 610 (1959).

(12) K. R. Ryan, Ph.D. Dissertation, University of New South Wales, 1962.

(13) K. J. Ivin and G. W. R. Steacie, *Proc. Roy. Soc.* (London), **A208**, 2680 (1951).

(14) C. A. Miller, *J. Chem. Phys.*, **28**, 1255 (1958).

(15) C. D. Wagner, *J. Phys. Chem.*, **64**, 231 (1960).

(16) T. J. Hardwick, *ibid.*, **64**, 1623 (1960).

(17) T. J. Hardwick, *ibid.*, **65**, 101 (1961).

yield would then depend rather on the radical–molecule reaction cited or the hydride ion transfer than on the hydrogen abstraction reaction.

The extent of ion–molecule reactions in the liquid state is uncertain but it seems that ion dissociation reactions, which are competitive, are quite important.[18] The mean lifetime of the allowed reactant fragment ions with respect to their reaction with the molecule, C_5H_{12}, is $1/kc$, where k for hydride ion transfer in pentane is 0.5×10^{-10} cc. molecule^{-1} sec.$^{-1}$. If the concentration of pentane molecules is approximately $5.2 \times$

10^{21} molecules cm.$^{-3}$, then the mean lifetime with respect to the ion–molecule reaction is 4×10^{-12} sec. If this is compared to the smallest estimates of the time for neutralization, which according to Samuel and Magee[19] is 10^{-13} to 10^{-14} sec., then it is obvious that the hydride ion transfer reaction competes unfavorably with neutralization processes and reactions of neutral species.

(18) T. F. Williams, *Trans. Faraday Soc.*, 57, 755 (1961).
(19) A. H. Samuel and J. L. Magee, *J. Chem. Phys.*, 21, 1080 (1953).

Kinetics and Mechanism of the Low-Cubic to Hexagonal

Phase Transformation of Silver Iodide[1]

by Gordon Burley

National Bureau of Standards, Washington, D. C. (*Received November 18, 1963*)

The transformation rates for the low-cubic to hexagonal irreversible phase change of silver Iodide have been determined at three temperatures by a powder X-ray diffraction technique. The reaction obeys first-order kinetics, with an activation energy of 10.3 ± 0.8 kcal./mole. This is interpreted in terms of a mechanism where the silver atoms initiate the transition by movement to interstitial sites and the iodine lattice then moves to attain the lowest lattice energy.

Introduction

Silver iodide is trimorphic at atmospheric pressure.[2a] Below 147° both a wurtzite-type hexagonal and a zincblende-type cubic structure can exist, but only the former is the stable modification in this temperature range. The cubic to hexagonal phase change is irreversible under ordinary conditions.[2b] At 147° both of these phases transform reversibly to a body-centered cubic phase, where the silver atoms exhibit high mobility.[3]

The speed of any polymorphic transformation depends primarily on the energy barriers opposing the process, and the energy change during a transformation corresponds to a change in bonding type or geom-

etry of the atoms. Structurally the least drastic kind of transformation involves no change in the coordination of nearest neighbor atoms, but a change only in the coordination of atoms further removed than the nearest neighbors is possible. Because of the greater distances involved the bond interactions are then weaker. Two mechanisms for a change in secondary coordination are possible. In a displacive-type transformation the structure is only distorted system-

atically. This is opposed by no energy barrier and consequently proceeds at high speed. In a reconstructive type of transformation the entire network is broken and then reconstructed to form a new and different network. A very high energy barrier exists for this mechanism and the transformation generally proceeds very sluggishly. The phase change involving the zincblende- and wurtzite-type structures of silver iodide is of this reconstructive form.

The magnitude of the energy barrier for silver iodide can be approximately determined from the kinetics of transformation. This follows directly from the Arrhenius rate equation

$$k = Ae^{-\Delta E/RT}$$

when values of the rate constant k are available at two or more different temperatures.

Procedure

Samples of the low-cubic phase with greater than 90% conversion were made from the hexagonal phase by (1) heating to just above the melting point and quenching in water and (2) compacting the material under a pressure of several hundred bars. A high-temperature powder X-ray diffraction apparatus, attached to a Norelco high-angle diffractometer, was used to obtain all data. The polycrystalline material was packed into the rectangular depression of an alumina sample holder, heated rapidly to a specific temperature, and maintained there for a number of hours. A frequent record of the diffraction pattern in the 2θ range from 20 to 40°, using copper radiation, was obtained on an attached recorder. Several different samples were run at each temperature.

Results

The phase transformation occurred irreversibly and at a reproducibly finite rate at all temperatures above 120°. The fraction of silver iodide converted to the hexagonal phase was estimated from the ratio of the integrated areas of the (100) and (101) reflections to that of the (110) reflection. The rate of conversion was determined at 120, 137, and 146°, and the experimentally determined values as a function of time are shown in Table I. The initial value of the fraction of the cubic phase was 0.70 in all cases, due to the difficulty of obtaining total conversion from the hexagonal phase as well as slight transformation during preliminary annealing at 100°.

The transformation was determined to be first order, in accordance with the $k = 1/t \ln \left[a/(a - x)\right]$ relation. The values of the three rate constants k_T were then determined graphically at each experimental tempera-

Table I : Experimental Data for the Face-Centered Cubic to Hexagonal Phase Transformation of Silver Iodide

Time, hr.	Hex., %	F.c.c., %	$a/(a - x)$	$\log \left[a/(a - x)\right]$
		120°		
0	30	70	1.00	0.000
2	32	68	1.04	0.017
4	34	66	1.07	0.028
8	37	63	1.11	0.048
15	41	59	1.20	0.080
24	45	55	1.30	0.115
		137°		
0	30	70	1.00	0.000
2	34	66	1.06	0.026
5	40	60	1.16	0.066
8	45	55	1.26	0.104
12	49	50	1.37	0.136
20	56	44	1.59	0.200
		146°		
0	30	70	1.00	0.000
2¹/₄	45	55	1.30	0.114
4¹/₂	53	47	1.49	0.173
5	55	45	1.55	0.190
5³/₄	57	43	1.63	0.212
6¹/₄	59	41	1.71	0.233

ture. From the slope of a graph of the logarithms of these calculated rate constants against the reciprocal absolute temperatures the activation energy is estimated to be 10.3 ± 0.8 kcal./mole (1 kcal. = 4.184 × 10^3 joules), the uncertainty indicating the mean deviation of the result.

Discussion

The low-cubic to hexagonal phase transformation for silver iodide has been shown to be irreversible. However, the low-cubic form can be prepared and kept for extended periods at room temperature. Only above 120° does the conversion rate even approach a measurable rate, but nowhere is the transformation extremely rapid. This phase change is thus very sluggish, irreversible, and does not readily go to conclusion.

The low-cubic phase of silver iodide, of the zincblende-type, and the hexagonal phase, of the wurtzite-type, may both be considered as layer structures and differ only in the stacking repeat. If only the iodine atoms are considered, this is analogous to the model close-packed cubic and hexagonal structures. The transition mechanism then must introduce one-dimensional stacking disorder. The relation of both the low-cubic and hexagonal phases to each other and to the high-cubic phase is shown in Fig. 1.

STRUCTURE.   bcc   hex   fcc
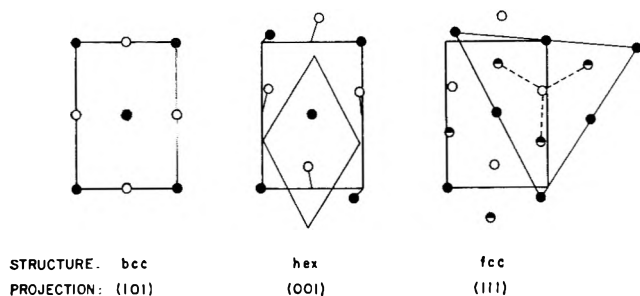PROJECTION: (101)   (001)   (111)

Figure 1.   Structural relationship of the three phases of silver iodide in projection, indicating required atomic shifts for transition. Open circles represent the A layer, filled circles the B layer, and half-filled circles the C layer.

The mechanism is similar to that of the diffusionless martensite-type transformation, with shear on the (111) cubic planes initiating the transition to the hexagonal lattice by a succession of identical glides on alternate parallel planes in the $[\bar{1}\bar{1}2]$ cubic directions. The dislocation node theory, developed by Seeger,[4] suggests that the transformation begins from extended dislocations (Shockley partials), which are anchored at a screw dislocation extending into the hexagonal region along the c-axis. Rotation of the half dislocation about the point of emergence of the screw advances the hexagonal region by two planes for each turn. The dislocation lines would have a screw component twice that of the (111) cubic interplanar distance and represent the nuclei of the hexagonal phase.

Experimentally it has been determined that slow cooling through the transition temperature at 147° yields the hexagonal phase, while rapid cooling produces the low-cubic phase.[2b] The latter probably involves the formation of a transition tetragonal structure, which then rearranges to the low-cubic form.[3]

The kinetics determined from the X-ray diffraction results represent an average transition rate for the system and cannot differentiate local inhomogeneity. The transformation may occur either at random sites or may be initiated at preferred sites and progress to neighboring areas. However, the range over which the transition occurs seems to preclude a purely homogeneous nucleation process. The observed isothermal transformation process can then be attributed either to the presence of structural heterogeneities leading to lower interfacial energies at specific sites, or to the creation of defect sites by thermal activation.

For silver iodide, the silver atoms are in tetrahedral coordination in both low-temperature structures, and the phase transformation involves a change of the relative positions of these atoms as well as that of the iodine atoms. A transition mechanism must therefore

differentiate between a model where the iodine atoms shift as layers and the silver atoms follow, and one where the silver atoms initiate the shift and the iodine lattice follows. No explanation of the specific mechanism of the low-cubic to hexagonal phase transformation has yet been proposed. An attempt will therefore be made to correlate other known properties with the kinetic results presented here.

Activation energies have also been previously derived from electrical conductivity and specific heat measurements of silver iodide. These can be associated almost entirely with the known rapid creation of thermally generated defects in the temperature region between 100° and the transition to the partially disordered high-temperature structure at 147°, and other effects can be neglected over this limited range.

The conductivity has been found to be purely ionic, with a temperature dependence

$$\sigma = \sigma_0 \exp\{-(E_f/2 + U)/RT)\} \text{ ohm}^{-1} \text{ cm.}^{-1}$$

where E_f is the energy required for the creation of one mole of defects and U is the energy barrier for transfer. From measurements at 100° and 1 atm. pressure an activation energy $E_f/2 + U = 11.2$ kcal./mole has been reported.[5]

The deviation of the specific heat in this temperature region from the extrapolated low temperature value has been equated to the rate of creation of thermal defects by

$$\Delta C_p = E_f \frac{d\epsilon}{dT}$$

and, combined with the temperature dependence of defect concentration, yielded a literature value for $E_f/2 = 8$ kcal./mole. The value of U is essentially temperature independent and was estimated as 2–4 kcal./mole.[6] The total activation energies measured by the conductivity, specific heat, and kinetic methods are thus is excellent agreement.

At this point the type of defects must be considered. It has been determined experimentally that the transport number of the Ag^+ in silver iodide is near unity, so that the entire current is carried by the cations.[7] The thermal creation of defects in the temperature range of interest here has been shown to lead predominately to the formation of Frenkel-type defects. This refers to the creation of interstitials, leaving a positive

(4) A. Seeger, Z. Metallk., 47, 653 (1956).

(5) K. H. Lieser, Z. Physik. Chem., 9, 302 (1956).

(6) K. H. Lieser, Fortschr. Min., 36, 96 (1958).

(7) F. S. Stone, "Chemistry of the Solid State," W. E. Garner, Ed., Butterworths Scientific Publications, London, 1955, Chapter 2.
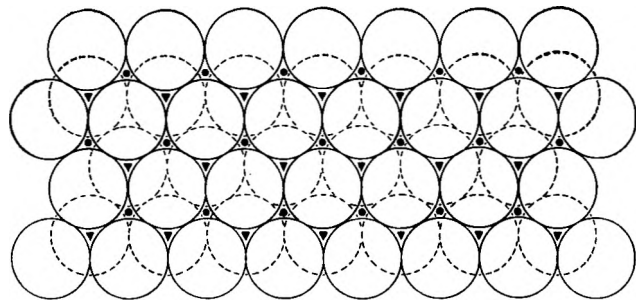
Figure 2. Schematic representation of the close-packed atomic arrangement. Dashed lines represent the first layer, and solid lines the second layer of iodine atoms. The arrangement of silver atoms required for the low-cubic progression is shown by triangles, and that for the hexagonal progression by small solid circles.

hole. The lattice of iodine atoms is thus essentially fixed and only the silver atoms are relatively mobile.

This mobility of the silver atoms, together with the similarities of the activation energies obtained from the kinetics and ionic conductivity experiments, suggests a more detailed picture for the transition mechanism in silver iodide than any proposed previously. The layer structure in the cubic (111) direction is shown in Fig. 2. The arrangement of the silver atoms between the second and third iodine layers is shown by circles for the low-cubic and triangles for the hexagonal structure. The required shift is $1/\sqrt{3}$ the distance between centers of iodine atoms and into an available interstitial site. The creation of one interstitial silver site leads to a local lattice instability and two factors then favor its propagation. First, the repulsive interactions of neighboring cation force fields favor their separation and, second, the creation of a number of adjacent identical defects is equivalent to a lattice

glide. These silver atoms will tend to move the adjacent iodine atoms of the next successive layer into the tetrahedral configuration. The tendency is toward the phase of lowest lattice energy, which in the case of silver iodide is the hexagonal form. The energy barrier measured by the kinetics experiments must thus be the sum of the energy required for the creation of an interstitial Frenkel-type defect and the energy to move a silver atom from its lattice site to the interstitial site. The transformation rate is temperature dependent, in agreement with the measured increase of defects at higher temperatures. The iodine atoms then move only in order to minimize the silver coordination number and no appreciable energy barrier exists for this.

Conclusions

The kinetic measurements for the irreversible low-cubic to hexagonal phase transformation of silver iodide have been interpreted in terms of a transition mechanism. An activation energy of 10.3 ± 0.8 kcal./mole was derived from the rate equation in the temperature range from 120 to 146°. By analogy with the results from conductance and heat capacity experiments this leads to the conclusion that the iodine lattice remains essentially stationary and the transition is initiated by the movement of silver atoms to interstitial sites. When a sufficient number have migrated to positions required for the hexagonal progression the adjacent iodine atoms of the next succeeding layer then shift. The transformation is regional and stepwise, since only local conditions are of importance, and the trend is always toward the more stable hexagonal phase. The specific mechanism may be analogous to that of the martensitic-type transition.

A Spectrophotometric Study of the Gaseous Equilibrium

between Cadmium and Cadmium(II) Chloride[1]

by Buddy L. Bruner and John D. Corbett

Institute for Atomic Research and Department of Chemistry, Iowa State University, Ames, Iowa
(Received November 22, 1963)

A Beckman DU spectrophotometer has been modified to permit investigation of gaseous equilibria at high temperatures, and the absorption spectra of the Cd-$CdCl_2$ system and its components have been measured between 545 and 780°. The mixture displays new bands due to the monochloride in addition to the transitions found with the pure components. $\Delta H°_{1000}$ for the reaction $Cd(g) + CdCl_2(g) = 2CdCl(g)$ was found to be $34.1_5 \pm 0.5$ kcal. mole^{-1} and, with the third-law entropy change, $\Delta F°_{1000}$ is 23.8 ± 0.5 kcal. mole^{-1}. Utilizing the solubility data for Cd in $CdCl_2(l)$, 83.9 and 32.6 kcal. mole^{-1} are obtained for $\Delta H°_{1000}$ and $\Delta F°_{1000}$, respectively, of the presumed reaction $Cd_2Cl_2(l) = 2CdCl(g)$. Values of 2.11 ± 0.03 and $0.02_7 \pm 0.01$ e.v. for $D°_0$ of CdCl and Cd$_2$, respectively, are also obtained. Analysis of the CdCl vibrational bands yields $334._5$ cm.$^{-1}$ for ω_e'' and 1.3 cm.$^{-1}$ for $x_e''\omega_e''$ of the $^2\Sigma$ ground state, and 397 cm.$^{-1}$ for ω_e' and 0.9 cm.$^{-1}$ for $x_e'\omega_e'$ of the $^2\Pi_{1/2}$ excited state. The 3181-Å. band is not observed and its previous assignment to CdCl is concluded to be erroneous.

Introduction

Although the solution of cadmium in its chloride has received considerable attention from investigators with regard to the nature of the solute species,[2,3] very little has been established about the gas phase equilibrium. Tarasenkov and Skulkova[4] reported that $CdCl_2$ was significantly less volatile in a Cl_2 stream than in one of N_2, and Walters and Barratt[5] assigned to CdCl the two new band systems that they observed in the spectrum of the cadmium metal on introduction of $CdCl_2$ at 500 to 800°. These two observations suggest that a stable subhalide may exist under equilibrium conditions.

The present paper reports a direct determination of the nature of the gas phase species above the solution of Cd in $CdCl_2$ and of the thermodynamic parameters of the equilibrium. Since the objective of this investigation required both identification and measurement of the equilibrium species, preferably over a range of temperature and concentration, the electronic absorption spectra of the system were studied. The use of absorption spectra not only provides a means of satisfying the minimum requirements of the investi-

gation but in principle permits simultaneous and essentially independent measurements of all the species present. Although in practice only the relative concentration of the product CdCl could be measured reliably, even this would have been achieved only with difficulty by conventional pressure-measuring methods.

Experimental

Materials. For accurate, unambiguous, and quantitative spectral measurements, it is necessary to use chemicals of high purity. Therefore, the materials used herein were transferred only under vacuum or in an argon-filled drybox after purification. Cadmium metal (A. D. MacKay, 99.999%) was fused under vacuum, cooled, and the resulting surface impurities

(1) Contribution No. 1411; work was performed in the Ames Laboratory of the U. S. Atomic Energy Commission.

(2) Summarized by J. D. Corbett, W. J. Burkhard, and L. F. Druding, *J. Am. Chem. Soc.*, **83**, 76 (1961).

(3) L. E. Topol, *J. Phys. Chem.*, **67**, 2222 (1963).

(4) D. N. Tarasenkov and G. V. Skulkova, *Zh. Obshch Khim.*, **7**, 1721 (1937).

(5) J. M. Walters and S. Barratt, *Proc. Roy. Soc.* (London), **A122**, 201 (1929).

(primarily CdO) dissolved in dilute HNO_3. The cleaned buttons were then distilled twice at 415° under dynamic vacuum (10^{-7} torr) in a Pyrex tube that had been degassed at 500°. The $CdCl_2$ was prepared by direct chlorination of the metal[2] and vacuum sublimed twice at 550° after being chlorinated for 1 hr. at 500°. After purification, both salt and metal were sublimed directly into the sample cell or into small glass fingers which were subsequently sealed off for storage.

Apparatus. A Beckman DU spectrophotometer equipped with a 1P28 photomultiplier detector and a H_2 source was modified for measurements on gas phase samples at high temperatures by rearranging the components of the instrument to provide the "reversed optics" necessary to minimize the effects of furnace radiation above 500°.[6,7] This and the enlargement of the sample compartment to contain the required furnace made it necessary to modify the cell compartment mounting block and the light source arrangement.

The mounting block was altered to accommodate the detector in a manner essentially identical to that described by Gruen and McBeth.[8] The source was modified by removing the condensing mirror and cutting a large hole in the housing wall so that the light beam entered the cell compartment directly from the source. Since this produced a divergent beam over the 58.5 cm. between the source and the monochromator slit, substantially reducing the effective intensity, two fused silica condensing lenses (Perkin-Elmer, 35-mm. diameter, 8-mm. thickness, 55-mm. focal length) were then mounted in adjustable holders at each end of the sample compartment to focus the beam. The wave length calibration was checked with a Hg discharge tube. The furnace compartment for the high temperature work was essentially a large box constructed from boiler plate, angle iron, and sheet metal with exterior Cu coils for water cooling, and was mounted to the monochromator through the alignment pegs of the modified mounting block. The source was mounted on the other end of this compartment. Access to the furnace and sample was attained by unbolting and removing one side and the top of the compartment.

The cells were of cylindrical, fused silica construction (Pyrocell, 100-mm. path length, 22-mm. diameter) with a finger on the sample cell perpendicular to the light path at the longitudinal midpoint. A 16-in. (40 cm.) hinged muffle furnace (Heavy Duty Electric) was rewired so that the 4-in. (10 cm.) end sections could be controlled separately from the central sections to allow compensation for the heat loss at the ends of the furnace. A set of appropriately drilled firebrick plugs was also used within the end sections for the same

purpose. A hole in the lower, central heating section permitted the installation of a third heater that was used to regulate the temperature of the liquid sample, if any, inside the finger of the cell during spectral measurements. A stainless steel block within the central section of the furnace acted as a holder for the absorption cells and as a body of large heat capacity to minimize temperature variations. The block was constructed in halves to permit easy access and was drilled out to accommodate both a reference cell and a sample cell with its finger. Grooves in the top of the block and adjacent to the sample cell held thermocouples for control of the central heating section and for the determination of the temperature along the length of the cell. Cells with 50-, 100-, or 150-mm. path lengths could be accommodated by the use of a set of steel inserts.

The small tubular heater positioned around the sample cell finger was fitted with a Lavite insulator and, at the bottom, with a small cylindrical stainless steel block. A well was drilled into the center of the block along its lateral axis to accommodate the finger, and a second hole at the base of and perpendicular to this well contained a measuring and controlling thermocouple. The temperatures of the central heaters of the furnace and of the small finger furnace, 15° below that of the main block, were regulated by two Brown proportioning controllers (Minneapolis Honeywell) while the end heaters were controlled by a Celectray off-on controller. Sample temperatures were measured with the aid of a Rubicon precision potentiometer. The entire furnace was on wheels and, as required by the Beckman instrument, was alternately positioned with sample and reference holes in the light path with the aid of preset stops.

The absorption cells were filled after a careful regimen of degassing and chlorination (except for those used for metal samples since chlorination or washing with HCl introduced spurious monochloride lines into the spectra). The samples necessary for condensed phase measurements were sublimed into the cells while the weighed samples for gas phase measurements were added directly to the cell in the drybox. In all cases the cells were evacuated and sealed off prior to measurements.

Data Correction. The difficulties of maintaining a closely matched reference cell prompted the use of the

(6) B. R. Sundheim and J. Greenberg, *Rev. Sci. Instr.*, 27, 703 (1956).

(7) B. R. Sundheim and J. Greenberg, *J. Chem. Phys.*, 28, 439 (1958).

(8) D. M. Gruen and R. L. McBeth, *J. Inorg. Nucl. Chem.*, 9, 290 (1959).

empty reference "hole" in place of the cell so that a correction procedure was required to obtain the actual sample absorbance. Since the low temperature measurements (approximately 100°) of a system essentially represented the transmission of an empty cell (sample absorptions were undetectable), these values were adopted as $I_{cell}/I_{reference}$. The actual corrections were obtained by drawing a calibration curve of $\%T$ (transmittance) vs. wave length for the low temperature values of each run and interpolating the correction values from this graph. This procedure implicitly corrected for any mismatching of the absorption cells in cases where a reference was employed as well as for other incidental errors such as a faulty positioning of the furnace blocks. The slight change in cell transmittance observed at higher temperatures was accommodated by shifting the transmission values of the correction curve so that these were identical with those of the sample in the blank 4000 to 5000-Å. region. The corrected transmittances were then obtained by dividing the measured transmittances by the values from the correction curve.

Results and Discussion

Spectral measurements of the gas phase above condensed Cd, CdCl₂, saturation solutions of Cd in CdCl₂, and of all-gas systems of Cd and of mixtures of Cd and CdCl₂ were made between 2000 and 5000 Å. In all cases the measurements were made from room temperature to at least 750°. The choice of the spectral region was made after preliminary measurements disclosed no interesting detail from 5000 to 20,000 Å., while temperatures above 800° were not used since at this temperature the absorption above condensed samples in a 100-mm. cell was already too large to be measured with good accuracy. Characteristic data for absorption peaks are tabulated in Table I for both all-gas and condensed phase samples.

The spectrum of the metal vapor, described in Table II, is in excellent agreement with previously reported observations.[9] The observed spectrum of gaseous CdCl₂ presented no interesting details. It first appears at 675°K. at a pressure of 3×10^{-3} torr and quickly forms a rather broad, structureless continuum centered at 2000 Å. and shaded to the red. With increasing pressure the band broadens and shifts to the red until at 60 torr (1025°K.) the transition is apparently centered at 2400 Å. and extends to 3600 Å.

Identification of CdCl. A typical vapor phase spectrum of the Cd–CdCl₂ mixture is presented in Fig. 1 with the source of the Cd and CdCl₂ lines marked for reference. The most notable feature of these spectra is the observation of two series of bands extending to

Table I : Spectral Data for Gaseous Cd and for Cd–CdCl₂ Mixtures (100-mm. Path Length)

T, °K.	%T (3261 Å.) (Cd)	%T (3172 Å.) (Cd₂)	P/T^b (Cd)	Absorbance^a (Cd₂)	%T (3070 Å.)
	Cadmium metal				
989.2	8.7	83.8	0.3167	0.076₈	
1008.0	8.8	84.1	0.3133	0.075₂	
1048.5	9.2	84.3	0.3080	0.0?42	
928.4	19.2	94.2	0.2052^c	0.0155	99.2
968.0	7.6	85.8	0.3412^c	0.066	98.9
987.8	4.8	80.5	0.4242^c	0.0835	98.7
1003.5	3.8	72.1	0.5062^c	0.142	98.6
1018.3	3.0	64.1	0.6037^c	0.194	98.5

T, °K.	%T (3261 Å.) (Cd)	%T (3070 Å.) (CdCl)	%T (3170 Å.) (CdCl)	Absorbance^a (CdCl, 3070 Å.)	P/T^{b,c} (Cd)
	Cadmium plus cadmium dichloride				
945.6^d	26.2	81.0	82.0	0.078	
965.6^d	26.5	78.1	77.6	0.094	
987.4^d	26.8	74.7	74.6	0.014	
1006.4^d	26.8	71.6	70.5	0.133	
1026.4^d	27.5	68.2	70.2	0.153	
955.6^e	28.2	74.7	75.4	0.107	
985.4^e	28.4	68.3	69.9	0.146	
1016.1^e	28.5	62.4	61.9	0.189	
1045.6^e	28.7	55.5	58.2	0.236	
951.9^f	26.2	75.8	76.0	0.102	
977.7^f	26.4	71.4	71.2	0.128	
1001.9^f	26.7	66.1	65.9	0.162	
1027.7^f	26.7	60.3	59.8	0.201	
1052.4^f	27.3	55.0	53.8	0.241	
817.6	74.7	98.0	98.1		0.039
869.1	52.5	94.3	94.6		0.089
902.3	34.3	86.2	85.0		0.144
936.3	18.6	69.1	68.0		0.227
968.7	6.1	43.9	43.8		0.340
993.2	3.3	25.0	25.0		0.451
1018.0	1.8	11.0	12.4		0.592

^a Corrected for background. ^b Torr deg.⁻¹. ^c Condensed phase run; P/T for Cd calculated from known vapor pressure data of F. D. Rossini, et al., "Selected Values of Chemical Thermodynamic Properties," National Bureau of Standards Circular 500, U. S. Govt. Printing Office, Washington, D. C., 1952. ^d Run A; 0.1884 and 0.0090 torr deg.⁻¹ of Cd and CdCl₂, respectively. ^e Run D; 0.1623 and 0.171 torr deg.⁻¹ of Cd and CdCl₂ respectively. ^f Run E; 0.1841 and 0.140 torr deg.⁻¹ of Cd and CdCl₂, respectively.

lower wave lengths from 3070 and 3170 Å. These values and their accompanying fine structure form a positive identification of the presence of CdCl in that they correspond well to the CdCl lines reported by Walters and Barratt[5] although the wave lengths ob-

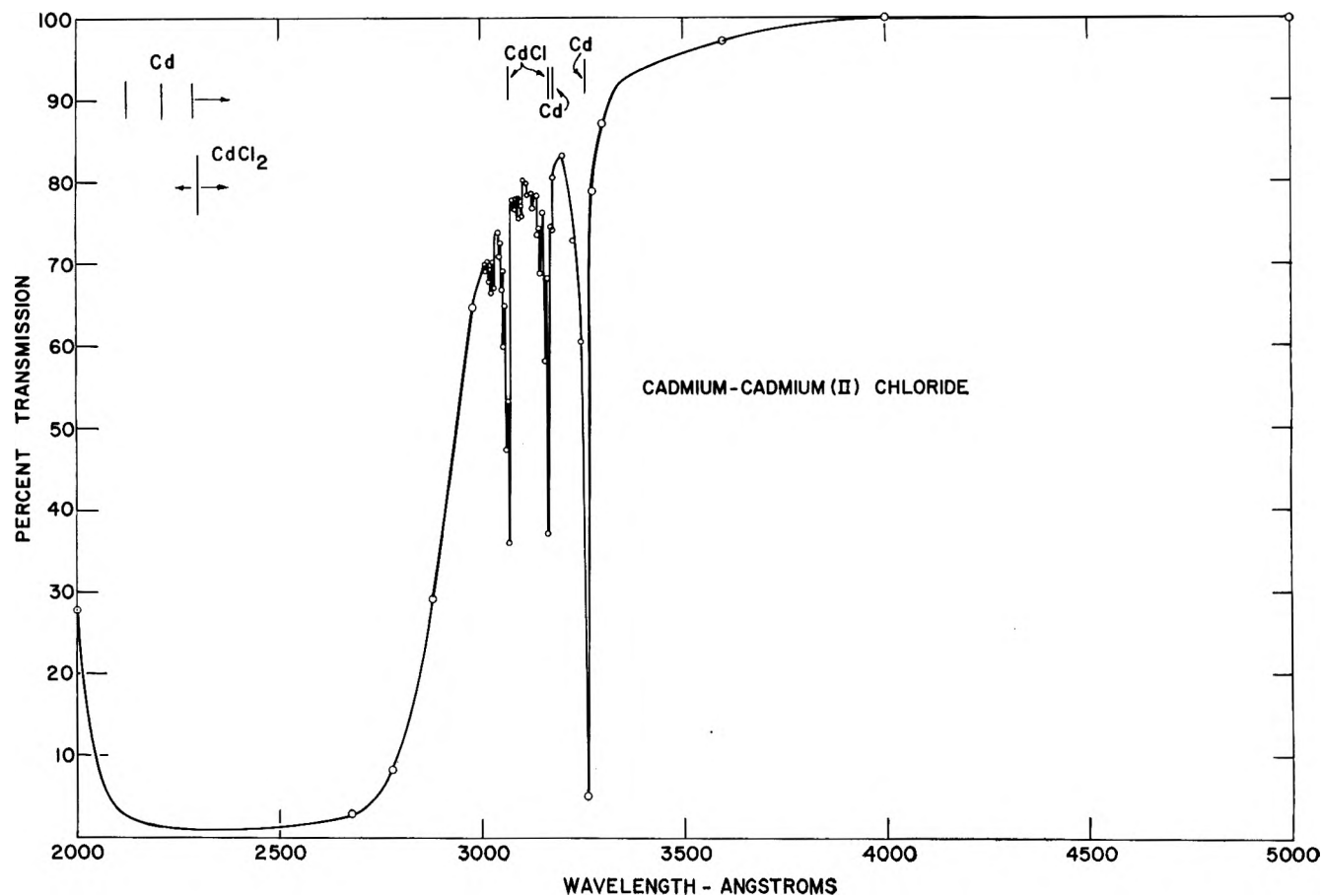(9) S. W. Cram, *Phys. Rev.*, **46**, 205 (1934).

Figure 1. Typical spectrum of gas phase mixtures of Cd and CdCl₂ (with P/T of
Cd and CdCl₂ equal to 0.2205 and 0.0187 torr deg.⁻¹, respectively; T = 1026°K.).

served in this study are consistently about 2 Å. smaller. The assignment of this doublet to CdCl is based on the predicted appearance of a doublet from the $^2\Pi-^2\Sigma$ transitions anticipated for such a species and the very fact that discrete bands are observable rather than more or less of a continuum to be expected for a polyatomic species such as Cd_2Cl_2. The inability to detect the previously reported transition at 3181 Å. is most likely due to an erroneous assignment to CdCl of a transition of Cd by Walters and Barratt.[5] Their failure to record the detection of the subsequently observed 3178-Å. line[9,10] supports this contention. No other continua or discrete bands could be found on careful scanning to 20,000 Å.[11] It therefore must be concluded that all other possible species are absent or present in undetectable amounts unless masked by the Cd + CdCl₂ continuum. It is unlikely that any other components, particularly Cd_2Cl_2, would exhibit no transitions in the normal ultraviolet–visible region. There is also no indirect stoichiometric evidence to suggest that any other species was present.

Vibrational Bands of CdCl. The aforementioned

discrepancies between the reported and observed CdCl vibrational bands indicated a need to re-examine the vibrational analysis presented by Howell[12] on the basis of the earlier values. To this end, Deslandres tables were prepared using weighted averages of the wave lengths observed in a number of measurements, one of which is given in Table III. Assuming that the CdCl systems observed were due to the $^2\Pi-^2\Sigma$ transition and that only the Q-heads were likely to be resolved, the intense 3070 and 3170 Å. transitions were assigned to the 0–0 transitions for the anticipated doublet. It was then possible to assign all of the other bands in a very consistent manner (using as a guide the value of 330.5 cm.⁻¹ for ω_e'' that Cornell[13] obtained

(10) S. Mrozowski, *Z. Physik*, **62**, 314 (1930).

(11) It is interesting to note that the spectra of empty cells that had previously been used for a run that contained the metal always exhibited the 2288-Å. resonance transition of Cd. The intensity corresponded to a pressure of some 10⁻³ torr of Cd(g), and this transition could not be eliminated by heating the cell under vacuum to 500° or by washing the cell with acids.

(12) H. G. Howell, *Proc. Roy. Soc.* (London), **A182**, 95 (1944).

(13) S. D. Cornell, *Phys. Rev.*, **54**, 341 (1938).

Table II : Spectral Systems of Gaseous Cadmium Metal

Transition	Appearance[a]	Description
2288 Å.	4.5 × 10⁻⁴ torr 475°K.	The major resonance peak, broadens slowly and symmetrically at the base (100% T) from 0.5 torr. By 10 torr the peak begins to broaden asymmetrically to the red and by 135 torr it has formed a sharp edge at 2200 Å. and a wing extends to 3000 Å. in the red
3261 Å.	0.8 torr 585°K.	The secondary resonance line broadens symmetrically from the base at 85 torr and asymmetrically to the red above 500 torr
2123 Å.	2.5 torr 700°K.	A sharp peak which broadens very slowly and symmetrically from its first appearance
2214 Å.	2.5 torr 700°K.	A sharp peak which is absorbed into the 2288-Å. band at 135 torr
3178 Å.	50 torr 840°K.	A sharp line which tends to be absorbed by the 3261-Å. line at pressures above 1 atm.

[a] Pressures and the corresponding temperatures for the minimum detection of the vapor spectrum through a 100-mm. path length.

from emission measurements in a different region). The results differ from Howell's assignments and yield apparent values of 334.5 and 1.3 cm.⁻¹ for ω_e'' and $x_e''\omega_e''$, respectively, of the $^2\Sigma$ ground state as well as 397 and 0.9 cm.⁻¹ for ω_e' and $x_e'\omega_e'$ of the $^2\Pi_{1/2}$ state. A value of 420 ± 10 cm.⁻¹ is suggested for ω_e' of the $^2\Pi_{3/2}$ state on the basis of the 0–1 transition observed.

Table III : Vibrational Band Heads of the CdCl Spectrum

Å.	Å.	Å.
3170 (10)[a]	3095 (1)	3052 (2)
3161 (4)	3089 (0)	3046 (0)
3150 (1)	3082+ (00)	3033 (1)
3141 (0)	3070 (10)	3027+ (1)
3128+ (00)	3064 (7)	3022 (00)
3102+ (1)	3058 (3)	3016 (00)

[a] Relative intensities in parentheses.

Calculation of Equilibrium Thermodynamics. A series of preliminary calculations indicated that the intended method of quantitatively analyzing the all-gas system on the basis of calibration curves for the metal and dichloride could not be applied, principally because
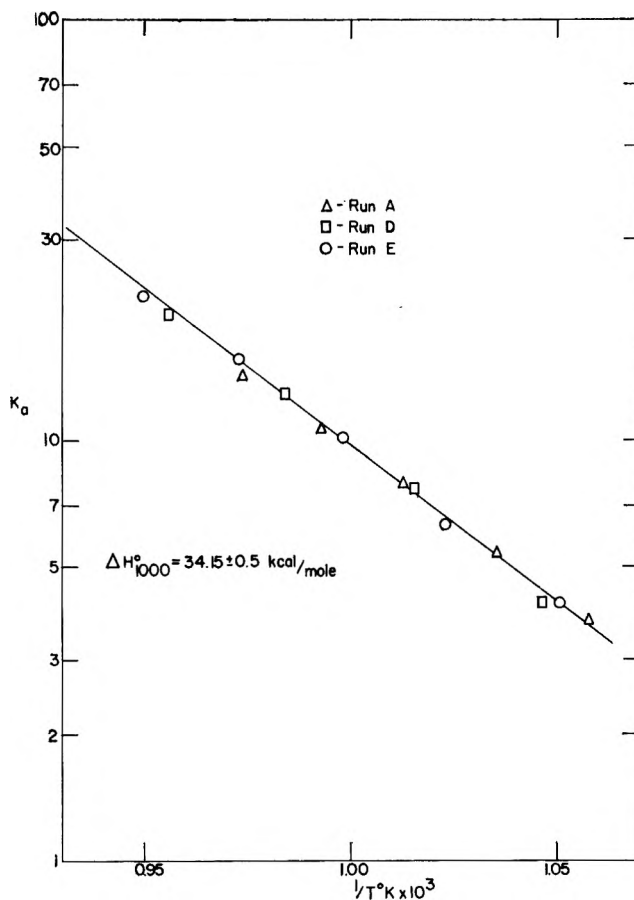
Figure 2. Plot of log K_a vs. $1/T$ for the reaction Cd(g) + CdCl₂(g) = 2CdCl(g).

of extensive line broadening of the CdCl₂ spectrum by Cd. Therefore the following procedure was adopted. The concentration of CdCl produced was assumed to be too small to decrease the initial, known concentrations of the reactants significantly. Acting on this assumption, a set of pseudo-equilibrium constants were calculated over a range of temperatures and concentrations from the relationship $K_a = (A_{CdCl})^2/(C_{Cd})(C_{CdCl_2})$, where A_{CdCl} is the absorbance of CdCl corrected for background absorption of Cd and CdCl₂ and the C quantities represent the concentration of the corresponding reactants calculated from the amount originally added to the cell.[14] A plot of log K_a vs. $1/T$ should yield a straight line parallel to such a plot of the true equilibrium constant but differing in the intercept by a value of 2 log ab since absorbance is the product of path length (b), absorptivity (a), and concentration. This plot of data for three separate

(14) The assumption here of substantially only monomeric CdCl₂ in the gas phase is confirmed by the recent vapor pressure study by F. J. Keneshea and D. Cubicciotti, *J. Chem. Phys.*, **43**, 1778 (1964).

experiments, Fig. 2 (Table I), yields an apparent heat of reaction of 34.1_5 kcal. mole^{-1} at 1000°K. for the reaction $CdCl_2(g) + Cd(g) = 2CdCl(g)$. The complete agreement between different experiments at varying pressures as well as the shape of the peaks support the presumption that $a(CdCl)$ is not affected by the other components.

The reliability of this measure of $\Delta H°_{1000}$ can be established by its internal variation or self-consistency and by the agreement between the original assumptions and the equilibrium concentrations calculated with the use of this heat and a third-law entropy for the reaction. A least-squares analysis of the data shown in Fig. 2 gives a 95% confidence limit of ±0.5 kcal. and a 99.5% level of ±0.75 kcal. for random errors in $\Delta H°_{1000}$. Utilizing the experimental heat and the statistical $\Delta S°_{1000}$ of 10.4 e.u.[15-19] for the reaction, $\Delta F°_{1000}$ is 23.8 kcal. mole^{-1}, from which K_P equals 6.3 × 10^{-6}. The latter value corresponds to a change of less than 1% in the concentrations of the reactants in the three runs and thus is consistent with the assumption that relatively little CdCl is produced. In principle, it would be possible to accommodate these small changes and to modify slightly the resulting $\Delta H°$, but such a correction (0.2 kcal.) is probably not too meaningful considering the magnitude of the over-all experimental error. The results of Taresenkov and Skulkova[4] that suggested a more substantial amount of a reduced species are thus inconsistent with the present findings as well as with recent studies of the vapor pressure of $CdCl_2$.[14,20]

It is possible to analyze similarly the absorbance of the 3178-Å. band of Cd_2[9] to obtain a value of $D°_0$ for this molecule. The experimental data yield a $\Delta H°_{1000}$ value of 1.6_7 ± 0.2 kcal. mole^{-1} for $Cd_2 = 2Cd$, which compares with 2.0 ± 0.5 kcal. mole^{-1} for $\Delta H°_{\sim 1225}$ obtained by Kuhn and Arrhenius[21] by essentially the same method. With $\Delta(H°_{1000} - H°_0) = (5 - 4.47)R$ kcal. ($\omega \sim 40$ cm.$^{-1}$ for Cd_2), the enthalpy change found here gives about 0.6 kcal. mole^{-1} or 0.02_7 e.v. for $D°_0$ of Cd_2.

Additional Thermodynamic Calculations. Having experimentally determined $\Delta H°_{1000}$ for the gaseous reaction of Cd with $CdCl_2$, it is worthwhile to consider some other reactions for which thermodynamic values may now be derived or improved. The enthalpy obtained in this study may be combined with that for other processes to give a much better value for the dissociation energy of CdCl than has heretofore been available. For the present reaction $CdCl_2(g) + Cd(g) = 2CdCl(g)$, the foregoing $\Delta F°_{1000}$ may be combined with −11.68 kcal. mole^{-1} deg.$^{-1}$ for $\Delta(F°_T - H°_{298})/T$ at 1000°K.[15,17-19] to give a $\Delta H°_{298}$ of 35.5 kcal.

Table IV: Heat of Atomization of CdCl(g) at 298°K.

	$\Delta H°_{298}$, kcal. mole^{-1}	Ref.
$2CdCl(g) = Cd(g) + CdCl_2(g)$	−35.5	This work
$CdCl_2(s) = Cd(s) + Cl_2(g)$	93.00	8
$CdCl_2(g) = CdCl_2(s)$	−43.6 ± 0.2	14
$Cl_2(g) = 2Cl(g)$	57.88	15
$Cd(s) = Cd(g)$	26.75	15
$2CdCl(g) = 2Cd(g) + 2Cl(g)$	98.53	

mole^{-1}. The reactions in Table IV give the heat of atomization of CdCl(g) at 298°K., and this together with $\Delta(H°_{298} - H°_0)$[15,22] yields 48.6 ± 0.7 kcal. mole^{-1} (2.11 ± 0.03 e.v.) for $D°_0$ of CdCl. The principal source of the estimated uncertainty is from the reaction studied here. This value of $D°_0$ compares with Gaydon's estimate of 2.0 ± 0.5 e.v.[23] and indicates that the 2.8 e.v. value obtained by a linear Birge-Sponer extrapolation[24] is too large.

A comparison of the $Cd-CdCl_2$ reaction in gaseous and liquid systems is also informative. Using the solubility data of Topol and Landis[25] a heat of reaction of 5.6_7 kcal. mole^{-1} at 1000°K. can be estimated for the presumed reaction of Cd(l) with $CdCl_2(l)$ to form an ideal solution of $Cd_2Cl_2(l)$. This combined with the heats of vaporization of Cd[15] and $CdCl_2$[14] and the heat determined for the gas phase reaction gives 83.9 kcal. mole^{-1} for $Cd_2Cl_2(l) = 2CdCl(g)$. A similar procedure yields $\Delta S°_{1000} = 51.3$ e.u. The former compares with 70.5 ± 3 kcal. mole^{-1} for $Hg_2Cl_2(l) = 2HgCl(g)$.[26,27] In principle, a comparative value of the corresponding $\Delta F°_{1000}$ could be de-

(15) D. R. Stull and G. C. Sinke, "Thermodynamic Properties of the Elements," American Chemical Society, Washington, D. C., 1956.

(16) $S°_{1000} = 85.55$ e.u. for $CdCl_2$ was calculated statistically from molecular constants given in ref. 17.

(17) L. Brewer, G. R. Somayajulu, and E. Brackett, *Chem. Rev.*, **63**, 111 (1963).

(18) K. K. Kelley, U. S. Bureau of Mines Bulletin 584, U. S. Govt. Printing Office, Washington, D. C., 1960.

(19) K. K. Kelley and E. G. King, U. S. Bureau of Mines Bulletin 592, U. S. Govt. Printing Office, Washington, D. C., 1961.

(20) J. L. Barton and H. Bloom, *J. Phys. Chem.*, **60**, 1413 (1956); **62**, 1594 (1958).

(21) H. Kuhn and S. Arrhenius, *Z. Physik*, **82**, 716 (1933).

(22) A value of 2316 cal. mole^{-1} for CdCl(g) was calculated statistically from molecular constants given in ref. 19.

(23) A. G. Gaydon, "Dissociation Energies and Spectra of Diatomic Molecules," 2nd Ed., Chapman and Hall, Ltd., London, 1953, p. 223.

(24) G. Herzberg, "Spectra of Diatomic Molecules," 2nd Ed., D. Van Nostrand Co., Inc., Princeton, N. J., 1950, p. 516.

(25) L. E. Topol and A. L. Landis, *J. Am. Chem. Soc.*, **82**, 6291 (1960).

(26) K. Newmann, *Z. Physik. Chem.*, **191A**, 284 (1942).

(27) S. J. Yosim and S. W. Mayer, *J. Phys. Chem.*, **64**, 909 (1960).

rived from the spectral measurements on liquid $CdCl_2$ saturated with Cd (Table I) with the aid of the absorptivity of CdCl calculated from the data for the gaseous equilibrium and the reported saturation limits for the melt. In practice, the aforementioned broadening of particularly the $CdCl_2$ band by Cd is so large because of the higher pressures of the components that the background correction for the CdCl bands is uncertain, or, in other words, the latter are not as well resolved as in the all-gas systems studied. Although such calculated results are in semiquantitative agreement with the gaseous systems, the spectral studies above the melts are generally not as useful for this study because of the dependence of solution composition on temperature as well as the higher pressures of the condensed components.

Finally, it would be most interesting to be able to derive thermodynamic data for the dissociation $Cd_2Cl_2(l) = 2CdCl(l)$ as well as its gas phase counterpart from the foregoing information on $Cd_2Cl_2(l) = 2CdCl(g)$. With condensation data for $InCl$[28] as a reasonable stand-in for those for CdCl, $\Delta H°_{1000}$ and $\Delta S°_{1000}$

for the liquid phase dissociation of Cd_2Cl_2 are estimated to be about 40 kcal. mole^{-1} and 3 e.u., respectively. This corresponds to $K_D = 10^{-8.1}$, in agreement with the lack of magnetic evidence for the monomer in these melts.[29] On the other hand, vaporization data for Cd_2Cl_2 necessary to consider the gaseous dissociation can only be guessed. However, if $\Delta S°_{1000}$ for this vaporization is taken to be a plausible 24 e.u., a 1% limit of detection of $Cd_2Cl_2(g)$ in the spectral studies gives a maximum value of 35 kcal. mole^{-1} for $\Delta H°_{1000}$ of the gas phase dissociation and a lower limit of 49 kcal. for vaporization of 1 mole of Cd_2Cl_2. The apparently complete dissociation in the gas phase vs. the opposite behavior in the melt thus appears to be mainly a consequence of a reasonable difference in the entropy change in the two cases, 27 vs. 3 e.u., respectively, rather than the result of any marked difference in the enthalpy.

(28) Refer to work of F. D. Rossini, et al., quoted in Table I, ref. c.

(29) N. H. Nachtrieb, J. Phys. Chem., 66, 1163 (1962).

Adsorbed Layers of Protein. I. Film Hysteresis of Ovalbumin[1]

by Laylin K. James, Jr., and John N. Labows, Jr.

Department of Chemistry, Lafayette College, Easton, Pennsylvania   (*Received November 26, 1963*)

The forces upon a rectangular wire frame have been determined during the extension and compression of the surfaces of ovalbumin solutions. The forces during extension and compression of the surface film were, in general, different and formed a hysteresis loop. The area of this loop was termed the "film hysteresis" and was determined at various pH values and in buffers of different ionic strengths. The hysteresis appears to arise from the development of viscoelastic characteristics in the surface layer.

Introduction

There exists a considerable body of information dealing with spread films or monolayers of protein, but fewer reports have appeared concerning the adsorption of proteins and, in particular, the properties of the adsorbed layer.[2,3] The purpose of the project to be described here was to attempt to gain greater insight into the nature of adsorbed films of proteins.

The experimental approach employed the technique of the laminometer of Matalon[4] which was based upon the work of Lenard and others.[5] In brief, the method involves measurement of the vertical pull upon a rectangular wire frame as it is raised progressively through and above the surface of a solution and subsequently lowered again to the initial position immediately below the surface. Lenard first showed that the meniscus which formed as the frame was raised above the surface could develop under certain conditions into a thin lamina of liquid. Matalon perfected the laminometer technique for investigating the properties of the lamina in connection with his studies of the foaming properties of solutions. He recognized that the form of the extension curve depended upon such factors as extension rate and surface tension or composition of the solution but did not present sufficiently detailed results for analysis. In the present work on ovalbumin solutions, the forces necessary to raise the wire frame and hence to extend the liquid lamina and the adsorbed films of protein stabilizing it were compared with the forces required to support the frame during its return to the original position causing compression of the surface films. We found, as Matalon did, that the forces for extension of the film were generally higher than those

during the subsequent return. Thus, the plot of force *vs.* distance for an extension–compression cycle forms a hysteresis loop. The magnitude of the area of the loop is termed the "film hysteresis." This parameter was measured for ovalbumin films of differing surface ages and from solutions of various pH values, compositions, and ionic strengths.

Experimental

The apparatus used for the film hysteresis experiments was a slightly modified Cenco duNouy interfacial tensiometer. Raising or lowering of the sample container, which changed the height of the liquid surface relative to the wire frame, was carried out manually in 0.05-cm. increments at 10-sec. intervals. (For the measurements by the ring method, the surface was extended almost continuously through a vertical distance of about 1 cm. at a rate of about 0.025 cm./sec.) Balancing of the force on the nearly stationary frame after each movement of the liquid surface was done in the usual way by manual manipulation of the torsion head with the null position of the pointer being observed with a magnifier. The sample container was closed

(1) Work supported in part by Research Grant A-4348(C1) from the National Institute of Arthritis and Metabolic Diseases, Public Health Service, Bethesda, Md.

(2) H. Neurath and H. B. Bull, *Chem. Rev.*, **23**, 391 (1938).

(3) C. W. N. Cumper and A. E. Alexander, *Rev. Pure Appl. Chem.* (Australia), **1**, 121 (1951).

(4) (a) R. Matalon, "Surface Chemistry," Butterworth's, London, 1949, p. 195; (b) *J. Soc. Cosmetic Chemists*, **3**, 216 (1952); (c) "Flow Properties of Disperse Systems," J. J. Hermans, Ed., Interscience, New York, N. Y., 1953, p. 323.

(5) (a) P. Lenard, R. V. Dallwitz-Wegener, and E. Zachmann, *Ann. Physik*, **74**, 381 (1924); (b) H. Lemonde, *J. Phys. Radium*, **9**, 505 (1938).

rather tightly during the experiment by two notched glass cover plates.

The frame was constructed of platinum wire of 19 and 22 gage with the joints sealed by epoxy cement. The length of the horizontal bar which was made of the 22 gage wire was 2.65 cm. The horizontal bar was generally raised about 1.0 cm. above the solution surface at the point of maximum extension of the lamina. No interference colors were seen for the extended protein films although they were noted in some instances with synthetic detergents.

The film hysteresis was computed by plotting the force upon the frame in dynes cm.$^{-1}$ vs. extension in cm. on graph paper. The outline of the hysteresis loop was transferred to heavy paper, cut out with scissors and weighed with the aid of a Mettler, Type H-15, analytical balance. The weight was then converted to area of the loop in units of dynes. The error in measurement of film hysteresis by this technique was $\pm 2\%$, which was much smaller than the variation between film hysteresis values found for duplicate experiments (an average of $\pm 10\%$).

The ovalbumin used was a Worthington Biochemical Corp. 2X crystallized, lyophilized, salt-free preparation. Inorganic salts were reagent grade and the buffer compositions were taken from the literature.[6] The water employed in preparing solutions was from a conventional commercial still. Water which had been further purified by demineralization with a commercial ion-exchange apparatus was rejected because unlike the ordinary distilled water, it contained film-forming contaminants when examined with the laminometer technique. Glassware was cleaned with chromic acid solution and rinsed thoroughly before using.

Solutions of ovalbumin were freshly prepared for each experiment and discarded after a single use. A uniform 30-min. period was allowed for dissolving the protein before forming the new surface. Care was taken to avoid transferring any of the surface film formed during dissolving of the protein to the dish in which the experiments were conducted. All measurements were carried out at room temperature, which ranged from 23.0 to 27.5° during the year, but which varied less than 1.0° during a single experiment.

The pendant drop apparatus was similar to others already described.[7] The drops were formed from the tip of a modified stainless steel hypodermic needle in a Pyrex optical cell. The cell was closed tightly by a polyethylene Caplug which fitted the cell neck and was pierced by a small hole for the hypodermic needle. A Hamilton gas-tight syringe was used and Apiezon L grease was employed to seal the joint between the needle and the syringe tip. Drop outlines were photo-

graphed on 35-mm. film and measurement of drop shapes was made by projection onto cross-section paper. Surface tensions were calculated by the method of the selected plane.[8]

Results and Discussion

The order of presentation will consist of a general description of the phenomenon of film hysteresis followed by data on its concentration and pH dependence. An explanation of the phenomenon will be given in terms of the flow behavior of the film and irreversibility of the adsorption process. Typical hysteresis loops
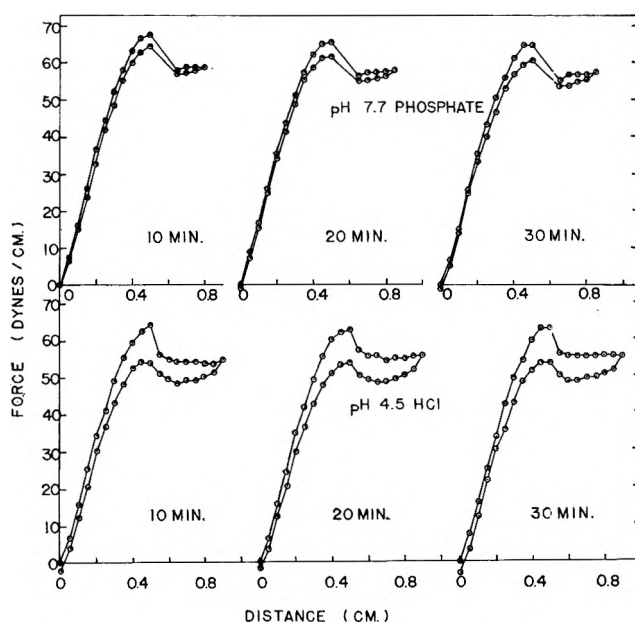

Figure 1. Typical hysteresis loops.

are shown in Fig. 1. Detailed explanations of the particular features of the curves have already been given. In general, during the upper or extension portion of the curve, the force rises to a maximum corresponding to the greatest deformation of the bulk meniscus followed by establishment of the thin lamina. This layer is extended under almost constant force up to the onset of compression. The compression curve follows the general shape of the extension portion but is displaced below it. Occasionally, with films showing lower film

(6) (a) P. Alexander and R. J. Block, "Analytical Methods in Protein Chemistry," Vol. 2, Pergamon Press, New York, N. Y., 1960, p. 202; (b) G. L. Miller and R. H. Golder, Arch. Biochem., 29, 420 (1950).

(7) L. K. James, Jr., Thesis, University of Illinois, 1958.

(8) (a) J. M. Andreas, E. A. Hauser, and W. B. Tucker, J. Phys. Chem., 42, 1001 (1938); (b) D. O. Niederhauser and F. E. Bartell, "Report of Progress—Fundamental Research on Occurrence and Recovery of Petroleum," American Petroleum Institute, Lord Baltimore Press, Baltimore, Md., 1950, p. 114.

hysteresis it was impossible to balance the force sufficiently for measurement during one or two increments of extension beyond the maximum force in the course of the cycle. In this region the film was at a critical point in the process of thinning to the lamina. Here the amount of movement necessary for balancing the force with the torsion arrangement was sufficient to vary the thickness of the lamina and hence change the force. In such cases the time sequence of extension– compression was retained, but the force was not recorded until it was again steady during measurement. The hysteresis loop was obtained by drawing straight lines between the measurable points.

The curves of Fig. 1 represent relatively high and low film hysteresis. The film on phosphate buffer, pH 7.7, gave hysteresis values of about 1.5 dynes while the sample at pH 4.5 in HCl–NaCl solution yielded about 5 dynes of hysteresis. In neither case did the form of the hysteresis loop change upon successive extension–compression cycles. This indicates that the processes taking place were generally quite reversible and could be repeated several times without collapse or rupture of the film occurring.

After the first cycle, the maximum peak height during extension was found to decrease slightly, probably due to the smaller force required to deform the film after the surface layer was saturated with adsorbed molecules during the initial compression. Often after compression the curves did not return exactly to the original starting point but fell several dynes below the original zero of force. This might reflect the incomplete desorption of excess protein from the layer during the return portion of the cycle or additionally might arise, in part, from changes in the wetting behavior of the solution on the frame. These points will be discussed subsequently.

The maximum distance of extension, of course, directly influenced the value of the film hysteresis. Generally, films were extended about 0.9 cm. above the starting point unless they were particularly unstable and did not maintain the liquid lamina sufficiently to permit such prolonged extension. Such films were extended as far as possible without causing them to break during the cycle. Generally, the weaker films were those which showed curves of return only slightly below those for extension. With regard to wetting effects, blank runs with the frame dipping into a protein solution but without a film being supported by the cross member indicated that differences in force between extension and compression of as much as 0.7–0.9 dyne/ cm. could be attributed to effects arising from nonzero contact angles during wetting and dewetting of the vertical parts of the frame. These differences were

noted for the surfaces of 0.1% ovalbumin solutions at pH 5.0 where protein adsorption was apparently at a maximum. An estimated film hysteresis of 0.7–1.0 dyne could thus arise from wetting effects alone.

Figure 2 presents data on the concentration dependence of the surface tension of ovalbumin in 0.10 ionic strength acetate buffer, pH 5.0, as measured by different techniques. Also shown is the concentration dependence of the film hysteresis at several ages of sur
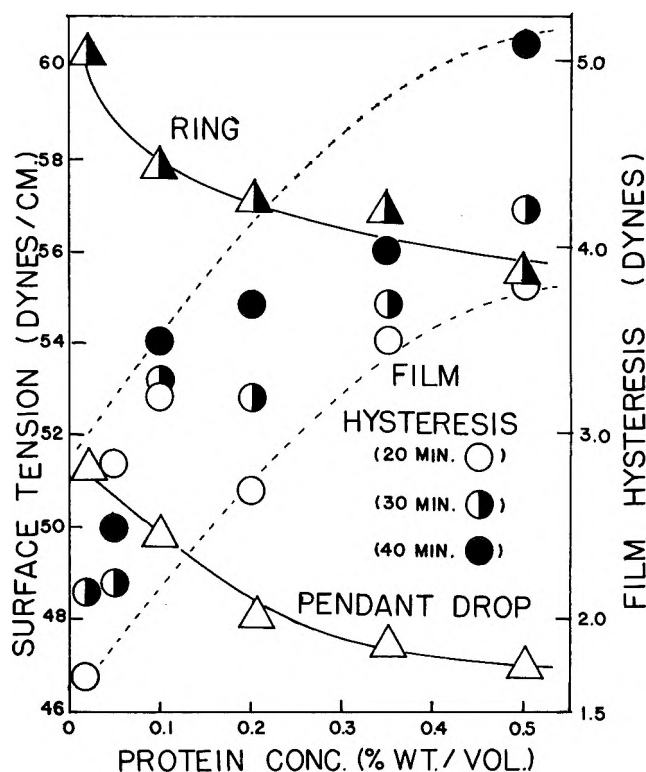

Figure 2. The concentration dependence of film hysteresis and surface tension.

face. Tensions by the ring method were measured after the final laminometer experiments upon the same surfaces. The pendant drop values are the static levels reached after relatively long undisturbed aging of the surface (ca. 1 hr.). Regardless of which method was used, the surface tension is seen to fall with increasing protein concentration although certain discrepancies are immediately apparent. The tensions obtained by the relatively static method, that of the pendant drop, are lower than the values obtained by actual detachment of a portion of the surface using the ring method. Furthermore, the differences between the values obtained by the two techniques become larger with increasing concentration of protein. The film hysteresis is seen to increase with concentration and to a slight ex

tent with repeated extensions and compressions of the surface.

The increase of film hysteresis with concentration which is observed suggests that diffusional limitations are not responsible for the higher tensions during extension of the frame. If diffusion of protein to the surface was the limiting factor in these measurements, it should become less important as the ovalbumin concentration in the bulk solution is increased.

Table I presents the results of typical measurements of the film hysteresis of 0.1% ovalbumin, in 0.1 ionic strength solutions either buffered or containing protein, dilute hydrochloric acid or sodium hydroxide, and sodium chloride. Some of the data from Table I are plotted in Fig. 3 which serves to point out several
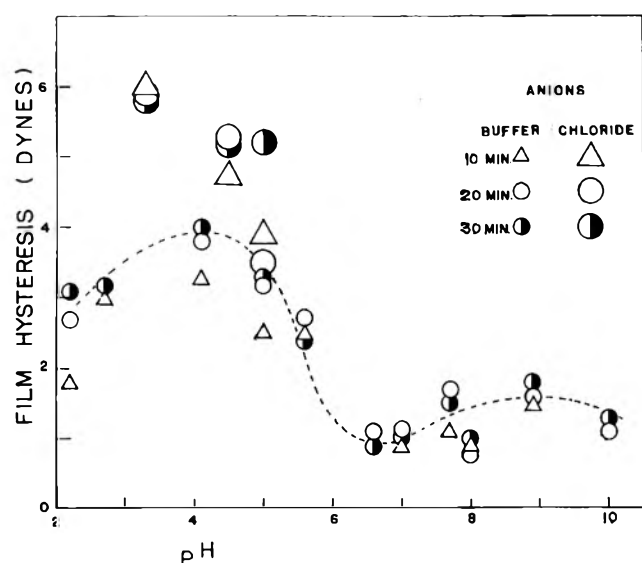
Figure 3. The pH dependence of film hysteresis of 0.1 ionic strength solutions.

interesting qualitative observations. In general, the film hysteresis is higher near the isoelectric point (ca. pH 4.6) and in acidic solutions. In these cases the film hysteresis usually increased with subsequent extension–compression cycles. The film hysteresis was found to be lower at pH values greater than 5.6 and did not show any regular behavior with subsequent cycles. Specific effects of interaction with buffer ions also seem to be present since the solutions containing only chloride as the added anion show much higher hysteresis than those containing acetate. Solutions containing phthalate are still lower in hysteresis as is reported in Table I. Table II lists the pH dependence of the film hysteresis of 0.1% ovalbumin solutions in buffers of 0.02 ionic strength. No particularly significant variations in

Table I: Film Hysteresis of 0.1% Ovalbumin Solutions, 0.1 Ionic Strength

pH	Buffer	Age of surface, min. 10	20	30	40
		Film hysteresis, dynes			
2.2	Glycine–HCl	1.8	2.7	3.1	
2.7	Glycine–HCl	3.0		3.2	2.8
4.1	Acetate	3.3	3.8	4.0	4.7
4.6	Phthalate	2.9	2.7	2.8	
5.0	Acetate	2.5	3.2	3.3	3.5
5.0	Phthalate	2.2	2.1	3.3	
5.6	Acetate	2.5	2.7	2.4	
6.6	Phosphate		1.1	0.9	
7.0	Phosphate	0.9	1.1	1.1	
7.7	Phosphate	1.1	1.6	1.5	
8.0	Veronal	0.9	0.8	1.0	
8.9	Veronal	1.5	1.6	1.7	
10.0	Glycine–NaOH		1.1	1.3	
	Unbuffered				
3.3	HCl–NaCl	6.0	5.9	5.9	6.5
4.5	HCl–NaCl	4.7	5.3	5.2	5.9
4.8	HCl–NaCl	4.9	4.9	5.9	5.8
5.0	NaOH–NaCl	3.9	3.5	5.2	4.7
10.0	NaOH–NaCl		1.2	1.1	

hysteresis are noted between pH 3.0 and 8.3. However, a rather marked fall in the property is noted at pH 10.

Table II: Film Hysteresis of 0.1% Ovalbumin Solutions, 0.02 Ionic Strength

pH	Buffer	Age of surface, min. 10	20	30	40
		Film hysteresis, dynes			
3.0	Glycine–HCl	2.8	3.2	3.5	
3.6	Glycine–HCl		2.8	2.7	3.0
4.3	Acetate	3.7		3.5	3.5
4.7	Acetate	2.3	2.4	2.9	
5.6	Acetate		3.4	3.1	
6.8	Phosphate	2.0	2.2	2.8	
7.7	Phosphate	1.9	2.0	2.3	
8.8	Veronal	2.3	2.5	2.5	2.7
10.0	Glycine–NaOH	1.3	1.5	1.3	

At this point it would seem appropriate to consider possible explanations for the phenomenon which is termed the "film hysteresis." Hysteresis phenomena with spread monolayers have been discussed in terms of aggregation within the film and interaction between aggregated and nonaggregated surface active molecules.[9] Dervichian has related hysteresis in force–area studies

(9) F. Krum, Kolloid Z., 153, 47 (1957).

of protein monolayers to time-dependent changes of molecular state with variation in area[10] and Joly[11] has given a general theory of phase transformations in monolayers.

It will be helpful first to consider the adsorbed films in this study in terms of flow characteristics. Film hysteresis might result from relaxation phenomena taking place in the surface layer during extension and compression. However, relaxation times of adsorbed films of ovalbumin do not appear to have been measured for the sorts of solvents and surface ages encountered in these experiments. With solutions of ovalbumin in distilled water relaxation times have been found to range from a few seconds to about 60 sec. depending upon the surface age and the concentration of the solution.[12]

Some laminometer experiments have been conducted so as to permit a qualitative measure of stress relaxation. In some trials the films were extended to the usual maximum extent and, immediately following the last increment of extension, motion was stopped and the force continued to be measured with time as the films remained supported upon the frame. Table III summarizes the results of this experiment. Films were from 0.1% solutions of ovalbumin in acetate buffer, pH 5.1, or phosphate buffer, pH 7.0, both of 0.1 ionic strength. As can be seen the force relaxed fairly rapidly at first and then more slowly. The form of the relaxation curve at pH 5.1 was approximately an exponential decay of force with time as predicted for viscoelastic bodies.

Table III: Stress Relaxation of Ovalbumin Solutions during Extension and Compression

Time after motion stops, sec.	Force, dynes/cm.			
	Extension		Compression	
	pH 5.1	pH 7.0	pH 5.1	pH 7.0
0	60.2	59.2	55.7	58.2
5	59.4	58.9		58.2
10			56.4	58.2
15	59.0			58.5
20		58.7	56.4	
25	58.8	58.5		58.2
40	58.6		56.0	58.0
60	58.3		55.8	

Relaxation values after the first compression were obtained in accompanying experiments on the surfaces of similar solutions. The films were extended on the laminometer in the usual way and after the first increment of compression, motion was stopped and the force

was measured against time. The force was found to be initially low, rising slightly for the solution in acetate buffer and then remaining relatively constant with time as shown in Table III.

The results of these experiments seem to indicate that the films are, indeed, viscoelastic and that relaxation occurs sufficiently slowly to become an important factor in determining the property of film hysteresis. It has been pointed out that the stress found for deformation of a viscoelastic body at constant rate of strain will be the sum of a series of partially relaxed stresses up to that instant.[13] When the forces during extension for films showing appreciable film hysteresis are examined in detail, they are often found to increase slightly during subsequent extensions in the region of the "plateau" rather than remaining constant. These increases disappear if the force is measured after 20–30-sec. intervals between extensions which permits greater time for relaxation.

Some qualitative effects of extension rate upon film hysteresis are given in Fig. 4. The hysteresis for films
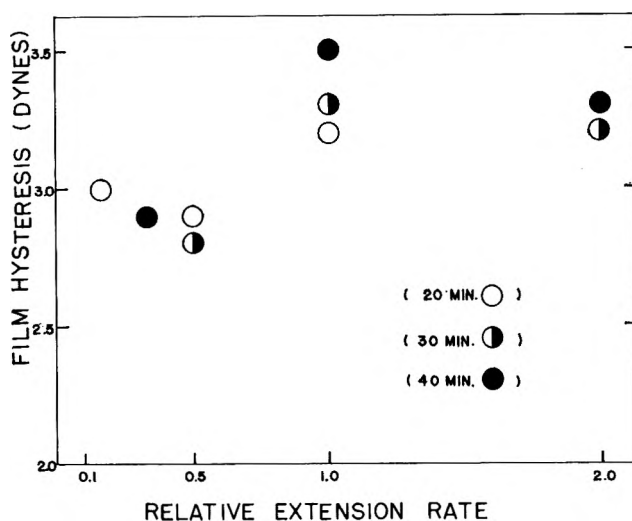
Figure 4. The effect of extension rate on film hysteresis.

of different ages is given for different rates of extension. In obtaining the results plotted in the figure, the runs at less than normal rate ($^1/_6$, $^1/_3$, $^1/_2$) were carried out with the usual increments of extension (0.05 cm.) separated by suitably increased time intervals (60, 30, or 20 instead of 10 sec.). Hence increased time was

(10) D. G. Dervichian, Kolloid. Z., 126, 15 (1952).

(11) M. Joly, J. Colloid Sci., 5, 49 (1950).

(12) H. Kimizuka, Bull. Chem. Soc. Japan, 26, 30 (1953).

(13) J. D. Ferry, "Viscoelastic Properties of Polymers," John Wiley and Sons, Inc., New York, N. Y., 1961, p. 57.

allowed for relaxation of the film between measurements and the film hysteresis was found to decrease as might be expected. At twice the normal rate, however, the film was extended or compressed twice the usual distance (0.1 cm.) each time while the usual 10-sec. interval between movements was retained. The opportunity for relaxation of the stresses in the film was thus comparable to that at normal rates of deformation of the surface and the hysteresis was not significantly changed.

The value of the film hysteresis thus seems to be calculated from forces during extension which may be elevated because of incomplete relaxation of stress while the film is extended and from forces for the return portion of the cycle which may be reduced resulting from incomplete relaxation during compression as well. The differences between the forces measured during extension and compression are thus increased as a result of the viscoelastic nature of the film and the sort of experimental method used. It is not possible at this stage to determine whether all of the film hysteresis arises from these causes, but it is likely that a major portion does.

The relatively small amount of stress relaxation found for the surfaces of solutions of ovalbumin in phosphate buffer, pH 7.0, is in qualitative agreement with the very small value of film hysteresis observed at this pH. This serves further to confirm the idea that film hysteresis has its primary origin in the development of viscoelastic properties in the films.

Another way to explain the film hysteresis might be in terms of some degree of irreversibility of the adsorption-desorption process arising from surface denaturation. That adsorption and desorption do not proceed at the same rate and that the process becomes more irreversible as aging of the surface proceeds may be seen from the following. About 30 min. is required for the static value of the surface tension (about 48 dynes/cm.) to be reached by adsorption of protein from a 0.2% solution of ovalbumin in acetate buffer, pH 5.1, as measured by the pendant drop method. If a fresh drop is aged for 2.5 min. and then reduced in volume, thus compressing the surface film on the drop, the static value is attained almost at once. If another drop is allowed to stand for 10 min. before compressing the surface by withdrawal of a portion of the drop into the capillary tip, the tension falls below the static value to about 36 dynes/cm. and rises again to about 48 dynes/cm. after 12 min. Following 90 min. of aging, withdrawal of liquid from a drop produces a low tension (about 35 dynes/cm.) with a value of only 45 dynes/cm. being reached after 10 min.

These results seem to indicate that adsorption and desorption do not proceed at the same rate and that desorption of protein proceeds more slowly as the film ages for longer periods. It is further suggested that the process may not be completely reversible if the film is aged a sufficiently long time. Of course, the retardation of desorption and eventual prevention of complete removal of protein from the surface during compression may well result from the same interactions between protein particles in the film which lead to the development of viscoelastic characteristics.

The qualitative features of the pH dependence of film hysteresis can be explained on the basis of interactions between protein molecules in the surface layer. In the isoelectric range, attractive forces between units are at a maximum due to the zero net charge on the particles accompanied by large numbers of positive and negative charges on the individual molecules. Biswas and Haydon[14] have studied the rheology of protein films at hydrocarbon–water interfaces and have found a maximum in the shear modulus at the isoelectric point. They concluded that relaxation of stress occurs mainly by rupture of hydrogen bonds and their reformation in a more relaxed state. Away from the isoelectric region expansion of molecules and repulsion of their over-all charges would reduce the attractive forces to varying degrees at different salt concentrations.

From several brief laminometer experiments which dealt with spread "monolayers," it was discovered that ovalbumin or β-lactoglobulin films spread from isopropyl alcohol–sodium acetate solutions did not show a degree of film hysteresis similar to adsorbed films until a two- or threefold excess of protein above the amount necessary to furnish 1 mg./m.^{2} of surface was added.[15] Joly and others[16] have pointed out that when molecules of protein are spread against a considerable pressure as is the case when an excess of spreading solution is added, spreading remains incomplete. This suggests that partially spread or even unspread molecules of native protein are a necessary part of the film if it is to show appreciable film hysteresis and tends to agree with the suggestion that hysteresis with spread monolayers is due to effects arising from both modified and unmodified, still surface-active molecules.[9]

Summary

The results presented here indicate that adsorbed films of ovalbumin show a hysteresis in force vs.

(14) B. Biswas and D. A. Haydon, Proc. Roy. Soc. (London), A217, 296, 317 (1963).

(15) L. K. James, Jr., unpublished observations.

(16) (a) M. Joly, Compt. rend., 208, 975 (1939); (b) D. F. Cheesman and O. Sten-Knudsen, Biochim. Biophys. Acta, 33, 158 (1958).

distance during extension and compression of the surface by the laminometer technique. The hysteresis appears to arise mainly from the development of a viscoelastic film of protein at the surface of the solution. The pH dependence of the film hysteresis can be explained, in part, on the basis of protein–protein interactions

in the film. The surface layer probably contains both denatured and undenatured protein.

Acknowledgment. The authors wish to thank Dr. John Holme of the Procter & Gamble Co., who proposed the original research program which inspired this work.

Temperature Jump Rate Studies of Polyborate Formation in

Aqueous Boric Acid[1]

by J. L. Anderson,[2] E. M. Eyring, and M. P. Whittaker

Department of Chemistry, University of Utah, Salt Lake City, Utah (*Received December 2, 1963*)

The chemical relaxation times of two boric acid polymerization equilibria in a 0.1 M aqueous $NaClO_4$ medium at 25° have been measured by the temperature jump method. Previously available equilibrium constants have been used to calculate rate constants for both polymerization reactions.

In recent papers Ingri[3-7] has reported equilibrium constants for the formation of polyborates in aqueous boric acid solutions having concentrations in the 0.01 to 0.6 M range. For total boric acid concentration c_B less than 0.01 M in a 0.1 M $NaClO_4$ medium the only important equilibrium is

$$B(OH)_3 + OH^- \underset{k_{21}}{\overset{k_{12}}{\rightleftharpoons}} B(OH)_4^- \qquad (1)$$
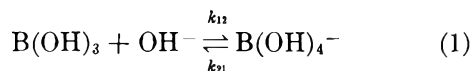
for which the equilibrium constant is[4]

$$\beta_1 = [B(OH)_4^-][B(OH)_3]^{-1}[OH^-]^{-1} =$$
$$10^{14.16-8.98} = 10^{5.18} \qquad (2)$$

since in Ingri's notation $*\beta_1 = [H^+][B(OH)_4^-] \cdot [B(OH)_3]^{-1} = 10^{-8.98}$ and $pK_w = 14.16$. Ingri's titrimetric data for $c_B = 0.01-0.20\ M$ in the pH 5 to 9 range can be satisfactorily explained in terms of only one additional species, $B_3O_3(OH)_4^-$, for which the formation equilibrium is

$$2B(OH)_3 + B(OH)_4^- \underset{k_{32}}{\overset{k_{23}}{\rightleftharpoons}}$$

$$B_3O_3(OH)_4^- + 3H_2O \qquad (3)$$
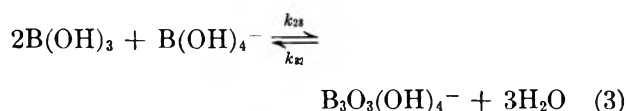
and the over-all stability constant in 0.1 M $NaClO_4$ is

$$\beta_{13} = [B_3O_3(OH)_4^-][B(OH)_3]^{-3}[OH^-]^{-\nu} =$$
$$10^{14.16-7.29} = 10^{6.87} \qquad (4)$$

In the 0.2 to 0.6 M boric acid range the additional species $B_5O_6(OH)_4^-$, $B_4O_5(OH)_4^{-2}$, and $B_3O_3(OH)_5^{-2}$ may all become important dependng upon c_B and pH.

(1) Supported in part by an equipment grant from the University of Utah Research Fund and Grant AM-06231-02 from the National Institute of Arthritis and Metabolic Diseases.

(2) National Science Foundation undergraduate summer research fellow.

(3) N. Ingri, G. Lagerström, M. Frydman, and L. G. Sillén, *Acta Chem. Scand.*, 11, 1034 (1957).

(4) N. Ingri, *ibid.*, 16, 439 (1962).

(5) N. Ingri, *ibid.*, 17, 573 (1963).

(6) N. Ingri, *ibid.*, 17, 581 (1963).

(7) N. Ingri, *Svensk Kem. Tidskr.*, 75, 199 (1963).

In the present study we have used the additional constants

$$\beta_{15} = \underline{B_5O_6(OH)_4^-}][B(OH)_3]^{-5}[OH^-]^{-1} =$$
$$10^{14.16-6.77} = 10^{7.39} \quad (5)$$

$$\beta_{24} = [B_4O_5(OH)_4^{-2}][B(OH)_3]^{-4}[OH^-]^{-2} = 10^{13.5} \quad (6)$$

$$\beta_{23} = [B_3O_3(OH)_5^{-2}][B(OH)_3]^{-3}[OH^-]^{-2} = 10^{11.7} \quad (7)$$

the latter two of which are only estimates from Ingri's boric acid constants for 0.6 M B(OH)$_4^-$ and 3.0 M NaClO$_4$ media.[3-5] The relative importance of the concentrations of various boric acid species over the 5 to 11 pH range is depicted in Fig. 1 for $c_B = 0.4\ M$.

The present study of boric acid polymerization was
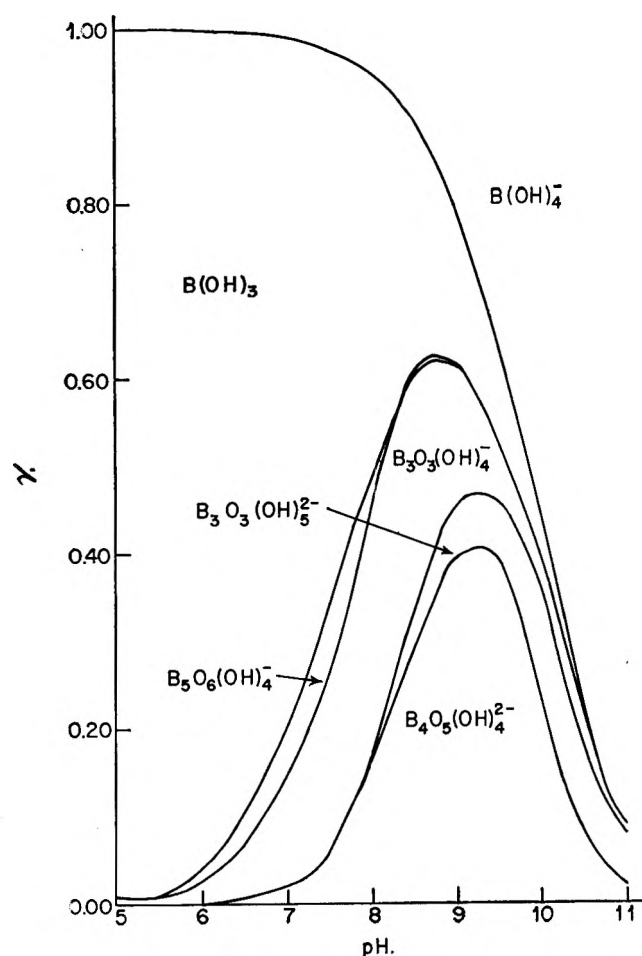
Figure 1. Distribution of boron between different ions in 0.1 M ionic strength medium (adjusted with NaClO$_4$) when total boric acid concentration $c_B = 0.40\ M$. At a given pH, the fraction of boron, γ, present as a given ion is represented by the length of a vertical line segment falling between curves.

carried out using the temperature jump relaxation method.[8,9] We are able to report over-all rate constants for two polymerization steps in aqueous boric acid.

Experimental

Weighed samples of Baker Analytical reagent grade boric acid were dissolved in doubly distilled, boiled water. The pH of the sample was adjusted with NaOH and determined with a Radiometer TTT-1 titrimeter. The ionic strength μ of each sample was made 0.1 M by the addition of concentrated NaClO$_4$. Depending upon the pH of the sample, methyl red, phenol red, cresol red, or phenolphthalein was added in a concentration not greater than $5 \times 10^{-5}\ M$ such that the optical absorbance at the appropriate wave length was in the range 0.3 to 0.8. A single beam temperature jump apparatus of the type described by Hammes and Steinfeld[10] was used to perturb the boric acid equilibria. The temperature jump from 15° to approximately 25° was effected in a few microseconds by discharging a 0.1 μf. capacitor charged to 30 kv. through the 1-ml. sample volume having a resistance of 100 ohms. The oscilloscope trace for each experiment, depicting change in optical absorbance as a function of time, was recorded photographically (see Fig. 2) and the relaxation times were obtained from such curves by looking for linearity in semilogarithmic plots of vertical deflection vs. time. To ensure the validity of our experimental results a "blank" system consisting of indicator and supporting electrolyte in the same concentrations and at the same pH was run in every case and found to give no relaxation in the time region of interest.
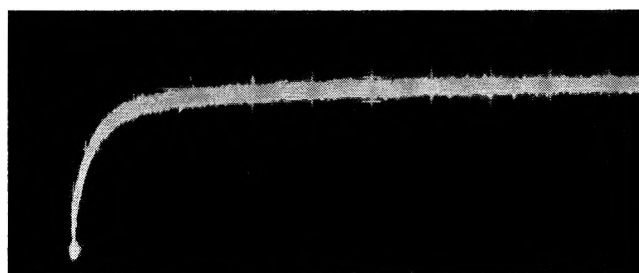
Figure 2. Oscilloscope trace displaying two relaxation times, $\tau_{32} = 0.60$ msec. and $\tau_{43} = 4.4$ msec. Total boric acid concentration $c_B = 0.5\ M$, pH = 6.1, 0.1 M ionic strength (adjusted with NaClO$_4$), 25°; the horizontal scale is 2 msec./major division; the vertical scale is in arbitrary units proportional to the absorbancy; $\lambda = 560\ m\mu$.

(8) G. Czerlinski and M. Eigen, Z. Elektrochem., 63, 652 (1959).

(9) M. Eigen and L. DeMaeyer, "Technique of Organic Chemistry," Vol. VIII, Part II, S. L. Friess, E. S. Lewis, and A. Weissberger, Ed., Interscience Publishers, New York, N. Y., 1963, Chapter 18.

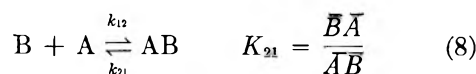(10) G. G. Hammes and J. I. Steinfeld, J. Am. Chem. Soc., 84, 4639 (1962).

Calculations

Table I presents the results of temperature jump experiments at pH 7.4. For c_B less than 0.20 M at this pH the only polyborate present in substantial amounts is $B_3O_3(OH)_4^-$. Thus there are only two coupled boric acid equilibria eq. 1 and 2 above, that must be considered in explaining the single observed relaxation time. Using von Smoluchowsky's equation for the specific rate of a diffusion-controlled reaction between one charged and one uncharged species,[11] we estimate a relaxation time for the equilibrium of eq. 1 that is much shorter than our instrument relaxation time of 10 μsec.; the predicted specific rate k_{12} is approximately 10^{10} M^{-1} sec.$^{-1}$.

Table I: Temperature Jump Data for Aqueous Boric Acid at pH 7.4

c_B,[a] M	τ_{32} (obsd.), msec.	k_{23},[b] 10^3 M^{-2} sec.$^{-1}$	τ_{32} (calcd.),[c] msec.	τ_{43} (obsd.), msec.	τ_{43} (calcd.),[d] msec.
0.06	12.9	3.22	14.6		
0.08	12.2	3.04	13.1		
0.10	11.65	2.74	11.6		
0.12	9.5	3.08	10.3		
0.14	9.0	2.89	9.2		
0.16	8.3	2.77	8.1		
0.18	8.0	2.54	7.2		
0.20	7.55	2.44	6.5		
0.30	3.6		4.6	13.5	14.6
0.40	2.8		3.5	12.8	13.0
0.50	2.4		2.9	12.5	11.9
0.60	2.0		2.5	10.0	11.5

[a] Total boric acid concentration in moles per liter. [b] Calculated using the observed τ_{32} in eq. 22. [c] Calculated using the low boric acid concentration average value of $k_{23} = 2.84 \times 10^3$ M^{-2} sec.$^{-1}$ in eq. 22. [d] Calculated using this same value of k_{23} and $k_{34} = 2.0 \times 10^2$ M^{-2} sec.$^{-1}$ in eq. 30.

Let us derive an expression for the specific rate k_{23} using the following notation: H = H^+, A = OH^-, B = $B(OH)_3$, AB = $B(OH)_4^-$, C = $B_3O_3(OH)_4^-$, D = $B_5O_6(OH)_4^-$, HIn is the acid form of the indicator (phenol red, cresol red, etc.), and In is the indicator anion where A denotes an instantaneous and $\bar{A}$ an equilibrium concentration, etc. (italic letter denotes concentration). We have not preserved Ingri's notation in its entirety because of the complicated nature of our subsequent equations. Thus in slightly basic solution we have the interdependent equilibria

$$B + A \underset{k_{21}}{\overset{k_{12}}{\rightleftharpoons}} AB \qquad K_{21} = \frac{\bar{B}\bar{A}}{\overline{AB}} \qquad (8)$$

$$2B + AB \underset{k_{32}}{\overset{k_{23}}{\rightleftharpoons}} C \qquad K_{32} = \frac{\bar{B}^2\overline{AB}}{\bar{C}} \qquad (9)$$

$$HIn + A \underset{k_{98}}{\overset{k_{89}}{\rightleftharpoons}} In \qquad K_{98} = \frac{\overline{HIn}\bar{A}}{\overline{In}} \qquad (10)$$
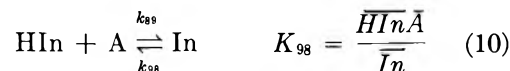
Making the safe assumption that the relaxation times of the first and third equilibria are both much shorter than that of the second, we write

$$\frac{dC}{dt} = k_{23}B^2AB - k_{32}C \qquad (11)$$

Making the substitutions $B = \bar{B} + \Delta B$, etc., and noting that

$$\frac{d(\bar{C} + \Delta C)}{dt} = \frac{d\Delta C}{dt} \qquad (12)$$

$$\frac{d\bar{C}}{dt} = 0 = k_{23}\bar{B}^2\overline{AB} - k_{32}\bar{C} \qquad (13)$$

and

$$\Delta B \Delta AB \sim 0, \text{ etc.} \qquad (14)$$

we obtain

$$\frac{d\Delta C}{dt} = k_{23}(\bar{B}^2\Delta AB + 2\bar{B}\overline{AB}\Delta B) - k_{32}\Delta C \qquad (15)$$

From the conservation equations

$$\Delta B + \Delta AB + 3\Delta C = 0 \qquad (16)$$

$$\Delta In + \Delta AB + \Delta C + \Delta A = 0 \qquad (17)$$

$$\Delta In + \Delta HIn = 0 \qquad (18)$$

for boron, charge, and indicator, respectively, it follows that

$$\Delta AB = -\frac{\Delta C}{1 + \dfrac{\Delta In + \Delta A}{\Delta AB}} = -\frac{\Delta C}{1 + \alpha} \qquad (19)$$

and

$$\Delta B = -\Delta C\left(3 - \frac{1}{1 + \alpha}\right) \qquad (20)$$

Substituting eq. 19 and 20 into eq. 15, we find that

$$\frac{d\Delta C}{dt} = -\Delta C\left[k_{23}\left(\frac{\bar{B}^2}{1 + \alpha} + 2\bar{B}\overline{AB}\left(3 - \frac{1}{1 + \alpha}\right) + K_{32}\right)\right] = -\frac{\Delta C}{\tau} \qquad (21)$$
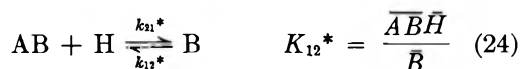
where

(11) Ref. 9, p. 1032.

$$\tau_{32} \equiv \left[k_{23} \left(\frac{\bar{B}^2}{1 + \alpha} + 2\bar{B}\overline{AB} \left(3 - \frac{1}{1 + \alpha} \right) + K_{32} \right) \right]^{-1} \quad (22)$$

is the experimental relaxation time. The factor

$$\alpha = \left(1 + \frac{\overline{HIn}}{K_{98} + \bar{A}} \right) \times$$

$$\left(- \frac{K_{32}\bar{A} + \bar{A}\bar{B}^2 + 2K_{21}\bar{B}\overline{AB}}{\dfrac{K_{32}\bar{A}\overline{HIn}}{K_{98} + \bar{A}} - 2\bar{B}^2\overline{AB} + K_{32}\bar{A}} \right) \quad (23)$$

corrects both for indicator concentration and for the fast boric acid equilibrium of eq. 8 in basic media. It may be neglected for $c_B < 0.2\ M$. The agreement between experimental and calculated relaxation times, where the latter are obtained with an average experimental $k_{23} = 2.84 \times 10^3\ M^{-2}$ sec.$^{-1}$ substituted in eq. 22, is excellent as is evident from Table I.

In acidic media the above process can be repeated using

$$AB + H \underset{k_{12}^*}{\overset{k_{21}^*}{\rightleftarrows}} B \qquad K_{12}^* = \frac{\overline{AB}\bar{H}}{\bar{B}} \quad (24)$$

and

$$H + In \underset{k_{89}^*}{\overset{k_{98}^*}{\rightleftarrows}} HIn \qquad K_{89}^* = \frac{\overline{HIn}}{\overline{HIn}} \quad (25)$$

in place of eq. 8 and 10. The resulting expression for τ is identical with eq. 22 except that α now denotes

$$\alpha = \left(1 + \frac{\overline{In}}{K_{89}^* + \bar{H}} \right) \times$$

$$\left(- \frac{K_{32}K_{12}^* + K_{12}^*\bar{B}^2 + 2\bar{B}\overline{AB}\bar{H}}{K_{12}^*K_{32} \left(1 + \dfrac{\overline{In}}{K_{89}^* + \bar{H}} \right) - 2\bar{B}\overline{AB}^2} \right) \quad (26)$$

Agreement between observed and calculated values of τ_{32} is good over the 5 to 8 pH range using the average values of k_{23} at the respective pH values given in Table II. For higher boric acid concentrations in the range $c_B = 0.3$ to $0.6\ M$ and pH 7.4 another equilibrium

$$2B + C \underset{k_{43}}{\overset{k_{34}}{\rightleftarrows}} D \qquad K_{43} = \frac{\bar{B}^2\bar{C}}{\bar{D}} \quad (27)$$
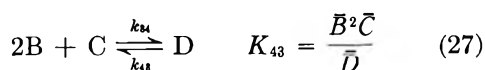
must be added to eq. 8, 9, and 10 to account for a second observed relaxation time. From the revised rate expressions

$$\frac{d\Delta C}{dt} = k_{23}(\bar{B}^2\Delta AB + 2\bar{B}\overline{AB}\Delta B) - k_{32}\Delta C +$$

$$k_{43}\Delta D - k_{34}(\bar{B}^2\Delta C + 2\bar{B}\bar{C}\Delta B) \quad (28)$$

Table II: Over-all Rate Constants for Boric Acid Polymerization as a Function of pH

pH	k_{23}, M^{-2} sec.$^{-1}$	k_{34}, M^{-2} sec.$^{-1}$
5	4×10^4	
6	7.6×10^3	4.8×10^2
7.4	2.8×10^3	2.0×10^2
8	3.2×10^3	
9	3.2×10^3	
10	3.6×10^3	

$$\frac{d\Delta D}{dt} = k_{34}(\bar{B}^2\Delta C + 2\bar{B}\bar{C}\Delta B) - k_{43}\Delta D$$

and the revised conservation relations

$$\Delta AB + \Delta A + \Delta C + \Delta D + \Delta In = 0$$

$$\Delta AB + \Delta B + 3\Delta C + 5\Delta D = 0 \quad (29)$$

$$\Delta HIn + \Delta In = 0$$

we obtain the relaxation times

$$\frac{1}{\tau_{32,43}} =$$

$$\frac{-(a_{11} + a_{22}) \pm \sqrt{(a_{11} + a_{22})^2 - 4(a_{11}a_{22} - a_{12}a_{21})}}{2}$$

$$(30)$$

using a standard method[12] where in this particular case

$$a_{11} = -k_{23} \left(\frac{\bar{B}^2}{1 + \alpha'} + \frac{4 + 6\alpha'}{1 + \alpha'} \bar{B}\overline{AB} + K_{32} \right) -$$

$$k_{34} \left(\bar{B}^2 - \frac{4 + 6\alpha'}{1 + \alpha'} \bar{B}\bar{C} \right)$$

$$a_{12} = -k_{23} \left(\frac{\bar{B}^2}{1 + \alpha'} + \frac{8 + 10\alpha'}{1 + \alpha'} \bar{B}\overline{AB} \right) +$$

$$k_{34} \left(\frac{8 + 10\alpha'}{1 + \alpha'} \bar{B}\bar{C} + K_{43} \right) \quad (31)$$

$$a_{21} = k_{34} \left(\bar{B}^2 - \frac{4 + 6\alpha'}{1 + \alpha'} \bar{B}\bar{C} \right)$$

$$a_{22} = -k_{34} \left(\frac{8 + 10\alpha'}{1 + \alpha'} \bar{B}\bar{C} + K_{43} \right)$$

The symbol α' denotes a correction factor that is substantially more complicated than eq. 23. For pH 7.4 it is negligible. However in acidic media where α' takes the form

(12) Ref. 9, p. 910.

$$\alpha' = -\left(\frac{\overline{In}}{\overline{H} + K_{89}{}^*} + 1\right) \times$$

$$\left(\frac{K_{12}{}^*K_{32}K_{45} + K_{12}{}^*K_{43}\overline{B}^2 + 2K_{43}\overline{B}\overline{AB}\overline{H} + 2K_{32}\overline{CB}\overline{H} + K_{12}{}^*\overline{B}^4 + 2\overline{B}^3\overline{AB}\overline{H}}{K_{12}{}^*K_{32}K_{43}\left(1 + \dfrac{\overline{In}}{\overline{H} + K_{89}{}^*}\right) - 2K_{43}\overline{B}\overline{AB}^2 - 2K_{32}\overline{CB}\overline{AB} - 2\overline{B}^3\overline{AB}^2}\right)$$

it becomes significant for pH 5 and 6, particularly for the lower boric acid concentrations.

Conclusions

Since over the 5 to 9 pH range the predominant polyborate species at low boric acid concentration is B_3O_3-$(OH)_4{}^-$, it is always possible to calculate the over-all rate constant k_{23} from the single observed relaxation time. The agreement of k_{23} over a range of values of c_B at a given pH is always good, and there is no significant pH dependence of k_{23} in the alkaline range (see Table II). The appreciable rise of k_{23} with increasing acidity suggests, however, that homogeneous acid catalysis may affect one or more of the intermediate steps in the over-all process. The word "over-all" deserves emphasis: one conceivable, though by no means unique, mechanistic explanation for the forward reaction of eq. 3 involves three discrete bimolecular steps. Unfortunately, we have too little information to estimate specific rates of individual steps in the manner adopted by Eigen and Kustin[13] for the case of halogen hydrolysis.

In the 5 to 7 pH range the second most concentrated boric acid polymer is $B_5O_6(OH)_4{}^-$ and the species B_3O_3-$(OH)_5{}^{-2}$ and $B_4O_5(OH)_4{}^{-2}$ can be neglected. Good

agreement between experimental and theoretical relaxation times τ_{43} (see Table I) is obtained at several concentrations at pH 7.4 using $k_{23} = 2.84 \times 10^3\,M^{-2}\,\text{sec.}^{-1}$ and $k_{34} = 2.0 \times 10^2\,M^{-2}\,\text{sec.}^{-1}$. No significance can be attributed to the difference in values of k_{34} at pH 6 and 7.4. A second experimental relaxation time is not observed reproducibly at pH 5.

Temperature jump results obtained in the 8 to 11 pH range at the higher boric acid concentrations illustrate the principal limitation of relaxation spectrometry. Although Ingri's equilibrium data indicate that B_3O_3-$(OH)_4{}^-$, $B_3O_3(OH)_5{}^{-2}$, and $B_4O_5(OH)_4{}^{-2}$ species are all present in significant concentration at $c_B = 0.4\,M$ (see Fig. 1), never more than one relaxation time is clearly distinguishable in the 10 μsec. to 1 sec. range of the instrument at pH 8 or above. We are therefore unable even to estimate over-all rate constants for formation of the species $B_3O_3(OH)_5{}^{-2}$ and $B_4O_5(OH)_4{}^{-2}$.

Ingri's inferences regarding equilibrium species are confirmed conclusively by our rate experiments only in the pH 6 region where two of the predicted three relaxation times are measurable and the third is virtually certain to be too short for detection with our equipment. The unobservability of multiple relaxation times in the 8 to 11 pH range for $c_B = 0.2$ to $0.6\,M$ cannot be construed as evidence for or against the existence of such species as $B_3O_3(OH)_5{}^{-2}$ and $B_4O_5(OH)_4{}^{-2}$.

(13) M. Eigen and K. Kustin, *J. Am. Chem. Soc.*, **84**, 1355 (1962).

Mechanism of the Pyrolysis of Propylene: The Formation of Allene

by Akira Amano and Masao Uchiyama

The Department of Applied Chemistry, Tohoku University, Sendai, Japan   (Received December 2, 1963)

Based on the evaluation of reaction rates of a number of related elementary reactions, the following free-radical chain mechanism is proposed for the pyrolysis of propylene at the conditions under which ordinary cracking reactions are practiced: $C_3H_6 \to$ allyl $+$ H, H $+$ $C_3H_6 \to$ n-propyl*, H $+$ $C_3H_6 \to$ H_2 $+$ allyl, n-propyl* $\to$ C_2H_4 $+$ methyl, methyl $+$ $C_3H_6 \to$ CH_4 $+$ allyl, allyl $+$ $C_3H_6 \to$ polymer $+$ H, allyl $\to$ C_3H_4 $+$ H, allyl $+$ methyl $\to$ C_4H_8, and allyl $+$ H $\to$ C_3H_6. The proposed mechanism reveals the existence of two distinctly different reaction zones. At lower temperatures and higher propylene pressures, the reaction is characterized by the formation of higher boiling materials and it obeys three-halves-order rate law. At higher temperatures and lower pressures, however, the formation of allene becomes important and the reaction obeys first-order rate law. Consistent results are obtained for each of the zones mentioned when existing data are critically analyzed for both product distributions and reaction rates in terms of the proposed mechanism. The analysis also indicates that the value of 78 kcal./mole formerly assigned for D(allyl–H) may be in error by a considerable amount. The formation of allene by a severe pyrolysis is discussed quantitatively resulting in a good agreement with observations reported recently.

Introduction

Although the pyrolysis of propylene has been a subject of many modern investigations, a number of controversial views have been raised for reaction mechanism depending on their experimental results obtained at different reaction conditions. According to Szwarc[1] the reaction was first order and its main products were allene, ethylene, and methane; whereas according to Laidler and Wojciechowski[2] it was three-halves order with no evidence of the allene formation. The disagreement such as typified above is inherent in the olefin pyrolysis in which decomposition and polymerization are simultaneously taking place in varying proportions according to the conditions used.

In the present paper, certain elementary free-radical reactions are selected on the light of the values of A-factor and activation energy for a number of related elementary reactions which have been discussed in our recent paper.[3] Table I shows the values of those kinetic parameters upon which the present discussion is based.

The mechanism consisting of the selected elementary reactions is capable of elucidating both decomposing and polymerizing phases of the pyrolysis. It thus offers in the most unified manner an explanation of the propylene pyrolysis at cracking temperatures ranging from 550 to 900°. The mechanism is then tested for both product distributions and reaction rates hitherto reported with special reference to the formation of allene.

Pyrolysis

Generalized Mechanism. Based on the evaluation of reaction rates using those kinetic parameters listed in Table I, the following reactions can be selected in a broad range of the ordinary cracking conditions.

$$C_3H_6 \longrightarrow \text{allyl} + H \qquad (1)$$

$$H + C_3H_6 \longrightarrow n\text{-propyl*} \qquad (5)$$

$$H + C_3H_6 \longrightarrow H_2 + \text{allyl} \qquad (6)$$

$$n\text{-propyl*} \longrightarrow C_2H_4 + \text{methyl} \qquad (7)$$

$$\text{methyl} + C_3H_6 \longrightarrow CH_4 + \text{allyl} \qquad (11)$$
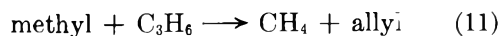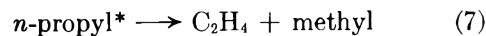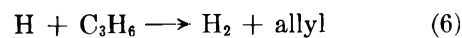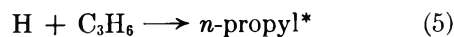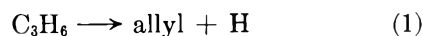
(1) M. Szwarc, *J. Chem. Phys.*, **17**, 284 (1949).

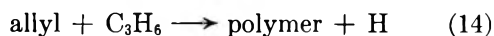(2) K. J. Laidler and B. W. Wojciechowski, *Proc. Roy. Soc.* (London), **A259**, 257 (1960).

(3) A. Amano and M. Uchiyama, *J. Phys. Chem.*, **67**, 1242 (1963).

Table I: Kinetic Parameters of Related Elementary Reactions[a]

Reactions		log A[b]	E, kcal./mole
$C_3H_6 \rightarrow$ allyl $+$ H	(1)	(15)	99.2 $- Q^c$
$C_3H_6 \rightarrow$ vinyl $+$ methyl	(2)	(15.6)	91.0
$2C_3H_6 \rightarrow$ allyl $+$ propyl	(4)	(8.5)	62.5 $- Q^c$
H $+$ $C_3H_6 \rightarrow$ n-propyl	(5)	10.1	1.5
H $+$ $C_3H_6 \rightarrow$ H_2 $+$ allyl	(6)	9.7	1.5
n-Propyl $\rightarrow$ C_2H_4 $+$ methyl	(7)	13.4	30.4
n-Propyl $\rightarrow$ C_3H_6 $+$ H	(8)	14.1	38.4
n-Propyl $\rightarrow$ H_2 $+$ allyl	(9)	(13)	(30)
Methyl $+$ $H_2 \rightarrow$ CH_4 $+$ H	(10)	8.7	10
Methyl $+$ $C_3H_6 \rightarrow$ CH_4 $+$ allyl	(11)	7.8	7.7
Methyl $+$ $C_3H_6 \rightarrow$ butyl	(12)	9.0	8.8
Allyl $+$ $H_2 \rightarrow$ C_3H_6 $+$ H	(13)	7.9	7.3 $+ Q^c$
Allyl $+$ $C_3H_6 \rightarrow$ polymer $+$ H	(14)	(6)	(15)
Allyl $\rightarrow$ C_3H_4 $+$ H	(15)	13.2	50.2 $+ Q^c$
2 allyl $\rightarrow$ diallyl	(16)	(7)	(0)
Allyl $+$ methyl $\rightarrow$ C_4H_8	(17)	(8)	(0)
Allyl $+$ H $\rightarrow$ C_3H_6	(18)	(9)	(0)

[a] The values in parentheses are those which are less accurate. [b] Units are sec.$^{-1}$ for unimolecular reactions and l./mole sec. for bimolecular reactions. [c] Q denotes the stabilization energy in allyl radical.

$$\text{allyl} + C_3H_6 \longrightarrow \text{polymer} + H \qquad (14)$$

$$\text{allyl} \longrightarrow C_3H_4 + H \qquad (15)$$

$$\text{allyl} + \text{methyl} \longrightarrow C_4H_8 \qquad (17)$$

$$\text{allyl} + H \longrightarrow C_3H_6 \qquad (18)$$
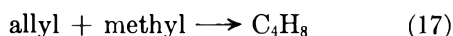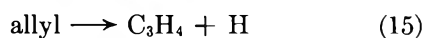
The asterisk indicates a *hot* radical. In the present case, the n-propyl radical produced by reaction 5 has an excess energy of about 35 kcal./mole corresponding to the amount of heat evolved by the reaction. The excess energy can then be utilized in part for its subsequent decomposition (reaction 7). Characteristic features of the *hot* n-propyl radical have been described in our recent paper.[3] The proposed scheme is a free-radical chain mechanism in which the chain is initiated by reaction 1 and terminated by reaction 17 and/or reaction 18.

In the above scheme, reaction 14 and reaction 15 are competing in propagating the chain. The former reaction represents the polymerization, whereas the latter the decomposition to form allene. The relative importance between these two reactions will be determined by the ratio $k_{15}/k_{14}(C_3H_6)$ and hence by both temperature and pressure at which the pyrolysis is studied. The ratio can be calculated by using the values of kinetic parameters assigned for these reactions assuming $Q = 20$ kcal./mole. As is illustrated in Fig.

1, the two zones characterized by the polymerization and the decomposition are separated by a smooth curve corresponding to $2k_{15} = k_{14}(C_3H_6)$ on the pressure-temperature diagram. The curve shifts toward the left on the diagram if smaller values are assumed for Q. Included in Fig. 1 are points corresponding to the conditions under which actual runs were carried out by a number of investigators to indicate that most of the studies were confined within the low temperature polymerization zone.

Low Temperature Zone. The mechanism of the pyrolysis in this temperature range can be obtained if reaction 15 is ignored in relation with reaction 14 in our generalized mechanism proposed above. A similar mechanism was proposed by Laidler and Wojciechowski[2] although they included reaction 9 instead of reaction 6. These two reactions are kinetically indistinguishable. Kinetic data available to test the proposed mechanism include those reported by Ingold and Stubbs,[4] Laidler and Wojciechowski,[2] Amano and Uchiyama,[3] and by Szwarc[1] for his runs carried out at lower temperatures (Fig. 1).
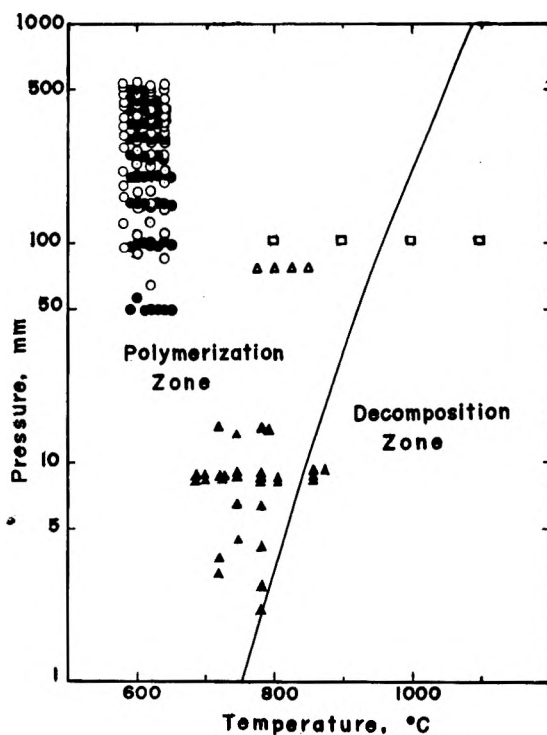

Figure 1. Pressure-temperature diagram: solid line, $2k_{15} = k_{14}(C_3H_6)$; empty circles, Laidler and Wojciechowski; filled circles, Ingold and Stubbs; empty triangles, Amano and Uchiyama; filled triangles, Szwarc; squares, Kunichika and Sakakibara.

(4) K. U. Ingold and F. J. Stubbs, *J. Chem. Soc.*, 1749 (1951).

Assuming the relation $k_5 = 0.4k_6$ reported by Darwent and Roberts,[5] the over-all stoichiometry of the proposed scheme can be expressed by the equation

$$3.8(C_3H_6) \longrightarrow 0.4(H_2) + (CH_4) + (C_2H_4) + \text{polymer}$$
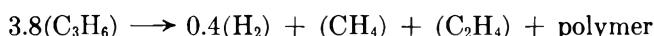
Laidler and Wojciechowski[2] reported that the amounts of hydrogen, methane, and ethylene formed were in the ratio of approximately 1:2:2, which is in good agreement with the product distribution expected from the equation. The similar product distribution has been reported in numerous other works. Since the amount of higher boiling products in the above equation corresponds to 1.4 moles of C_6 hydrocarbons, about 74% of the carbon atoms produced by the pyrolysis should be recovered in the higher boiling fraction. This was experimentally observed to be 50–70% by Ingold and Stubbs[4] and 30–55% by Laidler and Wojciechowski. The discrepancy may be caused by either the subsequent decomposition of the higher boiling materials or the coke formation.

By applying steady-state approximation to the proposed scheme, two different over-all rate expressions can be obtained depending on the mode of termination. If the chain part of the reaction is controlled by reaction 11 and is therefore terminated by reaction 17 (case I), the over-all rate of propylene consumption can be expressed by the equation

$$-\mathrm{d}(C_3H_6)/\mathrm{d}t = (361k_1k_{11}k_{14}/35k_{17})^{1/2}(C_3H_6)^{3/2}$$

If, on the other hand, propagation of the chain is controlled by reaction 5 and terminated by reaction 18 (case II), the rate can be expressed by the equation

$$-\mathrm{d}(C_3H_6)/\mathrm{d}t = (361k_1k_5k_{14}/35k_{18})^{1/2}(C_3H_6)^{3/2}$$

The reaction is thus, in agreement with Laidler and Wojciechowski,[2] three-halves order independent of the mode of termination.

In analyzing their data on the premise of first-order kinetics, Ingold and Stubbs[4] stated that the reaction order gradually changed from first to second as the initial pressure was decreased. By recasting raw data reported by Ingold and Stubbs to log (rate) vs. log (initial pressure) relationship, however, parallel straight lines are obtained for six different temperatures studied. This is illustrated in Fig. 2. Since the slope of these lines corresponds to about 1.4, their results can also be taken to indicate the three-halves-order reaction.

Szwarc[1] and Amano and Uchiyama[3] have also calculated rate constants at temperatures ranging from 680 to 870° assuming the reaction to be first order. As has already been discussed, however, most of these runs were carried out in the range of conditions where
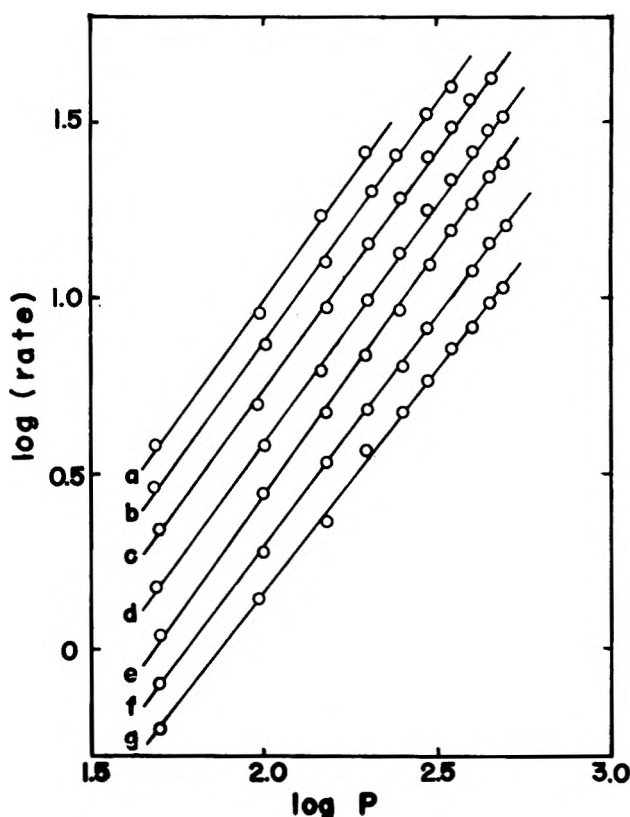
Figure 2. log (rate, mm./min.) vs. log (initial pressure, mm.) relationship: a, 650°; b, 640°; c, 630°; d, 620°; e, 610°; f, 600°; g, 590°.

the order of the reaction should effectively be three-halves. As will be seen later, an excellent fit to the Arrhenius equation is in fact obtained when the values of their first-order rate constants are readjusted for the three-halves-order rate law.

A further support for the proposed rate law can be obtained, if kinetic data reported by Szwarc[1] in his runs at 780° are used to calculate the rate constants. The values calculated are compared with the original figures in Table II. As was pointed out by Szwarc, there is a definite trend in the values of the Szwarc's constant (k_1) with respect to the change in initial pressure. The values of three-halves-order rate constant ($k_{3/2}$) are more consistent. Three runs reported by Szwarc at pressures below 5 mm. are intentionally omitted from the list of the table, since they belong to the borderline case.

Illustrated in Fig. 3 are the Arrhenius plots of the three-halves-order rate constants obtained from the four different sources discussed above. The solid

(5) B. deB. Darwent and R. Roberts, Discussions Faraday Soc., 14, 55 (1953).

Table II: Comparison between First-Order and Three-Halves-Order Rate Constants

Run	Pressure, mm.	Contact time, sec.	Conversion, %	$k_1 \times 10^2$, sec.$^{-1}$	$k^3/_2$, l./mole sec.
15	6.3	0.580	0.86	14.8	1.41
9	8.2	0.144	0.21	14.8	1.25
11	8.3	0.144	0.23	15.8	1.53
14	11.3	0.448	0.88	19.7	1.52
10	14.4	0.124	0.25	19.9	1.21

lines in Fig. 3, corresponding to the theoretical rate equations derived from the proposed mechanism, would indicate a general agreement between observed and calculated rates. Because of a better fit to the experiments, the case I mechanism is favored at present.

High Temperature Zone. At higher temperatures and lower pressures, unimolecular decomposition of allyl radical becomes increasingly important. The mechanism in the decomposition zone can be obtained when reaction 14 is ignored in relation with reaction 15 in our generalized mechanism. The resulting mechanism also involves a free-radical chain
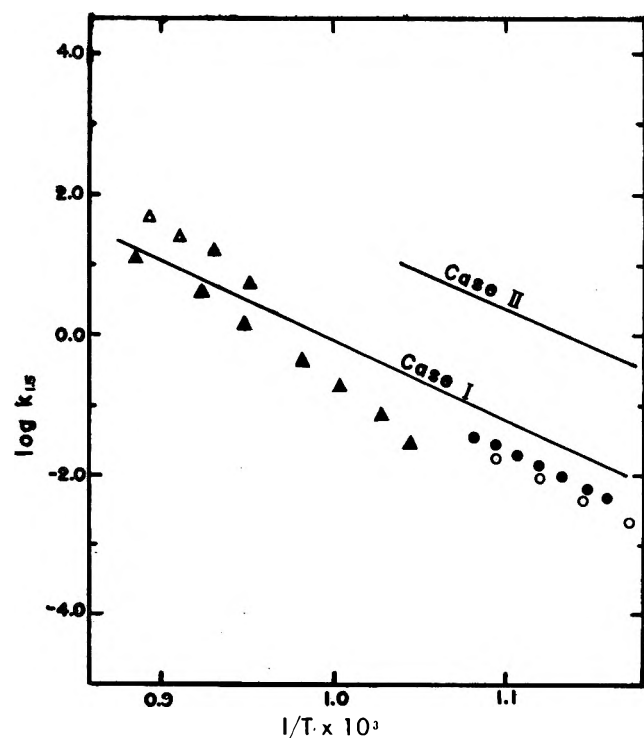
Figure 3. Arrhenius plots of the three-halves-order rate constants: empty triangles, Amano and Uchiyama; filled triangles, Szwarc; empty circles, Laidler and Wojciechowski; filled circles, Ingold and Stubbs.

and is characterized by the formation of an appreciable amount of allene as is indicated by the over-all stoichiometric relation

$$2.4(C_3H_6) \rightarrow 0.4(H_2) + (CH_4) + (C_2H_4) + 1.4(C_3H_4)$$

By applying steady-state approximation to the above mechanism, the following rate equation can be obtained.

$$-d(C_3H_6)/dt = (144k_1k_5k_{15}/35k_{18})^{1/2}(C_3H_6)$$

Thus the mechanistic transition from the low to the high temperature zones is reflected in the change of the reaction order. As can be seen in Fig. 1, data available to test the proposed high temperature mechanism are scarce. Furthermore such a simplified mechanism is only practicable in a limited temperature range. At temperatures exceeding about 900°, the splitting of propylene to vinyl and methyl radicals may become important and a large number of secondary reactions will also be involved.

In agreement with the above stoichiometry, Szwarc[1] reported that hydrogen, methane, ethylene, and allene were formed in the mole ratio of approximately 1:2:2:3 for the products obtained at about 860° and 8 mm. In spite of this agreement, our criticism to his paper lies in the fact that Szwarc analyzed his data covering a temperature as low as 680° based exclusively on the first-order rate equation. All the experimental runs, except those at his highest temperature mentioned above, were made at conditions where the three-halves-order rate equations should be used. The applicability of the latter rate law has been demonstrated by the linear plots illustrated in Fig. 3.

At 857°, which is well within the decomposition zone, the first-order rate constant recorded by Szwarc[1] was 0.13 sec.$^{-1}$, while the theoretical value based on our equation is found to be 2.5 sec.$^{-1}$. It should be noted that the kinetic analysis given by Szwarc was based on data obtained at contact times of about 0.12–0.15 sec. which are not much longer than the induction period (*ca.* 0.03 sec. at 850°) observed by Amano and Uchiyama.[3] The omission of the induction period in Szwarc's treatment as well as the overestimation of Q in our calculation may be major factors of the discrepancy between observed and theoretical rate constants. By the reasons described above, the value of 78 kcal./mole assigned by Szwarc for the bond dissociation energy between allyl radical and hydrogen atom is somewhat doubtful. The latest figure suggested is about 84 kcal./mole.[6]

(6) S. W. Benson, A. N. Bose, and P. Nangia, *J. Am. Chem. Soc.*, **85**, 1388 (1963).

Recently Kunichika and Sakakibara[7] observed appreciable amounts of allene and methylacetylene in the reaction products at 100 mm. and temperatures ranging from 800 to 1400°. Although both the low and the high temperature mechanisms are working simultaneously under the given conditions, the amount of allene expected in the products can be calculated by using two stoichiometric equations and the ratio $k_{15}/k_{14}(C_3H_6)$ assuming $Q = 20$ kcal./mole. The amount of allene calculated in the manner described above is listed in the second column of Table III for three different temperatures. Those observed values, also listed in the last column of the table, are the sum of allene and methylacetylene. A reasonable agreement is observed between the observed and the calculated values at lower temperatures at which any serious mechanistic complications are not expected. At the highest temperature listed, however, the amount of allene observed becomes considerably less than that calculated by the present mechanism. The discrep-

Table III: Formation of Allene at Varying Temperatures

Temp., °C.	Allene formed/propylene consumed, mole %	
	Calcd.	Obsd.
800	8	12–15
900	36	29
1000	54	30–34

ancy may be caused by the complication in the mode of initiation as well as the involvement of secondary reactions which would consume unsaturated compounds.

(7) S. Kunichika and Y. Sakakibara, 14th Annual Meeting of the Chemical Society of Japan, April, 1961; private communications.

Nucleation in Silver Bromide Precipitation

by C. R. Berry and D. C. Skillman

Research Laboratories, Eastman Kodak Company, Rochester, New York   (*Received December 4, 1963*)

Crystals formed during the first few seconds of silver bromide precipitation were examined in the electron microscope. Under those conditions where crystals smaller than 500 Å. in cube-edge length were formed, measurements of turbidity were also used to give information on the crystal size and the rate of change of size on standing. The turbidity measurements gave somewhat smaller values of size than the electron microscope and reasons are given why the smaller values are probably more reliable. Many precipitation variables were examined by the light-scattering method, which gives results with more facility than that using the electron microscope. A minor disadvantage of the turbidity measurements was that only an average crystal size could be obtained, however. At 50°, nuclei were produced by a double-jet scheme which were of about 275 Å. edge length. Lowering the temperature to 40° or having an excess of about 0.002 M potassium bromide decreased the nucleus volume by a factor of two. Adding 0.2 N ammonium hydroxide before precipitation increased the nucleus volume by about 200 times. Quantitative considerations of the data emphasize the fast rates at which some of the growth processes occur. The results are quite different from those obtained in homogeneous precipitation in dilute systems.

Introduction

In earlier reports[1] details were given of the structure, growth rates, and size distributions of silver bromide microcrystals precipitated in gelatin. Perfect crystals and singly and doubly twinned crystals were identified which were bounded by {200} faces, except when there was an excess of bromide ion producing {111} surfaces. During most of the precipitation time, only growth occurred, and the size distribution became more monodisperse with continued growth. The rate of volume increase of a crystal in the distribution was proportional to its surface area, except for the doubly twinned crystals which grew somewhat more rapidly. The object of the present work was to examine the sizes of crystals formed during the first few seconds of these fast precipitations.

According to the usual thermodynamic treatment for the formation of nuclei from ions in solution, the critical radius for stability is given by $r_0 = -2\gamma/\Delta G_v$, where γ is the specific surface energy and ΔG_v is the free energy of solution. A stable nucleus in this sense means that beyond a certain size of crystal, an ion added to the crystal causes a net decrease in

energy because the increase in surface energy is more than counterbalanced by the decrease in volume energy. For a crystal smaller than the critical size, the added ion increases the total energy. On this basis the critical radius for AgCl is only a few Ångstrom units. Experimentally, a value for the stable nucleus size in AgCl has been estimated from conductometric measurements by Klein, Gordon, and Walnut[2] to consist of five ions. The measurements were made in homogeneous systems where the chloride ion was slowly produced from hydrolysis of allyl chloride, and nucleation did not begin until about 100 min. had elapsed.

In the cases of both silver chloride and silver bromide, the thermodynamic values of nucleus size do not apply at all to fast precipitations, where the measurements indicate far larger sizes. On this account, it may be argued that for fast precipitations there is no nucleation process as ordinarily defined. However, the term "nucleation" has been frequently used in the literature in referring to fast precipitation, and we will use it to

(1) C. R. Berry and D. C. Skillman, *J. Appl. Phys.*, **33**, 1900 (1962); *Phot. Sci. Eng.*, **6**, 159 (1962); *J. Phys. Chem.*, **67**, 1827 (1963).

(2) D. H. Klein, L. Gordon, and T. H. Walnut, *Talanta*, **3**, 187 (1959).

refer to that part of the crystallization process where the number of new crystals is increasing at a rapid rate while the average size of the crystals present changes only slowly.

Measurements were made with the electron microscope, and for the smaller crystals (cubes with edge lengths less than 0.05 μ) the size was also determined from the turbidity. Since earlier comparisons of sizes of crystals in the range of 0.1 to 1.0 μ, when calculated from measurements of the turbidity and from electron micrographs, gave good agreement,[3,4] we have much confidence in the absolute value of sizes determined from the turbidity. The Rayleigh and Mie theories of light scattering are apparently obeyed quite closely for silver bromide suspensions, even when the suspensions are quite concentrated.[4] When the crystal size is less than 0.05 μ, the values of turbidity are undoubtedly more reliable than those from the electron micrographs because the time elapsed between precipitation and sampling is so small. Several difficulties are encountered in using the electron microscope for accurate size measurements of the very small crystals. Replication cannot be used because the thickness of the replica is confusing. Some photolysis inevitably occurs (with an unrefrigerated sample stage). The apparent crystal size may vary with the precision of focus of the electron microscope and with the photographic exposure in the electron microscope and in the printing process.

The onset of nucleation occurs so soon after the start of a precipitation and the amount of crystalline material present is so small that we have not made direct measurements of the size and number of nuclei present until after 3 sec. had elapsed. However, it is possible to use related published information to construct an approximate model of the first instants of precipitation.

Consider first the time required to build up the concentrations of silver and bromide ions so that nucleation may begin. Davies and Jones[5] have measured conductometrically the conditions for slow nucleation of AgCl and observed spontaneous nucleation when the product of the ionic concentrations is 1.7 times the solubility product. Assume that nucleation of AgBr begins when the product of the ionic concentrations is about twice the solubility product. The time required to achieve this concentration in a typical case may be obtained from the following data: a total of 11.1 g. of silver bromide is precipitated in 15 min. at 50° in a vessel originally containing 100 ml. of gelatin solution. Since the solubility product of silver bromide at 50° is given by Gledhill and Malan[6] as 7.5 × 10⁻¹² mole²/l.², it will require only 0.01 sec. to attain

twice this ion product concentration. If there is a slight excess of Ag^+ or Br^- before starting the addition, this time will be much reduced. For our purposes, we may consider the onset of nucleation to be instantaneous. Although it might be supposed that stirring conditions would be crucial to attaining reproducibility, it appears that in practice only rather poor stirring makes a noticeable difference.

The precipitates were made in 100 ml. of a 3% gelatin solution. A completed precipitation took 15 min., and, in this time, 10.00 g. of silver nitrate in 30 ml. of aqueous solution and an equivalent amount of potassium bromide were added simultaneously through two orifices. This precipitation scheme has often been termed the "double-jet method." When the nuclei were to be examined in the electron microscope, the addition of silver nitrate and potassium bromide was stopped and all of the precipitate was diluted with cold water and centrifuged. A separate precipitation was required for each experimental point. When the turbidity was to be measured, the precipitation was stopped and the material was run immediately into the cell in the spectrophotometer. There was a delay of less than 5 sec. from the stopping of precipitation until the turbidity was measured. The turbidity measurement could then be continued to allow the rate of grain growth by Ostwald ripening to be observed.

Observations

A comparison is given in Fig. 1 of the results obtained for two different conditions of balanced double-jet precipitation at 50° in 3% gelatin. The lowest curve was obtained from measurements of turbidity in precipitations where no solvent was present. The electron micrographs showed that the cube shape was produced, even for crystals as small as 0.030 μ. Details of the observations during the fine-grain precipitation will be discussed later, but some of the results are given here for comparison with the upper curve, which refers to measurements from electron micrographs for precipitations in the presence of 0.2 N ammonium hydroxide.

The nucleus size for the precipitate made in ammonia is much larger than that of the precipitate made without solvent present. This illustrates that there is no

(3) E. J. Meehan and W. H. Beattie, *J. Phys. Chem.*, **64**, 1006 (1960).

(4) C. R. Berry, *J. Opt. Soc. Am.*, **52**, 888 (1962).

(5) C. W. Davies and A. L. Jones, *Discussions Faraday Soc.*, **5**, 103 (1949).

(6) J. A. Gledhill and G. McP. Malan, *Trans. Faraday Soc.*, **50**, 126 (1954).
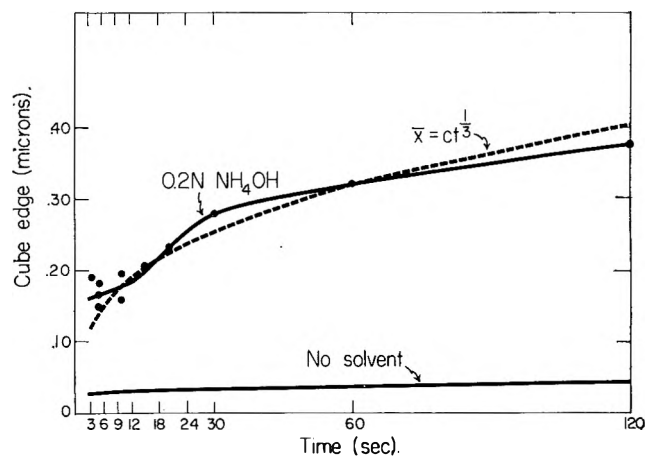
Figure 1. Average crystal size of AgBr during nucleation period. Upper curve (———) for precipitates in 0.2 N NH₄OH and 3% gelatin at 50°. Experimental points (●) are from carbon-replicated electron micrographs. The theoretical curve (- - - - - -), $\bar{x} = ct^{1/3}$, describes the condition for growth alone (no continuing nucleation). Lower curve (taken from turbidimetric measurements of Fig. 2) for precipitates in the absence of solvent.

fixed size of nucleus, but the size depends on the precipitation conditions. The average crystal sizes at 3 sec. are 0.160 and 0.0275 μ in the two cases. From a knowledge of the amount of AgBr precipitated and the time required for an average nucleus to reach a given size, values are readily obtained (Table I) which illustrate the rates of some of the nucleation phenomena. Of particular interest is the speed of addition of new layers. For the coarse-grain precipitate, completed layers of ions were added at the rate of more than 185/sec. This rapid addition of material emphasizes the difference between this system and those cases where equilibrium thermodynamic considerations may be applied.

Because of the rapid addition of layers, it seems likely that the layers do not add in an orderly fashion with one layer completed before the start of the next.

Table I: Characteristics of Double-Jet Precipitates at 3 Sec.

	Average length of cube edge, μ	Rate of nucleus formation, sec.⁻¹ cm.⁻³	Minimum average rate of layer addition, sec.⁻¹	Fraction of added material going into new nuclei, %
Coarse grain	0.160 (at 3 sec.)	4.6 × 10⁹	185	83
Fine grain	0.0275 (at 3 sec.)	9.1 × 10¹¹	32	91

There may well be some coalescence in the sense that groups of atoms have crystallized before attaching to the surface of larger crystals. Although the rate of growth during nucleation is so large that much imperfection could be anticipated, it is interesting to note that this is in fact not so. Earlier measurements[1] of the structure and imperfections of crystals made by the methods described here showed that the crystals were free of dislocations and twin planes except for a small percentage of twinned crystals found in precipitates made in ammonia. During the later stages of precipitation, when nucleation has stopped, the rate of addition of new layers is markedly smaller. For example (Fig. 1), with the grains precipitated in ammonia, the cube size changed from 0.320 to 0.378 μ between 60 and 120 sec. This corresponds to layer addition at the rate of only 1.7/sec.

After a certain period of time during the double-jet precipitation, nucleation ceases and only growth occurs. The end of nucleation can be established in principle by determining when the number of crystals present does not change. At any time, t, when the average crystal volume is $\bar{v}$, the number of crystals present is $n = (V/T)t/\bar{v}$, where V is the final total volume of AgBr produced in the time of a completed precipitation, T. When $dn/dt = 0$, $d\bar{v}/dt = \bar{v}/t$, or $d\bar{x}/dt = \frac{1}{3}\bar{x}/t$ which integrates to $\bar{x} = ct^{1/3}$. A curve of the form $\bar{x} = ct^{1/3}$ is shown in Fig. 1, where the constant c is chosen to give a good fit for the data with 0.2 N ammonium hydroxide at larger values of time than are shown in the figure. The experimental result oscillates around the ideal curve, presumably because of experimental fluctuations. Since there appears to be a coincidence of the two curves somewhere around 10 to 15 sec., we suppose that the nucleation was completed in about this time. For the fine-grain precipitate, the time when nucleation was completed is less well determined from the experimental data. The data are given in detail in Fig. 2 for both electron-microscopic and turbidimetric measurements of crystal size of the fine-grain precipitate. The experimental points for the electron-microscopic measurements are from single experiments, but each turbidimetric value is typically the average of about five separate runs. The electron-microscopic values of crystal size are somewhat larger and less reproducible than those obtained from the turbidity.

The values of crystal size designated in Fig. 2 as "rapid mixing, continuous flow" were for precipitates made by a different scheme from that discussed thus far and should not be compared directly with the other values in Fig. 2. In the rapid mixing scheme, measurements were actually made under steady-state condi-
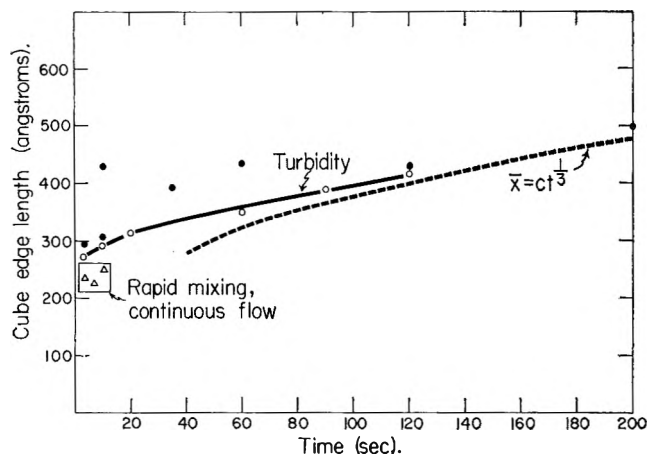
Figure 2. Electron-microscopic and turbidimetric determinations of crystal size during nucleation period for AgBr precipitates in 3% gelatin at 50° with no solvent present. The theoretical curve, $\bar{x} = ct^{1/3}$, describes the condition for growth alone (no continuing nucleation): ●, electron-microscopic measurements; O, turbidimetric measurements; Δ, turbidimetric measurements in a steady-state, continuous-flow system with rapid mixing.

tions. A continuous flow system was used, in which a solution of silver nitrate was mixed vigorously in a small chamber with a solution of potassium bromide and gelatin. The resultant precipitate flowed continuously through the spectrophotometer cell. The average time in the mixing chamber was 0.4˙ sec. and the precipitate was observed in the spectrophotometer 3.0 sec. later. For different runs, the concentrations of the silver nitrate and potassium bromide solutions were changed. All of the points for rapid mixing plotted at different times in Fig. 2 were actually obtained under the same conditions of flow and time. Although the plotted values of time are fictitious, they correspond to the times which would be required under our usual precipitation conditions to produce the same amount of silver bromide in a given volume of solution. In the limit of zero concentration in the continuous-flow system and zero time in the usual precipitation scheme, the values of nucleus size obtained by the two methods should coincide. They are, in fact, in fairly good agreement.

When only crystal growth occurs and the nucleation has stopped, the data should follow the curve $\bar{x} = ct^{1/3}$. The value of c in Fig. 2 was obtained from the more reliable electron-microscopic values at longer precipitation times. The turbidimetric values of crystal size are always above the curve $\bar{x} = ct^{1/3}$. Although this could indicate continuing nucleation, there is a systematic error which makes the turbidimetric values too high. The average grain volume is

given from the electron micrographs in terms of the cube edge, a, as $a^3 = \Sigma N_i a_i^3 / \Sigma N_i$. However, the measurement of turbidity for a fixed quantity of scattering material gives an average volume as $a^3 = \Sigma N_i a_i^6 / \Sigma N_i a_i^3$. For the distributions of grain size indicated by the electron micrographs, the average value of cube edge from the turbidity is about 15 to 20% too high. Such a correction, when applied to the turbidity measurements of Fig. 2, would indicate that nucleation has stopped after about 1 min. This is only an approximate value, and much more accurate data would be required to fix this point with confidence.

Nucleation Variables

Several variations in the conditions of nucleation were investigated. Although most of the precipitates were made in 3.0% gelatin solutions, many were also made in 1.5% gelatin. There was no definite difference in the results at these two gelatin concentrations. A further reduction of the concentration by a factor of two caused a definite increase in the nucleus size. Some results of Oliver and Ahmad[7] on the grain size of nuclear-track emulsions were presented in such a way as to indicate a strong dependence of grain size on gelatin concentration. This could be misleading in that the total addition of silver ion and bromide ion was varied in such a way as to keep the AgBr–gelatin ratio constant. Oliver's data can be interpreted equally as well by saying that the gelatin concentration (from about 1 to 13%) made no difference in the grain size but that the grain size increase was proportional to the cube root of the amount of silver bromide. This is equivalent to our curves: $\bar{x} = ct^{1/3}$.

When no potassium bromide was added but only silver nitrate, there was a precipitate which gave definite turbidity. X-Ray diffraction analysis of the product showed silver chloride. The chloride ion is presumably a constituent of the gelatin, and the turbidity observed for different additions of silver nitrate corresponds to the presence of a few milligrams of Cl^- per gram of gelatin. The presence of this amount of Cl^- would be expected to have little effect on the silver bromide nuclei which are formed when bromide ion is also present. As a confirmation of this assumption, it was found that addition of 20 mg. of chloride ion before the start of a 10-sec. run of silver nitrate and potassium bromide had a negligible effect on the turbidity of the silver bromide precipitate.

By contrast with this observation, the addition of a slight excess of bromide ion before a run caused a definite change in nucleus size. Effects of excess

(7) A. J. Oliver and I. Ahmad, U. S. Atomic Energy Commission, UCRL-6048-T, July 1, 1960.

bromide or excess silver ion on the turbidity are shown in Fig. 3. Since the optical density is proportional to the crystal volume, the measurements are effectively of crystal volume. When the bromide was started 10 sec. before the double-jet addition, the turbidity had a minimum value. In this case, there was an excess bromide concentration of 6.5×10^{-3} mole/l. corresponding to a pAg of 8.9. This is a substantially higher value than the minimum solubility at 50° $(1.25 \times 10^{-4}$ to 1.25×10^{-3} mole/l.). It is also much higher than the values of pAg (7.0 to 8.0) between which Klein and Moisar[8] found the minimum rate of ripening of silver bromide. This is apparently a further demonstration that equilibrium considerations do not apply in fast precipitations.

When the bromide ion was started 80 sec. ahead of the silver ion, the nuclei were of identical size with those obtained with no excess. This is at a potassium bromide concentration of 5.0×10^{-2} mole/l. or a pAg of 9.8. When precipitation was continued with this excess of potassium bromide to 7.5 min., the crystals had a variety of shapes (some cubes, some octahedra, and a fraction of a per cent of tabular types) and were obviously larger than a similar precipitate with no
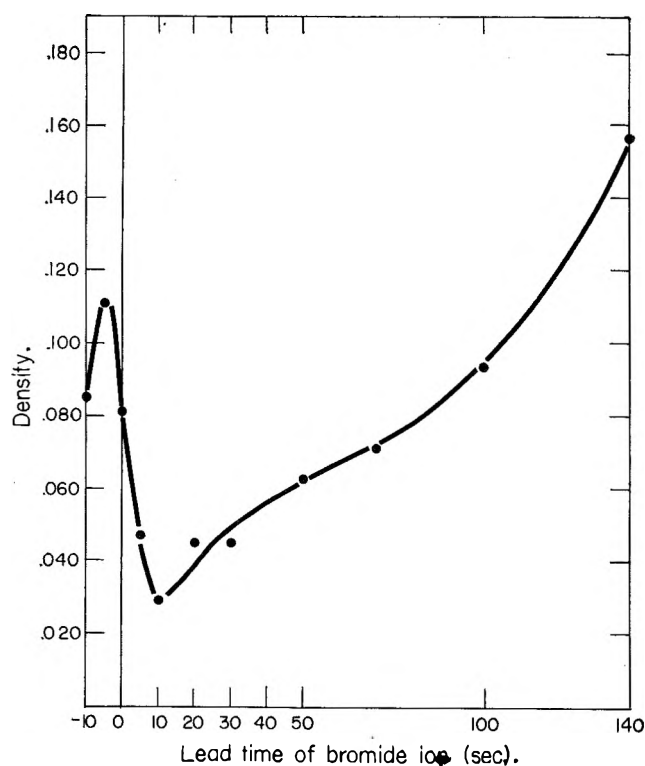
Figure 3. Turbidimetric measurement of optical density (proportional to crystal volume) after 10-sec. nucleations of AgBr in 3% gelatin at 50° as a function of the excess bromide or excess silver ion present.

excess potassium bromide. Thus, equivalence of size in the nucleation period does not guarantee equivalence during further growth.

Nuclei were precipitated at 40° rather than at 50°. This reduction in temperature caused the nucleus volume to decrease by about a factor of 2.0. Changes in optical density corresponding to changes in crystal volume were recorded on ripening the nuclei in the spectrophotometer. Some results are recorded in Table II for nuclei which were ripened at 50° for 1 min. following precipitation. It is observed that the

Table II: Increases in Average Volumes of Nuclei by Ripening for 1 Min. at 50°[a]

Nucleation condition	Volume increase by ripening, %
Reactants added for 3 sec.	60
Reactants added for 10 sec.	30
Reactants added for 60 sec.	6
Reactants added for 10 sec. but with various excesses of Br⁻ present	30 (Essentially independent of the Br⁻ excess)
After addition of AgNO₃ for 10 sec., the AgNO₃ and KBr were added simultaneously for 10 sec.	2

[a] Nuclei were produced by balanced double-jet additions at a fixed rate of AgNO₃ and KBr solutions to 3% gelatin solution at 50°.

per cent increase in volume is much larger for the nuclei present after 3 sec. compared with the nuclei produced during 60 sec. This emphasizes a limitation in obtaining reproducible electron micrographs for the shorter values of nucleation time, where the nuclei may grow during specimen preparation. Why the crystals after 60 sec. addition are so much more stable than those formed in 3 sec. is not clear because the difference in average crystal size in the two cases is not large. Possibly, the greater instability at shorter nucleation times could be accounted for by the existence of a wider distribution of sizes or by the occurrence of some coalescence. It was surprising that the amount of excess bromide (up to as much as 120 sec. lead time) made little difference in the per cent change in volume. This may be caused by a balancing of two effects: when the amount of bromide present tends to increase the rate of solution, it also produces somewhat larger (more stable) nuclei. Additions of small excesses of

(8) E. Klein and E. Moisar, Ber. Bunsenges. Physik. Chem., 67, 349 (1963).

silver ion before nucleation reduced the instability in the system quite markedly.

Conclusions

Fast precipitation of silver bromide in gelatin produces very large nuclei. Thermodynamic predictions of nucleus size agree only with results of slow nucleation as in homogeneous precipitation. In the presence of the solvent, 0.2 N ammonium hydroxide, nuclei were cube-shaped and had an average edge length of 0.160 μ. New layers of ions added at the rate of more than 185/sec. during the nucleation period and then dropped to less than 1% of this during the ensuing period of growth. In spite of the fast rate of some of these processes, most of the crystals produced were free of dislocations and twins, and moderate changes in stirring rate had little effect on the results.

Precipitates made in the absence of ammonia had cube-shaped nuclei of about 275-Å. edge length. At this size, the results of turbidimetric measurements were more reproducible and more accurate than the results from electron micrographs. Turbidimetric measurements of the nuclei made by our customary procedure after stopping the addition of silver nitrate and potassium bromide were nearly the same as results obtained in a continuous-flow system. Additions of excess bromide ion before the start of a precipitation caused changes in nucleus size, but there was no correspondence between the conditions for minimum nucleus size and minimum solubility. After the addition of silver nitrate and potassium bromide was stopped, the size of the nuclei continued to increase by Ostwald ripening. The ripening was much larger when the nucleation was stopped after a short time than after a longer time. An excess of bromide ions within a restricted range had little effect on the rate of ripening, but an excess of silver ions almost eliminated the ripening.

Coulometric Study of the Reaction of Diphenylpicrylhydrazyl

and Bromide Ion[1]

by Emanuel Solon and Allen J. Bard[2]

The Department of Chemistry, The University of Texas, Austin, Texas (*Received December 6, 1963*)

The rate of the reaction of diphenylpicrylhydrazyl (DPPH) and bromide ion in an acetonitrile medium was studied using the technique of controlled potential coulometric analysis. The rate of the reaction was second order with respect to both DPPH and bromide ion. A mechanism for the reaction was proposed and an integrated rate equation based on this mechanism was derived.

The electrochemistry of diphenylpicrylhydrazyl (DPPH), a stable free radical, has been described.[3] The study showed that acetonitrile solutions of DPPH
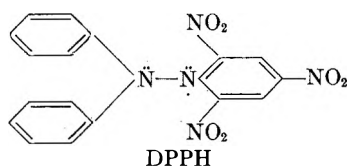
DPPH

containing tetra-*n*-butylammonium perchlorate (TBAP) were stable, and that DPPH was reduced at a platinum electrode in a reversible, one-electron, reaction ($E_{1/2}$ = 0.20 v. *vs.* s.c.e.)

$$R\cdot + e \rightleftharpoons R:^- \qquad (1)$$
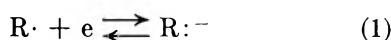
where R· is DPPH and R:⁻ is its reduction product. When tetra-*n*-butylammonium bromide (TBAB) was used as a supporting electrolyte, voltammetry showed that the cathodic wave height decreased and the anodic wave height increased with time (indicating a reaction resulting in conversion of R· to R:⁻), until the solution, originally purple in color, became brown, and only the anodic wave remained.

Since the potential of the bromine–bromide ion couple in acetonitrile is more positive than 0.5 v. *vs.* s.c.e., an oxidation–reduction reaction between DPPH and bromide ion appeared thermodynamically unfavorable, and a study of the reaction was undertaken. No recorded reaction of DPPH and bromide ion has appeared, although several authors mention a reaction of DPPH and bromine.[4]

Results

The rate of the reaction was studied by preparing acetonitrile solutions of DPPH and TBAB and determining the concentration of DPPH at various times after mixing using controlled potential coulometry. The theoretical treatment for the controlled potential coulometric electrolysis of a species undergoing chemical reaction prior to and during the electrolysis has been given.[5] By using a high speed coulometric apparatus,[6] the electrolysis times were kept short (less than 5 min.) and the amount of reaction occurring during the coulometric analysis was practically negligible.

The measured quantity was n_{app}^0, the apparent number of electrons involved in the reduction of DPPH based upon the initial concentration of DPPH in the stock solution, C_i

$$n_{app}^0 = \frac{Q}{FVC_i} = \frac{nC}{C_i} \qquad (2)$$

where Q is the number of coulombs involved in the electrolysis, n is the number of equivalents per mole of

(1) (a) Based on a thesis submitted by E. S. in partial fulfillment of the requirements for the degree of Ph.D., August, 1963; (b) presented at the 145th National Meeting of the American Chemical Society, New York, N. Y., September, 1963.

(2) To whom correspondence and request for reprints should be directed.

(3) E. Solon and A. J. Bard, *J. Am. Chem. Soc.*, **86**, 1926 (1964).

(4) R. H. Poiner, E. J. Kahler, and F. Fenington, *J. Org. Chem.*, **17**, 1437 (1952); S. Goldschmidt and K. Renn, *Ber.*, **55**, 628 (1922); J. A. Weil, private communication.

(5) A. J. Bard and E. Solon, *J. Phys. Chem.*, **67**, 2326 (1963).

(6) A. J. Bard, *Anal. Chem.*, **35**, 1121 (1963).

electroactive species reduced (1 for the reduction of DPPH), V is the volume of stock solution taken, and C is the concentration of DPPH at the start of the electrolysis. Typical results for the reaction of 0.1 M TBAB and 11.64 mM DPPH in acetonitrile are shown in Table I. For comparison, results for a TBAP–DPPH mixture are also given. Similar trials were also carried out with other concentrations of TBAB; in all cases the concentration of TBAB was larger than that of DPPH.

Table I : $n_{app}{}^0$ for Reduction of DPPH in Acetonitrile Solutions of Tetra-n-butylammonium Perchlorate (TBAP) and Bromide (TBAB)

Time elapsed after mixing stock soln., hr.	TBAP, 0.1 M^a	$n_{app}{}^0$ TBAB, 0.1 M^b
0.33	1.02	0.858
2.1		0.697
4.0		0.645
9.6		0.558
19.2	1.04	
24.0		0.419
44.0	1.03	
48.4		0.328
74.5	1.03	

^{a} The DPPH concentration was 7.95 mM. ^{b} The DPPH concentration was 11.64 mM.

The order of the reaction with respect to DPPH was established by plotting various functions of $n_{app}{}^0$ against the time, t. For a second-order reaction the following equation applies

$$\frac{C_i}{C} = 1 + C_i k' t \qquad (3)$$

or, using eq. 2

$$\frac{n}{n_{app}{}^0} = 1 + C_i k' t \qquad (4)$$

Plots of $n/n_{app}{}^0$ vs. t were nearly linear for all concentrations of TBAB (Fig. 1) indicating a reaction second order in DPPH. The limiting slopes of some of these plots at various concentrations of TBAB are shown in Table II. Considering

$$k' = k Z_i{}^b \qquad (5)$$

where Z_i is the initial concentration of TBAB, the data of Table II best fit eq. 5 for a value of b of 2, indicating that the reaction is second order with respect to bromide ion (or TBAB).

Voltammetry in solutions in which DPPH had reacted completely with bromide ion showed a limiting
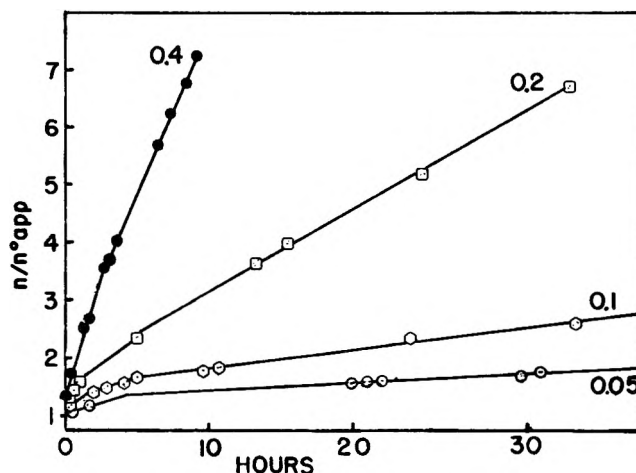
Figure 1. Variation of $n/n_{app}{}^0$ with time elapsed between mixing of DPPH–TBAB stock solution and coulometric determination. Concentrations of DPPH varied between 2.57 and 21.2 mM (see Table III). TBAB concentrations (M) are given on each curve.

Table II : Values of k' for Various Concentrations of DPPH and TBAB

DPPH concn., C_i (mM)	TBAB concn., Z_i (M)	$k' \times 10^2$	$k \times 10$ $\dfrac{k'}{Z_i}$	$\dfrac{k'}{Z_i{}^2}$
20.4	0.050	0.47	9.5	188
11.6	0.10	2.2	22	220
20.4	0.20	7.0	35	176
20.2	0.40	29	72	181
			Av.	191

anodic current about one-half as large as that of the original cathodic limiting current due to the reduction of DPPH. This indicated that one-half of the original DPPH was converted to its reduction product (R:$^-$) in the over-all reaction.

Discussion

A reaction scheme consistent with the above results is

$$\text{R} \cdot + \text{Br}^- \overset{K_1}{\underset{}{\rightleftharpoons}} \text{R}:^- + \text{Br} \cdot \quad (\text{fast}) \qquad (6)$$

$$\text{Br} \cdot + \text{Br}^- \overset{K_2}{\underset{}{\rightleftharpoons}} \text{Br}_2 \cdot^- \quad (\text{fast}) \qquad (7)$$

$$\text{R} \cdot + \text{Br}_2 \cdot^- \overset{k_3}{\longrightarrow} \text{RBr} + \text{Br}^- \quad (\text{slow}) \qquad (8)$$
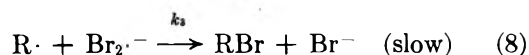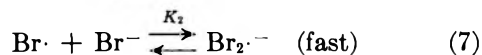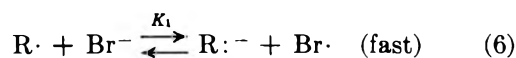
where K_1 and K_2 are the concentration equilibrium constants of eq. 6 and 7, respectively, k_3 is the rate constant of eq. 8, and RBr is a nonelectroactive product. The over-all reaction is as shown in eq. 9

$$2\text{R}\cdot + \text{Br}^- \longrightarrow \text{R}\!:^- + \text{RBr} \qquad (9)$$
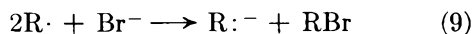
in agreement with the voltammetric data.

The rate equation for the over-all process is based on the rate equation of the slow step (reaction 8)

$$\frac{-\text{d}[\text{R}\cdot]}{\text{d}t} = k_3[\text{R}\cdot][\text{Br}_2\cdot^-] \qquad (10)$$

where brackets represent concentrations. From eq. 6 and 7

$$K_1 = \frac{[\text{R}\!:^-][\text{Br}\cdot]}{[\text{R}\cdot][\text{Br}^-]} \qquad (11)$$

$$K_2 = \frac{[\text{Br}_2\cdot^-]}{[\text{Br}\cdot][\text{Br}^-]} \qquad (12)$$

Combination of eq. 10, 11, and 12 yields

$$\frac{-\text{d}[\text{R}\cdot]}{\text{d}t} = k_3K_1K_2\frac{[\text{R}\cdot]^2[\text{Br}^-]^2}{[\text{R}\!:^-]} \qquad (13)$$

An expression for [R:$^-$] can be obtained from the over-all stoichiometry of the reaction

$$[\text{R}\!:^-] = (C_i - C)/2 \qquad (14)$$

Combining eq. 13 and 14 yields

$$-\frac{\text{d}C}{\text{d}t} = k\left(\frac{C^2Z^2}{C_i - C}\right) \qquad (15)$$

where Z is the bromide ion concentration and

$$k = 2k_3K_1K_2 \qquad (16)$$

The integrated form of eq. 15 is

$$C_i/C - 1 - \ln\,(C_i/C) = kZ_i{}^2t \qquad (17)$$

when the bromide ion concentration is in large enough excess to be assumed constant during the electrolysis and equal to its initial concentration, Z_i. When the bromide ion concentration is not much larger than the DPPH concentration, integration of eq. 15 can be performed using, from the stoichiometry of the reaction

$$Z = Z_i - (C_i - C)/2 \qquad (18)$$

The resulting equation is

$$(2Z_i - C_i)^2kt/4 = C_i/C + 2Z_i/(2Z_i + C - C_i) -$$

$$2 - \frac{2Z_i + C_i}{2Z_i - C_i}\ln\left(\frac{C_i(2Z_i + C - C_i)}{2Z_iC}\right) \qquad (19)$$

A plot of the right-hand side of eq. 19 vs. t, shown in Fig. 2, is linear, and allows calculation of k from its slope. The plots based on eq. 19 take account of the inverse order dependence with respect to R:$^-$; the deviations from linearity shown in Fig. 1 disappear when the data are plotted according to eq. 19. Values of k
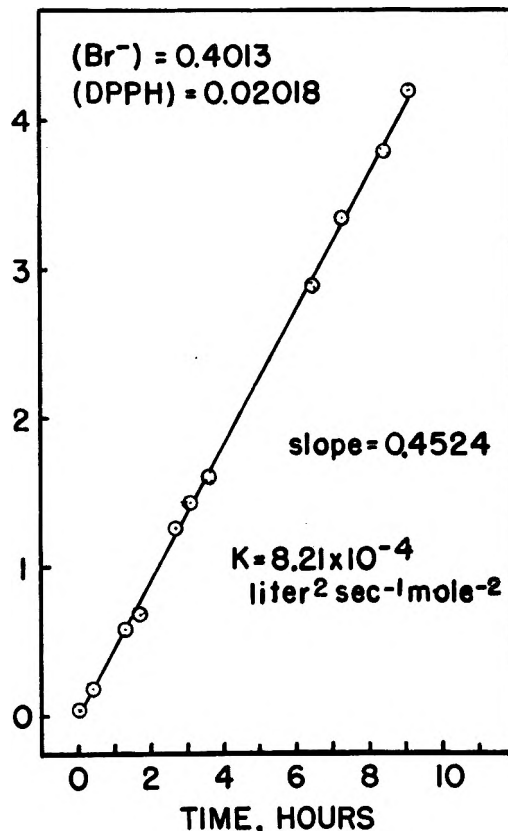
Figure 2.   Plot of DPPH–TBAB reaction according to eq. 19.   The ordinate is the right-hand side of eq. 19.

determined from plots such as that in Fig. 2 for different concentrations of DPPH and bromide ion are given in Table III.

Table III: Values of Over-all Rate Constant k for Various DPPH and TBAB Concentrations

DPPH concn., C_i (mM)	TBAB concn., Z_i (M)	$k \times 10^4$ (l.^{2} mole^{-2} sec.$^{-1}$)
2.57	0.05	9.3
11.8	0.05	6.3
20.4	0.05	7.4
21.2	0.10	6.1
20.4	0.20	7.7
20.2	0.40	8.2
	Av.	7.5 ± 0.7

The rate of the reaction of DPPH and bromide ion depends quite strongly upon the solvent medium. The reaction was about one order of magnitude slower when methanol rather than acetonitrile was used as the solvent.   This reaction was complicated by the

simultaneous reaction of DPPH and methanol itself. Addition of water to the acetonitrile also decreased the rate of the reaction. Similarly the reaction rate was very slow in a carbon tetrachloride medium.

The existence of the species Br_2^- has precedence in electrochemical studies. Llopis and Vazquez[7] in a study of the electroreduction of bromine at a platinum electrode postulated a one-electron primary step forming Br_2^-. Reaction 7 also was used in their mechanism and was assumed to be rapid compared to the electrode reaction, which had a rate constant (k^0) of about 0.05 cm./sec.

Experimental

Reagents. The acetonitrile (Matheson Coleman and Bell practical grade) was purified by several distillations from phosphorus pentoxide and a final distillation from anhydrous potassium carbonate. The TBAB and TBAP were polarographic grade (Southwestern Analytical Chemicals, Austin, Texas) and were oven-dried before use. The DPPH was obtained from Eastman Kodak Co. and was used as received.

Procedure. The general apparatus and techniques have been described.[3] Controlled potential coulometry was performed in a high speed apparatus[6];

to prevent the solution from heating up during the electrolysis ultrasonic stirring was not used. The reference electrode was an aqueous saturated calomel electrode (s.c.e.) with an agar–1 M potassium nitrate bridge. The auxiliary electrode, a silver wire coil, was separated from the working electrode by an agar–1 M KNO_3 plug and a sintered glass disk.

Stock solutions of known DPPH and TBAB concentration were prepared using acetonitrile which was previously deaerated with nitrogen and were mixed at $t = 0$. A deaerated acetonitrile solution containing TBAB in the coulometric cell was reduced at a platinum electrode at +0.015 v. vs. s.c.e. until the current decayed to a small background level. At time t an aliquot portion of the DPPH–TBAB stock solution was added, and the electroreduction of DPPH continued until the current decayed to the background level. The number of coulombs necessary for the electrolysis was noted and corrected for the background current. Electrolysis times were always less than 5 min.

(7) J. Llopis and M. Vazquez, *Electrochim. Acta*, **6**, 177 (1962).

Electronic Spectra of Organolithium Compounds.   III.

Effect of Methyl Substitution

by Richard Waack and Mary A. Doran

The Dow Chemical Company, Eastern Research Laboratory, Framingham, Massachusetts
(Received December 7, 1963)

Substitution of a methyl group on an odd-alternant anion [*e.g.*, benzyllithium, allyllithium, or styryllithium] causes, depending on position, either a red shift or a blue shift of the longest wave length absorption.   This behavior is identical with that of nonalternants and is consistent with the arrangement of the π-molecular orbitals of these molecules.   Explanations are given in terms of resonance theory and molecular orbital theory.

The effect of a methyl substituent on the spectrum of an even-alternant hydrocarbon or a nonalternant hydrocarbon (*e.g.*, azulene) is well-known.   There are no reports in the literature, however, describing the behavior of the spectra of odd-alternant molecules (which must be free radicals or ions) upon methyl substitution.   This paper is concerned with the effect of a methyl substituent on the spectra of the odd-alternant anions[1] benzyllithium, allyllithium, styryllithium, and 1,1-diphenyl-*n*-hexyllithium.   The observed spectral changes are analogous to those of the nonalternant hydrocarbons in that, depending on the position of the methyl substituent, either a red or a blue shift in absorption maximum from that of the unsubstituted species results.   A qualitative explanation of this finding is given in terms of resonance theory.   LCAO-MO calculations of relative transition energies are in qualitative agreement with the spectral shifts.   The use of molecular orbital coefficients to predict the shift direction, which was successful for even-alternants and nonalternants, does not give the correct shift for these odd-alternant anions.

Experimental

The spectra were measured in tetrahydrofuran (THF) solution using the absorption cell and the procedures described previously.[2]

Benzyllithium was prepared from tribenzyltin chloride and phenyllithium in diethyl ether or from dibenzylmercury and metallic lithium in THF.[3]   Allyllithium was prepared in hexane from *n*-butyllithium

and tetraallyltin.[4]   Solid allyllithium was washed with hexane and dissolved in THF. α-Methylbenzyllithium, *p*-methylbenzyllithium, α-methylallyllithium, γ-methylallyllithium,[5] and β-methylallyllithium were prepared from the corresponding triphenyltin compounds[6] in diethyl ether *via* transmetalation with phenyllithium.   Insoluble tetraphenyltin was filtered off the chilled reaction mixture.   Styryllithium, α-methylstyryllithium, *p*-methylstyryllithium, *o*-methylstyryllithium, and *m*-methylstyryllithium were formed from *n*-butyllithium and the respective monomer in THF solution.   The monomers were dried over calcium hydride and vacuum distilled.   The methyl-substituted 1,1-diphenyl-*n*-hexyllithium compounds were formed from the corresponding 1,1-ditolylethylenes[7] and *n*-butyllithium.   Phenyllithium and *p*-tolyllithium were prepared from metallic lithium and the corresponding bismercury compound in THF solution.   Phenyllithium was also prepared from chlorobenzene in THF solution.

(1)   For convenience we refer to organolithium compounds as anions although in solution they most probably exist as the ion pairs.

(2)   R. Waack and M. A. Doran, *J. Am. Chem. Soc.*, 85, 1651 (1963).

(3)   R. Waack and M. A. Doran, *J. Phys. Chem.*, 67, 148 (1963).

(4)   D. Seyferth and M. A. Weiner, *J. Am. Chem. Soc.*, 83, 3583 (1961).

(5)   Either α-methylallyltriphenyltin or γ-methylallyltriphenyltin results in the same organolithium compound, which is expected to be predominantly crotyllithium.

(6)   Kindly supplied to us by Dr. F. C. Leavitt and Miss Priscilla A. Carney of this laboratory.

(7)   Kindly supplied by Dr. Vernon Sandel of this laboratory.

Results

The wave lengths of the absorption maxima in THF solution of the parent lithium compounds, benzyllithium, allyllithium, styryllithium, 1,1-diphenyl-n-hexyllithium, and phenyllithium, and their methyl-substituted derivatives are listed in Table I.

Table I : Electronic Absorption Spectra of Odd-Alternant Organolithium Compounds and Their Methyl Derivatives

	λ_{max}, mμ
Benzyllithium	330
α-Methylbenzyllithium	333
p-Methylbenzyllithium	315
Allyllithium	315
α-Methylallyllithium	291
γ-Methylallyllithium	291
β-Methylallyllithium	330
Styryllithium	335
α-Methylstyryllithium	340
p-Methylstyryllithium	327
o-Methylstyryllithium	325
m-Methylstyryllithium	338
Phenyllithium	292, 268, 261
p-Tolyllithium	292, 273, 268
1,1-Diphenyl-n-hexyllithium	495, 315
1,1-Di-o-tolyl-n-hexyllithium	501, 328
1,1-Di-p-tolyl-n-hexyllithium	490, 318
1,1-Di-m-tolyl-n-hexyllithium	498, 310 (sh)

The following important features are shown by the data in Table I. A methyl group in a starred (or active) position[8] of the odd-alternant lithium compounds causes either a red shift or a blue shift of the absorption maximum, depending on the position of substitution. A methyl group in an inactive position, such that it is in cross conjugation with the π-system, causes only a red shift in absorption maximum. Larger shifts result from methyl substitution in a smaller molecule. When the methyl substituent is removed from the chromophoric site, and there is no formal delocalization, e.g., in phenyllithium, it causes little change in the spectrum. The deviation of o-tolyl-n-hexyllithium from the general pattern is likely due to steric effects.

Discussion

Methyl or alkyl substitution on an even-alternant hydrocarbon always causes a bathochromic shift of the conjugation bands.[9-11] On the other hand, methyl substitution of a nonalternant hydrocarbon, e.g., azulene,[12] causes either, depending on its location, a red shift or a blue shift of the longest wave length

absorption band. The spectral changes caused by methyl substitution of the odd-alternant organolithium compounds are like those of the nonalternants, in that either a red shift or a blue shift in absorption maximum may occur.

The perturbation of the parent molecule by a methyl group can be separated into a resonance effect (hyperconjugation) and an inductive effect. Considering the longest wave length absorption, hyperconjugation always produces a red shift independent of molecular structure, whereas the inductive effect can produce either a red shift or a blue shift[13,14] depending on the molecule. In an even-alternant hydrocarbon, because the antibonding molecular orbitals are a mirror image of the bonding molecular orbitals, both bonding and antibonding orbitals are shifted by equal amounts[13,14]; thus, the first-order inductive effect of a methyl group on the long wave length transition cancels out.[15] Red shifts caused by methyl substitution of even-alternant hydrocarbons result from hyperconjugation.[16] In non-alternant hydrocarbons (e.g., azulene) the shifts produced by methyl substitution are much larger and are mainly due to the inductive effect of the methyl substituent.[12,17]

In odd-alternant organolithium compounds because the highest occupied orbital (to a first approximation) is the central nonbonding orbital located between the lowest antibonding and highest bonding orbitals, both the hyperconjugative and inductive action of a methyl substituent influence the longest wave length transition. Thus, methyl substitution on an odd alternant would be expected, depending on the position of the methyl group, to produce both red and blue shifts

(8) An odd-alternant hydrocarbon is composed of two classes of carbon atoms, starred (the larger number) and unstarred, such that every other carbon atom belongs to a different class [A. Streitwieser, "Molecular Orbital Theory for Organic Chemists," John Wiley and Sons, Inc., New York, N. Y., 1961, pp. 45–46.

(9) G. W. Wheland, "Resonance in Organic Chemistry," John Wiley and Sons, Inc., New York, N. Y., 1955, p. 275.

(10) F. A. Matsen, "Technique of Organic Chemistry," Vol. 9, W. West, Ed., Interscience Publishers, Inc., New York, N. Y., 1956, p. 671.

(11) Unless steric effects result in changes in the geometry of the molecule.

(12) E. Heilbronner, "Non-Benzenoid Aromatic Compounds," D. Ginsberg, Ed., Interscience Publishers, Inc., New York, N. Y., 1959, p. 224.

(13) C. A. Coulson, Proc. Phys. Soc. (London), A65, 61 (1952).

(14) H. C. Longuet-Higgins and R. G. Sowden, J. Chem. Soc., 1404 (1952).

(15) Experimental evidence for the effectiveness of purely inductive effects in an even alternant is that the spectrum of anilinium ion, having a positive charge, absorbs at almost the same wave length as does benzene.[10]

(16) D. Peters, J. Chem. Soc., 646, 4182 (1957).

(17) B. Pullman, M. Mayot, and G. Berthier, J. Chem. Phys., 18, 257 (1950).

from the absorption maximum of the parent species, as is observed.

It has been shown for even-alternant hydrocarbons that the shifts produced by a methyl substituent are proportional to the reciprocal of the number of carbon atoms in a molecule.[12] This behavior is evident here, in that the shifts produced by methyl substitution on allyllithium are larger than those produced by substitution of benzyllithium.

In p-tolyllithium the methyl substituent is considerably removed from, and not in conjugation with, the anionic chromophore. It has no effect on the longest wave length transition of phenyllithium, which our evidence indicates may be due to an n → π*-type transition of an electron of the carbon–lithium bond. The methyl group can, however, interact with the π-electrons of the phenyl ring. The shorter wave length transitions, which probably involve the π-electrons, are moved to longer wave length by methyl substitution.

The first electronic transition of an odd (or even) alternant carbonium ion is predicted to be of similar energy to that of the corresponding carbanion.[2,18] The behavior to be expected from the molecular orbital arrangement in odd-alternant ions is that the inductive effect of a methyl group on the spectra of the carbonium ion should be opposite that of the carbanion. This will be illustrated in a following section.

Resonance Theory Interpretation of Spectral Shifts. In this section an explanation is given for the effect of a methyl substituent on the spectra of odd-alternant anions in terms of resonance theory, which permits by inspection the prediction of the direction of the spectral shift. The methyl group may be either on an "active" or "inactive" position.[8] A methyl substituent in an "inactive" position causes a red shift in absorption maximum of all three organolithium compounds, and may be considered the general behavior. When the methyl substituent is on an "active" position, shifts in absorption maximum either to the red or to the blue occur. To generalize this behavior, consider the electron-donating effect of the methyl group on the relative stabilities of the resonance structures of the odd alternants benzyllithium and allyllithium.

The electron distribution probabilities (to a first approximation) for the Kekulé structures of benzyllithium, allyllithium, and their methyl-substituted species are shown in Table II.[19] In the benzyl anion the probability of the primary Kekulé structure, *i.e.*, charge being in position 1, is four times greater than for structures 2, 3, or 4. Intuitively, owing to the electron-supplying behavior of a methyl group, the resonance structures of α-methylbenzyllithium in which

the charge is on the phenyl ring, *i.e.*, structures 2, 3, and 4, should be more nearly equivalent in energy to the primary resonance structure 1 than they are in benzyllithium; this is illustrated by their relative probabilities in Table II. As the consequence of the α-

Table II : Probabilities of Kekulé Resonance Structures of Benzyl and Allyl Carbanions

	Calculated LCAO-MO charge densities[a,b]				
	Position				
	1	2	3	4	$\Sigma q_i{}^c$
Benzyl	0.57	0.14	0.14	0.14	0.99
α-Methylbenzyl	0.41	0.16	0.18	0.16	0.91
p-Methylbenzyl	0.60	0.14	0.01	0.14	0.89
o-Methylbenzyl	0.59	0.00	0.14	0.16	0.89
Allyl	0.50	0.50			1.00
γ-Methylallyl	0.57	0.34			0.91

[a] Standard LCAO-MO methods and the conjugation–induction model of Streitwieser and Nair[19] were used. Secular determinants were diagonalized on a Burroughs 220 using a program written by Dr. James R. Scherer. [b] The charge densities, which are analogous to probability distribution, are for the anions. Although no allowance was made in these calculations for the effect of the negative charge on the effective electronegativity of the carbon atom skeleton, this should be similar in the methyl-substituted and nonsubstituted compounds and not alter the comparison between the two. [c] Charge distributed at unmarked positions results in the sum of the charges at positions 1 → 4 not being equal to unity.

methyl substituent, therefore, the four Kekulé resonance forms of α-methylbenzyllithium are more equivalent in energy than they are in benzyllithium. On the other hand, a methyl substituent in either the *ortho* or *para* position of benzyllithium would tend to push the charge out of the ring and thus make the primary Kekulé structure of lower energy (*i.e.*, more stable) than those forms having the charge on the ring. Although resonance lowers the ground state energy of a compound, it usually, because the contribution of resonance structures is greater in the excited state than in the ground state, has an even greater stabilizing effect on the excited state.[9,20] Thus, factors tending to

(18) D. P. Craig, Chemical Society Annual Report, 1958, p. 173.

(19) A. Streitwieser and P. M. Nair, *Tetrahedron*, **5**, 149 (1959).

(20) (a) E. A. Brande, "Chemistry of Carbon," Vol. I, E. H. Rodd, Ed., Elsevier Publishing Co., 1951, p. 83; (b) ref. 9, p. 676; (c) M. J. S. Dewar, Special Publication No. 4, The Chemical Society, London, 1956, p. 64; (d) W. Kauzmann, "Quantum Chemistry," Academic Press, Inc., New York, N. Y., 1957, p. 678.

favor resonance by making the resonance structures more equivalent in energy[21] should lower the excited state energy relative to the ground state energy and produce a red shift in absorption maximum. Conversely, factors tending to inhibit resonance by making one of the resonance forms of lower energy than the others should cause a blue shift in absorption maximum.

Identical reasoning applies to allyllithium and methylallyllithium. The two resonance forms of allyllithium are equal in energy. In butenyllithium the resonance forms are not equivalent in energy. The crotyllithium resonance form is expected to be considerably more stable than the α-methylallyllithium resonance form, since the secondary carbanion of this latter structure is more energetic than a primary carbanion. (See the charge density probabilities in Table II.) Nonequivalence of these resonance forms is substantiated by proton magnetic resonance studies of butenylmagnesium bromide by Roberts, et al.,[22] which establish that its predominant, if not exclusive structure is crotylmagnesium bromide. Thus, methyl substitution makes resonance less favorable in α- and γ-methylallyllithium, and its absorption is blue shifted relative to allyllithium.

This discussion leads to the general rule that when the position of a methyl substituent on a starred C atom of an odd-alternant organolithium compound is such that the principal resonance structures of the molecule are made more equivalent in energy, its absorption is shifted to longer wave length, but if methyl substitution is such as to inhibit resonance in that the principal resonance structures are made less equivalent in energy, the absorption is shifted to the blue from that of the parent compound.

Molecular Orbital Interpretation of Spectral Changes and Calculation of Spectral Shifts. By perturbation methods both Coulson[13] and Longuet-Higgins and Sowden[14] have shown that the change in the long wave length transition energy of even alternants or nonalternants due to the inductive effect of a substituent is given by[23]

$$\Delta(h\nu)_{induct} = [c^2_{n+1,r} - c^2_{n,r}]\delta\alpha_r \qquad (1)$$

where $c_{n,r}$ refers to the coefficient of atom r (which is substituted) in wave function n, where n is the highest occupied orbital. Because $\delta\alpha_r$ is positive for a methyl substituent, i.e., the methyl-substituted carbon has a decreased effective electronegativity, red shifts owing to methyl inductive effects are expected when $c^2_{n,r} > c^2_{n+1,r}$ and blue shifts when $c^2_{n+1,r} > c^2_{n,r}$. This formula, and a similar one to account for the red shifts owing to hyperconjugation, correctly predicts with

qualitative agreement the direction of spectral shifts in methyl-substituted azulenes.[12–14] This is not so with the odd-alternant anions. The shifts predicted according to eq. 1 from the coefficients of the highest bonding and lowest antibonding π-orbitals [LCAO-MO] of benzyllithium or allyllithium are not in the correct direction. (See Scheme I.) Successive iterations to allow for the negative charge, using the ω-technique,[19] does not, in either molecule,[24] alter the direction of the predicted spectral shift.

Scheme I: Direction of Spectral Shifts Predicted from Equation 1

Red (R)[a]

Blue (B)
Blue (R)
Red (B)

Benzyllithium

Blue (R)
Red (B)

Allyllithium
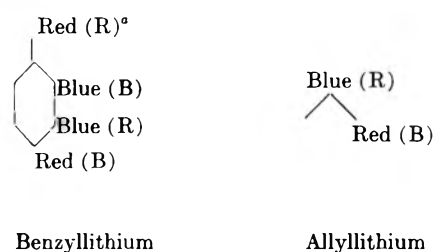
[a] Shift found experimentally.

The fact that the orbital coefficients do not predict the correct spectral shift is interpreted as indicating that the orbitals obtained from LCAO-MO are not, in these systems, an adequate approximation to the true molecular orbitals, even with iteration[19] to allow for the charge. Electron interaction, which is more important in ions,[25,26] presumably makes the simple description inadequate. The formulas derived via perturbation methods of LCAO-MO theory are not, therefore, expected to be generally applicable to the odd-alternant ions.

Pullman, Mayot, and Berthier[17] calculated qualitative relative transition energies for the methyl-substituted azulenes, using LCAO-MO methods and the parameters of Mulliken, et al.,[27] to describe the inductive and conjugative effect of methyl. Continuing

(21) Ref. 9, pp. 20–24.

(22) J. E. Nordlander, W. G. Young, and J. D. Roberts, *J. Am. Chem. Soc.*, 83, 494 (1961).

(23) Although odd-alternant molecules were not considered in these theoretical studies, there seems to be no reason that the same conclusions should not be valid for these species. We are indebted to Prof. C. A. Coulson for confirmation by personal communication.

(24) Unfortunately, as found for the benzyl cation,[19] the iterations of benzyl anion do not converge [ω = 1.4]. The allyl anion does converge.

(25) H. C. Longuet-Higgins and J. A. Pople, *Proc. Phys. Soc.* (London), A68, 591 (1955).

(26) A. Brinstock and J. A. Pople, *Trans. Faraday Soc.*, 50, 901 (1954).

(27) R. S. Mulliken, C. A. Rieke, and W. G. Brown, *J. Am. Chem. Soc.*, 63, 41 (1941).

this approach, using the inductive and conjugative parameters of Streitwieser and Nair[19] and iterating by the ω-technique to allow for the negative charge, the relative transition energies (in units of β) for benzyl and allyl anions in Table III are obtained. Two procedures were used to calculate relative transition energies: (1) combining the methyl group conjugation and induction parameters with a zeroth order Hückel calculation and (2) introducing the conjugation and induction parameters into the sixth iteration of the respective anion skeleton. The values given are averages of the first two iterations. Although for some molecules the individual iterations are somewhat extreme, the average of the first two iterations is expected to be a good approximation to the converged values. Streitwieser has shown that this is true for odd-alternant cations.[19,28] It is also true for allyllithium.[24]

Table III: Calculated Relative Transition Energies

	ν_{obsd} $\times 10^{-2}$ cm.$^{-1}$	Procedure 1 $\Delta E(\beta)$	ν_{calcd} ^{a,b}	Procedure 2 $\Delta E(\beta)$	ν_{calcd}
Allyllithium					
Unsubstituted	318	1.207	a	1.222	a
γ-Methyl	344	1.229	327	1.240	322
β-Methyl	303	1.114	294	1.122	292
Benzyllithium					
Unsubstituted	303	0.759	b	0.786	b
α-Methyl	301	0.760	304	0.783	302
p-Methyl	318	0.797	318	0.837	322
o-Methyl		0.749^c		0.790	
m-Methyl		0.703		0.762	

^{a} Transition energies are relative to allyllithium. ^{b} Transition energies are relative to benzyllithium. ^{c} This is the only value not qualitatively in agreement with observation.

The allyl anion transition energies are in qualitative agreement (i.e., correct order) for both calculation procedures. Since iteration of allyl anion converges, procedure 2, in which self-consistency of the negative charge was approached and then the effect of the methyl group introduced, might be preferred. The benzyl anion calculations are less satisfactory, possibly because the benzyl anion does not converge using ω = 1.4. A different value for ω should result in convergance,[28] and perhaps better agreement. Improvement might also be obtained if allowance were made for changing β[29] as well as α. These results indicate that LCAO-MO calculations are potentially useful for providing qualitative predictions of the spectral behavior

of odd-alternant ions, although further work is necessary. Assuming a value for β and calculating the relative magnitudes of the transitions shows that quantitative agreement of these simple calculations is poor, which is to be expected. These calculations of relative transition energies provide better agreement with experiment than the perturbation formulas based on LCAO-MO, indicating iteration by the ω-technique partially compensates for electron correlation.[28]

Comparison of the Effect of a Methyl Substituent on the Spectra of Cations and Anions. To a first approximation the bonding and antibonding molecular orbitals of odd alternants are mirror images of each other centered around a central nonbonding orbital. The lowest transition in the anion can be considered as a one-electron excitation from the filled nonbonding orbital to the lowest empty antibonding orbital, whereas the lowest energy transition in the cation will be from the filled highest bonding orbital to the empty nonbonding orbital. The coefficients of the lowest antibonding and highest bonding orbitals are equal. For the the anion the former is given a positive sign [in eq. 1] and the nonbonding coefficient has a negative sign. The situation is reversed for the cation. The inductive action of a methyl substituent, therefore, should have an opposite effect on the spectrum of the cation than it does on the anion. The limited data available on the electronic spectra of odd-alternant cations generally support this prediction.

For example, the absorption of α-methylbenzyl cation, λ_{max} 435 mμ,[30] is blue shifted relative to benzyl cation, λ_{max} 470 mμ.[30] The absorption of α,α-dimethylbenzyl cation is further blue shifted, λ_{max} 390 mμ. The absorption of butenyl cation, λ_{max} 290 mμ,[31] is red shifted relative to the allyl cation, λ_{max} 273 mμ.[31] The absorption of β-methylallyl carbonium ion, λ_{max} 256 mμ,[31] is blue shifted relative to allyl carbonium ion. These shifts are all opposite those of the corresponding carbanions. The shift of the latter two cations is also opposite that predicted from eq. 1. The absorption of o,o,p-trimethylbenzyl cation (I), λ_{max} 470 mμ, is strongly blue shifted by dimethyl substitution in the α position, λ_{max} 360 mμ,[32] again a behavior opposite that expected for the carbanion.

(28) A. Streitwieser, *J. Am. Chem. Soc.*, **82**, 4123 (1960).

(29) P. C. Den Boer-Veenendaal, J. A. Vliegenthart, and D. H. W. Den Boer, *Tetrahedron*, **18**, 1325 (1962).

(30) J. A. Grace and M. C. R. Symons, *J. Chem. Soc.*, 958 (1959).

(31) J. Rosenbaum and M. C. R. Symons, *ibid.*, 1 (1961).

(32) N. C. Deno, J. J. Jaruzelski, and A. Schriesheim, *J. Org. Chem.*, **19**, 155 (1954).

Methyl substitution of both *meta* positions of I causes a red shift, λ_{max} 380 mμ,[32] which is the only carbonium ion shift in the same direction as might be expected for the carbanion. Interestingly, the spectral shifts found

for benzyl carbonium ions on methyl substitution are larger than the corresponding shifts in the spectrum of benzyl carbanions, whereas the shifts in the allyl systems are of the same magnitude.

Temperature Dependence of Photoisomerization. III.[1]

Direct and Sensitized Photoisomerization of Stilbenes

by Shmuel Malkin and Ernst Fischer

Photochemical Laboratory, The Weizmann Institute of Science, Rehovoth, Israel   (*Received December 9, 1963*)

A quantitative and comparative study was made of the direct and sensitized photoisomerization and of the fluorescence of stilbene and several derivatives, in a wide temperature range. Quantum yields for all three processes were evaluated and their interdependence was studied. The yields of the direct *trans* → *cis* photoconversion and of the fluorescence were found to change sharply on cooling, probably owing to a potential barrier of close to 2 kcal./mole in the photoconversion. No such temperature dependence was observed in the photoisomerization sensitized by benzophenone, down to −140°. This indicates that the observed barrier is situated somewhere between the first excited singlet level and the active intermediate responsible for the actual isomerization. A comparison between stilbene and its *p*-bromo derivative makes it plausible that this barrier is due to the necessity, in stilbene, to pass a second, somewhat higher excited singlet level, unattainable directly, and by-passed in bromostilbene. The nature of this level is discussed.

Introduction

In earlier publications[1,2] from this laboratory, it was shown that the quantum yield of the *trans* → *cis* photoisomerization of aromatic azo compounds drops sharply with decreasing temperatures. These results were taken to indicate the existence of potential barriers somewhere along the path from the excited singlet *trans* molecule to the ground singlet *cis* molecule. Similar preliminary results were obtained with stilbene[1] and confirmed by Dyck and McClure,[3] thus indicating the existence of potential barriers also in this case.

The photoisomerization of stilbene has been investigated by several authors. all of whom conclude that the first excited singlet state, reached by light absorption, is not directly responsible for the isomerization, which

probably occurs in a lower excited state reached subsequently. Evidence that this intermediate state is a triplet was advanced by Schulte-Frohlinde,[4] Stegemeyer,[5] and Dyck and McClure,[3] the latter authors paying particular attention to the role of excited states as intermediates in the course of energy degradation. Commenting on the potential barriers observed by the present authors, Stegemeyer[5] suggests that these

(1) Part II: S. Malkin and E. Fischer, Symposium on Reversible Photochemical Processes, Durham, N. C., April, 1962; *J. Phys. Chem.*, 66, 2482 (1962).

(2) E. Fischer, *J. Am. Chem. Soc.*, 82, 3249 (1960).

(3) R. H. Dyck and D. S. McClure, *J. Chem. Phys.*, 36, 2326 (1962).

(4) D. Schulte-Frohlinde, H. Blume, and H. Güsten, *J. Phys. Chem.*, 66, 2486 (1962).

(5) H. Stegemeyer, *ibid.*, 66, 2555 (1962).
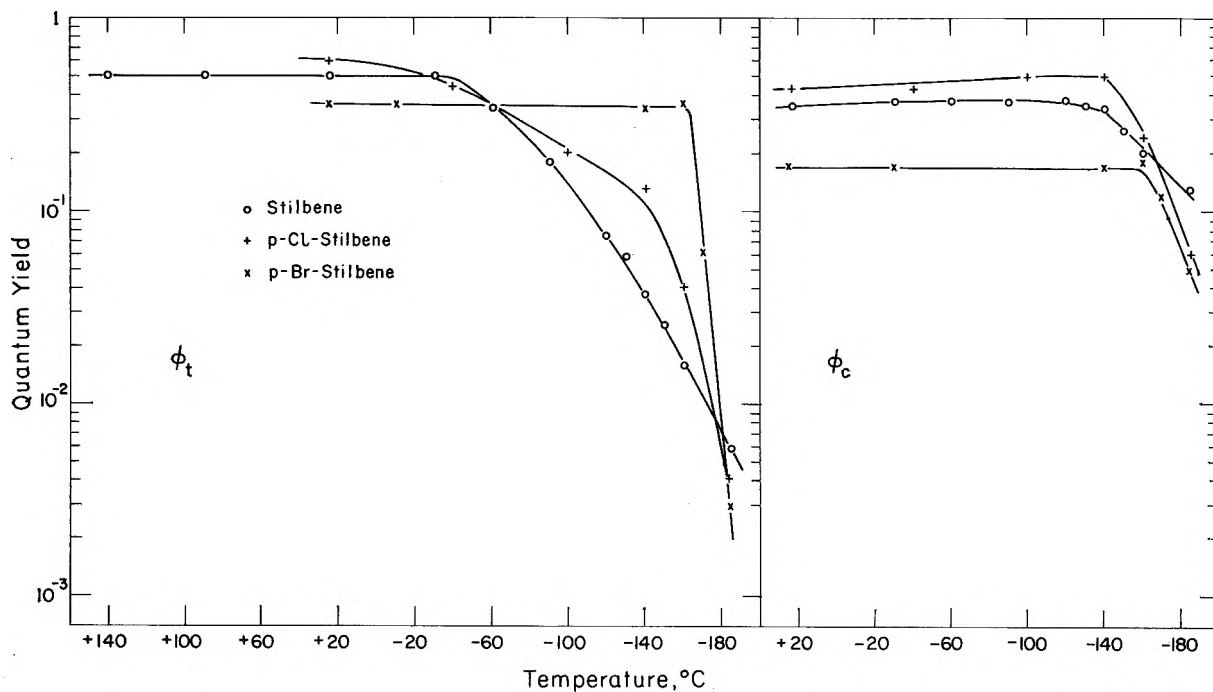
Figure 1.   Temperature dependence of the quantum yields in direct photoisomerization, ϕ_c (cis → trans) and ϕ_t (trans → cis). Solutions in methylcyclohexane–isohexane, at temperatures up to 25°, and in decalin at higher temperatures.

exist between excited (probably triplet) *trans* and *cis* states of the same multiplicity, while the other authors[3,4] believe that the barriers exist between the excited singlet and the triplet state of one isomer.   However, the evidence in all cases is not sufficiently accurate and complete to provide conclusive proof of either hypothesis.

The results to be reported here include a detailed and accurate investigation of the quantum yield of the *cis* ⇄ *trans* photoisomerization of stilbene and several derivatives over a wide range of temperatures, a parallel investigation of the fluorescence yield of the *trans* isomers, and, finally, a study of the quantum yield of photoisomerization of stilbene sensitized by benzophenone.[1,6]

Results

1.   Direct Photoisomerization.   Quantum yields were calculated[1] from the kinetics of the isomerization in both directions and the composition of the photostationary state attained after prolonged irradiation. Evaluation of the latter is somewhat complicated in stilbene, as compared with aromatic azo compounds, by the irreversible photocyclization and dehydrogenation of the *cis* isomer[7,8]: *cis*-stilbene $\xrightarrow{h\nu}$ (dihydrophenanthrene) → phenanthrene + 2H.   Fortunately, the yield of this reaction is much lower than that of the isomerization and practically vanishes at tempera-

tures below −50°.   Moreover, the quantity of phenanthrene formed can be estimated easily from its sharp absorption peak at 250 mμ, and the true spectrum of the photostationary mixture in the absence of cyclization evaluated.   The same holds also for *p*-chloro- and *p*-bromostilbene.   With the naphthyl analog, 1,2-di-(α-naphthyl)ethylene, irreversible photoreactions predominate over photoisomerization, and no quantitative measurements could be made, though the qualitative behavior of this compound is similar to that of the three stilbenes investigated, shown in Fig. 1.   Substitution of the naphthyl groups in the β-positions would probably prevent such cyclization.

The spectral changes involved in isomerization are exemplified in Fig. 2.   The temperature dependence of the quantum yields is characteristic of the compounds and varies only little with the viscosity and the chemical nature of the medium, as shown by observations on solutions in hydrocarbons, paraffin oil, alcohols, ethers, and plastic films (polystyrene).   In all cases ϕ_t, the quantum yield for the *trans* → *cis* isomerization, increases from very low values (about 0.002) at −180° to higher values at higher tempera-

(6)   S. Malkin, *Bull. Res. Council Israel*, **A11**, 208 (1962).

(7)   H. Stegemeyer, *Z. Naturforsch.*, **17b**, 153 (1962); H. Stegemeyer and H.-H. Perkampus, *Z. physik. Chem.* (Frankfurt), **39**, 125 (1963).

(8)   M. V. Sargent and C. J. Timmon, *J. Am. Chem. Soc.*, **85**, 2186 (1963), where previous literature is listed.

curves reflects competition among several deactivation pathways of the molecule, following primary excitation. One of these paths brings about isomerization and depends strongly on temperature, while the others do not cause isomerization and their rates do not change significantly with the temperature. This oversimplified scheme is shown in Fig. 3 and suffices to explain

Figure 2. Spectral changes resulting from irradiation of solutions in methylcyclohexane–isohexane at 313 mμ, for the periods indicated: parts a and b, at room temperature; c and d, at $-180°$; a and c, p-chlorostilbene (2.4 $\times$ 10^{-5} M); b and d, 1,2-di(α-naphthyl)ethylene (4 $\times$ 10^{-5} M).
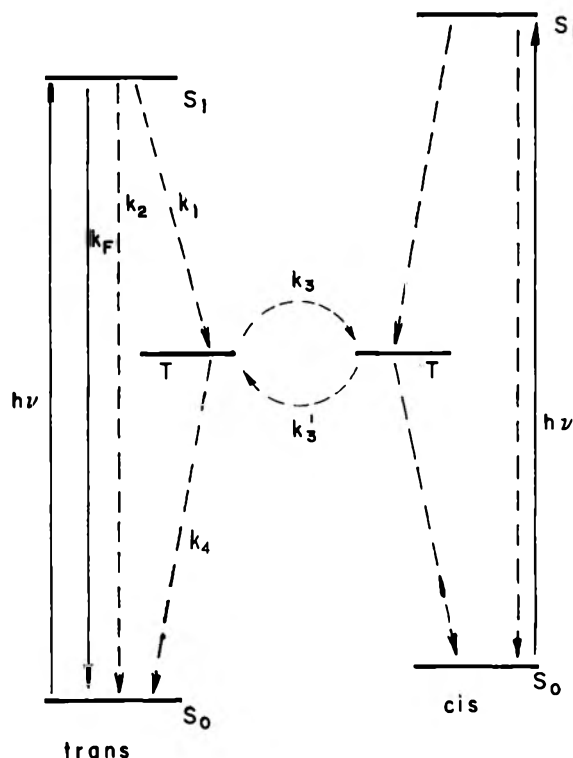
Figure 3. Scheme of energy levels involved in photoisomerization.

tures and eventually approaches a limiting value. The temperature at which this limiting value is attained varies greatly from compound to compound, e.g., $-160°$ for p-bromostilbene and $-30°$ for stilbene. This should be compared with azo compounds,[1] where a limiting value is not reached even at room temperature, and with azomethines and azoxybenzene, where ϕ_t does not change with temperature[9] down to $-180°$, suggesting that the observed value is the limiting one attained even at this low temperature.

The peculiar shape of the yield vs. temperature

the facts mentioned hitherto. If the rates of those steps which do not cause isomerization, k_F (fluorescence) and k_2 (nonradiative deactivation), do not change with the temperature, while those of the steps causing isomerization, i.e., k_1 and k_3, increase on raising the temperature, then at higher temperatures both ϕ_t and ϕ_c will reach limiting values because then $k_1 \gg k_F$, $k_1 \gg k_2$, $k_3 \gg k_4$. This means that an equilibrium between the excited forms of the two isomers will then be established rapidly, and the sum $\phi_t + \phi_c$ should approach unity. This is indeed the case for stilbene and p-chlorostilbene, but not for p-bromostilbene. The latter differs also in the shape of its ϕ_t vs. temperature curve, with ϕ_t staying constant down to $-160°$ and then dropping sharply on further cooling (Fig. 1).

(9) S. Malkin and E. Fischer, to be published.

Dyck and McClure,[3] whose observations are qualitatively similar to the above, suggest that the primarily reached excited state, S*, can pass into the excited state responsible for isomerization in two ways. One of these predominates in stilbene and the other in p-bromostilbene, probably because of the enhancement of singlet-triplet transitions by the heavy Br atom. This fact suggests that k_1, rather than k_3, in the above scheme changes with the temperature.

2. Fluorescence of trans-Stilbene. In order to test the above hypothesis, the temperature dependence of the fluorescence intensity was investigated. As seen in Fig. 3, the sharp decrease of ϕ_t on cooling should cause a concurrent rise in the yield of fluorescence. This was proved by Dyck and McClure[3] to be qualitatively true. The following results prove the quantitative interdependence of isomerization and fluorescence in stilbene.

The luminescence spectra of stilbene and p-chloro- and p-bromostilbene were measured over a wide range of temperature. The areas of the spectral curves, some of which are shown in Fig. 4, were assumed to be proportional to the quantum yields at each temperature. Table I summarizes the observations, with the quantum yields of fluorescence, ϕ_F, expressed as fractions of the highest quantum yield ϕ_F^∞, reached at $-183°$ with stilbene.

Table I: Temperature Dependence of ϕ_t and ϕ_F/ϕ_F^∞ in Solutions of Stilbene (0.8×10^{-5} mole/l.) and p-Chlorostilbene[a] (0.85×10^{-5} mole/l.) in Methylcyclohexane–Isohexane

T,	Stilbene		p-Chlorostilbene	
°C.	ϕ_t	ϕ_F/ϕ_F^∞	ϕ_t	ϕ_F/ϕ_F^∞
+25	0.50	0.08	0.60	0.11
−40	0.46	0.18	0.45	0.39
−65	0.31	0.50		
−80			0.29	0.62
−90	0.18	0.71		
−100			0.20	0.68
−105	0.12	0.74		
−123	0.07	0.90		
−140	0.04	0.97	0.13	0.70
−174			≈0.01	0.70
−183	0.006	1.00		

[a] For both compounds the fluorescence yields refer to ϕ_F^∞ of stilbene.

According to the scheme in Fig. 3, ϕ_t and ϕ_F may be expressed by

$$\phi_t = \alpha k_1/(k_1 + k_2 + k_F);$$

$$\phi_F = k_F/(k_1 + k_2 + k_F) \qquad (I)$$
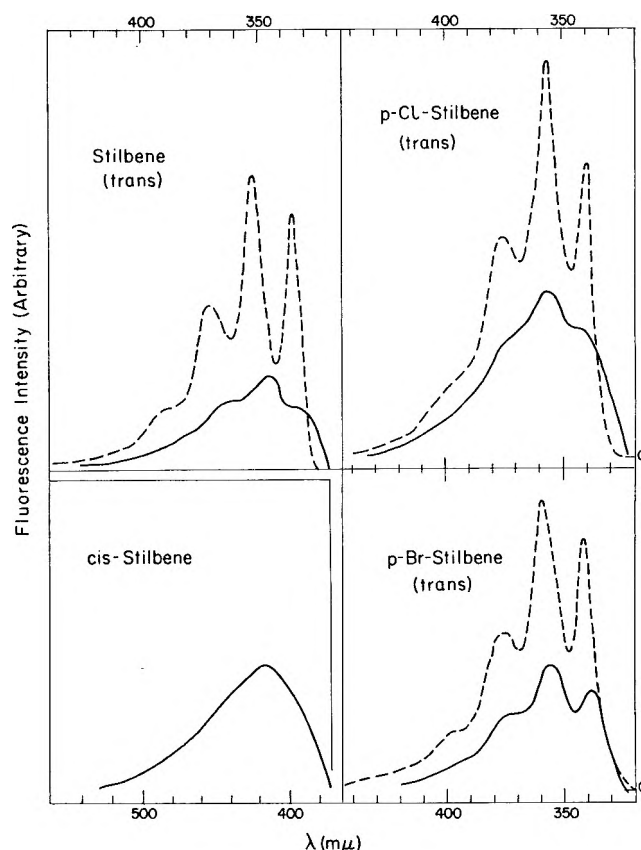
Figure 4. Emission spectra of stilbene and derivatives, excited with light at 313 mμ: full lines, at 25°; dashed lines, at −180°. The intensity scales at both temperatures are arbitrary. The emission of cis-stilbene was measured at −180° and corrected for the emission of traces of trans-stilbene accompanying the cis isomer.

where k_F and k_2 denote the rate constants of radiative and radiationless transitions from the excited to the ground singlet states, respectively, and α is a temperature-independent constant giving the probability of the excited intermediate (triplet?) to be transformed to the cis isomer. If ϕ' denotes the yield of the radiationless transition, given by $k_2/(k_1 + k_2 + k_F)$, the following expression will relate the various yields

$$\phi_F + \phi' + \phi_t/\alpha = 1 \qquad (II)$$

Dividing eq. II by ϕ_F^∞ in order to be able to use the relative fluorescence yields ϕ_F/ϕ_F^∞, we get

$$\frac{\phi_F}{\phi_F^\infty} = \frac{1 - \phi'}{\phi_F^\infty} - \phi_t \left(\frac{1}{\alpha \phi_F^\infty} \right) \qquad (III)$$

This equation leads to a linear relationship between the relative fluorescence yield and ϕ_t if $\phi_t \ll 1$. Figure 5 shows that such a relationship holds for stilbene and partly for p-chlorostilbene. From the slope of the
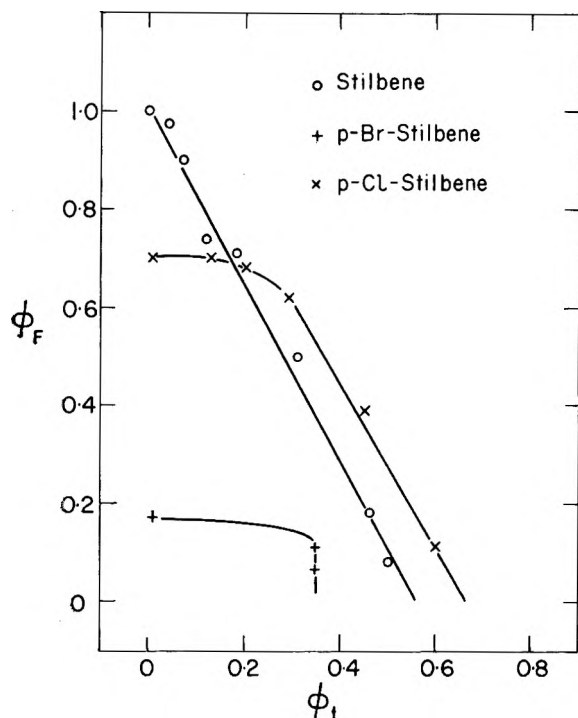
Figure 5. Interdependence of the quantum yields of fluorescence, ϕ_F, and of *trans* → *cis* photoisomerization, ϕ_t.

Table II : Temperature Dependence of ϕ_F and ϕ_t of a Solution of p-Bromostilbene in Methylcyclohexane–Isohexane (0.62 × 10⁻⁵ mole/l.)

T, °C.	ϕ_F	ϕ_t
+25	0.065	0.35
−40	0.08	0.35
−115	0.11	0.35
−135	0.12	0.35
−155	0.13	0.35
−183	0.17	0.003

straight lines and their intercepts with the vertical axis, $\alpha\phi_F{}^\infty$ and $\phi_F{}^\infty$ can be calculated. For stilbene the intercept is close to 1.0, and therefore $1/\phi_F{}^\infty \approx 1$, i.e., $\phi_F{}^\infty \approx 1$.

This conclusion was verified by a direct estimation of ϕ_F, by way of a comparison with the fluorescence of anthracene, the quantum yield of which is known to be between 0.22 and 0.28. The experimental results lead to $1 \leqslant \phi_F{}^\infty \leqslant 1.25$, with an experimental error of about 25%, thus justifying the above conclusion that the fluorescence yield of *trans*-stilbene approaches unity at low temperatures.

The slope of the curve for stilbene in Fig. 5 yields a value of $\alpha\phi_F{}^\infty = 0.55$, and therefore $\alpha \approx 0.55$. This means that the excited intermediate (triplet?) of stilbene has approximately the same chance of passing into the *cis* and the *trans* ground states, while the fact that $\phi' \approx 0$ shows that the rate of the radiationless transition from the excited to the ground singlet *trans* state is negligible in comparison with that of the radiative transition and the photoisomerization.

p-Bromostilbene shows a very different dependence of ϕ_F on temperature, as shown in Table II, where the absolute values of ϕ_F are given. These were calculated by comparison with the fluorescence of anthracene, as described above. The corresponding values for the photoisomerization yields are also tabulated.

The absence of any direct correlation between photoisomerization and fluorescence is evident. The sudden drop in ϕ_t below −160° without a concurrent rise in fluorescence yield is particularly striking and obviously cannot be due to a transition competing with fluorescence. It therefore appears that with this compound there exist transitions which are not allowed in stilbene.

p-Chlorostilbene occupies a position somewhere between stilbene and its p-bromo derivative, as seen in Fig. 5. Apparently, the assumption leading to a linear relationship between ϕ_t and ϕ_F holds only in a part of the temperature range. Together with the fact that $\phi_F{}^\infty$ is only 0.7 this indicates that $\phi' > 0$ and/or that other modes of deactivation exist.

In this context we could confirm Stegemeyer's[5] observation of luminescence of *cis*-stilbene. At temperatures below −160°, glasses of *cis*-stilbene solutions show not only a weak fluorescence spectrally identical with that of *trans*-stilbene, and attributable to traces of the latter, but also a broad emission peak at about 420 mμ (Fig. 4) with a quantum yield of about 0.05 at −180°. This may be due to phosphorescence of *cis*-stilbene, though according to Evans' direct measurements[10] of singlet → triplet absorption spectra, in the presence of oxygen at high pressure, this emission should appear at longer wave lengths.[10a] The observed luminescence is definitely not due to traces of phenanthrene.

3. Photosensitized Isomerization. The photosensitized *cis* ⇄ *trans* isomerization of stilbene in the presence of benzophenone, with light absorbed only by the latter, has already been reported in preliminary communications by the authors[1,6] and independently by Hammond and Saltiel.[11] The latter, following their extensive work on other photosensitized reactions, used a series of ketones and quinones as sensitizers.

(10) D. F. Evans, *J. Chem. Soc.*, 1351 (1957).

(10a) NOTE ADDED IN PROOF.—Very recently, Lippert proved that this is actually fluorescence (in press).

(11) G. S. Hammond and J. Saltiel, *J. Am. Chem. Soc.*, **84**, 4983 (1962).

The system stilbene–benzophenone is particularly convenient since the absorption of benzophenone extends to about 400 mμ, while stilbene absorbs only at wave lengths less than about 340 mμ (Fig. 6). Carefully filtered light at 365 mμ emitted by a mercury arc is thus absorbed only by the sensitizer. On the other hand, analysis is facilitated by the fact that in the region 290–320 mμ the spectral absorption of stilbene predominates (Fig. 6). Control experiments in the absence of benzophenone showed no isomerization of stilbene.
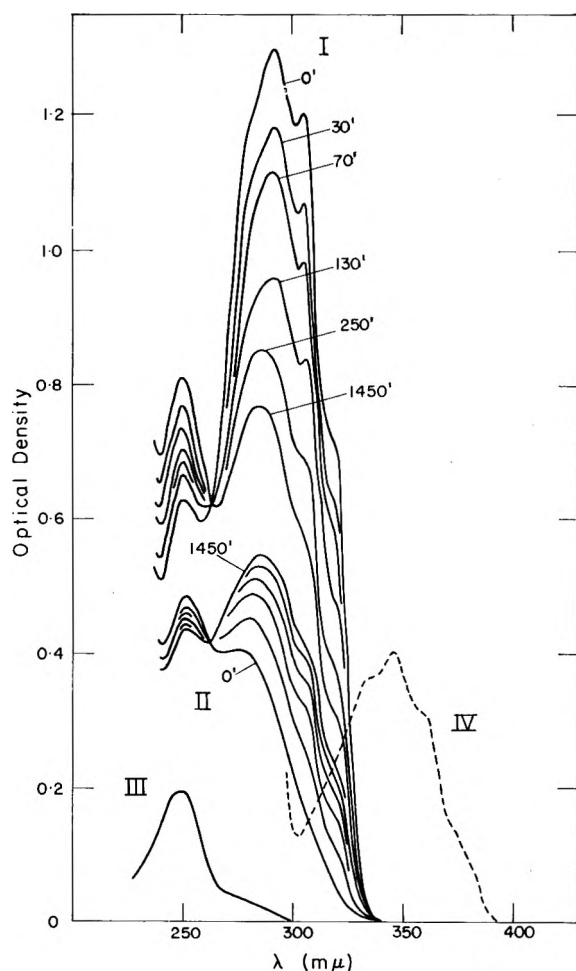
Figure 6. Photoisomerization of stilbene sensitized with benzophenone in methylcyclohexane. Spectra in 2-mm. cells: I, 2.4 × 10⁻⁴ M stilbene, 7 × 10⁻⁵ M benzophenone; II, 1.5 × 10⁻⁴ M stilbene, 7 × 10⁻⁵ M benzophenone; III, 7 × 10⁻⁵ M benzophenone only; IV, 3 × 10⁻² M benzophenone, 1-mm. cell. I and II are typical reaction mixtures after 100-fold dilution, III shows the absorption of benzophenone in these mixtures, while IV shows the absorption in the 365-mμ region. I and II depict gradual photoisomerization with light at 365 mμ, starting with trans- and cis-stilbene, respectively. Irradiation times were as indicated.

Extensive earlier work[12–14] has shown that irradiation of benzophenone results in formation of triplet benzophenone with a yield of close to unity, and that these triplet molecules can transfer their excitation energy to neighboring molecules with a high efficiency.

The following simple reaction scheme was used as a working hypothesis.

B + $h\nu$ ⟶ B* (singlet);

B* (singlet) ⟶ B** (triplet)

B** + trans-S $\xrightarrow{K_1}$ B + trans-S**;

B** + cis-S $\xrightarrow{K_2}$ B + cis-S**

B** $\xrightarrow{K_3}$ B

trans-S $\xleftarrow{K_3}$ trans-S** $\xrightarrow{K_4}$ cis-S;

cis-S $\xleftarrow{K_6}$ cis-S** $\xrightarrow{K_7}$ trans-S
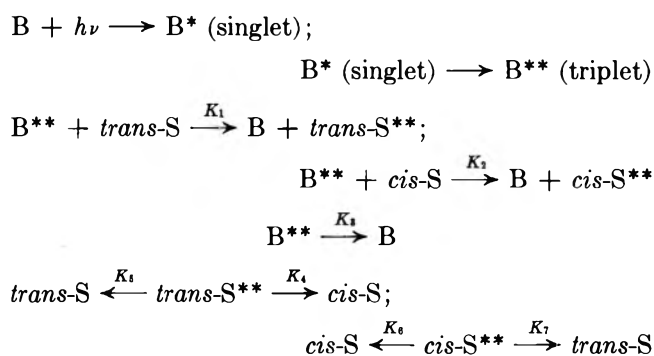
Here B = benzophenone, S = stilbene, * denotes the first excited singlet state, ** denotes the lowest triplet state, K_1 and K_2 are the rates of energy transfer from B** to cis- and trans-stilbene, while K_3 summarizes all other modes of deactivation of B**. The last two equations describe the deactivation of cis- and trans-S** to cis- and trans-stilbene in the ground state.

Let us denote by C_2 and C_1 the concentrations of cis- and trans-stilbene, respectively, by $C_0 = C_1 + C_2$ the total concentration of stilbene, by ϕ_1 the yield of formation of cis-stilbene from trans-S**, and by ϕ_2 that of formation of trans-stilbene from cis-S**. The ϕ's will be given by

$$\phi_1 = K_4/(K_4 + K_5); \quad \phi_2 = K_7/(K_6 + K_7) \quad (1)$$

and the relative rates of energy transfer from B** to trans- and cis-stilbene, respectively, by

$$K_1 C_1/(K_1 C_1 + K_2 C_2 + K_3);$$

$$K_2 C_2/(K_1 C_1 + K_2 C_2 + K_3) \quad (2)$$

Equations 1 and 2 lead to the following kinetic equation for the isomerization.

$$\frac{dC_1}{dt} = \frac{I}{V}\left(-\frac{\phi_1 K_1 C_1}{K_1 C_1 + K_2 C_2 + K_3} + \frac{\phi_2 K_2 C_2}{K_1 C_1 + K_2 C_2 + K_3}\right) \quad (3)$$

(12) H. L. J. Bäckström and K. Sandros, Acta Chem. Scand., 14, 48 (1960).

(13) G. Porter and F. Wilkinson, Proc. Roy. Soc. (London), A264, 1 (1961).

(14) G. S. Hammond, N. J. Turro, and P. A. Leermakers, J. Phys. Chem., 66, 1144 (1962).

Here V is the volume, in liters, of the solution undergoing reaction, and I denotes the rate of light absorption by benzophenone, in einsteins/sec. The solution of this difficult equation is greatly simplified by assuming that $K_1 = K_2$, i.e., that under otherwise identical conditions the probability of energy transfer from B** to cis- and to trans-stilbene is equal. As will be shown, the experimental results confirm the rate equation derived on the basis of this assumption.

Putting $K_1 = K_2 = K$ in eq. 3, we get

$$\frac{dC_1}{dt} = \frac{I}{V} \frac{K}{KC_0 + K_3} (\phi_2 C_2 - \phi_1 C_1) =$$

$$\frac{I}{V} \frac{K}{KC_0 + K_3} [\phi_2 C_0 - (\phi_1 + \phi_2)C_1] \quad (4)$$

This equation is similar to the rate equation for two opposing first-order reactions, and its solution is given by

$$\ln \frac{C_1 - C_1^\infty}{C_1^0 - C_1^\infty} = -\frac{I}{V} \frac{K}{KC_0 + K_3} (\phi_1 + \phi_2)t \quad (5)$$

where C_1^0 and C_1^∞ are the initial and the photostationary concentrations of trans-stilbene, respectively. Thus ln $(C_1 - C_1^\infty)$ should be a linear function of the time t. This was verified by experiments such as those described in Fig. 7, where the concentrations C_1 have been replaced by the optical densities δ at 305 mμ, which are linearly related to C_1. It is seen that eq. 5 holds over a wide range of concentrations of stilbene and benzophenone.

In order to find K, K_3, and $(\phi_1 + \phi_2)$, one may use the fact that the slopes of the straight lines depicted by eq. 5 are a function of C_0. Let X denote the observed slope, which according to (5) is given by

$$X = -\frac{I}{V} K(\phi_1 + \phi_2) \frac{1}{KC_0 + K_3}$$

or

$$\frac{1}{X} = -\frac{V}{I(\phi_1 + \phi_2)} C_0 - \frac{K_3 V}{IK(\phi_1 + \phi_2)} \quad (6)$$

The linear relationship between $1/X$ and C_0 was confirmed experimentally. The slope of this straight line gives $(\phi_1 + \phi_2)$. From the latter and the value of $1/X$ at the intersection of the line with the vertical axis, K/K_3 can be calculated.

Furthermore, in the photostationary state $dC_1/dt = 0$, and eq. 4 will result in

$$\phi_2 C_0 = (\phi_1 + \phi_2)C_1^\infty \quad (7)$$

making possible the calculation of ϕ_1 and ϕ_2.

By writing (7) in a different way, we have

$$\phi_1/\phi_2 = (C_0 - C_1^\infty)/C_1^\infty \quad (7a)$$

i.e., the isomeric composition at photoequilibrium does not depend on the total concentration of stilbene, C_0. This conclusion, too, was verified experimentally.

The numerical results calculated by the application of eq. 6 and 7 to the experimental data are summarized in Table III, together with the "limiting values" (at high temperatures) of the quantum yields ϕ_t and ϕ_c, measured for the direct photoisomerization as described in paragraph 1.

The ratio K_3/K is seen to be nearly constant for the three compounds (i.e., energy acceptors) investigated. Since K_3 is by definition independent of the acceptor, this means that K is almost the same for all three acceptors. This seems reasonable if it is assumed that the transfer of energy from benzophenone triplet to the acceptor is a diffusion-controlled process. If this is
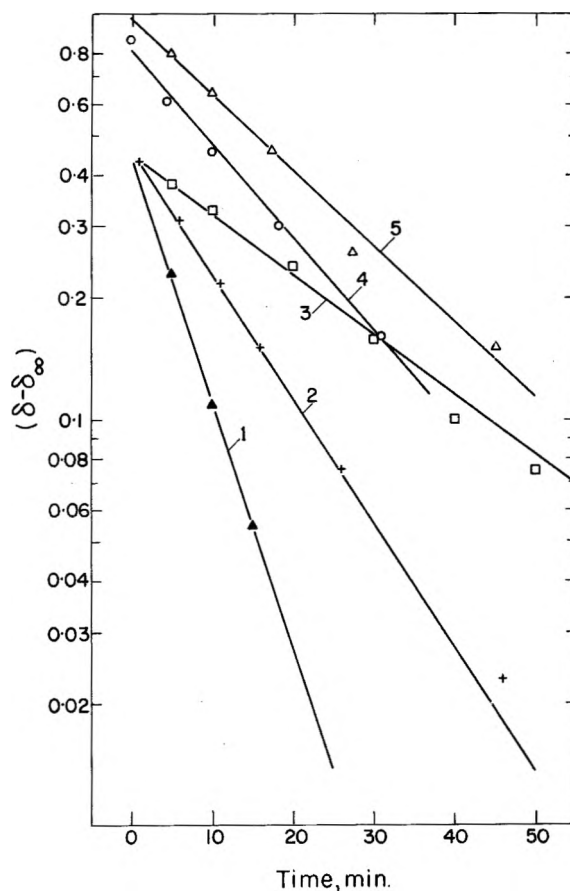
Figure 7. Kinetics of sensitized photoisomerization of trans-stilbene at 25° in methylcyclohexane. Stilbene concentrations: (1), (2), (3), 3.4 × 10⁻⁴ M; (4), 6.1 × 10⁻⁴ M; (5), 1.2 × 10⁻⁴ M. Benzophenone concentrations: (1), 2.1 × 10⁻² M (29% light absorption); (2), 0.95 × 10⁻² M (14.5% absorption); (3), 0.45 × 10⁻² M (7.2% absorption); (4), 1.03 × 10⁻² M; (5), 1.13 × 10⁻² M.

	ϕ_1	ϕ_t	ϕ_2	ϕ_0	$10^3 K_3/K$
Stilbene	0.50	0.50	0.27	0.30	0.58
p-Chlorostilbene	0.60	0.60	0.40	0.4–0.5	0.50
p-Bromostilbene	0.33	0.35	0.20	0.17	0.55

the case, K can be estimated from Smoluchowski's equation, making the further simplifying assumption that the effective radii of the colliding molecules are identical. The result is given by $K = 8RT/3000\eta \approx 3 \times 10^3$ l. mole^{-1} sec.$^{-1}$. Using the above result of $K_3/K = 0.5 \times 10^{-3}$, this leads to $K_3 \approx 1.5 \times 10^6$ sec.$^{-1}$, equivalent to a half-life of 0.5×10^{-6} sec., in reasonable agreement with 1.9×10^{-6} sec. calculated by Bäckström[12,15] by a different method for benzophenone in benzene solution.

The good agreement between the quantum yields of the direct and the sensitized isomerization is remarkable, in view of the considerable experimental errors involved. It may be tentatively concluded that the same intermediate state or states are involved in both processes. More specifically, in terms of the energy scheme in Fig. 3, state T is reached also by energy transfer from triplet benzophenone.

In view of the results regarding the temperature dependence of direct photoisomerization it would obviously by interesting to find out whether ϕ_1 and ϕ_2 also change with temperature. However, this is impractical experimentally for the following reason. Photosensitized isomerization in both directions is slowed down sharply on cooling, probably because K decreases. On the other hand, the solubility also decreases on cooling, so that with decreasing temperature and increasing viscosity one has to work under conditions for which $KC_0 \ll K_3$ in eq. 5, and therefore eq. 6 can no longer be used to calculate $(\phi_1 + \phi_2)$. However, as stated before, the ratio ϕ_1/ϕ_2, which equals the ratio C_2^∞/C_1^∞ (cf. eq. 7a) of the concentrations of the cis and trans isomers at photoequilibrium, is independent of the over-all concentration. This quantity could therefore be measured at low concentrations, where the rates of photoisomerization are reasonably fast. Measurements of the photostationary state were made at temperatures down to $-140°$, when this state was attained after several days of irradiation.[16] Within this temperature range, ϕ_1/ϕ_2 was found to be constant at about 1.8, while ϕ_c/ϕ_t in direct photoisomerization changes from 1.6 at 25° to 0.11 at $-140°$. While this observation does not prove that neither ϕ_1 nor ϕ_2

changes with temperature, it makes this conclusion plausible.

Exploratory measurements with solutions in paraffin oil, having a viscosity of about 150 times that of methylcyclohexane, gave further support for the conclusion that the reaction is diffusion-controlled. The initial rate of isomerization observed in this solvent was only about $\frac{1}{35}$ as high, indicating that the high viscosity reduces mainly K (cf. eq. 5).

Incidentally, the validity of the above equations could be checked in another way. According to eq. 4, the initial rate of photoisomerization cis → trans, when starting from pure cis isomer, i.e., $C_2 \gg C_1$, is given by $dC_2/dt = -(I/V)\phi_2 KC_2/(KC_0 + K_3)$, while when starting from pure trans, when $C_1 \gg C_2$, the rate will be $dC_1/dt = -(I/V)\phi_1 KC_1/(KC_0 + K_3)$. The ratio between the initial slopes of the two kinetic curves then gives approximately the ratio ϕ_1/ϕ_2. The latter was thus observed to equal that found from photostationary state measurements, well within the experimental error of about 10%.

4. Height of the Potential Barrier in Direct trans → cis Photoisomerization. In view of the results reported above, it seems plausible that it is step 1 in the scheme of Fig. 3 which is slowed down on cooling. Without as yet specifying what is meant by step (or steps) 1, one may calculate the potential barrier corresponding to the observed temperature dependence of ϕ_t, as follows: assuming an Arrhenius equation to hold for step 1, $k_1 = k_1^0 \exp(-E/RT)$, and substituting this for k_1 in eq. I, we have

$$\phi_t = \alpha \frac{k_1^0 \exp(-E/RT)}{k_2 + k_F + k_1^0 \exp(-E/RT)} \qquad \text{(IV)}$$

or

$$\frac{\alpha}{\phi_t} = 1 + \exp(E/RT) \frac{k_2 + k_F}{k_1^0}$$

and therefore

$$\ln\left(\frac{\alpha}{\phi_t} - 1\right) = \frac{E}{RT} + \ln\left(\frac{k_2 + k_F}{k_1^0}\right) \qquad \text{(V)}$$

Equation IV reduces at high temperatures to $\alpha/\phi_t = 1 + (k_2 + k_F)k_1^0$, showing that, provided $k_1^0 \gg k_2 + k_F$, α is the limiting value of ϕ_t at high temperatures. For stilbene, it was shown in paragraph 2 that α is

(15) K. Sandros and H. L. J. Bäckström, *Acta Chem. Scand.*, **16**, 958 (1961).

(16) At the lowest temperatures the low rate of isomerization made it impractical to achieve a stationary state. Instead, this state was approached from both sides, *i.e.*, by cis → trans and trans → cis, until the two states differed by 10%. The mean of the two states was then used as the correct value.

approximately 0.55, whereas according to Fig. 1 ϕ_t approaches 0.50 at high temperatures. Introducing $\alpha = 0.55$ into eq. V, linear plots of ln $[(\alpha/\phi_t) - 1]$ vs. $1/T$ were indeed observed, as shown in Fig. 8. From the slope of these lines and their intersection with the vertical axis, the following values were calculated.

	E, kcal./mole	$k_1^0/(k_2 + k_F)$
Stilbene	1.7	110
p-Chlorostilbene	1.8	250

A rough estimate of k_1^0 can be made by taking $k_F = 10^8$ sec.$^{-1}$, $k_2 = 0$, leading to $k_1^0 \approx 10^{10}$, which is normal for reactions not involving a change in multiplicity, but very high for a reaction involving such a change.

Discussion

In view of the results obtained with p-bromostilbene, both regarding fluorescence and direct photoisomerization, the scheme in Fig. 3 has to be modified as suggested in Fig. 9, where radiative and radiationless transitions are denoted by full and dashed lines, respectively. In stilbene, the sequence of events after the primary excitation is given by k_1 (involving a potential barrier), k_4, and k_6, leading to T′ in which the isomerization takes place. In p-bromostilbene ($k_1 + k_4$) is by-passed by k_5, a forbidden singlet-triplet transition whose probability is increased by the spin-orbital perturbation introduced by the bromine atom. The fact that the fluorescence yield is only slightly attenuated by this substitution shows that step k_1

Figure 9. Modified scheme of energy levels involved in photoisomerization.

is unaffected by this substitution, and therefore probably is a singlet-singlet transition, i.e., S_2 is a singlet level unattainable radiatively. Furthermore, since in p-bromostilbene the fluorescence yield does not exceed 17% even at $-180°$, when the isomerization yield is practically down to zero, it appears that there exists another triplet state in which isomerization does not occur and from which, under the influence of the bromine atom, a transition to the singlet trans ground state is possible (k_7 in Fig. 9). This is also borne out by the fact that the sum of the high temperature "limiting" values, ($\phi_c + \phi_t$), is only about 0.5. The sharp drop in ϕ_t from $-160°$ downward may be due to competition between k_6 and k_7, with the latter being favored at the lowest temperatures. In sensitized photoisomerization, energy transfer from the excited sensitizer seems to result in the direct formation of T, thereby causing the good agreement between the yields for direct and sensitized photoisomerization.

For p-bromostilbene, it is possible to estimate the yields of steps 1 and 5. It may be assumed that in this compound, as in stilbene proper, the nonradiative deactivation k_2 is negligible in comparison with the other deactivation processes.[16a] The fluorescence yield

Figure 8. Evaluation of the activation energy for trans → cis "direct" photoisomerization (see text and Fig. 1).

(16a) This assumption may be disputed.

will then be given by $\phi_F = k_F/(k_F + k_5 + k_1)$. If only k_1 is assumed to decrease on cooling, this equation will be reduced at low temperatures to $\phi_F \approx k_F/(k_F + k_5)$. Introducing the experimental ϕ_F's at 25 and $-115°$ we have $0.065 = k_F/(k_F + k_5 + k_1)$ and $0.13 = k_F/(k_F + k_5)$. Defining $\Sigma k = k_F + k_5 + k_1$ and rearranging we have $\Sigma k/(k_F + k_5) = 0.13/0.065$, and therefore at $25°$ $k_1 = k_F + k_5$, or $\Sigma k = 2k_1$. Defining the yields of steps 1 and 5 at $25°$ by $\phi_1 = k_1/\Sigma k$; $\phi_5 = k_5/\Sigma k$, we have $\phi_1 = k_1/2k_1 = 0.5$, and therefore $\phi_5 = 1 - \phi_F - \phi_1 = 0.435$. In other words, at room temperature the chances of step 1 and 5 are almost equal in p-bromostilbene.

The scheme of Fig. 9 is of course speculative, but suffices to explain the results obtained. The current investigation, as well as others in this field, may serve to emphasize how photoisomerization and related phenomena evoke more general theoretical problems, such as singlet–triplet transitions, evaluation of energy levels and potential curves, and transfer of excitation energy between molecules. A more thorough evaluation of current theories will be published separately, together with a comparison of the results in stilbene with those obtained in compounds containing lone electron pairs (aromatic azo and azoxy compounds, azomethines). At this point only a few general conclusions will be indicated. Dyck and McClure[3] have proved conclusively that the order of the central ethylenic bond in the lowest excited state of stilbene is only slightly lower than in the ground state. This rules out isomerization in the lowest excited singlet state, and also indicates that earlier LCAO–HMO calculations, leading to a much lower bond order in this state, are inaccurate. This leaves little choice but to assume that isomerization involves one or more of the triplet states possible in stilbene.

As to the nature of the intermediate singlet level S_2, one possible approach is using the concept of $+$ and $-$ levels introduced by Pariser[17] and others. Pariser assumes the operation of selection rules allowing only $+ \longleftrightarrow -$ nonradiative singlet–triplet transitions. If S_1 and T have the same sign and S_2 a different one, the transition $S_1 \rightarrow T$ would be forbidden and $S_2 \rightarrow T$ allowed, necessitating the sequence $S_1 \rightarrow S_2 \rightarrow T$, in which $S_1 \rightarrow S_2$ would involve passing a potential barrier. A reversal of the positions of S_1 and S_2 would then eliminate the need to pass such a barrier. This might well be the case in the cis isomer, although too small a barrier would escape detection in any case.

In azo compounds the $n-\pi^*$ transition might be involved. It is remarkable that the temperature dependence of ϕ_t was observed only in those compounds whose central part is symmetrical, i.e., stilbenes

and azo compounds, but not azomethines (—CH=N—) and azoxy compounds (—N=N—).[9]

$$\overset{\text{||}}{\underset{\text{O}}{}}$$

Experimental

Spectrophotometry, Irradiation, Actinometry, Analysis, and Calculation of Quantum Yields. All these were essentially as described in part II.[1] For the sake of better spectral definition, the 313-mµ group of mercury emission lines was isolated by a combination of a Corning filter No. 9863, 5 mm. of a solution of potassium chromate in water (300 mg./l.), and 10 mm. of a solution of potassium biphthalate[13] in water (25 g./l.). Most experiments were carried out with solutions in carefully dried methylcyclohexane–isohexane (1:1) mixtures. No difference in photoisomerization behavior was observed between air-saturated solutions and solutions in which the solvent was distilled under high vacuum from K–Na alloy onto the solute in the measuring cell, the latter then being fused off. A tiny magnetic stirrer served to ensure mixing of the solutions being irradiated, whenever their viscosity was not too high.

Sensitized Photoisomerization. Experiments at high concentrations were carried out in the above solvent mixture or in methylcyclohexane, in cells having a light path of 10 or 25 mm. Samples of 0.1 ml. were withdrawn after appropriate irradiation periods and diluted 100-fold. Their absorption spectra were then measured in 2-mm. cells in order to determine their isomeric composition (Fig. 6). At low concentrations the solutions were investigated directly in 1-mm. cells. At all temperatures the spectrum of the mixture of benzophenone and stilbene was found to be identical with the sum of the spectra of the component solutions, indicating that probably no complex formation between the two solutes in their ground state takes place.

Luminescence Spectra. These were measured at right angles to the exciting light. The latter was in all cases at 313 mµ, isolated from a Philips spectral lamp mercury arc by means of an interference filter transmitting 2.5% at 313 mµ and less than 0.05% at 302 mµ. The resulting low intensities of exciting light caused only little isomerization during the recording of the luminescence spectra. The latter were corrected accordingly. The light emitted by the solutions entered a Bausch and Lomb 500-mm. monochromator driven by a synchronous motor. A Type 6256Q E.M.I. photomultiplier was placed opposite the

(17) R. Pariser, *J. Chem. Phys.*, **24**, 250 (1956).

(18) R. E. Hunt and W. Davis, Jr., *J. Am. Chem. Soc.*, **69**, 1415 (1947).

exit slit and its anode current recorded directly by a Kipp & Zonen micrograph recorder having a maximal sensitivity of 0.1 μa. full scale. The spectral sensitivity of the photomultiplier over the range 302–405 mμ was found to be constant within 10%, and the experimental curves therefore were not corrected accordingly. The cell containing the luminescent solution was placed inside a copper block cooled by liquid or gaseous air and insulated by a quartz dewar. The luminescence intensities in a range of temperatures were assumed to be proportional to the areas beneath the recorded spectral curves. The relative luminescence yields were taken as proportional to the above intensities, after correcting them for the temperature dependence of the absorbance at 313 mμ. The latter was always smaller than 50%, the limit up to which the luminescence intensity was found proportional to the absorbance. The yields measured in this way were reproducible to within 10%.

(19) R. Anschütz, *Ber.*, **60**, 1320 (1927).
(20) W. Wislicenus and H. Wren, *ibid.*, **38**, 502 (1905).

Comparison of Various Liquid Theories with the Significant Structure Theory

by Teresa S. Ree, Taikyue Ree, and Henry Eyring

Department of Chemistry, University of Utah, Salt Lake City, Utah (*Received December 12, 1963*)

The significant structure theory of liquids is applied to calculate the compressibility factor of argon gas and the reduced excess entropy, energy, and heat capacity, the compressibility, and the thermal expansion coefficient of the liquids of inert gases and nitrogen in equilibrium with their vapor. The calculated thermodynamic data are compared with experiment and with the values calculated from other theories. It is found that the significant structure theory agrees best with experiment. The quantum effect in liquids of the elements of low atomic weight is discussed. It is pointed out that the significant structure theory accounts for this effect very well, whereas the cell model explains the effect only when some correction factors are introduced into the partition function.

I. Introduction

The free-volume theory of Lennard-Jones and Devonshire[1,2] is the most widely used theory of liquids. These authors assumed that the cells are singly occupied and that each molecule moves within its cell in the potential field of its neighbors fixed at the centers of their cells. Moreover, they artificially introduced the extra factor e^N into the partition function. Subse-

(1) J. E. Lennard-Jones and Devonshire, *Proc. Roy. Soc.* (London), A163, 53 (1937).
(2) R. H. Wentorf, R. J. Beuhler, J. O. Hirschfelder, and C. F. Curtiss, *J. Chem. Phys.*, **18**, 1484 (1950).

quently, the theory has been extended by several authors[3-6] by introducing holes into the lattice of liquids. In this way, they succeeded in introducing the factor, e^N, into the partition function. When applied to equations of state, however, these hole theories do not show much improvement over the previous free-volume theory. Another successful theory is the significant structure theory proposed by Eyring, Ree, and their associates.[7-14] The basis of this approach is the assumption that a molecule acquires gas-like properties as it jumps into a neighboring fluidized hole, while it acquires solid-like properties as it vibrates at an equilibrium site. It was shown[13] that when the significant structure theory is applied to the dense gaseous region, this theory is far better than the free-volume theory or the radial distribution method developed by Kirkwood.[15] Recently, Henderson proposed a hole theory of liquids[16,17] which gives better results than previous hole theories for the equation of state, but the results for thermodynamic properties of liquids at lower temperatures and higher densities were rather poor. In this paper, the significant structure theory is used to calculate thermodynamic properties in the region to which Henderson referred, and the results are compared with those obtained from Henderson's hole theory and from the free-volume theory of Lennard-Jones and Devonshire. Furthermore, the equation of state of the significant structure theory is compared with that obtained by Monte Carlo calculations and by previous hole theories.[18]

II. Calculations

According to the significant structure theory, the partition function, f, of a liquid is written as

$$f = (j_s)^{V_s N/V} (f_g)^{(V - V_s)N/V} \qquad (1)$$

Here, f_s and f_g are the partition functions of the solid and the gas, respectively, V is the molar volume of the liquid, V_s is the volume of the solid at the melting temperature, and N is Avogadro's number. For rare gas liquids, f_g and f_s in eq. 1 are written as[7,12,13]

$$(f_g)^{(V - V_s)N/V} = \left[\frac{(2\pi mkT)^{3/2}}{h^3} (V - V_s) \right]^{(V - V_s)N/V} \times$$

$$\left(\left(N \frac{V - V_s}{V} \right)! \right)^{-1} = \frac{(2\pi mkT)^{3/2}}{k^3} \frac{eV}{N} \qquad (2)$$

The form of eq. 2 follows from our model[12a,b] according to which the $3N(V - V_s)/V$ degrees of freedom associated with the $N(V - V_s)/V$ moving vacancies, or "gas-like molecules," communally share the excess volume, $V - V_s$.

In eq. 2

$$f_s = e^{E_s/RT} \psi^3 \left[1 + n \frac{V - V_s}{V_s} \exp \frac{-aE_s V_s}{(V - V_s)RT} \right] \qquad (3)$$

where[13]

$$\psi = \frac{1 - e^{-l\theta/T}}{1 - e^{-\theta/T}} + e^{-l\theta/T} \frac{(2\pi mkT)^{1/2}}{h} v_f^{1/3} \qquad (4)$$

if

$$l\theta \gg T$$

$$\psi = \frac{1}{1 - \exp(-\theta/T)} \qquad (5a)$$

which is an Einstein partition function. Here, θ is the Einstein characteristic temperature, E_s is the energy of sublimation of the solid at the melting point, a is a proportionality constant, n is approximately equal to the number of nearest neighbors, l is an integer determined from the relationship

$$\frac{E_s}{3R} \simeq l\theta \qquad (5b)$$

and v_f is the free volume of the solid found from the relation[13]

$$v_f = \left[\left(\frac{V_s}{N} \right)^{1/3} - \left(\frac{b}{4N} \right)^{1/3} \right]^3 \qquad (5c)$$

where b is the van der Waals constant. The nearest integer was chosen for l in eq. 5b. Equation 1 with 2 and 3 is employed for calculating equations of state and thermodynamic properties of rare gas liquids and gases. For nitrogen, the following partition function is used

(3) H. M. Peek and T. L. Hill, *J. Chem. Phys.*, **18**, 1252 (1950).

(4) J. S. Rowlinson and C. F. Curtiss, *ibid.*, **19**, 1519 (1951).

(5) G. Blomgren, *ibid.*, **34**, 1307 (1961).

(6) G. Blomgren, *ibid.*, **38**, 1714 (1963).

(7) H. Eyring, T. Ree, and N. Hirai, *Proc. Natl. Acad. Sci. U. S.*, **44**, 683 (1958).

(8) E. J. Fuller, T. Ree, and H. Eyring, *ibid.*, **45**, 1954 (1959).

(9) C. M. Carlson, H. Eyring, and T. Ree, *ibid.*, **46**, 333 (1960).

(10) T. R. Thomson, H. Eyring, and T. Ree, *ibid.*, **46**, 336 (1960).

(11) C. M. Carlson, H. Eyring, and T. Ree, *ibid.*, **46**, 649 (1960).

(12) (a) H. Eyring and T. Ree, *ibid.*, **47**, 526 (1961); (b) H. Eyring and R. P. Marchi, *J. Chem. Educ.*, **40**, 562 (1963).

(13) T. S. Ree, T. Ree, and H. Eyring, *Proc. Natl. Acad. Sci. U. S.*, **48**, 501 (1962).

(14) D. Henderson, H. Eyring, and D. Felix, *J. Phys. Chem.*, **66**, 1128 (1962).

(15) J. G. Kirkwood, V. A. Lewinson, and B. J. Alder, *J. Chem. Phys.*, **20**, 929 (1952).

(16) D. Henderson, *ibid.*, **37**, 631 (1962).

(17) D. Henderson, *ibid.*, **39**, 54 (1963).

(18) J. S. Dahler and J. O. Hirschfelder, *ibid.*, **32**, 330 (1960).

$$f = \frac{8\pi^2 IkT}{2h^2} (1 - e^{-h\nu/kT})^{-1}(f_s)^{V_sN/V}(f_g)^{(V-V_s)N/V}$$

$$(6)$$

where f_g and f_s are given by eq. 2 and 3, respectively; the first two terms on the right of eq. 6 have been factored out from the partition functions of the gas-like and the solid-like parts; I is the moment of inertia, and ν is the vibrational frequency.

The numerical values of all the parameters (n, a, E_s, V_s, θ, l, and b) for the liquids of the rare gases and nitrogen are found in an earlier paper[13] and are used in the present paper. For argon, the values of n and a are calculated from the model.[12b] In more complicated cases, the two parameters, n and a, may be chosen to fit the experimental data and subsequently explained in terms of molecular structure. We have not discussed our model in detail again here since it has been extensively discussed in the references cited.

(1)   The Equation of State. The equation of state derived from the significant structure theory is[13]

$$\frac{PV}{RT} = 1 + \frac{1}{x}\left[\gamma + \ln x + x\left(\frac{\partial \sigma^2}{\partial x}\right)_T - \sigma_2 - \sigma_1 - 1\right]$$

$$(7)$$

where

$$\sigma_1 = \frac{E_s}{RT} + 3 \ln\left[\frac{1 - e^{-l\theta/T}}{1 - e^{-\theta/T}} + \right.$$

$$\left. e^{-l\theta/T} \frac{(2\pi mkT)^{1/2}}{h} v_f^{1/3}\right]$$

$$(8)$$

$$\sigma_2 = \ln\left\{1 + n(x - 1)\exp\left[\frac{-aE_s}{(x - 1)RT}\right]\right\}$$

$$(9)$$

$$\gamma = \ln\left[\frac{(2\pi mkT)^{1/2}}{h^3}\frac{eV_s}{N}\right]$$

$$(10)$$

and

$$x = \frac{V}{V_s}$$

$$(11)$$

In Fig. 1, the compressibility factors of argon calculated from our theory at $T^* = kT/\epsilon = 2.74$ are plotted against $V^* = V/N\sigma^3$ and are compared with those given in the literature.[6,13] The values of ϵ/k and σ are obtained from the tabulated values of Hirschfelder, *et al.*[19] Here, our curve (I) is calculated by using eq. 7, while curve II is calculated by taking account of the fact that the pressure effect on V_s is not negligible under very high pressure in the region of interest. Thus, x in eq. 7 is generally represented by

$$x = \frac{V}{V_s'} = \frac{V}{V_s(1 - \beta\Delta P)}$$

$$(12)$$

where V_s' indicates the solid volume under pressure, β is the compressibility, ΔP is the pressure minus the vapor pressure at the melting temperature, and V_s has been defined. When eq. 12 is used with eq. 7, an iterative procedure is employed in order to obtain consistent compressibility factors as was done in a previous paper.[13] The compressibility, β, is obtained from the data for solid argon[20] by an interpolation to the pressure of interest. As is shown in Fig. 1, our significant structure theory does not apply to the region $V^* < 1.05$, while the other theories cover this region. However, for $V^* > 1.05$ the significant structure theory works better than other theories. Furthermore, it should be noted that the theories of Dahler and Hirschfelder and of Lennard-Jones and Devonshire are good for solids, whereas our theory and Blomgren's are good for liquids.
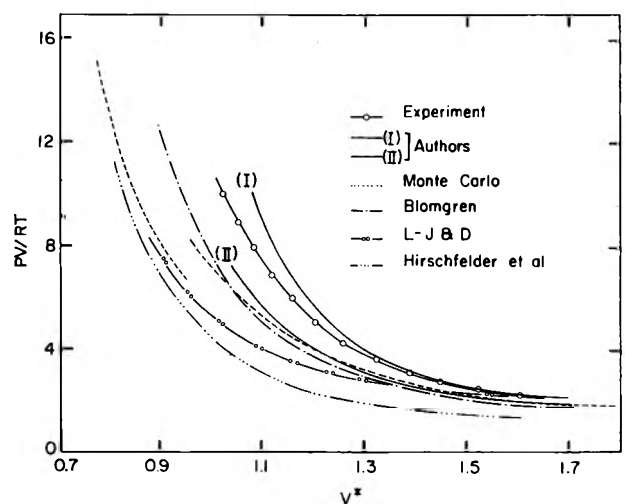
Figure 1.   Compressibility factors PV/RT vs. reduced volume, V^*. The experimental values of PV/RT over the high pressure region are due to P. W. Bridgman, *Proc. Am. Acad. Sci.*, **70**, 1 (1935); and those over the low pressure region are due to A. Michels, *et al., Physica*, **15**, 627, 689 (1949); **24**, 659, 769 (1958). The Monte Carlo curve is due to W. W. Wood and F. R. Parker, *J. Chem. Phys.*, **27**, 720 (1957). Blomgren's curve from ref. 6. Hirschfelder, *et al.*,'s curve and Lennard-Jones and Devonshire's curve are from ref. 18.

(2)   Thermodynamic Properties at Vapor Pressure Equilibrium. The following equations for the entropy, S, the internal energy, E, the specific heat at constant

(19) J. O. Hirschfelder, C. F. Curtiss, and R. B. Bird, "Molecular Theory of Gases and Liquids," John Wiley and Sons, Inc., New York, N. Y., 1954.

(20) E. R. Dobbs and G. O. Jones, *Rept. Progr. Phys.*, **20**, 516 (1957).

volume, C_V, the coefficient of thermal expansion, α, and the coefficient of compressibility, β, are derived from the significant structure theory

$$S = - \left(\frac{\partial A}{\partial T} \right)_V$$

$$= \frac{R}{x} \left[\sigma_1 + T \left(\frac{\partial \sigma_1}{\partial T} \right)_x + \sigma_2 + T \left(\frac{\partial \sigma_2}{\partial T} \right)_x \right] +$$

$$R \left(1 - \frac{1}{x} \right) \left[\gamma + T \left(\frac{\partial \gamma}{\partial T} \right) + \ln x \right] \quad (13)$$

$$E = kT^2 \frac{\partial}{\partial T} \ln f$$

$$= \frac{RT}{x} \left[T \left(\frac{\partial \sigma_1}{\partial T} \right)_x + T \left(\frac{\partial \sigma_2}{\partial T} \right)_x + \frac{3}{2} (x - 1) \right] \quad (14)$$

$$C_V = T \left(\frac{\partial S}{\partial T} \right)_V$$

$$= \frac{R}{x} \left[2T \left(\frac{\partial \sigma_1}{\partial T} \right)_x + T^2 \left(\frac{\partial^2 \sigma_1}{\partial T^2} \right)_x + 2T \left(\frac{\partial \sigma_2}{\partial T} \right)_x + \right.$$

$$\left. T^2 \left(\frac{\partial^2 \sigma_2}{\partial T^2} \right)_x \right] + R \left(1 - \frac{1}{x} \right) \left[2T \left(\frac{\partial \gamma}{\partial T} \right) + T^2 \left(\frac{\partial^2 \gamma}{\partial T^2} \right) \right]$$

$$(15)$$

$$\alpha = \frac{1}{V} \left(\frac{\partial V}{\partial T} \right)_P = - \frac{1}{V} \left(\frac{\partial P}{\partial T} \right)_V \Big/ \left(\frac{\partial P}{\partial V} \right)_T \quad (16)$$

and

$$\beta = \frac{-1}{V} \left(\frac{\partial V}{\partial P} \right)_T = - \frac{1}{V \left(\frac{\partial P}{\partial V} \right)_T} \quad (17)$$

where

$$\left(\frac{\partial P}{\partial T} \right)_V = \frac{R}{V_s x^2} \left\{ - \left[\sigma_1 + T \left(\frac{\partial \sigma_1}{\partial T} \right)_x \right] - \right.$$

$$\left[\sigma_2 + T \left(\frac{\partial \sigma_2}{\partial T} \right)_x \right] + x \left(\frac{\partial \sigma_2}{\partial T} \right)_T + xT \left[\frac{\partial}{\partial T} \left(\frac{\partial \sigma_2}{\partial x} \right)_T \right]_x +$$

$$\gamma + T \left(\frac{\partial \gamma}{\partial T} \right) + (x - 1) + \ln x \Big\} \quad (18)$$

and

$$\left(\frac{\partial P}{\partial V} \right)_T = \frac{RT}{V_s^2 x^3} \left[x^2 \left(\frac{\partial^2 \sigma_2}{\partial x^2} \right)_T - 2x \left(\frac{\partial \sigma_2}{\partial x} \right)_T + \right.$$

$$2\sigma_2 - x + 3 - 2(\gamma + \ln x - \sigma_1) \Big] \quad (19)$$

Using eq. 13, 14, and 15, the reduced excess entropy which is defined as

$$S_E^* = \left[S - R \ln \frac{e^{5/2} V}{Nh^3} (2\pi mkT)^{3/2} \right] \Big/ R \quad (20)$$

the reduced excess internal energy

$$U_E^* = (E - 3RT/2)/RT \quad (21)$$

and the reduced excess heat capacity

$$C_E^* = (C_V - 3R/2)/R \quad (22)$$

are calculated for argon and plotted in Fig. 2, 3, and 4 against reduced temperature T^*. For S_E^*, U_E^*, and C_E^*, our theory shows excellent agreement with the
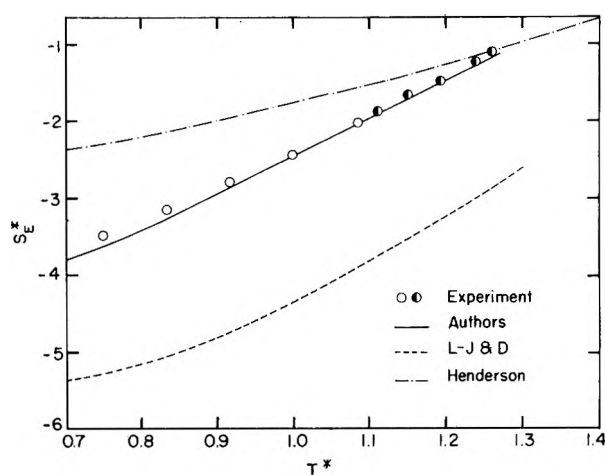
Figure 2. The reduced excess entropy, S_E^*, vs. reduced temperature, T^*. The experimental data of open circles are from ref. 21, those of half-shaded circles are due to A. Michel, et al., Physica, 24, 769 (1958). Henderson's curve and Lennard-Jones and Devonshire's curve are from ref. 17.
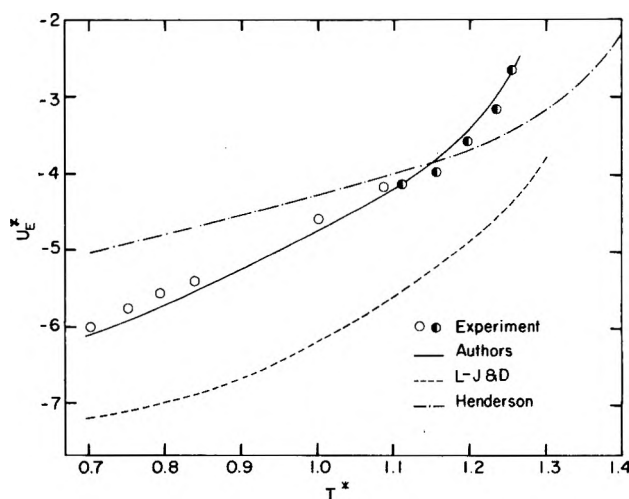
Figure 3. The reduced excess energy, U_E^*, vs. reduced temperature, T^*. The references for the experimental data, for Henderson's curve, and for Lennard-Jones and Devonshire's curve are the same as in Fig. 2.

Table I

T, °K.	Argon				T, °K.	Nitrogen			
	$\alpha_p \times 10^2$, deg.⁻¹ (theo.)	$\alpha_p \times 10^2$, deg.⁻¹ (exptl.)	$\beta_T \times 10^4$, atm.⁻¹ (theo.)	$\beta_T \times 10^4$, atm.⁻¹ (exptl.)		$\alpha_p \times 10^2$, deg.⁻¹ (teho.)	$\alpha_p \times 10^2$, deg.⁻¹ (exptl.)	$\beta_T \times 10^4$, atm.⁻¹ (theo.)	$\beta_T \times 10^4$, atm.⁻¹ (exptl.)
83.82ᵃ	4.72	4.37	1.75	2.03	63.18ᵃ	4.52	4.73	1.71	1.93
85	4.61	4.40	1.76	2.11	70	4.50	5.17	2.11	2.47
87.29ᵇ	4.51	4.49	1.84	2.27	75	4.86	5.53	2.62	2.96
90	4.48	4.58	1.94	2.45	80	5.44	5.92	3.35	3.53
95	4.61	4.80	2.24	2.91	85	6.14	6.44	4.30	4.3
100	4.89	5.09	2.64	3.42	90	7.11	7.2	5.67	5.5
105	5.29	5.43	3.16	4.02	95	8.57	8.2	7.86	7.2
110	5.88	5.9	3.92	4.8	100	10.7	9.5	11.4	10
120	7.63	7.8	6.35	7.8	105	14.1	11.2	17.3	13
130	12.4	12	13.5	16	115	81.8	20	14.5	30
140	62	22	96.4	40	120	-52.8	32	-116	60
150.72ᶜ	-8.2	∞	-38.6	∞	126.1	-81.6	∞	-49	∞

ᵃ Triple point. ᵇ Boiling point. ᶜ Critical point.
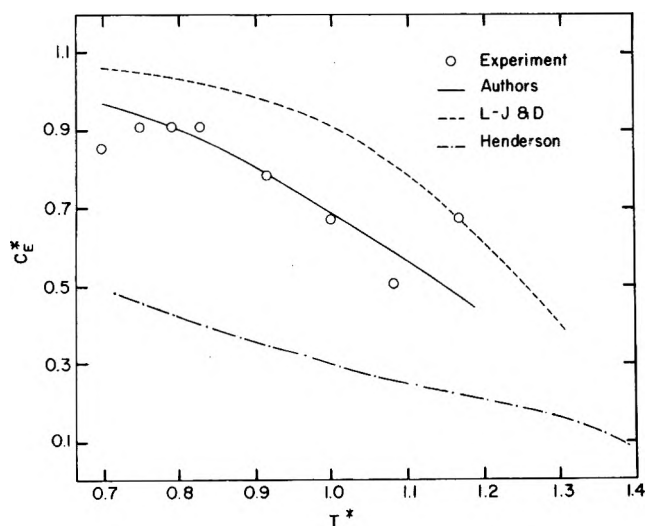
Figure 4. The reduced excess specific heat capacity, $C_E{}^*$, vs. reduced temperature, T^*. The experimental data are from ref. 21. Henderson's curve and Lennard-Jones and Devonshire's curve are from ref. 17.

experimental data[21] as compared to the theories of Lennard-Jones and Devonshire and of Henderson.[17] Here, since $C_E{}^*$ is sharply dependent on v_f, we used v_f tabulated by Wentorf, et al.[2] For calculating the terms, $\partial\sigma_1/\partial T$ and $\partial^2\sigma_1/\partial T^2$, which are involved in C_V, we have assumed that v_f is independent of temperature for convenience. The calculated coefficients, α and β, are tabulated in Table I for argon and nitrogen and are compared with the experimental data.[21] The agreement is very good except for temperatures near the critical value.

(3) The Reduced Equation of State. The use of reduced-state correlations have proved to be valuable

for the estimation of thermodynamic, volumetric, and transport properties. However, the validity of the law of corresponding states for condensed substances, in particular for the noble gases, has recently been the object of a number of investigators. de Boer and Bird[22] introduced a quantum-mechanical parameter, Λ^*, into the Lennard-Jones theory in order to account for the deviation due to the significant quantum effect. For hydrogen, by using the W.K.B.
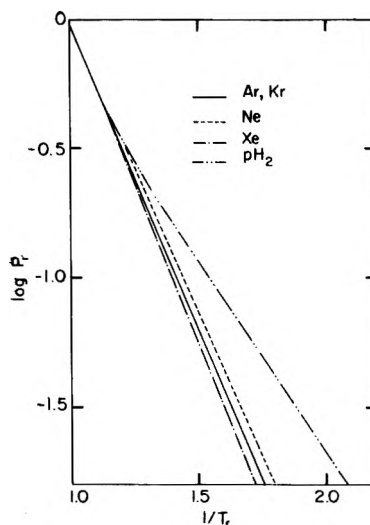
Figure 5. Plot of log P_r vs. $1/T_r$ for inert gases and hydrogen. Here $P_r = P/P_c$, $T_r = T/T_c$. The critical data for inert gases are from ref. 24. The pressure data for hydrogen calculated from the significant structure theory at various temperatures are from ref. 14.

(21) J. S. Rowlinson, "Liquids and Liquid Mixtures," Butterworths Scientific Publications, Ltd., London, 1959, Chapter II.

(22) J. de Boer and R. B. Bird, Phys. Rev., 83, 1959 (1951).

method, Henderson, Kim, and Eyring[23] obtained energy levels and the sum of the latter was used instead of the intergrated form of energy levels in the Lennard-Jones and Devonshire theory.

We calculate the reduced vapor pressure P_r for Ne, Ar, Kr, and Xe, where $P_r = P/P_c$, the P_c being the critical pressure. The pressure P is calculated by the usual procedure in the significant structure theory,[7] and the experimental P_c is used for the calculation of P_r. In Fig. 5, the values of log P_r are plotted against the reciprocal of the reduced temperature T_r, which equals T/T_c. The P_r data for hydrogen are due to Henderson, Eyring, and Felix,[14] who used the significant structure theory in their calculations.

By using experimental data, Hamrin and Thodos[24] have shown that Ar, Kr, and Xe produce a single straight line in a plot of log P_r vs. $1/T_r$, whereas the relationship for Ne is somewhat shifted to the right of the straight line because of the quantum effect of Ne. It is interesting to point out that the straight line for the experimental values of Ar, Kr, and Xe is located between the Xe line and the Ar–Kr line in our Fig. 5, and that the experimental data of Ne lie approximately on our Ne curve (for simplicity the experimental data are not shown in Fig. 5). One also notes that in Fig. 5 the curve for parahydrogen is far removed to the right from the inert gas group because of the quantum effect. Thus, one may conclude that the significant structure theory successfully explains the quantum effect.

(23) D. Henderson, S. Kim, and H. Eyring, *Proc. Natl. Acad. Sci. U. S.*, **48**, 1753 (1962).

(24) G. E. Hamrin, Jr., and G. Thodos, *J. Chem. Phys.*, **35**, 899 (1961).

Pulse Radiolysis Studies. V. Transient Spectra and Rate

Constants in Oxygenated Aqueous Solutions[1]

by Gideon Czapski and Leon M. Dorfman

Argonne National Laboratory, Argonne, Illinois (*Received December 13, 1963*)

The optical absorption spectra and reaction kinetics of transient species in oxygenated aqueous solutions have been investigated over the pH range 2 to 14 using the pulse radiolysis technique. The HO_2 radical spectrum has a maximum at 230 mμ with a molar extinction coefficient of $\epsilon_{HO_2}^{230} = 1150\ M^{-1}$ cm.$^{-1}$ at 25°. The O_2^- has a maximum at 240 mμ with $\epsilon_{O_2^-}^{240} = 1060\ M^{-1}$ cm.$^{-1}$. The pK of the hydroperoxy radical was found to be 4.5 ± 0.2. The absolute rate constants for the bimolecular disappearance of these transients at 25° were determined to be: $k_{HO_2 + HO_2} = 2.7 \times 10^6\ M^{-1}$ sec.$^{-1}$, and $k_{O_2^- + O_2^-} = 1.7 \times 10^7\ M^{-1}$ sec.$^{-1}$. In alkaline solution above pH 10, two new transient species were observed, one with a maximum at 240 mμ, the other with a maximum at 430 mμ. Both species decayed according to a first-order rate law with a pH-dependent half-life, the former in the range of seconds, the latter in the range of milliseconds. The possible identity of these transient species is discussed.

Introduction

The kinetics of the hydroperoxy radical in oxygenated aqueous solutions have recently been studied by several fast reaction techniques.[2-6] In these studies the radical has been generated by radiolysis,[2,6] by flash photolysis,[5] and by chemical means[3,4] from the reaction of ceric ion and hydrogen peroxide.

In the radiolysis of oxygenated aqueous solutions, the hydroperoxy radical is formed from the reducing species in two different ways

$$e_{aq}^- + H^+ = H \tag{1}$$

$$H + O_2 = HO_2 \tag{2}$$

$$e_{aq}^- + O_2 = O_2^- \tag{3}$$
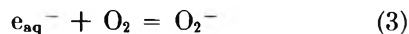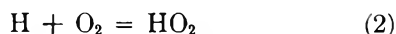
The relative importance of each reaction depends upon the pH and the oxygen concentration. The rate constants for (1) and (3) are accurately known from recent pulse radiolysis experiments.[7,8]

It was shown in the previous investigations[5,6] that the hydroperoxy radical exists in two forms: as HO_2 in acid solution and as O_2^-, the dissociated form, in basic solution. The pK of the hydroperoxy radical was found[6] to be 4.4 ± 0.4. The kinetics of the second-order

disappearance of the HO_2 and O_2^- were investigated and the bimolecular rate constants were determined at various values of the pH. There is some disagreement as to the rate constant[2,5,6] of $O_2^- + O_2^-$.

In the present investigation, we have used the pulse radiolysis technique[9] to determine the rate constants for the bimolecular disappearance of the HO_2 and O_2^- and have measured the pK of the hydroperoxy radical. The ultraviolet absorption spectra of these two species were obtained.

In the course of this work, new intermediates were observed in alkaline solution and the optical absorption spectra were determined. The kinetics of these new

(1) Based on work performed under the auspices of the U. S. Atomic Energy Commission.

(2) K. Schmidt, *Z. Naturforsch.*, 16b, 206 (1961).

(3) E. Saito and B. H. J. Bielski, *J. Am. Chem. Soc.*, 83, 4467 (1961).

(4) B. H. J. Bielski and E. Saito, *J. Phys. Chem.*, 66, 2266 (1962).

(5) J. H. Baxendale, *Radiation Res.*, 17, 312 (1962).

(6) G. Czapski and B. H. J. Bielski, *J. Phys. Chem.*, 67, 2180 (1963).

(7) L. M. Dorfman and I. A. Taub, *J. Am. Chem. Soc.*, 85, 2370 (1963).

(8) S. Gordon, E. J. Hart, M. S. Matheson, J. Rabani, and J. K. Thomas, *ibid.*, 85, 1375 (1963).

(9) L. M. Dorfman, I. A. Taub, and R. E. Bühler, *J. Chem. Phys.*, 36, 3051 (1962).

transient species were investigated over a broad range of pH.

Experimental

A detailed description of the pulse radiolysis method has already been presented.[9] A few modifications have been described in the later reports[7,10] in this series. In the present experimental study there have been some additional modifications in the optical detection technique.

Pulse Irradiation. A 14–15-Mev. electron beam from the linear accelerator was used throughout this work. The pulse duration ranged from 0.4 to 5 μsec. with the current in the range 50–180 ma. A 5-μsec. pulse at 100 ma. delivers a dose of approximately 1.9×10^{18} e.v./g. In most of the kinetic studies the electron beam had an incident diameter of 16 mm. and an emergent diameter of about 18 mm. for a 4-cm. cell. In the determination of absorption spectra, the cell was irradiated cross-wise, rather than end-on, at a position where the beam diameter was approximately 8 cm.

Optical Detection. Both the kinetic studies and the determination of spectra were carried out spectrophotometrically. A 1P28 photomultiplier tube was used to monitor the light from a steady lamp passing through the irradiated system.

Two different light sources were used. In most of the kinetic studies an Osram mercury lamp, Type HBO 107/1, was used, specifically with the 2537-Å. line. For spectral determination, where a continuum source was desirable, a 500-w. Osram xenon lamp, Type XBO 450W, was used.

A Bausch and Lomb grating monochromator, type 33-86-25, $f/3.5$, was used with a grating having a dispersion of 3.2 mμ/mm. In most of the kinetic studies an exit slit of 1.5 mm. was used. In the determination of absorption spectra, a slit width of 0.5–0.8 mm. was used, thus giving a band width of approximately 2 mμ for the determination of the optical density at a particular wave length. Below 260 mμ the scattered light becomes significant and increases in extent toward shorter wave lengths. A set of Corning filters was used to determine the magnitude of the scattered light at each wave length and to correct for any errors thus introduced. The scattered light, all of it above 3400 Å., amounts to 5% of the total at 2500 Å., 15% at 2300 Å., 40% at 2200 Å., and 60% at 2050 Å. Optical density measurements were extended to 205 mμ. The entire procedure used in the determination of spectra in this wave length region was checked using an aqueous solution of iodide ion for the determination of the iodide absorption spectrum. The spectrum obtained corre-

sponded in form, and within 2 mμ in wave length maximum, to the iodide spectrum in the literature.[11]

In the kinetic studies either a twofold or a fourfold optical path[9] was used with a 4-cm. cell.

Dosimetry. The dose was required only in connection with the determination of extinction coefficients from the optical density for a given transient. Consequently, the *in situ* dosimetry method previously described[7] was used. The dosimeter solution consisted of 10^{-2} M ferrous ion and 0.8 N sulfuric acid, saturated with oxygen and containing no chloride ion. The yield of ferric ion at high dose rates[12,13] is 15.6 molecules/100 e.v. The optical density was determined from a rate curve at 366 mμ and the calculation of dose based on the extinction coefficient $\epsilon_{302} = 2200$ M^{-1}cm.$^{-1}$. The extinction coefficient ratio was found to be $\epsilon_{302}/\epsilon_{366} = 9.1$, slightly higher than the previous determination.[7]

Materials. Solutions were degassed by pumping on a vacuum system and the cylindrical quartz cells were filled using a syringe technique.[14] The water used was triply distilled. All materials used were of analytical grade and were used without further purification.

Results and Discussion

Spectra. Since it has been shown[2,6] that the hydroperoxy radical exists in two forms, HO_2 and O_2^-, for which p$K = 4.4 \pm 0.4$, we recorded the optical absorption spectra of both transient species in the appropriate pH region over the wave length region 205 to 400 mμ. The spectrum of HO_2 was observed in oxygenated water containing 10^{-2} M perchloric acid. The spectrum of O_2^- was observed in neutral oxygenated water. The spectra are presented in Fig. 1, which shows the decadic molar extinction coefficient as a function of wave length. The extinction coefficient was determined only at 2537 Å. for both species.

The two spectra are very similar. The HO_2 has a maximum at 230 mμ with a peak half-width of about 50 mμ. The maximum for O_2^- is at 240 mμ, with a half-width of about 65 mμ.

An absorption, attributed to O_2^- in liquid ammonia,[15] has been reported with a maximum at 380 mμ.

In alkaline solutions of 2×10^{-2} N barium hydroxide, absorptions were found both in the far-ultraviolet region

(10) I. A. Taub and L. M. Dorfman, *J. Am. Chem. Soc.*, **84**, 4053 (1962).

(11) J. L. Weeks, G. M. A. C. Meaburn, and S. Gordon, *Radiation Res.*, **19**, 559 (1963).

(12) J. Rotblat and H. C. Sutton, *Proc. Roy. Soc.* (London), **A255**, 49 (1960).

(13) J. K. Thomas and E. J. Hart, *Radiation Res.*, **17**, 408 (1962).

(14) C. B. Senvar and E. J. Hart, *Proc. Intern. Conf. Peaceful Uses At. Energy*, **29**, 19 (1958).

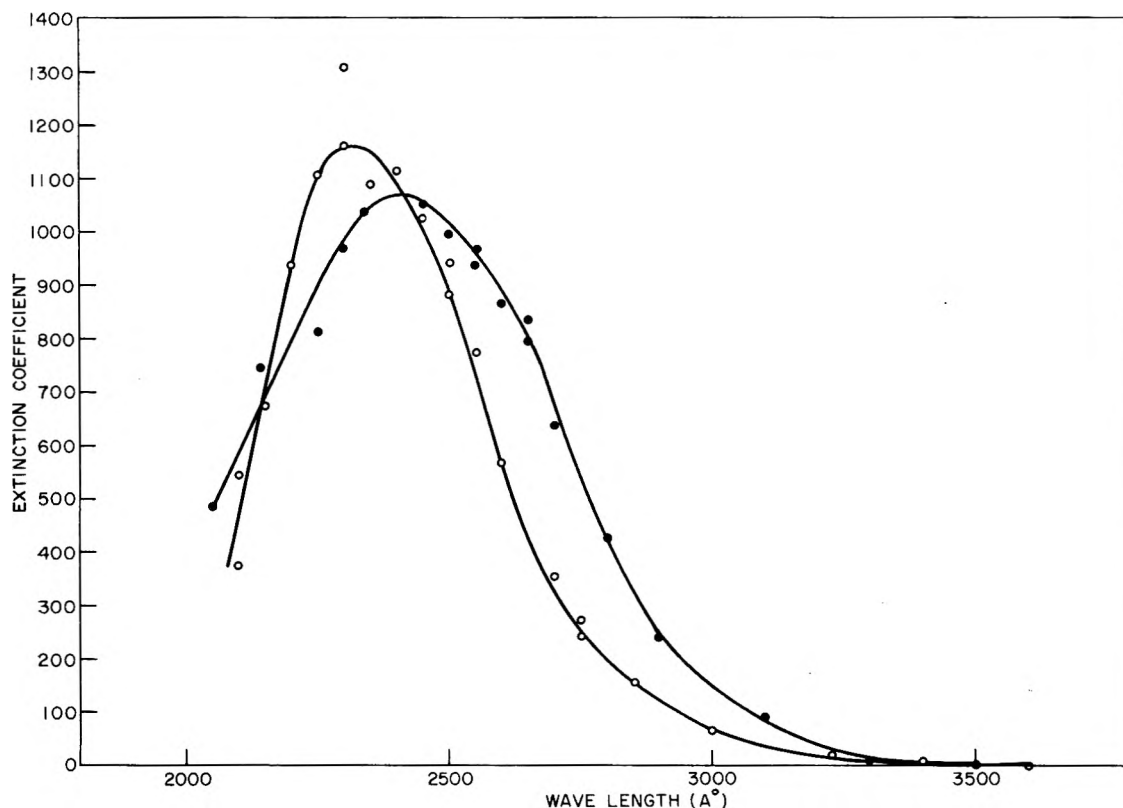(15) J. K. Thompson and J. Kleinberg, *J. Am. Chem. Soc.*, **73**, 1243 (1951).

Figure 1.   Absorption spectra of the HO_2 radical, O, in oxygenated 10^{-2} N perchloric acid solution, and the O_2^- radical-ion, ●, in neutral oxygenated water.   The ordinate values are the decadic molar extinction coefficient. The extinction coefficients are based on G_B = 3.3 for the HO_2 and $G_H + G_{e_{aq}^-}$ = 3.2 for the O_2^-.

as well as at longer wave lengths.   An absorption with a peak at 240 mμ did not differ significantly from the spectrum of O_2^-.   In 2 × 10^{-2} N barium hydroxide, an additional broader absorption was found with a peak at 430 mμ.   The spectrum of this transient is shown in Fig. 2.   As will be seen in the subsequent kinetic studies, the peaks at 240 and 430 mμ are to be assigned to two different species since their decay rates differ by more than an order of magnitude.   None of these transient spectra was observed in deaerated aqueous solutions.

No transient absorption which might be due to H_2O_3, previously postulated,[6] was observed in acid solution. Our failure to observe it does not contradict its possible existence.

Molar Extinction Coefficients.   Since the decay kinetics of the hydroperoxy radical consist of bimolecular radical–radical reactions, the concentration or molar extinction coefficient is necessary for the determination of absolute rate constants.   Most of the kinetic studies were done at 2537 Å.; hence, the molar extinction coefficient was determined at this wave length.   This was done in neutral water for the O_2^- and in 10^{-2} M perchloric acid for the HO_2.

The optical density for each transient was determined from rate curves immediately after a 1-μsec. 80-ma. pulse.   The dose was determined simultaneously in each case.   Under these conditions, the formation of HO_2 by reactions 1 and 2, and O_2^- by reactions 3 and 2, is more than 95% complete within 0.3 μsec. after the pulse, while the recombination of $HO_2 + OH$ and $O_2^- + OH$ is sufficiently slow that at 0.3 μsec. after the pulse only 2–3% or less of this reaction occurs.   There may be a small error in $\epsilon_{O_2^-}$ because of the following uncertainty.   There is a small contribution to O_2^- through the formation of HO_2 from the hydrogen atom yield.   Equilibration may be incomplete and an error on the order of 10% may be introduced.   Because of the compensating absorption of the HO_2, however, the final error in the extinction coefficient will amount to only 2–3%.

The data give, at 25°

$$\epsilon_{HO_2}^{2537} G_{HO_2} = 2750 \pm 400$$

and

$$\epsilon_{O_2^-}^{2537} G_{O_2^-} = 3140 \pm 470$$
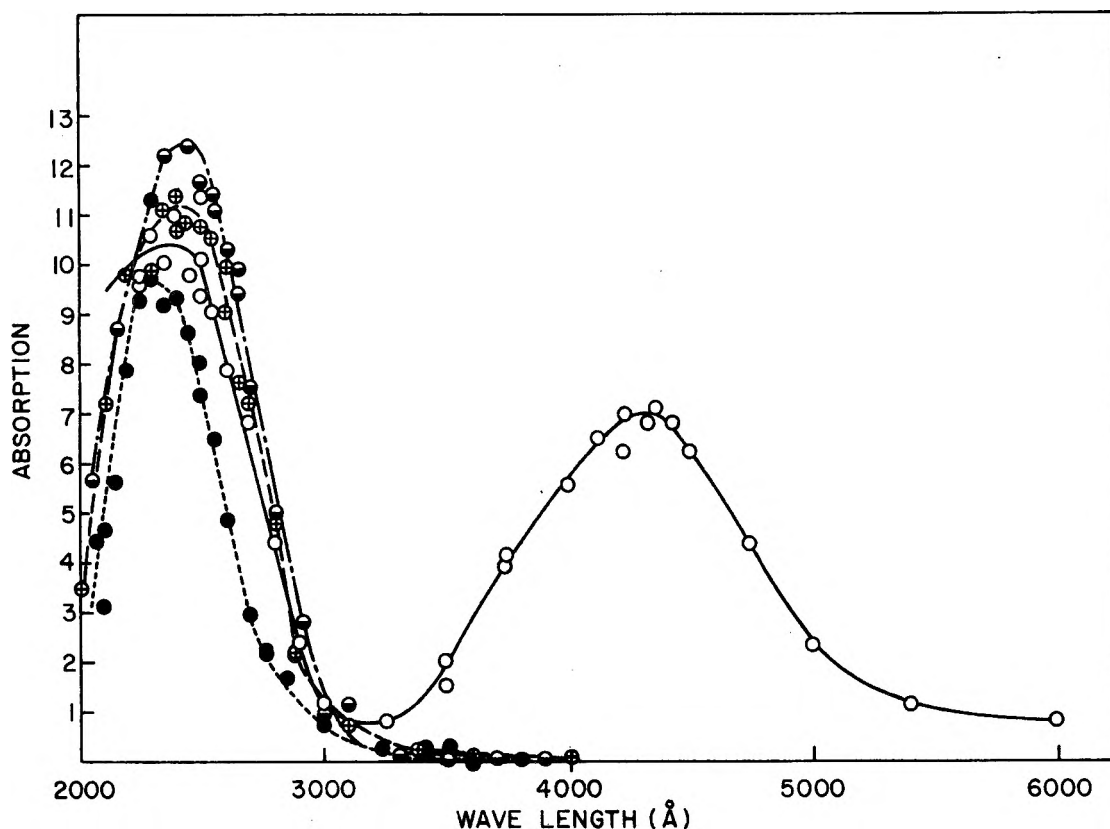
Figure 2. Absorption spectra of new transient species in oxygenated alkaline water. The new spectra are compared with those of HO_2 and O_2^-: O, $2 \times 10^{-2} N$ barium hydroxide; ⊕, $10^{-4} N$ barium hydroxide; ●, HO_2 in $10^{-2} N$ perchloric acid; ◒, O_2^- in neutral water. The optical density normalization is arbitrarily selected for illustrative purposes.

Taking[16] $G_H = 3.3$ molecules/100 e.v. at pH 2, and $G_H + G_{e_{aq}}^- = 3.2$ in neutral water,[17-20] we obtain

$$\epsilon_{HO_2}^{2537} = 830 \pm 125 \ M^{-1} \text{ cm.}^{-1}$$

and

$$\epsilon_{O_2^-}^{2537} = 980 \pm 140 \ M^{-1} \text{ cm.}^{-1}$$

The error limits do not include the uncertainties in the G-values.[21] These values for the extinction coefficients are considerably higher than the values 350 and 700 for the HO_2 and the O_2^-, respectively, reported in the flash photolysis work.[5]

The extinction coefficients at 2537 and 4300 Å. in alkaline solution could not be determined since the data obtained do not permit a reliable assignment of the spectra or a determination of the G-value of the species.

Kinetics of HO_2 and O_2^-. The decay kinetics of the hydroperoxy radical were observed both in acid solution and in neutral solution. In agreement with previous work,[2-6] the rate curves closely fit a second-order rate law. The decay kinetics correspond to the reaction

$$HO_2 + HO_2 = H_2O_2 + O_2 \tag{4}$$
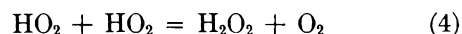
in acid solution, and the reaction

$$O_2^- + O_2^- \xrightarrow{(2H_2O)} H_2O_2 + O_2 + 2OH^- \tag{5}$$
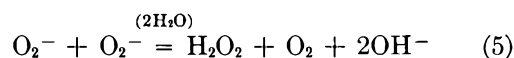
in neutral solution, and may be represented by the bimolecular rate expression

$$\frac{-d[R]}{dt} = 2k[R]^2 \tag{1}$$

Expressing [R], the concentration of the transient, in terms of its optical density the integrated form of eq. I reduces to

(16) W. G. Rothschild and A. O. Allen, *Radiation Res.*, **8**, 101 (1958).

(17) J. Rabani and G. Stein, *J. Chem. Phys.*, **37**, 1865 (1962).

(18) F. S. Dainton and D. B. Peterson, *Proc. Roy. Soc.* (London), **A267**, 443 (1962).

(19) G. Czapski and A. O. Allen, *J. Phys. Chem.*, **66**, 262 (1962).

(20) J. T. Allan and G. Scholes, *Nature*, **187**, 218 (1960).

(21) The value for $G_{e_{aq}}^-$ in neutral solution is not a matter of exact agreement in the literature. Values obtained tend to lie about a "high" value of 2.7 or the "lower" value of 2.3. The value 2.7 has been arbitrarily used here in calculating $\epsilon_{O_2^-}^{2537}$.

$$1/\log\,(I_0/I_{tr})_t = \left(\frac{2k}{\epsilon l}\right) t + 1/\log\,(I_0/I_{tr})_{t_0} \quad (II)$$

where t is the time, ϵ is the molar extinction coefficient of the transient, l is the length of the absorption path of the analyzing light beam, and the rate constant for the bimolecular disappearance is written as $2k$. A typical second-order plot of rate curves observed in neutral solution is shown in Fig. 3. As may be seen, the decay curves closely fit a second-order rate law over a fivefold variation in initial concentration of the transient.
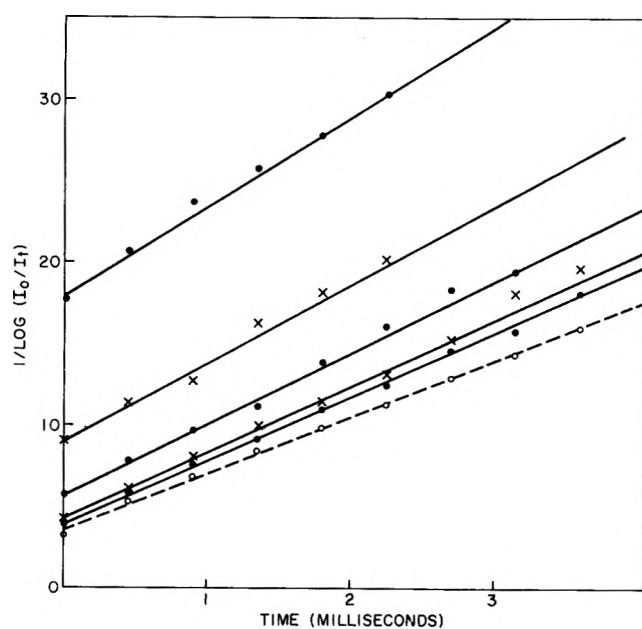
Figure 3. Test of second-order rate law for the decay of transient absorption at 2537 Å. in neutral water at 25°. The decay curves were measured using two passes through a 4-cm. cell. The upper five curves represent pulses of 0.4, 1.0, 2.0, 3.0, and 5.0 μsec., respectively, at about 120 ma. The dashed line represents a rate curve with 10^{-2} M methanol added and a 3-μsec. pulse.

Measurements were avoided at pH values close to the pK since the substantial difference in $\epsilon_{HO_2}^{2537}$ and $\epsilon_{O_2^-}^{2537}$ would make the interpretation of the rate curves complex. Most of the measurements were made at pH values differing by two units from the previously determined[6] pK of 4.4 ± 0.4.

The value of $k_4/\epsilon_{HO_2}^{2537}$ is constant over the pH range 1.7–3.0, while $k_5/\epsilon_{O_2^-}^{2537}$ was found to be constant over the range pH 5–7. The instantaneous pH change due to the formation of H$^+$ during the pulse was taken into account in calculating the pH which exists during the kinetic observations.

The values obtained for k_4 and k_5 are shown in Table I along with the values reported from the previous investigations. The uncertainty in our values of k/ϵ is considered to be less than ± 10%, the uncertainty in our absolute rate constants not more than ± 25%.

As may be seen from Table I, the values for k_4 obtained by the different methods are in good agreement with the exception of the flash photolysis[5] determination. Here the disagreement appears to depend only on the value of ϵ_{HO_2}, since the value obtained for k_4/ϵ_{HO_2} is in agreement with the present determination. The values for k_5 again seem to be in good agreement with the exception of the flash photolysis determination. But in this case, the values of $k_5/\epsilon_{O_2^-}$ differ by more than a factor of three.

Table I : Rate Constants for the Bimolecular Reaction of the Hydroperoxy Radical at 25°

Rate constant, M^{-1} sec.$^{-1}$	pH	This work	Previous values and ref. no.
k_4	0.5–1.5		2.4 × 10^6 (4)
	2.0–3.0		2.2 × 10^6 (6)
	1.7–3.0	2.7 × 10^6	
	2.7		1.25 × 10^6 (5)
$k_4/\epsilon_{HO_2}^{2537}$	1.7–3.0	3.3 × 10^3	
	2.7		3.5 × 10^3 (5)
k_5	5.0–7.0	17 × 10^6	
	5.0–8.0		15 × 10^6 (6)
	7.0		14.5 × 10^6 (2)
	7.0		120 × 10^6 (5)
$k_5/\epsilon_{O_2^-}^{2537}$	5.0–7.0	17 × 10^3	
	7.0		60 × 10^3 (5)

Addition of methanol to acid or neutral oxygenated solutions increases the yield of the absorbing species because of the added role of the hydroxyl radical as a precursor of peroxy radical

$$OH + CH_3OH = \cdot CH_2OH + H_2O \quad (6)$$

followed by

$$\cdot CH_2OH + O_2 = \cdot O_2CH_2OH \quad (7)$$
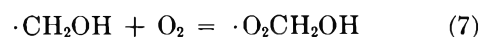
This also prevents the occurrence of the reaction OH + O$_2^-$. The decay curve again fits a second-order rate law as may be seen from the dashed line in Fig. 3 which also gives a similar slope in agreement with Baxendale.[5] However, the interpretation of the rate curves in the presence of methanol is uncertain since our data furnish no means of establishing whether $\cdot O_2CH_2OH$ has a stable existence and participates in

the kinetics, or whether reaction 7 is followed immediately by

$$\cdot O_2CH_2OH = HCHO + HO_2 \qquad (8)$$

pK of HO₂. The pK of the hydroperoxy radical has been estimated by Uri[22] from thermodynamic data to be p$K \sim 2$. A recent experimental determination[6] gave p$K = 4.4 \pm 0.4$. This was an indirect determination which involved a number of assumptions. In the present investigation the pK was measured in a more direct manner.

As may be seen from the absorption spectra in Fig. 1, $\epsilon_{HO_2}^{2700} < \epsilon_{O_2^-}^{2700}$ by about a twofold ratio. We therefore measured, under conditions of constant pulse current, the optical density at 2700 Å. of the HO_2 and O_2^- produced in the pH range 2–7. The results are shown in Fig. 4. Using a 1-μsec. pulse at approximately 80 ma. in these experiments, the initial radical concentration was approximately 5×10^{-6} M. Under these conditions, the radical recombination during the pulse is negligible and the initial concentrations of HO_2 and O_2^- can easily be determined from the measured optical density. From the data shown in Fig. 4 we obtain p$K = 4.5 \pm 0.2$ for the equilibrium $HO_2 \rightleftharpoons O_2^- + H^+$, in good agreement with the previous[6] determination. There may be a small error in this value due to incomplete equilibration between HO_2 and O_2^-. At pH > 4, most of the initial yield is in the form of O_2^- from reaction 3 which competes with reaction 1 followed by reaction 2. From the magnitude of the small change in optical density over the time range of a few microseconds where little of the reaction $OH + O_2^-$ occurs we estimate that the lack of complete
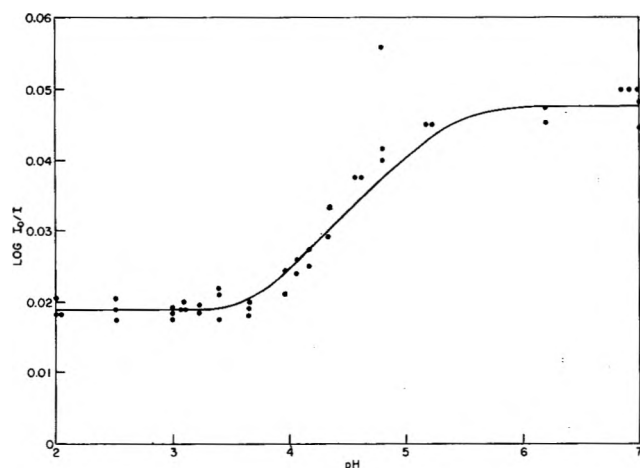
Figure 4. Optical density of transient species in oxygenated water at 2700 Å. as a function of pH. The curve gives p$K = 4.5 \pm 0.2$ for the hydroperoxy radical.

equilibration would produce an error of less than $+0.2$ pK unit in the value determined.

It is appropriate at this point to summarize briefly the basis for the identification of the observed absorption spectra with the hydroperoxy radical in its two forms. The transient is observed only when oxygen is present. The decay kinetics and the rate constants correspond closely with those determined by chemical initiation,[3,4] by radiolysis followed by chemical detection,[6] by e.s.r. detection,[4] and by conductivity measurement following radiolysis.[2] In these previous studies, as in the present, the identity of the active transient as the hydroperoxy radical is consistent with the accepted model for the radiolysis of oxygenated water. The previous conductivity studies[2] show that it is the species we observe at pH >4.5 which bears the charge. Finally, the very close agreement in the pK as determined optically, with that determined chemically,[6] further supports the identity.

Kinetics in Alkaline Solution. The kinetics of the transient species observed in aerated and in oxygen-saturated solutions were investigated over the pH range 9–14 using solutions of phosphate buffer, sodium hydroxide, and barium hydroxide. The transient spectra are shown in Fig. 2. The decay of these transients was observed at 2537 and 4300 Å. The lifetimes at these two wave lengths are very different, indicating that the two absorption bands are to be identified with different species.

The decay curves observed at 2537 Å. were found to fit a first-order rate law with a half-life which was markedly dependent upon pH. A first-order test of such a series of rate curves at 2537 Å. in 0.18 N barium hydroxide solution, over a sevenfold range of initial concentration of the transient, is shown in Fig. 5. As may be seen, this transient is very long-lived. The dependence of the half-life upon pH is shown in Fig. 6. The half-life is independent of the oxygen concentration and of the identity of the particular base or buffer used in the solutions. Experiments in which sodium perchlorate and barium perchlorate were added showed second-order decay of O_2^- as in neutral solution and ruled out any stabilization of the intermediates by the cation. No transient absorption was observed in degassed alkaline solutions at 2537 Å.

The data in Fig. 6 show considerable scatter, only part of which is due to lamp instability over the long time range and which we are unable to explain completely. The data of Baxendale[5] at pH 11, which upon replotting show a first-order decay, are in agreement. One point from these previous experiments[5] is included
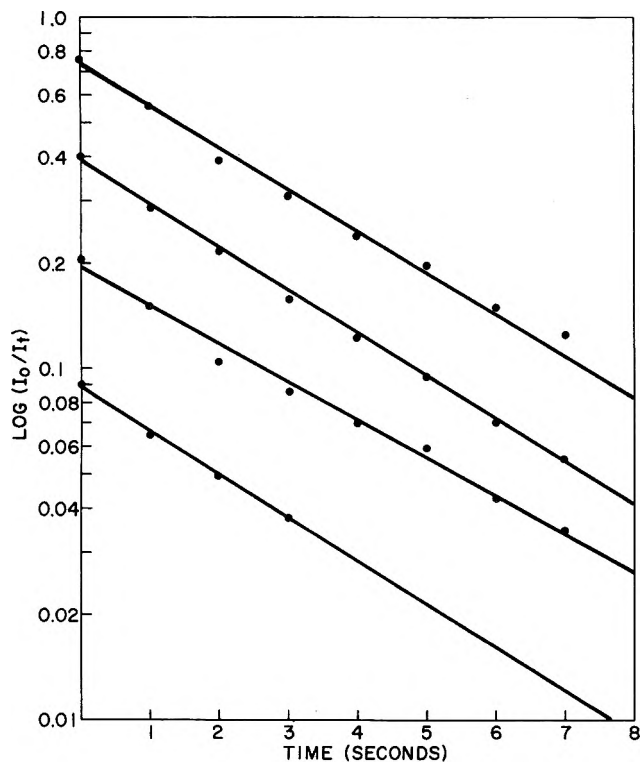
(22) N. Uri, *Chem. Rev.*, **50**, 375 (1952).

Figure 5. Test of first-order rate law for the decay of transient absorption at 2537 Å. in 0.18 N barium hydroxide solution saturated with oxygen. The separate decay curves are for electron pulses of 0.4, 1.0, 2.0, and 3.0 μsec. duration at approximately 120 ma.
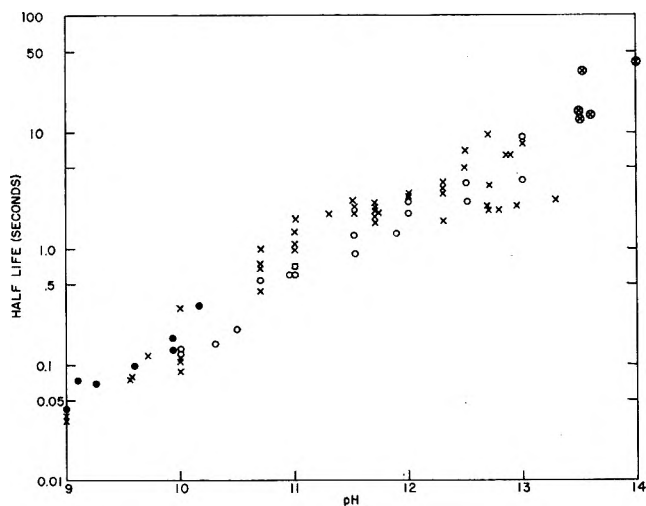

Figure 6. Half-life of transient absorption at 2537 Å. in oxygenated water as a function of pH: ●, phosphate buffer; ×, barium hydroxide; O, sodium hydroxide; ⊗, sodium hydroxide + 10^{-3} N barium hydroxide; □, calculated from ref. 5.

in Fig. 6 to indicate the agreement. If methanol is added at a concentration of 0.001–0.5 M, the same

decay characteristics are observed in agreement with Baxendale,[5] but the initial optical density is increased about twofold.

Another characteristic of the transient absorption at 2537 Å. is noteworthy. Within the first few microseconds after the pulse, a fast decay occurs because of the interactions OH + HO_2 and OH + O_2^-. After about 10 μsec., only the slower decay is occurring. In alkaline solutions, however, the fast decay disappears at pH ∼10, perhaps because O^- + O_2 is slow, and only a fast formation occurs at this and at higher values of the pH. The fast formation is then followed by the very slow decay. This behavior is shown in Fig. 7 in which the optical density at 2537 Å. is shown immediately after the pulse as well as 10 μsec. after the pulse as a function of pH.
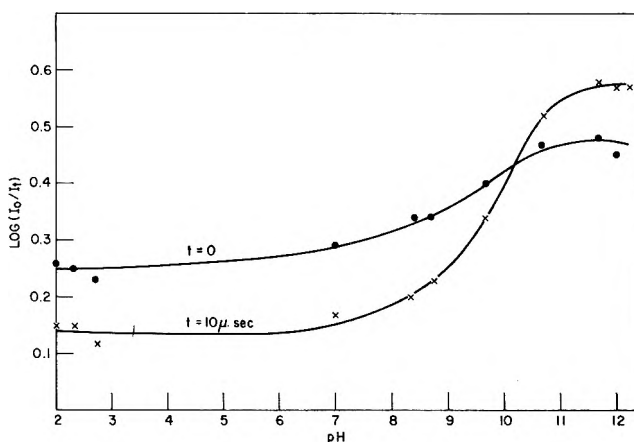
Figure 7. Optical density at 2537 Å. in oxygenated aqueous solutions immediately after the pulse ($t = 0$) and 10 μsec. after the pulse as a function of pH. A 1-μsec. pulse at 80 ma. was used with four passes through a 4-cm. cell.

The transient absorption with a maximum at 430 mμ which is found at pH >10 also shows a first-order decay. The half-life of this transient increases from 0.25 msec. at pH 10 to 4 msec. at pH 14. The pH dependence of the half-life is shown in Fig. 8. The initial optical density at 4300 Å. increases with pH, and appears to be leveling off at pH ⩾12. This is shown in Fig. 9. Addition of 10^{-2} M methanol eliminates this absorption completely. Addition of 10^{-4} M methanol decreases the absorption but does not affect the decay rate.

Identity of Transients in Alkaline Solution. The identity of the observed transient species in alkaline solution and their relationship to the HO_2 and O_2^- in acid and neutral solution is quite uncertain. The spectra of the HO_2 and O_2^-, as has been shown, differ
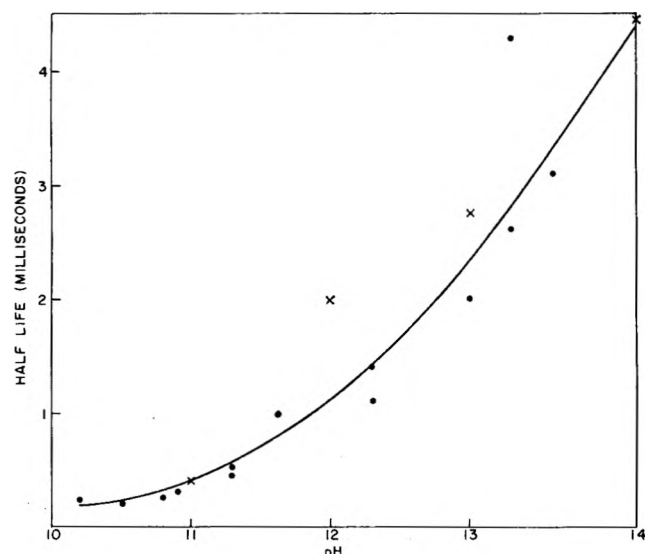
Figure 8. Half-life of transient absorption at 4300 Å. as a
function of pH: ●, barium hydroxide; ×, sodium hydroxide.
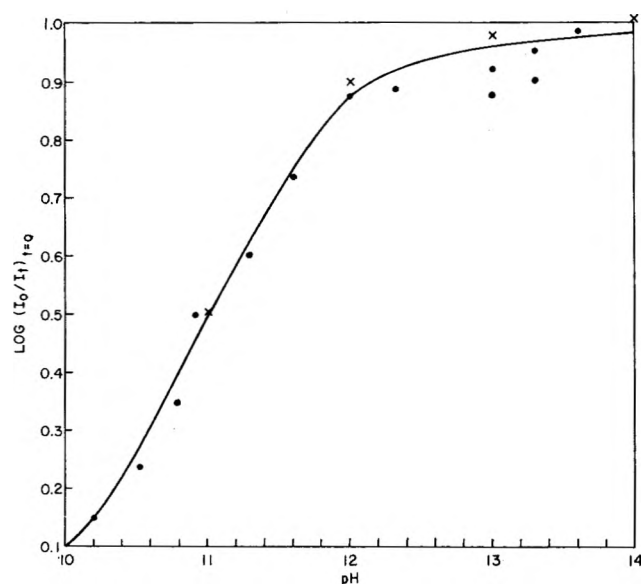
Figure 9. Initial optical density at 4300 Å. in
oxygenated solution as a function of pH: ●, barium
hydroxide; ×, sodium hydroxide.

only slightly. The spectrum of the ultraviolet absorbing species in alkaline solution, with a maximum at 240 mμ, is almost identical with that of the O_2^-.

In spite of this close similarity, the kinetic data exclude the possibility that the species absorbing at 240 mμ in alkaline solution is also the O_2^-, since the lifetime is several orders of magnitude too long for the value determined for k_5.

The evidence seems to indicate that the long-lived transient with a maximum at 240 mμ, observed at high pH, is a new species, probably formed from the O_2^- and hence an alkaline stabilized form of this radical-ion. Somewhat analogous behavior has previously been observed[23,24] by adding potassium superoxide to strong alkaline solutions.

The bimolecular disappearance, reaction 5, for which we have written only the stoichiometric reaction, may involve the formation of a doubly charged ion, O_2^{-2}, which is the new absorbing species

$$O_2^- + O_2^- = O_2^{-2} + O_2 \qquad (9)$$
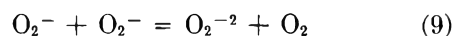
The O_2^{-2} then, depending upon pH, will disappear either by an acid-catalyzed decay or a natural decay

$$O_2^{-2} + H^+ = HO_2^- \qquad (10)$$

or

$$O_2^{-2} + H_2O = HO_2^- + OH^- \qquad (11)$$
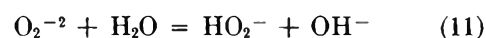
This mechanism would account for most of our results, predicting a second-order decay in neutral solution, where $k_{10}[H^+] \gg k_9$, and first-order in alkaline solution where the reverse is true. The formation of a doubly ionized dimer, O_4^{-2}, would fit this mechanism as well.

It is, of course, possible that a different mechanism obtains in which, instead of the occurrence of an acid-catalyzed decay of O_2^{-2}, this species is base-stabilized as HO_5^{-3} or HO_3^{-2}.

The species absorbing at 430 mμ is clearly different from the one absorbing at 240 mμ since the half-life is shorter by about three orders of magnitude. This species is formed only in the presence of oxygen in alkaline solution. It is noteworthy that the formation of the species is completely suppressed by the addition of 10^{-2} M methanol and partially suppressed by the addition of 10^{-4} M methanol, which, however, has no effect upon the decay rate. The effect of methanol suggests that the hydroxyl radical is a precursor, probably in the form O^- in strongly alkaline solution.

The absorption spectrum appears similar to that of O_3^- which has been observed[25,26] in liquid ammonia and in alkaline aqueous glass containing hydrogen peroxide where it shows a peak at 430 to 440 mμ. If this is the identity of the species, it may be formed in the reaction

$$O^- + O_2 = O_3^- \qquad (12)$$
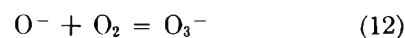
We are unable to advance a logical explanation for the

(23) P. George, *Discussions Faraday Soc.*, **2**, 196 (1947).

(24) J. Weiss, *Trans. Faraday Soc.*, **31**, 668 (1935).

(25) A. J. Kacmarek, J. M. McDonough, and I. J. Solomon, *Inorg. Chem.*, **1**, 659 (1962).

(26) A. D. McLachlan, M. C. R. Symons, and M. G. Townsend, *J. Chem. Soc.*, 952 (1959).

pH dependence of the half-life, but the pH dependence of the yield depends on ionization of OH to O$^-$. An alternative mode of formation from O$_2^-$ and an oxygen atom, of which the presence in irradiated water has been suggested,[27] would not account for the appearance of this species only at pH $\geqslant$ 10.

Another possible identity of the species would be O$_3^{-2}$, the doubly dissociated form of H$_2$O$_3$, which has been proposed in acid solution. In this case the pH dependence could be explained by a decay through HO$_3^-$.[28]

Acknowledgment. We are greatly indebted to Mr.

Douglas Harter, whose technical assistance has been very helpful to this investigation. We are grateful also to Mr. E. Backstrom, who operated the linac. The advice of Dr. S. Gordon concerning the use of the xenon lamp was very helpful. It is a pleasure to acknowledge the helpful discussions with our colleagues, Drs. J. Rabani and M. S. Matheson.

(27) A. O. Allen, *Radiation Res. Suppl.*, No. 4, 54 (1964).

(28) NOTE ADDED IN PROOF.—J. W. Boag, in a publication which has recently appeared [*Am. J. Roentgenol.*, 90, 896 (1963)], reports a transient absorption in oxygenated water with λ_{max} 2450 Å. Although no information is given concerning pH, it appears this is O$_2^-$, and is in close agreement with our observation.

Single Ion Conductances in Nonaqueous Solvents[1,2]

by Michael A. Coplan and Raymond M. Fuoss

Contribution No. 1752 from the Sterling Chemistry Laboratory, Yale University, New Haven, Connecticut
(Received December 14, 1963)

Conductances in methanol at 25° are reported for the following salts: sodium picrate, potassium picrate, tetra-*n*-butylammonium picrate and tetraphenylboride, and triisoamyl-*n*-butylammonium iodide, picrate, and tetraphenylboride. Using Gordon's transference data for sodium and potassium ions in their chlorides in methanol and Kunze's value $\lambda_0(\text{BPH}_4') = 36.50$, the following single ion conductances were derived: $\lambda_0(\text{Bu}_4\text{N}^+) = 39.36 \pm 0.14$, $\lambda_0(\text{Am}_3\text{BuN}^+) = 36.74 \pm 0.11$, and $\lambda_0(\text{Pi}') = 46.87 \pm 0.03$. Triamyl-butylammonium (TAB) tetraphenylboride is thus shown to be an electrolyte for which $\lambda_0^+ = \lambda_0^- = \Lambda_0/2$ within 1%, and may therefore be used as a reference electrolyte to establish single ion conductances in other solvents.

Two earlier approximate methods have been proposed to obtain single ion conductances in nonaqueous solvents by halving the limiting conductance of a salt made up of two large ions which were assumed to have equal conductances. Fowler and Kraus[3] used tetrabutylammonium triphenylborofluoride and triphenylborohydroxide, and Fuoss and Hirsch[4] the tetraphenylboride. A recent determination of the conductance of the tetraphenylboride ion in methanol[5] makes it possible to test the assumption. We have determined the conductance in methanol of sodium,

potassium, and tetrabutylammonium picrates, and used Gordon's values[6] for the single ion conductances

(3) D. L. Fowler and C. A. Kraus, *J. Am. Chem. Soc.*, 62, 2237 (1940).

(4) R. M. Fuoss and E. Hirsch, *ibid.*, 82, 1013 (1960).

of sodium and of potassium to evaluate the single ion conductance of the picrate and thence that of the tetrabutylammonium ion in methanol. The result is $\lambda_0(Bu_4N^+)$ = 39.36 ± 0.14, which is about 8% greater than Kunze's value $\lambda_0(BPh_4')$ = 36.50 ± 0.05.

In order to obtain a salt which would more satisfactorily permit the approximation $\lambda_0(+)$ = $\lambda_0(-)$ = $\Lambda_0/2$, we made triisoamylbutylammonium (TAB) iodide, picrate, and tetraphenylboride. From conductance measurements in methanol on these salts and other results, we find $\lambda_0(TAB)$ = 36.74 ± 0.11, well within 1% of the conductance of the tetraphenylboride. We plan to use this salt as our future reference for single ion conductances in nonaqueous solvents.

Experimental

Materials. Sodium picrate was prepared by neutralizing recrystallized picric acid with sodium hydroxide in ethanol. The product was recrystallized twice from absolute ethanol (7 g./100 ml.) and once from water (4 g./10 ml.). The monohydrate was dried in an Abderhalden drier at 132° (chlorobenzene) and 1 μ for 5 days (d 1.940). Potassium picrate was prepared in a similar fashion, and was recrystallized three times from water (10 g./100 ml.). This salt does not form a hydrate; it was dried at 100° and 1 μ for 1 day (d 1.852). Tetrabutylammonium picrate was from laboratory stock, m.p. 91.6–91.9°. It was dried at 58° (acetone) and 1 μ (d 1.116). Tetrabutylammonium tetraphenylboride from laboratory stock was recrystallized from petroleum ether (b.p. 60–80°)–acetone (1 g. of salt in 25 ml. of acetone, add ether to cloud point, filter, and add balance of 100 ml. of ether) to fine white needles, melting at 236.6–236.8° in a sealed capillary (d 1.023).

Triisoamylbutylammonium (TAB) iodide was prepared by heating Eastman triisoamylamine and n-butyl iodide in ethanol at 85° for 26 hr. (9.0 g. of amine, 7.3 g. of iodide, and 8 ml. of ethanol). Crude product was obtained by pouring the reaction mixture into 100 ml. of water; the dried precipitate was washed with petroleum ether and then dried at 50° for 4.5 hr. in the vacuum oven (yield, 60%). Heating a second batch for 46 hr. raised the yield to 80%. The salt was recrystallized three times from 3:1 ethyl acetate–petroleum ether (10 g./100 ml.), m.p. 119°, d 1.229. TAB picrate was prepared from the hydroxide (from the iodide and silver oxide) and picric acid. It was recrystallized three times from propanol (22 g./100 ml.); it is necessary to cool slowly or the salt may separate as an oil which congeals to lumps, m.p. 94.2–94.8°, d 1.139. TAB tetraphenylboride was prepared by adding a 3% solution of TAB iodide in methanol–

water to a 2% aqueous solution of sodium tetraphenylboride. The precipitate was thoroughly washed, and then recrystallized three times from 3:1 acetone–water (1.5 g./100 ml.), m.p. 274–275°, d 0.967.

Methanol was dried by refluxing 2-l. batches over 12.5 g. of aluminum foil and 2.5 g. of mercuric chloride for at least 6 hr. under nitrogen. A conductance cell on the end of the condenser monitored the solvent, which was distilled directly into a solvent storage flask, from which it was pumped into the conductance cell by dry nitrogen. The solvent conductance varied from 1 to 5 × 10^{-8}, d 0.78655 ± 2 at 25°.

Methods. Electrical equipment, cells, and general technique were as described by Lind and Fuoss.[7] All solutions were made up by weight; volume concentrations c (equivalents per liter of solution) are related to weight concentrations w (equivalents per kilogram of solution) through the density, c = wρ. At low concentrations, ρ = $\rho_0(1 + \gamma w)$. Values of γ were

Table I: Conductance of Picrates in Methanol at 25° (Superscripts Designate Series of Determinations)

10^4c	Λ	10^4c	Λ	10^4c	Λ
—NaPi—				—Bu₄NPi—	
		5.131[b]	93.13		
4.233[a]	87.03	10.346	90.39	4.150[a]	81.06
8.499	84.93	15.346	88.41	8.573	78.80
12.423	83.46	19.966	86.84	12.057	77.40
16.308	82.24	25.544	85.24	16.510	75.94
21.008	80.97	4.081[c]	93.85	20.655	74.76
4.571[b]	86.80	8.296	91.38	4.541[b]	80.81
9.179	84.60	12.177	89.64	8.710	78.69
13.635	83.00	16.420	88.08	12.729	77.15
17.996	81.71	20.638	86.69	16.206	76.01
22.646	80.52	4.713[d]	93.44	20.685	74.73
4.452[c]	86.94	9.522	90.83	3.653[c]	81.43
12.894	83.32	13.883	89.01	7.373	79.37
17.103	82.04	18.794	87.33	10.729	77.95
21.837	80.82	23.063	86.03	14.228	76.70
4.065[d]	87.20	8.524[e]	91.37	18.255	75.46
8.312	85.04	13.177	89.36	—Am₃BuNPi—	
12.106	83.59	17.133	87.92	3.589[a]	79.10
16.017	82.37	21.515	86.56	7.236	77.10
20.318	81.17	25.442	85.46	10.774	75.61
—KPi—		29.762	84.38	14.665	74.28
4.466[a]	93.48	33.687	83.47	17.616	73.36
9.038	90.90	38.564	82.41	5.230[b]	78.07
13.464	89.00	43.144	81.50	10.257	75.77
18.450	87.24			15.103	74.09
22.131	86.12			20.294	72.61
				25.404	71.36

(5) R. W. Kunze and R. M. Fuoss, *J. Phys. Chem.*, **67**, 385 (1963).

(6) J. P. Butler, H. I. Schiff, and A. R. Gordon, *J. Chem. Phys.*, **19**, 752 (1951); J. A. Davies, R. L. Kay, and A. R. Gordon, *ibid.*, **19**, 749 (1951).

(7) J. E. Lind, Jr., and R. M. Fuoss, *J. Phys. Chem.*, **65**, 999 (1961).

found as follows: NaPi, 0.184; KPi, 0.172; Bu₄NPi, 0.179; TABPi, 0.176; Bu₄N·BPh₄, 0.129; TAB·BPh₄, 0.164; TAB·I, 0.139. Cell constants were checked at the beginning and end of a series of runs on a given salt; constants were 0.15021, 0.11790, and 0.07260. The conductances of the salts in methanol at 25° are summarized in Tables I and II.

Table II: Conductances of Salts in Methanol at 25°
(Superscripts Designate Series of Determinations)

10^4c	Λ	10^4c	Λ	10^4c	Λ
⸺Bu₄N·BPh₄⸺		⸺Am₃BuN·BPh₄⸺			
				1.795[c]	69.99
1.966[a]	72.45	2.121[a]	69.74	3.657	68.52
3.728	70.96	4.412	68.09	5.402	67.46
5.529	69.76	6.637	66.86	7.345	66.46
7.406	68.70	8.750	65.88	9.158	65.66
2.883[b]	71.64	10.524	65.14	⸺Am₃BuNI⸺	
6.212	69.38	2.131[b]	69.89	4.362	93.68
9.296	67.80	4.324	68.25	8.654	91.22
12.114	66.57	6.375	67.07	12.777	89.38
15.429	65.32	8.827	65.88	16.782	87.90
		10.746	65.07	21.520	86.41

Discussion

The data of Tables I and II were analyzed by the IBM 709 computer, in order to obtain the constants of the conductance equation

$$\Lambda = \Lambda_0 - Sc^{1/2}\gamma^{1/2} + E'c\gamma \ln c\gamma + Jc\gamma - K_A c\gamma f^2 \Lambda \quad (1)$$

The results are summarized in Table III. The different runs for a given salt were made on samples subjected to varying times and temperatures of drying, and on successive crystallizations; no systematic variation was found within the experimental error of about 0.03% precision, so we consider the purity of the compounds to be established.

Single ion conductances were then computed. First, in order to have self-consistent figures, Gordon's data for sodium and potassium chlorides[6] and for potassium iodide[8] in methanol were extrapolated by means of eq. 1; the values found [$\Lambda_0(\text{NaCl})$ = 97.56, $\Lambda_0(\text{KCl})$ = 104.75, and $\Lambda_0(\text{KI})$ = 115.14] are 0.01–0.04 Λ-units lower than the limiting conductances obtained by the Shedlovsky extrapolation used by Gordon. Using Gordon's transference numbers 0.4634 for sodium and 0.5001 for potassium in the chlorides, we find $\lambda_0(\text{Na}^+)$ = 45.21 and $\lambda_0(\text{K}^+)$ = 52.38. Averaging the results of Table III for the alkali picrates, $\Lambda_0(\text{NaPi})$ = 92.05 and $\Lambda_0(\text{KPi})$ = 99.29, whence $\lambda_0(\text{Pi}')$ = 46.84 from the sodium salt and 46.91 from the

Table III: Constants of Conductance Equation
(Superscripts Designate Series of Determinations)

Run	Λ_0	K_A	J
NaPi[a]	92.03 ± 0.00	0	1097 ± 2
NaPi[b]	92.00 ± 0.01	0	1086 ± 7
NaPi[c]	92.06 ± 0.03	0	1101 ± 16
NaPi[d]	92.10 ± 0.02	0	1073 ± 13
KPi[a]	99.22 ± 0.01	15.4 ± 0.3	1383 ± 18
KPi[b]	99.27 ± 0.03	12.3 ± 1.7	1238 ± 85
KPi[c]	99.28 ± 0.06	12.8 ± 3.9	1281 ± 210
KPi[d]	99.28 ± 0.05	11.5 ± 3.1	1239 ± 158
KPi[e]	99.28 ± 0.03	9.9 ± 9.0	1188 ± 36
Bu₄NiP[a]	86.08 ± 0.03	8.8 ± 2.4	1105 ± 108
Bu₄NiP[b]	86.10 ± 0.04	11.8 ± 3.0	1233 ± 138
Bu₄NiP[c]	86.13 ± 0.02	8.4 ± 1.4	1082 ± 69
TAB·Pi[a]	83.71 ± 0.06	9.7 ± 6.2	1113 ± 292
TAB·Pi[b]	83.67 ± 0.01	10.2 ± 0.4	1146 ± 17
Bu₄N·BPh[a]	76.01 ± 0.01	40.0 ± 4.0	1364 ± 205
Bu₄N·BPh₄[b]	75.99 ± 0.02	34.8 ± 3.3	1148 ± 140
TAB·BPh₄[a]	73.21 ± 0.00	21.5 ± 0.2	1011 ± 7
TAB·BPh₄[b]	73.44 ± 0.01	29.0 ± 2.0	1163 ± 90
TAB·BPh₄[c]	73.19 ± 0.01	28.4 ± 2.1	1310 ± 100
TAB·I	99.39 ± 0.04	17.0 ± 2.6	1450 ± 135

potassium (average, 46.87 ± 0.03). The three runs on tetrabutylammonium picrate average to $\Lambda_0(\text{Bu}_4\text{NPi})$ = 86.10 ± 0.03, which is in exact agreement with Evers' result.[9] Combining this with the picrate conductance, we find $\lambda_0(\text{Bu}_4\text{N}^+)$ = 39.23.

A second approach to the conductance of the tetrabutylammonium ion was made through its tetraphenylboride. This salt has only a low solubility in methanol, and the solutions slowly turn yellow and finally red; indications are that the change is due to oxidation. Hence runs were made as rapidly as possible with this salt (no double checking on temperature equilibrium, no repeat frequency curves, etc.), with exclusion of air. The three runs made give $\lambda_0(\text{Bu}_4\text{N·BPh}_4)$ = 76.00 ± 0.02. (One run was omitted in Table II to save space.) The ±0.02 in Λ_0 shows excellent agreement on the extrapolated value, although the curves did not exactly coincide at the finite concentrations measured, as shown by the J values which were 1364, 964, and 1148. Using Kunze's value[5] for the tetraphenylboride ion, we obtain $\lambda_0(\text{Bu}_4\text{N}^+)$ = 39.50. The unweighted average of the picrate and tetraphenylboride figures is $\lambda_0(\text{Bu}_4\text{N}^+)$ = 39.36 ± 0.14.

We noted that the ratio $\lambda_0(\text{Bu}_4\text{N}^+)/\lambda_0(\text{BPh}_4')$ =

(8) R. E. Jervis, D. R. Muir, J. P. Butler, and A. R. Gordon, *J. Am. Chem. Soc.*, **75**, 2855 (1953).

(9) E. C. Evers and A. G. Knox, *ibid.*, **73**, 1739 (1951).

1.078, which shows that our earlier approximation[4] that $\lambda_0^+ = \lambda_0^- = \Lambda_0/2$ for this salt is out by about 8%. Evers[9] had reported the value of 82.5 for the limiting conductance of tetraisoamylammonium picrate in methanol, 3.6 Λ-units lower than the value for the tetrabutyl salt. In order to obtain a slower ion by about 2.9 units, to match the tetraphenylboride ion, we synthesized triisoamyl-n-butylammonium (TAB) iodide and then prepared the picrate and tetraphenylboride from it. The TAB ion is a little asymmetric, but probably can still be represented quite well by a charged sphere. Three values of λ_0(TAB) can be obtained from the figures in Table III. From the picrate (average Λ_0(TAB·Pi) = 83.69) and the single ion picrate conductance, we have λ_0(TAB) = 36.82. From the average Λ_0(TAB·BPh$_4$) = 73.28 and Kunze's value for the tetraphenylboride ion, λ_0(TAB) = 36.78. Finally, from the single iodide run, Λ_0(TAB·I) = 99.39. Using $\lambda_0(I') = 62.76$ from Gordon's results, this gives λ_0(TAB) =

36.63. The average over all three salts is 36.74; with a probable error of ± 0.11. The sum of the averaged single ion conductances of the TAB ion and the tetraphenylboride ion (36.74 + 36.50) is 73.24, in excellent agreement with the directly observed value of 73.28.

We now have a salt, triisoamyl-n-butylammonium tetraphenylboride, which has been shown to have cationic and anionic conductances which are equal to better than 1%. This salt, which is soluble in a wide range of organic solvents, will be used as the reference electrolyte in our future conductance studies, in order to establish single ion conductances. The implicit assumption is being made, of course, that the effect of solvent–solute interaction on limiting conductance is the *same* for these two ions, regardless of the solvent. This appears to be a plausible working hypothesis because both ions are large and have correspondingly weak fields at their "surfaces" and both are nearly centrally symmetric.

Electrolyte–Solvent Interaction. XV. The Isodielectric

Systems Methanol–Acetonitrile–Nitromethane[1]

by Michael A. Coplan[2] and Raymond M. Fuoss

Contribution No. 1751 from the Sterling Chemistry Laboratory, Yale University, New Haven, Connecticut
(Received December 14, 1963)

Conductances of solutions of triisoamyl-n-butylammonium (TAB) iodide, picrate, and tetraphenylboride have been measured in (nearly) isodielectric mixtures of the solvents methanol, acetonitrile, and nitromethane. The anionic Walden products (calculated on the assumption that the conductances of the two ions of TAB tetraphenylboride are the same in all solvents) are not constant. Selective solvation by monomeric methanol or by acetonitrile in preference to nitromethane is proposed to describe the observed changes in Walden product (and Stokes radius).

To first approximation, the limiting conductance of an ion varies inversely as the viscosity of the solvent, but as is well-known, the Walden product is not constant. One source of its variation is a relaxation effect produced by the motion of ions in a polarizable medium,[3,4] as a consequence of which the reciprocal Walden product depends linearly on the reciprocal dielectric constant. This is a volume effect, in that it can be calculated[5,6] by integrating over the entire medium surrounding the reference ion. If, however, specific interaction due to short-range interactions between ions and solvent dipoles occurs, then one might expect variation in the Walden product for a given ion in a series of solvents which had the same dielectric constant, but which varied in details of dipole structure. The purpose of this paper is to present examples of this situation. Mixtures of acetonitrile ($D = 36.0$), nitromethane ($D = 36.0$), and methanol ($D = 32.6$) are practically isodielectric. Still, the Walden products for the iodide, picrate, and tetraphenylboride ions in these mixtures varied considerably. Selective solvation by monomeric methanol or by acetonitrile is suggested as the explanation of the observed results.

Experimental

Preparation and purification of the salts are described in the preceding paper,[7] which also gives details of the purification of the methanol. Cells, electrical

equipment, and technique have all been described. Acetonitrile was refluxed over Drierite under nitrogen and then fractionated through an 80-cm. column which was packed with glass beads (conductance, $3\text{--}4 \times 10^{-8}$). Nitromethane (Matheson P 1240) was treated with Analabs 5A Molecular Sieve, filtered, and distilled at 40 mm. After discarding a forerun, nitromethane of conductance $2\text{--}6 \times 10^{-8}$ was obtained. The density ranged from 1.1230 to 1.1246, viscosity 0.6210 to 0.6218 cp. Low conductance unfortunately is not an adequate criterion of solvent purity. Our nitromethane is inferior to that which can be obtained by recrystallization,[8] which gives a product of density 1.13124 and viscosity 0.627. Distillation with an efficient column will give nitromethane of density 1.13064 and viscosity 0.608.[9] Vapor phase chromatog-

(1) This paper is based on part of a dissertation presented by Michael A. Coplan to the Graduate School of Yale University in June, 1963, in partial fulfillment of the requirements for the degree of Doctor of Philosophy.

(2) Grateful acknowledgement is made to the National Institute of Health for a fellowship held during 1962–1963.

(3) R. M. Fuoss, *Proc. Natl. Acad. Sci. U. S.*, 45, 807 (1959).

(4) D. S. Berns and R. M. Fuoss, *J. Am. Chem. Soc.*, 83, 1321 (1961).

(5) R. Zwanzig, *J. Chem. Phys.*, 38, 1603 (1963).

(6) R. H. Boyd, *ibid.*, 35, 1281 (1961).

(7) M. A. Coplan and R. M. Fuoss, *J. Phys. Chem.*, 68, 1177 (1964).

(8) A. K. R. Unni, L. Elias, and H. I. Schiff, *ibid.*, 67, 1216 (1963).

(9) C. J. Thompson, H. J. Coleman, and R. V. Helm, *J. Am. Chem. Soc.*, 76, 3445 (1954).

raphy showed later that our nitromethane contained about 1% each of a higher and a lower boiling impurity, which evidently form azeotropes with nitromethane.

Solvent mixtures were made up by weight. Their properties (density, viscosity, and dielectric constant) are given in Table I; w_1 is weight % of the first named member of a pair of solvents. Conductances of the three salts are given in Tables II, III, and IV, where the solvents are identified by the code numbers given in the first column of Table I. The sequence of mixtures is the same as the left-to-right sequence of points in Fig. 1.
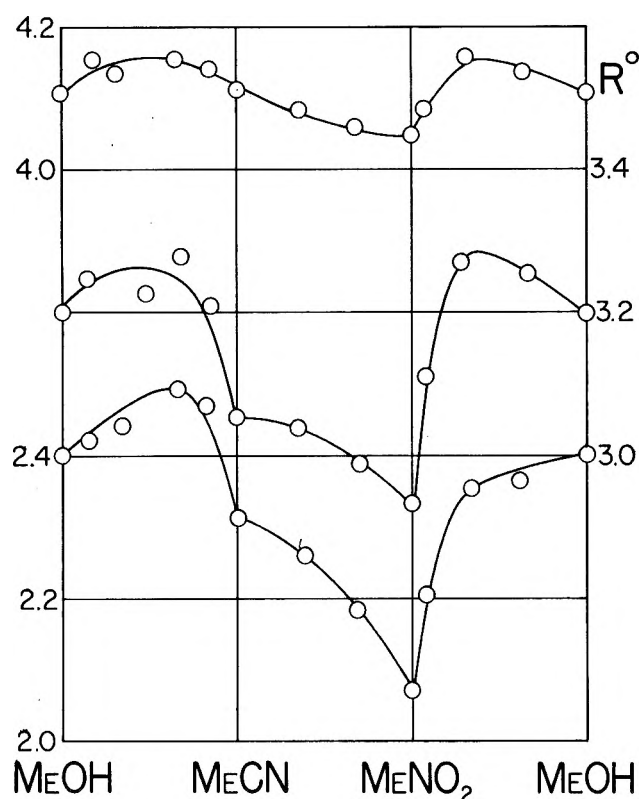
Figure 1. Dependence of Stokes radius of anions on composition of solvent: top, tetraphenylboride, ordinates left; center, picrate, ordinates right; bottom, iodide, ordinates left.

Discussion

The data conform to the conductance equation for unassociated electrolytes

$$\Lambda = \Lambda_0 - Sc^{1/2} + Ec \log c + Jc \qquad (1)$$

The values of the constants Λ_0 and J are summarized in Table V. The limiting conductances for a given salt cover a wide range of values as might be expected from the wide range of viscosities (0.00345–0.00622).

Table I: Properties of Solvents

No.	w_1	ρ	$10^3\eta$	D
Methanol–acetonitrile				
1	0.0	0.77686	3.45	36.01
2	14.5	0.77932	3.34	35.52
3	17.7	0.77970	3.33	35.47
4	32.2	0.78179	3.42	34.70
5	33.7	0.78198	3.43	34.96
6	35.4	0.78244	3.45	34.44
7	51.6	0.78438	3.69	34.16
8	65.8	0.78590	4.02	33.78
9	69.3	0.78682	4.19	33.78
10	82.8	0.78696	4.59	33.25
11	85.3	0.78703	4.69	33.15
12	86.0	0.78700	4.72	33.04
13	100.0	0.78655	5.45	32.63
Acetonitrile–nitromethane				
14	0.0	1.12460	6.22	36.00
15	30.1	0.99325	4.96	36.01
16	31.2	0.98872	4.92	36.07
17	31.7	0.98696	4.90	35.93
18	60.9	0.88498	4.13	35.96
19	64.4	0.87453	4.05	35.65
20	65.6	0.87080	4.03	35.98
Nitromethane–methanol				
21	34.4	0.88057	5.03	32.20
22	37.3	0.88914	5.02	32.24
23	37.5	0.88988	5.01	32.42
24	38.1	0.89173	5.00	32.20
25	65.2	0.98126	4.95	32.92
26	69.0	0.99513	4.97	33.01
27	72.4	1.00781	5.00	33.05
28	92.2	1.08880	5.50	34.74
29	92.3	1.08952	5.50	34.84
30	93.0	1.09251	5.54	34.91

In order to eliminate to first approximation the effect of viscosity, we shall consider the Walden products for the single ions, $\lambda_0^{\pm}\eta$.

The single ion conductances were obtained on the basis of the assumption that the limiting conductance of the triisoamyl-n-butylammonium ion, shown[7] to equal that of the tetraphenylboride ion in methanol, is the same as that of the latter ion in all solvents. Then we may set

$$\lambda_0(\text{TAB}^+) = \lambda_0(\text{BPh}_4') = (1/2)\Lambda_0(\text{TAB} \cdot \text{BPh}_4) \qquad (2)$$

for this salt, and construct from the data for the tetraphenylboride a plot of $\lambda_0^+\eta$ for the cation, from which values can be interpolated at the solvent compositions where the picrate and iodide were measured. Then subtracting $\lambda_0^+\eta$ for a given salt from its Walden product $\Lambda_0\eta$ gives the anionic product $\lambda_0^-\eta$. Cationic and anionic products obtained in this way are shown in Table V. It is immediately seen that the products

Table II : Conductance of TAB Iodide

10^4c	Λ	10^4c	Λ	10^4c	Λ
No. 13		No. 3		No. 14	
21.520	86.41	21.309	143.10	26.831	86.26
16.782	87.90	16.826	144.64	22.601	87.03
12.777	89.38	10.932	147.16	16.261	88.32
8.654	91.22	5.445	150.32	10.859	89.67
4.362	93.68			5.563	91.46
No. 11		No. 1		No. 28	
23.689	100.57	17.552	145.53	25.616	93.22
18.534	102.09	13.903	147.16	20.694	94.21
12.563	104.24	10.544	148.88	15.057	95.52
9.090	105.74	7.228	150.91	9.759	97.05
4.725	108.22	3.449	153.94	4.956	98.92
No. 8		No. 18		No. 25	
25.569	116.53	26.181	121.58	26.591	98.15
19.981	118.06	21.997	122.74	22.166	99.07
14.357	120.09	15.725	124.70	16.413	100.43
10.310	121.78	10.374	126.86	10.604	102.17
5.110	124.83	5.223	129.57		
No. 5		No. 16		No. 24	
23.575	137.06	27.796	104.58	26.372	95.84
19.998	138.11	22.851	105.69	21.816	96.89
16.026	139.39	16.540	107.29	15.349	98.58
10.096	141.92	11.195	109.00	10.217	100.27
5.059	144.94	5.587	111.37		

Table III : Conductance of TAB Picrate

10^4c	Λ	10^4c	Λ	10^4c	Λ
No. 13		No. 2		No. 14	
17.616	73.36	22.051	120.75	28.392	68.54
14.665	74.28	16.720	122.49	23.723	69.25
10.744	75.61	13.128	123.92	18.832	70.02
7.236	77.10	8.710	125.90	11.885	71.44
3.589	79.10	4.419	128.56	5.974	73.13
No. 12		No. 1		No. 29	
24.344	82.87	15.741	122.85	30.282	73.94
19.103	84.24	12.698	124.07	24.276	74.84
14.594	85.57	9.541	125.55	17.377	76.11
9.867	87.25	6.323	127.37	10.946	77.63
4.942	89.62			5.432	79.40
No. 7		No. 20		No. 27	
22.393	105.93	25.417	103.24	24.417	78.99
17.602	107.40	20.125	104.56	19.002	80.07
13.330	108.93	15.848	105.80	12.876	81.52
9.038	110.78	10.523	107.67	6.146	83.77
4.393	113.53	5.302	110.17		
No. 4		No. 15		No. 21	
23.880	115.26	29.242	84.41	25.543	77.22
18.556	116.77	24.656	85.19	21.016	78.20
15.098	117.94	18.690	86.44	15.080	79.72
9.975	120.05	6.056	90.30	9.970	81.33
5.023	122.90			5.001	83.54

Table IV : Conductance of TAB Tetraphenylboride

10^4c	Λ	10^4c	Λ	10^4c	Λ
No. 13		No. 2		No. 14	
10.524	65.14	24.215	104.05	26.517	57.10
8.750	65.88	18.040	105.74	21.535	57.78
6.637	66.86	9.709	108.77	16.268	58.61
4.412	68.09	4.794	111.33	10.445	59.74
2.121	69.74				
No. 10		No. 1		No. 30	
16.802	75.70	19.833	103.41	27.941	62.95
13.074	76.88	17.335	104.15	22.903	63.70
9.675	78.13	12.008	105.97	17.175	64.73
6.764	79.40	7.923	107.73	10.572	66.21
3.378	81.36	3.886	110.15	5.456	67.83
No. 9		No. 19		No. 26	
21.453	82.61	25.901	86.94	26.414	68.63
16.139	84.10	21.795	87.74	21.035	69.65
12.494	85.28	15.793	89.21	16.298	70.68
8.550	86.82	10.017	90.99	10.702	72.06
4.256	89.05	5.203	93.04	5.436	74.01
No. 6		No. 17		No. 22	
28.226	98.37	26.828	72.12	26.828	67.23
22.552	99.64	22.482	72.83	22.271	68.11
18.053	100.94	16.536	74.02	16.992	69.40
12.068	102.98	10.675	75.51	11.290	71.04
5.642	106.14	5.604	77.29	5.297	73.44

for a given ion depend on the composition of the solvent, the more sensitively the smaller the ion. Clearly, the simple model of spheres in a continuum is incapable of describing these systems.

In order to obtain a parameter with a simpler physical interpretation, let us consider the Stokes radii R for the anions, calculated as

$$R = \mathfrak{F}\epsilon/1800\pi\lambda_0^-\eta \qquad (3)$$

These are the radii of the spheres which are hydrodynamically equivalent to the ions; they are plotted in Fig. 1. The variation cannot be an electrostatic effect because the solvents all have nearly the same dielectric constant, and the s/D term[3] is small for dielectric constants of the order of 35. There is, however, some correlation between the variation of R with composition, and that of the viscosity, shown in Fig. 2. One might attempt to find a constant by considering a function of the form $\lambda_0\eta^\alpha$ with $\alpha \pm 1$, but this would be a completely empirical approach. A more satisfactory rationalization of the observations is to consider both the change of viscosity and the change of the Stokes radii with composition for the systems containing methanol to be consequences of the same origin.

Table V: Derived Constants

No.	Λ_0	J	$\lambda_0^+\eta$	$\lambda_0^-\eta$
TAB iodide				
13	99.39	1450	0.200	0.342
11	114.44	1275	0.198	0.339
8	132.00	1730	0.194	0.337
5	152.78	2295	0.196	0.329
3	158.69	2210	0.197	0.332
1	160.68	1440	0.199	0.355
18	136.46	1460	0.201	0.363
16	117.37	1300	0.202	0.375
14	96.24	1115	0.202	0.395
28	104.07	1500	0.201	0.372
25	110.48	1940	0.196	0.348
24	108.70	1845	0.197	0.347
TAB picrate				
13	83.69	1150	0.200	0.256
12	95.46	1225	0.198	0.253
7	120.19	1690	0.190	0.254
4	130.36	1985	0.196	0.250
2	135.83	2030	0.198	0.255
1	135.70	1550	0.199	0.269
20	116.69	1450	0.201	0.270
15	95.94	1220	0.202	0.274
14	77.61	1015	0.202	0.280
29	84.30	1310	0.200	0.264
27	89.60	1675	0.198	0.251
21	89.07	1420	0.197	0.252
TAB tetraphenylboride				
13	73.28	1200	0.200	0.200
10	86.09	1020	0.197	0.197
9	94.70	1320	0.198	0.198
6	113.62	1825	0.196	0.196
2	118.59	1940	0.198	0.198
1	116.26	1680	0.199	0.199
19	99.04	1550	0.201	0.201
17	82.42	1190	0.202	0.202
14	65.14	965	0.203	0.203
30	72.43	1120	0.201	0.201
26	79.34	1440	0.197	0.197
22	78.92	1195	0.198	0.198

Mecke[10] has summarized a large body of evidence from infrared spectroscopy that argues that methanol is polymeric, and that addition of other solvents causes depolymerization. More recent n.m.r. measurements[11] on mixtures of methanol and carbon tetrachloride substantiate Mecke's conclusions. In Fig. 2, a sharp drop in viscosity is observed when acetonitrile or nitromethane is added to methanol, far greater than could be accounted for on the basis of adding a more fluid component in the case of acetonitrile, and inexplicable on the basis of a mixture rule for the case of nitromethane because the latter has a higher viscosity than methanol. It is clear that a strong nonadditive interaction is taking place; direct evidence for such is the
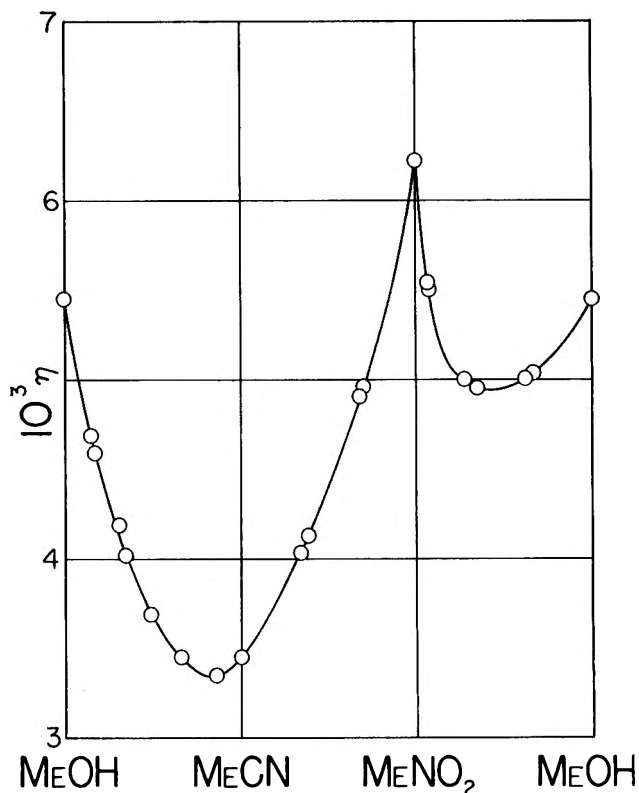
Figure 2. Dependence of viscosity on composition of solvent.

marked cooling which is observed when acetonitrile or nitromethane is added to methanol. If we assume that depolymerization occurs, we would expect a decrease in viscosity. Also, the behavior of the Stokes radii becomes plausible: monomeric methanol should act as a strong solvating molecule (especially for picrate ion), and it is seen that the Stokes radius does indeed increase when acetonitrile or nitromethane is added to methanol solutions of these salts (except, perhaps for the iodide plus nitromethane). Likewise, the Stokes radius increases very sharply when a little methanol is added to acetonitrile or nitromethane solutions of these electrolytes, especially the picrate and iodide. We would expect a dilute solution of methanol in another solvent to depolymerize; this would again supply monomers to act as solvating agents. Similar effects were observed on addition of methanol to solutions of tetrabutylammonium bromide in nitrobenzene[12]; likewise, addition of (nonpolar) heptane, benzene, or carbon tetrachloride to methanolic solutions of the same electrolyte[13] decreased the Walden product

(10) R. Mecke, Discussions Faraday Soc., 9, 161 (1950).
(11) J. Hyne and M. Saunders, J. Chem. Phys., 29, 1319 (1958).
(12) H. Sadek and R. M. Fuoss, J. Am. Chem. Soc., 72, 301 (1950).
(13) H. Sadek and R. M. Fuoss, ibid., 76, 5807 (1954).

(*i.e.*, increased the Stokes radius). Solvation by monomeric methanol provides a self-consistent description of these conductances, as well as the infrared and other observations.

A different model must, of course, be proposed to account for the acetonitrile–nitromethane mixtures, because these solvents are aprotonic, and here hydrogen bonds can play no role. In this case, the viscosity shows relatively small deviations from additivity (especially, no minimum, as in the case of the methanol mixtures). No solvent–solvent interaction seems likely here; both molecules have about the same dipole moment, yet all three anions are appreciably slower in acetonitrile than in nitromethane, the effect increasing with decreasing ion size. (The ratio of acetonitrile to nitromethane radius is 1.115 for iodide, 1.041 for picrate, and 1.016 for the tetraphenylboride.) Since both solvent molecules are dipolar, both presumably form ion–dipole solvates, but we would expect acetonitrile to be more effective than nitromethane, because the polar end of the molecule is smaller and hence the

field is more intense. In nitromethane, on the other hand, the negative part of the dipole is distributed over the two oxygen atoms, and the positive nitrogen is shielded. Hence for anion solvation, nitromethane should be less efficient than acetonitrile. In terms of the equivalent sphere, we would expect the Stokes radius to increase as acetonitrile is added to nitromethane, in accordance with observation. Nitromethane appears to be almost ineffective as a solvating agent; its effect on ionic hydrodynamics is primarily the long-range volume effect of polarization and relaxation. The low solubility of electrolytes[14] in nitromethane is another indication of its poor solvating ability, and Hammett[15] likewise concluded that it was so poor a solvating reagent that an extra molecule of acid was needed for acid–base reactions in nitromethane.

(14) A. J. Parker, *Quart. Rev.* (London), **16**, 163 (1962).

(15) H. V. Looy and L. P. Hammett, *J. Am. Chem. Soc.* **81**, 3872 (1959).

Thermodynamics of Solutions of Deuterium Chloride in

Heavy Water from 5 to 50°

by Robert Gary, Roger G. Bates, and R. A. Robinson

National Bureau of Standards, Washington, D. C.   *(Received December 14, 1963)*

The standard e.m.f. of the cell Pt; $D_2(g)$ at 1 atm., DCl in D_2O, AgCl; Ag has been determined from 5 to 50°. At 25° the standard e.m.f. is lower by 9.78 mv. (on the molality scale) or 4.31 mv. (on the mole fraction scale) than the standard e.m.f. of the corresponding cell with a hydrogen electrode and a solution of hydrochloric acid in ordinary water. Thermodynamic quantities have been calculated for the reaction $^1/_2D_2(g)$ + HCl(in H_2O) = $^1/_2H_2(g)$ + DCl(in D_2O). At 25°, $\Delta G°$ is 418 joules mole^{-1}, $\Delta H°$ is -611 joules^{-1}, and $\Delta S°$ is -3.5 joules deg.$^{-1}$ mole^{-1}, when all four substances are in the standard state on the mole fraction scale. The mean ionic activity coefficient and relative partial molal enthalpy of DCl at molalities from 0.01 to 0.05 in heavy water have been obtained and are compared with those for HCl in H_2O. The activity coefficient of DCl in D_2O is slightly smaller than that of HCl in H_2O at the same molality; at $m = 0.05$, $t = 25°$, the difference in log $\gamma_\pm$ is 0.0022.

Introduction

The standard e.m.f. of the cell

Pt; $D_2(g)$ at 1 atm., DCl(m) in D_2O, AgCl; Ag   (I)
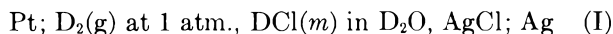
together with the known standard e.m.f. of the corresponding cell with a hydrogen electrode in a solution of hydrochloric acid in ordinary water furnishes a measure of the change in free energy of the reaction

$^1/_2D_2(g)$ + HCl(aq) = $^1/_2H_2(g)$ + DCl(in D_2O)
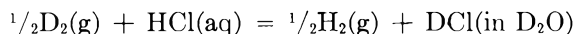
It is also of fundamental importance to the determination of dissociation constants and other thermodynamic properties of weak acids in deuterium oxide by means of the Harned–Ehlers cell[1] as well as to any effort to give meaning to pD measurements in deuterium oxide.

The silver–silver chloride electrode has had wide application in the determination of thermodynamic data for solutions in ordinary water.[2] In addition, this electrode has found use in establishing pH standards.[3]

In 1935 Abel, Bratu, and Redlich[4] used this electrode in solvents consisting of mixtures of light and heavy water, but only one measurement was made in a solvent containing more than 90 mole % of D_2O. It should be noted that these authors defined the

acid concentration, m', as moles of solute in 55.51 moles of (H_2O + D_2O). In the present paper concentrations are expressed in moles per kilogram of solvent, designated m.

Noonan and La Mer[5] made a more extensive study of cell I using solvents of compositions approaching pure deuterium oxide; some measurements were made over a range of temperatures. They also expressed acid concentrations in terms of a reduced molality m', that is, as moles of solute in 55.51 moles of solvent.

Renewed interest in the properties of acids and bases in heavy water has underscored the need for an operational scale for measuring conventional deuterium ion activities and, consequently, for pD standards with which to establish such a scale. As a first step, the standard e.m.f. of cell I must be determined.

(1) H. S. Harned and R. W. Ehlers, *J. Am. Chem. Soc.*, **54**, 1350 (1932).

(2) H. S. Harned and B. B. Owen, "Physical Chemistry of Electrolytic Solutions," 3rd Ed., Reinhold Publishing Corp., New York, N. Y., 1958.

(3) See R. G. Bates, *J. Res. Natl. Bur. Std.*, **66A**, 179 (1962).

(4) E. Abel, E. Bratu, and O. Redlich, *Z. Physik. Chem.* (Leipzig), **173A**, 353 (1935).

(5) E. Noonan and V. K. La Mer, *J. Phys. Chem.*, **43**, 247 (1939).

Deuterium gas is now available in comparatively large quantity. The measurement of the e.m.f. of cells of type I is relatively easy and we have now made a fresh study of the problem. This paper reports measurements of cell I at temperatures of 5, 15, 25, 35, 45, and 50° for five concentrations of deuterium chloride from 0.01 to 0.05 m. The data have been used to derive the standard electromotive force of cell I and the activity coefficients of deuterium chloride at these temperatures, as well as the relative partial molal enthalpy of DCl in D_2O at 25°. The difference between the standard electromotive force of cell I and that of the corresponding cell in ordinary water has been found to be 9.78 mv. at 25°. The data are shown to be consistent with the earlier data of Noonan and La Mer[5] when the same method of calculation is used.

Experimental

Materials. The heavy water had a density of 1.10416 g. ml.$^{-1}$ at 25°, indicating an isotopic purity of 99.7 mole %.[6] Its specific conductance was 3 $\times$ 10^{-6} ohm^{-1} cm.$^{-1}$ at 25°. The stock solution of deuterium chloride (about 0.05 m) was prepared by bubbling dry HCl gas, generated by adding concentrated H_2SO_4 to bromide-free NaCl, into heavy water. The amount of hydrogen added in this way was less than 0.1 mole % of the deuterium present.

Preparation of the Cells. The cells were of Pyrex glass throughout, except for Teflon stopcocks. The design was similar to that of Harned and his co-workers[7] and used by workers in this laboratory, except for the following features. Presaturation of the deuterium gas by portions of the same solution as that in the electrode compartments was achieved by a three-stage saturator with a sintered glass disperser in the middle stage. The glass joints were specially constructed with two seating surfaces separated by a groove 5 mm. wide to protect the solution from contamination by grease or by water from the thermostat. The deuterium electrodes were partially immersed in the solution, the upper half being exposed to the deuterium above the solution. The deuterium gas was stated by the suppliers to contain at least 99.7 mole % of D_2; before entry into the saturators and the cell it was passed through a Deoxo purifier to remove traces of oxygen. The silver–silver chloride electrodes were of the thermal-electrolytic type prepared according to the recommendation of Bates.[8]

Before the cells were filled, the electrodes were thoroughly washed and soaked in ordinary water and inserted into the empty cell vessels, which had been flushed with helium. The cells were then evacu-

ated and the vacuum maintained for about 30 min to dry the electrodes, after which the cells were filled with deuterium gas.

The cell solutions, deaerated and saturated with deuterium, were forced into the cell vessels by deuterium pressure, the cell being vented while the solution entered. Preliminary experiments with hydrogen and solutions in ordinary water showed that this technique gives stable, reproducible results in agreement with data obtained earlier in this laboratory.

The cell solutions were prepared by weight (vacuum corrections were applied) by dilution of the stock solution. The solutions were made up in air, transferred by pressure to helium-filled flasks, weighed, boiled at room temperature under vacuum, saturated with deuterium gas, and weighed again. The concentration of the solution was corrected for the loss of heavy water on boiling. The use of helium-filled flasks simplified the vacuum correction, since helium and deuterium have nearly identical densities.

Results

The e.m.f. of cell I at five molalities is recorded in Table I. The first measurements were made with a cell containing 0.02003 m DCl, and some instability of e.m.f. was found at 55°. Therefore, 50° was chosen as the highest temperature at which measurements of the other four solutions were made. The value in parentheses (at 50°) in Table I is an interpolated one. For purpose of comparison two cells with hydrogen electrodes and containing exactly 0.01 m HCl in *ordinary* water were measured; the e.m.f. values are also given in Table I.

The standard e.m.f. of the deuterium oxide cell (on the molality scale) was found by extrapolating to zero concentration the function

$$E_m^{\circ\prime} = E + 2k \log m - 2k \frac{A\,(md_0)^{1/2}}{1 + Ba^*(md_0)^{1/2}} \quad (1)$$

where k is written for $(RT \ln 10)/F$. The ion-size parameter,[9] a^*, was put equal to 4.3 Å. Values of $Ad_0^{1/2}$ and $Bd_0^{1/2}$, the constants of the Debye–Hückel equation, were calculated with the dielectric con-

(6) I. Kirshenbaum, "Physical Properties and Analysis of Heavy Water," H. C. Urey and G. M. Murphy, Ed., McGraw-Hill Book Co., Inc., New York, N. Y., 1951, p. 17.

(7) See H. S. Harned and J. O. Morrison, *Am. J. Sci.*, **33**, 161 (1937).

(8) R. G. Bates, "Determination of pH," John Wiley and Sons, Inc., New York, N. Y., 1964, p. 282.

(9) For their data in ordinary water, R. G. Bates and V. E. Bower [*J. Res. Natl. Bur. Std.*, **53**, 283 (1954)] put $a^* = 4.3$ Å. at 0 to 30° and 5.0 Å. at 35 to 55°. If we put $a^* = 5.0$ Å. at 50°, the present data for heavy water give an extrapolated $E_m^{\circ} = 0.19312$ v. at this temperature instead of 0.19310 v. with $a^* = 4.3$ Å.

Table I: Electromotive Force[a] of the Cell Pt; $D_2(g)$ at 1 atm., DCl(m) in D_2O, AgCl; Ag from 5 to 50°

m	5°	15°	25°	35°	45°	50°	55°
0.010015	0.45081	0.45305	0.45458	0.45547	0.45573	0.45562	
0.02003	0.41911	0.42031	0.42071	0.42048	0.41964	(0.41901)	0.41821
0.02999	0.40080	0.40135	0.40110	0.40027	0.39881	0.39783	
0.04001	0.38777	0.38784	0.38721	0.38580	0.38394	0.38280	
0.04998	0.37765	0.37739	0.37639	0.37473	0.37257	0.37120	
0.01000[b]	0.45962	0.46222	0.46425	0.46571	0.46656	0.46684	
$A d_0^{1/2}$	0.5232	0.5319	0.5413	0.5513	0.5622	0.5678	0.5736
$B d_0^{1/2}$	0.3429	0.3448	0.3467	0.3485	0.3504	0.3513	0.3523

[a] Electromotive force in volts.   [b] These results refer to the cell Pt; $H_2(g)$ at 1 atm., HCl (0.01 m) in H_2O, AgCl; Ag.

stants given by Malmberg[10] and the density data given by Chang and Tung.[11] Values of these constants are shown at the bottom of Table I. Table II gives the extrapolated values of the standard electromotive force on the molality scale, together with the standard deviation.

Table II: Standard Electromotive Force of the Cell Pt; $D_2(g)$ at 1 atm., DCl(m) in D_2O, AgCl, Ag from 5 to 50°

t, °C.	$E_m°$ (D_2O), v.	σ, mv.	$E_m°$ (H_2O), v.	$-\Delta E_m°$, mv.	$-\Delta E_N°$, mv.
5	0.22528	0.03	0.23420	8.92	3.81
15	0.21931	0.04	0.22862	9.31	4.02
25	0.21266	0.04	0.22244	9.78	4.31
35	0.20532	0.03	0.21574	10.42	4.76
45	0.19733	0.02	0.20839	11.06	5.22
50	0.19310	0.02	0.20456	11.46	5.53

The standard e.m.f. of the cell with ordinary water as solvent was calculated using the equation

$$E_m° = E + 2k \log m\gamma, \quad m = 0.01$$

together with the activity coefficient data of Bates and Bower,[9] which are in good agreement with the earlier data of Harned and Ehlers.[12] Values of this standard e.m.f. on the molality scale are also given in Table II together with the difference in standard e.m.f. between the ordinary water and the heavy water cells on both the molality (m) and mole fraction (N) scales

$$\Delta E° \equiv E°(D_2O) - E°(H_2O)$$

The difference in standard e.m.f. (on the mole fraction scale) can be expressed as a function of the temperature by the equation

$$-\Delta E_N° = 3.74 + (11.40 \times 10^{-3})t + (4.87 \times 10^{-4})t^2 \quad (2)$$

where t is in degrees Celsius and $\Delta E_N°$ is in millivolts. Alternatively

$$-\Delta E_N° = 36.96 - 0.2546T + (4.87 \times 10^{-4})T^2 \quad (3)$$

where T is in degrees Kelvin. Since $\Delta G° = -F\Delta E_N°$, where $\Delta G°$ is the free energy change of the reaction

$$^{1}/_{2}D_2(g) + HCl \text{ (in } H_2O) \to {^{1}/_{2}}H_2(g) + DCl \text{ (in } D_2O)$$
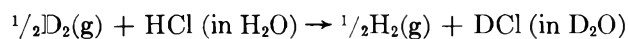
we can now calculate thermodynamic functions for this reaction

$$\Delta G° = 3566.4 - 24.57T + 0.04699T^2 \quad (4)$$

$$\Delta H° = 3566.4 - 0.04699T^2 \quad (5)$$

$$\Delta S° = 24.57 - 0.09398T \quad (6)$$

$$\Delta C_p° = -0.09398T \quad (7)$$

At 25°, $\Delta C_p° = -28$ joules deg.$^{-1}$ mole^{-1}. Values of the other functions are given in Table III, which also includes the change in electrostatic free energy,

Table III: Thermodynamic Functions[a] for the Reaction $^{1}/_{2}D_2(g) + HCl(\text{in } H_2O) = {^{1}/_{2}}H_2(g) + DCl(\text{in } D_2O)$

t, °C.	$\Delta G°$	$\Delta H°$	$\Delta S°$	ΔG_{el}
5	368	-69	-1.6	27
15	388	-335	-2.5	34
25	418	-611	-3.5	42
35	457	-896	-4.4	49
45	506	-1190	-5.3	56
50	534	-1331	-5.8	63

[a] $\Delta G°$ and $\Delta H°$ are expressed in joules mole^{-1} and $\Delta S°$ in joules deg.$^{-1}$ mole^{-1}.

(10) C. G. Malmberg, J. Res. Natl. Bur. Std., 60, 609 (1958).

(11) T. L. Chang and L. H. Tung, Chinese J. Phys., 7, 230 (1949).

(12) H. S. Harned and R. W. Ehlers, J. Am. Chem. Soc., 55, 2179 (1933).

Table IV: Activity Coefficients of DCl in D_2O Solutions[a]

m	5°	15°	25°	25°[b]	35°	45°	50°	$\bar{L}_2$ (25°)[c]
0.01	0.0440	0.0446	0.0454	0.0436	0.0464	0.0474	0.0479	290
0.02	0.0580	0.0591	0.0603	0.0578	0.0615	0.0626	0.0634	410
0.03	0.0674	0.0687	0.0701	0.0675	0.0714	0.0729	0.0736	470
0.04	0.0746	0.0757	0.0772	0.0747	0.0788	0.0805	0.0813	520
0.05	0.0795	0.0810	0.0827	0.0805	0.0847	0.0867	0.0878	630

[a] The negative logarithm of the molal activity coefficient is tabulated. [b] These values refer to HCl in H_2O at 25°. [c] In joules mole^{-1}.

calculated by the Born equation with $r_H = r_D = r_{Cl}$ = 2 Å. corresponding to the removal of hydrogen and chloride ions from ordinary water followed by the introduction of deuterium and chloride ions into heavy water. It will be observed that this change in electrostatic free energy is only about one-tenth of the total free energy change.

Discussion

We have recalculated the data of Noonan and La Mer[5] at 25° by converting their values of E to absolute volts and their values of m' to moles per kilogram of solvent (m). Our calculations give the following results:

m	0.01465	0.02596	0.04150
E	0.43588	0.40805	0.38545
E (calcd.)	0.43597	0.40810	0.38539

The values labeled E (calcd.) were obtained from the data of the present investigation. The results for 0.02955 m DCl (or 0.03282 m') are as follows:

	5°	15°	25°
E	0.40103	0.40189	0.40177
E (calcd.)	0.40145	0.40199	0.40180

and for 0.02695 m DCl (or 0.02991 m'):

	25°	35°	45°
E	0.40623	0.40563	0.40437
E (calcd.)	0.40629	0.40562	0.40432

With the one exception of the cell at 5°, the agreement is excellent, the average difference being only 0.06 mv.

Abel, Bratu, and Redlich[4] found an e.m.f. of 0.3492 v. for the cell Pt; 98.4 mole % D_2, 0.09007 m DCl in 97.0 mole % D_2O, AgCl; Ag at 21°. From our data we calculate an e.m.f. 0.4 mv. lower than theirs but some of this difference can be accounted for by the appreciable amount of hydrogen in their cell.

The values of $\Delta G°$ and related thermodynamic quantities in Table III are all based on $\Delta E_N°$ values, that is, they refer to transfers between HCl (in H_2O)

and DCl (in D_2O) when each is in its standard state on the mole fraction scale. The free energy on the molality scale will be different by

$$2RT \left\{ \ln \frac{1000}{w_{H_2O}} - \ln \frac{1000}{w_{D_2O}} \right\}$$

where w designates molecular weight.[13] This quantity becomes, on insertion of the appropriate numerical values, $1.765T$ joules mole^{-1}; thus, the values of $\Delta H°$ and $\Delta C_p°$ are the same on each scale but $\Delta G°$ becomes larger, e.g., 944 joules mole^{-1} at 25° on the molality scale compared with 418 on the mole fraction scale. Likewise, the entropy change is more negative by 1.8 joules deg.$^{-1}$ mole^{-1} at all temperatures, e.g., -5.3 joules deg.$^{-1}$ mole^{-1} at 25° on the molality scale compared with -3.5 on the mole fraction scale.

This discussion of scales of reference is pertinent to the work of Noonan and La Mer who employed neither the mole fraction scale nor the molality scale in its conventional sense. It can be shown that the free energy change on their scale is indeed the free energy change on the mole fraction scale, and this is true for the associated thermodynamic quantities. Our values (at 25°) of $\Delta G° = 418$ joules mole^{-1}, $\Delta H° = -611$ joules mole^{-1}, and $\Delta S° = -3.5$ joules deg.$^{-1}$ mole^{-1} compare with their values of $\Delta G° = 431$ joules mole^{-1}, $\Delta H° = -502$ joules mole^{-1}, and $\Delta S° = -3.1$ joules deg.$^{-1}$ mole^{-1}.

The activity coefficient of DCl in D_2O is given in Table IV, where the values at 25° are compared with the corresponding values for HCl in H_2O. The value of $\bar{L}_2$, the relative partial molal enthalpy of DCl in D_2O, is given in the last column of the table.

There is a difference of 0.002 to 0.003 in log $\gamma_\pm$, and it is of interest to note that this difference is less dependent on the dielectric constants of ordinary and heavy water than on the difference in the densities

(13) R. A. Robinson and R. H. Stokes, "Electrolyte Solutions," 2nd Ed., Butterworths, London, 1959, pp. 31 and 352.

of the two solvents. Thus the A constant of the Debye–Hückel equation is 0.5115 mole$^{-1/2}$ l.$^{1/2}$ for ordinary water at 25° and 0.5151 for heavy water, whereas $Ad_0^{1/2}$ is 0.5108 for ordina-y water and 0.5413 for heavy water. The value of $\bar{L}_2$ for DCl in D$_2$O is about 30% higher than for HCl in H$_2$O.[9,12]

The Kinetics of Reduction of Neptunium(VI) by

Vanadium(III) in Perchloric Acid[1]

by J. C. Sheppard

Hanford Laboratories, General Electric Company, Richland, Washington (*Received September 13, 1963*)

The rate law for the reduction of neptunium(VI) by vanadium(III) in perchloric acid obeys the expression, rate = $[\text{Np(VI)}][\text{V(III)}]\{k + k'/[\text{H}^+]\}$. At 25° and at an ionic strength of 2.0, the values for k and k' are 6.3 ± 1.2 M^{-1} sec.$^{-1}$ and 20.3 ± 0.5 sec.$^{-1}$, respectively. The corresponding energies and entropies of activation are 18.6 ± 1 kcal./mole and 5 e.u. for the hydrogen ion concentration independent path and 22 ± 4 kcal./mole and 19 e.u. for the hydrogen ion concentration dependent path.

The study of the kinetics of reduction of neptunium-(VI) by vanadium(III) in perchloric acid provides an opportunity to compare results obtained for other reactions involving the reduction of neptunium(VI).[2,3] Since neptunium(VI) is isostructural with plutonium-(VI), it is also of interest to compare the rates and kinetics of reduction of these ions with a common reducing agent, vanadium(III).

Preparation of Reagents. All reagents used in this investigation, unless specified otherwise, were reagent grade. Sodium perchlorate solutions were prepared by addition of an equivalent amount of perchloric acid to a sodium carbonate slurry. Perchloric acid solutions of vanadium(III) and vanadium(IV) were prepared in the following ways. Vanadium pentoxide, formed by the ignition of ammonium metavanadate, was suspended in 1 M perchloric acid and electrolyzed until vanadium(III) was formed.[4] A second preparation involved the dissolution of ammonium metavanadate in hot, dilute sodium hydroxide. The centrifuged solution was acidified with perchloric acid to precipitate the hydrated vanadium pentoxide.

The oxide was washed several times with dilute perchloric acid and then suspended in 1 M perchloric acid where it was electrolyzed to form vanadium(III).[5] Neptunium(VI) stock solutions were prepared by ozone or electrolytic oxidation of neptunium(V) in 1 M perchloric acid. The results of the kinetic experiments were not dependent on the mode of preparation of the reactants.

Analytical. The concentrations of vanadium(III) and vanadium(IV) in perchloric acid solutions were determined spectrophotometrically using a Cary Model 14 spectrophotometer and the molar extinction coefficients found by Appelman and Sullivan.[5] Total neptunium concentrations were determined by α-

(1) Work performed under contract AT-(45-1)-1350 between the General Electric Co. and the U. S. Atomic Energy Commission.

(2) (a) J. C. Sullivan, A. J. Zielen, and J. C. Hindman, *J. Am. Chem. Soc.*, **82**, 5288 (1960); (b) A. J. Zielen, J. C. Sullivan, and J. C. Hindman, *ibid.*, **80**, 5632 (1958).

(3) D. Cohen, J. C. Sullivan, and J. C. Hindman, *ibid.*, **76**, 352 (1954).

(4) S. W. Rabideau, *J. Phys. Chem.*, **62**, 414 (1958).

(5) E. H. Appelman and J. C. Sullivan, *ibid.*, **66**, 442 (1962).

assay as well as by coulometric analysis.[6] The composition of the neptunium(VI) stock solutions were established spectrophotometrically and were found to contain less than 1.5% neptunium(V). Radiochemical purity of the neptunium was determined by α-pulse analysis.

Apparatus. Reaction vessels for these experiments were 2.5-cm. silica absorption cells, each of which had a 10-cm. piece of plastic tubing connected to its neck. This allowed these cells to be immersed in the thermostated cell with a provision for the introduction of one of the reactants as well as providing for a needed air vent. The flow of water through copper coils which were inserted in the cell compartment maintained the temperature at $\pm 0.2°$ of that desired.

By the use of a syringe, the reaction was initiated by forcing one reactant solution from a storage vessel, through a Tygon tube, and into the absorption cell containing the second reactant where mixing took place. Experiments involving the neutralization of sodium hydroxide solutions indicated that the mixing time was less than 2 sec. Another experiment in which an equivalent amount of iron(II) in 1 M perchloric acid was injected into a neptunium(VI) solution showed that mixing and the reaction were complete in less than 2 sec. The reactant concentrations were $5 \times 10^{-4} M$ after mixing. Assuming that the iron(II)-neptunium(VI) reaction obeys second-order kinetics and has a half-time of less than 1 sec. at 25°, the specific rate constant is calculated to be greater than $2 \times 10^3 M^{-1}$ sec.$^{-1}$. Additional checks of this experimental setup involved the determination of the rates of the H_2O_2-U(IV)[7] and Np(VI)-U(IV) reactions. Within an experimental error of about 3%, the rate constants found for these reactions agreed with those reported.[1,7]

The progress of the reaction was followed by continuously monitoring the growth of the 980 mμ neptunium(V) peak with a Cary Model 14 spectrophotometer. To ensure that the vanadium(III) was not air oxidized during the course of the reaction, all solutions, previously purged of oxygen, were purged again by bubbling nitrogen through them for 5 to 10 min. just prior to their use.

Results

From the addition of an excess of neptunium(VI) solution to a vanadium(III) solution it was found that 1.96 ± 0.04 equivalents of neptunium(VI) were consumed for each equivalent of vanadium(III); consequently the net reaction is

$$V(III) + 2Np(VI) = V(V) + 2Np(V)$$
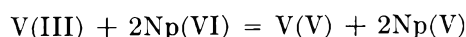
In addition, the rate data did not fit the reaction sequence

$$V(III) + Np(VI) \xrightarrow{k_1}$$
$$V(IV) + Np(V) \text{ (slow and rate determining)}$$
$$V(IV) + Np(VI) \xrightarrow{k_2} V(V) + Np(V) \text{ (rapid)}$$
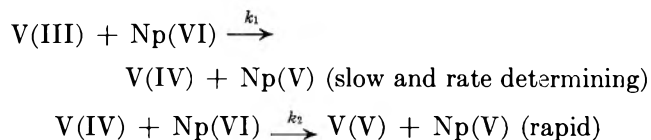
However, the data are consistent with the idea that two competitive, consecutive second-order reactions take place and that the specific rate constants, k_1 and k_2, have comparable values. Second-order plots of the data showed pronounced deviations in the later stages due to the competing vanadium(IV)-neptunium(VI) reaction. In 2.0 M perchloric acid and at 25°, the average rate constant for the vanadium(III)-neptunium(VI) reaction was found to be $17.5 \pm 1.6 \ M^{-1}$ sec.$^{-1}$ while the specific rate constant for the vanadium(IV)-neptunium(VI) reaction was estimated to be $30 \pm 15 \ M^{-1}$ sec.$^{-1}$. By direct determination of the rate of the vanadium(IV)-neptunium(VI) reaction under these conditions, it was found to obey second-order kinetics and have a specific rate constant of $13.3 \ M^{-1}$ sec.$^{-1}$. Further investigation of this reaction will be the object of future work. In view of the difficulties associated with the analysis of competitive, consecutive second-order reactions, only those points representing the initial 20-30% of the reaction were used to determine the rate constant for the vanadium(III)-neptunium(VI) reaction. This was done in an effort to eliminate or hopefully to minimize, as much as possible, the interference of the vanadium(IV)-neptunium(VI) reaction. Therefore, the data reported here should be regarded with some reserve, since the influence of the vanadium (IV)-neptunium(VI) reaction cannot be completely eliminated by this approach.

The rate data for these experiments are tabulated in Table I and as shown by Fig. 1 give a good fit when the observed specific rate constant $'k'$ is plotted against the reciprocal of the hydrogen ion concentration. Hence, over the range of hydrogen ion concentration studied these data are consistent with expression

$$'k' = k + k'/[H^+]$$

where k is the specific rate constant for the reaction between the unhydrolyzed reactants and k' is the specific rate constant for a path involving hydrolyzed species of either reactant. Possible reaction paths consistent with this equation are

$$V^{+3} + NpO_2^{+2} \xrightarrow{k}$$

(6) R. W. Stromatt, U. S. Atomic Energy Comm. Rept. HW-59447 (1959).

(7) F. B. Baker and T. W. Newton, *J. Phys. Chem.*, **65**, 1897 (1961)

and

$$VOH^{+2} + NpO_2^{+2} \xrightarrow{k''} products$$

or

$$V^{+3} + NpO_2OH^+ \xrightarrow{k'''}$$
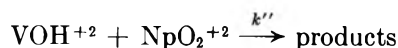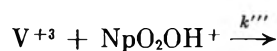
or combination of the last two reactions to give k'. On the basis of the extent of hydrolysis of the reactants alone, the VOH^{+2}–NpO_2^{+2} path would be expected to predominate. Table II includes the least-squares values for k and k' for the three temperatures at which the reaction was studied. The errors reported are in terms of standard deviations.

The activation energies for the hydrogen ion independent and dependent paths were calculated to be 18.6 ± 1 kcal./mole and 22 ± 4 kcal./mole, respectively. These values are close to activation energies found for other reactions involving the oxidation of vanadium(III).[4,5,8] The corresponding entropies of activation are 5 and 19 e.u., respectively.

Figure 1. Plot of the observed rate constant against the reciprocal of the hydrogen ion concentration.

Table I: Rate Data for the Neptunium(VI)–Vanadium(III) Reaction at an Ionic Strength of 2.0[a]

Temp., °C.	[H⁺], M	[V(III)] × 10^4, M	[Np(VI)] × 10^4, M	$'k'$, M^{-1} sec.$^{-1}$
25	2.00	12.0	12.0	18.3 ± 1.8[b]
	2.00	9.35	10.0	20.3 ± 2.0
	2.00	9.35	4.50	15.0 ± 1.6
	2.00	9.35	13.0	17.1 ± 0.8
	2.00	4.68	4.86	16.0 ± 0.8
	2.00	5.30	9.95	19.2 ± 0.8
	1.00	4.68	4.86	24.5 ± 1.1
	0.67	4.65	5.40	35.7 ± 3.5
	0.50	4.65	5.32	46.4 ± 2.8
	0.40	4.65	5.40	50.5 ± 3.2
	0.29	4.65	5.50	75.6 ± 7.6
	0.20	5.38	5.43	113 ± 11
17	2.00	4.65	5.15	9.0 ± 0.5
	1.00	4.65	5.48	12.5 ± 0.7
	0.60	6.51	5.43	24.0 ± 1.7
	0.40	6.51	5.43	35.3 ± 2.0
	0.30	6.51	5.43	41.3 ± 2.0
	0.25	5.38	5.44	52.3 ± 3.5
	0.20	6.51	5.48	62.0 ± 6.0
34	2.00	5.38	5.08	41.5 ± 2.0
	1.40	5.38	4.98	61.7 ± 5.7
	1.00	5.38	4.98	80.5 ± 8.0
	0.70	5.38	5.37	110 ± 15
	0.60	5.38	5.26	127 ± 17
	0.40	5.38	5.38	177 ± 25

[a] The ionic strength was adjusted with sodium perchlorate.
[b] These estimated errors undoubtedly reflect the contribution of the competing vanadium(IV)–neptunium(VI) reaction.

Table II: Summary of Rate Data for the V(III)–Np(VI) Reaction in Perchloric Acid[a]

Temp., °C.	k, M^{-1} sec.$^{-1}$	k', sec.$^{-1}$
17.0	2.4 ± 1.4	12.2 ± 0.5
25.0	6.3 ± 1.2	20.3 ± 0.5
34.0	12.4 ± 2.8	67.1 ± 3.1

[a] μ = 2.0, adjusted with sodium perchlorate.

It is of interest to compare the rate expressions for the neptunium(VI)–vanadium(III) and plutonium-(VI)–vanadium(III)[4] reactions, since plutonium(VI) and neptunium(VI) are isostructural and have a common reducing agent, vanadium(III). It seems likely that both reactions would obey the same rate law but have different specific rate constants. The rate laws for these reactions are

$$\text{rate} = [Pu(VI)][V(III)]\left(\frac{k'}{[H^+]} + \frac{k''}{[H^+]^2}\right)$$

and

$$\text{rate} = [Np(VI)][V(III)]\left(k + \frac{k'}{[H^+]}\right)$$

(8) W. C. E. Higginson and A. G. Sykes, J. Chem. Soc., 2841 (1962)

The rate laws for these reactions differ in that the path involving the unhydrolyzed reactants appears to be negligible in the case of the plutonium(VI)–vanadium(III) reaction.[4] But upon closer examination it was found that the data for the plutonium(VI)–vanadium(III) reaction could also be better fitted by the equation

$$\text{rate} = [\text{Pu(VI)}][\text{V(III)}]\left(k + \frac{k'}{[\text{H}^+]} + \frac{k''}{[\text{H}^+]^2}\right)$$

where the values for k, k', and k'' at 25° are 0.20 M^{-1} sec.$^{-1}$, 1.8 sec.$^{-1}$, and 0.19 M sec.$^{-1}$, respectively.

Accepting these specific rate constants for the plutonium(VI)–vanadium(III) reaction, the rate laws are the same except the missing third term for the neptunium(VI)–vanadium(III) reaction and it may be accounted for by the fact that this reaction was studied over a smaller hydrogen ion concentration range. Regardless of the rate law assumed for the plutonium(VI)–vanadium(III) reaction, the path involving the hydrolyzed species, the $1/[\text{H}^+]$ path, predominates as does the comparable path of the neptunium(VI)–vanadium(III) reaction.

It is not possible to make a detailed comparison of the entropies and energies of activation between the vanadium(III)–neptunium(VI) and vanadium(III)–plutonium(VI) reactions, since these activation parameters are not known for each path of the latter reaction.[4] Furthermore, the activation parameters for the former reaction, which have relatively large errors, indicate possible nonlinearity with respect to the Arrhenius plot. This may be due to a salt effect on the reaction and/or that the perturbing influence of the vanadium(IV)–neptunium(VI) reaction cannot be excluded. Comparison of the hydrogen ion concentration dependent paths of these reactions shows large differences in their activation parameters. Activation energies for these paths are 16 and 22 kcal./mole for the reaction of vanadium(III) with plutonium(VI)[4] and neptunium(VI), respectively, and the corresponding entropies of activation are -10 and 19 e.u. For very similar reactions these differences are larger than expected and are probably due to complications noted above.

Electrical Conductance and Density in Molten Molybdenum(VI)

Oxide–Alkali (Lithium, Potassium) Molybdate Systems[1]

by Kelso B. Morris and Press L. Robinson

Department of Chemistry, Howard University, Washington, D. C.   20001   (*Received May 28, 1963*)

Electrical conductance and density have been determined as functions of temperature for the two fused binary molybdate systems, K_2MoO_4–MoO_3 and Li_2MoO_4–MoO_3. Data for the two properties in both systems cover temperatures which range up to at least 100° above the melting point for each composition. For the single components, the ranges for specific conductances, in ohms cm.$^{-1}$, are 1.211 at 931.0° to 1.302 at 997.8° for K_2MoO_4; 4.017 at 790.6° to 6.761 at 939.0° for Li_2MoO_4; and 0.685 at 823.8° to 0.719 at 820.9° for MoO_3. Ranges for the densities, in g. cm.$^{-3}$, are 2.479 at 935.0° to 2.450 at 988.3° for K_2MoO_4; 2.888 at 781.2° to 2.802 at 963.4° for Li_2MoO_4; and 3.206 at 828.2° to 3.083 at 918.0° for MoO_3. When conductances for the first system, K_2MoO_4–MoO_3, are compared at corresponding temperatures that represent a fixed number of degrees above the melting points, resemblance is observed between the conductance–composition diagram and the phase diagram for this system. In plots of either specific conductances or equivalent conductances, at corresponding temperatures, *vs.* composition, two conductance minima and a single conductance maximum correspond, respectively, to the eutectic compositions and compound composition in the phase diagram for this system. A conductance–composition plot for the second system, Li_2MoO_4–MoO_3, in terms of the more familiar polytherms is also similar to the phase diagram for this system. Although the phase diagram for this system shows peritectic reaction and no compound formation, the composition for the single minimum or true eutectic in the system is the same as that for the conductance maxima in the polytherms. The two kinds of isotherms together with references to the observations of others suggest strongly that correlations may exist between conductance–composition diagrams and the phase diagrams for many molten binary systems. An explanation for the variation of conductance with composition in both systems is based on the nature and relative contributions of the constituent ionic species suggested by the phase diagram. Average activation energies, based on specific conductances, for the single substances and Na_2MoO_4 at corresponding temperatures that are 100° above the melting points decrease in the order $Li_2MoO_4 > Na_2MoO_4 > K_2MoO_4 > MoO_3$ or $MoO_2^{+2} \cdot MoO_4^{-2}$.

Introduction

In an earlier paper,[2] electrical conductance and density data were reported for the molten system, molybdenum(VI) oxide–sodium molybdate. The present report is concerned with measurements of the same properties, with superior scientific equipment and vastly improved experimental procedures, for two additional molten systems consisting of molybdenum-(VI) oxide and the molybdates of lithium and potas- sium. Density data and conductance data appear not to have been obtained previously for these two systems.

(2) K. B. Morris, M. I. Cook, C. Z. Sykes, and M. B. Templeman, *J. Am. Chem. Soc.*, **77**, 851 (1955).

However, Jaeger[3] has reported density data for pure K_2MoO_4.

Experimental

Chemicals. All molybdenum-containing chemicals were obtained on special order from the S. W. Shattuck Co., Denver, Colo., as reagent-quality anhydrous powders. A wet method of chemical analysis based on total molybdenum revealed these purities: MoO_3, 99.5%; Li_2MoO_4, 99.7%; and K_2MoO_4, 99.7%. Melting points, as determined by the method of thermal analysis for these substances, were in agreement with literature values. General qualitative spectrographic analysis of two chemicals at the National Bureau of Standards revealed impurities to be less than 0.01% for MoO_3 (Lab. No. 5.02–34726) and less than 0.1% for K_2MoO_4 (Lab. No. 5.02–34727).

Electrical Conductance. The experimental details employed were essentially the same as described in a recent report[4] on electrical conductance in another fused molybdate system. For the resistance measurements, the assembly consisted of a Leeds and Northrup Co. precision Jones conductivity bridge (Catalog No. 4666), a Hewlett-Packard Co. oscillator (20 c.p.s. to 20 k.c., Model 201-C), and a General Radio Co. tuned amplifier and null detector (Type 1232-A). All leads were shielded. The dip-type conductance cell of clear fused quartz was identical in basic design with that described by Van Artsdalen.[5] Calibration of each cell was carried out by using the technique suggested by others.[5] Platinum disk electrodes, each having a 3-mm. length of platinum–rhodium alloy wire (B. & S. gage 24), welded to the underside of the disk, rested on the shelf at the top of the capillary tubing in each arm of the quartz cell. The electrode leads, also of platinum–rhodium alloy wire (B. & S. gage 24), were covered with several refractory mullite insulators up to the point where they were joined to short copper leads just outside the furnace chamber. These insulators, each about 5 cm. in length, served to keep the electrodes seated firmly and to minimize the mutual inductance that otherwise might be caused by the close proximity to each other of the electrode leads. The calibrated conductance cells, with cell constants of the order 149–267 cm.$^{-1}$, were discarded after being used in no more than two runs because cumulative attack of the quartz by the molybdate melts was then significant. All resistance measurements were made at a frequency of 2000 cycles. In making a measurement, the power supply to the furnace was shut off temporarily in order to prevent the 60-c.p.s. current to the furnace from interfering with bridge balance. The furnace insulation was sufficient

to maintain constant temperature during this short interval.

Density. Measurements of density and the calibration technique for the specially designed density bob, machined from a single solid platinum cylinder and with a weight of the order 27.0000 g., were essentially the same as described by Janz.[6] The diameter of the platinum–rhodium alloy wire by means of which the bob was suspended from one arm of a Christian Becker chainomatic balance was 0.020 in. except at the point where the wire contacted the melt surface. For this point, a short length of platinum–rhodium alloy wire (of 0.01-in. diameter) was used between the large wire and the stem of the density bob. Therefore, surface tension corrections were negligible.

Temperature. A Marshall tubular testing furnace (6.35-cm. i.d., 30.84-cm. o.d., 40.70 cm. long), wound with platinum–rhodium alloy wire, was used for the heating and melting of all samples. The furnace temperature was controlled to 0.5° by means of a millivoltmeter pyrometer controller operating in conjunction with a Pt–Pt 13% Rh thermocouple located directly beneath the heating element and running the full length of the furnace chamber. A platinum–20% rhodium alloy crucible of 70-ml. capacity was used as container for all samples. Preliminary drying to constant weight as well as the melting, heating, and cooling of all samples were carried out in an atmosphere of pure argon gas. Temperatures of the melts were measured with an NBS-calibrated Pt–Pt 10% Rh thermocouple by means of a Leeds and Northrup Co. Type K-3 potentiometer (Catalog No. 7553-5) while the lower end of the thin-walled thermocouple protection tube was approximately 1 mm. (as determined by a B & S super vernier caliper, accurate to 0.001 in., in positioning the crucible and sample with a Cenco-Lerner Lab-Jack) above the surface of the melt.

One important aspect of the research was the development of a satisfactory procedure for determining the composition of the melts. Since the vapor pressure of pure molybdenum(VI) oxide is significantly high in the vicinity of its melting point, the vapor pressures of mixtures of this component and alkali molybdates are appreciable. A qualitative indication of the magnitude of this partial vapor pressure of the MoO_3 is obtained by observing the extent to which there is

(3) F. M. Jaeger, *Z. anorg. allgem. chem.*, **101**, 16 (1917); "International Critical Tables," Vol. 3, McGraw-Hill Book Co., New York, N. Y., 1928, p. 24.

(4) K. B. Morris, N. McNair, and G. Koops, *J. Chem. Eng. Data*, **7**, 224 (1962).

(5) E. R. Van Artsdalen and I. S. Yaffe, *J. Phys. Chem.*, **59**, 118 (1955).

(6) G. J. Janz and M. R. Lorenz, *Rev. Sci. Instr.*, **31**, 18 (1960).

smoking of the melts. The vapor pressures of the pure, molten alkali molybdates are negligible for the temperature ranges employed. Therefore, the composition of each sample changes slightly during the heating and cooling process because of the loss by volatilization of small amounts of MoO_3. Moreover, these changes in composition were found to depend principally upon the percentage of MoO_3 in each mixture, the temperature, and the duration of the heating and cooling period.

Now, if chemical analyses of mixtures such as these are to be meaningful, they must be made of melt portions taken at the precise times the properties, electrical conductance and density are measured. However, a sampling process of this kind followed by rapid quenching was not feasible for the experimental conditions employed. A decision was made to subject the

cooled mixtures to chemical analysis for total molybdenum (conversion of MoO_3 to molybdate ion, precipitation of molybdate with α-benzoin oxime, and subsequent ignition of the precipitate under appropriate conditions to the oxide which is then weighed). This well-known analytical procedure was found to be satisfactory for unheated samples and for cooled melts of the same initial composition. Subsequent investigation revealed that essentially the same information on final compositions of the mixtures could be obtained much more conveniently by carrying out a series of weight-loss-on-heating experiments. In using this technique, weighed samples of a given mixture were heated under the same conditions that prevailed when the properties were actually being measured. At certain time intervals, crucibles containing the melts were withdrawn

Table I: Specific Conductances for the System K_2MoO_4–MoO_3

Compn., mole % MoO₃	t, °C	κ, mhos cm.⁻¹	Compn., mole % MoO₃	t, °C	κ, mhos cm.⁻¹	Compn., mole % MoO₃	t, °C	κ, mhos cm.⁻¹
0.00	931.0	1.211	14.13	975.4	1.161	52.44	593.6	0.345
	938.7	1.233		985.7	1.170		598.5	0.354
	949.0	1.243		988.4	1.194		604.0	0.368
	955.8	1.256		994.7	1.215		609.7	0.377
	964.7	1.271					616.1	0.391
	972.6	1.280	30.13	882.2	0.882		625.0	0.407
	983.0	1.290		830.8	0.895		639.8	0.427
	990.6	1.299		838.0	0.908		649.8	0.443
	997.8	1.302		845.8	0.920		657.6	0.455
				853.7	0.933		667.1	0.465
14.13	876.8	0.992		862.7	0.945		674.5	0.473
	883.0	1.014		871.4	0.958		679.1	0.480
	897.2	1.020		877.2	0.968		682.8	0.486
	902.4	1.028		891.0	0.989		688.7	0.493
	910.0	1.041		900.0	1.002		697.8	0.502
	917.8	1.056		914.0	1.023		704.6	0.504
	926.8	1.071		928.6	1.037			
	931.3	1.083		933.8	1.044	60.20	642.0	0.434
	949.5	1.115					649.6	0.450
	964.7	1.144	52.44	583.3	0.325		656.6	0.463
				587.7	0.334			
60.20	664.0	0.473	68.64	689.0	0.540	77.35	765.3	0.653
	673.2	0.488		699.5	0.560		775.0	0.677
	682.1	0.503		705.6	0.576		786.3	0.699
	689.1	0.512		718.1	0.595		798.0	0.719
	701.0	0.532		727.5	0.616		809.1	0.733
	707.2	0.546		738.0	0.635		818.3	0.747
	719.3	0.565		754.0	0.660		826.8	0.760
	729.0	0.580		767.8	0.677		836.8	0.771
	739.5	0.597		771.4	0.687		845.8	0.778
	752.0	0.619		776.5	0.696			
	764.3	0.639		782.8	0.708			
	771.7	0.647						
	781.0	0.660						
	786.0	0.668						
	794.6	0.672						

Table I (*Continued*)

Compn., mole % MoO₃	t, °C.	κ, mhos cm.⁻¹	Compn., mole % MoO₃	t, °C.	κ, mhos cm.⁻¹	Compn., mole % MoO₃	t, °C.	κ, mhos cm.⁻¹
68.64	654.4	0.473	77.35	651.5	0.438	81.35	614.4	0.355
	662.0	0.486		662.5	0.462		619.0	0.367
	669.7	0.499		675.8	0.489		628.0	0.382
	679.2	0.521		685.5	0.509		639.4	0.407
81.35	738.0	0.589		699.5	0.538		650.9	0.428
	749.8	0.611		716.3	0.570		660.6[a]	0.446
	755.6[a]	0.625		728.4	0.590		674.5[a]	0.476
	766.7[a]	0.643		741.0	0.611		688.6[a]	0.505
	774.2	0.661					701.0[a]	0.531
	783.1[a]	0.677	100.00	823.8	0.685		716.4[a]	0.558
	793.0	0.693		838.0[a]	0.695			
	803.9	0.706		844.4[a]	0.699			
				856.4	0.705			
88.63	760.2	0.613		862.5	0.710			
	771.6	0.630		871.8	0.713			
	789.0	0.656		884.0	0.716			
	799.2	0.675		890.9	0.719			
	810.2	0.689						
	818.6[a]	0.699						
	827.8	0.712						
	838.0	0.720						
	845.8	0.729						
	852.2	0.737						
	859.0	0.742						
	869.0	0.747						

[a] Points not plotted due to space limitations.

from the furnace, cooled to room temperature, and then weighed in order to determine the change in weight. The compositions in the data tables which follow are final compositions based upon the weight-loss-on-heating experiments.

Results and Discussion

The Systems, K_2MoO_4–MoO_3 and Li_2MoO_4–MoO_3. Specific conductances and densities for these systems at various temperatures are listed in Tables I, II, III, and IV. Conductance and density equations for the pure compounds and for mixtures are given in Table V.

An important problem in molten salt research with which investigators have been confronted is the selection of a suitable temperature at which properties of various melts can be compared. For some substances, either the boiling point or some temperature related to the critical temperature has been found useful as a "corresponding temperature." It is possible that at some time in the future it may be found meaningful to compare physical properties of substances at a temperature that is the melting point plus some fraction of the liquid range for each pure substance under a

pressure of 1 atm. However, boiling point data for fused salts are either unreliable or not available. Researchers in the area of fused salts have used two general approaches in an effort to arrive at a satisfactory "corresponding temperature." Some investigators[7] have used conductance–composition plots for a given system at several arbitrarily chosen temperatures. These polytherms have been useful in an interpretation of the data. This is done in Fig. 2 of the present report on the molten system, Li_2MoO_4–MoO_3. Still others[8] have used conductance-composition plots at an arbitrarily defined "corresponding temperature." Van Artsdalen,[8] in his studies on molten salt systems, compared the properties of melts at equal fractions, θ, of the melting point on the Kelvin scale, where $\theta = T°K./T_m°K.$ and $T° > T_m°$. Recently, Reiss and his collaborators[9] obtained the same relation on theoretical grounds in connection with

(7) G. W. Mellors and S. Senderoff, J. Phys. Chem., 64, 294 (1960); E. F. Riebling and C. E. Erickson, ibid., 67, 307 (1963).

(8) E. R. Van Artsdalen and I. S. Yaffe, ibid., 60, 1125 (1956); G. J. Janz and M. R. Lorenz, J. Electrochem. Soc., 108, 1052 (1961).

(9) M. Reiss, S. W. Mayer, and J. L. Katz, J. Chem. Phys., 35, 820 (1961).

Table II: Densities for the System K_2MoO_4–MoO_3

Compn., mole % MoO_3	t, °C.	ρ, g. cm.$^{-3}$	Compn., mole % MoO_3	t, °C.	ρ, g. cm.$^{-3}$	Compn., mole % MoO_3	t, °C.	ρ, g. cm.$^{-3}$
0.00	935.0	2.478	14.13	962.0	2.426	52.44	581.7	2.854
	938.0	2.477		968.7	2.422		592.0	2.841
	944.0	2.474		977.7	2.416		604.0	2.826
	950.6	2.470					623.4	2.804
	956.8	2.467	30.13	783.5	2.607		646.6	2.778
	962.1	2.464		797.7	2.594		668.5	2.760
	969.7	2.459		815.6	2.582		676.0	2.752
	976.5	2.456		825.0	2.574		690.0	2.738
	981.9	2.453		833.7	2.567		699.6	2.730
	985.6	2.451		841.7	2.561		709.6	2.721
	988.3	2.450		854.5	2.552		718.0	2.712
				866.4	2.543		729.0	2.701
14.13	822.5	2.477		876.0	2.535		739.5	2.691
	891.2	2.471		885.5	2.530		748.6	2.682
	906.0	2.461		896.8	2.522		758.1	2.672
	919.5	2.453		915.8	2.510		765.5	2.684
	931.3	2.445		924.7	2.505			
	941.4	2.438		932.5	2.500	60.20	632.4	2.987
	954.4	2.432					638.0	2.981
			52.44	574.4	2.865			
60.20	648.5	2.970	68.64	712.2	2.988	77.35	747.6	3.037
	665.5	2.953		721.0	2.978		755.6	3.027
	681.0	2.937		735.4	2.960		765.5	3.015
	689.3	2.925		747.6	2.947		781.4	2.993
	700.7	2.917		756.5	2.936		799.3	2.975
	708.6	2.907		764.2	2.926		817.1	2.954
	721.1	2.895		770.5	2.916		832.6	2.937
	732.0	2.884		779.0	2.906		852.0	2.918
	738.0	2.877		791.8	2.894		870.2	2.898
	748.0	2.867					888.6	2.881
	756.8	2.855	77.35	642.3	3.156			
	764.5	2.848		649.6	3.145	81.35	614.4	3.263
	778.5	2.833		657.7	3.136		624.5	3.250
				669.8	3.124		636.7	3.236
68.64	673.2	3.030		685.5	3.103		647.7	3.224
	654.4	3.045		701.3	3.087		657.3	3.215
	666.0	3.034		719.4	3.065		667.0	3.205
	677.6	3.020		728.5	3.057		676.4	3.193
	700.8	2.999		738.5	3.047		682.8	3.185
81.35	694.8	3.171	100.00	828.2	3.206			
	709.0	3.156		835.3	3.195			
	718.0	3.146		840.6	3.188			
	727.5	3.135		845.5	3.178			
	740.8	3.123		850.8	3.169			
	750.4	3.116		861.3	3.151			
				866.6	3.138			
88.63	761.6	3.137		876.8	3.128			
	766.5	3.129		880.0	3.115			
	777.7	3.115		892.6	3.102			
	788.4	3.103		907.2	3.082			
	802.4	3.090		918.0	3.083			
	807.6	3.081						
	816.0	3.072						
	823.9	3.061						
	836.8	3.039						
	853.4	3.031						
	869.0	3.019						
100.00	820.8	3.219						

Table III: Specific Conductances for the System Li_2MoO_4–MoO_3

Compn., mole % MoO_3	t, °C.	κ, mhos cm.⁻¹	Compn., mole % MoO_3	t, °C.	κ, mhos cm.⁻¹	Compn., mole % MoO_3	t, °C.	κ, mhos cm.⁻¹
0.00	790.6	4.017	14.16 (10.55)ᵃ	835.6	2.324	22.12 (17.21)ᵃ	850.8	2.079
	803.7	4.162		840.2	2.365		851.4	2.091
	813.2	4.265		871.6	2.491		855.0	2.099
	829.4	4.414		879.6	2.513		858.6	2.108
	852.0	4.714		884.2	2.528		861.4	2.122
	860.2	4.880		888.4	2.551		871.8	2.137
	871.6	5.058		900.0	2.584	34.77 (32.68)ᵃ	845.4	1.519
	885.7	5.589		907.8	2.600		859.0	1.549
	904.0	5.923					869.6	1.570
	916.8	6.160	22.12 (17.21)ᵃ	764.0	1.746		880.4	1.601
	928.5	6.447		770.0	1.791		891.2	1.634
	939.0	6.761		776.0	1.827		906.1	1.667
14.16 (10.55)ᵃ	809.4	2.192		783.4	1.871		913.2	1.687
	813.4	2.209		791.8	1.896		919.4	1.702
	818.6	2.243		799.0	1.936		935.1	1.726
	824.0	2.266		812.0	1.979		941.3	1.738
	828.0	2.282		824.4	2.016		949.2	1.757
	830.8	2.297		835.4	2.045		956.0	1.777
				843.2	2.063			
47.49 (44.08)ᵃ	799.3	1.526	58.82 (54.18)ᵃ	804.0	1.340	72.44 (70.08)ᵃ	845.7	1.162
	817.0	1.573		815.6	1.361		852.4	1.179
	829.4	1.605		823.8	1.367		860.7	1.200
	839.3	1.638		829.5	1.417		867.8	1.224
	852.0	1.683		842.0	1.453		874.5	1.239
	859.0	1.711		853.8	1.487		892.5	1.262
	876.0	1.757		867.8	1.529		907.3	1.270
	890.0	1.796		881.7	1.560			
	910.6	1.835		898.6	1.588	83.97 (83.25)ᵃ	778.2	0.781
	931.0	1.885		905.0	1.601		782.6	0.794
	939.0	1.897		917.0	1.621		787.0	0.808
	943.0	1.911					791.5	0.821
	944.4	1.918	72.44 (70.08)ᵃ	800.0	1.055		801.0	0.838
				809.5	1.076		809.5	0.858
58.82 (54.18)ᵃ	768.0	1.222		821.0	1.101		818.5	0.926
	775.5	1.250		824.9	1.113		826.5	0.946
	781.3	1.274		832.7	1.129		835.8	0.957
	792.0	1.308		839.4	1.143		853.5	0.975
83.97 (83.25)ᵃ	869.0	1.007						
	885.7	1.031						
	894.1	1.043						
	903.6	1.053						
	917.0	1.064						
100.00	823.8	0.685						
	838.0	0.695						
	844.4	0.699						
	856.4	0.705						
	862.5	0.710						
	871.8	0.713						
	884.0	0.716						
	890.9	0.719						

ᵃ Corrected values based on weight-loss-on-heating.

Table IV: Densities for the System Li_2MoO_4-MoO_3

Compn., mole % MoO3	t, °C.	ρ, g. cm.^-3
0.00	781.2	2.888
	796.3	2.879
	809.5	2.872
	826.6	2.864
	851.0	2.850
	878.6	2.838
	894.0	2.834
	909.6	2.824
	923.5	2.816
	948.0	2.805
	963.4	2.802
14.16 (10.55)[a]	825.4	2.913
	852.2	2.899
	864.0	2.893
	874.6	2.886
	881.2	2.883
	891.4	2.880
47.49 (44.08)[a]	843.4	3.021
	853.9	3.014
	862.8	3.008
	866.4	3.003
	880.0	2.998
	902.2	2.982
	932.5	2.962
	949.5	2.951
	962.1	2.945
58.82 (54.18)[a]	760.0	3.152
	769.3	3.140
	785.5	3.131
	799.8	3.119
	810.5	3.109
	821.1	3.102
	832.5	3.093
	840.7	3.086
83.97 (83.25)[a]	912.0	3.128
	920.5	3.121
100.00	820.8	3.219
	825.2	3.206
	835.3	3.195
	840.6	3.188
	845.5	3.178
	850.8	3.169
	861.3	3.151
	866.6	3.138
	876.8	3.128
	880.0	3.115
	892.6	3.102
	907.2	3.082
	918.0	3.083

Compn., mole % MoO3	t, °C.	ρ, g. cm.^-3
14.16 (10.55)[a]	892.4	2.877
	898.8	2.875
	902.6	2.871
	907.6	2.869
	923.6	2.861
22.12 (17.21)[a]	781.8	2.993
	793.6	2.986
	810.4	2.975
	827.0	2.965
	843.6	2.955
	868.8	2.940
	877.8	2.934
	885.6	2.931
	893.8	2.925
	903.6	2.922
	905.4	2.920
58.82 (54.18)[a]	849.6	3.079
	858.6	3.070
	871.7	3.061
	888.4	3.047
	902.2	3.039
	914.5	3.031
	927.0	3.022
	933.7	3.017
72.44 (70.08)[a]	755.6	3.253
	771.6	3.237
	787.2	3.219
	810.5	3.200
	826.6	3.188
	838.0	3.181
	845.5	3.172
	858.8	3.162
	867.6	3.155

Compn., mole % MoO3	t, °C.	ρ, g. cm.^-3
34.77 (32.68)[a]	799.2	3.014
	816.0	3.003
	835.7	2.990
	845.6	2.986
	858.4	2.976
	865.2	2.972
	882.7	2.962
	891.2	2.956
	900.0	2.951
	906.2	2.947
	913.0	2.944
	918.2	2.939
	933.6	2.930
	941.8	2.925
	949.5	2.921
47.49 (44.08)[a]	802.6	3.005
	825.0	3.034
72.44 (70.08)[a]	874.5	3.149
	885.7	3.138
	896.8	3.128
	909.0	3.119
	923.5	3.108
83.97 (83.25)[a]	766.0	3.267
	780.5	3.252
	796.5	3.235
	809.2	3.225
	823.6	3.211
	836.8	3.197
	847.1	3.188
	858.8	3.176
	869.7	3.166
	878.5	3.156
	887.3	3.150
	898.2	3.139

[a] Corrected values based on weight-loss-on-heating.

Table Va: Specific Conductance Equations for MoO_3, K_2MoO_4, Li_2MoO_4, and Mixtures

Compn., mole %	Specific conductance $k = a + bt + ct^2$, mho cm.$^{-1}$			Std. dev., mho cm.$^{-1}$	Temp. range, °C.
	a	$b \times 10^2$	$c \times 10^6$		
100MoO₃	−5.7537	1.4563	−8.1949	0.002	82⅗–891
100K₂MoO₄	−21.0210	4.4823	−22.5066	0.005	931–998
100Li₂MoO₄	43.2596	−10.71	72.668	0.071	790–939

Mole % MoO₃					
		K_2MoO_4–MoO_3 system			
14.13	4.2506	−0.8537	5.5075	0.007	877–995
30.13	6.0644	−1.2999	8.1731	0.027	882–934
52.44	−2.7280	0.8329	−5.3073	0.002	583–705
60.20	−1.2083	0.3333	−1.2061	0.003	642–794
68.64	−1.9820	0.5345	−2.4426	0.003	654–783
77.35	−1.8458	0.4825	−2.0276	0.004	651–846
81.35	−1.3120	0.3365	−1.0589	0.003	614–804
88.63	−3.6606	0.9428	−5.0101	0.002	760–869
		Li_2MoO_4–MoO_3 system			
14.16 (10.55)ᵃ	−13.2305	3.2259	−16.322	0.007	809–908
22.12 (17.21)ᵃ	−21.3359	5.3686	−30.734	0.015	764–872
34.77 (32.68)ᵃ	−2.7958	0.7539	−2.887	0.005	845–956
47.49 (44.08)ᵃ	−4.6127	1.1832	−5.2117	0.007	799–945
55.82 (54.18)ᵃ	−4.0311	1.0289	−4.4897	0.001	768–917
72.44 (70.08)ᵃ	−7.4905	1.8153	−9.3589	0.008	800–907
83.97 (83.25)ᵃ	−10.4708	2.4981	−13.536	0.013	778–917

ᵃ Corrected values based on weight-loss-on-heating.

their development of reduced equations of state for ionic melts. Obviously, this is also a kind of isotherm that has merit. In Fig. 1 of the present report, the conductance–composition plot for the K_2MoO_4–MoO_3 system is one in which the "corresponding temperature" is defined as 100° above the melting point for each composition. There are several reasons why this choice of a corresponding state appears to be satisfactory. In the first place, the melting point itself is an excellent point for purposes of comparison provided that one is able to obtain conveniently the value of the property (conductance or surface tension or some other property) at the melting point. In the second place, it was shown in a previous report[4] that the shape of the conductance–composition plot is the same no matter whether the comparison is made at the melting point or at 80° above the melting point. This agrees with the view of Bockris[10] that under normal conditions of study (200–300° range above the melting point),

the structure of the molten electrolyte may be compared to that of its corresponding solid. Finally, the shape of the property–composition diagram based on the corresponding temperature defined in the present report is the same as that obtained when the Van Artsdalen[8]–Reiss[9] concept is employed.

In Fig. 1, which is concerned with the potassium system, the plots of both equivalent conductance (curve II) and specific conductance (curve III) vs. composition resemble strongly the phase diagram (curve I) of Hoermann[11] for this system. A more recent report for this system by Spitsyn and Kuleshov[12] reveals four eutectics at 467, 481, 553, and 547° containing 45, 53, 73, and 78 mole % MoO_3, respectively.

(10) J. O'M. Bockris, "Modern Aspects of Electrochemistry," Vol. 2, Butterworths Publications, London, 1959, p. 162.

(11) F. Hoermann, Z. anorg. Chem., 177, 145 (1928).

(12) V. I. Spitsyn and I. M. Kuleshov, Chem. Abstr., 46, 9006h (1952); J. Gen. Chem. USSR, 21, 445 (1951).

Table Vb: Density Equations for MoO_3,
K_2MoO_4, Li_2MoO_4, and Mixtures

Compn., mole %	Density $\rho = a - bt$, g./cc. a	$b \times 10^3$	Std. dev., g./cc.	Temp. range, °C.
$100MoO_3$	4.4436	1.4983	0.0065	821–918
$100K_2MoO_4$	2.9922	0.5491	0.0003	935–988
$100Li_2MoO_4$	3.2008	0.4152	0.0149	781–963

Mole %
MoO_3

K_2MoO_4–MoO_3 system

14.13	3.0360	0.6340	0.0007	882–978
30.13	3.1637	0.7146	0.0017	783–933
52.44	3.4282	0.9951	0.0059	574–766
60.20	3.6534	1.0529	0.0011	632–779
68.64	3.7813	1.1189	0.0029	673–792
77.35	3.0986	0.1007	0.057	658–852
81.35	3.9371	1.0997	0.0017	614–750
88.63	3.9974	1.1337	0.0042	761–869

Li_2MoO_4–MoO_3 system

14.16 (10.55)[a]	3.3520	0.5317	0.0009	825–924
22.12 (17.21)[a]	3.4559	0.5930	0.0010	781–905
34.77 (32.68)[a]	2.9856	0.0317	0.0257	799–950
47.49 (44.08)[a]	3.5641	0.6448	0.0014	802–962
55.82 (54.18)[a]	3.7359	0.7723	0.0018	760–934
72.44 (70.08)[a]	3.8951	0.8451	0.0020	755–924
83.97 (83.25)[a]	3.9932	0.9502	0.0014	766–921

[a] Corrected values based on weight-loss-on-heating.

Maxima, corresponding to $K_2Mo_2O_7$, $K_2Mo_3O_{10}$, and $K_2Mo_4O_{13}$, are found at 487, 567, and 559°, respectively. Two inflection points corresponding to $K_2Mo_6O_{19}$ and $K_2Mo_8O_{25}$ have calculated melting points of 589 and 649°, respectively. The authors of the present report have preferred using the earlier phase diagram as an overlay in Fig. 1 for three reasons, namely: (1) greater simplicity for the comparisons to be made; (2) the essentially indentical nature of the $K_2Mo_3O_{10}$ maximum in both diagrams; and (3) the inability of the conductance data to reflect the presence of polymolybdates other than $K_2Mo_3O_{10}$. The ranges of stability for $K_2Mo_2O_7$ and $K_2Mo_2O_{13}$ of the Spitsyn–Kuleshov report[12] are extremely narrow.

Now, it is not to be inferred that similarity between a conductance–composition plot of the kind described and the phase diagram will be observed for all possible systems. In our work, this has been found to exist

for only two systems, namely, the $Bi_2(MoO_4)_3$–Pb-MoO_4 system of a previous report[4] and the K_2MoO_4–MoO_3 system of the present report.

In view of the discussion up to this point, the structures of the melts in this system can be envisioned as a quasicrystalline arrangement in which the defects (of the solid) such as holes, interstitial ions, and other dislocations have increased. Since the corresponding temperature selected for purposes of comparison is 100° above the melting point for each composition, the structural forces within the melts would appear to be of the same relative order of magnitude as those present in the solid produced on freezing. Accordingly, the variation of conductance (at the corresponding temperature defined) with composition for this system in Fig. 1 can be interpreted in the light of the substances which the phase diagram indicates are present. For compositions corresponding to A, C, and E in Fig. 1, the phase diagram (curve I) reveals that the solid phases are K_2MoO_4, $K_2Mo_3O_{10}$, and MoO_3, respectively. Now, since the conductances (curves II and III) of Fig. 1 are for a corresponding temperature that is only 100° above the melting point of each substance, electrical conductance in the melts may be attributed to the presence of the following ion species: K^+ and $KMoO_4^-$ from K_2MoO_4; K^+ and $KMo_3O_{10}^-$ from $K_2Mo_3O_{10}$; and MoO_2^{+2} and MoO_4^{-2} from MoO_3 as $(MoO_3)_2$. It is postulated that the order of decreasing ionic conductance for these current-carrying species is $K^+ > MoO_2^{+2} > MoO_4^{-2} > KMoO_4^- > KMo_3O_{10}^-$. This order appears to be consistent with the conductances observed for the parent compounds at the corresponding temperature defined.

A qualitative model that accounts for the variation of conductance (at the corresponding temperature defined) with composition for composition A is

$$2K_2MoO_4 \longrightarrow 2K^+ + 2KMoO_4^-$$

Interaction as the composition changes from A to B (equivalent to $2K_2MoO_4 \cdot 2MoO_3$) gives

$$2K_2MoO_4 + 2MoO_3 \longrightarrow K^+ + 3KMoO_4^- + MoO_2^{+2}$$
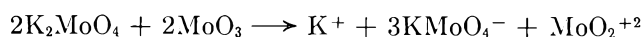
A decrease in conductance occurs because half of the potassium ions have been removed as $KMoO_4^-$ and replaced by the less mobile molybdenyl ions, MoO_2^{+2}. As the composition changes from B to C (the latter is equivalent to $2K_2MoO_4 \cdot 4MoO_3$ or $2K_2Mo_3O_{10}$), the interaction is

$$2K_2MoO_4 \cdot 2MoO_3 + 2MoO_3 \longrightarrow 2K^+ + 2KMo_3O_{10}^-$$
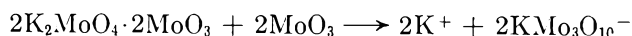
The conductance increases to a maximum at composition C. A change in composition from C to D (the latter is equivalent to $2K_2MoO_4 \cdot 8MoO_3$) results in
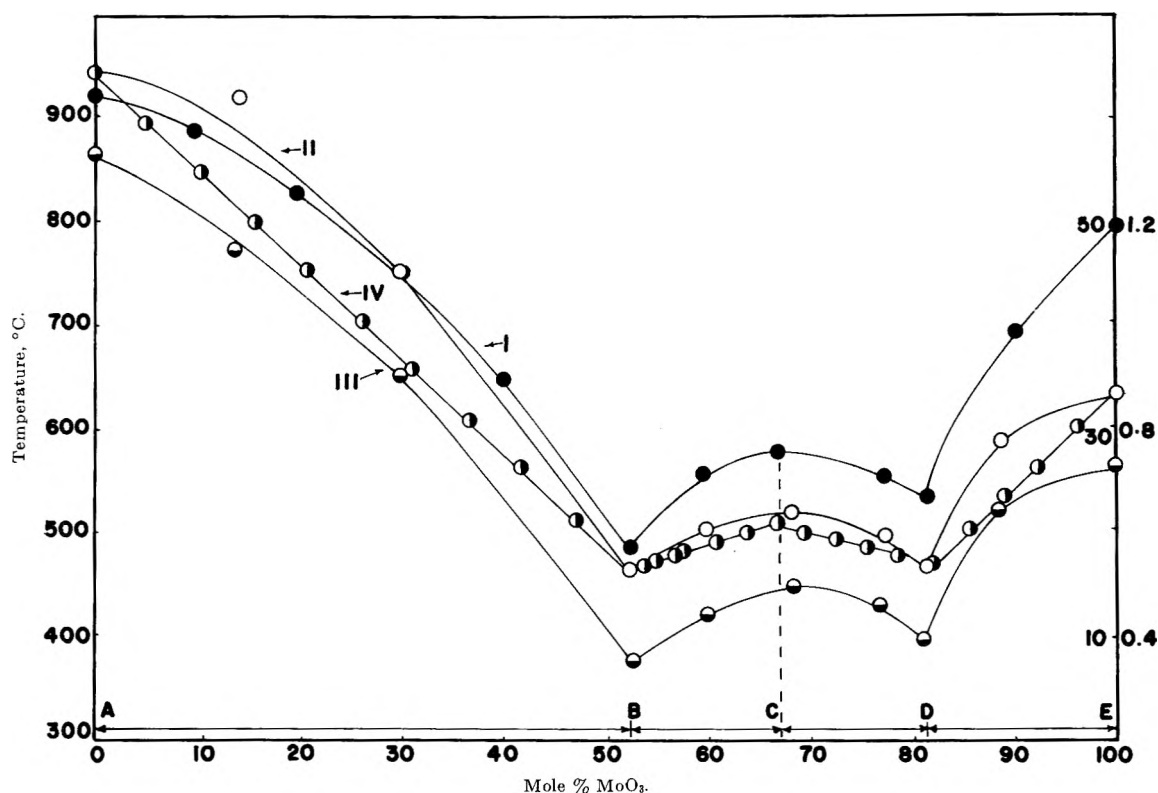
Figure 1. Specific conductance, equivalent conductance, and temperature as a function of composition in the molten system, K_2MoO_4–MoO_3. Equivalent weight of MoO_3 is taken as the molecular weight, equivalent to $(MoO_2^{+2} \cdot MoO_4^{-2})/2$. Curve numbers and symbols: I, ●, phase diagram; II, O, equivalent conductance vs. composition; III, ◒, specific conductance vs. composition; IV, ◐, additivity principle, $\Lambda = x_1\Lambda_1 + x_2\Lambda_2$. Equivalent and specific conductances in II and III are for mixtures at temperatures 100° above the melting point of each mixture.

a decrease in conductance because of the interaction

$$2K^+ + 2KMo_3O_{10}^- + 4MoO_3 \longrightarrow$$
$$4KMoO_4^- + 2MoO_4^{-2} + 4MoO_2^{+2}$$
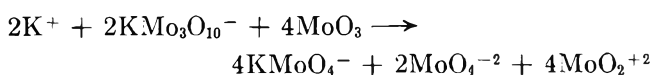
The increase in conductance as the composition changes from D to E is due to the gradual replacement of all ionic species by molybdenyl and molybdate ions of molybdenum(VI) oxide.

Curve IV in Fig. 1 is an application of the additivity principle, $\Lambda_{total} = x_1\Lambda_1 + x_2\Lambda_2$, where Λ_{total}, $x_{1 \text{ or } 2}$, and $\Lambda_{1 \text{ or } 2}$ represent total equivalent conductance, mole fraction of component 1 or 2, and conductance of pure component 1 or 2 at the corresponding temperature of the pure component, respectively. In using the additivity principle, the over-all abscissa, AE, which represents mole per cent MoO_3, is divided so that composition points A, B, C, D, and E refer to pure components in the calculations. For example, points B and C correspond to 52.2 MoO_3 and 66.7 MoO_3, respectively, on the over-all abscissa AE. On the division basis for the additivity calculations, the

eutectic composition corresponding to B is 100% B and the compound composition corresponding to C is 100% C. This does not mean that each eutectic composition is a single compound. Each eutectic, as customary, represents a fixed composition of two compounds with two distinct crystal lattices in the solid state. Since the cooling curve for a eutectic composition is like that for a pure compound, this is one justification for using a eutectic composition in the additivity principle as portrayed in curve IV. Although the additivity principle of conductivity in binary systems is generally applied isothermally to mixtures of compounds, it has been pointed out previously in this report that a conductance–composition plot based on the corresponding temperature defined in this report is itself a kind of isotherm. Polytherms of the more familiar type are not presented for the K_2-MoO_3–MoO_3 system because there is insufficient overlapping of the temperature ranges over which the data are valid. If curve IV is taken as a standard of reference, the positive deviations of equivalent conductance from additivity may be ascribed to increased mobility
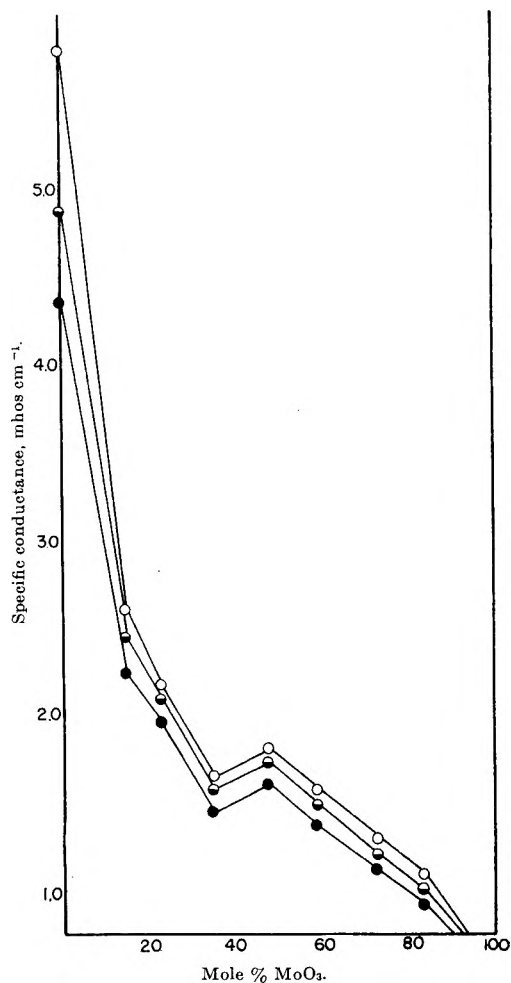
Figure 2. Specific conductance isotherms as a function
of melt composition in the system, Li_2MoO_4-MoO_3.
Temperatures, proceeding upward, are 820, 860, and 900°.

of the conducting species as a result of expansion of the quasicrystalline lattice.

In Fig. 2, specific conductance–composition data for the Li_2MoO_4-MoO_3 system are presented as polytherms. It is interesting to observe that the maximum at approximately 48 mole % MoO_3 corresponds to a eutectic or minimum in the phase diagram of Hoermann[11] for this system. Two peritectic reactions of this phase diagram are not indicated by the polytherms. Nevertheless, the slight similarity that exists here between the two types of diagrams constitutes additional support for the idea that there appears to exist some kind of correlation between the conductance (specific or equivalent or molar)–composition diagram and the corresponding phase diagram for certain systems of two components. Riebling and Erickson,[13] in presenting molar conductance isotherms as a function of melt composition for the molten salt system gallium monoiodide–gallium triiodide, point out the

presence of a maximum at the diiodide composition. The fact that Delimarskii and Markov[14] are able to illustrate the idea of similarity as observed for several molten binary systems suggests strongly that the similarity is more than coincidence.

Since the polytherms of Fig. 2 for the Li_2MoO_4–MoO_3 system all exhibit the same shape, it can be concluded that both the ionic species present in the melt and the nature of the conduction process remain the same for the temperature range of the polytherms. The principal ionic species present in the melts are Li^+ and MoO_4^{-2} from the Li_2MoO_4 and MoO_2^{+2} and MoO_4^{-2} from the MoO_3. For the melt consisting of ions from 100 mole % Li_2MoO_4, the conductance is high and the temperature with respect to the 820° isotherm is approximately 120° above the melting point. As the melts become increasingly richer in MoO_3, the conductance decreases continuously to the value for 100 mole % MoO_3, the poorer conducting component, for two chief reasons, namely (1) a decrease in the number of Li^+ carriers and (2) the insulating effect of MoO_3. Because of the fact that the conductances in a particular isotherm in Fig. 2 are for compositions that are different numbers of degrees above the respective melting points of the mixtures, one might suspect that a consideration of ionic mobilities is important in interpreting the polytherms. However, ionic mobilities appear to increase only very slightly as the temperature increases. This viewpoint is supported by the observation that plots (not shown) of conductance vs. temperature for various compositions in the Li_2MoO_4–MoO_3 system are lines that are almost parallel to the temperature axis. The effect of temperature on mobility for the ionic species may be important for the eutectic composition at about 47 mole % MoO_3 because the 820° isotherm is approximately 285° above the eutectic temperature.

The use of absolute reaction rate theory does not appear fruitful in an interpretation of the data for the pure components of both systems because calculated activation energies for conductance (ΔH_κ or ΔH_Λ) fluctuate up and down as the temperature changes in a given direction. However, the two activation energies in this research are generally of approximately the same magnitude for a given substance at the same temperature. This indicates that the αRT^2 term of the Martin[15] equation, $\Delta H_\Lambda - \Delta H_\kappa = \alpha RT^2$,

(13) E. F. Riebling and C. E. Erickson, J. Phys. Chem., 67, 307 (1963).

(14) Yu. K. Delimarskii and B. F. Markov, "Electrochemistry of Fused Salts" (translation by A. Peiperl and R. E. Wood), The Sigma Press, Publishers, Washington 7, D. C., 1961, pp. 22–40.

(15) R. L. Martin, J. Chem. Soc., 3246 (1954).

where α, the expansivity, is defined as $-1/\rho(d\rho/dt)$, is very small. This is in agreement with the fact that the rate of change of density (or specific or equivalent volume) with temperature is small.

When specific conductances for MoO_3 and the molybdates of Li^+, Na^+, and K^+ are compared at 100° above the respective melting points, the decreasing order of conductance is $Li_2MoO_4 > Na_2MoO_4{}^2 > K_2MoO_4 > MoO_3$. This is also the order for the average activation energies, ΔH_κ, based on specific conduct-

ances. This order for the activation energies is due perhaps to the fact that the polarizing powers of the cations and the coulombic forces between the ions of each substance are decreasing with increasing cation size. Quantitative interpretations of conductance data for molten molybdate systems must await the study of transport numbers for the conducting species.

The Photochemical Isomerization of α,N-Diphenylnitrone

by Kinko Shinzawa and Ikuzo Tanaka

Department of Chemistry, Tokyo Institute of Technology, Ohokayama, Meguro-ku, Tokyo, Japan
(Received September 28, 1963)

The photochemical isomerization of α,N-diphenylnitrone to α,N-diphenyloxazirane at 3130 Å. irradiation was confirmed by iodometry and ultraviolet and infrared absorption spectroscopy. The oxazirane produced in diluted cyclohexane solution isomerized thermally to benzanilide at high temperature (activation energy = 25.9 kcal./mole, frequency factor = 2.9×10^{11} sec.$^{-1}$). The oxazirane in concentrated solution decomposed to a substance having an aldehyde group even at room temperature. The infrared spectrum of the oxazirane was taken at 77°K. The quantum yield of the photoisomerization was independent of irradiation time, concentration of the nitrone, presence of oxygen, and temperature, but was affected by hydrogen bond formation. The quantum yield was 0.28 in the case of cyclohexane solution and 0.18 in ethanol solution in the temperature range from 30 to 75°. The *trans* → *cis* isomerization of the nitrone with irradiation could not be found. A mechanism of the reaction is proposed by consideration of the mobility of the oxygen attached to nitrogen and of *trans* → *cis* isomerization. At 2537 Å. irradiation the oxazirane was produced primarily just as in the case of 3130 Å. irradiation, but the oxazirane reacted futher by absorbing light of 2537 Å.

Introduction

Although there have appeared some reports[1-4] on the photochemical reaction of nitrones showing that their primary products were oxaziranes, the identity of the product in the case of α,N-diphenylnitrone has not been established and the mechanism of this reaction has not been discussed.

The chemical structure of α,N-diphenylnitrone is quite interesting. The features of its electronic

(1) M. Kamlet and L. Kaplan, *J. Org. Chem.*, **22**, 576 (1957).

(2) F. Kröhnke, *Ann.*, **604**, 203 (1957).

(3) J. S. Splitter and M. Calvin, *J. Org. Chem.*, **23**, 651 (1958).

(4) H. Shindo and B. Umezawa, *Chem. Pharm. Bull.* (Tokyo), **10**, 492 (1962).

structure are similar to those of pyridine N-oxide not only in the ground state but also in the excited state.[5] Pyridine N-oxide and picoline N-oxide were reported by Hata and Tanaka[6] to liberate oxygen at 2537 Å. irradiation, and the latter to isomerize to 2-pyridinemethanol at 3261 Å. irradiation. In addition, the nitrone has a double bond as has stilbene,[7] azobenzene,[8] and benzylidenephenylimine,[9] in which cases *trans* → *cis* photoisomerizations have been reported.

This paper describes the identification of the product as oxazirane, reports measurements of the quantum yield under various conditions, and includes a discussion of the mechanism of the photochemical reaction on the basis of the mobility of the oxygen attached to nitrogen and of *trans* → *cis* isomerization.

Experimental

Materials. α,N-Diphenylnitrone was synthesized and purified according to Foster, *et al.*[10] Cyclohexane was Nichiri Co. reagent grade product and was purified by passing through silica gel and by distillation. Ethyl alcohol was Kosō-Kagaku Co. reagent grade product.

Light Sources. A high pressure mercury lamp was used for 3130 Å. irradiation. The light was collimated and the stray radiation was prevented from entering the cell by a shielding box. The box was thermostated at experimental temperatures. For 3130 Å. irradiation a filter combination of cobalt sulfate–nickel sulfate solution and Hallio glass was used. The glass transmitted light of wave lengths longer than 3130 Å. A low pressure mercury resonance lamp containing neon was used for the 2537 Å. radiation source without filters, in which case the lamp was so separated from the cell that the 1849 Å. light from the lamp was negligible by absorption of oxygen in the air between them. A Hallio glass cell and a quartz cell were used for 3130 and 2537 Å. irradiation, respectively.

Light Intensity Measurement. The intensity of the incident light was measured periodically by the uranyl oxalate actinometric method.[11] The concentrations of the solutions were so adjusted that incident light was absorbed completely.

Spectroscopy. Ultraviolet absorption spectra at room temperature were taken with Shimazu QR-50 and Shimazu SV-50A spectrophotometers and infrared absorption spectra with a Perkin-Elmer Model 112 equipped with a special cell designed for low temperature measurements.[12] For reasons which will be apparent later, infrared spectra were taken both at low temperature and room temperature. For low temperature measurements, a disk of the sample, which was formed by pressing a mixture of the sample and KBr powder, was set in the cell, cooled by liquid nitro-

gen, and its spectrum taken. Then the disk together with the cell was put out of the spectrometer and irradiated at 77 °K. with 3130 Å. light for 2.5 hr. through a KBr window of the cell. Then the spectrum of the irradiated disk was taken again.

Results and Discussion

Formation of Oxazirane. The spectrum of the solution of α,N-diphenylnitrone changed markedly by irradiation with 3130 Å. light as shown in Fig. 1.
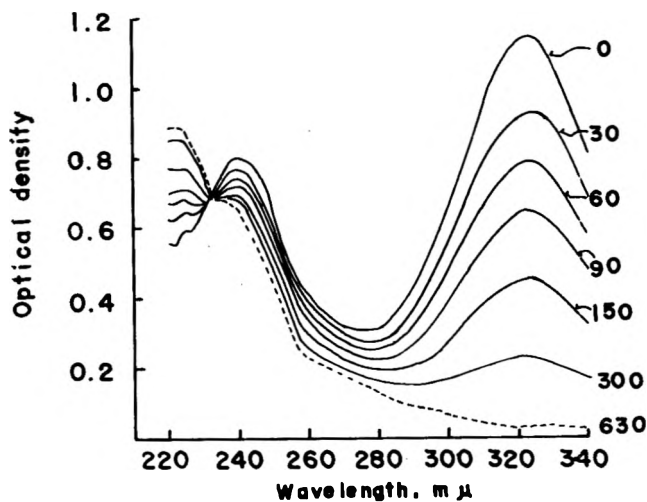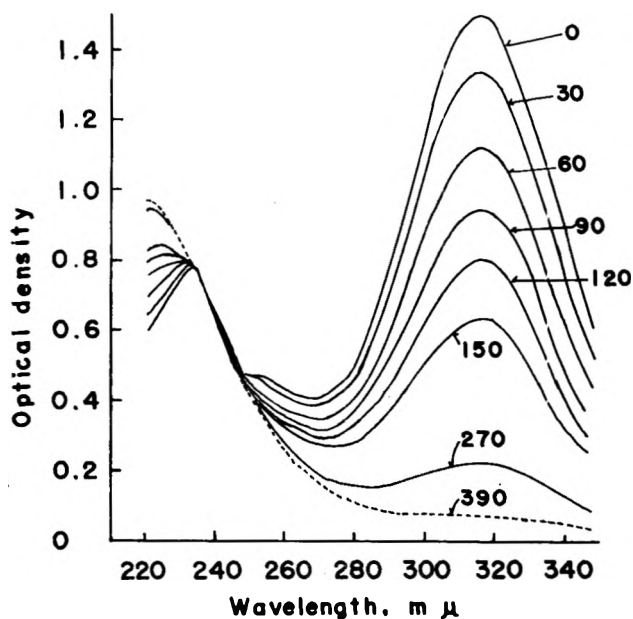

Figure 1. The progressive decrease of the spectrum of the nitrone at 3130 Å. irradiation in cyclohexane solution. Numbers refer to time of irradiation in seconds, and dotted line denotes a spectrum of the product at room temperature.

The first and second bands of the nitrone decreased and a new band with its maximum at 223 mμ appeared as the irradiation time increased, with an isosbestic point at 232 mμ. The reaction product has been considered to be α,N-diphenyloxazirane by the authors.[1,4] The oxazirane was so unstable that it could not be obtained by usual organic methods.[13] Consequently,

(5) T. Kubota and M. Yamakawa, *Bull. Chem. Soc. Japan*, **36**, 1564 (1963).

(6) N. Hata and I. Tanaka, *J. Chem. Phys.*, **36**, 2072 (1962); *Bull. Chem. Soc. Japan*, **34**, 1440, 1444 (1961).

(7) Z. Smakula, *Z. physik. Chem.*, **B25**, 90 (1934).

(8) G. S. Hartley, *Nature*, **140**, 281 (1937); *J. Chem. Soc.*, 633 (1938).

(9) E. Fisher and Y. Frei, *J. Chem. Phys.*, **27**, 808 (1957).

(10) (a) M. O. Foster and H. Folmes, *J. Chem. Soc.*, 242 (1908); (b) the authors are indebted to C. Shin for the preparation.

(11) G. S. Forbes and L. J. Heidt, *J. Am. Chem. Soc.*, **56**, 2363 (1934).

(12) The authors are indebted to the members of the laboratory of Prof. K. Kojima at Tokyo Institute of Technology for taking these spectra.

Table I[a]

Nitrone			Oxazirane		
Compound	λmax, mμ	εmax	Compound	λmax, mμ	εmax
(Ph)C(H)=N(→O)-Ph	322	20,000	(Ph)C(H)—N(Ph)—O (oxazirane)	223	14,000
Ph-C(H)=N(→O)-t-Bu	295	16,700	Ph-C(H)—N(t-Bu)—O	245	930
t-Bu-N(→O)=C(H)—C(H)=N(→O)-t-Bu	336	20,800	t-Bu-N—C(H)(O)—C(H)(O)—N-t-Bu	None	
NO₂-C₆H₄-C(H)=N(→O)-t-Bu	252, 362	11,400, 15,800	O₂N-C₆H₄-C(H)—N(t-Bu)—O	268	11,900

[a] The data except for those of α,N-diphenylnitrone and of its oxazirane are reprinted from Emmons' report.[13]

the formation of the oxazirane could not be confirmed by comparison of the properties of the products with oxazirane of another synthesis, but was confirmed by the following reasons.

Proof for the Formation of Oxazirane. 1. *Ultraviolet Absorption Spectrum.* In all the nitrones reported by Emmons, the absorption of oxazirane was at much shorter wave length than that of corresponding nitrone. Examples are shown in Table I. In the present work, the same relation was found between the spectra of nitrone and the reaction product.

2. Increase of Oxidizing Power. Oxaziranes are stronger oxidizers than nitrones.[13] The quantity of oxaziranes was determined by that of the iodine liberated from acidic potassium iodide.[13,14] An irradiated solution liberated iodine almost equivalent to the amount of converted nitrone. In contrast only 16% as much iodine was liberated from the unirradiated solution.

3. Thermal Isomerization to Benzanilide. Although the dilute cyclohexane solution of the photochemical reaction product was comparatively stable at room temperature, it showed a different absorption spectrum when heated at its boiling point for 15 min. (Fig. 2). After the solvent was evaporated, a white precipitate was obtained, which was identified as benzanilide by melting point and ultraviolet and infrared spectra. As benzanilide is an isomeric form of nitrone, this shows that the photochemical reaction product was also an isomer of the nitrone.
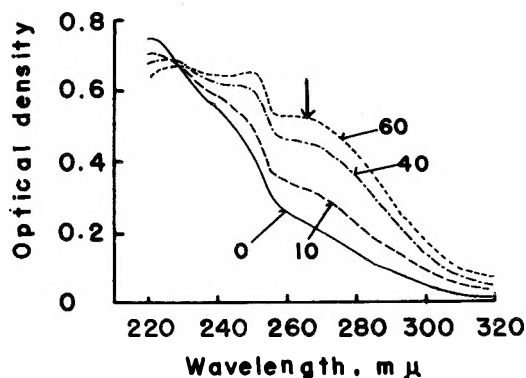
Figure 2. Spectral change of the oxazirane in cyclohexane solution with lapse of time at 80°. The maximum of the benzanilide absorption is indicated by an arrow. Numbers refer to the time at measurement in minutes.

4. Infrared Absorption Spectrum. In addition to the temperature dependence of the stability of the product, it was sensitive to concentration. A concentrated solution of product showed an irreversible change even at room temperature as revealed by ultraviolet spectra which was different from that of benzanilide and supposedly due to the decomposition of the product. The decomposition product was a dark brown oily substance which had a strong infrared absorption band due to the CHO group.

(13) W. D. Emmons, *J. Am. Chem. Soc.*, **79**, 5739 (1957).

(14) S. Siggia, "Quantitative Organic Analysis via Functional Groups," John Wiley and Sons, Inc., New York, N. Y., 1949, p. 100.

Table II

Nitrone		Irradiation products		Thermal decomposition products
ν, cm.⁻¹	Assignment[a]	ν, cm.⁻¹	Assignment	ν, cm.⁻¹
				1709 vs (aldehyde)
		1673 w		1652 m
				1624 w
1590 m	Ring A$_1$	1595 s		1594 s
1578 m	Ring B$_1$			
				1561 w
1547 s	C=N stretching			1534 m
		1524 w		
				1515 s
		1497 m		1485 s
1484 s	Ring A$_1$	1486 s		
1462 s $\}$ 1442 s	Ring B$_1$	1456 s		1454 s
		1438 w		1433 m
				1418 w
1396 vs	CH in plane bending	1394 vs		1392 m
				1364 w
1342 w				
1322 m				
1312 w		1312 m		1309 s
1296 s	Ring B$_1$	1296 m		
				1283 w
		1250 s	—C——N— / O	1258 w
1230 m	Ph–C stretching			
		1214 w		1204 vs
1189 s	Ph–N stretching			
1170 m	H bending A$_1$	1173 w		1167 s
1161 m	H bending B$_1$	1157 m		
		1149 m		
1079 s $\}$ 1077 s	H bending B$_1$			1102 w
1067 vs	N→O stretching	1074 s		1072 m
1025 m	H bending A$_1$	1024 s		1022 m
998 w	Ring A$_1$	1001 w		1000 w
988 w				
982 w	H bending A$_2$			
976 w				
925 s $\}$ 921 vs	H bending B$_2$	911 s		925 w
888 s	CH out of plane			
868 m	H bending A$_2$	866 s	—C——N—(?) / O	
848 w	Ph–N vibration	854 s		856 m
838 s		851 s		
		825 w		828 s
		818 w		
				794 w
773 vs $\}$ 762 s $\}$ 753 vs	H bending B$_2$	774 w / 757∼755 vs		776 s
		734 s	—C——N— / O	747 vs
694 vs	Ring B$_2$	698 vs		
687 vs		691 vs		691 vs

[a] H. Shindo, et al., Chem. Pharm. Bull. (Tokyo), **10**, 492 (1962).

In order to prevent the decomposition reaction, the infrared spectrum of the photochemical reaction product was taken at 77°K. by the method described above. The color of the disk was pale yellow both before and after irradiation at 77°K., but the irradiated disk suddenly darkened when brought to room temperature. The infrared spectrum of this substance was also taken. These are listed in Table II. The spectrum of the photochemical product was different from the spectra of both nitrone and the thermal decomposition product.

The band assignment of the nitrone in the first column was carried out by Shindo.[4] Accepting all the assignments, the bands of the nitrone which disappeared by irradiation were 1547 cm.$^{-1}$ (-C=N- stretching mode) and 1067 cm.$^{-1}$ (-N→O stretching mode), i.e., the bands associated with the structure of -C=N→O.

As the irradiation product was identified with a mono-substituted benzene by the existence of strong bands at 760~740 cm.$^{-1}$ and 690 cm.$^{-1}$,[15a] the bands considered to be due to the benzene ring can be related to those of the nitrone. Among the bands of irradiation products the 1250 and 734~714 cm.$^{-1}$ bands were characteristic ones which did not appear in the case of the nitrone or in the case of the thermal decomposition products.

Oxaziranes were reported by Krimm[16] and Shindo, et al.,[4] to have a strong absorption at about 1260 cm.$^{-1}$ which was assigned to the same ring breathing mode as that at 1266 cm.$^{-1}$ in ethylene oxide. The ring vibrations of the product with those of ethylene oxide, styrene oxide, and oxaziranes for comparison are listed in Table III. From the data, it can be deduced that 1250 and 734 cm.$^{-1}$ bands are due to the ring vibrations of oxazirane. In addition to these bands, 866 cm.$^{-1}$ might be due to another oxazirane ring vibration.

From the strong band at 1709 cm.$^{-1}$ of the thermal decomposition product shown in the third column in Table II, it is clear that an aldehyde group was formed by the thermal decomposition of oxazirane, but the other bands could not be assigned because of much decreased transmittance of the product.

Figure 3 shows the results of the nitrone in ethanol solution. Comparing Fig. 3 with Fig. 1, it is seen that the absorption of the nitrone shifted to shorter wave length while that of the product did not. The spectrum of the product in ethanol solution, in contrast with that in cyclohexane solution, showed a change, which seemed to be due to the decomposition of the oxazirane with a lapse of time at room temperature as shown in Fig. 4.

Quantum Yield of Nitrone → Oxazirane Reaction. The nitrone was converted to the oxazirane by 3130 Å.

Figure 3. The progressive decrease of the spectrum of the nitrone at 3130 Å. irradiation in ethanol solution. Numbers refer to time of irradiation in seconds, and dotted line denotes a spectrum of the product at room temperature.
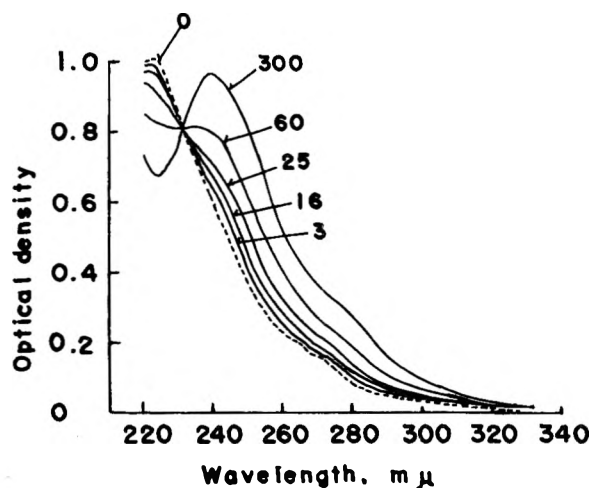
Figure 4. Spectral change of the oxazirane in ethanol solution with lapse of time at room temperature. Numbers refer to time at measurement in minutes, and dotted line denotes the spectrum of oxazirane.

irradiation without any side reaction as shown by the existence of the isosbestic point as shown in Fig. 1. The quantum yields were calculated from the ratio of the decrease in the number of nitrone molecules to

(15) L. J. Bellamy, "The Infrared Spectra of Complex Molecules," Methuen & Co., Ltd., London: (a) p. 76; (b) p. 308.

(16) H. Krimm, *Chem. Ber.*, 91, 1057 (1958).

Table III

Ring breathing A_1	1266'	1255	1259	1265	1250
Ring deformation A_2	877	877			(866?)
Ring deformation B_1	892	812			734-714

[a] R. C. Lord and B. Nolin, *J. Chem. Phys.*, **24**, 656 (1956). [b] W. A. Patterson, *Anal. Chem.*, **26**, 823 (1954). [c] From ref. 16. [d] From ref. 4. [e] Irradiation product in the present work. [f] All values in cm.$^{-1}$.
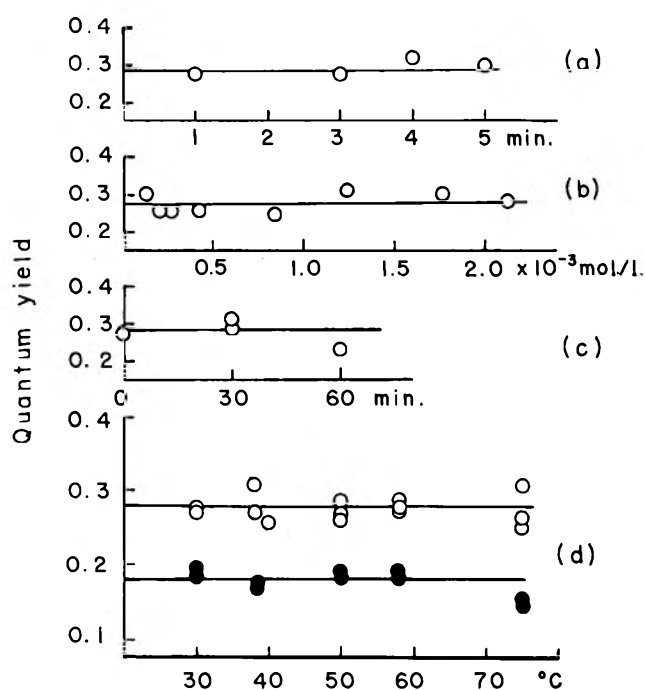
Figure 5. Dependence of quantum yield: (a), on irradiation time at 30° in cyclohexane with initial concentration of 3.71 × 10^{-4} mole/l.; (b), on concentration of nitrone at 30° in cyclohexane; (c), on deaeration by flushing with nitrogen at 30° in cyclohexane; (d), on temperature (O, in cyclohexane, concentration 4.85 × 10^{-4} mole/l.; ●, in ethanol, concentration 4.21 × 10^{-4} mole/l.).

the number of quanta absorbed by nitrone. The effects of various conditions on quantum yield were as follows.

1. Effect of Irradiation Time, Concentration, Oxygen, and Temperature on Quantum Yield. Quantum yields were obtained under various conditions (Fig. 5). The quantum yields of the reaction in cyclohexane did

not change with the variations of the irradiation time and the concentration of the nitrone at 30° (Fig. 5a and b).

The effect of oxygen dissolved in the cyclohexane solution on quantum yield was probably absent because there was no difference in quantum yields between an aerated solution and one deaerated by flushing with nitrogen at 30° (Fig. 5c).

The quantum yields in two solvents were independent of temperature in the range from 30 to 75°, as shown in Fig. 5d. Although the final product of irradiation was benzanilide at higher temperature and oxazirane at low temperature, it could be deduced from this temperature independence and the thermal isomerization of the oxazirane to benzanilide as stated above that the primary product of the reaction is the oxazirane even at high temperatures.

2. Effect of Solvent. Because the solvents affected considerably the quantum yields and ultraviolet spectra as shown above (Fig. 1, 3, and 5d), dependence of the yield on solvent was examined as follows.

The ultraviolet spectra of nitrone in ethanol-cyclohexane solution varied with the composition of the solvent as shown in Fig. 6. Some nitrones were revealed by means of ultraviolet and infrared spectra to form hydrogen bonds with solvents.[4,17] Assuming the same type of hydrogen bond between nitrone and ethanol in the present study, the equilibrium constant K of the bond formation was obtained to be 1.9 l./mole (Fig. 7).

In order to know the relation between quantum yield and hydrogen bond formation, the quantum yields were

(17) T. Kubota, M. Yamakawa, and Y. Mori, *Bull. Chem. Soc. Japan*, **36**, 1552 (1963).
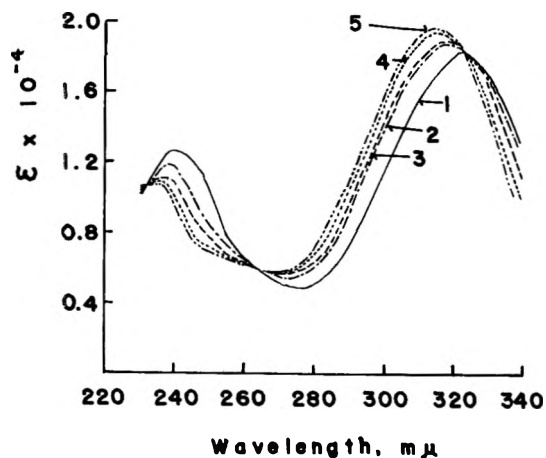
Figure 6. Spectra of nitrone in ethanol-cyclohexane mixture at room temperature. Ethanol concentrations are: 1, 0; 2, 0.569; 3, 1.14; 4, 5.70; and 5, 17.79 moles/l.
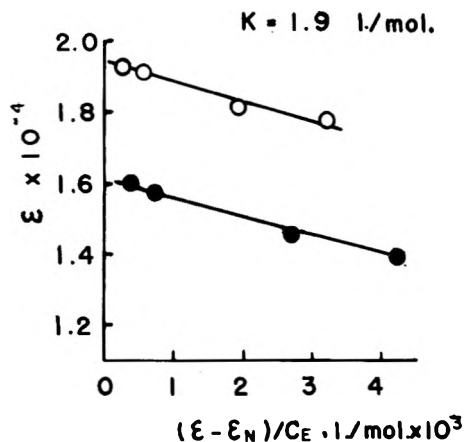
Figure 7. Plot of ε against $(\varepsilon - \varepsilon_N)/C_E$ to obtain the equilibrium constant K of the bond formation using the relation, $\varepsilon = -(\varepsilon - \varepsilon_N)/C_E K + \varepsilon_H$; slope of the curve indicates reciprocal value of K at room temperature; O, values for 310 mμ; ●, values for 330 mμ; ε, molar extinction of nitrone in ethanol-cyclohexane solution; ε_N, molar extinction of nitrone in cyclohexane; ε_H, molar extinction of hydrogen-bonded nitrone; and C_E, concentration of ethanol.

plotted in Fig. 8 against the fractions of the hydrogen-bonded molecules calculated from the K value. The linear relationship between them indicated that the decrease of the quantum yield in the case of ethanol solution was mainly caused by hydrogen bond formation of the molecule.

Reaction with Irradiation at 2537 Å. At 2537 Å. irradiation the ultraviolet spectra of a cyclohexane solution of the nitrone showed changes which were different from the case of 3130 Å. irradiation as shown in Fig. 9. It was found from the figure that the reaction had two steps, *i.e.*, the first change was the
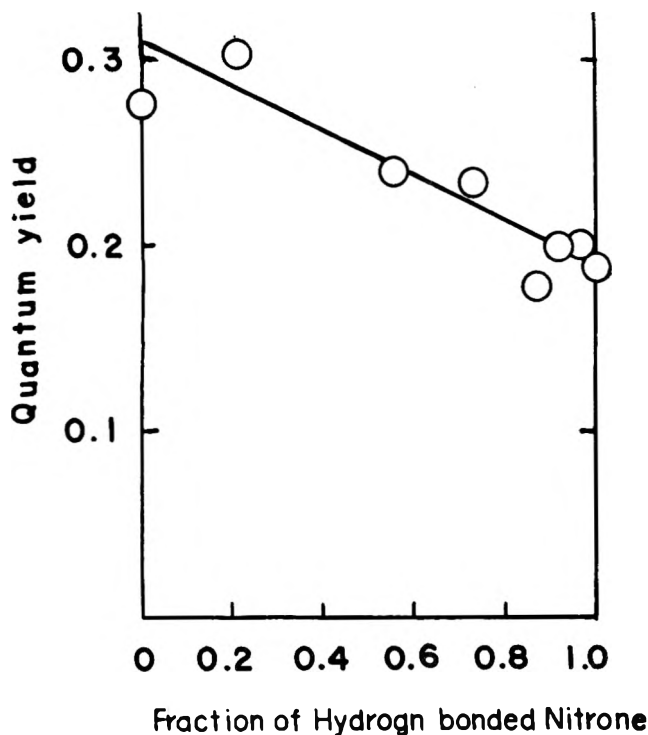
Figure 8. Plot of quantum yield against fraction of hydrogen-bonded nitrone molecules.
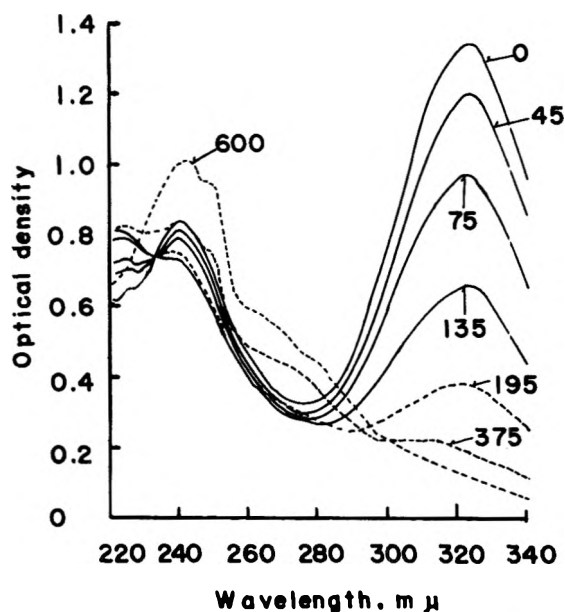
Figure 9. Change in spectrum caused by irradiating the nitrone solution with 2537 Å. light in cyclohexane. Numbers refer to time of irradiation in seconds.

decrease of the nitrone bands and the appearance of a new peak at 223 mμ with an isosbestic point at 230 mμ, and the second change was the decrease of the new peak and the rise of another peak at 242 mμ.

Comparing Fig. 9 with Fig. 1, it can be concluded that the oxazirane was produced primarily by the 2537 Å. light as well as in the case of 3130 Å., but the oxazirane reacted further by absorbing the incident light. The second change was confirmed by the fact that the oxazirane produced by 3130 Å. light showed the same spectral change by 2537 Å. light irradiation as that of the nitrone at the second step reaction (Fig. 10).

Thermal Isomerization of Oxazirane to Benzanilide. The oxazirane isomerized thermally into benzanilide. The reaction rates at several temperatures were determined by measuring the optical density at 267 mμ, where benzanilide had a maximum absorption, during the isomerization reaction. Assuming a first-order reaction, the activation energy and the frequency factor were calculated as 25.9 kcal./mole and 2.9 $\times$ 10^{11} sec.$^{-1}$, respectively, by the use of Fig. 11, in which logarithms of the specific rates were plotted against the reciprocals of the temperatures.

The comparatively smaller value of the activation energy than that of normal isomerization reactions indicates that the oxazirane has high potential energy.

Mechanism of Photochemical Reaction. The isomerization takes place at the lowest excited singlet state of the nitrone without considerable activation energy. The primary step of the reaction is not the twist of the two phenyl rings around the double bond but the movement of the oxygen atom to the α-car on atom.

The fact that the quantum yields do not depend upon the concentration of the nitrone below 2 $\times$ 10^{-3} mole/l., at which concentration the decrease of quantum yield was observed in *trans* $\rightarrow$ *cis* isomerization,[18] means that the reaction is so fast that it has finished
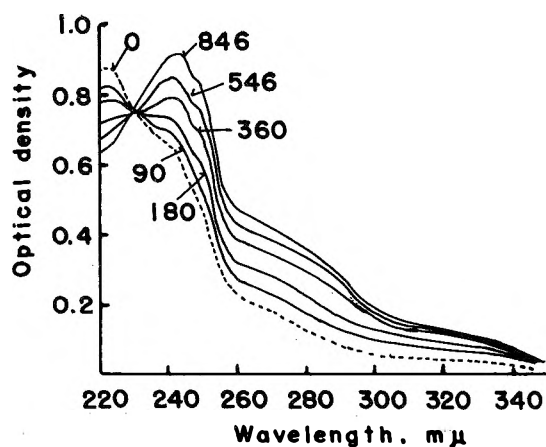
Figure 10. Change in spectrum caused by irradiating the oxazirane solution with 2537 Å. light in cyclohexane. Numbers refer to time of irradiation in seconds.
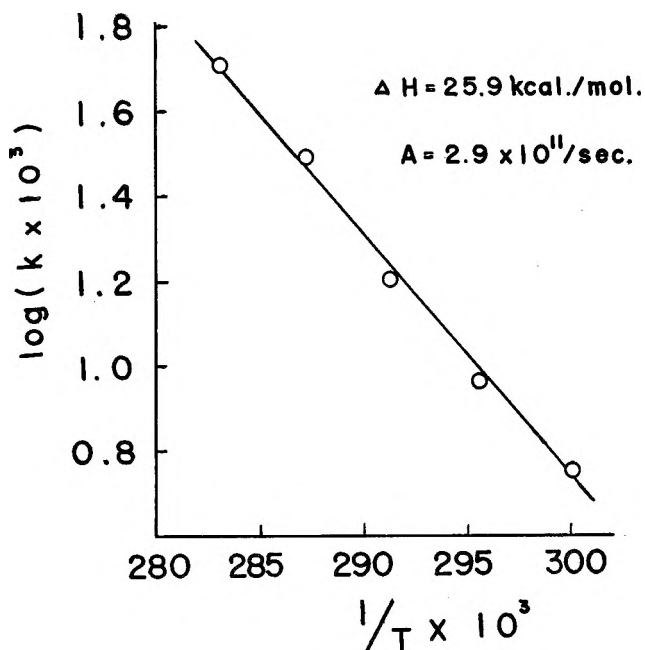
Fig. 11. Plot of logarithm of rate constant for thermal oxazirane $\rightarrow$ benzanilide reaction against reciprocal of temperature.

before deactivation of the excited nitrone molecule by collision with the ground state molecules occurs.

The linear relationship between the decrease of the quantum yield of the nitrone in ethanol-cyclohexane solution and the fraction of the hydrogen-bonded nitrone molecules in the ground state indicates that the reacting molecules when the isomerizations take place are surrounded with the solvent molecules in the ground state arrangement.

Considering the relaxation time in the solvents is about 10^{-11} sec.,[19] the lifetime of the excited nitrone molecule should be shorter than this value.

Lack of an activation energy in the nitrone $\rightarrow$ oxazirane reaction deduced from the temperature independence of the quantum yield is consistent with the fast reaction rate.

From the consideration of the facts that the nitrone used is known to be the *trans* form and that its *cis* form is assumed to have a different ultraviolet spectrum from that of the *trans* form, the existence of one isosbestic point in the spectral change of the reaction eliminates the possibility of a *trans* $\rightarrow$ *cis* isomerization.[20] It was considered that the photochemical

(18) D. Schulte-Frohlinde, H. Blume, and H. Güsten, *J. Phys. Chem.*, **66**, 2486 (1962).

(19) E. Lippert, *Z. Elektrochem.*, **61**, 962 (1957); *Z. Naturforsch.*, **10a**, 541 (1955).

trans → cis isomerization of the stilbene has a few kilocalories of activation energy and also needs the singlet–triplet conversion.[18] The absence of trans → cis isomerization indicates that the nitrone molecule has isomerized to the oxazirane before the slow trans → cis conversion takes place.

Reaction in the excited singlet state is also indicated by the independence of quantum yield on the presence of oxygen.

The labile character of the oxygen atom attached to the nitrogen atom in the nitrone may reasonably be assumed from the fact reported by Hata and Tanaka[6] that oxygen molecules were liberated from pyridine N-oxide and α-picoline N-oxide by 2537 Å. irradiation and that the α-picoline N-oxide isomerized to 2-pyridinemethanol with 3650 Å. irradiation.

The character of the oxygen in the nitrone may also be interpreted as due to a significant change in the dipole moment of the N→O bond on the excitation, and the free valence of carbon at the α-position in the excited state increased to 0.7800 from 0.5311 in the ground state.[5]

For the above reasons the oxygen atom moves rapidly to the carbon at the α-position whose free valence increases in the excited state to form a bond before the two phenyl rings twist around the double bond.

(20) If the thermal inverse reaction (cis → trans) is so rapid that most of the nitrone molecules are in the trans form at the photoequilibrium state of this temperature, the trans → cis isomerization cannot be observed.

Radiofrequency Measurements of Porous Conductive Plugs.

Ion-Exchange Resin–Solution Systems

by S. B. Sachs[1a] and K. S. Spiegler[1b]

Department of Chemistry, Technion-Israel Institute of Technology, Haifa, Israel
(Received November 22, 1963)

Measurements were made of the dielectric constants and electrical conductivities of the cation exchanger Amberlite IR-120 in the calcium form, immersed in distilled water and in calcium chloride solutions of different concentrations. An instrument based on a Schering bridge circuit was used, the alternating current frequency range being 20–90 Mc.p.s. The effects of the transmission line from the instrument terminals to the sample and the impedance effects of the electrodes were eliminated by measuring the capacitance and conductivity of columns of different height. The results showed that the apparent dielectric constant and apparent resistivity increase with decreasing frequency. This increase is particularly marked when the solutions are dilute. At the low frequencies, apparent dielectric constants of over 200 were measured in the resin–distilled water system. These measurements can be quantitatively interpreted if the column is approximated by a simple electric network which corresponds to a model used before to interpret the electrical properties of resin columns. This simplified model consists of three elements in parallel, namely (1) alternating layers of solution and ion-conductive solid, (2) solid, and (3) solution. Each part of the model is represented by a resistor and capacitor in parallel. Choosing the magnitudes of these components in accordance with the geometry of the model leads to quantitative agreement between the model theory and the results. The intrinsic dielectric constant of the wet solid resin is thus determined as 38 (25°).

Measurements of the dielectric properties of porous conductive media, *e.g.*, soils, biological membranes, porous water- or oil-bearing rocks, and ion-exchange resin columns, at radiofrequencies can be performed readily since several excellent instruments for the measurement of conductive media have been described and some are commercially available.[2,3] The interpretation of these measurements, however, is often quite difficult. The instrument readings can be easily converted to the apparent dielectric constant (the measured capacitance divided by the capacitance of the cell *in vacuo*) and apparent conductivity (the measured conductivity multiplied by the cell constant) but these two components of the complex conductivity are usually quite different from the true dielectric constants and conductivities of the components, or their weighted averages, and vary rapidly with the frequency. For instance, apparent dielectric constants larger than 1000

have been reported for *wet* soils and rocks[4] while the true dielectric constants of most *dry* soils and water are lower than 10 and 80, respectively. With increasing frequency, both the apparent dielectric constant and the apparent conductivity seem to approach limiting values. The present work demonstrates that these limits do not represent the weighted averages of the true constants of the pure components and that the decrease of both apparent dielectric constant and re-

(1) (a) The material for this paper is taken from the M.Sc. thesis of S. B. S., Technion-Israel Institute of Technology, 1961; (b) Willgoos Physical Chemistry Laboratory, Pratt & Whitney Aircraft, East Hartford, Conn.

(2) (a) H. Gerischer, *Z. Elektrochem.*, **58**, 9 (1954); (b) J. H. Mennie, "A Wide Range VHF Impedance Meter," "The Notebook," No. 2, Boonton Radio Corp., Boonton, N. J.

(3) R. Calvert, J. A. Cornelius, V. A. Griffith, and D. I. Stock, *J. Phys. Chem.*, **62**, 47 (1958).

(4) R. L. Smith-Rose, *Proc. Roy. Soc.* (London), **A140**, 359 (1923).

sistivity of these media in the radiofrequency range is primarily a consequence of their heterogeneous nature rather than a molecular phenomenon.

One of the problems of interpretation of the radiofrequency measurements of conductive porous media arises from the impedance of the components of the measuring circuit. The impedance of the wires and electrodes ("transmission line") is quite appreciable in the megacycle frequency range, even when all connections are as short as possible. Since the line impedance is primarily inductive, it decreases with decreasing frequency and becomes negligible at zero frequency. Measurements of dielectric constants at zero frequency (static) were indeed made and are described in the extensive contribution of Tarkov on conductive dry and wet rocks.[5] However, the electrochemical polarization effects at low frequencies complicate the interpretation of the conductance measurements at these frequencies. Because of this problem and since instruments for a.c. measurements are readily available offering the opportunity to cover a broad frequency range, most researchers have used a.c. methods for dielectric studies and tried to reduce the line effects to the absolute minimum and/or to compensate for them. This has also been done in the present research, in which the dielectric properties of the porous plugs consisting of ion-exchange resins and solutions were determined from the difference of measurements carried out at different distances between two plate electrodes confining the samples, all other conditions remaining equal. The frequency range 20–90 Mc.p.s. was chosen because at these frequencies the displacement current and the ionic conductance current passing the samples were roughly of the same order of magnitude, which condition is considered desirable when an ordinary, universal bridge instrument is used.

The other major problem arises from the heterogeneous nature of the media. While the dielectric constants of many homogeneous solutions are roughly the averages of those of the components, weighted by the respective volume fractions, this simple "mixing rule" does not at all hold for heterogeneous media, because of the complexity of the current path which crosses many phase boundaries. Maxwell[6] has derived a formula for the dielectric constant of a dilute suspension of spheres of one nonconductive dielectric in another, in terms of the dielectric constants of the components and their respective volume fractions. A large number of amplifications of his basic approach were published subsequently, many of which are reviewed by Tobias.[7] Wagner and others[8-11] have interpreted the frequency dependence of the dielectric constant of commercial dielectrics by assuming that

they are heterogeneous media. Maxwell's formula also describes the electrical conductivity of dilute suspensions of conductors in other conductive media, but is not strictly applicable to heterogeneous mixtures in which one component forms more than a small (volume) percentage of the mixture. In principle, it is possible to compute the dielectric constant and conductivity of mixtures of two components from the respective properties of the pure components, provided the geometrical shape of the phases is known. However, this problem is of less practical interest than the reverse one, namely, the determination of particle shape from the change of the complex conductivity with frequency. Although exact expressions for the complex conductivity of suspensions of ellipsoidal and cylindrical particles have been derived[12] which are even valid for more concentrated suspensions than those covered by the original Maxwell treatment, it was deemed desirable to search for a simple approximate formula to describe in terms of a minimum of empirical parameters the complex conductivity of a "suspension" as concentrated as a bed of conductive spheres immersed in a conductive liquid. In the present work the complex conductivities of porous plugs consisting of an ion-exchange resin and solutions of different concentrations in equilibrium with it were measured. The results were interpreted in terms of an a.c. network representing a simple model which had been used in the past to represent the change of low-frequency conductivity of these plugs[13] and of the electrical potential across them[14] with the solution concentration. Ion-exchange resins were chosen because of the prevalent interest in measurements of their dielectric constants in connection with the study of ion-exchange equilibria, and because of the similarity of the conduction mechanism which is ionic in both solid

(5) A. G. Tarkov, Leningrad Esoiusznyi Geologicheskii Institu Materialy: Geofizika, 12, 1 (1947).

(6) J. C. Maxwell, "Electricity and Magnetism," 3rd Ed., Oxford University Press, 1892.

(7) C. W. Tobias, Ed., "Advances in Electrochemistry and Electrochemical Engineering," Vol. 2, Chapter 2, John Wiley and Sons, Inc., New York, N. Y., 1962.

(8) K. W. Wagner, Arch. Elektrotechn., 2, 371 (1914).

(9) K. Sinjelnikoff and A. Walther, Z. Physik., 40, 786 (1927).

(10) A. Gemant, "Elektrophysik der Isolierstoffe," Springer, Berlin, 1930.

(11) B. V. Hamon, Australian J. Phys., 6, 304 (1953).

(12) H. Fricke, Phys. Rev., 24, 575 (1924); J. Phys. Chem., 57, 934 (1953); 59, 168 (1955).

(13) M. C. Sauer, P. F. Southwick, K. S. Spiegler, and M. R. J. Wyllie, Ind. Eng. Chem., 47, 2187 (1955).

(14) K. S. Spiegler, R. L. Yoest, and M. R. J. Wyllie, Discussions Faraday Soc., 21, 174 (1956).

and liquid phase, thus minimizing the complexity of charge transfer across the phase boundaries.

Experimental

Materials. The cation-exchange resin used was "Amberlite IR-120" (Rohm & Haas Co., Philadelphia, Pa.) which was preconditioned by alternating treatment with $CaCl_2$ and HCl solutions and finally converted completely to the pure Ca form according to established procedures.[15] After vacuum drying, the fraction in the size range 20–25 mesh (U. S. Standard, sieve openings 0.84 and 0.71 mm., respectively) was separated. Since it was deemed important to use particles of well-defined geometrical shape, only particles of perfect spherical appearance, when viewed under a magnifying glass, and without flaws or cracks, were handpicked. The resin sample made up of these particles was pretreated with water vapor at room temperature to effect gradual water uptake. It was then brought to equilibrium with demineralized distilled water and with solutions of reagent grade $CaCl_2$ of two different concentrations (0.0106 and 0.0421 M) for the different measurements described in the following paragraphs. The specific conductances of the two $CaCl_2$ solutions were 2.62×10^{-3} and 1.25×10^{-2} mho cm.$^{-1}$, respectively (25°). Microscopic examination after the equilibrations showed that only 0.2% of the particles in the sample were cracked.

The low-frequency specific conductance of the solid resin material was measured at 100 c.p.s. by the "isoconductance point method"[13,14] and found to be $(7.5 \pm 0.15) \times 10^{-3}$ mho cm.$^{-1}$ at 25.0° (Fig. 1). The water content of the resin in equilibrium with distilled water at the same temperature was determined from the weight loss on drying at 150° and found to be 47.0%. The porosity of the column was 0.37.

Instrument. The impedances were measured with an "RX Meter," Type 250 (Boonton Radio Corp., Boonton, N. J.). This instrument is essentially a Schering bridge[2] with a sensitive visual null indicator. The range of the instrument is from 0 to 0.067 mho and from -100 (inductive range) to $+20$ $\mu\mu f$. for the real and imaginary parts of the admittance, respectively. By introduction of calibrated inductances, the range of the instrument was extended to $+120$ $\mu\mu f$.

Series of measurements of the impedance of resin–solution columns were carried out within the frequency range 20–90 Mc.p.s. At each frequency the bridge was balanced with the cell and transmission line disconnected. The cell was then connected, the bridge balanced again, and the values of capacitance and resistance of an equivalent parallel circuit of these two components read directly on the instrument. Be-
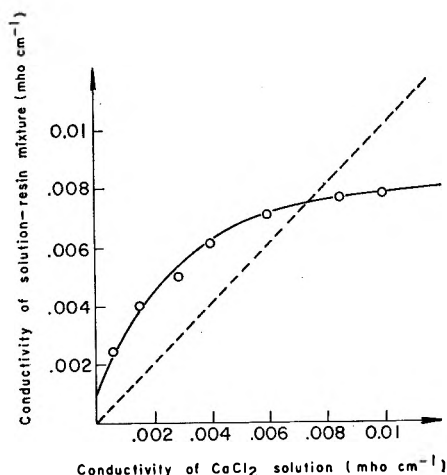
Figure 1. Specific conductance of ion-exchange column saturated with $CaCl_2$ solutions. Circles represent experimental data with Amberlite IR-120 cation-exchange resin (20–25 mesh, U. S. Standard Screen), 25°. Solid line is calculated from three-component model described in paper; 45° line (dotted) intersects curve at "isoconductance" point.

cause of the limitations imposed by the impedance range of the instrument and the considerable impedance of the connections between bridge and cell, the full frequency range could not be covered with all the samples, but the authors believe that the frequency range for each sample is wide enough for the significant comparison of the measurements with the postulates of the theory proposed in the Discussion.

Cell. The design of the cell and its connections to the bridge terminals enabled us to carry out measurements of resin–solution columns of different length and thus to eliminate, by computation, the very appreciable influence of the transmission line, the electrodes themselves, and the surroundings of the cell in general. The cylindrical sample was held between two flat circular electrodes. The distance between these electrodes could be changed and thus samples of different lengths could be measured, similar to the method used by Gillespie and Cole[16a] for the measurement of the dielectric constant of sulfuric acid and by Mandel for electrolyte and polyelectrolyte solutions.[16b] For the ion-exchange resin columns studied, this geometry was considered preferable to the use of coaxial cylinders as electrodes,[17] mainly because it is easier to

(15) (a) C. Calmon and T. R. E. Kressman, Ed., "Ion Exchangers in Organic and Biochemistry," Interscience, New York, N. Y., 1957; (b) F. Helfferich, "Ion Exchange," McGraw-Hill Book Co., Inc., New York, N. Y., 1962.

(16) (a) R. J. Gillespie and R. H. Cole, *Trans. Faraday Soc.*, 52, 1325 (1956); (b) M. Mandel, *Bull. Soc. Chim. Belges*, 64, 442 (1955).

(17) S. E. Lovell and R. H. Cole, *Rev. Sci. Instr.*, 30, 361 (1959).
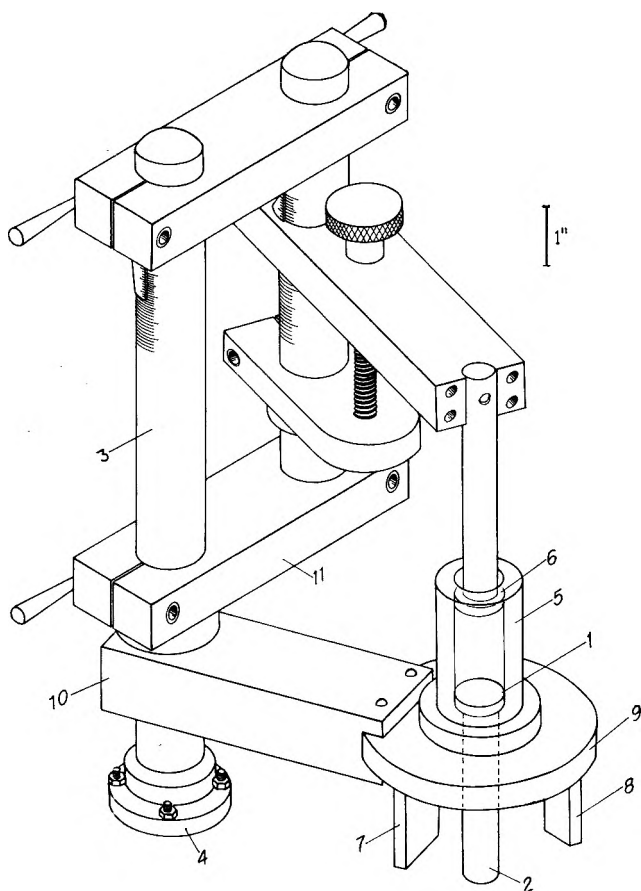
Figure 2. Transmission line and cell for impedance measurements. Assembly is mounted directly on top of "RX" meter. Lower electrode 1 makes contact with central ("hot") connector of "RX" meter at 2. Other connector is grounded to chassis making contact with column 3 through base plate 4. Cell 5 contains resin-solution mixture. In operation, upper electrode 6 is placed into cell 5, opposite lower electrode 1. All parts are metal (mostly brass) except cell 5, supports 7 and 8, supporting disk 9, and clamp 10, which are made of "Plexiglas," and clamp 11 (polystyrene).

Figure 3. Schematic representation of cell and transmission line at two different electrode distances. Figure shows that length ABCDEF = A'B'C'D'E'F' of transmission line is the same in both positions and basic geometry of line very similar. Cross-hatched parts are insulators. Lower electrode is connected to "hot" terminal, upper to other (chassis) terminal via transmission line.

fill the plate condenser uniformly and reproducibly with the sample. The cell is shown in Fig. 2.

Changing the electrode distance necessarily brings about some alteration of the transmission line from the instrument to the sample and hence some change of the impedance which is in series with the sample. Our cell design made it possible to change the electrode distance without changing the length of the transmission line and causing only a minor change in the geometry of the line, as illustrated in Fig. 3, which shows the transmission line at two different electrode distances. When changing the electrode distance, the position of the connector BC is readjusted so that the total length ABCDEF remains unchanged. The cell was mounted in a "Faraday cage" of wire mesh, directly

on top of the "RX meter" and connected to the top terminals of the latter.

Elimination of Extraneous Factors. The measured impedances were interpreted in terms of circuits of the type shown in Fig. 4 (a) and (c). These networks consist simply of two impedances in series, shunted by a parallel capacitor, C_t. One of the series impedances, Z_{tr}, represents the transmission line; the other, composed of a resistance and a capacitance in parallel (R_s, C_s and R_s/l, $C_s l$ in Fig. 4 (a) and (c), respectively) represents the sample. C_t represents the stray capacitance of the transmission line and the electrodes, i.e., the capacitance measured when there is no sample between the electrodes. It was measured as 4.24 $\mu\mu$f., independent of the frequency.[18,19]

Equating the expressions for the impedances of circuits (a) and (c) obtained from elementary network analysis[20] to those of (b) and (d), respectively, one obtains two

(18) It is surprising that networks as simple as those of Fig. 4 (a) and (c) represent the measured impedances, and that the analysis of the measurements does not necessitate the introduction of additional circuit elements between the two branches containing (Z_{tr} + sample) and C_t, respectively, at least up to 100 Mc.p.s. However, the simple network is strongly supported by an analysis of the equivalent circuit for the transmission line by means of measurements with objects of known impedance including standard solutions.[19] This analysis showed that the impedance of the transmission line itself can be represented as a very simple network of three components independent of the frequency, provided a constant capacitance of 4.24 $\mu\mu$f. is assumed to exist exactly in the position shown in Fig. 4.

(19) S. B. Sachs, M.Sc. Thesis, Technion-Israel Institute of Technology, Haifa, 1961.

(20) W. R. LePage, "Analysis of Alternating Current Circuits," McGraw Hill Book Co., Inc., New York, N. Y., 1952.

equations of complex variables from which the line Impedance, Z_{tr}, can be eliminated. The real and imaginary parts of the resulting single equation then lead to eq. 1 and 2 for the true resistance (ohms) and capacitance ($\mu\mu$f.) of the sample of unit length, respectively, at frequency f (sec.$^{-1}$).

Equations 1 and 2 contain R_p, C_p, R_p', and C_p' which are read directly from the "RX meter," the stray capacitance, C_t, determined previously when the sample is not in the circuit, and the angular frequency $\omega = 2\pi f$ at which the measurement is carried out. By performing these measurements at different frequencies, the source data for the test of the theory were obtained.

effects proved impractical because of the coarse heterogeneous nature of resin columns and also because of the limited capacitance and resistance ranges of the instrument. The geometrical cell constant, x_1/A, for a cylindrical resin column of length $x_1 = 5$ cm. and cross section $A = 3.14$ cm.^{2} is 1.588 cm.$^{-1}$, and, if there were no edge effects, the capacity of a condenser of the same dimensions would be $_gC_0 = 0.0556$ $\mu\mu$f. and the dielectric constant, ϵ', of a sample could be determined from

$$\epsilon' = \frac{C_s}{_gC_0} \text{ (for thin plate sample)} \qquad (3)$$

Since a column of these dimensions cannot be considered a thin plate with negligible edge effects, however, cor-

$$R_s = $$

$$\left[\frac{R_p^2(C_p - C_t)}{1 + R_p^2\omega^2(C_p - C_t)^2} - \frac{R_p'^2(C_p' - C_t)}{1 + R_p'^2\omega^2(C_p' - C_t)^2}\right]^2 \frac{[(1 + R_p^2\omega^2(C_p - C_t)^2)(1 + R_p'^2\omega^2(C_p' - C_t)^2)]l\omega^2}{[R_p(1 + R_p'^2\omega^2(C_p' - C_t)^2) - R_p'(1 + R_p^2\omega^2(C_p - C_t)^2)](l - 1)} +$$

$$\frac{[R_p(1 + R_p'^2\omega^2(C_p' - C_t)^2) - R_p'(1 + R_p^2\omega^2(C_p - C_t)^2)]l}{[(1 + R_p^2\omega^2(C_p - C_t)^2)(1 + R_p'^2\omega^2(C_p' - C_t)^2)](l - 1)} \qquad (1)$$

$$C_s = \left[\frac{(1 + R_p^2\omega^2(C_p - C_t)^2)(1 + R_p'^2\omega^2(C_p' - C_t)^2)(l - 1)}{R_s\omega^2[R_p(1 + R_p'^2\omega^2(C_p' - C_t)^2) - R_p'(1 + R_p^2\omega^2(C_p' - C_t)^2)]l} - \frac{1}{R_s^2\omega^2}\right]^{1/2} \qquad (2)$$
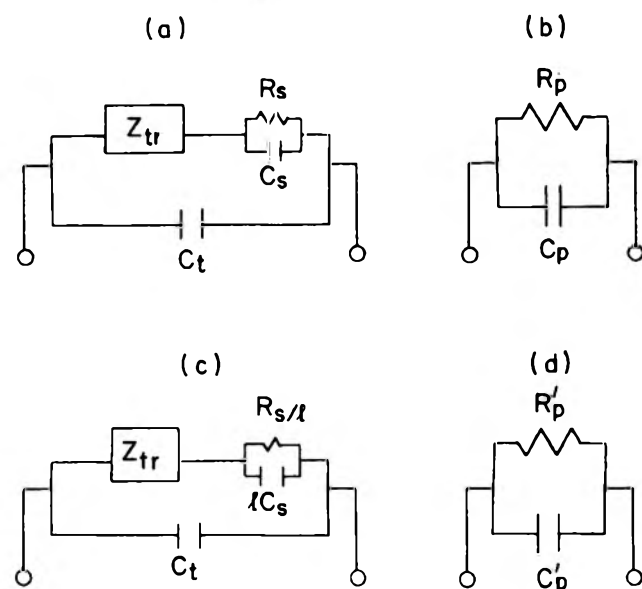
Fig. 4. Equivalent circuits for cell and transmission line. Networks (a) and (c) describe line impedance, Z_{tr}, stray capacitance, C_t, and impedance of material in cell, represented by a resistor, R_s, and capacitor, C_s, in parallel. Electrode distances in measurements represented by networks (a) and (c), respectively, are in ratio l. "RX" meter presents results in terms of (b) and (d), respectively.

Determination of Cell Constant. Measurement of thin disks of samples which exhibit negligible edge

rection is made for the deviation of the electrical field from ideal cylindrical geometry by introducing the correction factor β

$$\epsilon' = \frac{C_s}{_gC_0\beta} = \frac{C_s}{C_0} \qquad (4)$$

where $C_0 = {}_gC_0\beta$. The correction factors were determined separately for each of the three series of experiments involving a different interstitial liquid; in each case, the capacitance, C_s, of the cell filled with the respective interstitial liquid (but without resin) was determined by the same method as described for the resin–solution columns and divided by the product $_gC_0\epsilon'$ (eq. 4), the dielectric constants, ϵ', of the liquids being estimated from the work of Hasted, et al.,[21] as well as from our own measurements as described in the Discussion section. The correction factors are listed in Tables I–III. It was seen that they depend on the frequency and that their values range from 0.960 to 1.10.

The same correction factors were used to calculate the specific resistance, ρ' (ohm cm.) from the resistance, R_s (ohms)

$$\rho' = R_s \frac{A\beta}{x_1} \qquad (5)$$

(21) J. B. Hasted, D. M. Ritson, and C. H. Collie, *J. Chem. Phys.*, 16, 1 (1948).

Table I: Apparent Dielectric Constants, ϵ', and Specific Resistances, ρ', of Resin–Solution Columns. Resin in Pure Water[a]

| | Frequency, Mc.p.s. | | | | | | | |
	20	25	35	40	50	65	80	85
C_p	15.98	14.09	11.91	11.13	9.72	8.40	6.75	5.90
C_p'	24.80	20.29	16.39	14.89	11.93	7.75	0.87	−1.19
R_p	560	490	393	358	306	240	192	174.5
R_p'	333	280	220	197	158	120.5	100.3	100.5
C_s	12.21	10.72	8.44	7.67	6.24	5.52	4.72	4.71
R_s	507	476	419	392.8	370	324	304	272
β	0.980	0.984	0.989	1.007	1.017	1.072	1.095	1.095
ϵ'	224	196	154	139	110	93	77	77
ϵ'_{theor}	271	197	155	139	110	88	76	74
ρ'	330	308	272	254	240	211	198	192
ρ'_{theor}	356	315	261	253	232	220	208	200

[a]Resin: Amberlite IR-120, Ca form, 25°. Meaning of circuit elements, C ($\mu\mu$f.), and R (ohms), is illustrated in Fig. 4. Negative values of C indicate inductive impedance. Frequency is given in Mc.p.s. Column heights 5.00 and 2.90 cm. ($l = 1.724$), $C_t = 4.24$ $\mu\mu$f.

Table II: Apparent Dielectric Constants, ϵ', and Specific Resistances, ρ', of Resin–Solution Columns. Resin in $CaCl_2$ Solution[a]

| | Frequency, Mc.p.s. | | | | | |
	30	40	50	60	70	80
C_p	6.90	6.62	6.38	5.79	5.12	4.19
C_p'	6.28	5.31	3.97	2.29	0.12	−2.07
R_p	308	284	265	239	214	192
R_p'	170.5	156	144	132	123	122.5
C_s	4.27	4.18	4.23	3.95	3.79	3.55
R_s	334.7	318.7	316.4	294.2	274.8	249.5
β	1.061	1.061	1.061	1.061	1.061	1.061
ϵ'	72	71	72	67	64	60
ϵ'_{theor}	70	68	66	64	63	62
ρ'	211	200	199	185	173	157
ρ'_{theor}	195	192	189	187	184	182

[a] Specific conductance 2.62×10^{-3} mho cm.$^{-1}$; l and C_t as in Table I.

Table III: Apparent Dielectric Constants, ϵ', and Specific Resistances, ρ', of Resin–Solution Columns[a]

| | Frequency, Mc.p.s. | | | | |
	70	75	80	85	90
C_p	0.63	0.25	−0.17	−0.52	−0.90
C_p'	−21.87	0.82	−15.96	−13.47	−11.37
R_p	178	177.6	178	182	187
R_p'	204	242	290	350	428
C_s	4.36	4.44	4.57	4.38	4.25
R_s	84.23	82.1	79.09	77.8	76.0
β	0.96	0.96	0.96	0.96	0.96
ϵ'	50	51	52	50	49
ϵ'_{theor}	52	52	52	52	52
ρ'	86	84	81	80	78
ρ'_{theor}	96	93	90	87	85

[a] Specific conductance 1.25×10^{-2} mho cm.$^{-1}$. Column heights 3.00 and 1.00 cm. ($l = 3.00$). C_t as in Table I.

While the use of these correction factors involves rather sweeping simplifications, the authors felt that the factors are close enough to unity as not to warrant the involvement in a still more sophisticated correction procedure. It is known that in other conductive systems of high dielectric constants β is also close to unity.[16]

Results

The results of the measurements and the apparent dielectric constants and specific resistances of the three resin–solution columns at various frequencies are listed in Tables I–III. C_p, C_p', R_p, and R_p' are measured values. C_s and R_s represent the capacitance and resistance of the sample after elimination of transmission line and electrode effects, as calculated from eq. 2 and 1, respectively. The correction factor β was determined

by the procedure discussed under "determination of cell constant." The apparent dielectric constants ϵ' and apparent specific resistance ρ' were then calculated from eq. 4 and 5, respectively. The tables also list the values of ϵ'_{theor} and ρ'_{theor} calculated from the theory presented in the Discussion section, which utilizes only the conventional low-frequency conductivity measurements shown in Fig. 1. Figures 5 and 6 summarize the results, showing the apparent dielectric constants and apparent specific resistances obtained in this work as single points and the theoretical predictions as solid lines.

Discussion

Figures 5 and 6 demonstrate that the apparent dielectric constants and specific resistances of all three resin–solution columns decrease with the frequency and that the decrease is the more pronounced the less the concentration of the interstitial solution. To explain this result, the authors drew on a simplified model of heterogeneous porous media, proposed to explain the variation of the electrical conductivity of resin–solution columns with the conductivity of the components[13] and the electrical potential differences between two solutions of different concentration separated by such columns,[14] which has subsequently been applied also to heat transfer in catalyst beds.[22] This model is an approximation, imparting a simple physical meaning to the more complicated exact solution of the problem.

In the model, the transport of current was tentatively described as composed of three separate portions, illustrated in Fig. 7A, namely, current passing through (1) alternating layers of solution and solid, (2) solid particles only, and (3) solution only. In other words, the simple, square model of Fig. 7B was substituted for the complicated geometry of the porous medium.

The conductivity K_0 (ohm^{-1} cm.$^{-1}$), of this model is given by

$$K_0 = \underbrace{\frac{K_R K_w}{[K_R(1 - d)/a] + [K_w d/a]}}_{\text{element 1}} + \underbrace{bK_R}_{2} + \underbrace{cK_w}_{3} \tag{6}$$

where K_R and K_w are the conductivities of resin and solution, respectively. By changing the solutions systematically and measuring the conductivity of the resin–solution system at 60 and 1000 c.p.s., we obtained a plot of K_0 vs. K_w (Fig. 1) which was indeed well described by eq. 6 if the following values for the geometrical parameters were chosen: $a = 0.65$; $b = 0.02$; $c = 1 - a - b = 0.33$; $d = 0.90$. These values
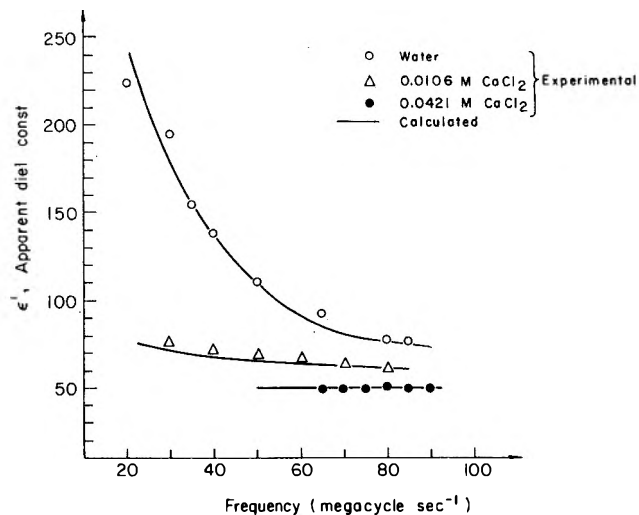
Figure 5. Apparent dielectric constants of ion-exchange resin columns saturated with different interstitial solutions.
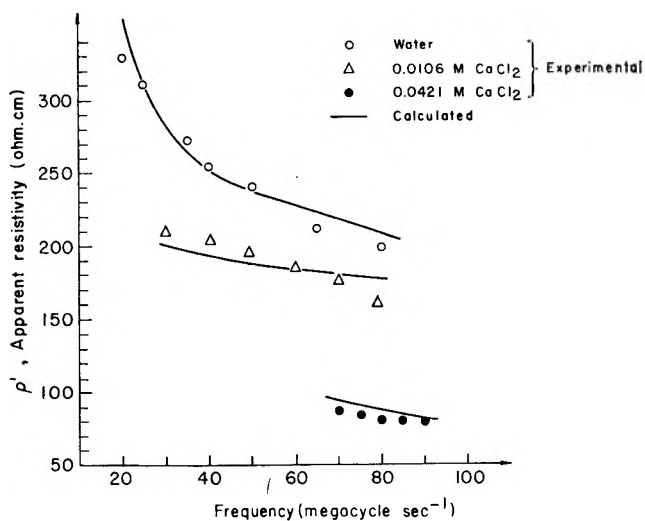
Figure 6. Apparent specific resistances of ion-exchange resin columns saturated with different interstitial solutions.

are almost the same as those obtained in previous work with different solutions and resins of different specific conductivity.[13,14]

Since the simple model describes the conductivity data at low frequencies very well, an attempt was made to explain quantitatively the frequency dependence of the dielectric constant and the conductivity of the same resin–solution systems at high frequencies.

When alternating current passes through parallel layers of resin and solution in series (element 1, Fig. 7B), alternating charge accumulation occurs at the interfaces of the two media, because their dielectric

(22) M. Kimura, Kagaku Kogaku, 21, 472 (1957).
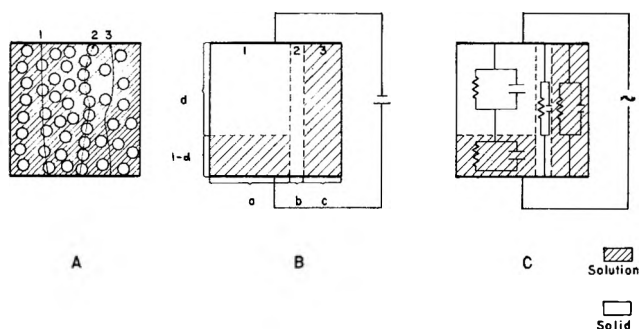
Figure 7. Model of porous plug: A, schematic representation of current path through plug. (1) Represents current through solution and spheres in series, (2) through spheres in contact with each other, (3) current through solution. B: simplified model for d.c. conductance, representing situation shown in A. Different zones represent separate resistors of dimensions shown. $a + b + c = 1$ cm. C: Extension of same model to a.c. properties. Each zone is represented by a parallel circuit of resistor and capacitor. Impedance of each zone is determined by its dimension (equal to those shown in B) and conductivity and dielectric constant of material forming the zone. Size of cubes shown is $1 \times 1 \times 1$ cm.

constants and conductivities are not equal. This dielectric polarization phenomenon can be described in network terms by representing each of the two layers in series as a parallel circuit of condenser and resistor, the first representing the dielectric polarization, the latter the ionic current. Elements 2 and 3 are also described by parallel capacitor–resistor circuits (Fig. 7C). The impedances of these circuit elements are uniquely determined by the geometrical parameters, a, b, c, and d, as given above, and by the dielectric constants, ϵ_R, ϵ_S, and specific resistances, ρ_r, ρ_w, of resin and solution, respectively. The specific admittance, Y, of the model of Fig. 7 can be calculated by elementary network analysis[20]:

Element 1: $Y_1 = \left[\dfrac{1 - d}{ak_s + j\omega\alpha\alpha\epsilon_s} + \right.$

$$\left. \dfrac{d}{(ak_r + j\omega\alpha\alpha\epsilon_r)} \right]^{-1}$$

Element 2: $Y_2 = bk_r + j\omega ab\epsilon_r$ \hfill (7)

Element 3: $Y_3 = ck_s + j\omega c\epsilon_s$

$$Y = Y_1 + Y_2 + Y_3$$

where α is the capacitance of the unit capacitor in the vacuum, i.e., 0.0885×10^{-12} f., and Y and k are given in ohm^{-1} cm.$^{-1}$, ω is the angular frequency (sec.$^{-1}$), and $j \equiv \sqrt{-1}$. Separating imaginary and real parts, the following expressions for the apparent dielectric constant ϵ'_{theor} and the apparent specific resistance ρ'_{theor} of the model are obtained

$$\epsilon'_{theor} = \frac{a}{d(1-d)S} \left[\frac{\epsilon_r k_s^2}{1-d} + \frac{\epsilon_s k_r^2}{d} + \right.$$

$$\left. \omega^2\alpha^2 \left(\frac{\epsilon_r \epsilon_s^2}{1-d} + \frac{\epsilon_r^2 \epsilon_s}{d} \right) \right] + b\epsilon_r + c\epsilon_s \quad (8)$$

$$(\rho'_{theor})^{-1} = \frac{a}{d(1-d)S} \left[\frac{k_r k_s^2}{1-d} + \frac{k_r^2 k_s}{d} + \right.$$

$$\left. \omega^2\alpha^2 \left(\frac{\epsilon_s^2 k_r}{1-d} + \frac{\epsilon_r^2 k_s}{d} \right) \right] + bk_r + ck_s \quad (9)$$

where

$$S = \left(\frac{k_s}{1-d} + \frac{k_r}{d} \right)^2 + \omega^2\alpha^2 \left(\frac{\epsilon_s}{1-d} + \frac{\epsilon_r}{d} \right)^2 \quad (10)$$

These values are listed in Tables I–III along with the corresponding experimental values, ρ' and ϵ', determined from the measured resistances (eq. 5) and capacitances (eq. 4) after correction for line effects. In these calculations the values of the specific conductances of the interstitial fluids were determined by us in the same cell and by the same method as the measurements of the resin–solution mixtures and were found to be $k_s = 1.0 \times 10^{-6}$ mho cm.$^{-1}$ for distilled water and 0.00262 and 0.0125 mho cm.$^{-1}$ for the 0.0106 and 0.0421 M CaCl$_2$ solutions, respectively. The dielectric constant for water was taken from the work of Hasted, et al.,[21] as $\epsilon_s = 78.0$ and the dielectric constant of the dilute CaCl$_2$ solution, which is very similar, was estimated from the work of the same authors as 77.7, equal to an equimolar MgCl$_2$ solution. The dielectric constant of the more concentrated CaCl$_2$ solution was determined by us, using the same procedure as described for the resin–solution mixtures, $\epsilon_s = 75.0$. The specific conductance of the resin was taken as $k_r = 0.0075$ mho cm.$^{-1}$, as determined at 1000 c.p.s., and the dielectric constant of the resin, ϵ_r, as 38 ± 1, as determined from Fig. 5 by extrapolation of the results to high frequencies. All these values were assumed to hold over the whole frequency range of our measurements. This is merely an approximation, but since both solutions were very dilute, we believe it is justified.

The agreement between theory and results can best be judged by consideration of Fig. 5 and 6. It is seen that the theory reproduces fairly well the sharp decreases with frequency of the apparent dielectric constant and specific resistance of the resin columns in distilled water, as well as the variation of these frequency–dispersion curves with the concentration of the interstitial solution. It is of particular interest that the model explains the high values of the apparent dielectric constants found for the resin–solution systems, which are much higher than the dielectric

constants of the two separate components. The specific resistances predicted by the theory are also close to the measured values except for some discrepancies in the resin–$CaCl_2$ solutions at high frequencies. These discrepancies are perhaps due to dielectric losses in the "Plexiglas" sample holder.

The determination of the dielectric constant, ϵ_r, of the solid wet resin by extrapolation of the curves in Fig. 5 was made by means of the following formula derived from eq.[8] 8

$$\lim_{\omega \to \infty} \epsilon'_{theor} = \frac{a\left(\dfrac{\epsilon_r \epsilon_s^2}{1-d} + \dfrac{\epsilon_r^2 \epsilon_s}{d}\right)}{d(1-d)\left(\dfrac{\epsilon_s}{1-d} + \dfrac{\epsilon_r}{d}\right)^2} + b\epsilon_r - c\epsilon_s \tag{11}$$

We used the lowest curve which could most readily be extrapolated and then calculated the theoretical curves of ϵ' vs. ω for the other two cases.

It is of interest that the dielectric constant of the resin was found somewhat lower than the weighted average by volume of the dielectric constant of water (when taken as 78) and of organic matrix (when taken as about 2) in the resin as predicted by Rice and Nagasawa.[23] This finding does not imply that the dielectric constant of the wet resin is completely independent of the frequency. Solid wet resin spheres are not strictly homogeneous, but represent colloid systems with heterogeneities on the scale of tens to hundreds of Ångstrom units. Therefore, their dielectric constant, ϵ_r, and the conductivity, k_r, may be expected to depend on the frequency similar to the situ-

ation in zeolites.[24] It appears, however, that in the radiofrequency range this variation with frequency is much less than the very large effects we observed in resin–solution mixtures, which result from the macroscopic heterogeneity of these systems. As a first approximation, ion-exchange resins have indeed often been treated as single phases, and this approach explains their electrochemical properties fairly satisfactorily.[15b] If one visualizes each resin particle as homogeneous, then ion displacement throughout the particle is assumed to occur by the same mechanism. Because of the relatively large size of the particles, bulk effects overshadow surface effects.

From the present measurements no conclusions should be drawn about the exact mechanism of relaxation within the particle; our interpretation rests on the assumption that the dielectric constants and conductivities of the separate solution and resin phases are constant in the frequency range investigated. This assumption leads indeed to fair agreement between calculated and observed dielectric constants and conductivities of the plugs composed of both phases.

(23) S. A. Rice and M. Nagasawa, "Polyelectrolyte Solutions," Academic Press, Inc., New York, N. Y., 1961, p. 470.

(24) A. Lebrun, R. Libaert, J. Fontaine, and A. Risbourg, *Compt. rend.*, **256**, 5334 (1963).

NOTES

A Simple Method for Determining the Cleanliness of a Platinum Anode

by Sigmund Schuldiner and Theodore B. Warner[1a]

United States Naval Research Laboratory, Washington, D. C.
(*Received November 3, 1963*)

Pearson and Butler[1b] showed that upon anodic charging of a platinum electrode a potential region is obtained which indicates the formation of a monolayer of oxygen atoms. A linear relation is shown between time (or coulombs of charge) and voltage in this region. Subsequent work by others verified this relation. Schuldiner and Roe[2] using high current density anodic pulses showed that this oxygen atom adsorption region was between 0.88 and 1.76 v. (*vs.* n.h.e.).

Recent work at this laboratory showed that the linearity of the voltage *vs.* time relation in the atomic oxygen adsorption region could be used as a reliable index of electrode cleanliness. Using a previously reported[2] experimental technique, data, such as shown in Fig. 1, were obtained for a platinum bead electrode in 1 *M* H_2SO_4. Figure 1a shows four typical oscilloscope traces that are the result of four successive single anodic constant current (0.45 amp./cm.[2]) pulses. The bottom curve was obtained with the platinum electrode after it had been partially covered with a small amount of carbon monoxide. The preparation of an electrode with only a fraction of its surface covered with CO was done by adding a small amount of CO to the electrolyte, lowering the partial pressure of the CO to zero by bubbling pure helium through the cell, and then removing the adsorbed CO by several anodic pulses. The minute amount of CO remaining in solution would then partially cover the Pt bead before the first anodic trace was taken.

For the bottom curve in Fig. 1a, the region (Pt–O) in which oxygen atoms are formed shows a break which indicates the oxidation of CO' to CO_2. After the removal of CO, the potential rises as the electrode surface is covered with a monolayer of oxygen atoms until the upper plateau, which shows the generation of molecular oxygen. The curve immediately above (second from the bottom) was taken 80 sec. after the first trace. This curve shows no evidence of CO on the electrode since the time interval between these first two pulses was not long enough to allow adsorption of a significant amount of CO from solution. The

amount of charge transferred in the oxygen atom formation region is equivalent to a monolayer of oxygen, within experimental error, and agrees well with numerous other determinations made on clean surfaces.[2] The shape of this curve is quite characteristic of the formation of a monolayer of atomic oxygen on a clean Pt surface. Here a very linear relation between potential and time is observed in the region for the formation of a monolayer of oxygen atoms. The time to gaseous oxygen evolution is longer in the bottom curve because extra charge is required to oxidize adsorbed CO.

The third curve from the bottom in Fig. 1a was taken 8 sec. after the second pulse. Compared with the second pulse, fewer coulombs are required for the formation of the oxygen atom monolayer. This indicates that the time interval between the second and third pulses was too short to allow removal of all the adsorbed oxygen formed during the earlier pulse. The third curve is also slightly convex in the oxygen atom region. This is believed to be due to oxygen dissolved in the surface layers of the platinum which could poison the discharge reaction. These characteristics are more evident in the top curve of Fig. 1a, which was taken about 0.5 sec. after the previous pulse. Here the oxygen adsorption region is even shorter and slightly more convex. This is because ever less time elapsed between the last two pulses and thus less oxygen was spontaneously lost from the surface. Also there was a greater buildup of oxygen dissolved in the metal owing to repeated pulsing.

The four successive curves in Fig. 1a hence demonstrate that an impurity on the electrode which is oxidizable in the atomic oxygen formation region will cause a break in the linearity and an increase in the length of this region. If atomic oxygen is present on the electrode surface before the anodic sweep, it will be shown as a shortening of the atomic oxygen adsorption region which gives a convex rather than straight line relation in the same region. Substances, such as hydrogen, which are oxidized before the atomic oxygen formation potential is reached will be indicated as plateau regions at lower potentials.[2]

Another, but less reliable, test of cleanliness of the electrode consists of a determination of the double

(1) (a) National Academy of Sciences Resident Research Associate; (b) J. D. Pearson and J. A. V. Butler, *Trans. Faraday Soc.*, 34, 1163 (1938).

(2) S. Schuldiner and R. M. Roe, *J. Electrochem. Soc.*, 110, 332 (1963).
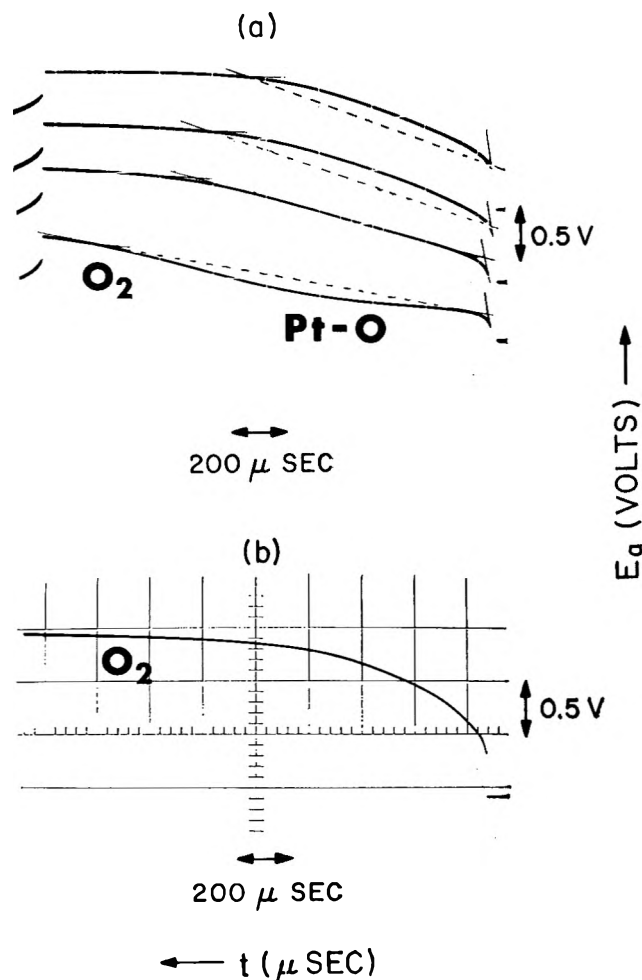
Figure 1. Typical anodic charging curves. a—reading from
bottom to top: first trace shows effect of partial coverage
of Pt electrode with CO, second trace taken 80 sec. later
shows characteristic trace of a clean electrode, third trace
taken 8 sec. later shows effects of oxygen poisoning, fourth
trace taken 0.5 sec. later shows additional oxygen poisoning
effects; b—poisoned with a nonoxidizable impurity (methane).
(The direction of the time scale is reversed from its
normal direction. Zero time is on the right-hand side
of the pulses. The time scale reads from right to left.)

layer capacitance in the sharply rising potential region
just before oxygen atoms are deposited. If a double
layer capacitance of about 40 μf./cm.[2] (on the basis
of true electrode area as defined by Schuldiner and
Roe[2]) is found, it indicates that the electrode surface
is clean. If the double layer capacitance is signifi-
cantly less than 40 μf./cm.[2], then the presence of an
impurity is indicated. If the double layer capacitance
is significantly greater than 40 μf./cm.[2], the presence
of a substance, such as hydrogen,[2] which is oxidizable
at potentials below the oxygen formation potential
is indicated.

This suggested test for surface cleanliness has an
additional benefit. As shown by Schuldiner and Roe,[2]
the length of the atomic oxygen adsorption region
can be used to define the true area of the clean platinum
electrode.

The effect of a nonoxidizable impurity on the anodic
charging curve is demonstrated in Fig. 1b. Here
methane was added to the solution. Adsorption of
this gas masked the surface so that no clear atomic
oxygen adsorption region was found. No indication
of oxidation of methane is apparent.

The importance of the test we have suggested in
kinetic investigations of the oxygen or other electrode
processes is apparent from a perusal of the literature
which shows such anodic charging curves. A careful
reading of such curves shows that the presence of
trace amounts of oxidizable impurities or of poisons
in the atomic oxygen formation region is the rule
rather than the exception. This test can undoubtedly
be extended to other noble metals.

On Kuhn's ω''-Molecular Orbital Method[1]

by A. Streitwieser, Jr., A. Heller, and M. Feldman

Department of Chemistry, University of California,
Berkeley 4, California   (Received November 9, 1963)

In several recent letters, Kuhn[2] has commented on
the ω-technique of simple molecular orbital theory[3]
and has pointed out some merits of a proposed exten-
sion. In the ω-technique, the coulomb integral, α,
of a carbon atom, r, is modified by the electron density,
q_r, according to

$$\alpha_r = \alpha_0 + (1 - q_r)\omega\beta_0 \qquad (1)$$

Kuhn comments that this procedure neglects the not
inconsiderable potential associated with neighboring
atoms and proposes what we will call herein the ω''-
technique

$$\alpha_r = \alpha_0 + (1 - q_r)\omega\beta_0 + \sum_s (1 - q_s)\omega'\beta_0 +$$

$$\sum_t (1 - q_t)\omega''\beta_0 \qquad (2)$$

(1) This research was supported by a grant from the United States
Air Force Office of Scientific Research of the Air Research and
Development Command.

(2) W. Kuhn, *Tetrahedron*, 19, Suppl. 2, 88, 389, 437 (1963).

(3) *Cf.* A. Streitwieser, Jr., "Molecular Orbital Theory for Organic
Chemists," John Wiley and Sons, Inc., New York, N. Y., 1961.

Table I: Variation of the Charge Distribution and the Dipole Moment in Azulene with Variation of ω and ω'

ω	ω'	q_2	$q_1 = q_3$	$q_9 = q_{10}$	$q_4 = q_8$	$q_5 = q_7$	q_6	μ, D. (calcd.)
0.5	0.33	−0.018	−0.147	+0.024	+0.132	−0.013	+0.121	5.0
0.5	0.5	−0.004	−0.147	−0.026	+0.145	−0.041	+0.140	4.6
1.0	0.67	0.000	−0.128	−0.021	+0.123	−0.033	+0.120	3.9
1.0	1.0	−0.009	−0.101	−0.056	+0.190	−0.137	+0.215	3.4
1.4	0.93	+0.008	−0.115	−0.021	+0.119	−0.048	+0.120	3.3
1.4	1.4	−0.265	+0.160	−0.237	+0.407	−0.440	+0.485	1.8
1.7	1.1	+0.010	−0.107	−0.021	+0.115	−0.052	+0.120	3.0
1.7	1.3	+0.003	−0.093	−0.039	+0.150	−0.105	+0.171	2.8
3.0	2.0				Divergence			

In eq. 2, the atoms s are the nearest neighbors bound to r, and t are the nearest neighbors of r once removed. By a simple electrostatic model, Kuhn suggests the values $\omega' = \omega/1.5$ and $\omega'' = \omega/2.2$, retaining the value $\omega = 1.4$.[3] Kuhn's method would allow, in effect, the incorporation of additional electron repulsion terms within the framework of the simple MO procedure and, if generally successful, would be a valuable contribution to quantum organic chemistry; consequently, we have undertaken a more extensive study of the method.

In the procedure used, the electron densities from one set of calculations are used to modify the α-values for a new iteration, the procedure being repeated until convergence or self-consistency is obtained. In such successive iterations, we found that Kuhn's ω''-technique gave convergence for allyl cation, cyclopropenyl cation, methylenecyclopropene, and tropylium cation. However, successive iterations diverged for fulvene, heptafulvene, azulene, and benzyl cation. Additional study showed that nonconvergence was associated with nonzero values for ω''; hence, the further study was made with the "ω'-technique"

$$\alpha_r = \alpha_0 + (1 - q_r)\omega\beta_0 + \sum_s (1 - q_s)\omega'\beta_0 \quad (3)$$

in which the effect is limited to nearest neighbors only.

This method gave convergence even for benzyl cation which does not converge for $\omega = 1.4$ in the simple ω-technique itself.[4] Variation of the two ω-parameters in eq. 3 showed that an increase in ω tended to lower the excess charge at various positions, whereas an increase in ω' caused stronger alternation of charges. This effect is shown in Table I in which the convergent values of electron densities are given for azulene with different assignments for ω and ω'.

On increasing ω and ω', the calculated dipole moment of azulene approaches the experimental value, 1.08 D.,[5] but the alternation of charges is far too strong at

high ω'-values. At very high ω- and ω'-values, successive iterations diverge. The "best" value for ω appears to be 1.4, the value used in the simple ω-technique, and the "best" value for ω' is about $\omega/1.5 = 0.93$ as suggested by Kuhn.[6]

In Table II, the charge densities obtained for these parameters are compared with other calculated values and with the charge distribution deduced "experimentally" from n.m.r. results.[7] The latter values must be too low, since the derived dipole moment is far too small. On the whole, the present ω'-technique gives a charge distribution more like those of "advanced MO" calculations than one gets from the HMO or ω-techniques.

The present ω'-technique has also been applied to fulvene and heptafulvene with the results summarized in Table III. Again, reasonable results are obtained; in particular, we may note that the direction of the dipole is still toward the ring in fulvene and away from the ring in heptafulvene.

The relatively successful application of the ω'-technique to nonalternant hydrocarbons suggested the further application to ionization potentials. Calculations were made for eight hydrocarbon radicals; the corresponding bonding energy differences (in units of β) between radical and cation, ΔM, fit the experimental electron impact ionization potentials, I, according to the equation

$$I = 10.13 \pm 0.51 - (1.020 \pm 0.065)\Delta M \quad \text{(e.v.)} \quad (4)$$

In the results summarized in Table IV, the standard

(4) A. Streitwieser, Jr., and P. M. Nair, *Tetrahedron*, **5**, 149 (1959).

(5) G. W. Wheland and D. E. Mann, *J. Chem. Phys.*, **17**, 264 (1949).

(6) It is interesting to note that Kuhn's ratio of 1/1.5 is similar to the ratio of coulomb repulsion integrals, $\gamma_{12}/\gamma_{11} = 0.69$, used in some SCF calculations[3]; cf. also A. Streitwieser, Jr., *J. Am. Chem. Soc.*, **82**, 4123 (1960).

(7) H. Spiesecke and W. G. Schneider, *Tetrahedron Letters*, **No. 14**, 468 (1961).

Table II: Comparison of the Charge Distribution and the Dipole Moment
Obtained by the ω'-Technique with Those Obtained by Other Methods

Method	$q_1 = q_3$	q_2	$q_4 = q_8$	$q_5 = q_7$	q_6	$q_9 = q_{10}$	μ, D.	Ref.
Experimental (n.m.r.)	−0.058	+0.023	+0.032	−0.043	+0.020	+0.048	0.11	7
Experimental	...	...	...	...	...	...	1.08	5
HMO	−0.139	−0.047	+0.145	+0.014	+0.130	−0.027	5.2	3
ω-Technique; $\omega = 1.4$	−0.118	−0.048	+0.095	+0.025	+0.084	−0.020	4.9	3
ω'-Technique; $\omega = 1.4$; $\omega' = 0.93$	−0.115	+0.008	+0.119	−0.048	+0.120	−0.021	3.3	
VESCF	−0.061	−0.021	+0.063	−0.009	+0.039	−0.009	2.3	a
Pariser–Parr	−0.096	−0.021	+0.021	+0.049	−0.052	−0.013	1.9	b
Nonempirical SCF	−0.049	+0.003	+0.092	−0.034	+0.062	−0.042	1.7	c

^{a} R. D. Brown and M. L. Heffernan, *Australian J. Chem.*, **13**, 38 (1960). ^{b} R. Pariser, *J. Chem. Phys.*, **25**, 1112 (1956). ^{c} A. Julg, *J. chim. phys.*, **52**, 377 (1955).

Table III: Charge Distribution and Dipole Moments of Fulvene and Heptafulvene

Fulvene

Method	$q_1 = q_4$	$q_2 = q_3$	q_5	q_6	μ, D.^{a}	Ref.
HMO	−0.092	−0.073	−0.047	+0.378	2.6	b
ω	−0.055	−0.029	−0.138	+0.306	2.0	c
ω'	−0.080	−0.019	+0.018	+0.181	0.9	..

Heptafulvene

Method	$q_1 = q_6$	$q_2 = q_5$	$q_3 = q_4$	q_7	q_8	μ, D.	Ref.
HMO	+0.058	+0.038	+0.047	+0.24	−0.3M	2.6	d
ω	+0.032	+0.008	+0.021	+0.094	−0.216	1.6	c
ω'	+0.060	−0.006	+0.027	−0.021	−0.142	0.9	..

^{a} Experimental value is 1.2 D (ref. 5). ^{b} A. Pullman, B. Pullman, and R. Rumpf, *Bull. soc. chim. France*, **15**, 757 (1948). ^{c} A. Streitwieser, Jr., and P. M. Nair, unpublished results. ^{d} E. D. Bergmann, E. Fischer, D. Ginsburg, Y. Hirshberg, D. Lavie, M. Manot, A. Pullman, and B. Pullman, *Bull. soc. chim. France*, **18**, 684 (1951).

Table IV: Ionization Potentials

Radical	Calcd. by eq. 4, e.v.	Obsd., e.v.
Methyl	10.13	9.95^a
Allyl	8.50	8.16^a
Pentadienyl	7.95	7.73^b
Benzyl	7.76	7.76^b
Cycloheptatrienyl	6.82	6.60^c
Diphenylmethyl	7.16	7.32^d
α-Naphthylmethyl	7.44	7.35^d
β-Naphthylmethyl	7.55	7.56^d

^{a} F. P. Lossing, K. V. Ingold, and I. H. S. Henderson, *J. Chem. Phys.*, **22**, 621 (1954). ^{b} S. B. Farmer, I. H. S. Henderson, C. A. McDowell, and F. P. Lossing, *ibid.*, **22**, 1948 (1954). ^{c} A. G. Harrison, L. R. Honnen, H. J. Dauben, Jr., and F. P. Lossing, *J. Am. Chem. Soc.*, **82**, 5593 (1960). ^{d} A. G. Harrison and F. P. Lossing, *ibid.*, **82**, 1052 (1960).

deviation of the fit, 0.17 e.v., is not quite as good as in the simple ω-technique,[8] but still represents a rather good performance. We conclude that the ω'-technique shows significant promise and further tests and applications with this method should be encouraged.

(8) A. Streitwieser, Jr., *J. Am. Chem. Soc.*, **82**, 4123 (1960).

The C–H Bond Dissociation Energy of Neopentane and Other Hydrocarbons

by J. W. Root and F. S. Rowland[1]

Department of Chemistry, University of Kansas, Lawrence, Kansas (Received November 13, 1963)

Bond dissociation energies of various chemical bonds have been obtained through numerous experimental

methods, and accurate values have been compiled for many molecules.[2,3] Our experiments with recoil tritium atoms have shown that the hot abstraction of H by reaction 1 is at least semiquantitatively dependent upon the bond dissociation energies of the C–H bonds involved.[4,5]

$$T^* + RH \longrightarrow HT + R \qquad (1)$$

The original correlation of hot HT yield with bond energy showed a substantial discrepancy[5] from the bond dissociation energy for reaction 2 as 95.5 ± 2.5 kcal./mole, measured through a photobromination procedure.[2,6,7]

$$neo\text{-}C_5H_{12} \longrightarrow H + C_5H_{11} \qquad (2)$$

A second measurement, also through the measurement of activation energies of bromination reactions, leads to the value 99.3 kcal./mole.[8,9] If the latter value is used, no appreciable discrepancy remains and the correlation between hot HT yields and bond dissociation energies is satisfactory within the errors of measurement. This correlation is shown in Fig. 1.
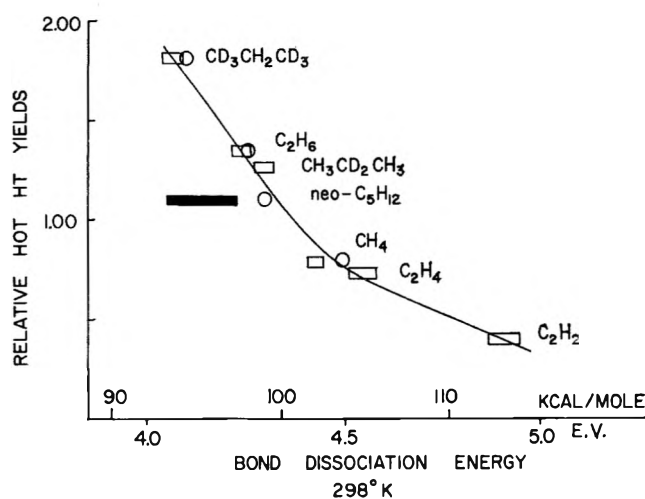
Figure 1 Correlation of hot HT yields with bond dissociation energies. HT yields from ref. 5. Bond dissociation energies: □, ref. 3; O, ref. 9; ■, ref. 6.

The measurement by Trotman-Dickenson, *et al.*, depends upon the evaluation of the activation energies of both the forward and reverse reactions of (3). The reverse reaction has, however, been estimated and not measured. If the correlation of Fig. 1 is assumed to display a valid relationship between hot HT yield and bond dissociation energy, the recoil tritium experiments confirm the accuracy of this estimate of

$$Br + RH \;\rightleftharpoons\; HBr + R \qquad (3)$$

the energetics of the reverse of reaction 3.

Further investigation of reaction 1 as a possible measure of bond dissociation energies is being carried out. If the present correlation is borne out by succeeding experiments, this approach would have the merits of ready application to a wide variety of molecular types. Interpolation of the measured HT yields for cyclopropane and cyclobutane leads to estimates of 101 and 96 kcal./mole for their respective C–H bond dissociation energies.

(1) This research has been supported by U. S. Atomic Energy Commission Contract No.-AT-(11-1)-407 and by a National Science Foundation Predoctoral Fellowship (J. W. R.).

(2) See, for example, T. Cottrell, "The Strengths of Chemical Bonds." 2nd Ed., Butterworth Publications, London, 1958.

(3) R. R. Bernecker and F. A. Long, *J. Phys. Chem.*, **65**, 1565 (1961).

(4) J. W. Root and F. S. Rowland, *J. Am. Chem. Soc.*, **85**, 1021 (1963).

(5) W. Breckenridge, J. W. Root, and F. S. Rowland, *J. Chem. Phys.*, **39**, 2374 (1963).

(6) E. I. Hormats and E. R. Van Artsdalen, *ibid.*, **19**, 778 (1951).

(7) B. H. Eckstein, H. A. Scheraga, and E. R. Van Artsdalen, *ibid.*, **22**, 28 (1954).

(8) G. C. Fettis, J. H. Knox, and A. F. Trotman-Dickenson, *J. Chem. Soc.*, 4177 (1960).

(9) G. C. Fettis and A. F. Trotman-Dickenson, *ibid.*, 3037 (1961).

Polarizability of the Closed-Cage Boron Hydride $B_{10}H_{10}^{-2}$

by Alexander Kaczmarczyk and Gerald B. Kolski[1]

Department of Chemistry, Dartmouth College, Hanover, New Hampshire (*Received November 15, 1963*)

The very large diamagnetism[2] of $B_{10}H_{10}^{-2}$ and the pseudo-aromatic chemical behavior of this ion[3] seem to indicate that the electrons on the cage are extensively delocalized. Preliminary calculations[4] suggest that the diamagnetic susceptibility would be compatible with a model in which the ten borons form a conducting sphere on which the 22 cage electrons are relatively free to move under the influence of an electric or magnetic field. The validity of such a model should also be reflected in other properties such as polarizability.

(1) National Science Foundation Undergraduate Research Assistant, summer, 1963.

(2) R. D. Dobrott and W. N. Lipscomb, *J. Chem., Phys.*, **37**, 1784 (1962); G. Eaton, A. Kaczmarczyk, and W. N. Lipscomb, unpublished results.

(3) W. H. Knoth, H. C. Miller, D. C. England, G. W. Parshall, and E. L. Muetterties, *J. Am. Chem. Soc.*, **84**, 1056 (1962).

(4) R. Hoffman, private communication.

Table I

Concn. of soln., M	Δn_{546} $\times 10^3$	Δn_{436} $\times 10^3$	$\Delta d \times 10^3$, g./cc.	R_{546}, cm.^{3}	R_{436}, cm.^{3}
		$K_2B_{10}H_{10}$			
0.20053	10.058	10.331	12.28	55.97	57.07
0.09827	4.958	5.090	6.41	55.37	56.43
0.06015	3.082	3.211	4.00	55.60	57.07
		$(NEt_3H)_2B_{10}H_{10}$			
0.1004	8.061	8.275	2.57	116.90	119.07
0.09958	8.074	8.256	2.47	117.18	119.16
0.04016	3.267	3.331	1.29	118.87	120.07

Is the molecular weight of the solute, and C the solute concentration in moles/l. The static polarizabilities were obtained from the relation $R_\infty = 4\pi N_A \alpha_\infty/3$, after extrapolating the values of R_{app} found at 436 and 546 mμ with the aid of the standard[6] form

$$R^{-1} = C^*(\lambda_0^{-2} - \lambda^{-2}) \qquad (2)$$

in which C^* and λ_0 are constants for a given species. The salts of $B_{10}H_{10}^{-2}$ exhibit no absorption bands between 200 and 800 mμ, so that extrapolation is justified.[6] The solution data (all for 25.0 ± 0.2°) are summarized in Table I. The extrapolated polarizabilities are shown in Table II.

Table II: The Refractive Indices and Polarizabilities

Compound or ion	n^{25}_D	d^{25}_4, g./cc.	α_D, Å.^{3} (solid salt)	α_∞, Å.^{3} (solution)
$K_2B_{10}H_{10}$ (biaxial)	$n_\alpha = 1.665$ $n_\beta = 1.667$ $n_\gamma = 1.676$	1.385 ± 0.005^a	21.0 ± 0.1	21.3 ± 0.1
$(NEt_3H)_2B_{10}H_{10}$ (biaxial)	$n_\alpha = 1.546$ $n_\beta = \ldots$ $n_\gamma = 1.582$	0.919 ± 0.003^a	45.4 ± 0.5	45.4 ± 0.1
K^+	$\ldots$	$\ldots$	1.33^b	1.20
NEt_3H^+	$\ldots$	$\ldots$	13.1 ± 0.1^c	12.8 ± 0.1
$B_{10}H_{10}^{-2}$		Average	18.8 ± 0.3	19.3 ± 0.1

^{a} Determined by the float method. ^{b} J. R. Tessman and A. H. Kahn, *Phys. Rev.*, **92**, 890 (1953). ^{c} Extrapolated from refractive index data for NEt_3 in J. Timmermans, "Physico-Chemical Constants of Pure Organic Compounds," Elsevier Publ. Co., Amsterdam, 1950, p. 524, and corrected for the addition of H^+ by the same amount as NH_4^+ *vs*. NH_3.

That the polarizability is indeed very large, as would be expected from the proposed model, has now been verified experimentally.

Since the two salts easiest to prepare and purify are $K_2B_{10}H_{10}$ and $(NEt_3H)_2B_{10}H_{10}$, aqueous solutions of these salts were made up and used in this study. The refractive index increments of several solutions in the 0.2–0.04 M concentration range were determined at 436 and 546 mμ with a Brice-Phoenix differential refractometer. The densities of every solution and of the water used here were determined individually with a Weld pycnometer. The refractive indices and the density differences were used to calculate the apparent molar refractions from the Lorenz–Lorentz equation for binary systems in the form[5]

$$R_{app} = \phi_0(\Phi + \Pi) \qquad (1)$$

where $\phi = (n^2 - 1)/(n^2 + 2)$; $\Phi = [M_1 - 1000C^{-1}\cdot(d - d_0)]/d_0$; and $\Pi = 1000(\phi - \phi_0)/\phi_0 C$. In these equations, the subscript zero denotes a property of the pure solvent, n is refractive index, d is density, M_1

As an independent check the refractive indices of solid $K_2B_{10}H_{10}$ and $(NEt_5H)_2B_{10}H_{10}$ were determined by the liquid immersion method with a petrographic microscope, and the results are summarized in Table II. The geometric average of the refractive indices was used in calculating α_D.

Considering that the crystals are optically anisotropic, and hence that the Lorentz factor is not strictly $4\pi/3$, that the crystal data are restricted to a single wave length (Na D-line), and that the ions in solution are in a different environment, one could hardly wish better agreement.

The refractive indices of $(NEt_3H)_2B_{20}H_{18}$ were also determined: $n_\alpha = 1.600$, $n_\beta = 1.606$, $n_\gamma = 1.710$; combined with the crystallographic density[7] they yield $\alpha_D = 66.1$ Å.^{3}. Subtracting the contributions of the NEt_3H^+ we obtain for the ion $B_{20}H_{18}^{-2}$ a polariz-

(5) W. Geffcken, *Z. physik. Chem.*, **B5**, 81 (1929).

(6) P. Wulff, *ibid.*, **B21**, 370 (1933); N. Bauer and K. Fajans, *J. Am. Chem. Soc.*, **64**, 3023 (1942).

ability of 39.9 Å.[3]. This figure is close to twice that for $B_{10}H_{10}^{-2}$, in agreement with its structure[7] of two linked B_{10} cages. It is interesting to note that the molar diamagnetic susceptibility of $B_{20}H_{18}^{-2}$ is also very close to double that of $B_{10}H_{10}^{-2}$ (-258×10^{-6} and -132×10^{-6} cm.[3] mole^{-1}, respectively).[8]

The only ionic boron hydrides whose polarizabilities are reported in the literature[9] are the alkali salts of BH_4^-, which yield an average value of 3.94 ± 0.07 Å.[3] for the anion, or 0.99 Å.[3] per B–H bond.

To estimate the polarizability of the cage proper, we subtract the contribution of the ten electron-pair covalent B–H bonds from the total value for $B_{10}H_{10}^{-2}$ and obtain 8.9 Å.[3]. Since the polarizability of a rigid conducting sphere is equal to the cube of its radius, a polarizability of 8.9 Å.[3] corresponds to an apparent radius of 2.07 Å. for the model mentioned earlier. The apical borons in $B_{10}H_{10}^{-2}$ (which is not strictly spherical) are 3.61 Å. apart,[2] which compares favorably with the apparent diameter of our hypothetical sphere. Better agreement might have been obtained if one allowed for the asymmetry of the cage, corrected for the electron correlations, and somehow determined the correct contribution from the B–H bonds in $B_{10}H_{10}^{-2}$. It should be pointed out that the B–H bonds in $B_{10}H_{10}^{-2}$ are much less hydridic than those in BH_4^- and also that the effects of a -2 charge are distributed over ten such bonds.

Work is currently in progress on a number of halogenated $B_{10}H_{10}^{-2}$ and $B_{12}H_{12}^{-2}$ salts and other closed-cage hydrides.

Acknowledgments. The authors thank Professor W. H. Stockmayer for valuable suggestions and Professor R. E. Stoiber for the determination of the refractive indices of the solids.

(7) A. Kaczmarczyk, R. Dobrott, W. N. Lipscomb, *Proc. Natl. Acad. Sci.*, **48**, 729 (1962).

(8) S. Shulman and W. N. Lipscomb, private communication.

(9) W. H. Stockmayer, D. W. Rice, and C. C. Stephenson, *J. Am. Chem. Soc.*, **77**, 1980 (1955).

Electron Spin Resonance Study of X-Ray Irradiated, Oriented Polypropylene

by Ramdas P. Gupta[1]

Institut für Electrowerkstoffe, Freiburg im Breisgau, Germany
(*Received March 6, 1963*)

Paramagnetic resonance investigation on stretched polypropylene, irradiated by X-rays, has been performed to study the effect of stretching on molecular orientation. The effect of radiation on polypropylene has been studied by the e.p.r. method in this as well as in other laboratories,[2-18] using different sources of irradiation, but so far, little information has been gathered about peroxy radical orientation which is formed by the reaction of atmospheric oxygen. The object of the present investigation, therefore, has been to get some information about the angular orientation of the peroxy radical formed by irradiating a stretched specimen of polypropylene by a weak X-ray source and then exposing it to atmospheric air.

Experimental

Investigation of electron spin resonance in a polypropylene specimen has been performed using a Varian spectrometer, Model V-4500 (x-band 100-kc. modulation) with a 15-cm. electromagnet. Measurements have been done at room temperature. Samples of polypropylene were stretched in the form of thread and then irradiated by a weak X-ray source to 0.5×10^6 r. A few pieces of irradiated polypropylene thread were put in a quartz tube, axially parallel to each other. The quartz tube containing the polypropylene thread was mounted on the crystal holder, which was properly fitted in the radiofrequency cavity. The e.p.r. derivative line shapes were registered for several angular orientations of the specimen in the magnetic field. The experiment was performed after

(1) The Royal Institute of Technology (Physical Chemistry), Stockholm, Sweden.

(2) A. A. Millor, *J. Phys. Chem.*, **63**, 1755 (1959).

(3) S. Ohnishi, Y. Ikeda, S. Sugimoti, and I. Nitta, *J. Polymer Sci.*, **47**, 503 (1960).

(4) B. R. Loy, *ibid.*, **44**, 341 (1960); **50**, 245 (1960).

(5) E. J. Lawton, J. S. Balwit, and R. S. Powell, *ibid.*, **32**, 257 (1958).

(6) H. Fischer and K. H. Hellwage, *ibid.*, **56**, 33 (1962).

(7) E. Libby, M. G. Ormerod, and A. Charlesby, *Polymer*, **1**, 212 (1960).

(8) S. Ohnishi, Y. Ikeda, M. Kashiwagi, and I. Nitta, *ibid.*, **2**, 219 (1961).

(9) W. Gordy, I. Miyagawa, N. Watabe, and K. M. Wilbur, *Proc. Natl. Acad. Sci. U. S.*, **44**, 613 (1958).

(10) R. H. Sands, *Phys. Rev.*, **99**, 1222 (1955).

(11) B. Bleaney, *Proc. Phys. Soc.* (London), **A63**, 407 (1950).

(12) J. W. Searl, R. C. Smith, and S. J. Wyard, *ibid.*, **74**, 491 (1959).

(13) W. Low, *Solid State Phys. Suppl.* **2**, 12 (1960).

(14) R. P. Gupta, *J. Phys. Chem.*, **66**, 849 (1962).

(15) M. Nisenoff and H. Y. Fan, *Phys. Rev.*, **128**, 1605 (1962).

(16) R. J. Abraham and D. H. Whiffen, *Trans. Faraday Soc.*, **54**, 1291 (1958).

(17) S. Ohnishi, S. Sugimoto, and I. Nitta, *J. Chem. Phys.*, **37**, 1283 (1962).

(18) E. Libby and M. G. Ormerod, *J. Phys. Chem. Solids*, **18**, 316 (1961).
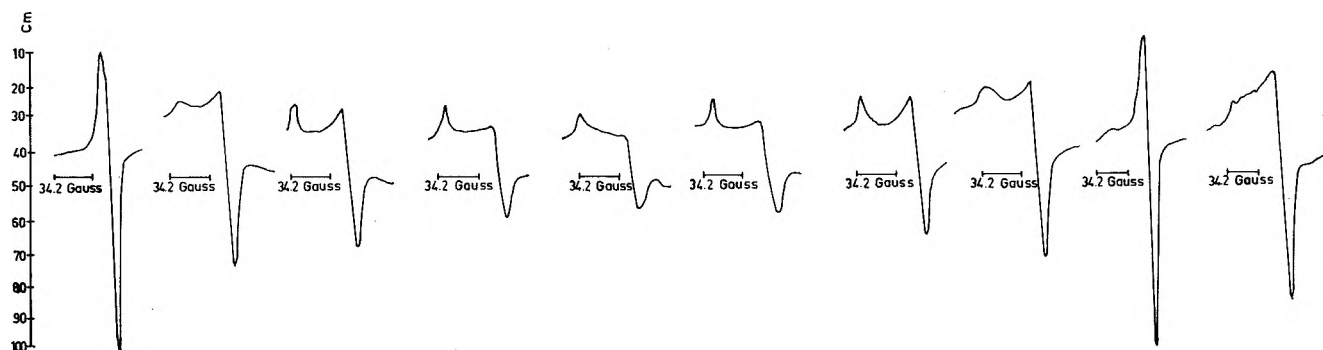
Figure 1. Electron paramagnetic resonance line shape for stretched polypropylene, having draw-axis orientation 0, 22, 45, 67, 90, 112, 135, 157, 180, and 187°, respectively, with magnetic field. The angular alignment has an error of ±3°.

every 24-hr. interval and when the line shape became stable after about 2 days, it was registered. The determination of the magnetic field and calibration of the sweep field were done using DPPH and Mn specimens. The signal level, sweep amplitude, and gain have been kept constant for relative intensity comparison. The error in angular adjustment is about ±3°. The sample was rotated in the magnetic field and a better angular adjustment could not be achieved; this is why the line shapes corresponding to 0 and 180° are not exactly similar.

Results and Discussion

Figure 1 shows the e.s.r. line shapes for stretched polypropylene irradiated to 0.5 × 10⁶ r. by weak X-rays. The above line shapes were taken several days after the samples were irradiated and correspond, respectively, to different angular orientations of the axis of stretch with respect to the direction of the magnetic field. The line shape changes with the change in the orientation of the draw axis of the polypropylene specimen with respect to the direction of the magnetic field. The change in line intensity with orientation is quite marked. There is a symmetrical change in intensity with respect to the intensity observed at the 90° orientation. The line intensity is at a maximum for the 0° orientation and decreases continuously as the orientation angle increases, until 90°, at which it is at a minimum. Then it increases again until 180°, where the intensity is at a maximum once more. This symmetry in the change of intensity about the 90° orientation is very distinct.

The g-factor variation, with the orientational direction of the draw axis with respect to the direction of the magnetic field, is shown in Table I. For the 45° orientation, there are two peaks corresponding to $g_\perp$ and $g_\parallel$ and these two peaks are equally pronounced, as

Table I

Angle between the stretched axis and the magnetic field, deg.[a]	$g\perp$	$g\parallel$
0	2.122	2.097
22	2.112	2.090
45	2.117	2.091
67	2.050	2.091
90	2.117	2.092
112	2.117	2.090
135	2.118	2.091
157	2.114	2.091
180	2.114	2.092

[a] The error in the adjustment of angle is about ±3°.

shown in Fig. 1c. For about 33° orientation of the draw axis, the peak due to $g_\parallel$ decreases and at the same time the peak due to $g_\perp$ increases. For an orientation of 22°, there is a further increase in $g_\perp$ intensity and a decrease in the intensity of the $g_\parallel$ component. Corresponding to 90° axial orientation, we observe only one distinct peak which appears due to the parallel component of g. From the line shape corresponding to 22 and 112° axial orientation, it is obvious that the intensity for $g_\perp$ in the first case is higher and for $g_\parallel$ it is lower, whereas in the second case (for a 112° orientation) the intensity for the peak due to $g_\parallel$ is higher and for the peak due to $g_\perp$ is lower.

To e.s.r. line shape was reproducible for several days except for decay in the spectral intensity due to lapse of time, but the nature of the line shapes was preserved. The e.s.r. spectrum observed in this case may be due to the peroxy radical, produced due to interaction of atmospheric oxygen. The mechanism of formation of the peroxy radical has been discussed by Whiffen.[16]

In view of the fact that the splitting between the lines is not due to hyperfine interaction, the spectrum may be analyzed using a simple form of the spin Hamiltonian

$$\mathcal{H} = \beta H g S \qquad (1)$$

where $S = \frac{1}{2}$, β is the Bohr magneton, and g is a tensor. The resonance condition is given by

$$h\nu = g\beta H \qquad (2)$$

By pulling the specimen in the form of thread, there is molecular orientation along the draw axis. If each ion has axial symmetry, then $g_x = g_y = g_\perp$; $g_z = g_{||}$; and $g^2 = g_{||}^2 \cos^2\theta + g_\perp^2 \sin^2\theta$, where θ is the azimuthal angle.[11]

The symmetrical variation in intensity of the spectrum due to the peroxy radical in stretched polypropylene with respect to angular orientation suggests that corresponding to the $0°$ orientation, it has the highest field and lowest center of gravity, g_1. This strongly suggests that the $-O-O$ bonds of the peroxy group are perpendicular to the draw axis. The highest g is expected to be nearly parallel to the $O-O$ bond.

Acknowledgment. The author is thankful to Prof. R. Mecke for permission to use the e.p.r. instrument.

Decarboxylation. I. Kinetic Study of the Vapor Phase Thermal Decarboxylation of 3-Butenoic Acid

by Grant Gill Smith and Sullivan E. Blau[1]

Department of Chemistry, Utah State University, Logan, Utah
(Received September 28, 1963)

Decarboxylation is an important reaction in many branches of organic chemistry, *e.g.*, synthetic organic, mechanism studies, and many life processes in both plants and animals. Most studies have been in the condensed phase under catalytic conditions. Several reviews have appeared, some very recently, dealing with the decarboxylation under acidic and basic conditions.[2] Less is known about how structural changes influence vapor phase thermal decarboxylations.

In condensed phase systems where solvent, catalysts, and other environmental conditions markedly influence the rate of the reaction it is difficult to evaluate the individual influences. A better understanding of the details of decarboxylation can be obtained through a

fundamental approach on a carefully defined system. Homogeneous vapor phase reactions provide this system. This is the first of a series of kinetic studies on the effect of structure on the ease of decarboxylation of organic acids in the vapor phase.

Experimental

Reagents. 3-Butenoic Acid. 3-Butenoic acid was prepared by hydrolyzing 67 g. (1.0 mole) of allyl cyanide (Matheson Coleman and Bell, practical grade) with 100 ml. (1.2 moles) of concentrated hydrochloric acid according to the method of Reitz.[3] The purified acid was collected at 88-90° (34 mm.), n^{19}D 1.4242. Literature values are 69-70° (12 mm.) and n^{15}D 1.4257.[4]

Cyclohexene. Cyclohexene (Matheson Coleman and Bell) was stored 3 days over sodium and distilled from sodium through a 20-in. Stedman column. After discarding a 10% forecut, cyclohexene was collected at 77.5° (645 mm.), n^{27}D 1.4441. Reported values are 81° (725 mm.) and n^{25}D 1.4441.[5]

Kinetics. 3-Butenoic acid was injected with a microsyringe and needle into a stainless steel reaction chamber as a 1:6 mole ratio solution in cyclohexene. The increase in pressure as the reaction progressed was plotted continuously on a 2-mv. strip chart recorder. The apparatus is described in detail elsewhere.[6] The temperature was constant during a run to $< \pm 0.2°$, being measured with two chromel-alumel thermocouples in series mounted in the aluminum thermostat on either side of the reaction vessel; these thermocouples were calibrated to $\pm 0.1°$ against a platinum resistance thermometer.

Homogeneity. The homogeneity of the reaction was checked by packing the reaction chamber with a stainless steel sponge (Gottschalk No. 725) which increased the surface area more than ten times while leaving the volume essentially unchanged.

Product Analysis. The products of the reaction were collected in a trap cooled in liquid nitrogen as they were removed from the reaction vessel after a run.

(1) This study is abstracted from a thesis presented to the Graduate School, Utah State University, by S. E. Blau in partial fulfillment of the requirements for the degree of M.S., Sept., 1963.

(2) (a) B. R. Brown, *Quart. Rev.* (London), **5**, 131 (1952); (b) E. M. Kosower, "Molecular Biochemistry," McGraw-Hill Book Co., New York, N. Y., 1962, p. 71; (c) L. L. Ingraham, "Biochemical Mechanisms," John Wiley & Sons, Inc., New York, N. Y., 1962, p. 58.

(3) E. Reitz, *Org. Syn.*, **24**, 96 (1944).

(4) I. M. Heilbron, "Dictionary of Organic Compounds," Vol. 4, Oxford University Press, New York, N. Y., 1953, p. 665.

(5) A. J. Streiff, J. C. Zimmerman, L. F. Soule, M. T. Butt, V. A. Sedlak, C. B. Willingham, and F. D. Rossini, *J. Res. Natl. Bur. Std.*, **41**, 357 (1948).

(6) (a) G. G. Smith and F. D. Bagley, *Rev. Sci. Instr.*, **32**, 703 (1961); (b) G. G. Smith and D. A. K. Jones, *J. Org. Chem.*, **28**, 3496 (1963).

Several 0.3 to 0.4-ml. samples of vapor were withdrawn from the trap by means of a hypodermic syringe and an 11-in. needle as the trap slowly warmed up from liquid nitrogen to Dry Ice temperature; the products were separated on a 2-m. long silica gel gas chromatograph column maintained at 241°. Identification of the products was made by comparing their retention times with CO_2 from Dry Ice and propene obtained from the phosphoric acid anhydride dehydration of isopropyl alcohol.

Results

Kinetics of the Decarboxylation of 3-Butenoic Acid. Determinations of the rates of decarboxylation of 3-butenoic acid were made at temperatures ranging from 334.6 ± 0.2° to 378.4 ± 0.2°. The rate constants for the reaction were obtained by plotting log $(E_\infty - E_t)$ against time, where E is equal to the output of the pressure transducer as plotted on the strip chart recorder and is proportional to the pressure inside the reaction chamber.

Even though product analysis by vapor phase chromatography showed only two products (CO_2 and propene) there was apparently a very slow secondary reaction (*ca.* $1/_{50}$ the rate of the decarboxylation) that caused the pressure to increase beyond that expected from the decarboxylation. For this reason E at 8 half-lives[7] (98.7%) was taken as E_∞. Where this value of E_∞ was used in determining the rate, straight lines were obtained in first-order plots through 75–90% of the reaction. The data for these determinations are shown in Table I.

The rate of the reaction at a given temperature was found to be independent of the initial pressure. This confirmed the order of the reaction indicated by the straight lines obtained in the first-order plots.

The data in Table II demonstrate that the reaction was essentially homogeneous. The surface:volume ratio was increased in excess of ten times while the ratio of the rate in the packed reaction vessel to that of the unpacked vessel was 1.20, which is considered satisfactory.[8]

The Arrhenius plot obtained by treating the data by the method of least squares gave $E_a = 39.3 \pm 1.6$ kcal./mole and $\Delta S^* = -10.2 \pm 2.5$ e.u. at 650°K.

Product Analysis. Three peaks were obtained when the products were separated in the gas chromatograph. The first peak was nitrogen which was used to flush out the reaction chamber. The retention times of the other two peaks corresponded to the retention times of known samples of CO_2 and propene. The retention times for the reaction products and the known compounds are shown in Table III.

Table I: Kinetic Data for the Decarboxylation of 3-Butenoic Acid

Run	Temp., °C.	$10^3/T$	$-\log k$	10^3k, sec.$^{-1}$	Av. $10^3 k$	Std. dev.
122	369.6	1.556	2.03	9.31		
123	369.6	1.556	2.06	8.78		
124	369.6	1.556	2.05	8.89	9.08	0.28
125	369.4	1.556	2.03	9.33		
128	358.8	1.582	2.23	5.85		
129	358.8	1.582	2.24	5.74	5.83	0.08
130	358.6	1.583	2.23	5.90		
132	348.6	1.609	2.45	3.53		
133	348.3	1.609	2.48	3.32		
134	347.8	1.611	2.46	3.46	3.44	0.09
135	348.0	1.610	2.46	3.46		
138	334.8	1.645	2.77	1.71		
139	334.7	1.645	2.77	1.73	1.71	0.02
140	334.2	1.646	2.77	1.69		
146	378.6	1.534	1.80	16.0		
147	378.5	1.535	1.81	15.4	15.6	0.28
148	378.5	1.535	1.81	15.5		
149	378.2	1.536	1.81	15.5		

Table II: Homogeneity of Decomposition

Run	Temp., °C.	10^3k, sec.$^{-1}$ Unpacked	Packed
216	369.6	1.01	
217	369.6	1.00	
218	369.6	0.99	
222	369.6		1.20
223	369.6		1.18
224	369.6		1.22

Table III: Retention Times of the Products of the Reaction

Compound	Retention times, min. Standards	Reaction products
N_2	0.71	0.71
CO_2	1.28	1.27
Propene	2.68	2.68

Discussion

Thermal decarboxylation of β,γ-unsaturated acids in the vapor phase proceeds smoothly to olefin and

(7) The half-life used was obtained by a method of approximation. The first approximation of the half-life was $t_{1/2}'$, at $\Delta E/2$. The second approximation was $t_{1/2}'' = E/2$ where E was taken at $8 \times t_{1/2}'$. The third approximation to E_∞ was set equal to E at $8 \times t_{1/2}''$. Further approximation did not significantly change the value of E_∞.

(8) A. Maccoll and P. J. Thomas, *J. Chem. Soc.*, 979 (1955).

carbon dioxide. It has been suggested[9] that this decomposition reaction takes place via a transition state of type I. It is significant to note, however, that this conclusion is only valid theoretically if the mechanism can be proved to be both homogeneous and unimolecular, and have a negative entropy of activation.

$$
\begin{array}{c}
\text{CH} \\
\diagup\!\!\diagdown \\
\text{CH}_2 \quad\quad \text{CH}_2 \\
\vdots \qquad\quad | \\
\text{H} \qquad\quad \text{C}\!=\!\text{O} \\
\diagdown\quad\diagup \\
\text{O}
\end{array}
\xrightarrow{\text{heat}} \text{CH}_3\!-\!\text{CH}\!=\!\text{CH}_2 + \text{CO}_2 \quad (1)
$$

I
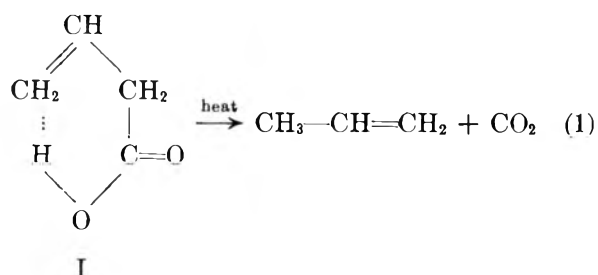
This study clearly demonstrates that the thermal decomposition of 3-butenoic acid follows first-order kinetics and that the rate constants are independent of the initial pressure and are essentially independent of the volume to surface ratio. The products of the reaction, as measured by gas phase chromatography, are propene and carbon dioxide, and the rate of their formation shows no inductive periods. These facts are adequate to exclude radical or radical-chain mechanism and to establish that the reaction is a true homogeneous, unimolecular reaction which proceeds with a negative entropy of activation (-10.2 e.u.). These data provide the strongest support for the cyclic transition state mechanism (I) for this decarboxylation suggested by Arnold, et al.,[9] who have suggested that α,β-unsaturated acids first rearrange to β,γ-unsaturated acids before decarboxylating. A number of reactions have been reported which give products consistent with this mechanism.[10] Preliminary studies show that the isomer of 3-butenoic acid, crotonic acid, pyrolyzes at a much slower rate than 3-butenoic acid. A determination of the rate of decarboxylation of crotonic acid will be, therefore, a measure of the rearrangement of crotonic acid to 3-butenoic acid.

A similar mechanism has been proposed for the condensed phase decarboxylation of a number of alkylidene malonic acid derivatives in pyridine.[11] It was proposed that the α,β-unsaturated acids tautomerize to the β,γ isomer which subsequently loses carbon dioxide as the anion (eq. 2). The rates of decarboxylation of the β,γ acids are found to be faster than their α,β isomers.

The thermal decarboxylation of 3-hexendioic acid (eq. 3) has been recently reported,[12] and, though no kinetic studies were made, the mechanism

$$
\begin{array}{c}
\text{CH}_3 \quad\quad \text{COOH} \\
\diagdown\quad\diagup \\
\text{C}\!=\!\text{C} \\
\diagup\quad\diagdown \\
\text{CH}_3 \quad\quad \text{COOEt}
\end{array}
\xrightarrow{\text{C}_5\text{H}_5\text{N}}
\begin{array}{c}
\text{O} \\
\| \\
\text{CH}_2 \quad\quad \text{C}\!-\!\text{O}^- \\
\diagdown\!\!\diagup \\
\text{C}\!-\!\text{CH} \\
\diagup\quad\diagdown \\
\text{CH}_3 \quad\quad \text{COOEt}
\end{array}
$$

$$\downarrow -\text{CO}_2$$

$$
\begin{array}{c}
\text{CH}_2 \\
\diagdown\!\!\diagup \\
\text{C}\!-\!\text{CH}_2\!-\!\text{COOEt} \\
\diagup \\
\text{CH}_3
\end{array}
\xleftarrow{\text{H}^+}
\begin{array}{c}
\text{CH}_2 \\
\diagdown\!\!\diagup \\
\text{C}\!-\!\text{CH} \\
\diagup\quad\diagdown \\
\text{CH}_3 \quad\quad \text{COOEt}
\end{array}
\quad (2)
$$

$$\swarrow \text{H}^+$$

$$
\begin{array}{c}
\text{CH}_3 \\
\diagdown \\
\text{C}\!=\!\text{CH}\!-\!\text{COOEt} \\
\diagup \\
\text{CH}_3
\end{array}
$$
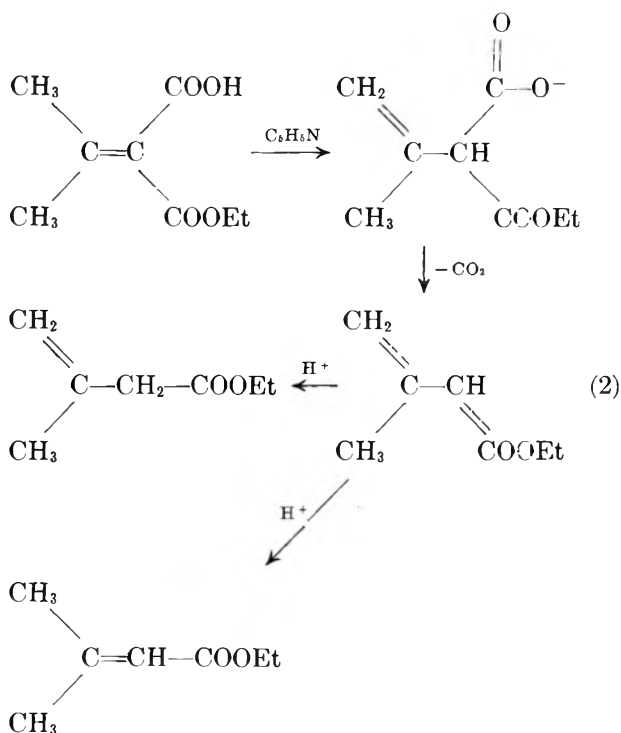
suggested by the investigators is a two-step process equivalent to the one-step process proposed by Arnold, et al.[9]
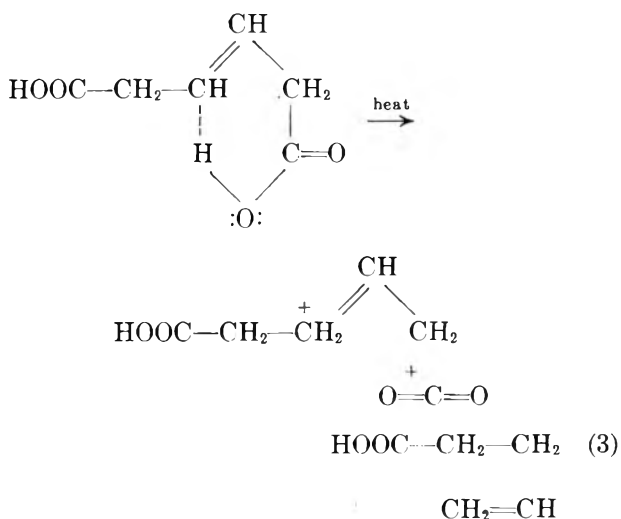
$$
\text{HOOC}\!-\!\text{CH}_2\!-\!
\begin{array}{c}
\text{CH} \\
\diagup\!\!\diagdown \\
\text{CH} \quad\quad \text{CH}_2 \\
| \qquad\quad | \\
\text{H} \qquad\quad \text{C}\!=\!\text{O} \\
\diagdown\quad\diagup \\
:\text{O}:
\end{array}
\xrightarrow{\text{heat}}
$$

$$
\text{HOOC}\!-\!\text{CH}_2\!-\!\overset{+}{\text{CH}_2}
\begin{array}{c}
\text{CH} \\
\diagup\!\!\diagdown \\
\quad\quad \text{CH}_2 \\
\\
\overset{+}{\text{O}}\!=\!\text{C}\!=\!\text{O}
\end{array}
$$

$$\text{HOOC}\!-\!\text{CH}_2\!-\!\text{CH}_2 \quad (3)$$

$$\text{CH}_2\!=\!\text{CH}$$

(9) R. T. Arnold, O. C. Elmer, and R. M. Dodson, J. Am. Chem. Soc., 72, 4359 (1950).

(10) (a) R. T. Arnold and M. J. Danzig, ibid., 79, 892 (1957); (b) E. E. Blaise and A. Courtot, Compt. rend., 139, 292 (1904); (c) O. Wallach, Ann., 353, 304 (1907); (d) O. Wallach, ibid., 360, 68 (1908); (e) W. J. le Noble and P. J. Crean, J. Org. Chem., 27, 3875 (1962).

(11) E. J. Corey, J. Am. Chem. Soc., 74, 5897 (1952); 75, 1163 (1953).

(12) F. Bennington and R. D. Morin, J. Org. Chem., 26, 5210 (1961).

ministered by the American Chemical Society, and to the Utah State University Division of University Research for partial support of this research.

Isotope Exchange in Gaseous Nitrogen under X-Ray and Cobalt-60 γ-Irradiation

by M. Anbar and P. Perlstein

The Weizmann Institute of Science and the Soreq Research Establishment, Rehovoth, Israel (Received October 3, 1963)

The radiolytically induced isotopic exchange reaction between $N_2^{14,14}$ and $N_2^{15,15}$ was investigated by Klein and Hörl,[1] who irradiated solid $N_2^{14,14}$–$N_2^{15,15}$ mixtures at 4.2 and 20°K. with 15–20 kev. electrons. An isotopic exchange was observed with a low G value ($G_{N_2}^{14,15} = 0.1$–0.3). On the other hand, nitrogen atoms (active nitrogen) produced in a condensed discharge were found not to undergo any isotopic exchange with nitrogen molecules in the gas phase.[2]

We have found that nitrogen undergoes isotopic exchange in the gas phase under radiolytic conditions. The present work was undertaken to study this isotopic exchange reaction and possibly to elucidate its mechanism.

Experimental

Radiation Sources. X-Ray irradiations were performed with a Picker Vanguard X-ray unit, with a Machlett EG-302 tube. The tube was operated at 280 KVP with a current of 20 ma. The γ-irradiations were performed with a 3.5-kc. cobalt-60 source (in a Gammacell 200 produced by The Atomic Energy of Canada Ltd.) with a dose rate of 5.75×10^5 rads/hr.

Irradiation Vessels. All the vessels were made of Pyrex glass with break-off tips. The vessels were washed with hot concentrated nitric acid and then with triple-distilled water. Then they were outbaked in a vacuum oven at 140°. Finally they were outgassed on a vacuum line at 500°. Silica wool-filled irradiation vessels were treated alike and the outgassing was rechecked by successive pressure determinations, until no gas could be desorbed from the silica.

The volume of the vessels was approximately 12 cc.; the walls were of 1.5–2 mm. thickness. Spherical irradiation vessels were used in the X-ray irradiations and vessels of cylindrical shape were irradiated in the Co^{60} γ-experiments.

Materials. The nitrogen-15 was obtained from Isomet Corp., Palisades Park, N. J., with a stated N^{15} content of 95.5 and 97.4%, which was confirmed by us. Normal nitrogen as well as oxygen and hydrogen were AirCo research grade reagents. All gases were passed through traps immersed in suitable freezing mixtures to remove any condensable impurities eventually present.

Dosimetry. The nitrous oxide system was used for the determination of the absorbed dose. A value of 12 for G_{-N_2O} was adopted for the dose calculations[3]; the proportions between $N_2:O_2:NO_2$ formed were taken as $1:0.14:0.48$. The pressure of products, noncondensable in liquid nitrogen, was measured after irradiating N_2O in the same vessels.

Procedure. The preparation of gas mixtures as well as the filling of the irradiation vessels were performed on a vacuum line at 10^{-5} mm. The filling was carried out using a manifold on which up to eight irradiation vessels could be simultaneously filled by means of a Toepler pump and then sealed off. The filling pressures were determined by means of a mercury manometer. A special cold trap was attached to the filling manifold and held in a CO_2–acetone bath ($-78°$) to remove mercury vapor originating from the Toepler pump and from the manometer.

One of the mixtures was prepared in the presence of a sodium mirror condensed on the walls of the vessel to assure the elimination of any trace of oxygen. The vessel was first flushed with pure nitrogen to remove any hydrogen which might have been formed from the reaction between sodium and traces of water absorbed on the walls.

The composition of the mixtures was in most experiments approximately $1:1$ $N_2^{14,14}/N_2^{15,15}$. The initial amount of "scrambled" nitrogen, $N_2^{14,15}$, was between 2.3 and 4.2%.

In the X-ray irradiations, the dose rates applied were 0.64×10^6 rads/hr., 2.5×10^6 rads/hr., and most runs were carried out at 6.23×10^6 rads/hr. The total doses varied between 1.16×10^7 rads and 1.25×10^8 rads.

In the γ-irradiations, the dose rate measured was 5.75×10^5 rads/hr. and the total doses varied from 1.84×10^7 rads to 1.06×10^8 rads.

The temperature in the Co^{60} γ-irradiations was 33° while in the X-ray irradiations it was 25° initially, but it rose to about 60° for the high dose rate experiments.

Analysis. Analyses were performed with a CEC

(1) R. Klein and E. M. Hörl, *J. Chem. Phys.*, **32**, 307 (1960).

(2) R. A. Back and J. Y. P. Mui, *J. Phys. Chem.*, **66**, 1362 (1962).

(3) P. Harteck and S. Dondes, *Nucleonics*, **14**, 66 (1956).

21-401 analytical mass spectrometer. The masses 28 ($N_2^{14,14}$), 29 ($N_2^{14,15}$), and 30 ($N_2^{15,15}$) were measured as well as masses 32 (O_2) and 40 (Ar) to check on possible contamination.

From the measured peaks the ratio

$$R = \frac{N_2^{14,15}}{N_2^{14,14} + N_2^{15,15}}$$

was calculated.

The stoichiometry of the isotopic exchange is given by the equation

$$aN_2^{15,15} + bN_2^{14,14} + x_0 N_2^{14,15} + cA \longrightarrow$$

$$\left(a - \frac{x_t}{2}\right) N_2^{15,15} + \left(b - \frac{x_t}{2}\right) N_2^{14,14} +$$

$$(x_t + x_0)N_2^{14,15} + cA$$
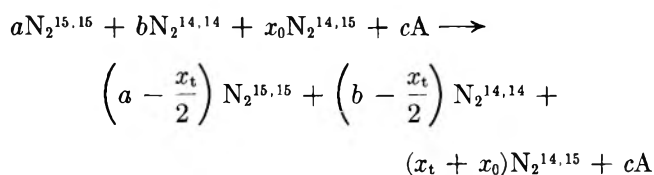
$$R_0 = \frac{x_0}{a + b}$$

$$R_t = \frac{x_t + x_0}{a + b - x_t}$$

If it is assumed that no energy is transferred from the additive A to nitrogen, the experimentally observed G value for the exchange reaction is

$$G_{N_2^{14,15}}^{obsd} = (a + b) \frac{R_t - R_0}{1 + R_t} \frac{100N}{(a + b + x_0)dW}$$

where R_0 and R_t are defined above; a, b, and x_0 are moles of $N_2^{15,15}$, $N_2^{14,14}$, and $N_2^{14,15}$ in the initial mixture; x_t = moles of $N_2^{14,15}$ formed by the radiolytic exchange; N = Avogadro's number; d = total dose absorbed in e.v./g.; and W = the molecular weight of nitrogen.

If complete energy transfer from the additive to nitrogen is assumed, $G_{N_2^{14,15}}^{obsd}$ should be corrected accordingly. In order to get from the observed G value of "scrambled" nitrogen ($G_{N_2^{14,15}}^{obsd}$) the real G value of exchange including all nitrogen molecules which have undergone reaction, including those reacting with an isotopically identical species ($N^{14} + N^{14}$, $N^{14} + N_2^{14,14}$, $N^{15} + N^{15}$, $N^{15} + N_2^{15,15}$), the following formula was derived. If $N_2^{14,14}/N_2^{15,15} = y$ ($y > 1$), then the ratio, for a large number of molecules, is

total number of molecules that have undergone exchange

number of molecules that have undergone scrambling

$$= \frac{(y + 1)^2}{2y}$$

and the corrected G value becomes

$$G_{exch} = G_{N_2^{14,15}}^{obsd} \frac{(y + 1)^2}{2y}$$

Obviously this formula is applicable for $N_2^{15,15} > N_2^{14,14}$ with $y = N_2^{15,15}/N_2^{14,14}$.

Results and Discussion

The radiolytically induced isotopic exchange between $N_2^{14,14}$ and $N_2^{15,15}$ has been carried out at different dose rates, pressures, and sources of radiation. The results are given in Table I. It has been found that the radiolytic yield of exchange is independent

Table I: Radiolytically Induced $N_2^{14,14}$-$N_2^{15,15}$ Exchange[a]

Pressure, mm.	Dose rate, rads/hr. × 10⁶	Dose, rads × 10⁷	R_0 × 10³	R_t × 10³	$G_{exch.}$	Remarks
440	0.575	5.05	44.10	48.75	9.6	γ-rays
200	6.23	2.49	44.5	48.25	9.5	X-rays
200	6.23	3.74	44.5	49.95	9.1	X-rays
200	6.23	4.98	49.5	52.05	9.5	X-rays
200[b]	6.23	6.23	44.5	53.89	9.5	X-rays
200	6.23	7.48	44.5	55.94	9.5	X-rays
200	6.23	9.38	44.5	59.77	10.1	X-rays
200	6.23	12.45	44.5	63.45	9.5	X-rays
200	0.64	1.16	44.73	46.51	9.6	X-rays
200	2.5	1.51	44.73	47.01	9.5	X-rays
200	0.575	2.68	44.04	48.15	9.6	γ-rays
200	0.575	5.25	44.04	51.78	9.1	γ-rays
200	0.575	6.81	44.04	54.31	9.3	γ-rays
200	0.575	9.48	44.04	58.64	9.5	γ-rays
200	0.575	10.6	44.04	60.29	9.5	γ-rays
200[c]	0.575	5.05	44.10	46.37	6.7	γ-rays
100	0.575	5.05	44.10	48.61	9.5	γ-rays
33.0	0.575	5.05	44.10	49.82	11.1	γ-rays

[a] $N_2^{14,14}$:$N_2^{15,15} = 1$. [b] Sodium mirror experiment. [c] Silica wool added.

of pressure from 440 to 100 mm.; $G_{exch} = 9.5 \pm 0.25$. The G value was found independent of dose rate between 5.75×10^5 and 6.23×10^6 rads/hr. and was equal for X-rays and Co^{60} γ-rays. As has been stated in the Experimental section, the X-ray irradiations were carried out at about 60° and the Co^{60} irradiations at 33°; this means that the G value found shows little temperature dependence in the given range of temperatures. A certain wall effect has been demonstrated as may be seen from the effect of added silica wool (350 mg.) to the irradiated gas. In this case, a decrease to $G_{exch} = 6.7$ has been observed.

The independence of G_{exch} on dose rate and pressure, in the measured range, excludes the existence of an isotopic exchange by a chain mechanism via N_3, in analogy to the O_2–O_2 exchange.[4] Further, it is improbable, in view of these findings, that any bimolecular process between two reactive species takes place.

It has to be concluded that the mechanism of exchange involves reactive species formed under radiolysis which do not react with each other and which do not act as chain carriers. The experimental results may be interpreted in terms of the following mechanism.

It is suggested that the primary species formed is nitrogen in an excited state (N_2^*) at a level of excitation higher than its dissociation energy (7.35 e.v.)[5] yet lower than its ionization potential (15.59 e.v.).[6] Such excited states were observed by spectroscopy at around 14.5 and 12.5 e.v. and at lower energies down to 8.5 e.v.[7,8]

$$N_2 \xrightarrow{\quad} N_2^+ + e^- \longrightarrow N_2^* \qquad (1)$$

$$N_2 \xrightarrow{\quad} N_2^* \qquad (2)$$
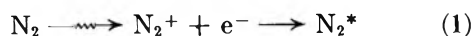
The first isotope exchange mechanism to be considered is by reaction 3

$$N_2^* + N_2 \longrightarrow 2N_2^x \qquad (3)$$

where N_2^x denotes isotopically exchanged molecules $N_2^{15,15} + N_2^{14,14} \rightarrow 2N_2^{14,15} = 2N_2^x$.

This reaction is conceivable, as far as energetic requirements are concerned,[9] for excited states of nitrogen molecules starting from ^3E_u (6.18 e.v.).[7] This mechanism is, however, rather unlikely in view of the finding that no nitrogen isotopic exchange is induced by nitrogen atoms and excited nitrogen molecules formed by condensed discharge.[2]

N_2^* may, however, undergo dissociation to nitrogen atoms on collision with a N_2 molecule

$$N_2^* + N_2 \longrightarrow N_2 + 2N \qquad (4)$$
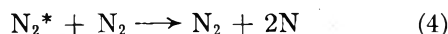
The nitrogen atoms formed will be at their ground state ^4S. Nitrogen atoms at their ground state (active nitrogen)[8] were shown not to undergo isotopic exchange with nitrogen molecules[2]

$$N + N_2 \xrightarrow{\quad/\quad} N + N_2^x \qquad (5)$$
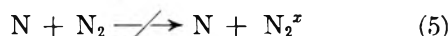
thus the exchange may proceed only by recombination of nitrogen atoms

$$N + N + (M) \longrightarrow N_2^x + (M) \qquad (6)$$
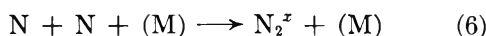
The effect of surfaces is to quench N_2^*

$$N_2^* + (W) \longrightarrow N_2 + (W) \qquad (7)$$
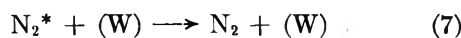
which explains the effect of silica wool on G_{exch}. At pressures over 100 mm., the walls of the irradiation vessels used had no appreciable effect on G_{exch} as no change was observed with change of pressure. The G value obtained for the isotopic exchange $G_{exch} = 9.2$ is not far from the values obtained in the decomposition of CO_2 ($G = 8.5$)[10] or N_2O ($G = 12$).[3] It is, however, surprising to get such a high G value for a decomposition of a stable molecule like N_2. This high G value implies that reaction 1, namely the ionization of N_2 to N_2^+, $G_{N_2^+} = 2.88$ (calculated from $W_{N_2} = 34.7$ e.v.),[11] contributes only about one third of the dissociated N_2 molecules. The energy left for excitation amounts to 55%, which gives for reaction 2 an average energy of excitation of 8.7 e.v. This is still sufficient to induce the dissociation of a nitrogen molecule to nitrogen atoms at their ground state.

Certain gases were added to the isotopic nitrogen mixture including oxygen and hydrogen. The results are summarized in Table II. It can be seen from this table that oxygen and hydrogen at small concentra-

Table II: Radiolytic $N_2^{14,14}$–$N_2^{15,15}$ Exchange in the Presence of Additives[a]

Mole % additive	Dose, rads × 10^7	R_0 × 10^3	R_t × 10^3	G_{exch}
0.5% O_2	2.26	43.15	45.32	6.1
0.5% O_2	4.15	43.15	46.99	6.0
0.5% O_2	6.3	43.15	48.87	5.8
0.5% O_2	8.4	43.15	51.04	6.0
0.5% O_2	10.45	43.15	52.87	6.0
			$G_{exch} = 6.0 \pm 0.11$	
0.5% H_2	1.84	24.03	26.17	7.6
0.5% H_2	3.03	24.03	28.00	8.4
0.5% H_2	4.46	24.03	28.96	7.3
0.5% H_2	6.02	24.03	30.50	7.0
0.5% H_2	8.45	24.03	33.45	7.3
			$G_{exch} = 7.52 \pm 0.56$	

[a] $N_2^{14,14}/N_2^{15,15} = 1:1$, pressure 200 mm., dose rate 5.75 × 10^6 rads/hr., γ-ray irradiation.

(4) R. A. Ogg, Jr., and W. T. Sutphen, *Discussions Faraday Soc.*, 17, 47 (1954).

(5) T. L. Cottrell, "The Strength of Chemical Bonds," Butterworth & Co., London, 1958.

(6) R. E. Honig, *J. Chem. Phys.*, 16, 105 (1948).

(7) R. E. Worley, *Phys. Rev.*, 64, 207 (1943).

(8) G. G. Mannella, *Chem. Rev.*, 63, 1 (1963).

(9) S. W. Benson, "The Foundations of Chemical Kinetics," Mc-Graw-Hill Book Co., New York, N. Y., 1960, p. 317.

(10) P. Harteck and S. Dondes, *J. Chem. Phys.*, 26, 1727 (1957).

(11) R. J. Weiss and W. Bernstein, *Radiation Res.*, 6, 603 (1957).

tions (0.5%) diminish the radiolytic yield of exchange from $G_{exch} = 9.5$ to 6.0 and 7.52 for O_2 and H_2, respectively. The sodium mirror experiment shows that traces of oxygen present in the nitrogen do not affect G_{exch} at all.

The effect of oxygen and hydrogen may be explained by their action as scavengers of nitrogen atoms. The possibility of reaction between O_2 or H_2 and N_2^* is excluded by their low concentration and the limited lifetime of N_2^*.

$$N + O_2 \longrightarrow NO_2 \qquad (8)$$

$$N + H_2 \longrightarrow NH_2 \qquad (9)$$
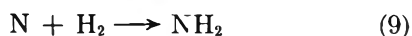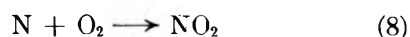
Reactions 8 and 9 compete with reaction 6, the bimolecular recombination of nitrogen atoms. From their effects on G_{exch} the specific rate of reaction 8 seems to be about twice that of reaction 9, in other words, oxygen is a superior scavenger for N atoms. Preliminary experiments with NO as scavenger showed this gas to be about twice as effective as oxygen.

The radiation-induced isotope exchange in nitrogen is the only known example of a gas phase radiolytic isotope exchange reaction which proceeds without any chemical change by a nonchain mechanism. Hydrogen–deuterium exchange is a chain process, so are also the oxygen–oxygen and the CO_2–CO_2 reactions. The latter two reactions are accompanied by the formation of radiolytic products, O_3 and $CO + O_2$, respectively. Other exchange reactions like CO–CO and NH_3–NH_3 are even more complex as far as the mechanism and radiolytic products are concerned. As the behavior of this system is predictable up to complete isotopic equilibration, it may be suitable for the dosimetry of radiation over a wide range of doses. As nitrogen-15 has a very low cross section for neutrons, mixtures of $N_2^{15,15}$ with $N_2^{14,14}$ may be used for γ-dosimetry in the presence of neutron fluxes.

Specific Rearrangements in the
Mass Spectra of Short Chain Esters

by D. R. Black, W. H. McFadden, and J. W. Corse

Western Regional Research Laboratory, Western Utilization Research and Development Division, Agricultural Research Service, U. S. Department of Agriculture, Albany, California
(*Received October 11, 1963*)

Previous studies of the mass spectral rearrangement processes of aliphatic esters have utilized both series of esters and deuterium-labeled compounds. Information concerning the proton-transfer processes has been obtained by Sharkey, *et al.*,[1] and Colomb, *et al.*,[2] from the study of the mass spectra of series of short chain esters and Beynon, *et al.*,[3] from the high resolution spectra of series of esters. McLafferty,[4] Colomb,[2] and Godbole and Kebarle[5] have used deuterated compounds to indicate the availability of the protons along the carbon chain in the transfer processes. An interesting rearrangement involving a cyclic intermediate with the resultant loss of a hydrocarbon fragment from the center of the molecular ion was detected by Ryhage and Stenhagen[6-8] and Guriev and Tikhomirov[9,10] in their studies of a series of long chain methyl esters. Subsequently Dinh-Nguyen, *et al.*,[11] using deuterated esters established that the group most frequently lost in this process originated next to the carbonyl group. However, these rearrangements are still not fully understood, and this study on selectively deuterated butyl acetates and propionates was carried out to clarify these processes.

Experimental

Sample Preparation. Synthesis and nuclear magnetic resonance (n.m.r.) analysis of 4-deuterio-1-butanol and 3-deuterio-1-butanol have been described.[12] Synthesis of 3-deuterio-1-butanol yielded 4-deuterio-2-butanol as a by-product. To obtain 1,1-dideuterio-1-butanol, the acid chloride was reduced with $LiAlD_4$.[13] To synthesize 1,1,1-trideuterio-2-butanol, CD_3I was added to magnesium and the CD_3MgI treated with propionaldehyde.[14,15]

(1) A. G. Sharkey, Jr., J. L. Shultz, and R. A. Friedel, *Anal. Chem.*, 31, 87 (1959).

(2) H. O. Colomb, B. D. Fulks, and V. A. Yarborough, 10th Annual Meeting, ASTM Committee E-14, New Orleans, La., June, 1962.

(3) J. H. Beynon, R. A. Saunders, and A. E. Williams, *Anal. Chem.*, 33, 221 (1961).

(4) F. W. McLafferty, *ibid.*, 31, 82 (1959).

(5) E. W. Godbole and P. Kebarle, *Trans. Faraday Soc.*, 58, 1897 (1962).

(6) R. Ryhage and E. Stenhagen, *Arkiv Kemi*, 15, 332 (1960).

(7) R. Ryhage and E. Stenhagen, *ibid.*, 15, 291 (1960).

(8) R. Ryhage and E. Stenhagen, *ibid.*, 13, 523 (1959).

(9) M. V. Guriev and M. V. Tikhomirov, *Zh. Fiz. Khim.*, 32, 2731 (1957).

(10) M. V. Guriev, M. V. Tikhomirov, and N. N. Tunitsky, *Dokl. Akad. Nauk SSSR*, 123, 120 (1958).

(11) N. Dinh-Nguyen, R. Ryhage, S. Stallberg-Stenhagen, and E. Stenhagen, *Arkiv Kemi*, 18, 393 (1962).

(12) W. H. McFadden, D. R. Black, and J. W. Corse, *J. Phys. Chem.*, 67, 1517 (1963).

(13) R. F. Nystrom and W. G. Brown, *J. Am. Chem. Soc.*, 69, 1197 (1947).

(14) N. L. Drake and G. B. Cooke, "Organic Syntheses," Coll. Vol. II, John Wiley and Sons, Inc., New York, N. Y., 1943, pp. 406-407.

Acetic anhydride was obtained commercially, and the acetyl and propionyl acid chlorides were made by refluxing the desired acid in phthaloyl chloride and distilling over the acid chloride.[16] High purity commercial CD_3COOD was used to prepare CD_3COCl.

All esterifications were carried out by adding an excess of either anhydride or acid chloride to the desired alcohol. The excess was subsequently hydrolyzed to the acid and then neutralized with carbonate. The ester was taken up in ether, dried, and then purified using a Carbowax 20M g.l.c. preparatory column.

Mass Spectrometry. A Bendix Time-of-Flight mass spectrometer (T.O.F.) using continuous ionization produced the mass spectra. The electron accelerating voltage was 70 e.v. Temperature was not measured in the ionization chamber but the source end of the mass spectrometer was $100 \pm 5°$.

The mass spectra obtained are presented in partial form pertaining to the rearrangement processes discussed. The complete mass spectra will be submitted to the ASTM File of Uncertified Mass Spectra.

Isotopic Purity. The isotopic purity of compounds was checked by n.m.r. and, where feasible, by mass spectra of the deuterated alcohol or ester. Only compounds whose isotopic purity was better than 95% in the labeled position are reported. No corrections were made for the isotopic impurities detected by n.m.r., and no corrections were made for natural isotopic species. In all cases the conclusions are based on observed effects that exceed any contributions from isotopic impurities.

Results and Discussion

The principal features of the mass spectra of the deuterated esters are, for the most part, those that would be predicted from previous studies of the undeuterated esters.[1,3] However, certain peaks in the former spectra, in spite of their low intensities, give new information on the rearrangement processes of these esters. One of these rearrangements is the well-known transfer of two protons from the butyl group in the formation of the $(CH_3COO + 2H)^+$ ion. Another rearrangement is the apparent loss of a CH_2O fragment from the center of the molecule with retention of the two end groups by the ion. A third rearrangement, observed with 2-butyl acetate, seems to involve an unexpected rearrangement in the formation of the apparently simple $C_4H_9O^+$ ion.

The partial spectra of the deuterated 1-butyl acetates and 1-propionates in the mass range 86-90 and 100-103 (Table I) and the partial spectra of the deuterated

Table I: Partial Mass Spectra of Deuterated 1-Butyl Acetate and 1-Butyl Propionate

	C	C	C	C	CD₃	C	C
	C=O	C=O	C=O	C=O	C=O	C=O	C=O
	O	O	O	O	O	O	O
	C	CD₂	C	C	C	C	CD₂
	C	C	C	C	C	C	C
	C	C	CD	C	C	C	C
	C	C	C	CD	C	C	C
	116	118	117	117	119	130	132

m/e	Total ionization, %						
86	0.31	0.34					
87	0.47	0.02	0.76	0.79			
88	0.05	0.02	0.08	0.07			
89		0.44	0.04	0.03	0.33		
90					0.47		
100						0.21	0.19
101						0.44	0.04
102						0.05	0.03
103							0.42

Table II: Partial Mass Spectra of Deuterated 2-Butyl Acetates

	C	C	C	C	C	CD₃
	C=O	C=O	C=O	C=O	C=O	C=O
	O	O	O	O	O	O
	C—C	C—C	C—C	CD—C	C—CD₃	C—C
	C	C	CD	C	C	C
	C	CD	C	C	C	C
	116	117	117	117	119	119

m/e	Ionᵃ	Total ionization, %					
		T.O.F.ᵇ	T.O.F.ᵇ	Mag-neticᶜ,ᵈ	Mag-neticᶜ,ᵈ	T.O.F.ᵇ	T.O.F.ᵇ
72	$C_4H_8O^+$	0.46			0.34	0.48	
73	$C_4H_9O^+$	2.55	0.43	0.34	0.16	1.60	0.77
74		0.18	2.30	1.94	1.23	0.12	0.60
75			0.14	0.15		0.12	0.47
76						1.75	1.00

ᵃ See ref. 1. ᵇ T.O.F. = Bendix Time-of-Flight mass spectrometer. ᶜ Magnetic = Consolidated Electrodynamics Corporation Type 21-103C. ᵈ F. W. McLafferty and M. C. Hamming, *Chem. Ind.* (London), **42**, 1366 (1958).

(15) J. D. Roberts, W. Bennett, R. E. McMahon, and E. W. Holroyd, Jr., *J. Am. Chem. Soc.*, **74**, 4283 (1952).

(16) J. D. Cox and H. S. Turner, *J. Chem. Soc.*, 3176 (1950).

2-butyl acetates (Table II) give evidence of these rearrangements.

Both the T.O.F. data and that obtained with the magnetic instrument (Table II) give evidence for the second rearrangement mentioned above. The ions of interest are those that result from loss of 30 m.u. from the molecular ions of the undeuterated 1-butyl esters at mass 86 and mass 100 (Table I) and the one that results from loss of 44 m.u. from the molecular ion of undeuterated 2-butyl acetate at mass 72[10] (Table II). The mass spectra of those compounds deuterated in the 3 or 4 positions of the butyl groups show that the ionization normally observed at masses 72 or 86 is absent, indicating retention of the terminal ethyl group. However, in the spectra of esters with deuterium on the C-1 of the 1-butyl group or on either the C-1 or C-2 of the 2-butyl group, no shift of the ionization is evident at masses 86 or 100 (Table I) or at mass 72 (Table II) thus indicating loss of those carbons. Furthermore, if the acetyl group is completely deuterated, a corresponding mass shift of 3 m.u. in the spectra occurs, although this is somewhat speculative in the spectrum of 2-butyl acetate. Evidently this mode of ionization results from cyclization of the molecular ion followed in each case by loss of the group immediately adjacent to the carbonyl group: CH_2O from the 1-butyl esters and CH_3CHO from the 2-butyl acetate. This is contrary to the usual suggestion that loss of 30 or 44 m.u. is due to loss of C_2H_6 or C_3H_8. One possible mechanism for this rearrangement would be
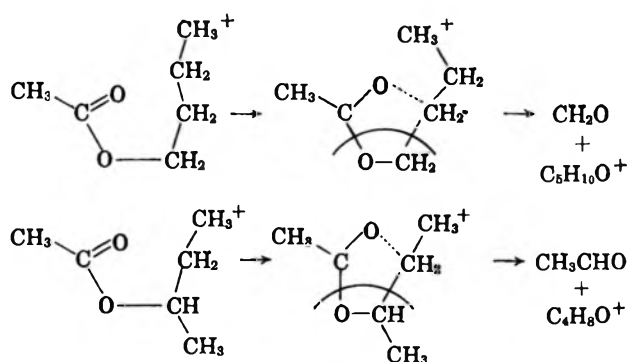
Other cyclic intermediates are also possible. Guriev, et al.,[9,10] Ryhage and Stenhagen,[6-8] and Dinh-Nguyen, et al.,[11] detected similar rearrangements in the mass spectra of long chain esters. The possibility of cyclical intermediates has been suggested as an explanation of observations in the mass spectra of many other compounds.[2,12,17,18]

The ionizations observed at mass 87 in the spectrum of undeuterated 1-butyl acetate and at mass 101 in the

spectrum of 1-butyl propionate are known to be due to loss of $C_2H_5\cdot$ from their high resolution spectra.[3] The data in Table I confirm this and indicate that reactions occur with very little hydrogen–deuterium exchange.

In addition to the above rearrangement, the spectra of the deuterated 2-butyl acetates (Table II) indicate that an unexpected exchange process occurs prior to the formation of the mass 73 ion in the deuterated compound. From high resolution mass spectra[3] this ion is known to have the formula $C_4H_9O^+$. The mass spectral data of the esters in which the 2, 3, or 4 position of the 2-butanol has been deuterated would seem to confirm the expectation that this ion occurs by a simple bond break. However, data obtained from the ester deuterated on C-1 of the 2-butanol show the ionization due to this mode in two places: approximately one-half the ions retain the deuterium (mass 76) and one-half lose the deuterium (mass 73). Since very little ionization is observed at masses 74 and 75, H–D exchange cannot explain this observation. Apparently an exchange of the methyl groups is occurring, by some mechanism. The mass spectra of $CH_3COOCH(CD_3)CD_2CH_3$ and $CH_3COOCD(CD_3)CD_2CH_3$ also confirm this observation but the data for these compounds are not presented because of uncertain chemical purity. As shown in the last column of Table II, deuteration on the acetyl moiety is also only partly lost to give the mass 73 ion and partly retained to give the mass 76 ($C_4H_6D_3O^+$) ion. (In this case there appears to be some H–D exchange leading to the m/e 74 ion and, in addition, the ion formed by loss of CH_3CHO presumably occurs at m/e 75 as previously discussed.) Thus, the formation of the $C_4H_9O^+$ ion apparently involves a complex intermediate in which the acetyl methyl and the 2-butanol methyl (1 position) become indistinguishable. The $C_4H_9O^+$ ions could be formed by a variety of processes including formation of part of the ions by a simple mechanism; cyclization followed by relatively simple H–D rearrangements, or even rearrangement of an entire CH_3 group onto an adjacent oxygen. Further study seems to be indicated.

In the rearrangement process resulting in the formation of the $(CH_3COO + 2H)^+$ ion, the origin of the two protons of 1-butyl acetate is of interest and is indicated in the mass spectra of the deuterated esters (Table III). The ionization resulting from transfer of the protons is seen at mass 61 in the spectrum of the

(17) W. H. McFadden, M. Lounsbury, and A. L. Wahrhaftig, Can. J. Chem., 36, 990 (1958).

(18) J. H. Beynon, R. A. Saunders, A. Topham, and A. E. Williams, J. Phys. Chem., 65, 114 (1961).

undeuterated ester, and that ionization resulting from transfer of the deuterium is seen at mass 62 in the other spectra. The mass 62 peak in the second spectrum represents only 8% of the total ionization due to this process and shows that the availability of the protons on the terminal methyl group is less than statistical. In the third spectrum the mass 62 peak is more intense; it makes up 37% of the total ionization due to the rearrangement process, indicating that the protons on the carbon δ to the carbonyl group are favored. The mass 62 peak in the last spectrum represents only 16% of the total intensity of the mass 61 and mass 62 peaks. This result indicates that direct transfer of a proton to the adjacent oxygen is not highly favored, a result also indicated by the data of McLafferty[4] on deuterated 2-butyl acetate.

Table III: Effect of Deuteration on the Acetate Rearrangement Peaks of 1-Butyl Acetate

m/e	Ionization, %			
59	0.08			
60	0.16	0.14	0.15	0.10
61	5.42	5.09	3.45	5.14
62	0.16	0.48	2.03	1.01
63	0.05	0.08	0.07	0.10

The 2-monodeuterio-1-butyl acetate was not synthesized but the availability of this hydrogen for the rearrangement can be surmised. As shown above, the deuterium on the dideuterated C-1 and the monodeuterated C-3 and C-4 are available for transfer 16, 37, and 8% of the time, respectively, for a total of 61%. The second two values would be considerably greater if each position were fully deuterated (approximately 37% X 2 and 8% X 3); consequently the transfer of a proton (deuteron) from the C-1 would not seem to be significant. These results indicate that in this rearrangement of the 1-butyl acetate the protons on C-3 of the butyl group participate to a greater extent than do those on the C-1 or C-2, contrary to the observation of Colomb, et al., from the mass spectra of deuterated hexyl butyrate and valerate.[2]

In addition, data exist for deuterated ethyl acetates which indicate that deuteration on the C-1 of the ethanol[5] or the C-2[19] leads to a nearly statistical selection of deuterium in formation of this rearranged ion. Thus, it is possible that for some molecules the two-proton transfer process proceeds by a mechanism different from that proposed by McLafferty.[4] The present data suggest a selective transfer of one proton from C-3 followed by a random selection of the second proton from the other protons in the alcohol moiety. Such a random selection will always occur if the second transfer proceeds at a rate significantly less than the rate of H–D exchange within the alcohol group.

(19) Unpublished data of authors.

(20) Reference to a company or product name does not imply approval or recommendation of the product by the U. S. Department of Agriculture to the exclusion of others that may be suitable.

Long-Range Metal–Proton Coupling Constants in Vinyl Metallic Compounds

by S. Cawley and S. S. Danyluk

Department of Chemistry, University of Toronto, Toronto 5, Canada (October 12, 1963)

Metal–proton spin–spin coupling constants for metals with spin $1/2$ have shown several interesting features in compounds of the type $(C_2H_5)_nX$.[1] In all cases, except the fluoro compound,[1] vicinal coupling constants are of greater magnitude than geminal couplings and are of opposite sign. For ethyl fluoride the absolute magnitudes are reversed with $J_{CH_2-F} > J_{CH_3-F}$ and the relative signs are identical.

Several mechanisms, including contributions arising from electron–orbital interaction[2] and involvement of d-electrons in the C–X bond[1] in addition to Fermi contact interaction, have been proposed to account for these coupling constants. Recently Maher and Evans[3] interpreted long-range thallium(Tl^{205})–proton coupling constants qualitatively in terms of a Fermi contact interaction arising from a large effective nuclear charge on the thallium atom. A similar coupling mechanism was suggested for other metal alkyls.[3]

(1) S. L. Stafford and J. D. Baldeschwieler [*J. Am. Chem. Soc.*, **83**, 4473 (1961)] gave a summary of metal–proton *J* values for ethyl derivatives.

(2) P. T. Narasimhan and M. T. Rogers, *J. Chem. Phys.*, **34**, 1049 (1961).

The coupling mechanism for long-range metal–proton coupling constants in vinyl metallics is less certain and in order to clarify this we have measured coupling constants at 60 Mc./sec. for vinyl metallics of the type $X(CH=CH_2)_n$ where $X = Si^{29}$, Sn^{117}, Sn^{119}, or Pb^{207}. These results along with data for vinyl fluoride,[4] trivinylphosphine,[5] and thallium vinyl cations[3] are summarized in Table I. Metal–proton coupling constants were obtained from an analysis of satellite multiplets observed in spectra for neat vinyl metallics. For example, the three Pb^{207}–proton coupling constants are readily picked out by inspection of the satellites superimposed on the 60 Mc./sec. proton spectrum for tetravinyllead, Fig. 1. Comparison of calculated and observed spectra shows that relative signs for gem-, cis-, and trans-Pb^{207}-proton couplings are identical (assumed positive, cf. Fig. 1) and of the same sign as the cis and trans proton–proton coupling constants.[5,6] Similar results have been noted for trivinylphosphine[5] at 60 Mc./sec. and tetravinyltin (Sn^{119}).

Table I : Metal–Proton Coupling Constants for Vinyl Metallics $X(CH=CH_2)_n$

Compound	$J_{X-H(cis)}$[a]	$J_{X-H(trans)}$	$J_{X-H(gem)}$	Ref.
$F^{19}(CH=CH_2)$	±19.8[b]	±52.7	±84.6	4, 8
$Si^{29}(CH=CH_2)_4$	±8[c]	±22[c]		6
$P^{31}(CH=CH_2)_3$	±13.62	±30.21	±11.74	5
$Sn^{117}(CH=CH_2)_4$	±86.1	±174.1	±91.2	
$Sn^{119}(CH=CH_2)_4$	±90.4	±183.0	±96.0	
	±90.4[d]	±183.1	±98.3	7
$Hg^{199}(CH=CH_2)_2$	±159.5	±296.4	±128.3	
	±159.6[d]	±295.5	±128.5	7
$Pb^{207}(CH=CH_2)_4$	±161.7	±330.1	±212.4	
$Tl^{205}(CH_2=CH)Tl^{++}$	±1806	±3750	±2004	3
$(CH_2=CH)_2Tl^+$	±805	±1618	±842	3

[a] cis, trans, and gem refer to the orientation of the proton relative to the metal atom. [b] All measurements were made at 60 Mc./sec. unless otherwise stated. [c] Estimated from α-chlorovinyltrichlorosilane. [d] 40 Mc./sec.

Several features of the vinyl couplings are of interest. The three metal–proton coupling constants each show an increase in magnitude with increasing atomic number although the rates of increase differ, with the trans coupling constant showing the largest change. A linear correlation of coupling constants with atomic number was only observed for compounds within a given group of the periodic table, e.g., group IV-B. Somewhat surprisingly the increase in magnitude for J_{X-H} values in going from group II-B to group IV-B elements within a given period is of the same order as that observed in going from elements in one period
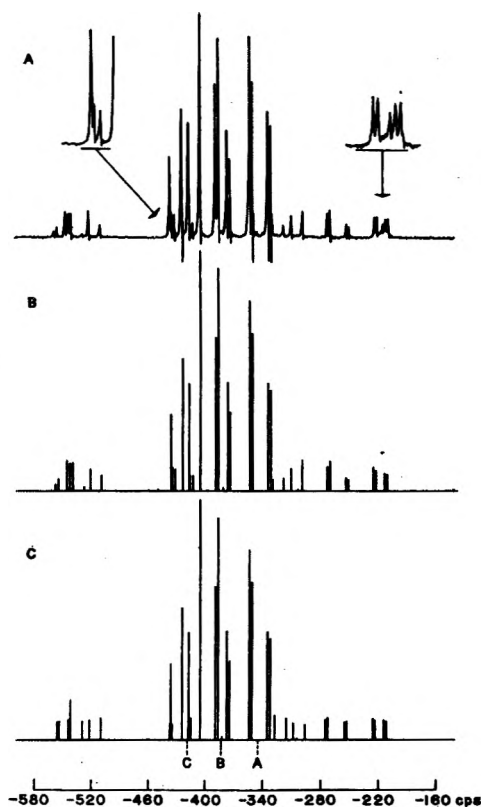
Figure 1. Observed and calculated proton magnetic resonance spectra for tetravinyllead (Pb^{207}): A, observed spectrum for neat tetravinyllead at 60 Mc./sec. Tetramethylsilane used as an internal reference. The small signal at 217 c.p.s. is due to a trace impurity of a lead alkyl derivative. B, calculated spectrum with all $J_{Pb^{207}-H}$ coupling constants positive. The letters A, B, and C refer to protons cis, trans, and gem to the metal atom. C, calculated spectrum with $J_{Pb^{207}-H}(gem)$ assumed negative and of opposite sign to the cis and trans coupling.

to elements in the adjacent period.[7] The increase in J_{X-H} values within a given period parallels a corresponding increase in effective atomic number, Z_e.

Of additional interest are the relatively large gem metal–proton coupling constants for vinyl groups bonded to heavier elements in groups III to VI. $J_{X-H}(gem)$ is larger than $J_{X-H}(cis)$ in the majority of vinyl metallics studied. In contrast, the magnitudes of proton–proton coupling constants for all of the vinyl metallics fit into the normal sequence observed for vinyl groups, i.e., $J_{trans} > J_{cis} > J_{gem}$.

(3) J. P. Maher and D. F. Evans, Proc. Chem. Soc., 176 (1963).

(4) C. N. Banwell and N. Sheppard, Proc. Roy. Soc. (London), A263, 136 (1961).

(5) W. A. Anderson, R. Freeman, and C. A. Reilly, J. Chem. Phys., 39, 1518 (1963).

(6) S. Cawley and S. S. Danyluk, to be published.

(7) D. W. Moore and J. A. Happe, J. Phys. Chem., 65, 224 (1961).

The relative magnitude and signs for proton–F[19] coupling constants in vinyl fluoride have been interpreted[4,8] in terms of Fermi contact interaction as the predominant coupling mechanism. Considering the other vinyl compounds the contact contribution to the X–H coupling would vary with the electron densities at the X and H nuclei and would be proportional to $Z_{eX}^3 Z_{eH}^3 \gamma_X \gamma_H$. The electron densities of ns valence electrons at the nucleus, $|\psi_{ns}(0)|^2$, increase in going from group II-B to group V in any given period and parallel a corresponding increase in Z_e.[9] An increase of $|\psi_{ns}(0)|^2$ would also be expected with increasing atomic number within a given family, i.e., group IV-B.[10] Accordingly, the trends in magnitude for metal–proton couplings in vinyl metallics indicate, at least qualitatively, that the contact contribution predominates in these systems also. Additional factors such as changes in hybridization in going from group II to group V compounds and d_π–p_π interaction along the C–X bond would also affect J_{X-H} although in the case of the latter any effect on the coupling constant would be relatively small.[11]

The reasons for the large gem coupling constants in vinyl derivatives of heavier elements are not readily apparent. Although a wide variety of factors (electronegativity, bond angle, substituents) are known to influence the relative signs and magnitudes of geminal and vicinal proton–proton coupling constants[12] these do not change sufficiently within a given family (e.g., group IV-B) to account for the observed changes of $J_{X-H}(gem)$ and $J_{X-H}(cis)$. However, it is of some interest to note that the ratio $J_{X-H}(gem)/J_{X-H}(cis)$ increases with increasing s-electron density on the X nucleus. It is possible that an additional contribution to J_{gem} results from direct coupling "through space" analogous to the mechanisms proposed for unusually large vicinal couplings in metal alkyls[13] and saturated fluorine compounds.[14] Such an interaction would decrease rapidly with increasing interaction distance and would be less important for cis and trans couplings.

Mechanism of the Dependence of Yields upon pH and Solute Concentration in the γ-Irradiation of Water

by E. Hayon

Service de Chimie-Physique, C.E.N. Saclay (Seine et Oise), France
(Received October 23, 1963)

It was shown[1] in the radiolysis of water that the yields of oxidizing and reducing species, as well as the total decomposition of water, increase on going from neutral to acid solutions. Thus the 100-e.v. yield of total reducing species G(red.) in dilute solutions increases from 2.85 at neutral pH to 3.7 at pH 0.5, that is an increase of $\sim$30%. G(red.) is equal to $G(H_2O)_n^- + G_H$, the sum of the two reducing entities formed from the water by the action of ionizing radiations. On irradiation of chloro compounds it was suggested,[2] and later shown,[3] that the increase of G(red.) with $[H^+]$ and/or solute concentration is due mainly to an increase of reducing species which are initially produced in the form of electrons $(H_2O)_n^-$. The effect of the acid is to reduce in the spurs (radical scavenging by the solute) the back reaction to form water

$$(H_2O)_n^- + OH \longrightarrow nH_2O + OH^- \qquad (1)$$
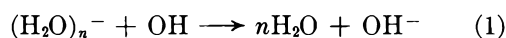
possibly also

$$(H_2O)_n^- + (H_2O)^+ \longrightarrow (n+1)H_2O$$
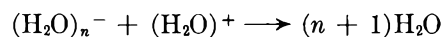
and consequently increase the yield as follows

$$(H_2O)_n^- + H^+ \xrightarrow{k_2} H + nH_2O \qquad (2)$$
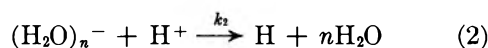
The same increase[3] can be obtained in neutral solution when certain electron-accepting solutes are present in concentrations equivalent to $[H^+]$ at low pH

$$(H_2O)_n^- + S \xrightarrow{k_3} S^- + nH_2O \qquad (3)$$
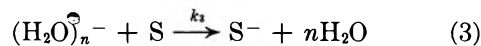
(8) M. Karplus, J. Chem. Phys., 30, 11 (1959).

(9) G. Klose, Ann. Physik, 9, 262 (1962).

(10) L. W. Reeves and E. J. Wells, Can. J. Chem., 41, 2698 (1963).

(11) W. G. Schneider and A. D. Buckingham, Discussions Faraday Soc., 34, 147 (1962).

(12) M. Karplus, J. Am. Chem. Soc., 84, 2458 (1962).

(13) G. Klose, Ann. Physik, 8, 220 (1961).

(14) L. Petrakis and C. H. Sederholm, J. Chem. Phys., 35, 1243 (1961).

(1) W. G. Rothschild and A. O. Allen, Radiation Res., 8, 101 (1958); F. S. Dainton and D. B. Peterson, Proc. Roy. Soc. (London), A267, 443 (1962).

(2) E. Hayon and J. J. Weiss, Proc. Second Intern. Conf. Peaceful Uses At. Energy (Geneva), 29, 80 (1958).

(3) E. Hayon and A. O. Allen, J. Phys. Chem., 65, 2181 (1961).

In this way it is possible to account for the values of G(red.) in neutral solution greater than 2.85 which have recently appeared in the literature.[3-5] The full curve in Fig. 1 is of G(red.) vs. $-\log$ [H⁺] as given by the authors of ref. 1. By taking values for k_2/k_3 from the literature it is possible to normalize with reference to [H⁺] the various solutes used in neutral solution on the basis of their concentration and reactivity toward $(H_2O)_n^-$. The points on the curve (Fig. 1) are for
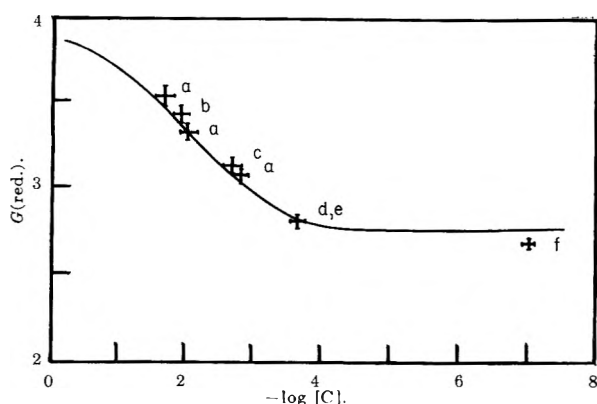
Figure 1. Full curve is G(red.) vs. $-\log$ [H⁺], and crosses are G(red.) values in neutral solution vs. $-\log$ solute concentration normalized with reference to H⁺: a, 10^{-2}, 5×10^{-2}, 10^{-1} M chloroacetate, $k_2/k_3 = 7.0$; b, 1.6×10^{-2} M N₂O, 10^{-3} M 2-propanol, $k_2/k[(H_2O)_n^- + N_2O)] = 1.6^4$; c, 2×10^{-3} M NO, $k_2/k_3 = 1.0^5$; d, 10^{-3} M H₂O₂, $k_2/k_3 = 2.0^{11}$; e, 490 μM O₂, 550 μM H₂, $k_2/k_3 = 1.0^{11}$; f, 0.1 M methanol, neutral pH 7.

chloroacetate,[3] N₂O + 2-propanol,[4] NO,[5] H₂ + O₂,[6] H₂O₂,[6,7] and methanol[8] systems. The good agreement shown in Fig. 1 provides strong support to the earlier suggestion that the effect of H⁺ and/or solute concentrations is due to scavenging of electrons in the spurs, and hence to a reduction of the back reaction (eq. 1).

It remained to be shown whether G_H varied with [H⁺]. Using two-solute systems,[9] one solute to react with electrons (KNO₃ or acetone) and another to react with H atoms (2-propanol) to give H₂, H + RH₂ → H₂ + RH, one can by measuring H₂ determine G_H. In acid solution a competition between reactions 2 and 3 sets in, and one has

$$G(H_2) = G_{H_2} + G_H + \frac{G(H_2O)_n^-}{1 + \dfrac{k_3[S]}{k_2[H^+]}} \quad (4)$$

Acetone and KNO₃ are known to react very slowly with H atoms so that at the concentrations used all the H atoms reacted with 2-propanol. Furthermore any electron scavenging in the spurs by KNO₃ or acetone would not lead to H or H₂ formation. The solutions

(ca. 10 ml.) were thoroughly degassed and irradiated with Co⁶⁰ γ-rays, and the hydrogen gas was determined by gas chromatography. Table I gives the H₂ yields

Table I

[iso-ProH], M	[Solute], M	pH	$G(H_2)$obsd.	$G(H_2)$calcd
1.0	0.5ᵃ	5.2	0.73	0.73
1.0	0.5ᵃ	2.1	0.79	0.82
1.0	0.5ᵃ	1.5	1.04	1.07
1.0	0.5ᵃ	1.2	1.20	1.30
1.0	0.5ᵃ	0.9	1.63	1.73
0.1	1.0ᵇ	5.1	0.68	0.68
0.1	1.0ᵇ	2.1	0.72	0.75
0.1	1.0ᵇ	1.7	0.76	0.80
0.1	1.0ᵇ	1.4	0.90	0.95
0.1	1.0ᵇ	1.0	1.20	1.28
0.1	1.0ᵇ	0.85	1.30	1.37
0.1	1.0ᵇ	0.6	1.60	1.80
0.1	5 × 10⁻⁴ᵇ	5.2	1.03	
0.1		0.6	4.10	
	10⁻³ᶜ	5.5	0.45	

ᵃ KNO₃.   ᵇ Acetone.   ᶜ KBr.

obtained from linear plots up to a dose of 3×10^{13} e.v./g., dose rate 7.22×10^{16} e.v./g./min. The $G(H_2)$ values given in column 5 were calculated according to eq. 4 taking G(red.) at each acidity from the curve in Fig. 1, assuming $G_H = 0.55^{3,9}$ and that it does not vary with pH. The ratio $k[(H_2O)_n^- + NO_3^-]/k[(H_2O)_n^- + CH_3COCH_3] = 2.5$ was arrived at by comparison of the scavenging of "molecular" H₂ by nitrate[10] and by acetone and $k_2/k[(H_2O)_n^- + NO_3^-]$ taken[11] as 2.0. No correction was made for the salt effect on the rate constants, and the values in column 5 were not lowered to account for the reduction[12] in the yield of "molecular" H₂ from 0.45 in neutral pH to 0.40 at pH 0.6. The agreement between observed and calculated values (Table I) is fair and this indicates that $G_H = 0.55 \pm 0.05$ is independent of pH, at least between pH 0.6 and 7.

(4) G. Scholes, M. Simic, and J. J. Weiss, *Discussions Faraday Soc.*, in press.

(5) W. A. Seddon and H. C. Sutton, *Trans. Faraday Soc.*, **59**, 2323 (1963).

(6) C. J. Hochanadel, *J. Phys. Chem.*, **56**, 587 (1952).

(7) E. Hayon, *Trans. Faraday Soc.*, in press.

(8) J. H. Baxendale and R. S. Dixon, *Proc. Chem. Soc.*, 149 (1963).

(9) J. T. Allan and G. Scholes, *Nature*, **187**, 218 (1960); J. Rabani, *J. Am. Chem. Soc.*, **84**, 868 (1962).

(10) H. A. Mahlman, *J. Chem. Phys.*, **31**, 993 (1959).

(11) A. O. Allen, "Radiation Chemistry of Water and Aqueous Solutions," D. Van Nostrand Co., Inc., Princeton, N. J., 1961.

(12) E. Hayon, *J. Phys. Chem.*, **65**, 1502 (1961).

The precursors[13] of "molecular" H_2 are mainly electrons and the yields in 0.5 M KNO_3[10] and 1.0 M acetone are 0.15 and 0.16, respectively. In neutral solutions containing 2-propanol, Table I, $G(H_2)$ is 0.73 in 0.5 M nitrate and 0.68 in 1.0 M acetone, that is $G(H_2) \simeq G_{H_2} + G_H$. Since addition of relatively high concentrations of electron scavengers such as nitrate ions and acetone reduces considerably G_{H_2} but has no effect on G_H, one must conclude that the main precursor of the H atom is not an electron which reacts in the spur with H^+ (reaction 2).[14] This is supported by recent work[7] which provides further arguments in favor of an excited water molecule as the precursor of H atoms.

(13) E. Hayon, Nature, 194, 737 (1962).

(14) A very small contribution from this process cannot be excluded at present.

Desorption of Hydrogen from Platinum Catalysts

by Yutaka Kubokawa, Seisuke Takashima, and Osamu Toyama

Department of Applied Chemistry, University of Osaka Prefecture, Sakai, Osaka, Japan   (Received October 29, 1963)

It has been shown in previous work[1] that not only can desorption rate measurements yield unambiguous information on the energy relation for a given chemisorption system, but in addition they lead to definite conclusions regarding the heterogeneity of the surface and the existence of two types of chemisorption. Although several workers[2] have investigated hydrogen chemisorption on reforming catalysts such as platinum supported on alumina, complete information on the energy relation for such catalysts has not yet been reported. Therefore, in the present work desorption rate measurements have been carried out for hydrogen chemisorbed on platinum catalysts.

Experimental

Materials. Alumina which had been sintered at 750° was impregnated without evacuation with a solution of platinum chloride and dried at 100°. Subsequently, it was reduced with hydrogen at 370° for 21 hr. The reduced catalyst contained 1.15 weight % platinum. The weight of the catalyst was 10.17 g. The alumina used in this study was the material for chromatographic use manufactured by the Wako Junyaku Kogyo Co. It has a B.E.T. surface area of 190 m.[2]/g. Platinum supported on silica gel was

prepared in the same manner. Silica gel for chromatographic use obtained from commercial sources was employed. Platinum black was prepared as described by Feulgen.[3] Hydrogen was purified by passing it through a heated palladium thimble.

Apparatus and Procedure. The method for measuring the rate of desorption has been described in the previous paper[1] and will be repeated here only in outline. The chemisorbed gas was desorbed by making use of a mercury diffusion pump and the desorbed gas was collected in a McLeod gage whose pressure was followed at definite intervals. During the desorption rate measurements, the temperature of the adsorbent was lowered abruptly and the rates before the temperature drop were extrapolated to those for the small amounts adsorbed when the measurements were carried out after the temperature drop. Thus, the rates at the two temperatures corresponded to the same amount adsorbed and the activation energy of desorption could be obtained.

Results and Discussion

After hydrogen was allowed to chemisorb on the catalyst at about 300°, the system was cooled down to −52° in hydrogen. Then the temperature of the catalyst was raised to 300° in stages, at each of which the activation energy of desorption was determined as described previously. The results with platinum supported on alumina are shown in Fig. 1. It is seen that
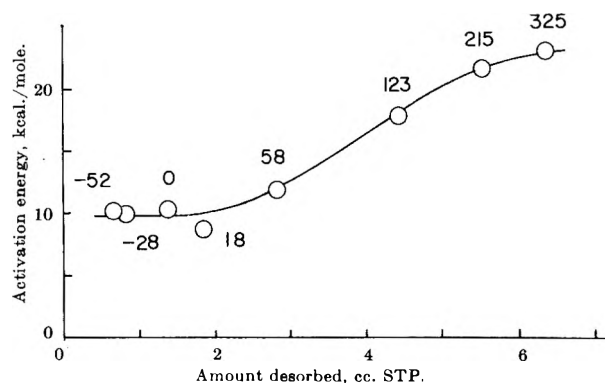
Figure 1. Activation energy of desorption of hydrogen chemisorbed on platinum supported on alumina. Figures indicate the temperature of desorption. The amount adsorbed at −52° before desorption was 6.67 cc. The amount adsorbed when the ratio of hydrogen atoms adsorbed to platinum atoms in the catalyst is one was calculated to be 6.71 cc.

(1) (a) Y. Kubokawa, Bull. Chem. Soc. Japan, 33, 546, 550, 555, 739, 747, 936 (1960); J. Phys. Chem., 67, 769 (1963); (b) Y. Kubokawa and O. Toyama, Bull. Chem. Soc. Japan, 35, 1407 (1962).

(2) (a) L. Spenadal and M. Boudart, J. Phys. Chem., 64, 204 (1960); (b) S. F. Adler and J. J. Keavney, ibid., 64, 208 (1960).

(3) R. Feulgen, Ber., 54B, 360 (1921).

in the range below room temperature the activation energy is almost constant, being equal to 10 kcal./mole, while above room temperature it increases with increasing desorption temperature to 23 kcal./mole. These activation energies of desorption may be assumed to be equal to the heats of adsorption, since with platinum supported on silica gel both values were found to be equal[4] and also adsorption equilibrium was rapidly established on all the platinum catalysts. From the amount adsorbed at $-52°$ before the desorption experiment, the ratio of hydrogen atoms chemisorbed to platinum atoms in the catalyst was found to be close to 1, suggesting an extremely high order of metal dispersion in the catalyst as pointed out by several workers.[2] Furthermore, it may be concluded that the energy values obtained in this work are associated with the whole range of coverage from very low θ-values to a nearly fully covered surface.

From the rate of desorption R and the activation energy of desorption E, values of $\log A$ $(R = Ae^{-E/RT})$ were calculated with the results shown in Fig. 2. It is seen that the plot of $\log A$ against the amount adsorbed shows a minimum as well as a maximum. Although it is very difficult to predict the behavior of the change in $\log A$ with coverage, it seems that such a behavior as represented in Fig. 2 would be unexpected for the case where only one type of adsorption is operating. Scholten, et al.,[5] and Taylor and Langmuir[6] have investigated the desorption of nitrogen from an iron catalyst and of cesium from tungsten, respectively, in both of which cases one type of adsorption seems to operate under their experimental conditions. They have found that with decreasing coverage $\log A$ decreases monotonically or passes through a maximum and then decreases. In addition, the results of desorption measurements carried out by the present authors showed that when two types of adsorption are oper-

ating, a minimum was always observed in the plot of $\log A$ vs. coverage. The considerations described above suggest that in Fig. 2 the type of adsorption is different on each side of the minimum. From the study of infrared spectra of hydrogen chemisorbed on platinum supported on alumina, Pliskin and Eischens[7] have concluded that the weakly chemisorbed hydrogen which can be removed by evacuation at room temperature differs in the type of adsorption from the strongly chemisorbed hydrogen. It might therefore be concluded that in this system two types of adsorption are operating, one corresponding to the desorption below room temperature with the heat of adsorption about 10 kcal./mole, and the other to that at higher temperatures with increasing heat of adsorption up to 23 kcal./mole. Similar experiments were carried out with platinum black and platinum supported on silica gel. It was found that the minimum and maximum heats of adsorption are nearly the same for all three catalysts and two types of adsorption of hydrogen are exhibited by the three catalysts.

Acknowledgment. The authors wish to express their sincere thanks to Professor P. H. Emmett of Johns Hopkins University for his helpful discussion.

(4) Adsorption equilibrium measurements were carried out only with platinum supported on silica gel. It was found that the heat of adsorption obtained from the adsorption isotherms between 278 and 226° is 16 kcal./mole at $\theta = 0.6$, being almost equal to the activation energy of desorption at the same coverage. ($\theta = 1$ is defined as $H_{ads}/Pt = 1$.)

(5) J. J. F. Scholten, P. Zwietering, J. A. Konvalinka, and J. H. de Boer, *Trans. Faraday Soc.*, **55**, 2166 (1959).

(6) J. B. Taylor and I. Langmuir, *Phys. Rev.*, **44**, 423 (1933).

(7) W. A. Pliskin and R. P. Eischens, *Z. physik. Chem.* (Frankfurt), **24**, 11 (1960).

Oxygen Exchange between Chemisorbed Carbon Monoxide on Catalytic Nickel

by J. T. Yates, Jr.[1]

Department of Chemistry, Antioch College, Yellow Springs, Ohio
(Received November 1, 1963)

Studies of the infrared spectrum of adsorbed CO on supported nickel surfaces have led to the postulate that two distinct adsorbed species exist on the heterogeneous surface. These are a bridged CO between two adjacent Ni atoms and a linear CO bonded to one surface Ni atom.[2-4] The interpretation of the existence
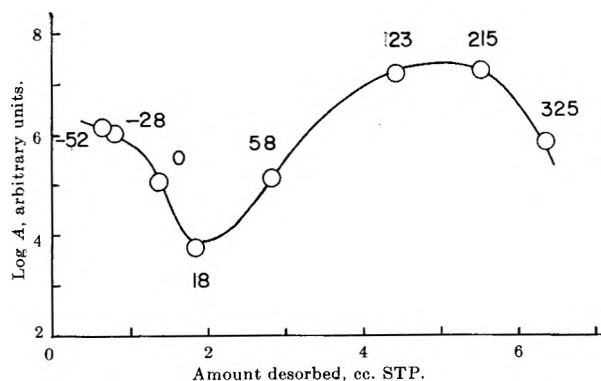
Figure 2. Values of $\log A$ for hydrogen chemisorbed on platinum supported on alumina.

(1) National Bureau of Standards, Washington, D. C.

of these two species is made by analogy with the spectra of metal carbonyls.

Because of the insensitivity of the infrared method, it is possible that other adsorbed CO species could exist undetected on Ni surfaces. The purpose of this investigation was to examine this possibility by using a technique first employed by Webb and Eischens[5] in their study of CO adsorption on catalytic iron surfaces. A mixture of $C^{12}O^{18}$ and $C^{13}O^{16}$ was adsorbed on a Ni surface and portions of the CO were removed with a diffusion pump and analyzed for $C^{13}O^{18}$. At room temperature oxygen exchange occurred. The data indicate that exchange proceeds most extensively when the equilibrium gas phase is at high pressure and contact time is of the order of many hours. Various possibilities are suggested for an exchange intermediate which forms at high coverage.

Experimental

Apparatus. A conventional glass high vacuum adsorption apparatus was employed. The system was evacuated through a liquid nitrogen trap with a two-stage fractionating oil diffusion pump using Octoil-S fluid. The system was capable of maintaining a pressure of less than 1×10^{-6} torr. Baking of some sections of the apparatus was achieved at 250° using heating tape and infrared lamps.

The powdered Ni sample was held on a glass support consisting of three trays each of which had a volume of about 1 cm.[3]. The sample and its support were held inside a vertical 2.5-cm. diameter Vycor furnace which was connected to the vacuum manifold *via* a high conductance stopcock. The temperature of the support was monitored by a thermocouple which passed up a Vycor finger mounted vertically along the axis of the furnace tube.

Carbon monoxide which had been chemisorbed on the Ni surface could be desorbed from the sample through a two-stage mercury diffusion pump which was connected to the vacuum manifold *via* a liquid nitrogen trap and a high-conductance stopcock. The mercury diffusion pump was backed by a 600-cm.[3] removable bulb which could be pumped out with the oil diffusion pump prior to a desorption experiment. The pressure of the collected gas in the bulb was monitored with a Pirani gage protected from mercury vapor by a Dry Ice trap. Once the bulb had been filled to a desired pressure, it could be disconnected and carried to the mass spectrometer for analysis. Desorption could be continued in an uninterrupted manner by using additional bulbs.

Materials. $C^{13}O^{16}$ was prepared from $C^{13}O_2$[6] by reduction over Baker 99.8% zinc dust according to the

procedure of Bernstein and Taylor.[7] Residual CO_2, if any, was condensed using liquid nitrogen on a side arm which was then sealed off. The mass spectrum showed less than 0.01% $C^{13}O_2$. $C^{12}O^{18}$ was obtained from the Weizmann Institute[8] and was used without further purification.

In each experiment a mixture of the two enriched CO samples was prepared in a dosing system connected to the vacuum manifold. A typical analysis of the CO mixture is shown in Table I.

Table I: Analysis of CO Mixture

H_2	1.5%
HD	1.0%
D_2	0.3%
H_2O	0.1%
$C^{12}O^{16}$	21.8%
$C^{13}O^{16} + C^{12}O^{17}$	22.4%
$C^{12}O^{18}$	52.2%
$C^{13}O^{18}$	0.73%
CO_2	0.03%
	100.0%

Sample Preparation. Nickel(II) oxide obtained from Prof. R. J. Kokes at Johns Hopkins University was used as a source of Ni in this research. This sample, prepared in the manner of Best and Russell,[9] was of high purity and similar to that used by Emmett and Hall in their work on ethylene and benzene hydrogenation.[10] This is referred to as sample VIII in their papers.

Approximately 1 g. of the NiO was placed in the weighed glass support which, after reweighing, was lowered into the furnace tube. The furnace was evacuated overnight, and purified hydrogen[11] was ad-

(2) R. P. Eischens, S. A. Francis, and W. A. Pliskin, *J. Phys. Chem.*, **60**, 194 (1956).

(3) J. T. Yates, Jr., and C. W. Garland, *ibid.*, **65**, 617 (1961).

(4) C. E. O'Neill and D. J. C. Yates, *ibid.*, **65**, 901 (1961).

(5) A. N. Webb and R. P. Eischens, *J. Am. Chem. Soc.*, **77**, 4710 (1955); *J. Chem. Phys.*, **20**, 1048 (1952).

(6) Obtained from Isomet Corp., Palisades Park, N. J. CO_2 analysis was 56.7% C^{13}. After reduction the CO was 56.0% $C^{13}O^{16}$.

(7) R. B. Bernstein and T. I. Taylor, *Science*, **106**, 498 (1947).

(8) Labeled 89.7% $C^{12}O^{18}$. Our analysis showed 88.5% of the CO to be $C^{12}O^{18}$.

(9) R. J. Best and W. W. Russell, *J. Am. Chem. Soc.*, **76**, 838 (1954).

(10) W. K. Hall and P. H. Emmett, *J. Phys. Chem.*, **62**, 816 (1958); **63**, 1102 (1959).

(11) Hydrogen for reduction of the samples was Airco electrolytic grade. It was passed through a Deoxo catalytic purifier and then through a liquid nitrogen trap. In some reductions, a prebaked Spheron charcoal trap, maintained at liquid nitrogen temperature, was employed in the hydrogen stream as suggested by Hall and Emmett. No enhancement of the specific CO adsorption was achieved with these samples compared to samples prepared without the charcoal trap.

mitted. When the pressure reached 1 atm., the furnace was gradually warmed; reduction began at about 200°. After the majority of the water had been liberated, as judged by condensation in the cool part of the exit tube, the temperature was raised to 350–400° and reduction with flowing hydrogen was continued for periods ranging from 16 to 53 hr. at a flow rate of 1.0 l. STP/hr.

After reduction, the sample was outgassed for 20–30 hr. at the reduction temperature using the trapped oil diffusion pump. The dynamic pressure at the end of the outgassing period was 2×10^{-6} torr or lower; on cooling the dynamic pressure dropped below 1×10^{-6} torr.

At the end of an experiment the Ni sample and the holder were reweighed. The loss in weight observed corresponded to the empirical formula $Ni_{1.00}O_{1.06}$, and the variation employed in reduction time and temperature in the various experiments did not affect the weight loss observed per unit weight of sample within experimental error.

CO Adsorption. Adsorption of the known mixture of isotopic CO was carried out at 25° in stepwise fashion by addition of known quantities of CO followed by pressure measurements; the adsorption could be followed with the McLeod gage to pressures of about 1×10^{-3} torr. Up to 50×10^{-3} torr, uptake was measured with a calibrated Pirani gage. Above this pressure, the dead space correction was appreciable and uptake measurements became impractical.

Analysis of the Desorbed Gas. The gas desorbed from the sample through the mercury diffusion pump was collected in a bulb until the pressure reached about 100×10^{-3} torr in the bulb. The bulb was then disconnected from the vacuum system and a portion of the gas was transferred by expansion to the sampling system (about 500 cm.³ volume) of a Consolidated Engineering mass spectrometer, Model 21-401. The precision in duplicate analyses was ±2%.

A sample of CO of known composition was retained in the mercury diffusion pump for approximately 9 hr. as a blank to check that exchange was not occurring on long exposure to the heated mercury vapor. No exchange was detected.

Experimental Results

Oxygen Exchange. Four experiments are reported in Table II. In the first portion of the table the highest CO pressure employed in the initial adsorption and the STP volume of CO adsorbed per gram of Ni at this pressure are given, as well as the contact time allowed at this pressure.

The lower entries show the CO volume per gram of

Ni as pumped from the sample in successive fractions. For each of these fractions desorbed, there are given two factors related to the increase in the $C^{13}O^{18}$ concentration ratio due to oxygen exchange between CO molecules. In addition, the $C^{12}O^{18}$–$C^{13}O^{16}$ concentration ratios in the initial gas and the desorbed gas are given.

It can be seen that in each experiment the concentration ratio of $C^{13}O^{18}$ in the desorbed gas has increased from that observed in the CO mixture prior to adsorption. This increase varies from about 30% in experiment I to 100% in the latter part of experiment III. Satisfactory checks (±1.2%) are obtained in the factor increase in the $C^{13}O^{18}$ concentration ratio when evaluated either as

$$\left(\frac{n_{31}}{n_{30}}\right)_{d} \bigg/ \left(\frac{n_{31}}{n_{30}}\right)_{0}$$

or as

$$\left(\frac{n_{31}}{n_{29}}\right)_{d} \bigg/ \left(\frac{n_{31}}{n_{29}}\right)_{0}$$

The other possible ratio involving the concentration of $C^{12}O^{16}$ is not shown since the accuracy of the mass 28 peak is considerably poorer than peaks at mass 29, 30, and 31 due to a nitrogen background problem in the mass spectrometer.

No discernible difference in the rate of desorption of $C^{12}O^{18}$ and $C^{13}O^{16}$ is seen, since the value of $(n_{30}/n_{29})_{d}$ remained the same as $(n_{30}/n_{29})_{0}$ within experimental error in each of the four experiments.

The data in Table II support the following qualitative observations relative to oxygen exchange between chemisorbed CO molecules.

(a) The highest extent of exchange is achieved by long contact with the gas phase at relatively high CO pressure. Thus, experiments III and IV show the highest extent of exchange and these two experiments employ the highest CO pressure and the longest contact time. Experiments II and III involve comparable CO pressure and by comparing these two experiments it may be seen that long contact time favors a higher extent of exchange.

(b) The extent of exchange observed does not vary appreciably in the successive fractions removed from the surface during desorption (experiment III).

(c) The gas phase at the higher pressure is in equilibrium with the adsorbed gas after 17 hr. contact insofar as the concentration of $C^{13}O^{18}$ is concerned. This may be seen from experiments III and IV where the $C^{13}O^{18}$ concentration in the gas which was pumped away in less than 1 min. is the same as in the desorbed

Table II: Adsorption and Desorption of $C^{12}O^{18} + C^{13}O^{16}$. Isotope Abundance Ratios in the CO[a]

	Experiment no. I	II	III	IV
Wt. of Ni sample, g.	1.3299	0.5884	1.3219	1.2188
Adsorption data				
P_{CO} at highest coverage, μ	0.65	59	60	380
V_{CO} adsorbed/g. of Ni, cc.	0.088	0.292	0.336	. . .
Contact time at highest P_{CO}, hr.	10	1	17.5	17.3
Desorption data				
V_{CO} desorbed/g. of Ni at T, °C.		0.137 cc.; 25[ob]	0.063 cc.; 25[ob]	0.103 cc.; 25[ob]
$\left(\dfrac{n_{31}}{n_{30}}\right)_d \Big/ \left(\dfrac{n_{31}}{n_{30}}\right)_0$		1.32	1.81	1.78
$\left(\dfrac{n_{31}}{n_{29}}\right)_d \Big/ \left(\dfrac{n_{31}}{n_{29}}\right)_0$		1.33	1.94	1.80
$\left(\dfrac{n_{30}}{n_{29}}\right)_0 ; \left(\dfrac{n_{30}}{n_{29}}\right)_d$		2.34; 2.35	2.35; 2.51	2.32; 2.36
V_{CO} desorbed/g. of Ni at T, °C.	0.065 cc.; 85°	0.048 cc.; 25°	0.046 cc.; 25°	. . .
$\left(\dfrac{n_{31}}{n_{30}}\right)_d \Big/ \left(\dfrac{n_{31}}{n_{30}}\right)_0$	1.30	1.47	1.95	1.80
$\left(\dfrac{n_{31}}{n_{29}}\right)_d \Big/ \left(\dfrac{n_{31}}{n_{29}}\right)_0$	1.29	1.45	1.89	1.81
$\left(\dfrac{n_{30}}{n_{29}}\right)_0 ; \left(\dfrac{n_{30}}{n_{29}}\right)_d$	2.30; 2.29	2.34; 2.30	2.35; 2.28	2.32; 2.36
V_{CO} desorbed/g. of Ni at T, °C.			0.083 cc.; 85°	
$\left(\dfrac{n_{31}}{n_{30}}\right)_d \Big/ \left(\dfrac{n_{31}}{n_{30}}\right)_0$			1.99	
$\left(\dfrac{n_{31}}{n_{29}}\right)_d \Big/ \left(\dfrac{n_{31}}{n_{29}}\right)_0$			1.96	
$\left(\dfrac{n_{30}}{n_{29}}\right)_0 ; \left(\dfrac{n_{30}}{n_{29}}\right)_d$			2.35; 2.32	
V_{CO} desorbed/g. of Ni at T, °C.			0.026 cc.; 85°	
$\left(\dfrac{n_{31}}{n_{30}}\right)_d \Big/ \left(\dfrac{n_{31}}{n_{30}}\right)_0$			2.02	
$\left(\dfrac{n_{31}}{n_{29}}\right)_d \Big/ \left(\dfrac{n_{31}}{n_{29}}\right)_0$			1.97	
$\left(\dfrac{n_{30}}{n_{29}}\right)_0 ; \left(\dfrac{n_{30}}{n_{29}}\right)_d$			2.35; 2.30	

[a] n_{31} = concentration of $C^{13}O^{18}$. n_{30} = concentration of $C^{12}O^{18}$. n_{29} = concentration of $C^{13}O^{16}$ + small amount of $C^{12}O^{17}$. $(n_{31}/n_{30})_0$ = concentration ratio in the initial gas. $(n_{31}/n_{30})_d$ = concentration ratio in the desorbed gas. $(n_{31}/n_{30})_d /(n_{31}/n_{30})_0$ = factor increase in concentration ratio due to exchange. [b] Pumping time less than 1 min. This gas is primarily from the equilibrium gas phase.

gas collected after long pumping. Experiment II, where contact time was only 1 hr., is a borderline case since it may be seen that the second fraction of CO removed from the adsorbed layer by long pumping is slightly more enriched in $C^{13}O^{18}$ than the first fraction which was primarily from the gas phase present in the apparatus. This difference in $C^{13}O^{18}$ enrichment during the initial stages of the surface exchange process indicates that interchange of CO between the adsorbed layer and the gas phase is a slow process.

(d) Increasing the sample temperature to 85° during the latter stages of desorption does not markedly increase the extent of oxygen exchange between CO molecules (latter part of Experiment III).

(e) In the exchange times employed here, achievement of statistical equilibrium is far from complete. If complete exchange had occurred, a 16-fold increase in the concentration of $C^{13}O^{18}$ would have been observed. The maximum increase obtained here is about twofold.

Residual Hydrogen Problem. By deuterium exchange studies, Hall[12] has ascertained that Ni catalyst VIII, very similar to the one employed in this work, retains hydrogen after reduction and evacuation. A particular sample prepared by Hall by reduction at 350° and outgassing at 350° for 2 hr. retained 0.10 cm.^{3} of hydrogen/g. The B.E.T. surface area of the same sample corresponded to a monolayer *nitrogen* capacity of 0.59 cm.^{3}/g.

In agreement with Hall's observations, strongly bound hydrogen was encountered in the present investigation even though the outgassing procedure employed here was considerably more strenuous. It was found that as desorption proceeded, the collected gas became richer in hydrogen. Table III shows data from experiment III.

Discussion

The evidence for oxygen exchange between chemisorbed CO molecules is in disagreement with recent results reported for CO on clean evaporated Ni films by Suhrmann and co-workers.[13] These workers were primarily interested in studying surface heterogeneity of the Ni film prepared under ultrahigh vacuum conditions, but they report that no oxygen exchange between CO was observed. Several important differences between Suhrmann's work and this work should be pointed out.

(a) Approximately three-fourths of the CO in equilibrium with Suhrmann's Ni films was $C^{12}O^{16}$, at the highest coverages employed, where the pressure was several microns. Any small degree of exchange might remain undetected since the initial concentration of $C^{12}O^{18}$ and $C^{13}O^{16}$ is fairly low compared to the present work.

(b) Suhrmann's tables indicate that contact times of the order of 1 hr. were employed at the highest coverages. This short time, coupled with the concentration factor, may have led to an undetectable extent of exchange.

(c) The situation on an evaporated film prepared under ultrahigh vacuum conditions is certainly very different from the samples employed in the present work. Thus it has been established that hydrogen contamination exists in these most carefully outgassed powdered samples. In addition, it is probable that the Ni surface is contaminated with adsorbed oxygen, and at the present time the possibility that these contaminants somehow are involved in the exchange cannot be ruled out.

Probably the most important observation in this work is that exchange seems to stop when the high pressure equilibrium gas phase is pumped away. This is excellent evidence for the absence of a dissociative process for CO chemisorption on Ni, since exchange should continue at all coverages by such a mechanism. The fact that exchange stops must mean that only at the highest coverage does an exchange intermediate form. At the present time it is impossible to decide whether this intermediate involves structures like those proposed by Eischens,[5] *viz.*
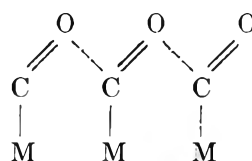
or a hypothetical two-point-attachment structure
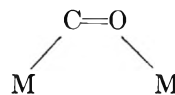
which, when formed next to another structure of the same type oriented in the opposite direction, could result in an intermediate favorable to exchange. A possible variation on this would be an exchange intermediate
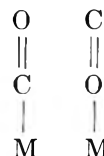
and it is conceivable that such a structure could begin to form at the highest coverage by insertion of CO molecules bonded through the oxygen atom into a surface layer predominantly composed of carbon-bonded CO.

Table III: Mole % Hydrogen in the Four Successive Desorption Samples from Experiment III

Pumping time	Sample temp., °C.	%H$_2$
30 sec.	25	0.7
4.9 hr.	25	29.9
8 hr.	85	52.8
49 hr.	85	83.1
61.9 hr. total		

(12) W. K. Hall, private communication. See also W. K. Hall, F. J. Cheselske. and F. E. Lutinski, *Actes Congr. Intern. Catalyse 2e, Paris,* 2199 (1960).

(13) R. Suhrmann, H. J. Heyne, and G. Wedler. *J. Catalysis,* 1, 208 (1962).

Oxygen exchange between chemisorbed CO molecules on Ni surfaces is somewhat analogous to experimental observations made with CO on catalytic Fe by Webb and Eischens.[5] These workers observed that on Fe appreciable oxygen exchange occurred at $-78°$ and that statistical equilibrium was achieved at about $160°$. They also showed that the presence of the gaseous phase at relatively high pressure (300 torr) increased the rate of approach to statistical equilibrium on the Fe surface.

Heats of Formation of
Dioxane–Halogen Complexes

by C. A. Goy and H. O. Pritchard

Chemistry Department, University of Manchester,
Manchester 13, England   *(Received November 1, 1963)*

The existence of a liquid complex between bromine and 1,3-dioxane[1] and of solid 1 : 1 complexes of both bromine and iodine with 1,4-dioxane[2] has been known for a long time. No thermodynamic study of these substances has been reported, although both equilibrium[3] and calorimetric[4] studies have been made on the solutions of iodine and 1,4-dioxane. The structure of the solids has recently been determined by X-ray methods, and it was found that the halogen molecules act as a bridge between the oxygen atoms of different dioxane molecules[5] in contrast to the theoretical description given by Mulliken.[6]

Spectroscopic Studies. It was found that the equilibrium

$$I_2(g) + 1,4\text{-dioxane}(g) \rightleftharpoons$$
$$[1,4\text{-dioxane} - I_2](s) \quad (1)$$
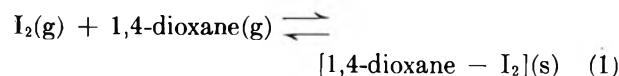
could readily be studied spectroscopically in the temperature range 35–60°. Known amounts of 1,4-dioxane (about 2–4 cm. pressure) and iodine were in-

troduced into a 5-cm. spectroscopic cell, and the concentration of I_2 present at any temperature was determined from the absorption at 4500 Å. (see ref. 7 for further details). Below about 35°, solid complex could be seen and since there was always an excess of dioxane, the concentration of I_2 was too low to measure satisfactorily. After each change of temperature, sufficient time was allowed for equilibrium to be attained. In each experiment, iodine concentrations were measured at successively higher temperatures until dissociation was complete (50–60° depending on relative concentrations) and the values were remeasured (and found to agree) as the temperature was being lowered; the equilibrium constants were then calculated from the initial pressure of dioxane and the measured concentration of iodine at complete dissociation. Various forms of equilibrium constant expression were explored, but the most satisfactory one was found to be

$$K_c = 1/[I_2][\text{dioxane}]$$

corresponding to the equilibrium 1. The heat of reaction 1 was determined from the slope of the plot of $\log K_c$ against $1/T$ using

$$\partial \ln K_c / \partial \left(\frac{1}{T}\right) = -2\bar{T} - \Delta H/R$$

Similar measurements were made with Br_2 and 1,4-dioxane, and with I_2 and 1,3-dioxane, where a liquid complex is formed: measurements could not be made

Table I: Spectroscopic Study of the Equilibria between Halogens and Dioxanes

Complex	Temp. range, °C.	No. of detn.	Mean log K_c at 25°, mole^{-2} l.^{2a}	Mean ΔH for reaction 1, kcal./mole^a
1,4-Dioxane–I_2(s)	36–60	10	8.4 ± 0.2	-27.4 ± 1.5
1,4-Dioxane–Br_2(s)	23–42	10	6.3 ± 0.2	-26.1 ± 1.5
1,3-Dioxane–I_2(l)	30–60	4	7.6 ± 0.1	-14.4 ± 1.5

[a] The errors quoted are such that all determinations lie within these limits.

(1) H. T. Clarke, *J. Chem. Soc.*, **101**, 1788 (1912).

(2) H. Rheinholdt and R. Boy, *J. prakt. Chem.*, **129**, 273 (1931).

(3) J. A. A. Ketelaar, *J. Phys. Radium*, **15**, 197 (1954); D. L. Glusker and H. W. Thompson, *J. Chem. Soc.*, 471 (1955); R. S. Drago and N. J. Rose, *J. Am. Chem. Soc.*, **81**, 6141 (1959).

(4) K. Hartley and H. A. Skinner, *Trans. Faraday Soc.*, **46**, 621 (1950).

(5) O. Hassel and J. Hvoslef, *Acta Chem. Scand.*, **8**, 873 (1954).

(6) R. S. Mulliken, *J. Am. Chem. Soc.*, **72**, 600 (1950).

(7) C. A. Goy and H. O. Pritchard, *J. Mol. Spectry.*, **12**, 38 (1964).

Table II: Calorimetric Study of Halogen–Dioxane Systems

System	Final concn., g./l.	ΔH(soln.) halogen, kcal./mole	ΔH(soln.) complex, kcal./mole	Calcd. ΔH for reaction 1 at 25°, kcal./mole
1,4-Dioxane–I₂	8.0	+1.88 ± 0.08	+6.62 ± 0.08	−28.6 ± 0.3
1,4-Dioxane–Br₂	4.5	−2.84 ± 0.08	+7.00 ± 0.10	−26.2 ± 0.3
1,3-Dioxane–I₂	8.4	+2.35 ± 0.15		

for Br_2 and 1,3 dioxane because the bromine was rapidly decolorized slightly above room temperature. The results are summarized in Table I; the difference in heats of formation of the two iodine complexes is consistent with the fact that one is solid and the other liquid.

Calorimetric Studies. Heats of solution were measured at 25° in a 100-ml. capacity dewar calorimeter of the kind which has been described previously.[8] 1,4-Dioxane was purified by refluxing with dilute HCl, dried by treatment with KOH, and fractionated from sodium[9]; 1,3-dioxane is not so easily purified and was simply fractionated. For the determination of the heats of solution of the solid complexes of 1,4-dioxane with I_2 and Br_2, fresh samples were prepared before each run by the method described by Rheinholdt and Boy[2]; the iodine and bromine used were of analytical grade. The quantities were adjusted so that the final solution was the same, independent of whether the heat of solution of the halogen or its complex had been measured; three determinations were made for each heat of solution, and all determinations fell within the limits quoted. No satisfactory heat of solution of Br_2 in 1,3-dioxane could be determined because a slow reaction occurred. A summary of the results is given in Table II.

In the final column of Table II, we give the calculated heat of reaction 1 based on the calorimetric measurements quoted and the latent heats of vaporization of the halogens[10] and 1,4-dioxane.[11] It is seen that the agreement with the figures obtained in Table I is quite satisfactory and strongly supports our choice of expression for the equilibrium constant; it also gives some confidence in our estimate for the heat of formation of the liquid complex between iodine and 1,3-dioxane.

Acknowledgment. We wish to thank Dr. H. A. Skinner and Dr. G. Pilcher for the use of their calorimetric equipment.

(8) H. O. Pritchard and H. A. Skinner, *J. Chem. Soc.*, 272 (1950).

(9) E. Eigenberger, *J. prakt. Chem.*, 130, 75 (1931).

(10) National Bureau of Standards Circular 500.

(11) Much of the relevant work on 1,4-dioxane in the literature has been done with dioxane which has been simply treated with sodium[12] or calcium chloride[13] and, unfortunately, could not be more than about 97% pure. However, in their vapor pressure determinations, Crenshaw, *et al.*,[14] did rigorously purify their dioxane, and for this reason we derive our latent heat of vaporization from their data, giving λ_{vap} = 9.0 ± 0.1 kcal. at 25°.

(12) A. F. Gallhaugher and H. Hibbert, *J. Am. Chem. Soc.*, 59, 2421 (1937).

(13) C. G. Vinsen and J. J. Morton, *J. Chem. Eng. Data*, 8, 74 (1963).

(14) J. L. Crenshaw, A. C. Cope, N. Finkelstein, and R. Rogers, *J. Am. Chem. Soc.*, 60, 2308 (1938).

Surface Areas from the V/n Ratio for Marine Sediments

by W. H. Slabaugh and A. D. Stump

Department of Chemistry and Department of Oceanography, Oregon State University, Corvallis, Oregon
(*Received November 4, 1963*)

We have recently made a series of determinations of the B.E.T. (Brunauer–Emmett–Teller) surface areas and pore-size distribution of marine sediments obtained from the continental terrace off the coast of Oregon by the research vessel Acona of Oregon State University. Our results showed good agreement between surface areas calculated by the B.E.T. method and by the use of the ratio V/n, where V denotes the volume absorbed at a certain relative pressure and n is the statistical number of molecular layers calculated from Frenkel–Halsey–Hill equation[1,2] for nitrogen adsorption.

Experimental

Apparatus. The adsorption isotherms were determined gravimetrically on a conventional gravimetric adsorption balance with quartz helical springs. The balance had a sensitivity of about 1 mm. extension

(1) C. Pierce, *J. Phys. Chem.*, 63, 1076 (1959).

(2) C. Pierce, *ibid.*, 64, 1184 (1960).

per mg. and a capacity of 400 mg. The spring extension was projected optically on a wall chart for an over-all sensitivity of ±0.04 mg. for a 200-mg. sample. The sensitivity of our apparatus was within ±5% for a B.E.T. surface area over 14 m.²/g., ±7% between 14 and 10 m.²/g., and ±10% between 10 and 7 m.²/g. For surface areas below 4 m.²/g., little reliability was attached to our results.

Sample Preparation. All samples were dried in a vacuum oven for 24 hr. at about 2 torr and at a temperature below 124°. The samples were hand ground with a mortar and pestle until they passed through a 170-mesh sieve (35 openings per cm.).

Procedure. Approximately a 200-mg. portion of each sample was outgassed for 36 hr. at 10^{-4} torr at room temperature. The apparent weight loss was measured by the adsorption balance and the weight loss was subtracted from the original weight to obtain a weight "*in vacuo.*" Adsorption isotherms were made with nitrogen at $-196 \pm 0.1°$, and the samples were equilibrated at each step for about 20 min.

Results and Discussion

Verification of the Frenkel–Halsey–Hill Equation. From the independent work of Frenkel,[3] Halsey,[4] and Hill,[5] an equation has been derived by Pierce[2] as follows

$$n^s = \frac{K}{\log P_0/P} = \left(\frac{V}{V_m}\right)^s \tag{1}$$

In this expression s and K are constants related to the adsorbate and adsorbent. It is remarkable that, for N_2 adsorption, the values of K for several solids are almost constant, and the present study further supports this finding and expands the usefulness of the F.H.H. relationship. If a material has only a free surface and if the above relationship is true, then for any gas for which s and K are known, V_m could be evaluated at any P/P_0 value by

$$V_m = \frac{V}{n}$$

where V_m is the volume of gas required to produce a monolayer and V is the volume of gas adsorbed at pressure P. A plot of V/n vs. P/P_0 for nitrogen adsorption on anatase, using $s = 2.75$ and $K = 1.305$, is shown in Fig. 1. Each point on the plot is the average of eight samples. If no capillary condensation occurs, the curves should be linear for P/P_0 between 0.2 and 0.9. Above $P/P_0 = 0.9$, deviation can be attributed to condensation between the particles.[2] As shown in Fig. 1, experimental deviation from the average within the same P/P_0 range was
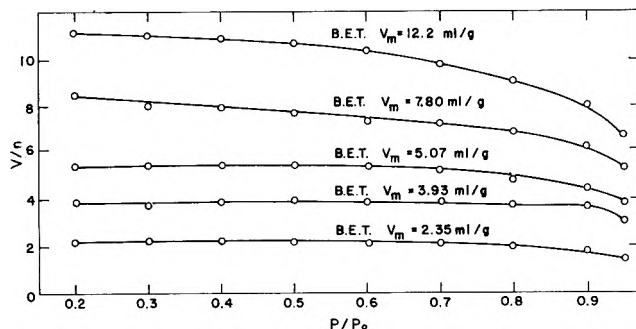
Figure 1. Correlation of V/n plots with B.E.T. values.

small (within ±10%). The average V_m value obtained from this method is about 8% higher than the B.E.T. value but within the accuracy of the apparatus for low surface area materials.

The Use of V/n for the Determination of Surface Areas. It is much simpler to determine surface areas from gaseous adsorption data by means of eq. 2 than by calculating them from B.E.T. plots, because eq. 2 requires a measurement of adsorption at only one pressure. An adsorption balance could be constructed to regulate the pressure automatically at a predetermined amount and allow the system to reach equilibrium. The weight of adsorbed gas could be observed and V_m calculated directly from eq. 2.

The feasibility of this procedure for nitrogen surface areas of marine sediments was investigated and multiple isotherms were derived from 45 samples. The P/P_0 value of 0.2 (152 torr) was selected as the best value for these measurements, because (1) it is somewhat above the B.E.T. B point, (2) no capillary condensation has occurred up to this point, (3) 152 torr is a pressure that can be conveniently measured, and (4) the n value at this point is small (1.25). Surface areas of terrigenous marine sediment samples calculated from V/n values at $P/P_0 = 0.2$ and by the B.E.T. relationship for isotherms are compared in Table I. For the series of 45 isotherms the V/n value averaged 1.7% higher than B.E.T. values for V_m, and the only deviation greater than ±10% was the one case where the V_m value was below the sensitivity range of the apparatus. Only 12 samples showed deviations greater than ±5%, which is the approximate reproducibility of B.E.T. measurements.

(3) J. Frenkel, "Kinetic Theory of Liquids," Oxford University Press, London, 1946.

(4) G. D. Halsey, *J. Chem. Phys.*, 16, 931 (1948).

(5) T. L. Hill, "Advances in Catalysis," Vol. IV, Academic Press, New York, N. Y., 1952, p. 211; *J. Chem. Phys.*, 14, 263, 441 (1946); 15, 767 (1947); 17, 520, 668 (1949).

| Description | | N₂ surface area, m.²/g. | | Deviation, |
Color	Depth, fathoms	B.E.T.	V/n	%
Tan	50	2.7	2.4	11.6
Tan	70	10.6	10.9	2.3
Gray	80	13.0	13.4	3.0
Gray	90	19.9	20.1	0.7
Green	200	43.8	43.5	0.8
Green	200	45.7	45.3	0.8

The results of this investigation substantiate the use of V/n values in determining surface areas of marine sediments.

Acknowledgment. This work was partially supported by National Science Foundation grant G.P.622.

Tantalum Substitution in the Hexagonal Tungsten Bronzes

by Francis Galasso and Wilda Darby

*United Aircraft Corporation Research Laboratories,
East Hartford, Connecticut* (*Received November 19, 1963*)

Most of the alkali tungsten bronzes with the general formula $A_x(W^V_xW^{VI}_{1-x})O_3$ ($x < 1$) have been found to adopt either the perovskite, the tetragonal tungsten bronze, or the hexagonal tungsten bronze type structure depending on the size of the A ion and the value of x.[1] These phases are characterized by their colors and low electrical resistivities, both of which can be attributed to the presence of pentavalent tungsten ions in their structures. It therefore was of interest when some new phases with the tetragonal tungsten bronze structure and others which may have structures similar to the hexagonal tungsten bronzes were prepared by substituting tantalum ions for the pentavalent tungsten ions in the corresponding bronzes.[2] Since only preliminary studies were made on those phases which appeared to have the hexagonal structure, it was felt that further work should be carried out at these laboratories on these phases in order to determine the effect of tantalum substitution in the hexagonal bronzes on cell size, color, electrical conductivity, and thermal expansion characteristics. The purpose of this note is to report the experimental procedures and results of this study.

Experimental

K_2CO_3, Rb_2CO_3, $CsNO_3$, Ta_2O_5, and WO_3 used in these preparations were reagent grade chemicals. Samples were prepared by mixing the constituent powders in appropriate proportions to give products having the general formula $A_{0.3}(Ta_{0.3}W_{0.7})O_3$, A = K, Rb, or Cs. The mixture was fired in alumina combustion boats at 1100° for 24 hr. Powder X-ray photographs were taken of the products using a Philips 57.3-mm. radius camera. High intensity copper $K\alpha$ radiation was used with settings of 40 kv. 30 ma. for 4 hr. High temperature X-ray diffractometer tracings were made up to 1000° using a Norelco diffractometer with an attached HX-2A furnace made by Tem-Pres Inc. These studies were carried out in air with no evidence of sample decomposition.

Samples of the phases were analyzed by Ledoux & Company of Teaneck, N. J. The analyses confirmed that the amount of tantalum ion substituted in each phase corresponded to the general formula $A_{0.3}(Ta_{0.3}W_{0.7})O_3$. *Anal.* Calcd. for $K_{0.3}(Ta_{0.3}W_{0.7})O_3$: K, 4.83; Ta, 22.36; W, 53.03. Found: K, 4.30; Ta, 23.70; W, 51.77. Calcd. for $Rb_{0.3}(Ta_{0.3}W_{0.7})O_3$: Rb, 9.99; Ta, 21.15; W, 50.16. Found: Rb, 9.64; Ta, 21.88; W, 48.77. Calcd. for $Cs_{0.3}(Ta_{0.3}W_{0.7})O_3$: Cs, 14.72; Ta, 20.04; W, 47.52. Found: Cs, 14.30; Ta, 20.57; W, 46.73.

Discussion and Results

The phases obtained were cream-white in color, indicating that the elements in them were present in their highest oxidation state. This is in contrast with the deep blue color of the bronzes which contain tungsten ions alone in the octahedral sites of the hexagonal bronze structure. The powder X-ray photographs of the phases in which tantalum ions were substituted for part of the tungsten ions resembled those of the hexagonal bronzes so their X-ray patterns were indexed on the basis of similar hexagonal unit cells. Table I gives the indexing data for $Rb_{0.3}(Ta_{0.3}W_{0.7})O_3$, and compares the observed intensities of the $Rb_{0.3}$-$(Ta_{0.3}W_{0.7})O_3$ and $Rb_{0.29}WO_3$ patterns. The d calculated values were obtained using a cell size of $a = 7.342$, $c = 7.715$ Å. Since tantalum and tungsten have about the same atomic scattering factors, the satisfactory agreement between the intensities of the two compounds indicates that $Rb_{0.3}(Ta_{0.3}W_{0.7})O_3$ does have the hexagonal tungsten bronze structure. The cell sizes of the potassium, rubidium, and cesium tantalum-tungsten bronzes are given in Table II.

(1) A. Magneli and B. Blomberg, *Acta Chem. Scand.*, 5, 372 (1951).
(2) F. Galasso, L. Katz, and R. Ward, *J. Am. Chem. Soc.*, 81, 5898 (1959).

Table I : X-Ray Data for $Rb_{0.3}(Ta_{0.3}W_{0.7})O_3$

hkl	d calcd.	d obsd.	$Rb_{0.3}(Ta_{0.3}$ $W_{0.7})O_3$ I obsd	$Rb_{0.29}WO_3^a$ I obsd.
100	6.36	6.34	m	m
002	3.86	3.84	s	s
110	3.67	3.66	w	w
111	3.31			vw
102	3.30			
		3.29	s	s
200	3.18	3.18	vs	vs
112	2.66	2.65	m	s
202	2.453	2.45	s	s
211	2.294	2.297	w	w
300	2.119	2.116	w	w
212	2.040	2.037	m	m
004	1.929	1.925	m	m
302	1.858	1.858	w	w
104	1.846			
		1.833	s	s
220	1.836			vw
310	1.764			
		1.763	w	w
213	1.756			vw
311	1.719			
		1.705	w	w
114	1.707			vw
222	1.657			
		1.649	s	s
204	1.649			s
312	1.604	1.604	w	m
400	1.590	1.590	w	m
402	1.470	1.470	m	s
320				vw
313				w
321				vw
304	1.426	1.425	w	vw
410	1.388	1.389	vw	vw
411	1.366			
		1.363	m	vw
322	1.364			m
224	1.330	1.329	m	s
412	1.306			
		1.304	w	w
314	1.301			w
006	1.286	1.285	vw	vw
106	1.260	1.260	w	w
404	1.227	1.226	m	s
116	1.214			
		1.213	vw	vw
331	1.209			vw
420	1.202	1.201	m	m
206	1.192	1.192	w	w
332	1.166			
		1.162	vw	vw
324	1.163			vw
422	1.147	1.146	m	s

^{a} A. Magneli, *Acta Chem. Scand.*, **7**, 315 (1953).

Table II : Lattice Constants for Tetragonal and Hexagonal Bronzes

Compound	a_0, Å.	c_0, Å.	c/a
Tetragonal			
$K_{0.48}WO_3^a$	12.285	3.833	0.312
$K_{0.5}(Ta_{0.5}W_{0.5})O_3^b$	12.36	3.90	0.316
Hexagonal			
$K_{0.3}WO_3^c$	7.385	7.513	1.02
$K_{0.3}(Ta_{0.3}W_{0.7})O_3$	7.333	7.685	1.05
$Rb_{0.27}WO_3^c$	7.394	7.516	1.02
$Rb_{0.3}(Ta_{0.3}W_{0.7})O_3$	7.342	7.715	1.05
$Cs_{0.31}WO_3^c$	7.406	7.608	1.03
$Cs_{0.3}(Ta_{0.3}W_{0.7})O_3$	7.450	7.821	1.05

^{a} M. J. Sienko and S. Morehouse, *Inorg. Chem.*, **2**, 485 (1963). ^{b} See ref. 2. ^{c} See ref. 3.

Calculation of the tungsten–oxygen interatomic distances from the atomic positions found by Magneli for $Rb_{0.29}WO_3$ showed them to be longer in the a–b plane, indicating that the oxygen octahedra are flattened. It is felt that this distortion may be partially due to the presence of some pentavalent tungsten in the octahedral sites (Jahn–Teller distortion). Therefore, when the larger tantalum ions replace the pentavalent tungsten ions in this hexagonal structure there is an elongation of the c-axis and, in the potassium and rubidium bronzes, a contraction of the a-axis in an attempt to minimize the distortion of the octahedra. Because the large cesium ion probably causes a closer packing of oxygen ions in the a–b plane, tantalum substitution in the cesium–tungsten bronze causes expansion along both axes, but significantly more in the c direction so that c/a for all the $A_{0.3}(Ta_{0.3}W_{0.7})O_3$-type bronzes is the same. This anisotropic expansion agrees quite well with that observed when tantalum ions were substituted for the pentavalent tungsten ions in the tetragonal tungsten bronze structure. A summary of these data is given in Table II.

Thermal expansion characteristics of the hexagonal bronzes as reported by Werner, Kierkegaard, and Magneli[3] appear to reflect the loose packing in the a–b plane by exhibiting nonlinear expansion in the a direction for the potassium and rubidium compounds (Table III). The tantalum–tungsten hexagonal bronzes studied in our laboratory showed nonlinear thermal expansion along the c-axis. It appears that since the c-axis has been lengthened, the oxygen ions become more

(3) E. Werner, P. Kierkegaard, and A. Magneli. *Acta Chem. Scand.*, **15**, 427 (1961).

Table III: Thermal Expansion Data[a]

| Compound | a-axis | | c-axis | |
	Temp., °C.	Exp. coeff. × 10⁶	Temp., °C.	Exp. coeff. × 10⁶
$K_{0.3}WO_3$[b]	20–545	(6 ± 1)	20–750	(15 ± 3)
	545–750	−(12 ± 3)		
$K_{0.3}(Ta_{0.3}W_{0.7})O_3$	20–900	+12.1	20–600	21.2
			~600–900	−11.0
$Rb_{0.27}WO_3$[b]	20–500	(7 ± 2)	20–970	(12 ± 3)
	700–900	0		
	900–970	−(6 ± 3)		
$Rb_{0.3}(Ta_{0.3}W_{0.7})O_3$	20–900	+14.3	20–600	+22.0
			~600–900	−10.4
$Cs_{0.31}WO_3$[b]	20–720	(2 ± 0.7)	20–720	(4 ± 1.0)
$Cs_{0.3}(Ta_{0.3}W_{0.7})O_3$	20–900	+7.6	20–500	+1.64
			~500–900	−9.4

[a] Calculated from X-ray data.   [b] See ref. 3.

loosely packed in this direction and thus more irregular in their c-axis thermal expansion.

The introduction of tantalum ions in the hexagonal bronzes also affects their electrical resistivities. Since the presence of pentavalent tungsten probably causes the low resistivity of the bronzes, its replacement by tantalum should result in phases with much higher resistances. This result was observed. The resistivities of pellets of the tantalum–tungsten bronzes are given in Table IV.

Table IV: Resistivity Data

Compound	Resistivity, ohm. cm.[a]
$K_{0.3}(Ta_{0.3}W_{0.7})O_3$	2 × 10⁸
$K_{0.31}WO_3$[b]	5 × 10⁻²
$Rb_{0.3}(Ta_{0.3}W_{0.7})O_3$	7 × 10⁸
$Rb_{0.29}WO_3$[b]	2.8 × 10⁻²
$Cs_{0.3}(Ta_{0.3}W_{0.7})O_3$	2 × 10⁷
$Cs_{0.30}WO_3$[b]	6.7 × 10⁻²

[a] At room temperature.   [b] See ref. a in Table I.

In summary, since the pentavalent tungsten ion has a 5d electron which probably causes the blue color and low resistivity and contributes to the distortion of the oxygen octahedra in the hexagonal tungsten bronzes, substitution of pentavalent tantalum, which has no 5d electron, for the pentavalent tungsten ions produces cream color phases, with high resistivities and less distortion of the octahedra in their structures.

Influence of Temperature on the Radiation-Induced Branching of Polyisobutene Molecules

by D. T. Turner

Camille Dreyfus Laboratory, Research Triangle Institute, Durham, North Carolina   (Received November 20, 1963)

The stoichiometry of polymer degradation is conveniently studied by measurement of solution viscosity with reference to an appropriate molecular weight relationship established for linear fractions. This procedure is clearly not valid in cases where branching occurs and this possibility must be given careful attention when degradation is caused by exposure to high energy radiation since this almost certainly results in the formation of potential cross-linking sites on the polymer molecules, for example, by the elimination of hydrogen atoms. It is difficult to estimate, and perhaps even to detect, a small degree of branching in a polymer, but the theories of Zimm, Stockmayer, and Fixman[1,2] have been applied to studies of the radiation-induced degradation of polyacrylates and polymethacrylates by Shultz, Roth, and Rathmann.[3] A careful comparison of solution viscosity and light scat-

(1) B. H. Zimm and W. H. Stockmayer, J. Chem. Phys., 17, 1301 (1949).

(2) W. H. Stockmayer and M. Fixman, Ann. N. Y. Acad. Sci., 57, 334 (1953).

(3) A. R. Shultz, P. I. Roth, and G. B. Rathmann, J. Polymer Sci., 22, 495 (1956).

tering data as a function of radiation dose failed to reveal branching in polymers which, by structural analogy with polymers which yield cross-linked networks on irradiation, would be expected to form some cross links.[4]

Recently, Kilb has extended the earlier theoretical treatments to include the more relevant case of a polydisperse polymer with a random distribution of tetrafunctional cross links and has suggested that the most practicable method of estimating branching is by comparison of the ratio of the limiting viscosity numbers of branched and linear polymers of the same weight average molecular weight.[5] There follows an account of the application of this method to a study of the influence of temperature on the radiolysis of polyisobutene.

Experimental

Commercial samples of polyisobutene (M_w in the range 6–12 × 10^5) were purified by double precipitation from petroleum ether (b.p. 40–60°) with methanol. Solvent then was pumped out of the polymer at 60° during several weeks. Polymers of lower molecular weight were prepared by polymerization of isobutene with boron trifluoride at low temperatures[6] and purified similarly. The high molecular weight polymers were thoroughly degassed and sealed *in vacuo* in glass ampoules for exposure to a 4 Mev. beam of electrons from a linear accelerator at a dose rate of the order 1 Mrad/min. Ampoules were cooled during irradiation by immersion in water (20°) or in liquid nitrogen (−196°).

Polyisobutene was found to have a refractive index increment in *n*-hexane at 22° of 0.1567 ± 0.00056 ml./g. (Mr. F. Rogers, Imperial Chemical Industries Ltd., Welwyn Garden City, England). Turbidity measurements were made with a Brice-Phoenix light scattering photometer and M_w was calculated from a Zimm diagram. Polymer was recovered from aliquots of solution, by total evaporation of *n*-hexane, and redissolved in toluene for determination of limiting viscosity number at 25° with an Ubbelohde viscometer.

Calculations

Figure 1 shows plots of [η] against M_w for linear polymers ($\gamma = 0$) calculated from the relationship [η] = 2.15 × $10^{-4}M_v{}^{0.67}$ which is derived from data of Fox and Flory for linear fractions of polyisobutene.[7] The broken curve is for the case where all the polymer molecules are of the same length, *i.e.*, $M_v = M_n$, and the topmost full curve is for polymer molecules of random length distribution, *i.e.*, $M_w = 2M_v/1.85$. The full curve has been used to generate a family of curves with the parameter γ, a cross-linking index which
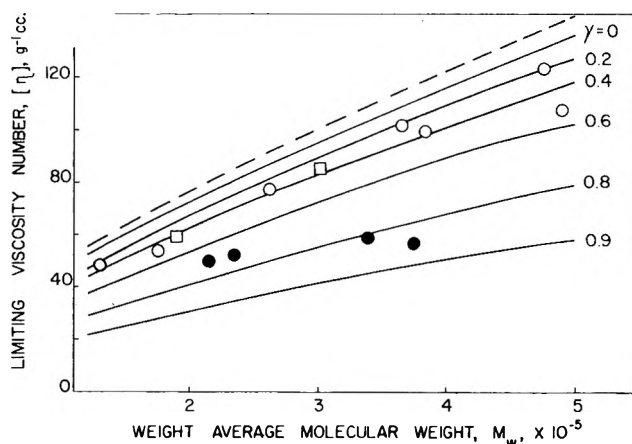
Figure 1. Relationship between M_w and [η] for various polyisobutenes: □, polymer prepared by polymerization of isobutene with boron trifluoride; O, polyisobutenes irradiated at 20° (doses 0.3–4.0 Mrads); ●, polyisobutenes irradiated at −196° (doses 4–10 Mrads).

rises toward unity at the gel point. Ratios of limiting viscosity numbers of the same weight average molecular weight for various values of γ were taken from Table III of Kilb's paper.

Discussion

The fact that the unirradiated polyisobutenes have (M_w, [η]) coordinates which lie below the curves for $\gamma = 0$ implies that they are either branched or else have a wider length distribution than corresponds to either of the two distributions considered in Fig. 1. Branching cannot be excluded definitely but the latter possibility seems the more likely. Kilb has suggested that his method of estimating branching is not very sensitive to length distribution and this may be seen by a comparison of the two curves for $\gamma = 0$ in Fig. 1. Nevertheless, this factor will assume importance when an attempt is made to estimate low degrees of branching. In these circumstances analysis of the results obtained at 20° is deferred pending the establishment of a curve for $\gamma = 0$ which takes appropriate account of length distribution.

The (M_w, [η]) results obtained after irradiation at −196° lie sufficiently below those obtained at the higher temperature to demonstrate unequivocally that the polymers are extensively branched. However, a decision as to whether the cross-linking reaction itself

(4) A. R. Shultz, P. I. Roth, and J. M. Berge, paper presented at the 135th National Meeting of the American Chemical Society, Boston, Mass., 1959.

(5) R. W. Kilb, *J. Polymer Sci.*, **38**, 403 (1959).

(6) R. M. Thomas, W. J. Sparks, P. K. Frolich, M. Otto, and M. Müller-Cunradi, *J. Am. Chem. Soc.*, **62**, 276 (1940).

(7) T. G Fox and P. J. Flory, *J. Phys. Colloid Chem.*, **53**, 197 (1949).

increases on lowering the temperature of irradiation or whether the number average of branches per molecule is merely enhanced by depression of the fracture reaction must again await precise knowledge of the extent of cross linking at the higher temperature.

From the above findings it now clearly emerges that the puzzling linear relationship reported between the yield cf fractures in polyisobutene and the temperature of irradiation in the range -196-$20°$ is an artifact, because it was based on the analysis of viscosity data on the assumption that the polymer is linear.[8,9] Presumably, other data concerning radiation damage in various biological systems, which has been adduced to make a case that this unusual temperature dependence may be a rather general effect in radiation chemistry, also require reappraisal. In this respect it is noted that Pollard has interpreted the temperature dependence of the inactivation of a number of biological systems on irradiation as a plateau effect.[10]

(8) P. Alexander, R. M. Black, and A. Charlesby, *Proc. Roy. Soc.* (London), **A232**, 31 (1955).

(9) D. T. Turner, *J. Polymer Sci.*, in press.

(10) E. Pollard, *Advan. Biol. Med. Phys.*, **3**, 153 (1953).

Decomposition Pressure of TcZn6[1]

by Ewald Veleckis and Irving Johnson

Argonne National Laboratory, Chemical Engineering Division, Argonne, Illinois (*Received December 9, 1963*)

Studies[2] of the technetium–zinc system have revealed the existence of two intermediate phases: a zinc-rich phase which contains approximately 5.5 atom % technetium and a technetium-rich phase which corresponds to the formula TcZn6. The free energy of formation of this latter compound has been determined from the measurement of the vapor pressures of zinc in equilibria

$$TcZn_6(s) = Tc(s) + 6Zn(g) \qquad (1)$$

by the Knudsen effusion method.

Experimental

Vapor pressures were measured by the use of a continuous weighing effusion balance.[3] A tantalum effusion cell, with two opposing orifices (approximately 0.01 cm. in diameter) located in the cell wall, was employed for all of the measurements.

To prepare the alloy (15 atom % Tc), arc-melted technetium and high purity zinc (99.999%) were heated together at 600° for 31 days. Approximately 150-mg. samples of the powdered (200 mesh) alloy were used in each experiment. Zinc was evaporated isothermally until no further changes in weight were observed. The weight loss *vs.* time graph had one sharp break at the sample weight which corresponded to TcZn6. The break was followed by a straight line indicative of the heterogeneous region TcZn6–Tc. The decomposition pressure of TcZn6 is proportional to the constant rate of weight loss in this region and was computed using the Knudsen equation

$$P_{mm} = 17.14(KA)^{-1}(T/M)^{1/2}(\Delta w/\Delta t) \qquad (2)$$

in which P_{mm} is the vapor pressure of zinc in mm.; K, the Clausing short channel correction factor; A, the area of the orifice in cm.^{2}; T, the absolute temperature in °K.; M, the atomic weight of zinc; and $\Delta w/\Delta t$, the rate of weight loss in grams per second. The effective orifice area, $KA = 1.62 \times 10^{-4}$ cm.^{2}, of the cell was determined by calibration with pure solid zinc. The vapor pressure of zinc, reported by Barrow, *et al.*,[4] was used.

Because of the low volatility of technetium only zinc contributes significantly to the vapor. Mass spectrometric[5] and torsion effusion[6] studies have shown that zinc vapor consists mainly of monatomic zinc. The small value of the ratio (orifice area) : (sample area) renders the corrections for nonequilibrium conditions within the cell negligible. Assuming that the evaporation coefficient of Zn from Tc–Zn alloys is approximately the same as that of Cd from U–Cd alloys,[7] the correction to the vapor pressure is estimated to be less than 0.5%.

(1) Work performed under the auspices of the U. S. Atomic Energy Commission.

(2) M. Chasanov, I. Johnson, and R. V. Schablaske, *J. Less-Common Metals*, in press.

(3) E. Veleckis, C. L. Rosen, and H. M. Feder, *J. Phys. Chem.*, **65**, 2127 (1961); the balance in the original apparatus has been replaced by an Ainsworth, Model RVA-AU-2, recording vacuum balance.

(4) R. F. Barrow, *et al.*, *Trans. Faraday Soc.*, **51**, 1354 (1955).

(5) K. H. Mann and A. W. Thickner, *J. Phys. Chem.*, **64**, 241 (1960).

(6) G. M. Rosenblatt and C. E. Birchenall, *J. Chem. Phys.*, **35**, 788 (1961).

(7) E. Veleckis, H. M. Feder, and I. Johnson, *J. Phys. Chem.*, **66**, 362 (1962).

Results and Discussion

The observed decomposition pressures of $TcZn_6$ are listed in column 3 of Table I. These data may be represented by the empirical equation

$$\log P_{mm} = 9.853 - 8242T^{-1}$$

$$(\pm 0.024, \text{ std. dev.}) \quad (3)$$

In spite of the relatively high vapor pressures (above 1 mm.) reached at the highest temperature, no evidence of deviation from molecular flow was observed. At 570° the ratio of the mean free path to the orifice diameter is 1.5. Vapor pressure measurements for mercury[8] have demonstrated the persistence of molecular flow at similar ratios.

Table I: Decomposition Pressure and Standard Free Energy of Formation of $TcZn_6$

Temp., °C.	$\dfrac{\Delta w}{\Delta t} \times 10^6$, g./sec.	P_{mm} (obsd.)	$-\Delta G_f^\circ$, kcal./g.-atom
470.0	0.165	0.0592	3.02
480.0	0.217	0.0778	3.03
488.4	0.306	0.110	2.89
500.0	0.429	0.156	2.85
510.0	0.554	0.203	2.86
520.0	0.813	0.299	2.68
530.0	0.988	0.366	2.75
541.7	1.59	0.594	2.47
552.4	2.10	0.789	2.43
560.0	2.42	0.914	2.46
570.0	2.94	1.114	2.50

The standard free energy of formation of $TcZn_6$, listed in column 4 of Table I, was computed with the relation ΔG_f° (cal./g.-atom) $= x_{Zn}RT \ln (P/P^0)$, in which x_{Zn} is the atom fraction of zinc in the compound $(^6/_7)$; P, the decomposition pressure of the alloy at temperature T; and P^0, the vapor pressure of pure liquid zinc. Values of P^0 were calculated using the equation given by Barrow and his co-workers.[4] The free energy may be represented by the empirical equation

$$\Delta G_f^\circ \text{ (cal./g.-atom)} = -7823 + 6.43T$$

$$(\pm 75, \text{ std. dev.}) \quad (4)$$

$TcZn_6$ is reported to decompose peritectically into pure technetium metal and a saturated liquid zinc solution at about 950°.[2] Extrapolation of eq. 4 indicates that $\Delta G_f^\circ = 0$ at 944°, which, in view of the long extrapolation, is in satisfactory agreement with the thermal analysis result.

The partial molal excess free energy of technetium in saturated solutions, $\bar{G}^{XS}$, may be computed from the free energy of formation of $TcZn_6$ and the solubility of technetium in liquid zinc. At 500° $\bar{G}^{XS} = -3.2$ kcal./g.-atom of Tc indicating moderate negative deviation from ideal solution behavior. The low solubility of technetium in liquid zinc (6×10^{-3} atom % at 500°) is therefore due to the great stability of $TcZn_6$ ($\Delta G_f^\circ = -20.0$ kcal./mole at 500°) rather than a large positive deviation from ideality.

Acknowledgment. We wish to thank E. Van Deventer and P. D. Hunt for technical assistance, and Dr. H. M. Feder for helpful discussions.

(8) K. D. Carlson, P. W. Gilles, and R. J. Thorn, *J. Chem. Phys.*, 38, 2725 (1963).

The Electrical Conductivity of Aqueous Electrolytic Solutions near the Freezing Point

by R. A. Horne and R. A. Courant

Arthur D. Little, Inc., Cambridge, Massachusetts

The activation energies of aqueous solutions of strong electrolytes are in the range 3–4 kcal./mole at 10° and increase with decreasing temperature, while that of ice is 10–12 kcal./mole.[1] Unfortunately, the precision conductivity measurements of Jones and Bradshaw[2] and Gunning and Gordon[3] on aqueous KCl solutions were repeated at too few low temperatures to permit reliable calculation of activation energies of conduction as the freezing point is approached. However, their data do show deviation from linearity in the conductance *vs.* temperature curve, and the change in slope evidences changes in the activation energy.

We have noted elsewhere[4] that the activation energy of electrical conduction is very sensitive to structural changes in the solution, and, on the basis of changes in density, it is well-known that water undergoes important structural changes near 4°. The behavior of the activation energy of conduction as the freezing

(1) R. S. Bradley, *Trans. Faraday Soc.*, 53, 687 (1957).

(2) G. Jones and B. C. Bradshaw, *J. Am. Chem. Soc.*, 55, 1780 (1933).

(3) H. E. Gunning and A. R. Gordon, *J. Chem. Phys.*, 10, 126 (1942).

(4) R. A. Horne, B. R. Myers, and G. R. Frysinger, *ibid.*, 39, 2666 (1963).

Figure 1. Specific conductance of an aqueous
0.100 M KCl solution at low temperatures.

in resistance accompanied by a slight increase in cell
temperature as the phase change finally occurred.

Results and Discussion

The temperature dependence of the specific con-
ductance of an aqueous 0.100 M KCl solution over
the temperature range -1 to $+9°$ is shown in Fig. 1.
The activation energies of conduction were calculated
from the curve in Fig. 1 using the integrated form of
the Arrhenius equation

$$E_a = (\log K_2 - \log K_1)4.576T_2T_1/(\Delta T) \quad (1)$$

The results are shown in Fig. 2. As the tempera-
ture decreases, E_a increases slowly, goes through a
maximum at about $3°$, and then drops off sharply.

Unfortunately, due to the supercooling, we were
not able to calculate reproducible E_a values at the
freezing point. Presumably E_a goes through a mini-
mum near the freezing point and then rises very
rapidly to its ice value.

At higher temperatures the activation energy of
electrical conduction of aqueous solutions decreases
with increasing temperature due to thermal destruc-
tion of the order in liquid water. The E_a of viscous
flow in water and of self-diffusion behave in a parallel
manner, and this is taken as evidence of a common
mechanism for all three processes, namely, the forma-

point of the solution is approached is, therefore, of
interest.

Experimental

The precision conductivity bridge and the thermo-
static bath have been described earlier.[5] The con-
ductivity cell used had parallel plate electrodes of
platinized platinum. For those runs in which the
temperature was reduced below the freezing point
expendable cells of a capillary type with electrodes
consisting of snarls of platinized platinum wire were
used. This precaution proved unnecessary because
freezing did not damage the cells.

The temperature variation in the thermostatic
bath was $\pm 0.05°$ which corresponds to ± 0.000011
conductivity unit. The temperature variation in the
cell is less than in the bath. Thus the deviation in the
experimental conductivity values should be less than
0.14%. However, the measured average deviation
was actually slightly larger, for example, 0.28%,
at 2.64°.

Supercooling occurred in all runs and was indicated
by the continuation of the gradual increase in resistance
down below the freezing point, then an abrupt increase

Figure 2. Activation energy of electrical conductance of an
aqueous 0.100 M KCl solution at low temperatures.

(5) R. A. Horne and G. R. Frysinger, *J. Geophys. Res.*, **68**, 1967 (1963).

tion of a "hole" in the solvent followed by the jump of a nearby solvent molecule or solvated ion into the "hole."[6]

Recently Némethy and Scheraga[7] have made quantitative estimates of the temperature dependence of the size and concentration of the Frank–Wen "flickering clusters" in water. As temperature increases, the concentration of clusters increases but their sizes decrease. Figure 3 shows that relative cluster size, S_T/S_0, estimated from the results of Némethy and Scheraga[7]; the relative viscosity of water, η_T/η_0; and the reciprocal of the relative limiting equivalent conductivity, $(\Lambda_T/\Lambda_0)^{-1}$, from the table of values quoted by Robinson and Stokes,[8] vary with temperature in much the same manner, thus providing a striking illustration of the dependence of transport processes on the structure of the liquid. It is interesting to notice that the important factor appears to be cluster size rather than cluster concentration.

The temperature of maximum density of an aqueous 0.100 M KCl solution is also about 3°. Estimates of E_a for conduction of sea water, based on the conductivity data of Thomas, Thompson, and Utterback,[9] have shown that for sea water up to 5°/oo chlorinity, the temperatures of maximum density and of maximum E_a of conduction very nearly coincide, but at larger concentrations, the latter becomes increasingly larger than the former.[10] These changes in density and E_a
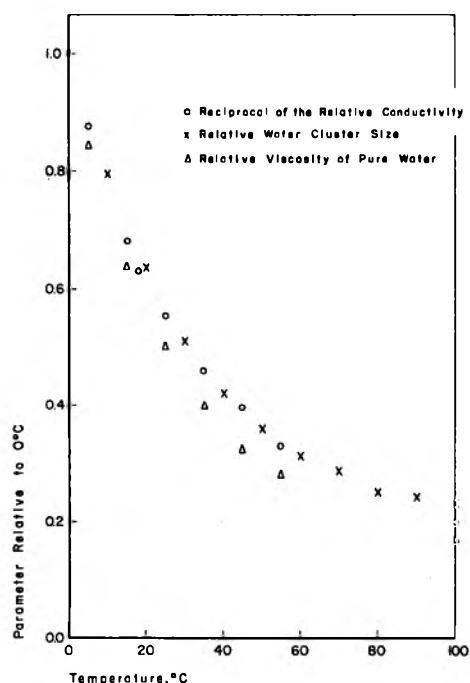
of electrical conduction arise from structural changes in water in the neighborhood of 4°. Above 4° the structure of water is believed to be quartz-like (water II) but below 4° ice–tridymite-like forms (water I) are present.[11] The density of the former is 1.08 but the density of water I is only 0.91.[11] E_a of conduction is the same as E_a of "hole" formation in water, thus the rapid drop-off of E_a of conduction below 4° (Fig. 2) is due to the relatively greater ease of "hole" formation in "the relatively empty ice-like structure of water I"[11] in contrast with the more dense and closely knit water II.

It is interesting to note that E_a of conduction in the more open water I falls to a value comparable to the energies estimated by Morgan and Warren[7,12] for the breaking of H bonds in liquid water, 1.4 compared to 1.3–2.6 kcal./mole.

Acknowledgment. This work was supported in part by the Bureau of Ships, Department of the Navy, Contract NObsr-81564 S-7001-0307. The authors wish to acknowledge valuable discussions with Prof. D. E. Carritt of M.I.T., Prof. R. M. Fuoss of Yale, and Dr. J. D. Birkett of Arthur D. Little, Inc.

(6) See S. Glasstone, K. J. Laidler, and H. Eyring, "The Theory of Rate Processes," McGraw-Hill Book Company, Inc., New York, N. Y., 1941, pp. 505, 520, 523, 557, and 562.

(7) G. Némethy and H. A. Scheraga, *J. Chem. Phys.*, 36, 3382 (1962).

(8) R. A. Robinson and R. H. Stokes, "Electrolyte Solutions," 2nd Ed., Butterworths Scientific Publ., Ltd., London, 1959, p. 465.

(9) B. D. Thomas, T. G. Thompson, and C. L. Utterback, *Conseil Perm. International p. l'Explor. de la Mer, J. du Conseil*, 9, 28 (1934).

(10) R. A. Horne and R. A. Courant, *J. Geophys. Res.*, 69, 1152 (1964).

(11) J. D. Bernal and R. H. Fowler, *J. Chem. Phys.*, 1, 515 (1933).

(12) J. Morgan and B. E. Warren, *ibid.*, 6, 666 (1938).

Solid–Liquid Phase Equilibria in Binary Mixtures of p-Dioxane with Anisole and Several Related Compounds

by N. F. Mangelson, J. R. Goates, and J. B. Ott

Department of Chemistry, Brigham Young University, Provo, Utah
(Received December 16, 1963)

In the course of conducting some exploratory solid–liquid phase equilibria studies, it was observed that mixtures of dioxane and anisole formed a solid compound. Since both of these substances are generally considered to be strong electron donors, their intermolecular compound was quite unexpected. This note reports the solid–liquid phase diagram for the p-di-

Figure 3. Comparison of the temperature dependence of the conductive, structural, and viscous properties of aqueous electrolytic solutions.

oxane–anisole system and several related systems. The latter were investigated principally to help in the understanding of the type of interactions involved between dioxane and anisole.

Experimental

Chemicals. Spectro grade *p*-dioxane and reagent grade anisole, N,N-dimethylaniline, diphenyl ether, and phenetole were further purified by fractional distillation in a 70-cm. vacuum-jacketed column, packed with glass helices and operated at a reflux ratio of approximately 50:1. The center third cut was retained for use.

The purified reagents contained the following amounts of liquid soluble–solid insoluble impurities as determined by the change of freezing point as a function of the fraction melted: *p*-dioxane, 0.06 mole %; anisole, 0.01 mole %; N,N-dimethylaniline, 0.16 mole %; diphenyl ether, 0.19 mole %.

Several other chemicals were used in exploratory measurements to check on the presence or absence of solid intermolecular compounds. These chemicals were reagent grade or better and were used without further purification.

Apparatus and Temperature Scale. The freezing point apparatus has been described previously.[1] Temperatures were measured with a strain-free platinum resistance thermometer (laboratory designation T-2) in conjunction with a Leeds and Northrup high precision resistance bridge. The Leeds and Northrup calibration of this resistance thermometer was checked by us at the time of the measurements. Details are given in a previous paper.[2] On the basis of these checks, the temperature scale is considered accurate to within ±0.05° over the temperature range of the measurements.

Measurements and Accuracy. Both cooling and warming curves were made. Freezing points were obtained by extrapolation across the supercooled region. Agreement within a few hundredths of a degree between freezing and melting points was generally obtained.

The accuracy of the freezing points of the pure substances was estimated to be ±0.05°, and that of the solutions was ±0.1°. The invariant temperature values where stirring was possible are also considered accurate to within ±0.1°.

Results and Discussion

The freezing point data for the dioxane–anisole system are recorded in Table I, and the phase diagram for this system is shown in Fig. 1.

Table I: Freezing Points of Pure Compounds and Their Binary Solutions

Mole fraction of dioxane	Freezing point, °K.	Mole fraction of dioxane	Freezing point, °K.	Mole fraction of dioxane	Freezing point, °K.
		p-Dioxane–anisole			
0.0000	235.99[a]	0.3349	246.81	0.5964	262.25
.0492	234.17	.3925	248.05	.6950	268.09
.0978	232.22	.4122	248.53	.7959	273.51
.1472	237.19	.4425	251.17	.8678	277.75
.1943	240.82	.4658	253.10	.9298	281.10
.2476	243.77	.4905	254.90	1.0000	284.95[a]
.2920	245.52				
		p-Dioxane–N,N-dimethylaniline			
0.0000	275.57[a]	0.4331	253.20	0.7506	271.80
.1138	270.02	.5023	258.10	.7996	274.33
.2248	264.26	.5915	263.60	.9904	279.67
.3252	258.52	.6749	268.15	1.0000	284.95[a]
.4014	253.88				
		p-Dioxane–diphenyl ether			
0.0000	300.04[a]	0.5056	270.57	0.7597	271.59
.0975	295.58	.5900	263.29	.8014	273.87
.2162	289.58	.6124	263.00	.8992	279.37
.3314	282.93	.6704	266.52	1.0000	284.95[a]
.4094	277.86				

[a] Corrected to zero impurity.

As can be seen in the diagram, an incongruently melting 1:1 compound forms. The composition was obtained from the maximum in a plot of length of meritectic halt *vs.* mole fraction.

The meritectic point is at 0.408 mole fraction dioxane and 248.18°K. The eutectic occurs at 0.104 mole fraction dioxane and 231.98°K. The invariant temperature line at the right of the diagram is the solid state transition in dioxane.

In order to find out more about the interactions between dioxane and anisole, a number of other related systems were investigated. Two of these, dioxane with N,N-dimethylaniline and with diphenyl ether, were studied over the entire composition range. The freezing point data for these systems are recorded in Table I. Since both are single eutectic systems, the phase diagrams are not given. The eutectic points are at 0.422 mole fraction dioxane, 252.35°K. in dioxane–N,N-dimethylaniline and at 0.601 mole fraction, 262.16°K. in the dioxane–diphenyl ether system.

Ten other systems were investigated at only three compositions, 0.3, 0.5, and 0.7 mole fractions. When

(1) J. R. Goates, J. B. Ott, and A. H. Budge, *J. Phys Chem.*, **65**, 2162 (1961).

(2) J. R. Goates, J. B. Ott, and N. F. Mangelson, *ibid.*, **67**, 2874 (1963).
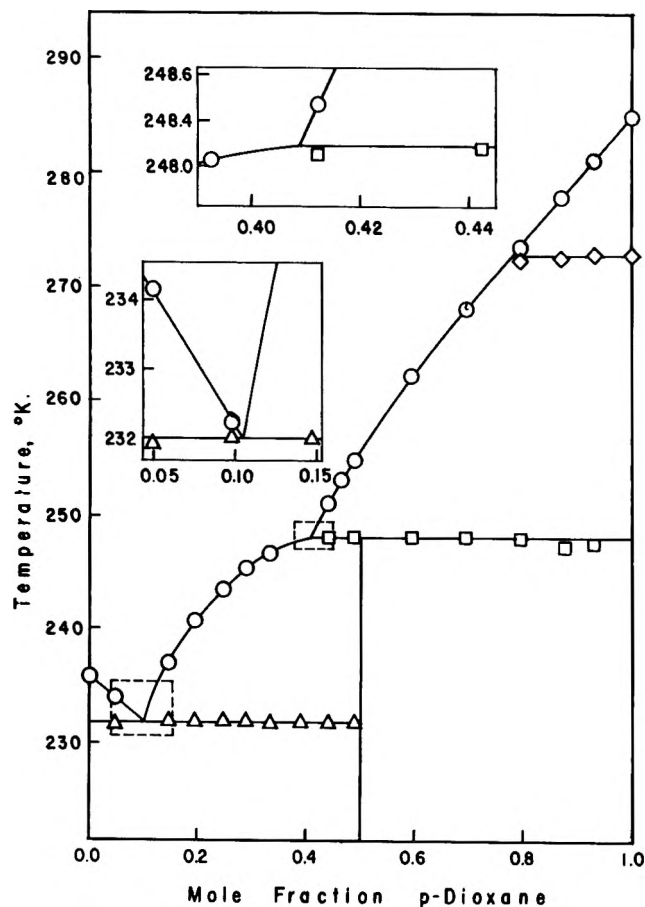
Figure 1. Phase diagram for p-dioxane–anisole.

the same eutectic was observed at each composition and no other temperature halts or irregularities were observed in the cooling curves, the conclusion was made that no compounds were present between the extreme compositions studied. The composition was chosen to include mixtures corresponding to 1:2, 1:1, and 2:1 molecular ratios.

One would expect that the most likely bonding site on the dioxane molecules would be the oxygen atoms. Any one of at least three parts of the anisole molecule might be involved: (1) the ring, (2) the oxygen, or (3) the methoxy hydrogens. Substances related to anisole but chosen to enhance the activity of each of the three sites mentioned above were then investigated.

Inasmuch as anisole has a high electron density in the ring, other aromatic compounds of varying ring electron density were studied. No compound formation was observed in mixtures of dioxane with nitrobenzene, α,α,α-trifluorotoluene, chlorobenzene, benzene, toluene, o-, m-, and p-xylenes, and N,N-dimethylaniline. Since the electron density in the ring of anisole is less than in N,N-dimethylaniline but greater than in the rest of the compounds, it would appear that

the ring is not significantly involved in the dioxane–anisole interaction.

Anisonitrile and 2-methoxypyridine were chosen as compounds similar to anisole in size and structure, but with more electropositive methoxy hydrogens. Neither of the two formed a compound with dioxane. This fact appears to be evidence against the possibility of attachment through the methoxy hydrogens.

Diphenyl ether and phenetole were used to study the effects of replacing the aliphatic radical of the mixed ether with another group which would in one case enrich and in the other case deplete the electron density around the oxygen. Neither substance formed an addition compound with dioxane, which fact implies that the extent of electronegativity of the oxygen in anisole is not significant in the formation of the anisole–dioxane compound. Finally, mixtures of tetrahydrofuran and anisole were studied, and even in this system, no addition compound formed.

On the basis of these results, it appears likely that the formation of the dioxane–anisole 1:1 compound may be caused more by a favorable crystal geometry than a strong specific interaction. The activity coefficients of the dioxane in the liquid mixtures give support to this conclusion. A comparison of the freezing point depression of dioxane in the three systems for which the information is available (dioxane with anisole, diphenyl ether, and N,N-dimethylaniline) shows slightly less interaction for dioxane in anisole than in diphenyl ether and only slightly more interaction than in dimethylaniline.

The Ultraviolet Spectra of Transients Produced in the Radiolysis of Aqueous Solutions[1]

by S. Gordon, E. J. Hart, and J. K. Thomas

Chemistry Division, Argonne National Laboratory, Argonne, Illinois (Received December 27, 1963)

The spectra of several transients have been observed in the radiolysis of aqueous solutions by 15-Mev. electrons by a pulse radiolysis method similar to that

(1) Based on work performed under the auspices of the U. S. Atomic Energy Commission.

already reported by Gordon, *et al.*[2] In the latter experiments, it was impossible to observe spectra below 3000 Å. except for 2537 Å. Now with an improved light source and simplified optical arrangement we have extended this range to 2000 Å.

In the present work a 450-watt X130, 450 W/p Osram xenon lamp was used in conjunction with a regulated d.c. power source. This gave a strong continuous light output from 8000 to 2000 Å. The light from this lamp was focused by a built-in quartz lens of 5-cm. focal length through a 4-cm. quartz irradiation cell to a mirror from which it was reflected back through the cell, hence giving an effective light path of 8 cm. The resultant light after a 45° reflection was then focused by a 30-cm. focal length quartz lens into an *f* 3.5 Bausch and Lomb grating monochromator. Interchangeable gratings covering the 180–400- and the 350–800-mμ spectral regions were used. A IP28 photomultiplier tube was placed at the exit of the monochromator and the output for this tube was amplified and photographed on a Tektronic oscilloscope No. 551. The lenses in the system were adjusted to give the best photomultiplier output for the particular wave length region that was of interest with a minimum of scattered light (Table I). The procedure for filling the 4-cm. cell has been described.[2] For the work cited here, 0.4-μsec. electron pulses of varying currents were used, yielding from 1 to 3 μmoles of H and OH radicals per pulse. The dosimetry was carried out by observing the hydrated electron absorption band at λ 5770 Å. in deaerated water where the molar extinction coefficient is 10,000 M^{-1} cm.$^{-1}$.[2]

The solutions studied were aerated 0.1 *N* sulfuric acid and unbuffered aqueous isopropyl alcohol, aqueous acetone, and aqueous *o*-, *m*-, and *p*-phthalate ions. Figures 1 and 2 show the observed spectra.

A transient with a maximum at 235 mμ was observed in the aerated 0.1 *N* H_2SO_4.[3a] No transient was observed in the absence of oxygen. It was suspected that this species was the HO_2 radical as reported by Baxendale.[3b] Two decay curves were observed for this species at 2500 Å. The first is a fast decay with $T_{1/2} \sim 2$ μsec. and a slower decay of $T_{1/2} \sim >10^{-3}$ sec. This is precisely the behavior predicted[4] for the HO_2 via

$$OH + HO_2 \xrightarrow[\substack{T_{1/2}(\text{sec.}) \\ 2 \times 10^{-2}}]{\text{fast}} H_2O + O_2$$

and

$$HO_2 + HO_2 \xrightarrow[\sim 1 \times 10^{-3}]{\text{slow}} H_2O_2 + O_2$$
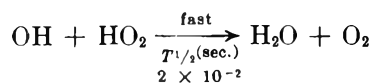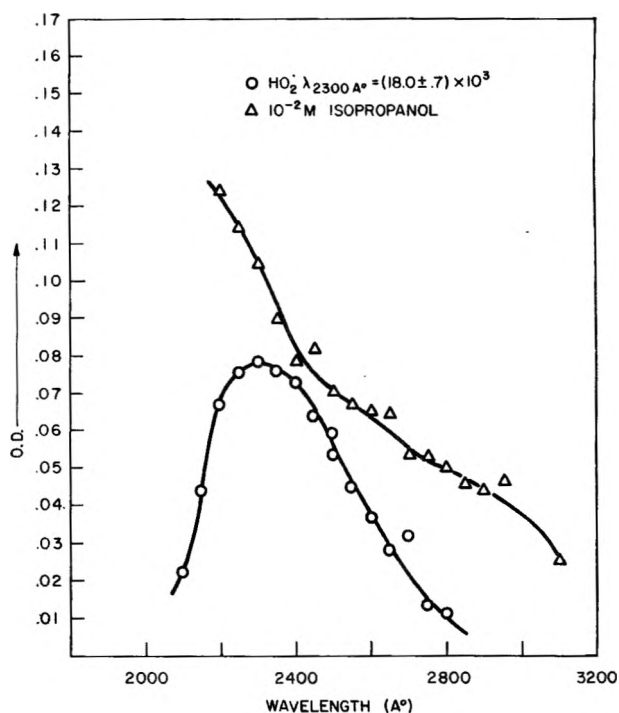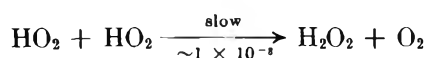
Figure 1. The absorption spectra of the HO_2 and isopropyl radicals at 25° with an 8-cm. path length using a Bausch and Lomb *f*/3.5 grating monochromator with slit width of 1 mm.
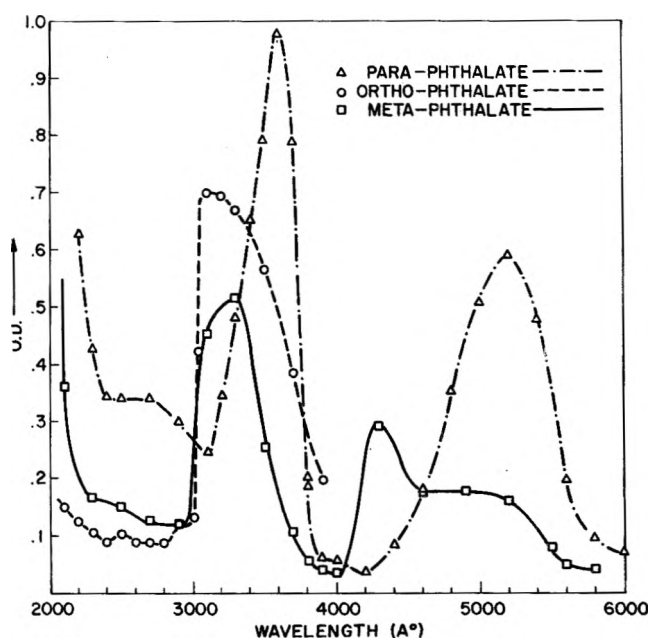
Figure 2. The absorption spectra of the transients produced in the radiolysis solutions of *o*-, *m*-, and *p*-phthalate ions. Experimental conditions as in Fig. 1.

(2) S. Gordon, E. J. Hart, M. Matheson, J. Rabani, and J. K. Thomas, *J. Am. Chem. Soc.*, **85**, 1375 (1963); *Discussions Faraday Soc.*, **36**, 193 (1964).

(3) (a) This bond has been reported by G. Czapski and L. Dorfman, *J. Phys. Chem.*, **68**, 1169 (1964); (b) J. H. Baxendale, *Radiation Res.*, **17**, 312 (1962).

The rate of appearance of the transient at λ 2400 Å. was also observed in solutions of 0.1 N H_2SO_4 with oxygen concentrations varying from 20 to 100 μM. The rate of appearance of the species was first order and the result of determinations gave $k_{H+O_2} = 2.1 \times 10^{10}\ M^{-1}\ \text{sec.}^{-1}$. This agrees very well with previous estimates of 1.2×10^{10}, 2.6×10^{10}, and 1.9×10^{10} for this reaction.[4-6]

Solutions of isopropyl alcohol were irradiated in the absence of oxygen. A transient with an absorption band from 2000 to 3000 Å. was observed. The spectrum exhibited an absorption in the same wave length region as the CH_3-$\overset{.}{C}H$-OH radical reported by Dorfman and Taub.[7] [No absorbing species was detected after irradiation of deaerated $10^{-2}\ M$ methanol solutions where the $\overset{.}{C}H_2OH$ radical is expected.] We attribute the observed absorption to the $(CH_3)_2\overset{.}{C}OH$ formed by H abstraction by the OH radical and the H atom.

Aqueous deaerated solutions of acetone were irradiated and gave a transient absorbing at 2000–3000 Å. This spectrum was very similar to that obtained with the isopropyl alcohol radical. Previously,[2] we have observed that the hydrated electron, which would be formed in the above solutions, reacted rapidly with acetone. The reaction scheme may be

$$(CH_3)_2C{=}O + e_{aq}^{-} \longrightarrow (CH_3)_2\overset{.}{C}{-}O^{-} \xrightarrow[H_2O]{H^+}$$

$$(CH_3)_2\overset{.}{C}{-}OH$$
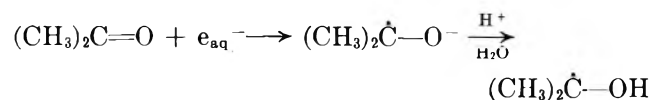
This would account for the similar spectra for the acetone and isopropyl alcohol solutions.

In following the decay of the hydrated electron at 5770 Å. in solutions of o-, m-, and p-phthalate ions at pH 13, it was noted that for the meta and para compounds, composite decay curves were obtained. These were due to the simultaneous e_{aq}^{-} decay and transient build up. If it is assumed that the transient results from reaction of the solute with e_{aq}^{-}, the curves can be treated as a parent–daughter relationship with $T_{1/2}\ e_{aq}^{-} \ll T_{1/2}$ transient. In this way, good pseudo-first-order plots were obtained at two different initial concentrations of the phthalate ions. The second-order rate constants calculated from these curves are: o-phthalate, $1.8 \times 10^9\ M^{-1}\ \text{sec.}^{-1}$; m-phthalate, $3.0 \times 10^9\ M^{-1}\ \text{sec.}^{-1}$; and p-phthalate, $7.3 \times 10^9\ M^{-1}\ \text{sec.}^{-1}$.

From these curves, it was possible to calculate the ratio of the extinction coefficients at 5770 Å. for these ions to that of the hydrated electron. These values were ϵ (hydrated electron)/ϵ (p-phthalate) = 4.76 and ϵ (hydrated electron)/ϵ (meta-phthalate) = 12.0.

These values suggested that the spectra of the isomer transients might exhibit a wave length shift due possi-

bly to their difference in symmetry. The spectra of the ortho and para compounds were determined from 2100 to 6000 Å. by the technique described. These are shown in Fig. 2. It can be seen that there is a shift in the absorption peaks.

The transient absorptions of a 1 mM solution of m-phthalate ion saturated with N_2O and without N_2O were measured at a number of wave lengths. This indicated that a saturated solution (0.03 M N_2O) reduces the transient absorption by a factor of two, suggesting the phthalate ion transient is a species created by capture of the hydrated electron.

Table I: Percentage of Scattered Light

Wave length, mμ	% Scattered light
280	1.0
270	1.5
260	2.0
250	5.0
240	6.5
230	10
220	25
210	43

(4) J. K. Thomas, J. Phys. Chem., **67**, 2593 (1963).

(5) H. Fricke and J. K. Thomas, Radiation Res. Suppl., **4**, 35 (1964).

(6) J. P. Sweet and J. K. Thomas, J. Phys. Chem., in press.

(7) L. M. Dorfman and I. A. Taub, J. Am. Chem. Soc., **84**, 4053 (1962).

High Temperature Mechanism of the System Hydrogen–Hydrogen Iodide–Iodine

by Osamu Horie, Yutaka Ishii,[1] and Akira Amano

The Department of Applied Chemistry, Tohoku University, Sendai, Japan   (Received December 30, 1963)

In the reaction system $H_2 + I_2 \rightleftharpoons 2HI$, Benson and Srinivasan[2a] were the first to show by calculation that I atom-catalyzed chain mechanism would become more important than the classical bimolecular mechanism of the type developed by Bodenstein at higher

(1) On leave from the Defense Ministry.

(2) (a) S. W. Benson and R. Srinivasan, J. Chem. Phys., **23**, 200 (1955); (b) J. H. Sullivan, ibid., **30**, 1292, 1577 (1959); **36**, 1925 (1962).

temperatures and lower iodine concentrations. This was subsequently confirmed experimentally by Sullivan[2b] over a range of temperatures between 633 and 800°K Thus the atomic chain mechanism would account for about 10% of the over-all hydrogen iodide formation at 633°K., 27% at 738°K., and 95% at 800°K. when the initial pressure of iodine was 0.5 atm. The mechanism can then be written more generally in terms of the following elementary reactions.

$$H_2 + I_2 \underset{2}{\overset{1}{\rightleftharpoons}} 2HI$$

$$I_2 + M \underset{}{\overset{}{\rightleftharpoons}} 2I + M$$

$$I + H_2 \underset{4}{\overset{3}{\rightleftharpoons}} HI + H$$

$$H + I_2 \underset{6}{\overset{5}{\rightleftharpoons}} HI + I$$
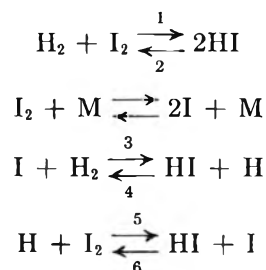
In sharp contrast with the conclusion drawn above, Graven[3] in his paper on the rate of the forward and the reverse reactions stated that the bimolecular mechanism was still paramount for both reactions even at temperatures ranging from 873 to 1048°K. However, the discussion put forward by the latter in support of the classical theory was based on a somewhat doubtful kinetic treatment. Included in Tables I and II are the experimental results reported by Graven for reactions at 973°K. As can be seen in the tables, there are more than twofold variations in the values of Graven's bimolecular rate constant (k_G listed in the fifth column). The variations are more pronounced for decomposition and have a definite trend with the degree of approach to the equilibrium composition. A more serious difficulty arises in the values of E_1 and E_2 which were reported to be 41.0 and 49.2 kcal./mole, respectively. The difference between these values is implausibly larger than the maximum value of $\Delta H_{2,1}$ (973°K.) = 3.66 kcal./mole estimated from the best available thermodynamic data of the relevant molecules.

The purpose of the present note is to show that the raw data reported by Graven can be conversely and more consistently used in support of the atomic chain mechanism. As will be seen later, the data are in fact quite useful to assign values for both k_3 and k_4/k_5. In our present analysis, any ambiguity in the observed quantities which might be caused by the type of apparatus and procedures used by the original author will be ignored.

Applying steady-state hypothesis to the atomic chain mechanism described above, the instantaneous rate of the reactions can be expressed by the following differential form

Table I : Rate of HI Decomposition

$(HI)_i$, mmoles/l.	$(H_2)_i$, mmoles/l.	(I_2), mmoles/l.	t, sec.	k_G, l./mole sec.	$k_3 \times 10^{-3}$, l./mole sec.
0.811		0.00368	0.486	23.1	3.56
1.62		0.0189	0.486	30.4	4.20
2.43		0.0435	0.486	31.6	4.41
3.24		0.0710	0.486	29.2	4.34
4.05		0.110	0.486	29.5	4.47
4.86		0.154	0.486	29.0	4.53
5.67		0.201	0.486	28.0	4.55
3.19		0.0906	0.486	39.3	5.22
4.26		0.257	0.867	39.1	4.60
4.26		0.345	1.30	38.8	4.17
4.26		0.552	2.59	61.2	5.87
3.21	0.200	0.0722	0.486	31.1	4.50
3.21	0.401	0.0701	0.486	31.0	4.69
3.21	0.802	0.0674	0.486	31.4	4.49
3.21	1.60	0.0648	0.486	33.4	4.72
3.21	2.40	0.0612	0.486	34.6	5.07
3.19	3.99	0.0532	0.486	33.0	5.25
3.19	4.79	0.0508	0.486	34.5	5.63

Table II : Rate of HI Synthesis

$(I_2)_i$, mmoles/l.	$(H_2)_i$, mmoles/l.	(HI), mmoles/l.	t, sec.	K_G, l./mole sec.	$k_3 \times 10^{-3}$, l./mole sec.
4.88	0.407	0.410	0.486	605	4.18
4.88	0.814	0.872	0.486	695	4.41
4.88	1.63	1.66	0.486	675	4.52
4.82	2.41	2.46	0.486	729	4.82
4.82	3.21	3.22	0.486	761	4.81
4.82	4.02	4.00	0.486	812	3.69
1.10	4.41	1.16	0.444	835	5.22
2.14	4.28	1.93	0.432	754	3.08
3.02	4.54	2.94	0.457	813	3.95
3.78	4.54	3.61	0.457	843	4.55
5.29	4.54	4.48	0.457	781	5.08
5.71	4.28	4.26	0.432	743	5.07
4.79	4.11	4.95	0.818	753	4.57
5.01	4.01	5.72	1.20	733	4.78
4.54	4.54	4.00	0.457	752	3.97
4.34	4.34	5.93	2.59	512	5.52

$$\pm d(HI)/dt = 2K_1 k_3 (I_2)^{1/2} \lvert (H_2)(I_2) - K_{2,1}(HI)^2 \rvert /$$
$$[(I_2) + K_{4,5}(HI)]$$

where plus sign stands for synthesis and minus sign for decomposition. Upon integration, the following equation can be obtained

(3) W. M. Graven, *J. Am. Chem. Soc.*, **78**, 3297 (1956).

$$At = \frac{D_3 - D_1}{\sqrt{D_1}(D_1 + D_2)}\left[\tan^{-1}\frac{y}{\sqrt{D_1}} - \tan^{-1}\frac{\sqrt{(I_2)_i}}{\sqrt{D_1}}\right] +$$

$$\frac{D_2 + D_3}{2\sqrt{D_2}(D_1 + D_2)}\ln\left|\frac{y + \sqrt{D_2}\sqrt{(I_2)_i} - \sqrt{D_2}}{y - \sqrt{D_2}\sqrt{(I_2)_i} - \sqrt{D_2}}\right|$$

In the equations above, the following abbreviations are used

$$D_1 = \left[\left\{\frac{4K_{2,1}[(HI)_i + 2(I_2)_i] + (H_2)_i - (I_2)_i}{2(1 - 4K_{2,1})}\right\}^2 + \right.$$

$$\left.\frac{K_{2,1}[(HI)_i + 2(I_2)_i]^2}{1 - 4K_{2,1}}\right]^{1/2} +$$

$$\frac{4K_{2,1}[(HI)_i + 2(I_2)_i] + (H_2)_i - (I_2)_i}{2(1 - 4K_{2,1})}$$

$$D_2 = \left[\left\{\frac{4K_{2,1}[(HI)_i + 2(I_2)_i] + (H_2)_i - (I_2)_i}{2(1 - 4K_{2,1})}\right\}^2 + \right.$$

$$\left.\frac{K_{2,1}[(HI)_i + 2(I_2)_i]^2}{1 - 4K_{2,1}}\right]^{1/2} -$$

$$\frac{4K_{2,1}[(HI)_i + 2(I_2)_i] + (H_2)_i - (I_2)_i}{2(1 - 4K_{2,1})}$$

Figure 1. The relation between k_3 and k_4/k_5 for the synthesis and the decomposition.

$D_3 = K_{4,5}[(HI)]_i + 2(I_2)_i]/(1 - 2K_{4,5})$, $A = K_1k_3 \cdot (1 - 4K_{2,1})/2(1 - 2K_{4,5})$, $y = [(I_2)_i - (HI \text{ formed})/2]^{1/2}$ for synthesis and $[(I_2)_i + (HI \text{ decomposed})/2]^{1/2}$ for decomposition, $K_I = (I)/(I_2)^{1/2} = 5.00 \times 10^{-3}$ $(\text{mole/l.})^{1/2}$ at $973°K.$, $K_{2,1} = k_2/k_1 = 0.03396$ at $973°$ $K.$,[4] and $K_{4,5} = k_4/k_5$.

The value of k_3 can be calculated from the integral rate expression and the observed rate data for each fixed ratio of k_4/k_5 as a parameter. The results of the calculation are illustrated in Fig. 1. The value of k_3 is an increasing function of the ratio k_4/k_5 for both reactions, but it is only for the decomposition that the value is highly sensitive to the change in the ratio. This permits one to estimate the most probable ratio as being about 0.06 from the intersection of the two lines illustrated in Fig. 1. The ratio thus determined in turn gives a group of k_3 values of the minimum standard deviation. From the latter values, also listed in the last column of the tables, 4.6×10^3 l./mole-sec. is estimated for k_3.

The corresponding values at $973°K.$ computed from the kinetic constants reported by Sullivan are $3.6 \sim 6.8 \times 10^3$ l./mole sec. for k_3 and $0.07 \sim 0.20$ for k_4/k_5. The values obtained from the two independent sources are in excellent agreement, and this can be taken as an evidence for the atomic chain mechanism. It should be noted that the evaluation of the kinetic constants was carried out by Sullivan on the basis of the rate of synthesis where the value of k_3 is practically unaffected by the change in k_4/k_5. The ratio of k_4/k_5 was estimated by Sullivan in relation with k_3 and therefore may include considerable uncertainty.

(4) G. Murphy, *J. Chem. Phys.*, 4, 344 (1936); see also ref. 3.

Conductivities and Viscosities of Fused Salts in Fritted Disks[1]

by Benson Ross Sundheim and Alexandre Berlin

Department of Chemistry, New York University, Washington Square, New York, N. Y.
(Received January 18, 1964)

We have recently been examining the conductivity of fused salts held in sintered disks so as to explore the nature of the conduction process near surfaces. In connection with these experiments, we have made several observations which may be of general interest.

Table I: Specific Conductivities and Viscosities of $AgNO_3$ and $TlNO_3$

Temp., °C.	AgNO₃ Spec. cond. Cell A[a]	Spec. cond. Cell B[b]	Visc.[c] Cell C	TlNO₃ Spec. cond. Cell A	Spec. cond. Cell B	Visc. Cell C	Visc.[d] Cell D
213.3	0.6631	0.6519	51.56	0.3649	0.3342	38.81	...
216.4	0.6793	0.6768	50.13	0.3713	0.3424	38.02	...
218.7	0.6885	0.6801	48.75	0.3802	0.3499	37.22	37.33
238.5	0.7847	0.7821	41.51	0.4321	0.4059	32.10	32.39
259.3	0.8793	0.9011	36.15	0.4806	0.4570	28.45	28.16
278.5	0.9660	1.0262	32.43	0.5356	0.5161	25.63	24.97
298.2	1.0806	1.1676	29.70	0.5954	0.5976	23.03	22.68
313.0	...	...	...	0.6363	...	...	21.13
318.3	1.1848	1.4783	27.62	0.6517	0.7947	21.10	...

[a] Specific conductance in mhos cm.⁻¹ in a conventional conductivity cell (platinum electrodes and a 5-mm. long capillary (2-mm. diameter) linking the two electrode compartments). [b] Specific conductance in a similar cell except that the capillary was replaced by a Pyrex medium fritted disk 10 mm. in diameter and 2 mm. thick. [c] Absolute viscosities in millipoises as measured in a regular Ostwald-type viscosimeter. [d] Absolute viscosities measured in a modified Ostwald-type viscosimeter. A Pyrex medium fritted disk 10 mm. in diameter was placed at the end of the long capillary tube.

The conductances of $AgNO_3$ and of $TlNO_3$ were determined in conventional semicapillary cells and in cells with "medium" porosity Pyrex fritted disks over the temperature range 214–318°. A Leeds and Northrup precision Jones bridge was used at frequencies from 2500 to 15,000 c.p.s. The measured resistances varied less than 1% for the conventional cells but up to as much as 7% for the cells with fritted disks. The resistance in the conventional cells was a linear function of $(freq.)^{-1/2}$ but was a linear function of $(freq.)^{-1}$ for the cells with the fritted disks. Large capacitances were required in the parallel equivalent circuits of the fritted disk cells and increases rapidly with decreasing frequency.

1. In conventional conductivity cells we obtained results for $AgNO_3$ which compare favorably with previously published ones.[2-4] The values for $TlNO_3$ agree with those obtained by other workers[5] as far as they go; we have extended the temperature range up to 318° and find that the graph of $\log k$ vs. $1/T$ continues to be reasonably linear in this range.

2. Below 280° the values for the conductivity of $AgNO_3$ in cells containing fritted disks are the same as those obtained without disks. In the same region, the conductivity of $TlNO_3$ is 5–8% less than that found in the absence of such disks. (These values are obtained after prolonged evacuation and flushing of cells and are reproducible and independent of time.) Reducing the pressure above the melt in both electrode compartments of the conductivity cell with a fritted disk produces a decrease in the measured electrical conductance. With a pressure above the melt of less than 5 mm., the decrease in the case of $TlNO_3$ was 3% at 220° and 6% at 320°. Upon returning to atmos-

pheric pressure, the electrical conductance comes back to its original value. This seems to indicate that air bubbles are always entrapped in the frit, in spite of continuous evacuation above the melt and flushing of the melt through the frit.

3. The increase in the apparent specific conductance for both $AgNO_3$ and $TlNO_3$ in fritted disks above 280° is accompanied by detectable inclusion of the cation in the glass. These results together with the absence of any effect of the Pyrex frit on the viscosity of $TlNO_3$ at these temperatures (see below) can tentatively be interpreted as being due to ion exchange of the salt with the glass under the influence of an electric field.

4. In quartz fritted disks, the ratio of the conductance of $TlNO_3$ to that in conventional cells rises regularly above 280° without the abrupt changes shown in Pyrex cells. However, the conductance vs. temperature curves displayed a sort of hysteresis in that the resistance did not return to its initial values upon returning to the lower temperature region. Also, gas bubbles formed in the quartz much more rapidly than in Pyrex so that a clear-cut inference could not be drawn.

5. We conclude that below 280° the behavior of $TlNO_3$ in fine-pore disks is somewhat different from that in the bulk, whereas that of $AgNO_3$ is the same as that in the bulk. Furthermore we note that the

(2) R. C. Spooner and F. E. W. Wetmore, Can. J. Chem., **29**, 134 (1962).

(3) V. D. Polyakov, Akad. Nauk SSSR, Izv. Sekt. fiz.-chim. anali., **26**, 191 (1955).

(4) W. T. Davies, S. E. Rogers, and A. R. Ubbelohde, Proc. Roy. Soc. (London), **A220**, 14 (1953).

(5) J. P. Frame, E. Rhodes, and A. R. Ubbelohde, Trans. Faraday Soc., **55**, 2039 (1959).

result of the transference number experiments above 280° with Pyrex or quartz fritted disks[6,7] must be viewed with suspicion.

6. The conventional shear viscosities of $AgNO_3$ and $TlNO_3$ have been determined over the same temperature range as the conductivities. The viscosity of $AgNO_3$ was found to be somewhat higher than that previously determined,[4] while the temperature range for the viscosity of $TlNO_3$ has been extended.[5] In the case of $TlNO_3$, the viscosity was also determined using a modified Ostwald type viscosimeter in which the flow rate was determined by a Pyrex medium fritted disk located at the end of the conventional long capillary tube. The viscosities determined by these two methods gave the same results.

7. A calculation of the self-diffusion coefficients using the Stokes–Einstein relation and the viscosity values just determined leads to a calculated D_{NO_3}- much larger in $TlNO_3$ than in $AgNO_3$ and almost similar D_{Tl^+} and D_{Ag^+} values. A combination of the self-diffusion values thus calculated with the Nernst–Einstein relation gives a calculated equivalent conductance larger for $TlNO_3$ as compared with $AgNO_3$. Experimentally, however, we find the equivalent conductance of $TlNO_3$ to be about 60% of that of $AgNO_3$.

(6) F. R. Duke and G. Victor, in press.

(7) I. G. Murgulescu and D. Topor, Z. Physik. Chem., 219, 134 (1962).

COMMUNICATIONS TO THE EDITOR

The Use of Flash Heating to Study the Combustion of Liquid Metal Droplets[1]

Sir: Investigations of the combustion of liquid metal droplets are important in order to understand basic oxidation processes,[2] to disperse toxic or radioactive metals safely during high-speed ablative entry into the earth's atmosphere,[3] to control metal fires,[4] or conversely to use metal flames for achieving high temperatures[5] or large thrusts in propulsion devices.[6]

In earlier studies, metal droplets have been produced in flames,[6–8] plasma torches,[9] or burning propellant strands.[7] These experiments have had limitations imposed on the oxidizing atmospheres by the source of heat used to prepare the droplets. Clearly, it would be desirable to use a means of heating that does not itself modify the atmosphere in which the oxidation is to be carried out. Furnaces operating above the melting point of the metal satisfy this requirement to some extent,[10,11] although it may be difficult to obtain sufficiently large energy transfer rates to melt the more refractory metals.

Flash heating[12,13] seems to offer considerable promise as an atmosphere-independent method of preparing droplets of the higher melting metals. In this technique, an intense pulse of light from a capacitor discharge lamp is used to heat solids with high specific areas rapidly to very high temperatures. A number of refractory metals in the form of thin wires, foils, and fine powders have been melted or vaporized this

way.[12–14] The pulses of light normally have millisecond durations, with radiant energies of 10–30 joules/cm.[2] flash.[15] These previous experiments indicate that droplets of any of the metals may be prepared by flash heating in atmospheres that may vary widely

(1) Work was performed under the auspices of the U. S. Atomic Energy Commission.

(2) E. M. Mouradian and L. Baker, Jr., Nucl. Sci. Eng., 15, 388 (1963).

(3) I. L. Branch and J. A. Connor, Jr., Nucleonics, 19, No. 4, 64 (1961).

(4) L. Liebowitz, L. Baker, Jr., J. G. Schnizlein, L. W. Mishler, and J. D. Bingle, Nucl. Sci. Eng., 15, 395 (1963).

(5) A. V. Grosse and J. B. Conway, Ind. Eng. Chem., 50, 663 (1958).

(6) D. A. Gordon, "Solid Propellant Rocket Research," Academic Press, New York, N. Y., 1960, p. 271; W. M. Fassell, C. A. Papp, D. L. Hildenbrand, and R. P. Sernka, ibid., p. 259; W. A. Wood, ibid., p. 287.

(7) R. Friedman and A. Macek, "Ninth Symposium (International) on Combustion," Academic Press, New York, N. Y., 1963, p. 703.

(8) C. M. Drew, A. S. Gordon, and R. H. Knipe, A.I.A.A. Conference on Heterogeneous Combustion, Palm Beach, Fla., Dec , 1963.

(9) Private communication, A. E. Levy-Pascal, Astropower, Inc., Newport Beach, Calif.

(10) H. M. Cassell and I. Liebman, Combust. Flame, 3, 467 (1959).

(11) Private communication, J. L. Beal, Cornell Aeronautical Laboratory, Buffalo, N. Y.

(12) J. Eggert, Physik. Bl., 10, 549 (1954);   J. Phys. Chem., 63, 11 (1959).

(13) L. S. Nelson and J. L. Lundberg, ibid., 63, 433 (1959).

(14) L. S. Nelson and N. A. Kuebler, Rev. Sci. Instr., 34, 806 (1963).

(15) N. A. Kuebler and L. S. Nelson, J. Opt. Soc. Am., 51, 1411 (1961).

in composition and pressure, and may be neutral, ionized, or dissociated.

We report here on the use of flash heating to form single droplets of molten zirconium (melting point 1855°) with highly reproducible diameters between 100 and 500 μ. The droplets were prepared from carefully cut squares of foil dimensions: 0.2 to 2.0 mm. square, 16 μ thick). Oxidations were performed in air at pressures between 50 and 629 torr.

The apparatus in which the oxidations were performed is shown in Fig. 1. It consisted of a vertical glass oxidation tube, the upper end of which was surrounded with a helical capacitor discharge lamp. At the top of the tube, a mechanism operated by a rotary solenoid released single squares of zirconium foil which fell downward toward the flash heating region. Just as the foils passed through, the lamp was triggered; the resulting thermal emission melted the zirconium and formed brilliantly incandescent droplets. The behavior of the glowing droplets as they fell was recorded by high speed photography.

The flash lamp was powered by a Trion PS-100 laser
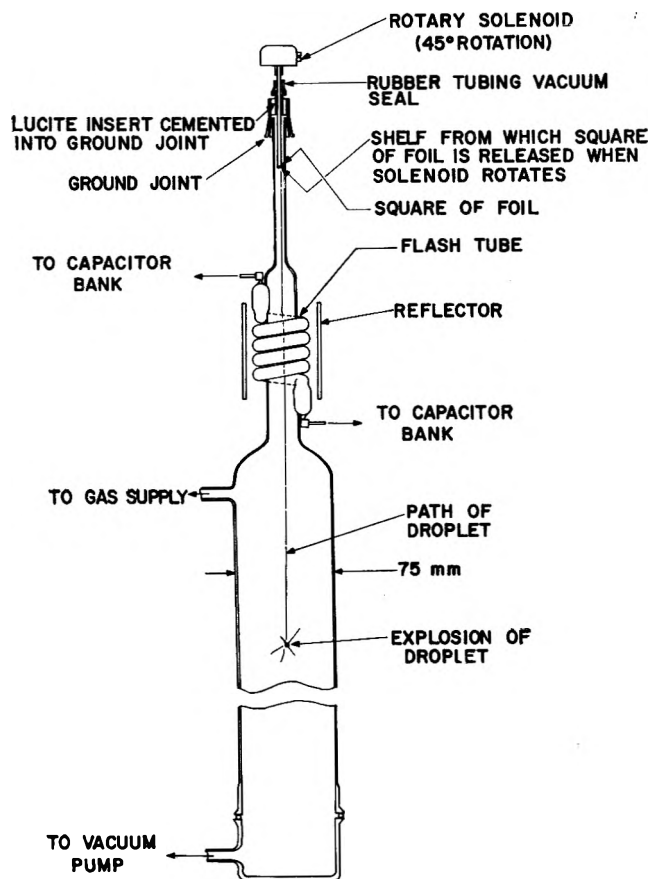
Figure 1. Flash heating apparatus for studying the oxidation of freely-falling metal droplets. To load square of foil onto shelf, rotary release mechanism is raised above ground joint.
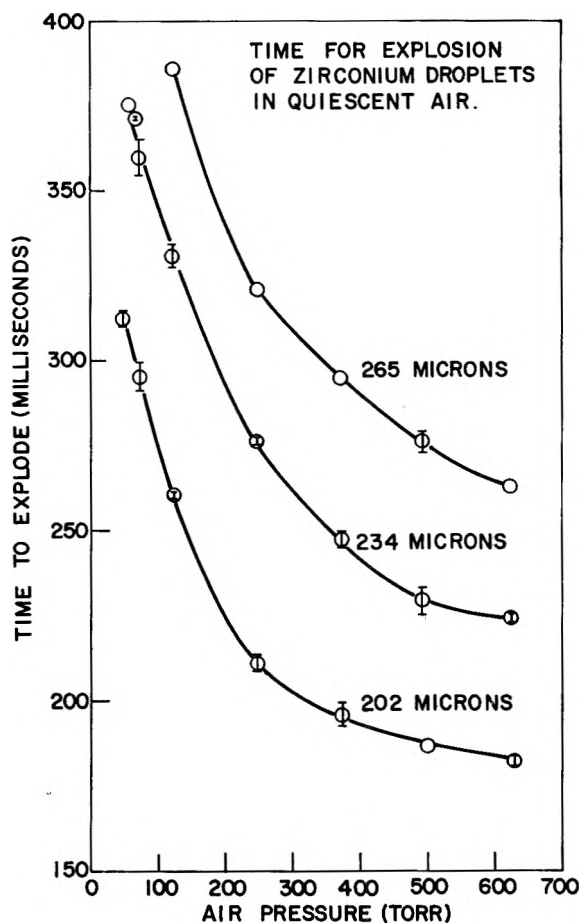
Figure 2. Time required for zirconium droplets to explode during free fall in quiescent air, measured from start of heating flash. Points with vertical bars are averages of from three to five separate determinations; average deviation is indicated by distance from point to end of bar.

stimulator which operated at 4 kv. and delivered 3600 joules. The fused quartz flash lamp was surrounded by an externally silvered cylindrical glass reflector. A cylindrical volume approximately 30 mm. in diameter and 65 mm. long was illuminated.

Several results obtained with zirconium droplets will be presented here to illustrate the capability and accuracy of the method. A more complete report will be presented later.

The most impressive feature of the combustion of a zirconium droplet falling freely in air is the explosion or sparking that occurs a short time after the droplet is formed. This is easily seen in a darkened room with the unaided eye and appears plainly on motion picture frames recorded at 5000 frames/sec. This effect has been observed by others in zirconium and other metals,[6–9,11,16] both directly and by inference from the presence of shattered hollow spheres after the combustion.

We have found that the induction period before explosion is quite sensitive both to air pressure and to the diameter of the droplet. A plot of the time interval between the start of the heating flash and the explosion observed on our films is shown in Fig. 2. Each point is the average of three to five separate determinations. The average deviation between points is about ±3 msec., or about ±2%. It will be noted that the induction period increases with increasing particle diameter and with decreasing air pressure.

Collection of particles in glass dishes inserted at various heights in the oxidation tube enabled us to follow the oxidation process as the droplets fell. This is based upon the observation that the incandescent droplets apparently quench rapidly when they strike a glass surface. Table I summarizes the appearance of residues collected at various levels in the oxidation tube when $265\text{-}\mu$ diameter droplets fell through air at 625 torr. The normal distance for explosion of droplets with this diameter was 32 ± 2 cm., measured downward from the midpoint of the flash lamp's helix.

The cause of the explosions is not known at present, but the films show a rapidly expanding luminous burst in the first frame or two (0.2–0.4 msec.) at the start of the explosion. It is thus likely that the driving force is the expansion of a gas at high pressure. The explosions may also be related to the change from the

---

Table I: Appearance of Residues Collected at Various Distances when a $265\text{-}\mu$ Zirconium Droplet Falls in Air at 625 Torr (Explosion Distance = 32 ± 2 cm.)

Distance below flash lamp, cm.	Appearance of residue[a]
<2.5	Dull gray metal sphere surrounded by smoky white deposit on collection dish
20.0	Gray particle with thin transparent glass-like coating. Metal spattered on dish
27.5	Thicker transparent coating on gray particle
30.0	Still thicker transparent coating that contains large patches of glossy white material. Some particles were completely coated with the white material
32.5	Fragmented hollow spheres of white vitreous material. Thickness of the shells about half the radius of the sphere. Many thin transparent spherical bubbles that show interference colors. Bubbles are much smaller than original droplet
42.5	Jagged pieces, many tiny bubbles
60.0	Jagged pieces, many tiny bubbles

[a] In each experiment, a few streamers of fine fluffy white crystals were found in the dish. This is presumably due to oxidation of zirconium vapor, followed by crystallization from the vapor phase. Also a few tiny bubbles were found in some dishes placed above the explosion level.

---

transparent to the opaque white coating on the particle near the fragmentation level as described in Table I.

Acknowledgment. The authors wish to thank Dr. H. S. Levine for stimulating discussions during the course of this work.

(16) P. D. Harrison and A. D. Yoffe, *Proc. Roy. Soc.* (London), A261, 357 (1961).

SANDIA LABORATORY   L. S. NELSON
ALBUQUERQUE, NEW MEXICO   N. L. RICHARDSON

Purification of Lecithin

Sir: In a recent contribution from Blei and Lee,[1] reference is made to work reported by Elworthy and Saunders[2] in which they claim that we have not paid adequate attention to metal cations present in lecithin preparations. The authors wish to direct attention to the fact that in our paper mentioned above we stated that all lecithin sols were treated with ion-exchange resins to remove ionized impurities and to reduce their specific conductances to very low values. We have found that it is preferable to carry out the ion-exchange process on aqueous lecithin dispersions in which the lipid is present in micellar form; in organic solvents decomposition of the phospholipid is more likely to occur. The method of removing cationic impurities described by Blei and Lee seems unsatisfactory because the cations are replaced by hydrogen ions causing the preparation to become acidic; we find that this treatment increases the specific conductance of lecithin sols. The acidity may account for the more rapid attainment of solubilization equilibrium with the salts of the dye used by Blei and Lee, reported in their paper.

The statement by Blei and Lee that the metal cation content of their impure lecithin was over 20% suggests that their lecithin preparation must have contained large amounts of anionic lipids, perhaps free fatty acids and phosphatidic acids. The normal salt content of egg lecithin is, we find, of the order of 2%, giving a 4% aqueous sol a specific conductance of 150 μmhos cm.$^{-1}$. Treatment of the sol with mixed ion-exchange resins reduces the specific conductance to 5 μmhos cm.$^{-1}$.

(1) I. Blei and R. E. Lee, *J. Phys. Chem.*, 67, 2085 (1963).
(2) P. H. Elworthy and L. Saunders, *J. Chem. Soc.*, 330 (1957).

SCHOOL OF PHARMACY   L. SAUNDERS
UNIVERSITY OF LONDON   S. D. HOYES
BRUNSWICK SQUARE, LONDON W. C. 1
ENGLAND

RECENT PROGRESS IN SURFACE SCIENCE

In Two Volumes

Edited by **J. F. Danielli**, **K. G. A. Pankhurst**, and **A. C. Riddiford**

Volume 1, May 1964, 397 pp., $16.00

Volume 2, Summer 1964, about 500 pp.

These volumes contain critical reviews of the different disciplines in the general field of surface science. Particular stress is laid on significant advances and problems raised from 1956–1961.

CHELATING AGENTS AND METAL CHELATES

Edited by **F. P. Dwyer** and **D. P. Mellor**

May 1964, 530 pp., $17.00

This important treatise presents fundamental data on the structure and properties of these compounds. Included is an intensive treatment of the metal-ligand bond, followed by full discussions of optical activity of metal chelates (with special references to stereospecificity and absolute configuration) and of redox potentials of metal chelate systems.

SILICATE SCIENCE

In Five Volumes

By **Wilhelm Eitel**

Volume 1, **Silicate Structures**

June 1964, 666 pp., $24.00

*Subscription price, $21.00

* Subscription prices valid on orders for the complete set received before publication of the last volume

This treatise provides a source of information on silicate science in the fields of basic chemistry of the silicates, their natural and industrial significance in glass, ceramic, and construction material practice.

SPECTRA-STRUCTURE CORRELATION

By **John P. Phillips**

May 1964, 172 pp., $6.00

This book presents a balanced survey of the data of absorption spectroscopy for organic compounds in all regions of the spectrum from far ultraviolet to far infrared. Classification of compounds according to functional groups is the basic indexing system employed.

POSITRONIUM CHEMISTRY

By **James Green** and **John Lee**

June 1964, 105 pp., $5.50

Positronium Chemistry presents a new field of chemistry, thoroughly grounded in fundamental physical theory—theoretical, nuclear, and solid state. The development of this study is from the theory of positron electron interactions, through experimental nuclear and atomic physics, scattering, solid state through to the theory of chemical bonding, free radical and triplet state chemistry.

MOLECULAR ORBITALS IN CHEMISTRY

A Tribute to R. S. Mulliken

Edited by **Per-Olov Löwdin** and **Bernard Pullman**

Late Spring 1964, about 575 pp.

This tribute to R. S. Mulliken who pioneered in the development of the molecular orbital theory is composed of 33 papers written by the most outstanding world specialists in the numerous fields in which this method can presently be used. Simple and sophisticated approximations are presented and critically evaluated.

INORGANIC ADDUCT MOLECULES OF OXO-COMPOUNDS

By **Ingvar Lindqvist**

A Springer-Verlag title published in the U.S.A. and Canada by Academic Press

1963, 129 pp., $6.50

This book describes the systematic chemistry of all molecular adducts between inorganic electron pair acceptors and oxo-compounds acting as donors. The author begins with a summary of the present state of experimental knowledge, including new results which are published here for the first time.

CHEMICAL TRANSPORT REACTIONS

By **Harald Schäfer**

Translated by **Hans Frankfort**

May 1964, 158 pp., $6.80

Presented is an extensive survey of the literature covering such aspects as experimental and theoretical principles, the transport of solid substances and its special applications, information of the reaction process in the gas phase, chemical transport processes as an aid in preparative chemistry, and the use of transport experiments in the determination of thermodynamic values.

Detailed information available upon request
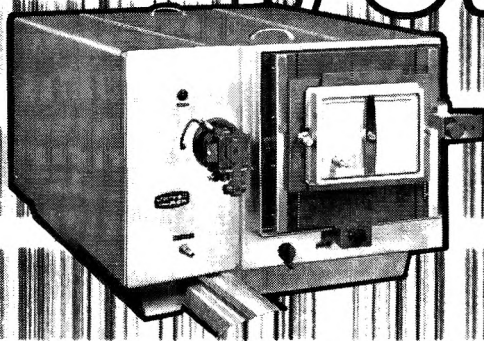
f/6.3 SPECTROGRAPH

HIGH SPEED SCANNING

MICROSECOND
EXPOSURE MEASUREMENT
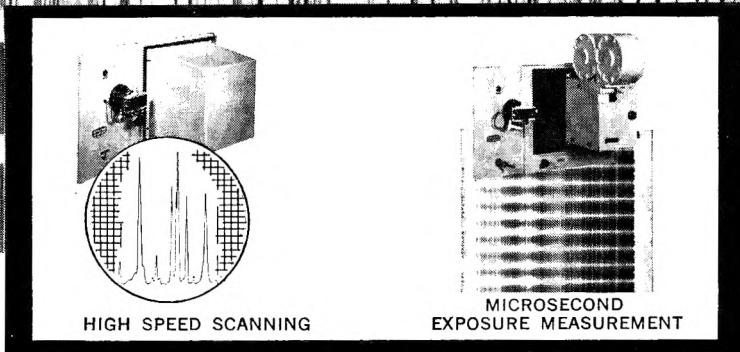
high speed · good dispersion · versatility

The Jarrell-Ash f/6.3 Spectrograph is being used in combustion and shock tube investigations, gas discharge and free-radical studies, and, time-resolved spectroscopic research.

This spectrograph's flat focal field permits very high speed photography. For example, by adding a moving film camera, exposures can be measured in microseconds. Alternatively, the addition of a photomultiplier attachment makes possible photoelectric recording. An optional rotating refractor-photomultiplier assembly with the aid of an associated oscilloscope permits time-resolved studies.

A variety of gratings are available to extend the spectral range to 20,000 angstroms; to resolve lines 0.4 angstroms apart; or to achieve 11 angstroms per millimeter dispersion.

For further information, write for bulletin 75-000.

Jarrell —Ash

Dedicated to excellence in the research, development and manufacture of precision analytical instrumentation.

JARRELL-ASH COMPANY
590 LINCOLN STREET, WALTHAM, MASSACHUSETTS, 02154
TELEPHONE: 617-899-4300   CABLE: JACO-WALTHAM

THE JOURNAL OF
PHYSICAL CHEMISTRY

Volume 68, Number 5   May, 1964

NOTES

$8.58* 250ml
11000

$4.66* 50ml
12940

$4.74* 24/40
16560

$11.83* 250ml
14980

If you use clear fused quartz, ... check these prices

This is VYCOR® brand labware. Compare it with fused quartz:

You can work continuously at 900° to 1000°C. (1652° to 1832°F.) with this 96% silica ware.

It will even go to 1200°C. (2102°F.) for short periods.
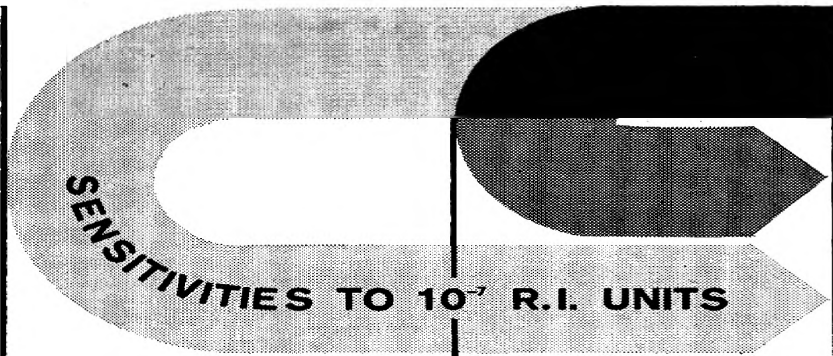
It will withstand a 900°C. thermal shock without a shudder.

But it costs considerably less.

The line is quite complete. You'll find 72 items in beakers, crucibles, dishes, flasks, ground joints, heaters, tubes; 33 different sizes of tubing. They're all listed and indexed in our regular PYREX® brand ware catalog. If you don't have a copy, write for one.

*All the prices above are net each. You can get the prices even lower since we give our regular labware quantity discounts which range as high as 28%.

If you have any questions, write to Laboratory Glassware Dept., 7805 Crystal St., Corning, N. Y.

CORNING
CORNING GLASS WORKS

No. 31 in the
Advances in Chemistry Series

CRITICAL SOLUTION TEMPERATURES

by **Alfred W. Francis,** consultant to Socony Mobil Oil Co., Inc.

This volume, written by an authority on hydrocarbon chemistry
and liquid-liquid phase relations, lists over 6000 critical solution
temperatures (the minimum temperature for mixing of two sub-
stances in all proportions *as liquids*). Also included are about
800 aniline point observations; methods for determining CST;
guides to using CST data and to estimating the CST for untested
systems.

Among uses of CST are: screening possible extraction solvents
for selectivity; approximating liquid solubility at any temperature
below the CST; characterizing hydrocarbons; analysis of mix-
tures, especially where water is one component, and providing an
insight into molecular structure.

CONTENTS

Introduction and six Figures . . . Tables: Critical Solution Tem-
peratures . . . Aniline and Furfural Points . . . Lower Critical Solu-
tion Temperatures . . . Mutual Miscibility of Liquids (tabulations
of numerical CST data from charts in five published compila-
tions) . . . Bibliography.

246 pages.   **Cloth bound.**   **Price: $5.00**

Order from:

Special Issues Sales, American Chemical Society
1155 Sixteenth Street, N. W., Washington 6, D. C.

High Temperature Mechanism of the System Hydrogen–Hydrogen Iodide–Iodine
. . . **Osamu Horie, Yataka Ishii, and Akira Amano** 1264

Conductivities and Viscosities of Fused Salts in Fritted Disks
. . . **Benson Ross Sundheim and Alexandre Berlin** 1266

COMMUNICATIONS TO THE EDITOR

The Use of Flash Heating to Study the Combustion of Liquid Metal Droplets
. . . **L. S. Nelson and N. L. Richardson** 1268

Purification of Lecithin . . . . **L. Saunders and S. D. Hoyes** 1270

AUTHOR INDEX

No. 29 in the ADVANCES IN CHEMISTRY SERIES

PHYSICAL PROPERTIES OF CHEMICAL COMPOUNDS—III

This handbook of basic data contains 456 full-page tables on 434 aliphatic compounds and 22 miscellaneous compounds and elements—all carefully worked out by R. R. Dreisbach of The Dow Chemical Co.

It is a sequel to **PHYSICAL PROPERTIES—II** (Advances No. 22), which covers 476 organic straight-chain compounds, and **PHYSICAL PROPERTIES—I** (Advances No. 15), which presents data on 511 organic cyclic compounds.

This series provides you with a breadth of data that you can get in no other way. For each compound 15 physical properties are given: purity—freezing point—vapor pressure—liquid density—vapor density—refractive index—rate of change of boiling point with pressure—latent heat of fusion—latent heat of evaporation—critical values—compressibility—viscosity—heat content—surface tension—solubility. Parameters are also furnished for interpolating and extrapolating determined data for almost all the compounds. To get this information by ordinary means you would have to seek out many sources.

PHYSICAL PROPERTIES—III offers the extra advantage of a cumulative index to **all three volumes** (1443 compounds and elements). Use it and the earlier compilations to save yourself hours of laboratory time, and to answer questions quickly.

489 pages.	Cloth bound.	Price: $6.50

PHYSICAL PROPERTIES—II — *491 pages* ● *cloth bound* ● *price:* *$6.50*
PHYSICAL PROPERTIES—I — *536 pages* ● *cloth bound* ● *price:* *$5.85*

Order from:

Special Issues Sales/American Chemical Society/1155 Sixteenth Street, N.W./Washington 6, D.C.